Ribbed moraines and subglacial geomorphological signatures of interior-sector palaeo-ice sheet dynamics

Kaleb Wagner, B.Sc. (Honours)

Department of Earth Sciences

Submitted in partial fulfillment

of the requirements for the degree of

Master of Science

Faculty of Mathematics and Science, Brock University

St. Catharines, Ontario

Table of Contents

Abstract

Transverse, subglacial bedforms (ribbed moraines) occur frequently in southern Keewatin, Nunavut, Canada, where they record a complex glacial history, including shifting centers of ice dispersal and fluctuating basal thermal regimes. Comprehensive mapping and quantitative morphometric analysis of the subglacial bedform archive in this sector reveals that ribbed moraines are spatially clustered by size and assume a broad range of visually distinct forms. Results suggest that end-member morphologies are consistent with a dichotomous polygenetic origin, and that a continuum of forms emerged through subsequent reshaping processes of variable intensity and duration. Translocation of mobile, immobile and quasi-mobile beds throughout the last glacial cycle conditioned the development of a subglacial deforming bed mosaic, and is likely responsible for the patchy zonation of palimpsest and inherited landscape signatures within this former core region of the Laurentide Ice Sheet. Comparison against field evidence collected from central Norway suggests that bedforming processes can be locally mediated by pre-existing topography.

Keywords: ribbed moraines, subglacial bedforms, spatial analysis, Keewatin, deforming bed mosaic

Acknowledgements

There are a number of names deserving of mention, whose support was critical in putting together this thesis. Above all I wish to thank my supervisor, Dr. John Menzies, whose patient guidance and unfathomable depth of knowledge granted me the basis and flexibility to pursue new avenues with this research. I am grateful also to my committee members, John Delgaty and Dr. Jacob Napieralski, whose insightful reviews contributed much to the readability of this manuscript and the arguments presented herein. Thanks to Marty Ouellette for his thin section work, and to Dr. Daryl Dagesse for lending me his time, direction and use of equipment in his sediment laboratory. Thanks to a number of my professors over the years, Dr. Alec Aitken, Dr Ívar Örn Benediktsson and Dr. Ólafur Ingólfsson, whose passions for Quaternary science and glacial geology incited my own interests in these fields.

This research was funded by a Natural Sciences and Engineering Research Council of Canada (NSERC) CGS-M award, as well as an Ontario Graduate Scholarship (OGS) supplied by the Government of Ontario, in addition to the financial support provided by Brock University and various internal scholarship donors, for which I am tremendously grateful.

I extend my thanks to all of the friends and acquaintances I've met during my studies at Brock, who have provided many (necessary) distractions, and helped to shape my overall graduate experience. Thanks to my housemates (at both Norman and Lampman), Geoclub, the Volley Llamas, everyone at NSI, fellow trivia night enthusiasts, Matt, Fernando, Eddy, Alicia, Mags, Matea, and the Alphie's crew. Jessey, I couldn't have asked for a better labmate; thanks for showing me the ropes as a TA, and later for the epic Zookeeper battles, impeccable humour, and for putting up with an endless barrage of digitization mouse clicks in the office. Thanks also to my friends outside of the Brock community, back in Saskatchewan and scattered elsewhere, who have maintained their amity from afar. Lastly – Mom, Dad, Marisha – I am forever appreciative of your unfailing support and encouragement.

To anyone I may have missed (there are bound to be many), thank you for any help and/or guidance you have provided over the past two years. It's been a meandering journey but I'm glad to have finally arrived at the destination.

-K.W.

List of Tables

Chapter 4

Chapter 5

Chapter 6

List of Figures

Chapter 3

Chapter 4

Chapter 5

Chapter 6

Chapter 7

List of Appendices

List of Abbreviations

In alphebatized order:

AKID	Ancestral Keewatin Ice Divide
ALOS	Advanced Land Observing Satellite
ANND	Average Nearest Neighbour Distance
ANOVA	Analysis of Variance
BP	Before Present
BRIE	Bed Ribbing Instability Explanation
CDED	Canadian Digital Elevation Data
CIS	Cordilleran Ice Sheet
CSA	Canadian Space Agency
CSR	Complete Spatial Randomness
DEM	Digital Elevation Model
DF	Draping Facies
DLIS	Dubawnt Lake Ice Stream
DLR	German Aerospace Centre
DN	Digital Number
DRF	Distal Ridge Facies
DSM	Digital Surface Model
DTM	Digital Terrain Model
EM	Electromagnetic
EOS	Earth Observing Satellite
ER	Elongation Ratio
ESA	European Space Agency
ETM+	Enhanced Thematic Mapper Plus
FASC	Full Aperature Solar Calibrator
FCC	False Colour Composite
FIS	Fennoscandian Ice Sheet
Ga	Giga-annum
GIS	Geographic Information System
GISc	Geographic Information Science
GSC	Geological Survey of Canada
GTZ	Glacial Terrain Zone
HCA	Hierarchical Cluster Analysis
HCPC	Hierarchical Clustering of Principal Components
IC	Internal Calibrator
IFOV	Instantaneous Field of View
InSAR/IfSAR	Interferometric Synthetic Aperture Radar
IR	Infrared
JAXA	Japan Aerospace Exploration Agency
Ka	Kilo-annum
KID	Keewatin Ice Divide
LDCM	Landsat Data Continuity Mission

LGM	Last Glacial Maximum
LiDAR	Light Detection and Ranging
Lins	Lineation Flowset
LIS	Laurentide Ice Sheet
LISA	Local Indicators of Spatial Autocorrelation
LZ	Lineation Zone
Ma	Mega-annum
MSGL	Mega-scale Glacial Lineation
MSS	Multi-spectral Scanner
NASA	National Aeronautics and Space Administration
NNA	Nearest Neighbour Analysis
NNR	Nearest Neighbour Ratio
NRN	National Road Network
NTDB	National Topographic Database
NTS	National Topographic System
OIS	Oxygen Isotope Stage
OLI	Operational Land Imager
OLS	Ordinary Least Squares
PALSAR	Phased Array type L-band Synthetic Aperture Radar
PASC	Partial Aperture Solar Calibrator
PC	Principal Component
PCA	Principal Component Analysis
PCILC1	Control Points for Landsat 7 Imagery, Canada, Level 1
PCS	Phase Change Surface
PRF	Proximal Ridge Facies
RBV	Return Beam Vidicon
RGB	Red Green Blue
Rm	Ribbed Moraine Flowset
RMZ	Ribbed Moraine Zone
RS	Remote Sensing
SAR	Synthetic Aperture Radar
SLC	Scan Line Corrector
SRTM	Satellite Radar Topography Mission
TIROS	Television and Infrared Observation Satellite
TIRS	Thermal Infrared Sensor
TM	Thematic Mapper
USGS	United States Geological Survey
UTM	Universal Transverse Mercator
VNIR	Visible and Near Infrared

List of Symbols

In order of appearance:

v_p	p-wave velocity
v_s	s-wave velocity
n	porosity | sample size
N	effective pressure
ε	strain rate
τ	shear stress
c	cohesion
P_n	component of normal stress
P_w	internal porewater pressure
$tan\varphi$	coefficient of friction
T_0	satellite orbital period
R_p	planet radius
H'	altitude of remote sensor above datum
g	gravitational constant
m	slope
γ	incidence angle
D_{obs}	observed distance
D_{exp}	expected distance
A	area
d	distance | diameter
d_i	distance between feature i and nearest neighbouring feature
$K(d)$	Ripley's K function
ϑ	density of instances
E	number of additional events within a distance (d) of a randomly selected event
$L(d)$	variance stabilized Ripley's K function
$k_{(i,j)}$ | $w_{(i,j)}$	spatial weight matrix
I	Moran's I
S_0	sum of spatial weights
G	Getis Ord General G
I_j	Local Moran's I
p	calculated probability value
z	elevation
$\bar{x}$	sample mean
$\bar{X}$	population mean | global mean
L	length
H	height
W	width
λ	gradient of above-mode exponential decay
β_0	area-normalized y-intercept
ϕ	mode
s	sample standard deviation
s^2	sample variance

p	fluid density
r	particle radius
t	time
η	viscosity
C	concentration
C_0	dry weight of sample
$\boldsymbol{\theta}$	sedimentation rate | basal temperature
T	temperature
V_1	principal eigenvector
S_1	principal eigenvalue
U	ice velocity
a_b	surface ablation rate

1. Introduction

1.1 *Background*

Subglacial processes are important because they influence the fundamental behaviours of glaciers and ice sheets, yet owing largely to their complexity, comprehensive understandings of the relationships between these processes and their geomorphic products have yet to be obtained (Clarke, 1987, 2005). Knowledge of subglacial processes forms a crucial prerequisite to the geomorphic reconstruction (e.g., Dyke and Prest, 1987; Kleman at al., 1997; Greenwood and Clark, 2009b; Hughes et al., 2014) and numerical modeling (e.g., Andrews and Mahaffy, 1976; Hindmarsh et al., 1989; Huybechts and T'siobbel, 1995; Tarasov and Peltier, 2004, 2007; Stokes et al., 2012) of past continental ice sheets and associated palaeoclimatic and palaeoceanic regimes. Ensuring the integrity of these models is critical, as they serve to guide and contextualize studies of modern glaciers and ice sheets, as well as inform predictions of chryosphere response under various scenarios for future climate change and sea level rise. The study of ancient sediments and landforms is a useful method for developing knowledge of subglacial processes. Subglacial bedforms, in particular, are a common focus of these investigations, as they are remarkably ubiquitous across formerly glaciated regions, and retain a wealth of information related to the style and direction of palaeo-ice flow. Recently, geophysical methods have confirmed the existence (King et al., 2007) and growth (King et al., 2009) of bedforms beneath the Antarctic Ice Sheet, thus establishing a crucial link between glacial geology and contemporary glaciology that places better constraints on ancient bedforming environments.

One of the most ambiguous subglacial bedforms which occurs across large areas of former ice sheet beds is the ribbed (a.k.a. "Rogen") moraine. These are arcuate, occasionally anastomosing ridges, oriented with their long-axes transverse to former ice flow, often with concave plan-forms arching in a down-ice direction. Ribbed moraines exhibit a relatively widespread distribution, and are found commonly within the former interior regions of the Laurentide, British-Irish, and Fennoscandian Ice Sheets (Hättestrand and Kleman, 1999; Dunlop and Clark, 2006b). Characteristically, ribbed moraines tend to exhibit either a gradual up- and/or down-ice transition to streamlined terrain (Lundqvist, 1969, 1989), though lateral transitions are also common in areas of low relief (cf. Aylsworth and Shilts, 1989a,b; Trommelen et al., 2014). Stemming from a lack of focused research, and an apparent discord between existing theories in the literature, the formative process (or processes) of ribbed moraines remain largely enigmatic. Hypotheses of formation have led to interpretations of these ridges as, *inter alia*, simple networks of end moraines (Frödin, 1913; 1925); active-ice marginal features (Cowan, 1968); end-members of a subglacial bedform continuum (Sugden and John, 1976; Lundqvist, 1981; 1989; Boulton, 1987; Menzies and Shilts, 1996; Knight and McCabe, 1997); glacio-fluvial infillings of meltwater ripples carved out during catastrophic, subglacial mega-floods (Fisher and Shaw, 1992; Shaw, 1983, 2002); accretional melt-out deposits of compressionally-stacked deformation planes in debris-rich basal ice (Shaw, 1979; Bouchard, 1989; Lindén et al., 2008); fragments of an extensionally fractured and re-moulded pre-existing drift sheet (Lundqvist, 1969; Hättestrand, 1997; Hättestrand and Kleman, 1999; Kleman and Hättestrand, 1999; Sarala, 2006); and more recently, a response to the development and propagation of instabilities at the ice/bed interface (Dunlop et al., 2008; Chapwanya et al., 2011).

Widely diverging evidence of structural, compositional and morphological properties has precluded the formation of a unifying theory of ribbed moraine formation. One outcome of these inconsistent observations has been the development of several independent classification schemes. Among others, these include Aylsworth and Shilts' (1989a) 'classic Rogen moraine', 'blocky ribbed

moraine', 'fish-scale ribbed moraine' and 'dune-shape ribbed moraine'; Hättestrand's (1997) 'Rogen moraine', 'hummocky ribbed moraine', 'Blattnick moraine' and 'minor ribbed moraine'; and Dunlop and Clark's (2006b) more elaborate 12-fold categorization. Whether differences in these naming schemes are merely a question of semantics, or rather, if each distinctive morphology can be linked to a unique genetic history remains to be determined. Many of these reported variations in ribbed moraine properties exist between studies that have considered Scandinavian and North American ribbed moraines separately (Lundqvist, 1997). It may thus be instructive to establish comparisons between these populations, using the unique glacial history of each region as a means to isolate potential formative controls.

One of the largest and least studied assemblages of ribbed moraines is found in the central and southern Kivalliq Region (formerly the District of Keewatin), Nunavut, Canada, over the western Canadian Shield. This region – often referred to as the 'Keewatin Sector' of the Laurentide Ice Sheet (LIS) (Prest, 1970) – occupied the periphery of the Keewatin Ice Divide (cf. Lee, 1959) throughout the last glacial cycle (Shilts et al., 1979; Shilts, 1980; Dyke and Prest, 1987; Dyke et al., 2002), and retains a complex, highly fragmented geological record of translocating dispersal centers and shifting ice flow vectors (Boulton and Clark, 1990a,b; McMartin and Henderson, 2004). Ribbed moraines in this area have been traditionally regarded as strictly deglacial features (e.g., Lee, 1959; Prest, 1968, 1970; Prest et al., 1968; Dyke and Prest, 1987; Kleman and Hättestrand, 1999), formed during the last and most recent phase of ice flow across this region, however their intricate association with streamlined landforms, involving adjacent zones of exclusivity and oblique re-moulding/overprinting (Aylsworth and Shilts, 1989a), remains unexplained and does not befit a single-stage formation hypothesis. Recent applications of remote sensing technologies have had much utility for characterizing the morphology and spatial distribution of ribbed moraines by enabling the mapping of diverse areas and collection of large sample sets (cf. Dunlop and Clark, 2006b), however this largest assemblage within south-central Keewatin, which supports a confounding variety of morphologies, has yet to be objectively assessed. The ability to better associate individual bedform morphologies with specific palaeoglaciological processes could foster a more complete knowledge of the glacial history of the central LIS. Such information could be used to facilitate more targeted prospecting for diamond and mineral exploration within palimpsest dispersal trains in Canada's North (cf. McClenaghan et al., 2001; Paulen and McClenaghan, 2013).

1.2 *Summary of Research Aims & Objectives*

Palaeoglaciology has seen many conceptual and methodological advances in recent decades which have caused a widespread shift in how past-glaciated landscapes are interpreted. Specifically, many components of the glacial system are now considered to be extremely variable throughout time and space, including basal thermal zonation, subglacial hydrology, ice streaming behaviour, and internal ice sheet dynamics (e.g., surging) (Kleman et al., 2006). Associatively, rheological properties of the subglacial bed are also increasingly being conceived within new frameworks that regard them as highly dynamic and transitory systems (e.g., van der Meer, 2003; Piotrowski et al., 2006). Most importantly with respect to the geomorphological archive, it is now understood that ice sheets produce *and preserve* a metachronous record of sediments and landforms that can no longer be explained using simplified models of the past (Clark et al., 2000, 2012; Greenwood and Clark, 2006b; Trommelen et al., 2012; Hughes et al., 2014).

The complex subglacial landscape in south-central Keewatin has yet to be re-interpreted within a modern palaeoglaciological paradigm. This thesis aims to accomplish such a re-interpretation by focusing on the spatial and morphological properties of the expansive glacial bedform record in this

region, and by evaluating methods of linking these properties to past subglacial dynamics. Comprehensive mapping of the bedform record in south-central Keewatin will allow for these important properties to be assessed in objective ways. This research has several aims which together converge on the ultimate goal of reconciling subglacial geomorphological signatures with interior-sector palaeo-ice sheet dynamics:

1. Quantitatively assess the spatial and morphological characteristics of ribbed moraines in south-central Keewatin;
2. Elucidate controls on ribbed moraine formation and development;
3. Contribute additional field-based observations of ribbed moraine internal structure and composition;
4. Determine the extent of convergence between morphologic and genetic ribbed moraine classifications;
5. Interpret the glacial history of south-central Keewatin within a modern palaeoglaciological framework.

1.3 *Outline & Structure of Thesis*

This thesis is provided in monograph format, with individual topics addressed as separate chapters. A brief synopsis of the history and mechanics of deforming subglacial beds is offered in Chapter 2, followed by an extensive review of the existing literature pertaining to the spatial, morphological and sedimentological properties of ribbed moraines in Chapter 3. A backgrounder to remote sensing and geographic information systems (GIS) technologies is provided in Chapter 4, with a focus on applications in glacial geomorphology. Chapter 5 contains information on the glacial geology of the southern Nunavut study area, as well as an overview of the methodologies used for bedform mapping and analyses in this study. The results section of this chapter is divided into two parts, one which presents outcomes of GIS-based ribbed moraine spatial and morphological analysis, and the other which outlines a reconstruction of the glacial history of south-central Keewatin based on a glacial geological inversion scheme using the mapped bedform record. Chapter 6 comprises field results from central South Norway. Ribbed moraine sections were invstigated at three separate field sites in order to collect information on their internal composition and structure and establish morphological comparisons with the features mapped in the Nunavut study area. An overview of field and laboratory methodologies, and information on the glacial geology of central Norway, which provides context for field results, are also contained in Chapter 6. A discussion of Chapters 5 and 6 is provided in Chapter 7, which considers results in light of the existing literature on ribbed moraines, deforming subglacial bed mosaics, and the glacial history of south-central Keewatin. Chapter 8 provides a brief summary of the overall findings presented within this thesis.

2. Deforming Subglacial Beds

Glacial sediments and landforms comprise widespread and important evidence of glaciation across much of the northern hemisphere, yet despite this abundance of information, subglacial erosional and depositional processes (including those which are bedforming) remain poorly understood. Nevertheless, major advances have been made in recent decades through laboratory tests and direct observations from beneath contemporary ice sheets. Considering the extent that modern bedforming hypotheses have come to rely on mechanisms of subglacial substrate deformation, a brief discussion of this theory and its background is warranted in this thesis.

The influence of subglacial processes on ice-sheet flow mechanics has only recently been fully recognized. Early field-based investigations of subglacial processes and sediments were typically conducted in alpine settings (cf., Kamb and La Chappele, 1964). Characteristically in these environments, ice slides directly over a low-permeability bedrock surface – typically mediated by a thin layer of pressure-generated meltwater (e.g., an '*Ha*'-type bed, cf. Menzies, 1989a,b) – motivating early studies to overemphasize the importance of lodgement processes by extrapolating their observations to ancient ice sheets (Boulton, 1986; Evans et al., 2006). More developed understandings of glacial substrates led to the notion that glacier beds locate along a rheological continuum, encompassing a broad array of geotechnical properties. This continuum includes at least some systems wherein basal ice is coupled to saturated and deformable sediments. In these latter systems, the substrate itself provides a mechanism of enhanced glacier flow, wherein rheologically soft basal sediments respond, via mobilization and deformation, to stresses imparted by overriding ice (Boulton, 1986).

Following his expedition to the Norwegian Arctic, Gripp (1929) became one of the first authors to suggest the existence of a viscous flow property in subglacial tills, based upon observations of sub-vertically oriented englacial moraine bands in Spitsbergen glaciers. Here it was suggested that partially saturated sediments could be upwardly injected into basal crevasses, either motivated by ice overburden pressures, or else as a thrust response to residual ice movement. Hoppe (1952, 1957) further expanded upon this hypothesis, proposing that a similar mechanism was responsible for the development of comparably shaped ridges (as well as dead-ice hollows and 'morainic plateaus') in the Veiki region of northern Sweden. Effectively, the implication of Hoppe's theory was that hummocky moraine (as we presently refer to it) is in fact a variety of subglacial squeeze moraine. Boulton (1970b) expressly disputed this hypothesis, prompting him also to question the mobilized till mechanism itself which underlay this idea (a position, however, he later retracted, cf. Boulton, 1971).

The application of high-resolution seismic survey techniques throughout the mid-1980's uncovered a wealth of new information concerning subglacial interfaces in Antarctica and their influence on ice motion. Much of this early work was focused on the large outlet glaciers of West Antarctica, and thus was chiefly concerned with describing ice streaming behaviour and associated mechanisms of fast glacier flow (Murray, 1997), and later with validating physical models of these phenomena (e.g., Alley et al. 1987b). In one such seismic reflection study, Blankenship et al. (1986, 1987) resolved a meters-thick layer of material beneath Ice Stream B, West Antarctica, through which compressional (P-wave) and shear (S-wave) velocities (v_p and v_s respectively) were found to be anomalously low. In porous, saturated, materials, v_p is primarily a function of porosity, and correspondingly, bulk density. Alternatively, v_s is most responsive to intergranular friction and effective pressure, such that both porosity and pressure can be estimated for a material given v_p and v_s, which are derived by inverting seismic travel times sourced from a wide-angle sounding. Using this relationship, Blankenship et al. (1986, 1987) were able to demonstrate that the material forming the layer of seismic

anomaly was highly porous ($n \approx 0.4$), water saturated, and exhibited substantial porewater pressure, offset only marginally by local overburden pressures, thus ultimately yielding trivial effective pressure ($N \approx 50$ kPa). Alley et al. (1986, 1987a,b) interpreted these results against those collected by Boulton (1979) and Boulton et al. (1974a,b) on the geotechnical properties of subglacial tills from the recently exposed Breiðamerkurjökull forefield, southeast Iceland. In view of its location at the ice/bed interface, apparent erosive capacity, and the above seismically derived parameters, the porous, saturated layer beneath Ice Stream B was identified as a highly-dilated glacial till, subject to large stress concentrations, and therefore consistent with an actively deforming subglacial substrate (Alley et al. 1986, 1987a,b). These speculations were validated by analyzing cores retrieved during subsequent borehole investigations (Engelhardt et al., 1990), though Engelhardt and Kamb (1998) later argued that most deformation within this layer proceeded within only the uppermost 5 cm, as opposed to the up to 12 m thick deforming layer as originally proposed.

Critical to the deformation mechanism in most subglacial tills is the existence of a debris-rich layer of basal ice which immediately overlies the ice-substrate contact. This layer of regelation ice may contain debris in concentrations up to 50% by volume, though above this, suspended debris concentrations are negligible, save for local accumulations within basal and/or englacial thrust planes. The presence of debris-rich basal ice is typical of warm-based and polythermal ice masses, and behaves as a dominant mode of transport for basally-derived debris (Boulton, 1979). Large clasts representative of the coarsest basal debris fraction protrude from the glacier sole and either collide with lodged particles in the basal substrate during ice motion, or experience a more constant frictional drag as they plough through underlying materials, both of which contribute to shearing of the substrate and thus dilation at particle contacts. Dilative effects are not localized at the interface, however, as inter-particle stress transmission can enable subjacent till dilation, even well beneath the ice-substrate contact (Boulton, 1979). Ultimately, a high void ratio ($n > .30$) is affected throughout the till by driving stresses associated with overriding ice movement, lowering the density of the material, and vertically stacking particles along a series of sub-horizontal micro-shear planes. This latter effect attributes a high coefficient of compression, and prevents dilatant tills from supporting any appreciable overburden pressures, thereby promoting lateral stress transmissions (i.e., the response to which is strain and deformation) (Boulton et al., 1974b). Dilative properties of certain tills have recently been invoked to explain the regular patterning of subglacial bedforms (including ribbed moraine) on a palaeo-ice sheet scale (Hindmarsh, 1998a,b,c; Fowler, 2000; Schoof, 2007; Dunlop et al., 2008; Clark, 2010; Chapwanya et al., 2011) (see section 3.4.4).

Boulton's understandings of subglacial stress transmission and substrate deformation contributed to development of the earliest 'subglacial till flow law'; namely the Boulton-Hindmarsh model:

$$\varepsilon = K\left(\tau - \tau_{yield}\right)^{a} N^{b} \left(\tau > \tau_{yield}\right)$$

where ε is strain rate, τ shear stress, N effective pressure (effective normal stress) and K, a and b are all empirically derived constants. τ_{yield} is given by the basic Mohr-Coloumb equation:

$$\tau_{yield} = c + N \tan \varphi$$

in which c represents cohesion, and $\tan\varphi$ the coefficient of friction. The Boulton-Hindmarsh model assumes an inverse relationship between strain rate and effective pressure, and increasing rates of strain for progressively greater shear stresses above a critical yield value (Boulton and Hindmarsh, 1987). When experimentally fitted to the sediment data obtained from the Breiðamerkurjökull forefield

(Boulton, 1979; Boulton et al., 1984a,b), the exponential constant *a* remained close to unity, which is suggestive of a Bingham (non-linear) viscous rheology for the till. Subsequent laboratory testing of subglacial tills using shear-box, ring shear, and triaxial shear apparatuses have demonstrated that this relationship may not properly characterize subglacial tills, indicating instead a nearly Coloumb-plastic rheology (e.g., one in which materials undergo sudden failure upon reaching a critical τ_{yield}, and where applied shear stress, or shear strength, increases linearly with *N*) (Kamb, 1991; Iverson et al., 1997, 1998; Tulaczyk et al., 2000). The applied research of Kavanaugh and Clarke (2006) appears to confirm this hypothesis. More recently, it has been shown that a viscous or pseudoviscous property could also characterize basal tills prior to the onset of plastic deformation (i.e., at stresses below 90%), thus partially reinstating the importance of the original power flow law (Rathbun et al., 2008).

The results obtained from Ice Stream B, and the subsequent models developed to explain them, were instrumental in overturning the highly idealized belief that all ice masses overlay rigid and fundamentally immobile beds. In effect, it was discovered that subglacial substrates may in fact comprise rheologically soft basal sediments which are, themselves, capable of deformation, and can therefore significantly contribute to observable ice velocities at the surface. Just as importantly, deformable subglacial sediments have since been acknowledged as potential contributors to subglacial erosional and depositional processes carried out at the ice/bed interface. Further studies conducted on the geotechnical properties of substrates underlying the Antarctic Ice Sheet have enabled even better characterizations of these materials and their influence on ice velocity (Peters et al., 2006). Nevertheless, the continued relevance of the early Antarctic geophysical studies cannot be overstated; and indeed they acted as the catalyst to what is now commonly referred to as the "paradigm shift in glaciology" (Boulton, 1986). This "paradigm shift" was very much a shift in international research focus, and subsequently the solutions to a number of pre-existing, unsolved problems surrounding glacier flow mechanics were ascribed to the existence of deformable subglacial tills. Associations were also made to ancient tills in this regard, and the theory of soft sediment deformation was used to fill numerous gaps in knowledge; *viz*., how considerable ice discharges might be explained in the presence of frequently low driving stresses; how substantial volumes of ice might respond rapidly to external climate forcing; how previously unexplainable rates of volumetric ice sheet growth and decay could have been achieved in the past such as to be properly rendered within contemporary ice sheet models; etc. (Boulton et al. 1985). Perhaps most significant of all, this "paradigm shift" presented subglacial bedforms within a new light, and studies – which quite plausibly found their modern beginnings in the work of Smalley (1966), and Smalley and Unwin (1968) – began to focus on the nature and strength of subglacial materials as potential explanatory variables in bed-formation, rather than just strictly morphology (Stanford and Mickelson, 1985).

3. Ribbed Moraines

3.1 *Introduction & the Early Literature*

Ribbed moraines have been recognized as a distinct category of glacial landform for well over a century. A thorough review of these features has been compiled by Hättestrand and Kleman (1999) which summarizes known spatial, sedimentological and morphological properties, and provides insight into the early Scandinavian literature. The following section benefits extensively from this review while providing updates from the more recent literature.

Högbom (1885, 1894) is often cited as the first researcher to have described ribbed moraine features from observations in central Sweden. At this early stage, attention was drawn only to the inconsistent composition and structure of the ridges, and no method of formation was conjectured. Throughout the early 20th century, increasing interest was generated around classifying independent moraine morphologies, particularly within areas of northern Sweden where numerous forms appeared to occur within close spatial proximity. Tanner (1914) provided a preliminary assessment of these, proposing the use of a crude classification scheme to differentiate "radial moraines" (which, mistakenly, also included drumlins) from end moraines, lateral moraines and "hummocky moraine land" (a term that, soon after, came to be synonymous with the genetic terms, 'dead-ice' and 'ablation' moraines). Informed by the state of 20th century knowledge, this author, as well as several others (Frödin, 1913, 1925; Högbom, 1920; Beskow, 1935), displayed a proclivity for classifying all transverse ridges as end moraines. Later, in conjunction with the discovery of wastage processes, this classification bias shifted rather to attributing ablationary origins to morainic forms. Lundqvist (1943) advanced a ternary classification system for this type of moraine, one which distinguished between sharply crested boulder-rich till ridges and hillocks; gently rounded forms with boulder contents ranging from moderate to low, and; conspicuous ridge forms, with long-axes trending at right-angles to palaeo-ice flow. So-called "Rogen moraines" were considered in parallel with the latter grouping, and it has been suggested by Hoppe (1952) that these types were initially subject to misclassification as end moraines more frequently than any other morphology.

Tanner's (1914) original discussion of "hummocky moraine land" constrained the development of these forms to within the pro-marginal zone. Morainic forms were thought to be shaped throughout glacial recession, specifically by the funneling of supra- and englacial debris into holes and clefts in ablating marginal ice. Upon melt, this debris remained to comprise a series of ridges and hillocks on the landscape, punctuated by topographic hollows and depressions marking the former locations of buried stagnant ice blocks. This perception of hummocky moraine development is very much in line with present-day understandings, although the author's failure to genetically separate regularly spaced transverse ridges from standard dead-ice features revealed a lack of understanding with respect to controlled moraine origins. A clearer example of this is exemplified by Lundqvist (1935) who echoes Tanner's (1914) model of hummocky moraine formation, and intentionally extends it to all Rogen forms as well (Lundqvist, 1937, 1943, 1951).

Mannerfelt (1945) later reiterated the importance of stagnant ice in shaping pro-marginal landscapes, though is notable in that he proposed a separate mode of formation for Rogen-type deposits, considering them as active ice-frontal accumulations, and invoking annual climatic fluctuations as a means of explaining their characteristic spacing. Yet despite placing them at the margin of a retreating ice lobe, this author was reluctant to definitively classify Rogen-type forms as *sensu stricto* end moraines (Mannerfelt, 1945, p. 154). Shortly thereafter, the term "Rogen moraine" was formally introduced to the literature by Hoppe (1952, 1959) to refer to landforms of the widely studied terrain

surrounding Lake Rogen in Härjedalen, west-central Sweden (henceforth considered the type locality of the Rogen moraine). Apart from coining this term, Hoppe's contribution is marked by being among the first workers to suggest a subglacial origin for the Rogen moraine, based on observations of superimposed eskers throughout Härjedalen. The largest and most prominent of these eskers was previously described by Frödin (1925), though no associations were made with respect to the underlying ridges, or any potential formational sequence. Observations of lodgement till within Rogen-type forms (Holmsen, 1935; Rasmusson and Tarras-Wahlberg, 1951; Kujansuu, 1967), and reports indicating the common drumlinization of ridges (Lee, 1959; Prest, 1968) led Lundqvist (1969) to propose the first modern, and widely reproduced theory of Rogen moraine formation. The majority of studies since this time have appealed to subglacial modes of development.

3.2 *Spatial & Morphological Properties*

3.2.1 **Morphological Characteristics**

Knowledge concerning the morphology of ribbed moraines has continued to evolve since the earliest studies, and radically so following the advent of aerial, and later, space-borne imaging technologies. In general, ribbed moraines are ridges of glacigenic material that are oriented with their long axes transverse to the direction of palaeo-ice flow. They are often described as being arcuate, with their 'horned' extremities and concave face trending down-ice (cf. Lundqvist, 1968; 1989). Unfortunately, Sugden and John (1976) appear to have mistakenly inverted this characteristic in their popular text, depicting ribbed moraines with down-ice facing convexities. Occasionally, ridges are noted to be sinuous and anastomosing, other times angular and well-defined. Of the numerous studies that concern the morphology of ribbed moraines, Aylsworth and Shilts (1989a) and Hättestrand, (1997) present separate classification schemes to relate variations in ridge shape within the North American and Scandinavian populations respectively (Fig. 3.1).

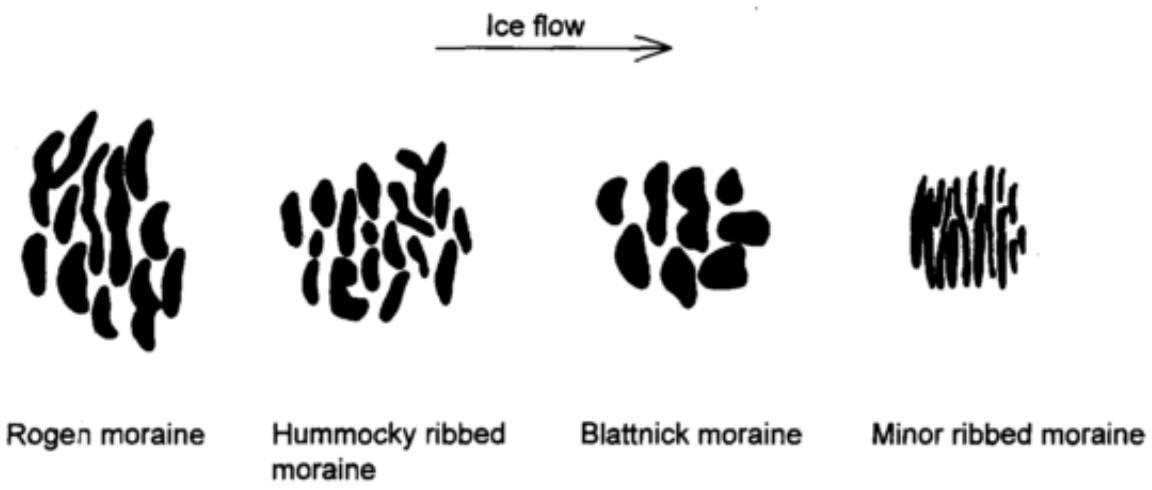

Fig. 3.1 – Classification of ribbed moraine morphologies in Sweden according to Hättestrand (1997).

Based on review of the previous literature, Hättestrand and Kleman (1999) propose typical ranges for the basic morphological properties of ribbed moraines, specifying that individual ridges can vary from 300-1,200 m in length, 150-300 m in width, and 10-30 m in height. These authors also suggest that moraine wavelengths (crest-to-crest distances) are closely spaced, though neglect to provide a numerical range for this parameter. Other writers cite more specific dimensions based on local-scale observations from detailed field studies. Bouchard (1989) (from observations in northern Québec) conservatively estimates average widths of 50-200 m, and heights of 5-20 m, insisting also that ridges are usually irregularly spaced, from 20 m to >200 m apart. Marich et al. (2005) (from observations on the Avalon Peninsula, Newfoundland) record values of 5-25 m for height, 100-400 m for width, and 5-5,000 m for length. In contrast to Bouchard's (1989) observations, these authors contend that ridges are evenly spaced, and usually at distances that approximate their average individual widths. Other writers make similar statements regarding ridge spacing (e.g., Lundqvist, 1969; Lindén et al., 2008) and some consider this property central to explaining the ridges' origins (e.g., Dunlop et al., 2008). Although morphometric properties appear to be relatively similar between the Swedish and North American distributions, ribbed moraines elsewhere (particularly in Finland) are commonly found at a much smaller scale (e.g., Aario, 1977b; Kurimo, 1980; Tikkanen, 2002; Sarala, 2006; Sutinen, 2009). Most field studies report site-specific ranges for morphometric parameters (e.g., Hughes, 1964; Shaw, 1979; Fisher and Shaw, 1992; McCabe et al., 1999; Knight, 2006).

Many descriptions of ribbed moraines in the literature note that they have asymmetric cross-profiles. Ridges are frequently reported to display a steeply dipping lee surface and a gently sloping proximal face (e.g., Shilts, 1977; Minell, 1980; Aylsworth and Shilts, 1989a,b; Bouchard, 1989; Hättestrand, 1997; Knight and McCabe, 1997; Hättestrand and Kleman, 1999; Raunholm et al., 2003; see also Andrews, 1963, 1969 and Shaw, 1983). However, Möller (2010) provides examples from southern Sweden where ribbed moraine cross-profiles vary between symmetric and asymmetric within the same field, suggesting that asymmetry may not be a universal characteristic.

Current research has underscored the need for large sample sizes and diverse site selections in order to accurately estimate size parameters of glacial bedforms (e.g., Clark and Meehan, 2001; Greenwood and Clark, 2009a,b; Greenwood and Kleman, 2010; Spagnolo et al., 2014). In particular, Dunlop and Clark (2006b) have developed findings from large sample sizes that directly challenge widely-held assumptions of ribbed moraine morphology which are pervasive throughout the earlier literature. A combined area of 81,000 km^2 across Canada, Ireland and Sweden was mapped for that study, within which 33,000 individual ribbed moraine ridges were digitized, and their basic morphological properties assessed. With respect to ridge morphology, their results suggested that ribbed moraines need not always be arcuate in planform, anastomosing, or concave downstream; commonly feature undulating, multiple subcrests; have a much broader range of dimensions, ranging in length from 45-16,214 m, 17-1,116 m in width and 1-64 m in height, with wavelengths between 12 and 5,800 m; and may have either symmetric or asymmetric cross-profiles.

3.2.2 **Inter- & Intra-field Patterning & Spatial Organization**

Much like other types of subglacial bedforms, ribbed moraines are known to occur in close spatial association, typically in what are described as 'fields' or 'swarms'. Many ribbed moraine fields are elongate in the direction of ice flow (Bouchard, 1989), and have been referred to as 'ribbons', 'narrow tracks' or 'bands' depending on their width (Aylsworth and Shilts, 1989a; Dunlop and Clark, 2006b; Greenwood and Kleman, 2010) (Fig. 3.2). In Nunavut, Shilts (1977) describes the tendency for ribbed moraines to occur in 'belts' that together parallel the regional ice flow. These are typically many

times longer (<60 km) than they are wide (<8 km), and are analogous in plan-form to glacial dispersal trains. The tendency for ribbed moraines to arrange themselves in fields is an exclusive property that is everywhere observed (Hughes, 1964). Ribbed moraine fields occur at a wide variety of scales, and it is therefore possible and instructive to assess morphometry at this level (cf. Trenhaile, 1975). Although this type of investigation has been qualitatively conducted in the past (Dunlop and Clark, 2006b), quantitative methods could provide a more objective basis for comparing different fields across different terrains. Similar measures have previously proven useful in identifying spatial tendencies among other classes of bedforms. For instance, statistical assessment of drumlin spacing (the perpendicular distance between contiguous drumlins) has revealed instances of both uni- and multi-modal distributions within individual fields, and a high degree of variability between fields (Reed, 1962; Menzies, 1979). Similarly, measures of drumlin density (drumlin frequency per unit area) have shown substantial inter- and intra-field variability, and an array of directional tendencies (Menzies, 1979). In other fields, some indications of periodicity (Reed, 1962), and possible non-random 'zonations' associated with former ice flow patterns (Vernon, 1966) have been uncovered. Smalley and Unwin (1968) used nearest-neighbour metrics to resolve random intra-field drumlin distributions, though Unwin (1996) later criticized this study for failing to incorporate the effects of arbitrary study area determination. Trenhaile (1968) used multiple tests to quantify the spatial arrangement of drumlins in southern Ontario and concluded that, generally, drumlin distributions range between random and 'more regular than random' within a given field. As Menzies (1979) suggests, however, quantitative measures of bedform morphometry are perhaps not informative on their own, yet, when integrated and evaluated against various controlling parameters (e.g., topography, glaciological factors, substrate properties, etc.), this type information can be enlightening of formative processes.

A number of contested observations petition the development of quantitative measures for ridge spacing, density and degree of spatial randomness within ribbed moraine fields. Möller (2010) observes closely spaced ridges that vary greatly in size within particular fields at his study site in southern Sweden. Hättestrand and Kleman (1999) also report the tendency for individual ribbed moraine ridges to be closely spaced within fields, though they argue in addition that these ridges are usually of similar size. Dunlop and Clark (2006b) present contradictory evidence, suggesting that most fields support a diverse spectrum of ridge sizes, yet that adjacent ridges are frequently of similar dimension. Conclusions within all the above studies have been drawn from visual observations alone, and have not been supported by objective quantitative analysis. A further point of contention in the literatures relates to the supposed 'jigsaw' matching of forms, whereby the shapes of neighboring ribbed moraine ridges are alleged by some authors to 'fit together', much like pieces in a jigsaw puzzle. This idea is advocated by Hättestrand and Kleman (1999), and has also been suggested earlier by Lundqvist (1969) and Bouchard (1989). Van Landeghem et al. (2009) depict a similar tendency among submerged ribbed moraines off the coast of Anglesey, North Wales. Dunlop and Clark (2006b), however, found no evidence for this as a widespread property within their large dataset of features.

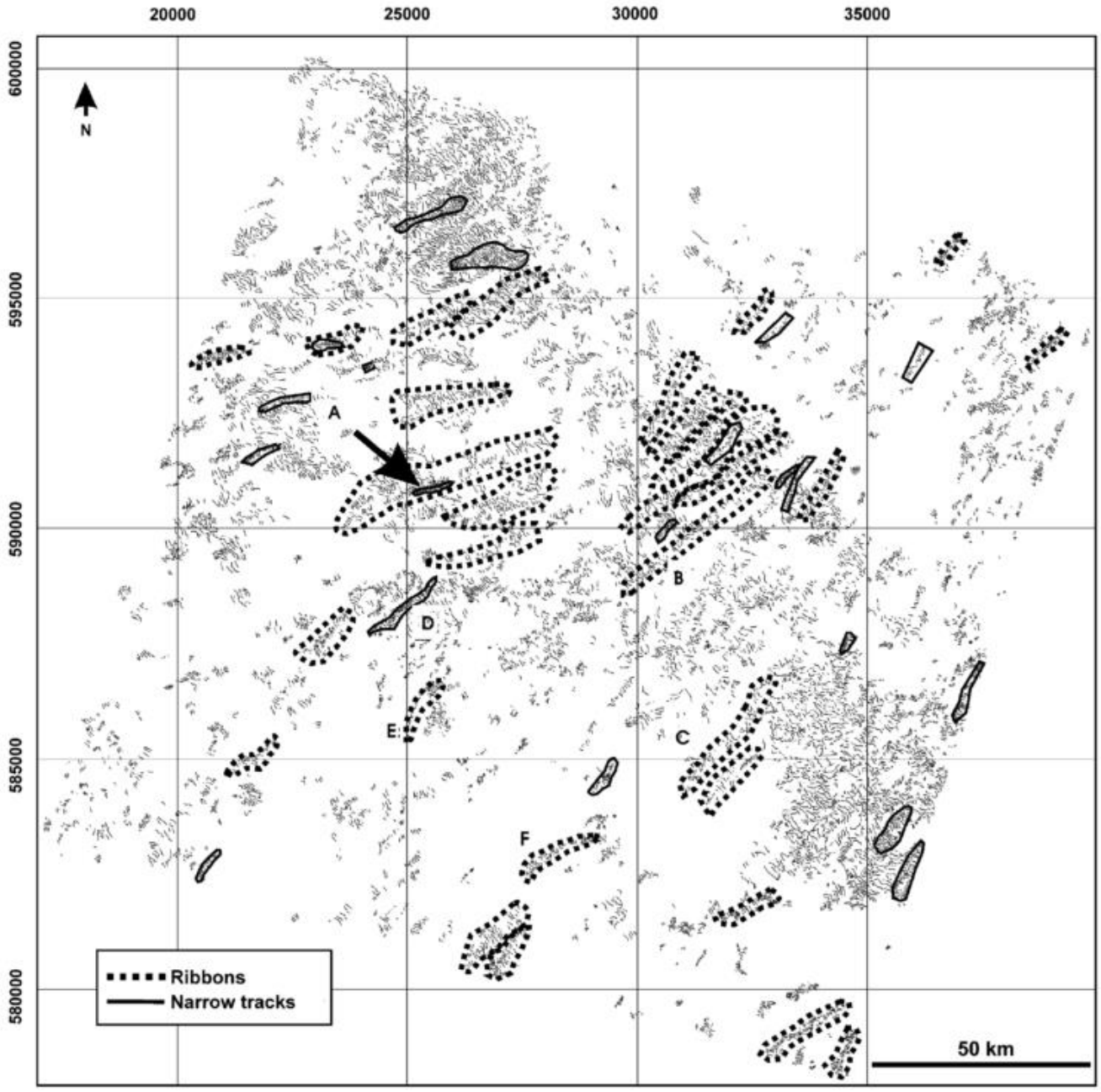

Fig. 3.2 – Examples of ribbed moraine field shapes in northern Québec. A-C are large 'ribbon'-type fields ~45 km in length. D-F are smaller 'ribbon'-type fields between 12 and 18 km in length (Dunlop and Clark, 2006b).

Bouchard (1989) observes a conspicuous quality among ribbed moraines in central Québec, insisting that a hypothetical line positioned across the uppermost surface of adjacent ridges along a flow-parallel transect would demonstrate very little relief. Earlier measurements conducted by the same author (Bouchard, 1980) substantiate this claim, revealing topographic variations of <3 m over horizontal distances spanning >1 km along ribbed moraine transects. This quality – so termed the "accordant-summit" characteristic (Bouchard, 1989, p. 300) – was interpreted as evidence of post-formational ridge planation (i.e., the development of a subsole décollement surface). The existence of such a shear plane may also be useful in explaining the drumlinization that is often observed of many

ridges. Lundqvist (1969) described a similar accordant crest-height trend among the Rogen forms in Härjedalen, Sweden, though notes also that ridge sediments are thickest (up to 30 m) near the centers of topographic basins and progressively thin out towards encompassing valley walls. Hättestrand and Kleman (1999) suggest that ridge planation cannot account for all instances of "accordant summits" because this tendency is also observed on sharp-crested ridges. Dunlop and Clark (2006b) statistically tested this theory using spatial regression and found that this characteristic applied only to roughly 10% of their sampled fields.

3.2.3 **Global Distribution**

The largest coherent fields of ribbed moraines occur within the former core-interior sectors of the Laurentide and Fennoscandian ice sheets, primarily in central Canada and Scandinavia (Hättestrand, 1997; Hättestrand and Kleman, 1999) (Fig. 3.3). Recently, large assemblages have also been identified from northern and central Ireland (Knight and McCabe, 1997; McCabe et al., 1999; Clark and Meehan, 2001; Smith et al., 2005; Dunlop and Clark, 2006b; Greenwood and Clark, 2008, 2009a,b), and the UK (Bradwell et al., 2008; Finlayson and Bradwell, 2008; Van Landeghem et al., 2009; Hughes et al., 2010, 2014). Reports extend also to coastal Denmark (Jensen, 1993), central Latvia (Lamster, 2012), and Russia (Hättestrand and Clark, 2006), though these appear very much to be outliers with respect to the global population. Contemporary investigations suggest that ribbed moraine fields exist often in close spatial association with the locations of former (and potentially highly migratory) ice divides (Kleman and Hättestrand, 1999; McMartin and Henderson, 2004; Trommelen et al., 2012). Although there are presently no confirmed instances of ribbed moraines in the southern hemisphere, it is probable that they do exist beneath the Antarctic Ice Sheet, and improved geophysical remote sensing techniques may be useful in detecting these in the future. For instance, King et al. (2007) have identified a single 'drumlinized transverse ridge' from beneath the Rutford Ice Stream, though its isolated occurrence suggests it is genetically distinct from ribbed moraines, which characteristically occur in fields. Sergienko and Hindmarsh (2013) have identified rib-like "tiger stripes" beneath the Pine Island and Thwaites glaciers in Antarctica, although these features have characteristically large dimensions (>40 km long) that are not matched by ridges in the geological archive (although see Greenwood and Kleman, 2010).

The Swedish ribbed moraine population is the longest and, perhaps, most comprehensively studied, with landforms distributed across an area spanning Värmland County in the south, to south-central Norrbotten County in the north. Recently, fields of transverse ridges near Lake Åsnan have been re-interpreted as ribbed moraines (Möller, 2010), hence extending the Swedish distribution as far south as southern Småland. Ribbed moraines in Sweden are less frequent in the extreme north, moving further from the past center of the ice sheet (Granlund, 1943; Mannerfelt, 1945; Lundqvist, 1969; Hättestrand, 1997). Elsewhere in Scandinavia, fields of ribbed moraines have been identified throughout central regions of South Norway, as well as the Finnish Lapland (e.g., Aario et al., 1974; Punkari, 1984; Sollid and Sørbel, 1984, 1994; Raunholm et al., 2003). A detailed overview of the Norwegian assemblage is provided by the glacial geological map of Norway (Sollid and Torp, 1984) and described in further detail in section 6.2.

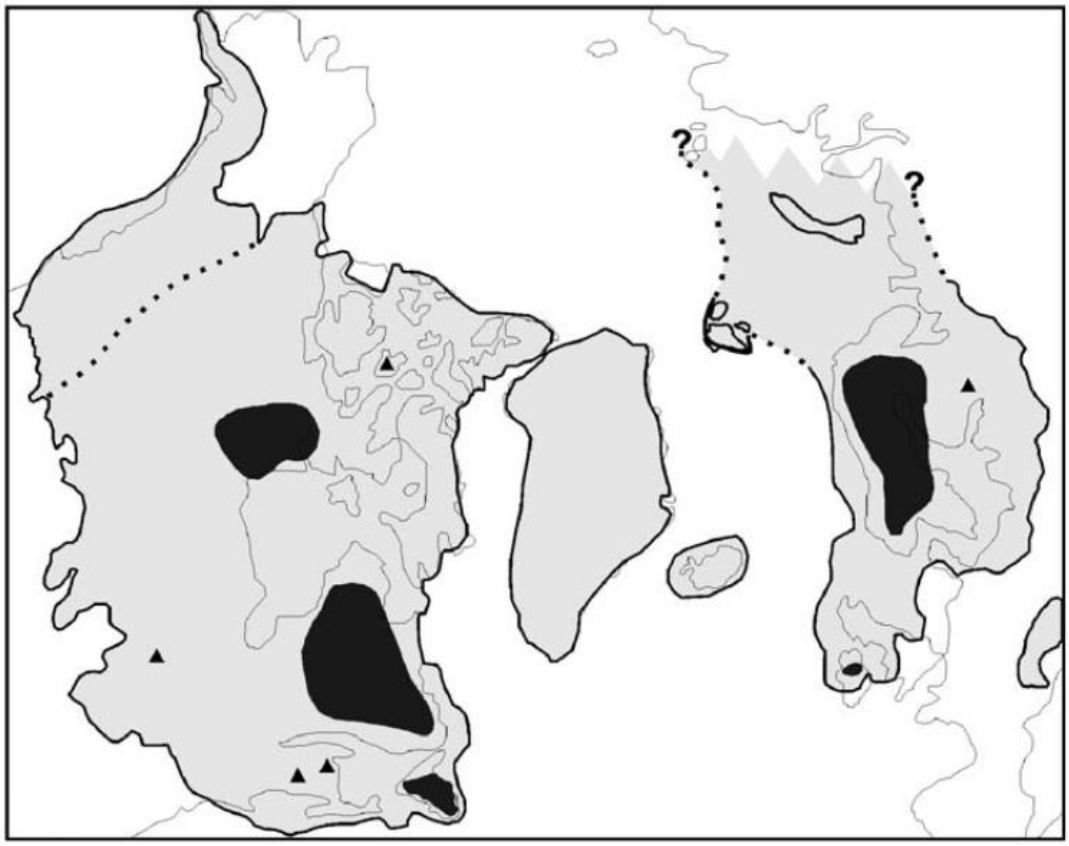

Fig. 3.3 – Currently known global distribution of ribbed moraines. Ice cover at LGM is shown in light grey. Dark shaded regions show areas where ribbed moraines occur commonly. Outlying fields are indicated with black driangles (modified from Dunlop and Clark, 2006b).

Whereas in Scandinavia, "Rogen moraine" has, until recently, been utilized as the preferred terminology, analogous ridges in North America have conventionally been referred to as "ribbed moraine" after their fish-scale, or rib-like appearance in high altitude aerial photographs (Hughes, 1964; Aylsworth and Shilts, 1989a), though Lundqvist (1989) proposes that this term may also describe transverse ridges that lack downstream transition to drumlins. Earlier papers in the North American literature have described this morphology as "ribble till" (Douglas and Drummond, 1953), "rippled till" (Ives, 1956), "Roxie Lake Moraines" (Ignatius, 1958), "ripple-till" (Hare, 1959), "cyclical moraines" (Henderson, 1959) and "ribbed minor moraines" (Lee, 1959, 1960b). Bouchard et al. (1989) provides a detailed account of the progression in this terminology. The present term, "ribbed moraine", was coined by Lee (1959), though did not gain ascendancy in the literature until its usage and defense by Hughes (1964).

In North America, the largest populations of ribbed moraines occur within the Keewatin district of south-central Nunavut, southeastern Northwest Territories, and northern Manitoba (e.g., Shilts, 1977; Aylsworth and Shilts, 1989a,b; Stokes and Clark, 2003; Stokes et al., 2006, 2008; Greenwood and Kleman, 2010; Trommelen et al. 2012, 2014) as well as throughout the Jamésie and Kativik regions of Nord-du-Québec (e.g., Bouchard, 1985, 1989; Clark et al., 2000; Jansson et al., 2002; Jansson, 2005; Dunlop and Clark, 2006a,b). Well-developed fields are manifest across central Labrador (Ives, 1956, Cowan, 1968), and surrounding the interior Avalon Peninsula in Newfoundland (Rogerson and Tucker, 1972; Fisher and Shaw, 1992; Marich et al., 2005). Brown et al. (2011) identify relatively large swaths

of ribbed moraines northwest of Great Slave Lake, Northwest Territories. A smaller zone of minor ribbed moraines is known also from southern New Brunswick, below the speculated position of the Miramichi Ice Divide. Isolated and outlying patches of ribbed moraines in the U.S.A., which must necessarily occur nearer to the former margin of the LIS, have been reported in Maine (Thompson and Borns, 1985), Wisconsin (Attig, 1985), and the St. Lawrence Valley, New York (Carl, 1978). Dyke et al. (1992) present an interesting example of ribbed moraines on Prince of Wales Island, Arctic Canada and, likewise, Storrar and Stokes (2007) provide evidence of possible ribbed moraine forms on Victoria Island in the Canadian Arctic. Shaw et al. (2010) appear to confirm these instances, and also point out isolated fields on King William Island, and adjacent the MacKenzie Delta, Yukon. De Angelis (2007) maps patches of ribbed moraines surrounding Amadjuak Lake and along the Brodeur Peninsula, south Baffin Island. Similarly, Andrews (1963, 1969) and Andrews and Smithson (1966) describe 'cross-valley' moraines from north-central Baffin Island, suggesting that they "bear a morphological resemblance to […] the minor moraines, ribbed, and straight-ribbed minor moraines of east and west Hudson Bay and the Canadian arctic coastal plain" (p. 272), as first identified by Lee (1959) and Craig (1961). A useful overview of the Canadian feature set is offered on the Glacial Map of Canada (Prest et al., 1968) and Shaw et al.'s (2010) Flowline Map of Canada. Larger-scale, regional maps are available for north-central Québec and Labrador (Jansson, 2005; Dunlop and Clark, 2006a), central Keewatin (Aylsworth and Shilts, 1989a; Stokes et al., 2006) and northern Manitoba (Trommelen and Ross, 2010), as well as the northwestern mainland (Brown et al., 2011) and east-central Canadian Arctic (De Angelis, 2007).

3.2.4 **Relationship to Aspect and Topography**

It is frequently observed that ribbed moraines occupy topographic lows – including valleys, swales, basins and depressions – and more explicitly, the concave proximal-facing slopes within these depressions (e.g., Andrews, 1963, 1969; Sugden and John, 1976; Shaw, 1979; Markgren and Lassila, 1980; Menzies and Shilts, 1996; Marich et al., 2005). Möller (2006) contends that this relationship does not apply to ribbed moraine assemblages within North America, though others provide contradictory evidence (e.g., Bouchard, 1989). Many hypotheses of ribbed moraine formation rely heavily on the existence of this association (e.g., Bouchard, 1989; Lundqvist, 1969, 1989; Minell, 1980; Sollid and Sørbel, 1994). There is, however, inherent difficulty in discriminating between what constitutes topographic versus other forms of bedforming control (e.g., geological, glaciological) in most types of environments. Moreover, attempts to isolate topographic influences on bed-formation often determine these controls to be ambiguous, since topography is very much a scale-dependent parameter. While topography might indeed predict localized bedforming patterns, its influence is less significant when assessed at regional or broader scales.

High-relief topography has been suggested to dominantly determine regional palaeo-ice flow direction and bedform orientation in Sweden (e.g., Lindén et al., 2008). Möller (2006) observes the tendency among ribbed moraines in the Indån Valley of central Sweden to align transverse to local valley axis, even in areas where this does not reflect the regional ice-flow direction recorded by striations on outcropping bedrock at high-elevations. Other examples suggest that local relief may play a role in determining the extent of bedform overprinting. Finlayson and Bradwell (2008) report multiple instances in northern Scotland where the degree of drumlin superimposition on ribbed moraines appears to increase down-valley. These authors also impute directional offsets in ridge orientation to strong lateral basal ice velocity gradients affected by the form of the valley.

Greenwood and Clark (2010) provide an explicit investigation of constraints on subglacial bed-formation across Ireland, wherein the degree of topographic influence is considered with respect to both geological (i.e., bedrock lithology) and glaciological controls. The study determined that ice dynamics are the principal influence which dictate the spatial expression of subglacial bedforms, though are locally outstripped by (generally third order) substrate controls, with topography consistently exerting a second order, though occasionally uncertain effect. Nevertheless, it may not be possible to accurately isolate the effects of these controls. For example, it has been compellingly demonstrated that bedrock lithology can mediate basal ice velocities (and therefore glaciological control), as in the case where sedimentary bedrock promotes more rapid flow than crystalline lithologies (Anandakrishnan et al., 1998; Wellner et al., 2006; De Angelis and Kleman, 2008; Larter et al., 2009; Phillips et al., 2010). Patterson and Hooke (1995) detail previous efforts to correlate subglacial bedform incidence with topography and the lithology of both the bedforming substrate and underlying bedrock. Finding none, it was determined that these variables do not exert appreciable effects on formation. Similarly, Greenwood and Kleman (2010) evince little support that either bedrock lithology, topography or drift substrate might account for first-order morphological characteristics of mega-scale subglacial landforms in Nunavut. Given these conflicting results, there exists a clear need to develop more precise means of isolating the effects of controlling variables on bed-formation.

3.2.5 **Bedform Transitions & Overprinting Relationships**

One of the most widely reported characteristics of ribbed moraines is their distinctive spatial association with streamlined subglacial bedforms (Lundqvist, 1969). This relationship is commonly expressed in the overprinting of landforms, and/or the transition from ribbed moraines into flutes or drumlins (Aario, 1977a,b; Aysworth and Shilts, 1989b; Bouchard, 1989, Clark and Meehan, 2001; Stokes et al., 2013b). Lundqvist (1989, p. 283) denotes this transition a defining feature of Rogen moraines, suggesting that where "it does not occur the term 'Rogen' should be avoided", otherwise ridges "are simply transverse moraines that can be formed in many different ways". Drumlins are often reported to grow progressively truncated downstream, wherein the convexity of their lee-side profile becomes inverted and is replaced by a concave stump (Fig. 3.4). In certain instances, these individual, crescent-shaped bedforms eventually 'line up' in a quasi-lateral, *en échelon* fashion, such as to collectively form a single transverse ridge. The staggered distribution of individual drumlins within a field contributes often to the development of diagonal 'cross-ribs' that join two or more individual ridges together (Sugden and John, 1976). Möller (2010) reports a similar situation, where closely spaced ridges link together to form dense 'ridge-nets'. Dunlop (2004) and Dunlop and Clark (2006b) describe these as 'lattice-structured' ridges.

Markgren and Lassila (1980) examined 'truncated drumlins' from the Blattnicksele area in Västerbottens, Swedish Lappland, interpreting them as drumlinized Rogen moraine, and coining the term "Blattnick moraine" to describe them. Compared to the pristine Rogen morphology, the asymmetric cross-profile of Blattnick moraine is typically exaggerated, supporting a steeper ice-proximal face, though lacking a sharp ridge crest. Similar to Blattnick moraine, some ridges are formed by parallel sequences of short, intact drumlins that retain their distal convexities (Lundqvist, 1989). Finlayson and Bradwell (2008) note the presence of both of these features at Coir' an Laoigh and Strath Grudie in northern Scotland, where they are superimposed by drumlinoid forms, and at Strath Tirry, where they grade further down-ice into "equant drumlin-like features" (p.613).

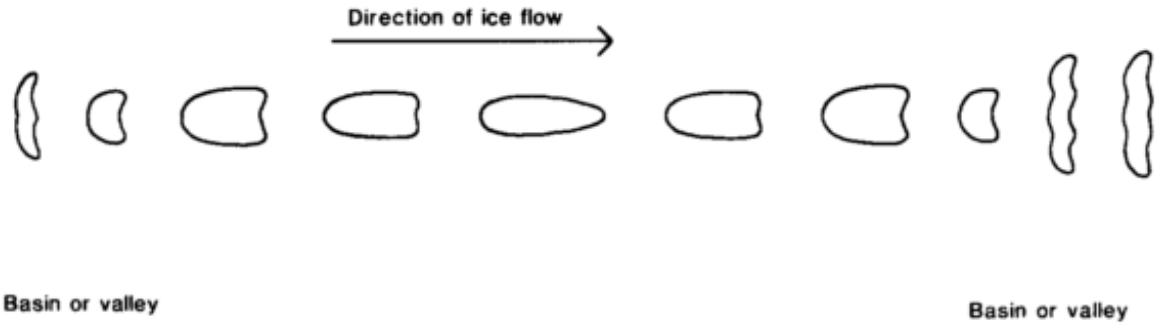

Fig. 3.4 – Proposed down-ice transition from Rogen moraines into drumlins and back into Rogen moraine, mediated by local topography (Lundqvist, 1989).

This type of 'bedform continuum' model has been advocated by a selection of other writers in the past, and has since evolved into the focus of much mathematically-driven research (e.g., Hindmarsh, 1998a,b,c; Fowler, 2000; Schoof, 2007; Dunlop et al., 2008; Clark, 2010; Chapwanya et al., 2011). Menzies (1987) provides an explicit treatment of the continua hypothesis (with a view to contextualizing drumlin formation), and convincingly links bedform development to transmissions of subglacial interface instabilities which arise due to fluctuations in basal thermal regime and stress response within the substrate. Aario (1977a,b, 1987) employs a continuum framework to describe the relationship between drumlins and Rogen moraines in northeast Finland, suggesting, alternatively, that transitions are primarily motivated by local-scale glaciological parameters. Stokes et al. (2013b) repurpose this model to incorporate ice flow velocity as a determining factor on bedform shape (Fig. 3.5).

Several reports from Ireland depict patchy down-ice overprinting and re-moulding of ribbed moraine ridges (Knight and McCabe, 1997; McCabe et al., 1999) which Knight et al. (1999) also explains using a bedform continuum model. Specific to this model is the idea that ribbed moraines post-formatively affect ice flow dynamics by reorganizing the nature of the ice/bed contact, implying that meltwater accumulated, and was stored within the hollows between individual ridge crests. Much like Kamb's (1987) linked cavity model, hydrostatic pressure generated by water storage at the base of the ice sheet would promote basal decoupling, sudden ice advance and meltwater release. Accordingly, Knight et al. (1999) determined the progressive drumlinization of ridges in this continuum to have been affected by sudden evacuations of meltwater at the base of the ice sheet. It should be noted that is unclear whether bedforms composed of deformable subglacial till would be capable of restraining the enormous hydrostatic pressures implied by this model without succumbing to failure and reorganization.

Recently, new landform associations have been discovered between ribbed moraines and palaeo-ice stream tracks. De Angelis and Kleman (2008) report a field (>100 km^2) of ribbed moraines on the Brodeur Peninsula, south Baffin Island, situated within a palaeo-ice stream trunk approximately 20 km down-ice from its onset. Stokes and Clark (2003, 2006, 2008) identified 1 km^2 to 2677 km^2 patches of ribbed moraines which overprint mega-scale glacial lineations across approximately 7% of the Dubawnt Lake palaeo-ice stream bed in central Keewatin. Dyke et al. (1992) map and discuss ribbed moraines located within the onset zone of the Transition Bay palaeo-ice stream, Prince of Wales Island. Similarly, Bradwell et al. (2008) map a small ribbed moraine field within the onset zone of the Ullapool palaeo-ice stream in northwest Scotland. In modern ice streams, onset zones are marked by at least an order of magnitude increase in downstream ice velocity (Stokes and Clark, 2001). There is thus great likelihood that the occurrence of ribbed moraines in these areas is associated with sharp velocity and basal temperature gradients, as has been recorded within ice stream onset zones in Antarctica (Engelhardt and Kamb, 1998; Bamber et al., 2000; Vaughan et al., 2006).

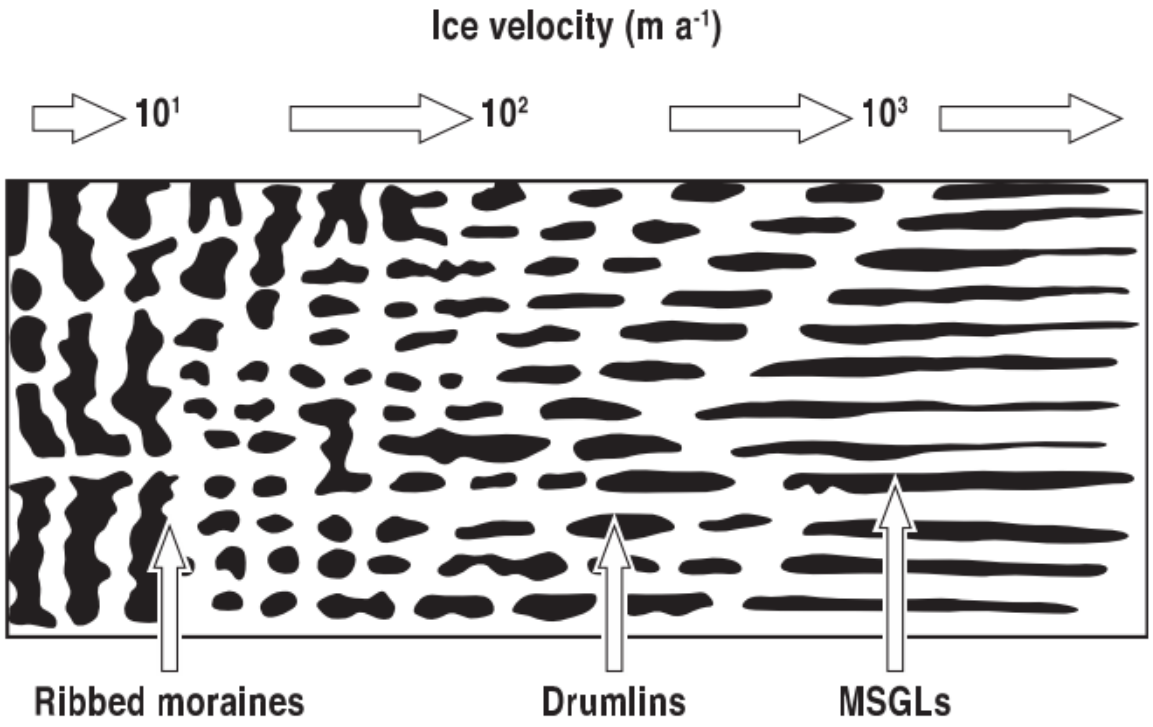

Fig. 3.5 – Schematic diagram depicting a subglacial bedform continuum, involving a downstream transition from transverse to progressively elongate flow-parallel bedforms, primarily motivated by increases in ice velocity (Stokes et al., 2013a). Diagram modified from Aario (1977a).

3.3 *Sedimentological Properties*

In comparison with the reasonably extensive literature that concerns ribbed moraine morphology, relatively few studies systematically recount findings on internal composition and structure. Of those that do, few report mutually consistent observations, and only occasionally are observations made from deep sections. Reports of textural constituents have ranged from stratified sands (Cowan et al., 1968), to glaciofluvial gravels (Aylsworth and Shilts, 1989a; Fisher and Shaw, 1992), to semi-consolidated lodgement tills interbedded with layers of sorted meltwater sediments (Lundqvist, 1997). Likewise, the internal *structure* of ribbed moraines has been equally confounding (e.g., in failing to provide a uniform diagnostic criterion or reliable facies model), though evidence of glaciotectonism (e.g., folds, shear planes, dipping strata) appears to be commonly detected (Hoppe, 1952; Cowan, 1968; Minnel, 1977, 1980; Shaw, 1979; Dredge et al., 1986; Bouchard, 1989; Fisher and Shaw, 1992; Lundqvist, 1997). Additional acquisitions of site-specific information of this nature are crucial to determining the specific bedforming processes that may have operated at particular geographic localities, and just as importantly, appreciating whether or not these are unique. Moreover, analysis of internal ridge properties can lead to the acceptance or refutation of models of ribbed formation (see section 3.4) that have been proposed on the basis of ridge morphology alone.

It has long been recognized that ribbed moraine ridges are characteristically composed of a wide assortment of materials (Högbom, 1885, 1894). In an early study of North American ribbed moraines, Cowan (1968, p. 1156) remarked that they may "be composed of almost any materials available". More recently this compositional diversity has been re-examined and interpreted in several ways. For instance,

it has been argued that: A) a lack of representative facies associations/matrix granulometries/structures implies that the internal composition of ribbed moraine ridges is an inconsequential factor in determining their origin, and thus all such ridges must be created through a similar process; or alternatively, B) diverse internal compositions must relate to multiple unique formational mechanisms, and thus the existence of ribbed moraine ridges may be owing to a wide variety of processes dependent upon specific geological and glaciological parameters.

Though ribbed moraines need not be composed of till, or even unsorted sediments, the most commonly reported materials occurring within such ridges are indeed varieties of basal till. Typically, these are coarse grained and rich in boulders and cobbles where developed in areas of crystalline bedrock, and relatively finer-grained, with lower frequencies of boulders and large clasts in areas where bedrock is either 'soft' or disaggregated (Lundqvist, 1969; Aylsworth and Shilts, 1989a). Certain observations from Scandinavia have revealed associations between coarser grained, stony basal tills in ridges located within valley basins, compared to those in higher topographic situations which more commonly feature matrices composed of silts and clays (Lundqvist, 1969). Lundqvist (1969, 1997) and Hättestrand (1997) describe sections from numerous locations in west-central Sweden that feature "ordinary basal tills" with properties that largely reflect the composition of surrounding (non-ribbed) deposits. Textural and/or geochemical similarities in ribbed and surrounding non-ribbed surficial deposits have also been noted in Finland (Sarala, 2006; Sarala and Peuraniemi, 2007), north-central Québec (Henderson, 1959) and northern Manitoba (Trommelen et al., 2013, 2014).

Nevertheless, ribbed moraines formed by sediments other than "ordinary basal tills" have also been reported. One of the earliest tills to be associated with the ribbed moraine was described from northern Sweden by Beskow (1935) who, though mistakenly misclassifies the features' morphologies, noted their tendency to be composed of a particular type of basal till, denoted the "Kalix" (also "Kalixpinmo") till. The Kalix till consists of bi-modally distributed, poorly sorted, over-consolidated coarse silty-sandy diamicton with dispersed cobbles and boulders, interbedded with compact, slightly disturbed stratified, sorted sediments. The presence of the latter interbeds implies primary deposition by meltwater currents, whereas the compaction and deformation structures in these materials suggest either active subglacial deposition or post-depositional reworking. In areas, these deposits appear as lenses and/or flow noses/nodules of coarser materials. Ridges constructed entirely of the Kalix till occur frequently in valley basins across northern Sweden (especially within the Kalix and Råne river valleys of Norbotton), and are referred to as "Kalixpinnmo ridges" or "Kalixpinnmo hills" in the early Swedish literature (Hoppe, 1959; Fromm, 1965). Lundqvist (1981) speaks of these features as "Niemisel moraine", advocating for their distinction from Rogen moraine on the basis of a unique topographic and spatial distribution, and lack of drumlinoid transitions. In a later paper, however, this author concedes that Niemisel moraine are "now considered a type of Rogen moraine" (Lundqvist, 1997, p. 35), perhaps in recognition of the broader contemporary morphological application of this term (cf. Dunlop and Clark, 2006b).

Lindén et al. (2008) provide a detailed analysis of the interior sediment facies and architecture of Niemisel-type Rogen moraine from five re-excavated road-cuts in the Råne River valley, northeast Sweden. These sections revealed a complex glacial/fluvioglacial stratigraphy consisting of ten unique sedimentary facies organized in elaborate lateral and vertical sequence successions. Exposures also displayed both overprinted and synsedimentary glaciotectonic deformation signatures. Based on internal facies relationships, individual assemblages were assigned to one of three architectural ridge components: Proximal Ridge Element (Promixal Ridge Facies (PRF) 1-5), Distal Ridge Element (Distal Ridge Facies (DRF) 1-3), or Draping Element (Draping Facies (DF) 1-2). Facies of the Proximal Ridge Element were the most compositionally varied, ranging from massive sandy, silty diamict (PRF 1) to

sorted and stratified silt, fine sand and gravel interbeds (PRF 4) and wedge structure infills (i.e., clastic dykes) (PRF 5). The Distal Ridge Element consisted primarily of massive to stratified (DRF 1), and purely stratified (DRF 3) sandy to silty diamict with sorted fine sand and silty (occasionally sandy-gravelly) interbeds (DRF 2). Irregular gravel lags and scour-fills formed coarser horizons in the Distal Ridge Element, though thicker and more continuous cobble-gravel beds also graded continuously, in places, into massive or parallel-laminated sand, and normally-graded gravelly sand. The latter units were seen to form bedsets with ripple-laminated sand in stacked sequences up to 2 m in thickness. The final Draping Element comprised massive (DF 1) to internally stratified (DF 2) silty, sandy diamict, occasionally exhibiting glaciotectonically deformed laminae (DF 1).

Ribbed moraines with similar complex stratigraphies have also been reported from several other locations. Bouchard (1989) describes ridges from the Québec portion of the Canadian Shield consisting of massive to stratified, matrix supported, fine-grained diamictons, which alternate across gradational contacts with laminated sands and gravels. Confirmed field observations from this region indicate that Kalix till-like deposits are not endemic to Scandinavia. Diamict fractions of the ribbed moraines studied by Bouchard (1989) are manifest as lenticular beds, with encompassing sorted materials occurring as thin bands of partitioning sediment. Both layers (sorted and unsorted) are laterally extensive, though discontinuous, and taper along protracted planes, thus attributing the till with apparent stratification at the macro scale. Laminations in the sorted beds are conformative to the boundaries of outsized clasts, a relationship traditionally interpreted as a primary signature of melt-out deposition (e.g., Shaw, 1979; Lawson, 1981; Haldorsen and Shaw, 1982; Shaw, 1982; Piotrowski and Tulaczyk, 1999; Munro-Stasiuk, 2000), and argued likewise by Bouchard (1989). These architectural signatures from Québec are consistent with the late-stage melt-out/downwasting style of ridge preservation advocated by a number of workers (e.g., Lundqvist, 1969, 1997; Sollid and Sørbel, 1994). More importantly, they discount any alternative means of formation involving active sediment displacement (e.g., near marginal subglacial processes) which would reorganize and thus obscure such primary relationships between internal architectural elements.

Bouchard (1989) relates his observations to those made from ribbed moraine sections in central Sweden by Shaw (1979), though mistakenly suggests that these Swedish ridges are formed of a specific till, known locally as the "Sveg till", when in fact Shaw (1979) addresses these topics separately in his paper. Shaw's (1979) investigations revealed internal ridge structures comprising folded and attenuated packages of predominantly local tills, displaced along visible thrust planes, and interbedded with thin, discontinuous horizontal laminae. Shaw's (1979) findings belong to a larger collection of studies in the literature that detail complex internal glaciotectonic structures in ribbed moraines (e.g., Raunholm, 2003; Möller, 2006; Lindén et al., 2008), including those which have analyzed radar facies and suggest the presence of inclined thrust structures (Stokes et al., 2008) or folds (Trommelen et al., 2014). In other examples, it is possible that deformational structures have been made difficult to discern given the common high proportion of local materials found in these landforms. Nevertheless, certain complexities in ribbed moraine stratigraphy are noted even in the absence of tectonic disturbance (e.g., Fisher and Shaw, 1992).

Boulders blanketing the surfaces of ribbed moraines are frequently reported (e.g. Ives, 1956; Lundqvist, 1958; Henderson, 1959; Shaw, 1979; Aylsworth & Shilts, 1989; Sarala, 2007; Möller, 2010; Sutinen et al., 2010; Trommelen et al., 2012, 2014) and could provide evidence of melt-out-style preservation, if these deposits are understood as being sourced supraglacially. Stokes et al. (2008), however, contend this phenomenon is best interpreted as a lag deposit, affected post-glacially by winnowing of fines at the surface. Boulders occupying inter-crestal hollows may then be likely

emplaced by the same method as those resting atop ridge crests, though have been sheltered from much erosive activity, and subsequently obscured by the in-filling of bog deposits.

3.4 *Existing Hypotheses of Formation*

Considering that the formation of ribbed moraines has not been directly observed beneath modern glaciers or ice sheets, it is necessary that hypotheses and models be generated in order to explain their presence across former ice sheet beds. Generally, these frameworks seek to explain and associate those various characteristics of the landform that *are* observable post-formation (e.g., spatial patterning, internal structure, size, composition, etc.), and thus speculate heavily within the process-form domain. According to Dunlop and Clark (2006b, p. 1669), "[t]he most successful hypothesis will be the one that provides the most complete explanation of ribbed moraine characteristics"; however, this type of statement is strongly biased towards the possibility of there being a single, unifying theory to account for all instances of the landform. This has yet to be proven, and in reality, a myriad of hypotheses may accurately describe multiple individual formation mechanisms.

Most recent hypotheses proposed to explain the existence of ribbed moraines have considered the influence of basal ice-flow dynamics, basal thermal regime, subglacial hydrology and/or substrate composition and topography as paramount to elucidating their origin. Many of these hypotheses attempt to decipher also the nature of the spatial association of ribbed moraines with streamlined bedforms, in addition to their widely cited overprinting relationships (see section 3.2.4). Models of formation have been informed by empirical evidence and, more recently numerical simulations. These are based variously on ribbed moraine internal composition/structure and morphology; however, given their variability, few explanations have been successful in reconciling these two lines of evidence.

Despite the variety of hypotheses of ribbed moraine formation offered to date, only several persist within the contemporary literature. Supraglacial and ice-marginal geneses were regularly suggested in early writings (see section 3.1), though have since ceded favour to subglacial modes of origin. These mechanisms are outlined below.

3.4.1 **Extensional Drift Sheet Fracture**

The theory of ribbed moraine formation by subglacial fracturing and extension of a pre-existing till sheet has been supported by a number of researchers, primarily based on observations from Scandinavia and central Canada (Lundqvist, 1969; Hättestrand, 1997; Hättestrand and Kleman, 1999; Kleman and Hättestrand, 1999; Sarala, 2006). This idea supposes the existence of a "phase change surface" (PCS) – functionally, a pressure melting isotherm – within a subglacial substrate, separating frozen sediment which overlies rigid bedrock from "thawed"/deformable materials nearer the ice/bed interface. During deglaciation, the PCS dips up-ice and intersects the glacier bed at an acute angle. Coincident with ice margin contraction, this zone of intersection transgresses inwards towards the ice dispersal center as the PCS migrates upwards through the subglacial substrate in response to thinning ice/reduced glaciostatic pressure and/or climatic amelioration. Intersection of the PCS with the bedrock/drift sheet interface, in conjunction with overriding glaciodynamic stress, results in the development of a strong, longitudinal tensile stress component, ductile deformation (shearing) along the interface, and the growth of sub-vertical fractures in the overlying frozen drift sheet (Fig. 3.6). Continued extensional ice movement serves to partially re-mould the tabular blocks of the drift sheet, and transport them down-ice to the point where the PCS intersects the ice/bed boundary. Beyond the latter intersection zone, pervasive soft-sediment deformation, rapid warm-based basal ice movement and

drift streamlining take place. As this area contracts, it overprints the former zone of fracture, causing fluting and/or drumlinization of the earlier-developed ribbed moraine. Subaerial exposure following deglaciation renders newly-formed ridges susceptible to fluvial, aeolian and mass wasting processes and serves to reduce their angular appearance (Hättestrand, 1997; Hättestrand and Kleman, 1999). This model is modified by Sarala (2006) to include consideration of strain response in the frozen bed prior to completed block detachment, and also includes a physical means for the input and redistribution of materials into inter-crestal troughs. In this latter model, a series of folds in basal ice and an adfrozen subjacent drift sheet are hypothesized to arise under cold-based conditions, where ice movement proceeds largely by internal deformation. Extensional flow after basal thawing promotes fold-fracturing and the transportation of sediment blocks or 'ribs' down-ice. This behaviour is preferred by Sarala (2006) over the 'boudinage' mechanism proposed earlier by Hättestrand, 1997.

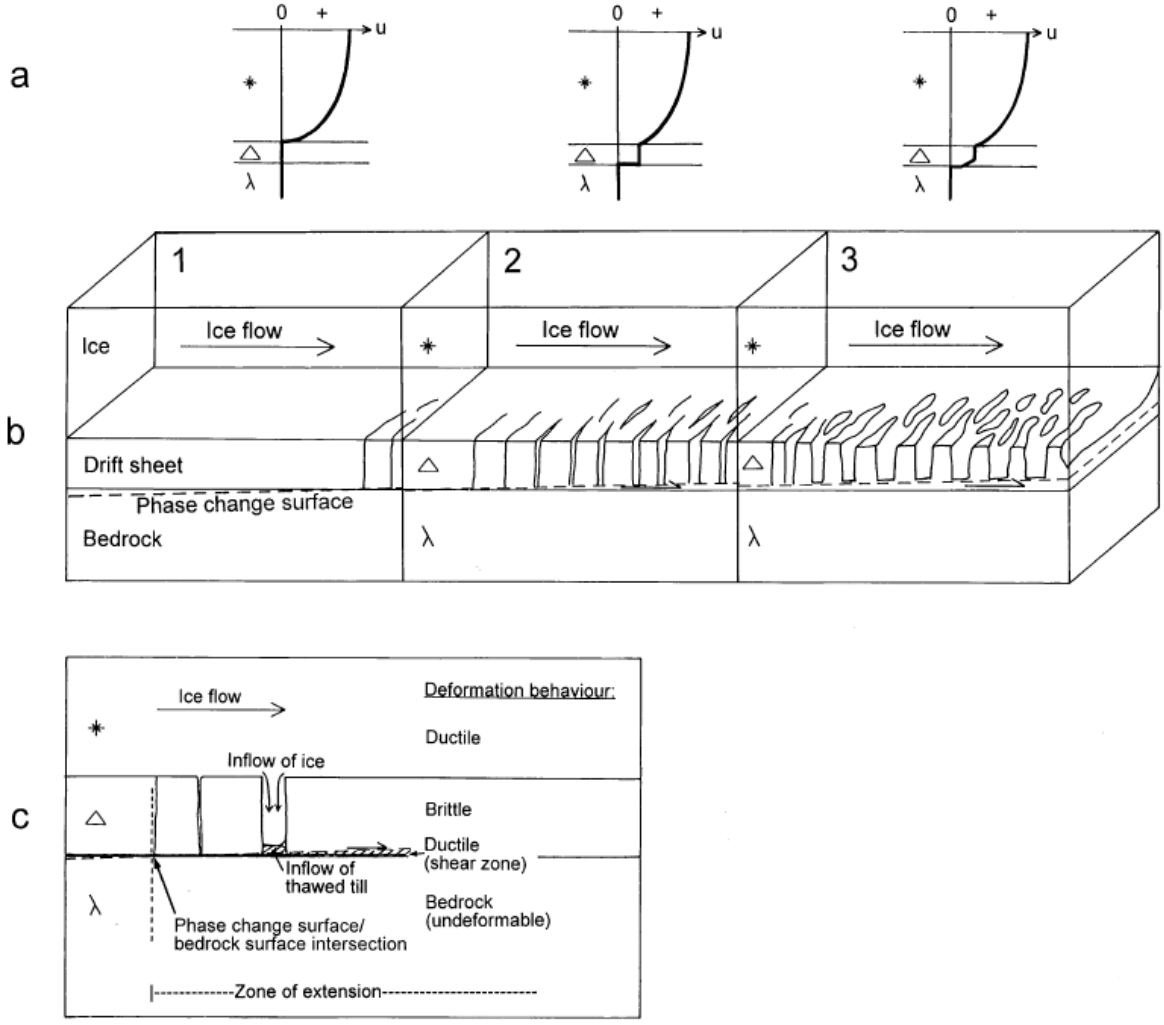

Fig. 3.6 – A model of ribbed moraine formation by fracture and extension of a pre-existing, coherent drift sheet. A) 2-dimensional ice-flow velocity (*u*) profiles for bedrock, basal ice and subglacial substrate, shown for the time steps outlined in B. B) Chronological progression (1-3) detailing the modification of an intact drift sheet to form ribbed moraines. Frozen blocks of drift are produced by fracturing and detached along a bedrock-sediment décollement plane when the pressure melting isotherm intersects the bedrock surface. C) Enlarged view of the fracture zone during brittle sediment fracture and block detachment. Fields of ribbed moraine are generated inward-transgressively as the phase change surface migrates up-ice (Hättestrand and Kleman, 1999).

Conviction in the accuracy of this hypothesis is tempting for a number of reasons, not the least of which stems from its simplicity, and its seemingly universal applicability. Most persuasive, however, is the spatial affinity of ribbed moraines with relict terrains, and their concentric arrangement around late-glacial ice retreat centers (cf. Kleman and Hättestrand, 1999; section 3.2.3) that appears to corroborate the most fundamental implication of this model (i.e., that ribbed moraines are formed during a transition from frozen to thawed basal thermal regime). A secondary implication of this model is that sediment composition is a non-controlling parameter in the ribbed moraine formative process. Indeed, supporters of this hypothesis point to observations (e.g., Lundqvist, 1997) of ribbed moraine structure and stratigraphy that suggest these aspects are highly variable (see section 3.3), and on this basis argue that there can be no representative facies/facies association which is genetically related to the process of ribbed moraine generation (Hättestrand and Kleman, 1999; Kleman and Hättestrand, 1999). That most sediments identified in ribbed moraine ridges are compositionally similar to the surrounding surficial geology appears to substantiate this claim (Hättestrand, 1997; Sarala, 2006; Trommelen et al., 2014).

Glaciotectonic structures indicative of compressive internal sediment deformation, however, have been identified in many fields of ribbed moraine (e.g., Shaw, 1979; Aylsworth and Shilts, 1989a; Bouchard, 1989; Dyke et al., 1992; Lindén et al., 2008) and are not readily explained by the "fracture and extend" model of formation, which invokes a tensile stress regime. Additionally, ridge preservation throughout deglaciation, assuming overriding by warm-based ice subsequent to formation, is unlikely a plausible scenario, though is a requirement of this particular model of ridge emplacement. Van Landeghem et al. (2009), however, effectively invoke the fracture-and-extend model to explain the presence of pristine submarine ribbed moraines identified offshore Anglesey, north Wales, arguing that a halting of the migrating frozen-thawed boundary at the edge of these ribbed moraine fields, and subsequent flotation/ice-bed decoupling of the overlying Irish Sea Ice Stream, led to the well-preserved present-day morphologies of the ridges. Similarly, Raunholm et al. (2003) convincingly fit the development and preservation of ribbed moraines to the deglaciation chronology of the Norwegian Channel Ice Stream using a fracture-and-extend framework.

Further criticism of the extensional drift sheet fracture model pertains to the need to explain variations in drift thickness. In many areas, drift is substantially thicker beneath ribbed moraine ridges than on the surrounding terrain, indicating a need for relief amplification in the ridge formation process that the "fracture and extend" model does not provide (Lundqvist, 1969, 1997; Wastenson, 1983; Trommelen et al., 2014). Initial evidence used to support the extensional drift sheet fracture mode of ribbed moraine generation was based on the apparent conformable alignment of ridges along a flowline. It has been purported (i.e., Hättestrand and Kleman, 1999; Kleman and Hättestrand, 1999) that neighbouring ridges 'fit together', much like pieces of a jigsaw puzzle, and that this may provide evidence that individual features once belonged to a single, coherent drift sheet (Fig. 3.7). For example, Finlayson and Bradwell (2008) identify areas of apparent jigsaw matching between a small number of ribbed moraines in upper Strath Grudie and Strath Tirry, northern Scotland, and they use this to infer a possible fracture-and-extend mode of origin. Dunlop and Clark (2006b), however, replicated this test using a larger dataset (~33,000) of ribbed moraines digitized from remotely sensed data and found little evidence to support claims that this is a widespread characteristic. Further, they highlight the fact that occasional "jigsaw matched" ridge morphologies in no way proves a mechanism of formation by extension and fracture. Möller (2006) also attacks this hypothesis on grounds that it demands implausible sediment mechanics, and is not thoroughly supported by geomorphological observations.

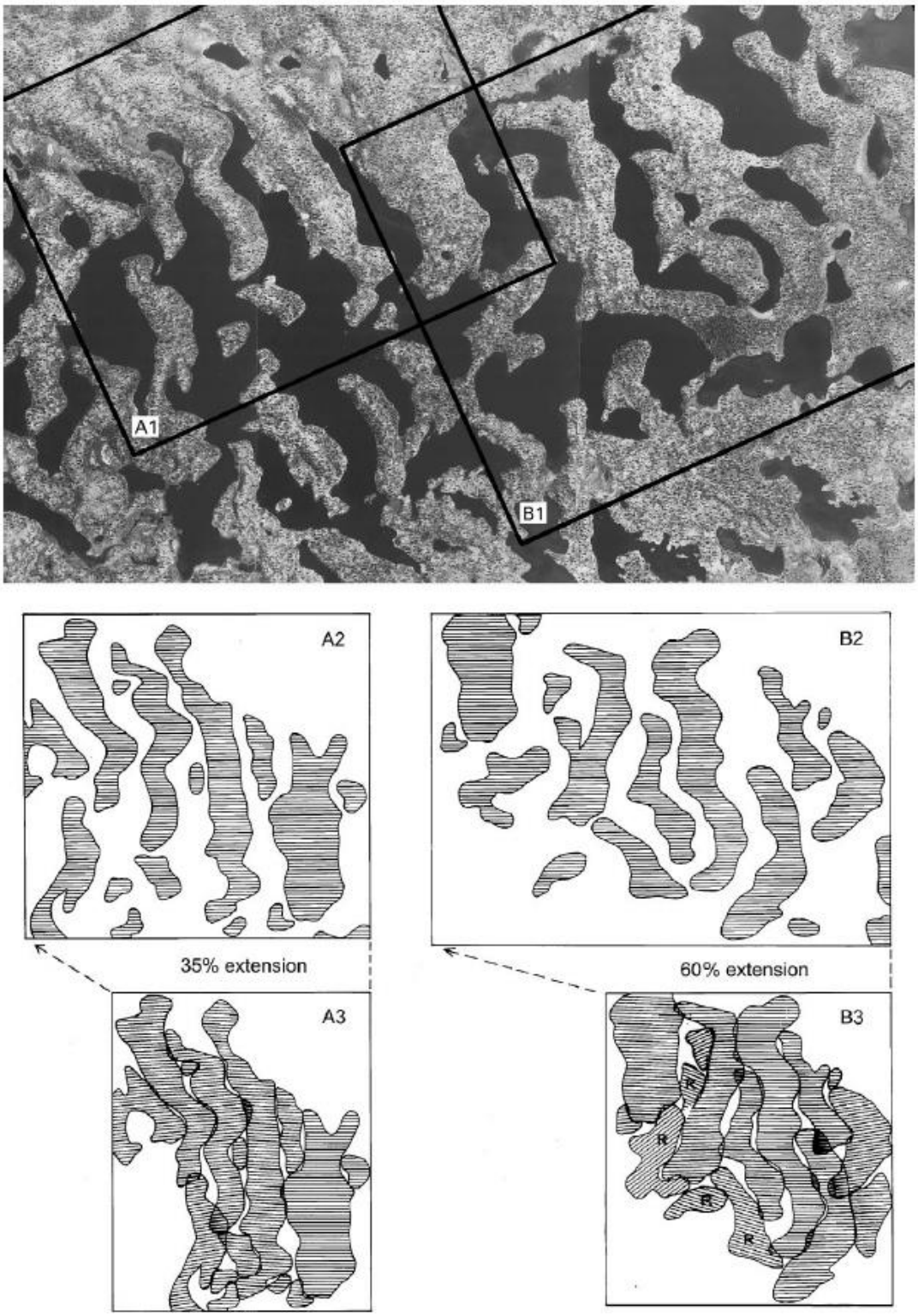

Fig. 3.7 – Alleged "jigsaw-matching" of ribbed moraine ridges, with an example from Lake Rogen, west-central Sweden. Morphological scenarios illustrated in boxes A2-3 and B2-3 are interpreted to depict 35% and 65% localized drift sheet extension respectively. Hatched pattern represents faint, overprinting/fluting. "R" symbology in B3 indicates blocks that are interpreted to have rotated during passive re-emplacement. Overlap of ridge horns is thought to result from drumlinization subsequent to drift sheet extension (Hättestrand and Kleman, 1999).

3.4.2 **Shear-and-stack**

Shear-and-stack models of transverse ridge formation are numerous and have been both developed for a variety physical settings and used to explain a diverse assortment of glaciodynamic behaviours. Shaw (1979) provides one of the earliest *explicit* considerations of this mechanism though it was before, and has since been *implicitly* advocated by a large number of other works (e.g., Lee, 1959; Minell, 1977, 1980; Shilts, 1977; Markgren and Lassila, 1980; Punkari, 1984; Sollid and Sørbel; 1984, 1994; Dredge et al., 1986; Aylsworth and Shilts, 1989, b; Dyke et al., 1992; Lindén et al., 2008; Stokes et al., 2008). Fundamentally, this model involves entrainment of englacial and/or basal debris via upward-thrusting and minor folding of bands of subglacial sediment in zones of compressive ice flow, as strongly informed by the early theoretical work of Boulton (1970a,b; 1971; 1972). These sediment bands are progressively attenuated during passive down-ice transport, though experience eventual folding when upglacier bands contact distal bands in stagnant or low-velocity ice. Cumulative folding leads to buckling at the fold hinge and sequential low-angle thrusting of limbs atop one another. During subsequent ice recession, these stacks are re-emplaced via ice-surface lowering as an englacial/subglacial melt-out deposit.

Differences between shear-and-stack models primarily reflect different understandings of how compressive flow is generated within the ridge-forming environment (and associatively, *where and when* the ridges are formed with respect to ice sheet geometry and stage of glaciation). Shaw's (1979) investigations of ribbed moraine deposits in central Sweden led him to interpret a close association between the englacial stacking (inferred from the presence of internal shear planes) of debris-rich basal ice in topographic depressions (i.e., zones of compressive flow) and subsequent transverse ridge development and exposure by undermelt/downwasting processes associated with syngenetic permafrost development (Fig. 3.8). The attribution of compressive flow to the encountering of topographic obstacles by basal ice is made also by several other authors, including Minell (1980) who identifies high concentrations of local bedrock material within arcuate ribbed moraines of northern Sweden, and interprets this as evidence of on-freezing and melt-out in topographic basins. Bouchard (1989) presents a similar model of basal-ice shear plane development and depression infill by debris-rich ice, though considers also the development of a decollément plane, beneath which neighbouring ridge surfaces are 'leveled off' to an accordant height (Fig. 3.9). Comparable ideas with respect to a melt-out/surface-lowering origin are put forth by Shilts et al. (1987) and Aylsworth and Shilts (1989a,b), though the nature of compressive flow in these cases owes to zones of reduced plasticity within debris-rich basal ice, rather than topographic obstruction, and the placement of ribbed moraine genesis in time and space is located much later in the glaciation phase, and much further from the ice sheet margin than in other shear-and-stack theories, respectively.

Many authors link ribbed moraine development to zones of transition across a basal thermal boundary. Unlike the "fracture-and-extend" model of formation (see 3.4.1), which implicates basal thawing and high tensional stress, the switch that is inferred here is one from warm- to cold-based basal ice – namely, one that is associated with the up-glacier development of high compressional stress. Stokes et al. (2008) connect this hypothesis to a sediment-landform association from the northwestern Canadian Shield, where fields (1 km^2 – 2500 km^2) of minor ribbed moraines are superimposed atop highly elongate mega-scale glacial lineations (MSGLs) over the Dubawnt Lake palaeo-ice stream bed. These observations, combined with stratigraphic and geophysical analyses, led the authors to identify two significant phases of ice movement in the region; the earliest characterized by extensional, and the latest by compressional ice flow. Outcropping sediments along a cut bank of the nearby Thelon River revealed two till sequences. On the basis of clast fabrics, the underlying unit was interpreted as a

lodgement till and attributed to the phase of ice flow responsible for MSGL development beneath the Dubawnt Lake palaeo-ice stream. The younger, overlying till with a perpendicular fabric was believed to correspond to ribbed moraine formation coincident with substrate porewater evacuation during basal freezing and/or ice stream collapse. Although this interpretation does well to explain the geomorphological evidence, it is weak from a strictly sedimentological perspective. Construal of the uppermost fabric as a product of compressive flow, transverse to ice movement (as opposed to a secondary ice flow trajectory) was made on the exclusive basis of the "freshest" striae found on *embedded* clasts (i.e., subject to rotation) which reportedly paralleled the nearby MSGL orientation. No conclusive evidence is presented as to ensure that sedimentary units identified in the studied exposure correspond to the nearby landform sequence. The interpretation of the two tills identified in the exposure as being emplaced along a single ice flowline is also suspect, given the volume of previous work which has geochemically sourced the multiple-till stratigraphy of central Keewatin to distinctive zones of provenance (see section 5.2).

Lindén et al. (2008) are able to much more convincingly link ribbed moraine development to basal thermal regime transitions and associated subglacial sediment porewater fluctuations (mediated by seasonal porewater/piezometric gradient alterations) within a shear-and-stack model framework, based on thorough sedimentological examinations of ribbed moraine exposures in coastal Norbotten, Sweden. The consideration of ribbed moraine-creating events as quasi-annual phenomena allowed these authors to connect rib-forming processes also to proximal De Geer moraine development. Given regular glaciotectonic stress transmission towards the ice terminus within the near-marginal zone (cf. Maltman and Bolton, 2003), ribbed moraines are hypothesized to arise under compressional stacking at an inward-propagating ductile/brittle subglacial sediment interface, nearing the end of a melt season (i.e., at the head of a 'subglacial sediment conveyor belt'), whereas De Geer moraines represent the distal extent of this sediment advection, and are formed at a subaqueous ice margin, as per Lindén and Möller (2005). Important to note, however, is that subglacial bed-formation over such a brief (i.e., annual) time interval is not supported by recent modeling efforts which predict much longer phases of growth (e.g., Dunlop et al., 2008; Chapwanya et al., 2011). Rose (1989) suggests that bedform development could take place over a period ranging between 4 and 400 years.

Dyke et al. (1992) also invoke a subglacial thermal transition to explain the localized presence of ribbed moraines in Arctic Canada. Here, alternating stick/slip conditions were thought to foster the infolding and stacking of entrained basal debris layers along a patchy, poorly-defined boundary where cold-based interior Innuitian sector ice became warm-based within the onset zone of the Transition Bay palaeo-ice stream, Prince of Wales Island. Similar to the mechanism proposed by Stokes et al. (2008), compressive flow was hypothesized to derive from internal glaciological factors, rather than topographical controls. An alternative model presented by Sollid and Sørbel (1994) combines these two sources. Möller (2010) puts forward a process of so-called "Åsnen-type" (southern Sweden) ribbed moraine development that closely parallels the shear-and-stack concept of Shaw (1979), however, compressive flow in this more recent hypothesis derives from basal thermal regime fluctuations, placing ridge inception well behind the ice margin. Unlike in Shaw (1979), no post-depositional deformational events or glaciotectonic behaviours are described.

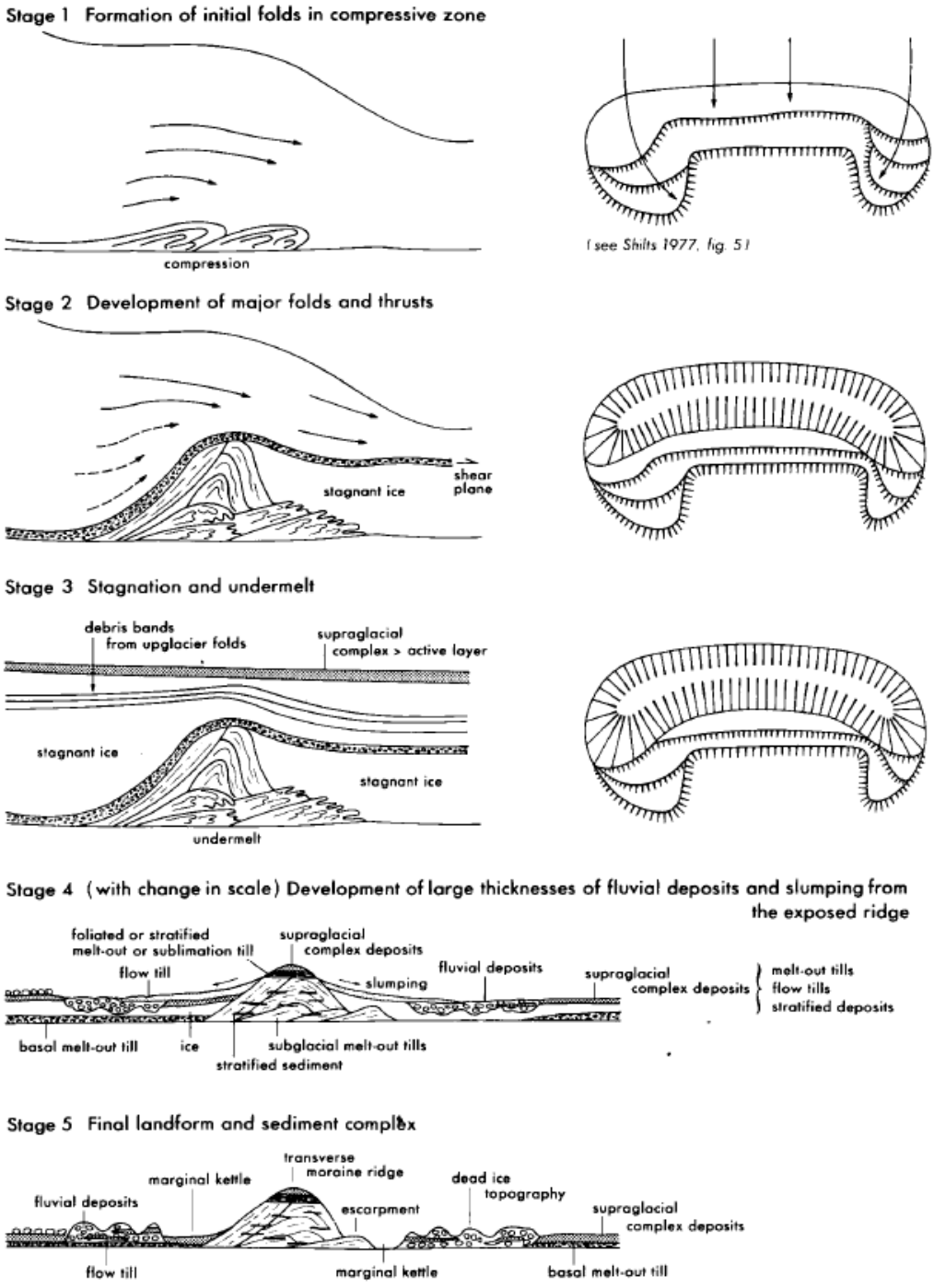

Fig. 3.8 – A model of ribbed moraine formation by stacking and subsequent melt-out of englacial debris bands. (I) Debris rich basal ice is folded and entrained into englacial ice within a zone of compressive flow. (II) Major folds are developed in debris bands leading to eventual buckling and basal ice overthrusting. Regions of stagnant ice develop in sheltered positions in the lee of thrust blocks, while continued ice flow atop these blocks transforms into a (high velocity) extensional flow regime, associated with the development of a vertical series of englacial debris bands. (III) Downwasting in stagnant zones exposes debris bands at the ice surface and contributes to the development of a supraglacial debris complex, eventually of greater thickness than the regional active layer, thus augmenting the relative contribution of undermelt processes to deglaciation. (IV and V) Final landsystem development following complete undermelt and fluvial modification (Shaw, 1979).

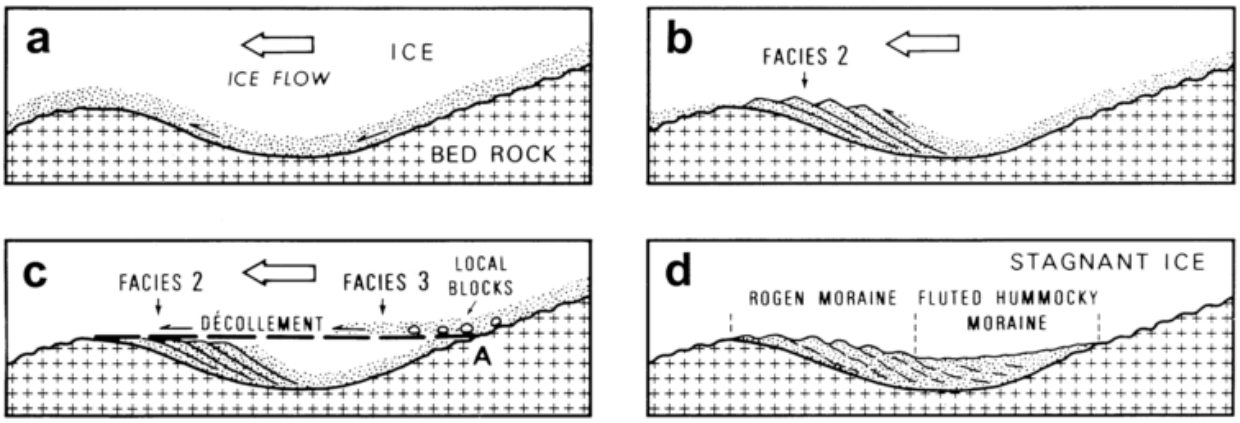

Fig. 3.9 – A model of ribbed moraine formation by basin infill, layered-debris stacking, and the development of a subglacial décollement plane (Bouchard, 1989). A,B) Stacking of debris-rich bands proceeds on the proximal face of an obstacle by the development of upglacier dipping shear planes in basal ice. C) Subsequent ice flow atop immobilized, debris-rich ice within the basin results in the generation of a subglacial décollement plane, constituting a new effective bed surface. Fluting and drumlinization of ridge surfaces is hypothesized to occur throughout this stage. D) Preservation and exposure of ridges is facilitated by gradual downwasting of stagnant ice.

3.4.3 **Multiple-step**

Step-wise mechanisms to explain the formation of ribbed moraines have traditionally been well-supported, and are intimately associated with other models of bedform generation/evolution through the recognition of these features as belonging to a spectrum or "continuum" of bed-formation (e.g., Aario, 1977a,b, 1987; Menzies, 1987; Rose, 1987; Menzies and Shilts, 1996). Fundamentally, multiple-step hypotheses propose the existence of a precursor ridge/landform of unconsolidated materials that is progressively reshaped by active, warm-based ice into a convex up-ice, transverse ridge. Though advanced independently by several workers, this concept has perhaps most plainly been demonstrated by Boulton (1987), who argues that flow-parallel subglacial landforms (i.e., drumlins, flutes) generated during earlier glacial advances or episodes may be subsequently reworked into transverse ridges following significant migrations of a dispersal center, thus leading to large shifts in flowline orientation (ca. 90˚). The precursor ridges in this model are assumed to be composed of deformable sediments with variable yield stress, implying the emergence of a series of resistant knobs along the ridge long axis around which horns and extremities are deformed and preferentially transported down-ice. Continuous non-uniform deformation acts to reshape the ridge into a classically-shaped, concave and undulating ribbed/Rogen moraine morphology, though sustained attenuation of the substrate will result in the production of a series of landforms comprising short, crescentic ridges, through barchanoid drumlins and into ellipsoidal/ovoid drumlins and flutes further down ice. The implications of Boulton's (1987) theory are that ice divides must have existed at, and migrated between, various locations throughout the last glacial cycle. While recent studies do suggest that late last glacial dispersal centers were highly migratory (e.g., Boulton and Clark, 1990a; McMartin and Henderson, 2004; Livingstone et al., 2010), it is problematic to assume that multiple migrations would condition the concentric patterns that ribbed moraines display around the final interior ice retreat centers (e.g., Kleman and Hättestrand, 1999).

Boulton's (1987) theory is closely paralleled by Lundqvist (1989, 1997), yet the latter author does not interpret the precursor ridge to constitute an original drift lineation. Although Lundqvist (1989, 1997) fails to determinately specify any means by which the precursor ridge is formed, he suggests one of two alternatives, either: (a) it arises subglacially and is later modified by supraglacial and/or

extraglacial processes during the same glacial episode, or else (b) it is a primary supraglacial deposit that is later overridden and restructured by active, warm-based ice readvance. One variant of the argument put forth in (a) follows a reasoning wherein the pre-existing landform is interpreted as a product of an earlier glaciation. This concept derives from stratigraphic evidence of Early Weichselian inheritance within the delicate Veiki moraine landforms of northern Scandinavia, originally noted by Lagerbäck (1988a,b) and Lagerbäck and Roberts (1988). Finalyson et al. (2010) similarly suggests that ribbed moraines from west-central Scotland were first emplaced during a build-up phase preceding LGM and later overridden and morphologically defined. Sutinen et al. (2010) provide evidence of a two-step construction process based on electrical-sedimentary anisotropy of ribbed moraine sequences near Lake Rogen in Sweden.

Möller (2006) envisions a similar origin for the ribbed moraine forms of the Indån and Våmån river valleys in central Sweden. The presence of undisturbed, sub-horizontal primary bedding, comprised of homogeneous diamicton units coupled to basal shear zones, was interpreted as a signature of sediment gravity-flow deposits. This intact bedding within the core is cut sharply along the proximal face of these ridges, and is replaced by steeply-inclined beds and folds across their lee-side surfaces, which the author interprets as a product of supraglacial/englacial melt-out and down/backwasting. Based on these observations, Möller (2006) maintains that topographically-associated ribbed moraines of central Sweden reflect stacked sequences of flow-till deposits (cf. Paul, 1983), possibly produced during Early Weichselian (i.e., the penultimate) deglaciation as a series of controlled moraines near the glacier margin in response to the earlier compressional folding and thrusting of debris-rich basal ice onto the ice surface (Boulton, 1972). Möller (2006) argues also that the subsequent deformational event required to reshape each ridge into its characteristic arcuate planiform (Fig. 3.10) must have been both short-lived and spatially localized, given the presence of sedimentological structures (e.g., sheath folds) indicative of high strain, and the variable degree of down-ice concavity displayed among individual ridges within a single field. Spatially variable, short-lived deformation events (as opposed to uniform, pervasive subglacial sediment deformation) might be attributed to a mosaic of deforming/non-deforming sediments far inside an ice margin (cf. Piotrowski and Kraus, 1997; Piotrowski et al., 2004; Trommelen et al., 2012, 2014), or alternatively, to subglacial processes in the marginal zone which are also short-lived in the sense that they terminate more quickly following deglaciation.

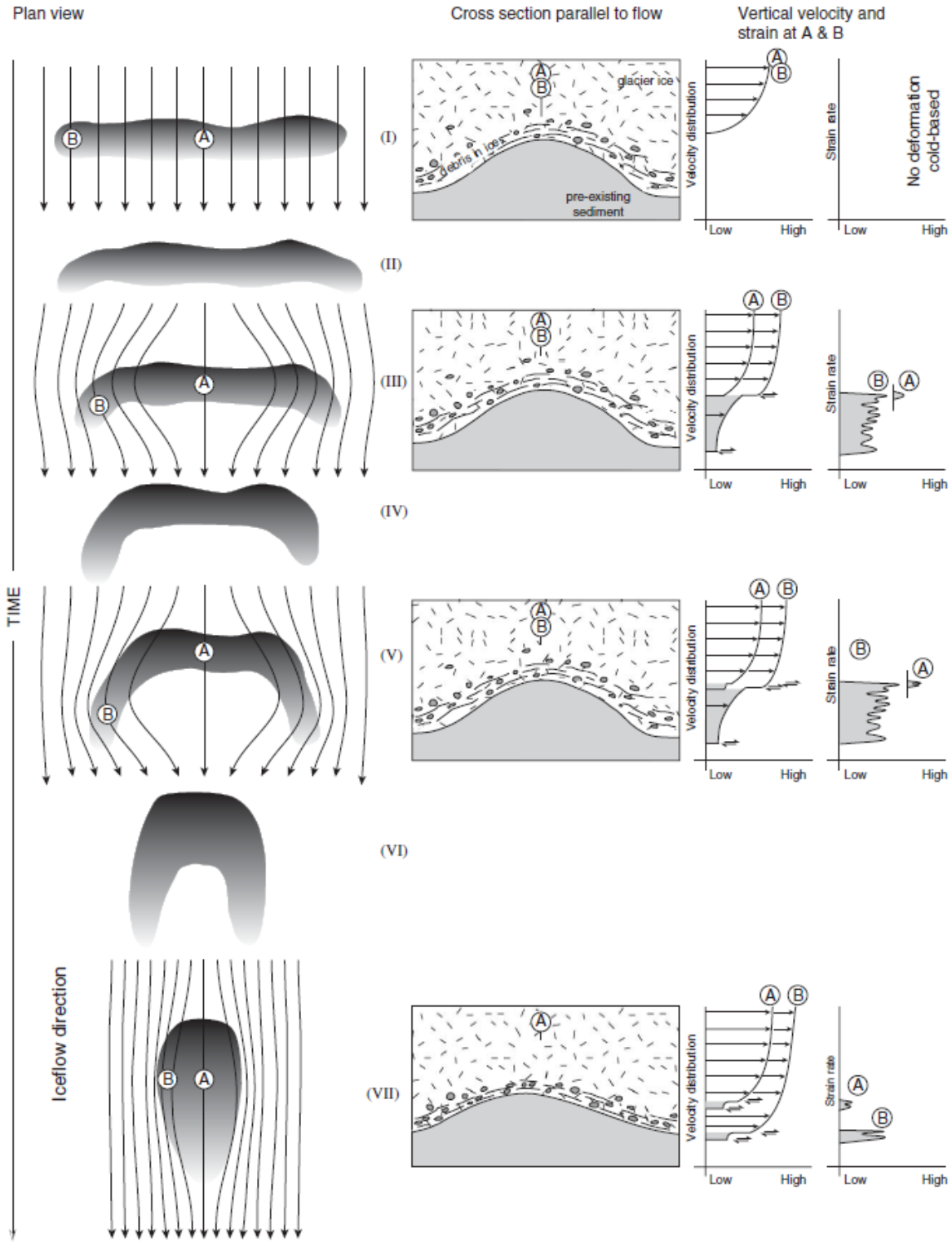

Fig. 3.10 – A model of ribbed moraine development and reshaping from a precursor transverse ridge, based on field observations from the Indån river valley, Sweden. An originally transverse landform (I) is progressively reformed by overriding active ice, conceivably resulting in the generation of parabolic (VI) or elliptical (VII) drumlins. Variations in strain rate and velocity distribution with time are demonstrated for both mid-ridge (A) and lateral extremities (B). Curving flow lines detail the effect of the ridge element as a gradually diminishing obstacle to ice flow (Möller, 2006).

3.4.4 **Bed-ribbing Instability**

One model of bedform development that has gained prominence in the contemporary literature proposes the emergence and propagation of a rheological instability within a layer of subglacial deforming sediment, in response to the regular coupled flow of ice and till. Positive relief is assumed to amplify through sediment accumulation, whereas patches of low relief will be preferentially eroded, producing regular pattern over a terrain, evinced by the positioning of subglacial bedforms (Stokes et al., 2013a). In essence, this concept represents an empirical extension of a recent body of mathematical work which demonstrates that interfacial instabilities are viable within deforming subglacial till (Hindmarsh, 1998a,b,c; Fowler, 2000, 2009, 2010; Schoof, 2007; Chapwanya, 2011). Recent measurements of ribbed moraine morphometric characteristics (length, height, width, wavelength) from large remote sensing datasets (cf. Dunlop and Clark, 2006b; this thesis) have revealed unimodal distributions for each of these parameters, in addition to remarkably consistent wavelengths (i.e., down-flow crest-to-crest distances) within individual fields. On the basis of this consistency, a number of authors have purported the existence of a single formational mechanism that may have operated non-discriminately over large areas at the base of the last continental ice sheets. Similar high-consistency patterns are known from other geomorphic environments (e.g., fluvial, aeolian), where bedform development (e.g., dune propagation) has been conclusively linked to the interaction of fluid-flow with an underlying sediment bed. Since these processes are driven by instabilities, where a given perturbation amplifies and ignites further change within the system, on the basis of form-analogy, comparable processes have been envisioned for the development of regularly-spaced subglacial bedforms with high-degrees of intra-field uniformity (Hindmarsh, 1998b, c). Fisher and Shaw (1992) also appeal to form analogy, in their case, to support a subglacial megaflood origin for ribbed moraines which involves fluvial and debris-flow deposition into carved subglacial cavities, though this particular theory has faced much opposition in the more recent literature (e.g., Benn et al., 2005; Clarke et al., 2005; Eyles, 2006; Finlayson and Bradwell, 2008; Benn and Evans, 2010).

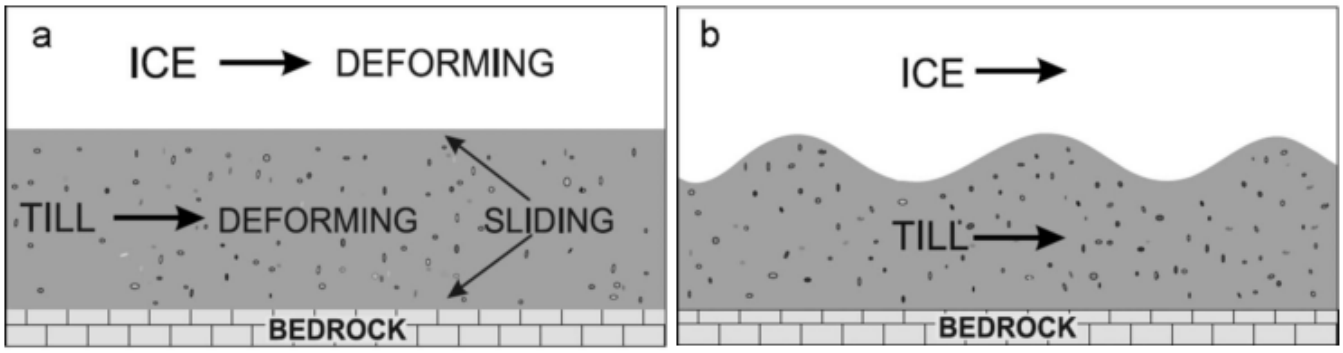

Fig. 3.11 – Schematic diagram illustrating the proposed Hindmarsh-Fowler instability. The model permits deformation in both ice and sediment, which corresponds to an environment that is prone to the development of instabilities. A) Model runs are initiated with a planar ice/bed interface, though under certain flow parameter combinations, waveforms are generated at the till surface (modified from Clark, 2010).

Dunlop et al. (2008) outline the instability theory as it applies to the genesis of ribbed moraines and present a numerically-based ice- and till-flow model, the Bed-Ribbing Instability Explanation (BRIE), which predicts ribbed moraine patterns and wavelengths that are agreeable with known ranges in nature (Dunlop and Clark, 2006b). The results of this modeling should be critically regarded,

however, as physical constraints on ribbed moraine formation (i.e., the parameter values in BRIE) remain poorly-understood. As a means of circumventing this issue, BRIE was run using numerous physical parameter combinations within pre-defined, glaciologically plausible ranges, and the basic assumption was made that all observed ribbed moraines (i.e., those belonging to the empirical dataset) were subject to a similar range of conditions at the time of their formation (Dunlop et al., 2008). Compilation of 2,116,800 model runs revealed predictions of instability-linked ribbed moraine formation at order of magnitude wavelengths between 100 and 1000 m, which compares with (though overestimates) the actual range of values (12–5,400 m) extracted from the empirical dataset (Dunlop and Clark, 2006b). Wavelength overestimation by the model likely implies that ribbed moraines emerge within a narrower (i.e., more specific) range of glaciological conditions in nature than was permitted by the selected range of parameter values. Nevertheless, this work revealed a strong concentration of power at preferred wavelengths, effectively demonstrating non-random ribbed moraine distributions. These findings agree well with underlying theory that predicts exponential growth of the instability, and consequently the dominance of a wavelength of maximum growth rate that determines the expression of the bedform pattern (Dunlop et al., 2008; Clark, 2010).

Whereas BRIE does not output true map plane (i.e., three-dimensional) surfaces, it does predict the downstream ribbing instability wavelengths that should arise from the action of coupled ice/deforming till flow, according to the framework detailed in Hindmarsh (1998c). Schoof (2007) also analyzed the Hindmarsh (1998c) model of till instability (alongside subsequent work by Fowler, (2000)), though determines its two-dimensionality (which suggests the development of finite-amplitude bedform morphology) unaccommodating of existing theories of bedform generation. Countering this, Fowler (2009) demonstrated that products of the instability theory (i.e., finite-amplitude, two-dimensional waveforms) may feature also secondary transverse instabilities, thus forming drumlins which do in fact grow to finite-amplitude. Chapwanya et al. (2011) use spectral approximations to develop full three-dimensional solutions to BRIE. Their calculations suggest that empirical ridge spacing and morphology is well simulated by the model, but that it remains incapable of producing genuine three-dimensional bedforms. The version of the model presented by Chapwanya et al. (2011) assumes passive hydraulic drainage, which lacks any influence on ice flow, though these authors speculate that the inclusion of an active stream flow model, which permits the generation of rilling and ribbing instabilities (Fowler, 2010), may in fact be capable of forming fully three-dimensional bedforms.

4. Remote Sensing, Geographic Information Systems, & Glacial Geomorphology

It is clear that concepts such as scale variation, time and space representation, feature identification and interrelation, data management, and process visualization have come to form fundamental considerations within the field of glacial geomorphology. Increasingly, it is also being recognized that many of these core considerations are shared with the broader fields of geomatics and geographic information science (GISc), whose practical applications are frequently mediated by remote sensing (RS) and GIS (Napieralski et al., 2007). GISc lends itself to the synthesis of regional (and larger) datasets, and performs well also when integrating information across broad spatial and temporal domains. For instance, sub-continental scale ice sheet reconstructions are increasingly being built from interpretations of RS datasets which are ingested into, managed, and processed within a GIS (e.g., Boulton and Clark, 1990a; Kleman et al., 1997, 2002, 2006, 2010; Clark et al., 2000; Jansson et al., 2002; Jansson and Glasser, 2005; Greenwood and Clark, 2009a,b; Evans et al., 2009; Livingstone et al., 2010, 2012; Clark et al., 2012; Finlayson et al., 2014; Hughes et al., 2014). In the past, the development and organization of this level of information relied extensively on field mapping and the manual construction of contour maps (e.g., Rose and Letzer, 1975). Though these methods remain central to detailed (fine-resolution), large-(map)scale mapping efforts, their relatively high-cost, and ability to survey only limited areas on the ground, have made them somewhat prohibitive to regional-scale investigations (Smith et al., 2000). To a certain extent, these methodologies have been supplanted by RS-GIS techniques (Smith et al., 2006); yet importantly, for most applications, ground-truth persists as the most reliable source of information. In any case, travel to study locations is often necessary in order to obtain samples, observe processes and/or conduct experiments at spatial and temporal resolutions that current RS systems are unequipped to handle (Walsh et al., 1998).

Early ventures into remote sensing in the geosciences began shortly following World War I, with the introduction of aerial photography and the development of photogeological reconnaissance methods. These applications involved largely qualitative analyses, and only later, the exploitation of quantitative photogrammetric procedures (Smith and Pain, 2009). With spatial resolution on the order of a few metres, and the ability to classify landscape features with high accuracy at scales ~1:20,000, aerial photography revolutionized the geologist's cartographic approach, particularly in remote and/or otherwise inaccessible terrains; nevertheless, a number of caveats relating to aerial photographic acquisition are to be noted. The relative usefulness of information displayed on aerial imagery is highly dependent upon the solar elevation at time of capture, and is often hampered by a suite of terrain cover aspects (e.g., snow, vegetation), or by poor processing quality of the prints (Clark, 1997). Moreover, regional-scale orthophoto acquisitions, and/or strict field surveys, require enormous time and monetary investments, and must necessarily be completed by large teams of individuals, each with varying biases and levels of experience, thus introducing the potential for inconsistent methodologies to affect final research outcomes. The traditional practice of aerial photographic interpretation involves examination of stereographic pairs of images under a stereoscope, affording the ability to visualize terrain in 3-dimensions. Annotations are typically hand-sketched onto transparencies over stereopair aerial photos in an analog fashion and later digitized for storage and subsequent manipulation in a computational environment, thus involving multiple steps and the potential for propagation of error. Important to note, however, is the recent proliferation of "soft-copy" digital photogrammetric systems, which enable direct digitization on-screen. Such technology has ensured the continued relevance and usefulness of air photo media as a data source (Fryer et al., 2008).

Alternatively, individual satellite images and digital elevation datasets demonstrate large areal coverage (commonly several tens to hundreds of km^2), and can thus be compiled and utilized by a single interpreter to map regions at synoptic scale. This small scale mapping affords better detection of large and/or overprinted landforms than traditional combined aerial photography/field surveying, and has enabled identification of previously unrecognized landscape patterns and "mega-scale" landforms (Fig. 4.1) (e.g., subglacial lateral shear-margin moraines (Dyke and Morris, 1988), and mega-scale glacial lineations and cross-cutting relationships (Boulton and Clark, 1990a.b; Clark, 1993, 1994)). With particular application to ribbed moraines, Clark and Meehan (2001), using Landsat TM imagery, and a photogrammetrically-derived digital elevation model (DEM), discovered transverse ridges in Northern Ireland an order of magnitude larger than previous records in the literature. Similarly, Greenwood and Kleman (2010) identified large transverse ridges in central Keewatin, Nunavut, Canada, which they interpreted variously as "mega-scale" ribbed moraines and massive, overprinted end moraines dating to the penultimate glaciation. Dunlop and Clark (2006b) utilized photogrammetrically derived DEMs, 1:60,000 stereopair aerial photographs, high-resolution ASTER, and panchromatic (ETM+) and multispectral (MSS) Landsat imagery to digitize over 33,000 individual ribbed moraine features in a GIS throughout Canada, Ireland and Sweden. Information concerning size, shape, pattern and distribution was collected. This broad-scale level of analysis prompted the authors to refute several classically-held assumptions pertaining to ribbed moraines, and further, to propose a new classification encompassing twelve morphologically distinct groupings.

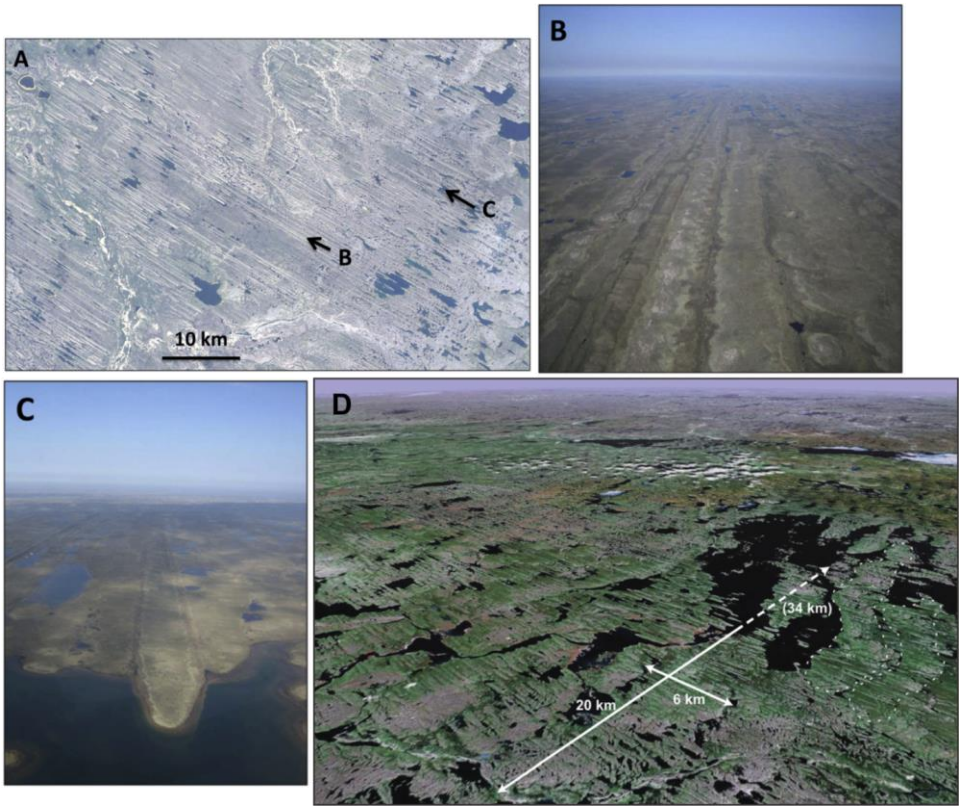

Fig. 4.1 – "Mega-scale" glacial landforms identified using satellite imagery. A,B,C) Landsat 7 ETM+ natural colour composite (NCC) image depicting mega-scale glacial lineations imprinted onto the bed of the Dubawnt Lake palaeo-ice stream, Nunavut, Canada (Stokes et al., 2013b). D) Oblique view of Landsat 7 ETM + natural colour composite image showing mega-scale transverse till ridges overprinted by drumlins and mega-scale glacial lineations, central Keewatin, Nunavut, Canada (Greenwood and Kleman, 2010).

Mapping from RS datasets proceeds quickly and efficiently, as data are stored digitally and are thus readily archivable and easily handled at multiple scales. In glacial geomorphology, features mapped from RS data are often digitized directly, thus permitting discrete, though related categories of landform data to be stored as separate data layers in a geographic information system (GIS). These layers can be manipulated individually and assembled as required in order to elucidate themes of landscape development (Fig. 4.2). Pre-existing field data found in published hardcopy maps and reports can be digitized and incorporated with new remote mapping (e.g., Clark et al., 2004; Evans et al., 2005). Moreover, data separation according to absorption, reflectivity, or emissivity characteristics of returns – an essential capacity of most Earth observing satellites (EOS) – simplifies identification of particular targets by exploiting their inherent spectral properties through the customizable assembly of multi-band ternary images. Lastly, most image products served to end-users are available georectified from well-maintained control points, thus eliminating additional and potentially time-consuming steps in the data preparation process. These aspects, combined with increasing availability, high temporal resolution, and low cost, position EOS RS as a useful supplement or alternative to traditional aerial photographic and field-based mapping for many geomorphological purposes.

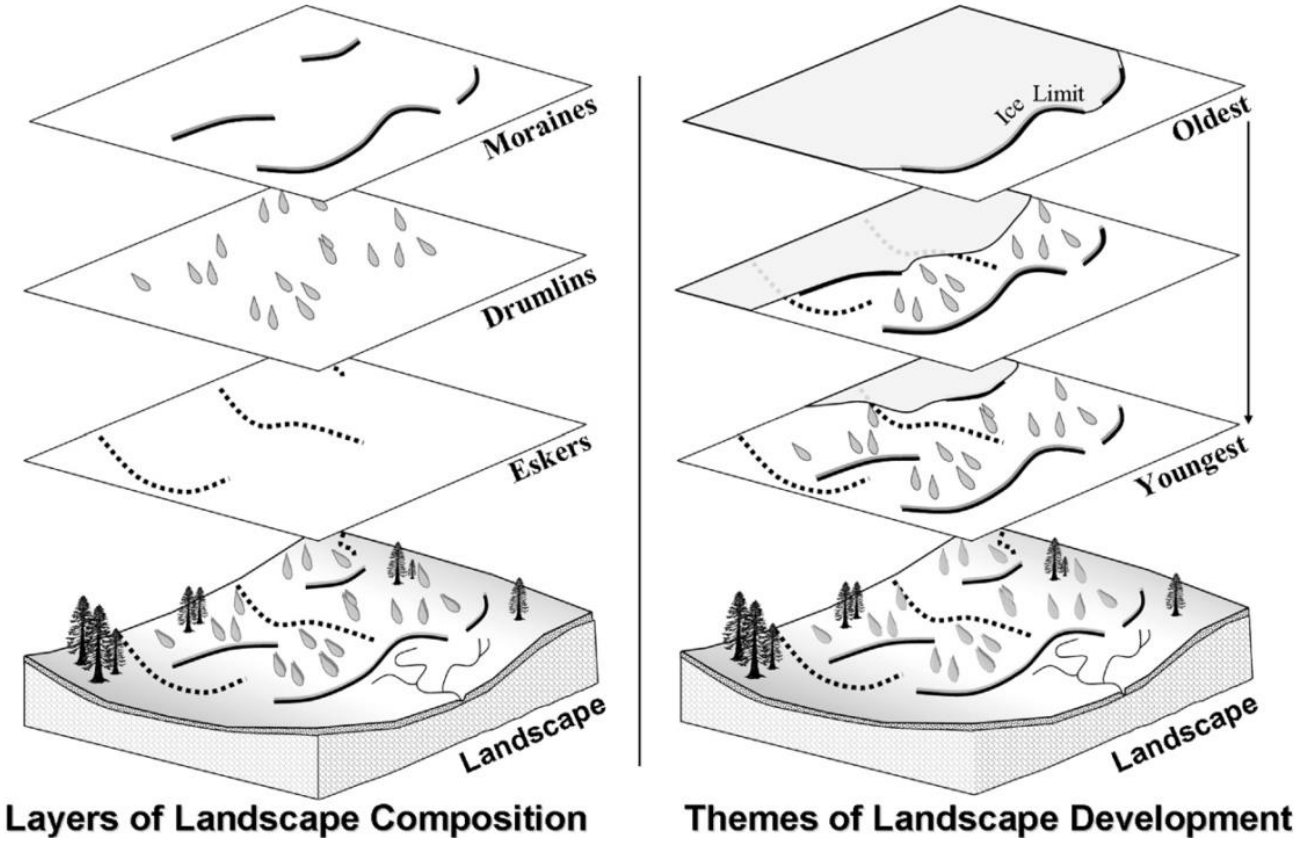

Fig. 4.2 – Schematic diagram illustrating the capabilities of GIS for storing various glacial landsystem components as separate data layers. These can be variously "stripped" away, or combined, to facilitate spatial and temporal analysis of landscape development (Napieralski et al., 2007).

4.1 *Remote Sensing of Glaciated Terrains*

Satellite RS systems collect and relay data of the Earth's surface at various spectral, temporal, radiometric, and (increasingly detailed) spatial resolutions, as is controlled by each system's sensing device, and the orbital path of its reconnaissance platform (Walsh et al., 1998). Spatial resolution (a.k.a. ground element, ground resolution cell, or cell width) refers to the smallest measurable area on the ground – the Instantaneous Field of View (IFOV) – that can be simultaneously sensed by a particular detector. A sensor's spectral resolution defines the span of the range of wavelengths (λ_1~λ_2) within the electromagnetic spectrum over which it is equipped to collect data. Associated with the latter is a sensor's spectral bandwidth (i.e., the width of its band pass), which is given by the width of λ at 50% of the sensor's maximum response level (Fig. 4.3). Temporal resolution is controlled by a sensor's swath width alongside the orbital parameters of its sensing platform; together these determine the periodicity (return interval) at which a fixed area on the ground is successively imaged by the space-borne sensor. RS systems that are placed within orbital paths more distant from the Earth's surface will have finer temporal (though typically coarser spatial) resolutions than those placed within nearer orbital paths. This is determined by:

$$T_0 = 2\pi\left(R_p + H'\right)\sqrt{\frac{R_p + H'}{g{R_p}^2}}$$

Where T_0 is satellite orbital period (s), R_p is planet radius (km; for Earth, ~6,800), H' is altitude of the sensor above datum (km), and g is the gravitational constant ($6.67384 \cdot 10^{-11}$ $m^3 \cdot kg^{-1} \cdot s^{-2}$).

Lastly, radiometric resolution describes the total number of quantization levels used by a sensor (e.g., its bit-depth, or the range of digital numbers (DNs) it is capable of natively displaying) (Gupta, 2003). Captured data, bound by these four resolutions, is manipulated to generate imagery of the Earth's surface. For certain applications, repeat imaging enables landscape change detection over periods extending from days to years. The digital collection, storage and distribution of RS data, in conjunction with its near-global coverage, provides Earth scientists with an extremely powerful toolset for landscape analysis that is unrivaled in its accessibility (Walsh et al., 1998).

Despite considerable and continued advancement, the technical and technological limitations of present-day RS systems pose real restrictions on the application of remotely collected data to glacial geomorphological research. In this regard, limitations in spatial resolution are much more readily managed than are those associated with temporal resolution: digital/analog conversions, and raster resampling, correction and transformation procedures are generally available in image processing and/or GIS software packages to facilitate the integration of spatial data from various RS systems. Management of temporal resolution is much less flexible, as this is pre-established by satellite orbit specification and the length of the sensor's imaging archive. Integrating satellite, airborne, and terrestrial RS systems, however, will often present a level of detail that is sufficient for most applications.

4.2 *Earth Observation Systems*

Although there are a large number (~1,000) of operational EOS sensors, only a handful produce imagery that is suitable for glacial landform mapping (see Table 4.1). These systems have been used extensively in recent years for mapping the geomorphology of formerly glaciated areas, including Landsat Thematic Mapper (TM) (McCabe et al. 1999, Clark and Stokes 2001, Stokes 2002), Landsat

Multispectral Scanner (MSS) (Boulton and Clark 1990a,b; Clark 1994; Clark and Stokes 2001; Jansson et al. 2003), SPOT HRV-IR (Smith et al. 2000), Landsat Enhanced Thematic Mapper Plus (ETM+) (Stokes and Clark 2003; Jansson and Glasser 2005; Greenwood and Clark, 2008), and ERS Synthetic Aperture Radar (SAR) (Clark et al. 2000; Clark and Stokes 2001). The majority of sensors utilized in glacial geomorphological mapping can be categorized into those which collect in the visible and near-infrared (VNIR) ranges of the electromagnetic (EM) spectrum, vs. those which collect in the microwave portion (i.e., radar) (Fig. 4.4). These instruments have been utilized in glacial geomorphology for only ~30 years. In contrast, the application of EOS remote sensing to geoscientific interests *in general* began as early as 1960, with the launch of the first Television and Infrared Observation Satellite (TIROS) by the U.S. National Aeronautics and Space Administration (NASA). TIROS and its successors were designed as monitoring platforms to capture images of Earth's continuously fluctuating meteorological phenomena. It wasn't until 1972, following the launch of NASA's Earth Resources Technology Satellite (ERTS; later renamed Landsat 1), that satellite imagery was applied specifically to geological topics.

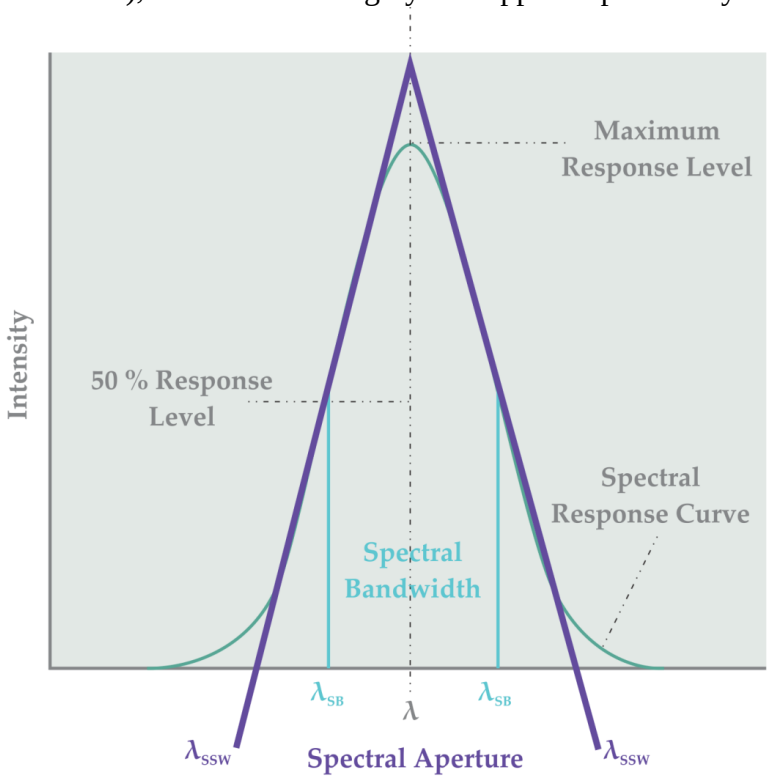

Fig. 4.3 – Generalized plot of the spectral bandwidth (spectral resolution) of a detector. Spectral range is determined from the difference of spectral boundaries (λ_{SB}) at 50% of the detector's maximum response level. The spectral aperture, or slit width of the detector, is shown with respect to its response curve above, and is calculated as the difference of λ_{SSW}.

Landsat 1, deployed into a polar, sun-synchronous orbit at 900 km altitude, carried two independent sensors, Return Beam Vidicon (RBV) and MSS, the latter of which provided imagery in four VNIR spectral bands at 80 m spatial resolution (production systems now resample this to 60 m). MSS was responsible for generating the most widely-used data throughout its lifespan, though was later superseded by the TM sensor onboard the Landsat 4 and 5 platforms. TM witnessed an improved spatial resolution of 30 m and expanded spectral resolution across 7 VNIR wavebands. Six years following the failed launch of Landsat 6 in 1993, Landsat 7 was deployed, carrying the ETM+ sensor which, to a large degree, replicated the capacities of TM, though also provided additional thermal infrared (IR) (band 6,

60 m resolution) and panchromatic (band 8, 15 m resolution) sensing bands. Moreover, the platform carried 3 on-board sensor calibration devices (Internal Calibrator, IC; Partial Aperture Solar Calibrator, PASC; Full Aperture Solar Calibrator, FASC), making it the first Landsat to support onboard, full aperture, 5% radiometric calibration. Permanent mechanical failure of the Scan Line Corrector (SLC) onboard ETM+ has somewhat reduced the sensor's utility throughout the past decade, however a number of algorithms have since been derived and have proven successful in filling SLC gaps using alternate scenes (cf. Chen et al., 2011). Deployed February, 2013, the Landsat Data Continuity Mission (LDCM; later renamed Landsat 8) is the most current operational platform in the long-standing Landsat series. This system houses two sensors, the Operational Land Imager (OLI), which collects and transmits data across eight VNIR spectral bands at 30 m ground resolution and one panchromatic band at 15 m ground resolution, and the Thermal Infrared Sensor (TIRS), which collects and transmits in two additional IR bands at 100 m ground resolution.

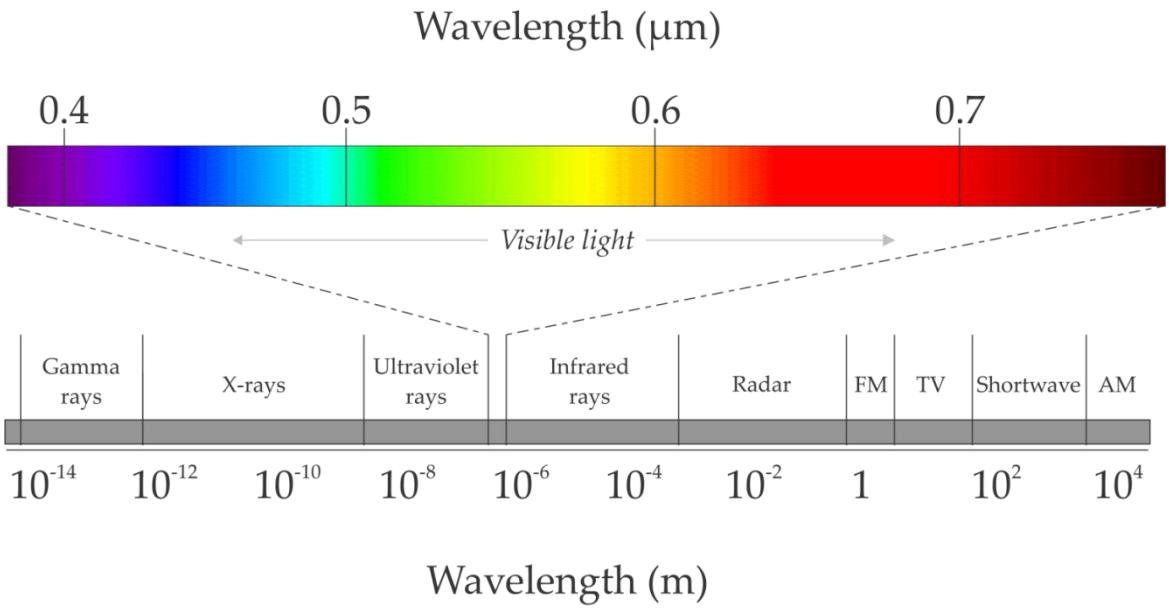

Fig. 4.4 – Wavelengths spanned by various portions of the electromagnetic spectrum. Note the small range within which visible light occurs.

A number of commercial VNIR sensors have also entered the market in recent years. These instruments provide very high spatial, though often only limited spectral, resolutions. Such sensors, including SPOT, CORONA, IKONOS, Quickbird, Rapideye, WorldView, and GeoEye produce panchromatic-band imagery at similar (spatial) resolution to aerial photographs. Cost, access, and data availability remain significant constraints on imagery use in glacial geomorphology, however, and in these categories, commercial sensors are typically unable to compete with freely available datasets, i.e., Landsat and Terra ASTER. Thus, despite launching prior to the 21st century, many moderate-resolution multi-spectral sensors remain important data sources, owing largely to their extensive imagery archives, high repeat-pass coverage (useful for monitoring purposes), low cost, ease of access, and large individual scene footprints (Smith and Pain, 2009).

In contrast to VNIR sensors, radar-derived (microwave band) imagery has experienced only niche use within glacial geomorphology. This application was first demonstrated by Ford (1981) who concluded that Seasat synthetic aperture radar (SAR) imagery was a preferable data source over Landsat MSS scenes for mapping drumlins and moraines, owing to higher spatial resolution and a lack of

azimuth biasing effects. Heiser and Roush (2001) utilized ERS-1 SAR imagery to map end moraine sequences in Chukotka, Russia, and interpreted multiple Pleistocene glaciations from their results. Pixel-based slope calculations and surface degradation indices allowed for the determination of relative moraine ages, revealing the most recent ice margin positions to have been most restricted within this record. These observations permitted correlation of local glacial history with previously known periods of ice cover in the Bering Strait. Clark and Stokes (2001) also utilized ERS-1 SAR imagery (in conjunction with elevation data, air photos and several Landsat MSS and TM scenes) to map the geomorphology of the M'Clintock Channel palaeo-ice-stream, off the east coast of Victoria Island, Canadian Arctic Archipelago (Fig. 4.5). An earlier study exclusively used SAR imagery to map eskers and glacial lineations across the Labrador sector of the former LIS (Clark et al., 2000). Analysis of relict lineation assemblages led to re-envisioned estimates of palaeo-ice divide migration coinciding with phases of rapid ice sheet drainage into Ungava Bay.

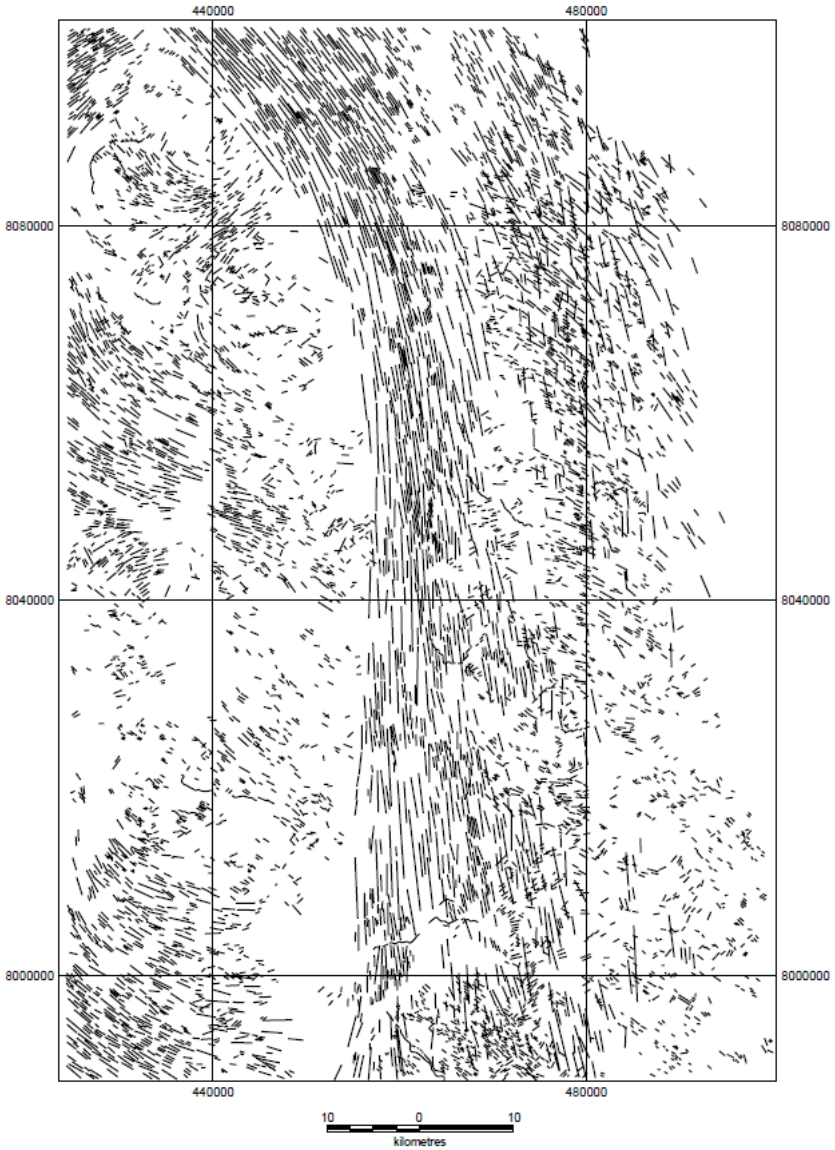

Fig. 4.5 – Glacial lineations mapped from Landsat TM and ERS-1 SAR imagery on the M'Clintock Channel palaeo-ice stream bed, Victoria Island, Canada (Clark and Stokes, 2001).

Table 4.1 – Select Earth observation satellites with data products potentially suitable for glacial landform mapping. Orange fill indicates publically available data; green fill designates commercial sensing systems.

Sensor	Platform	EM Span	Spatial Resolution (m)	Spectral Bands	Operator
MSS	Landsat 1-5	VNIR	80 (60)	4	NASA/USGS
TM	Landsat 4-5	VNIR	30	6	NASA/USGS
		Thermal	120	1	
ETM+	Landsat 7	Panchromatic	15	1	NASA/USGS
		VNIR	30	6	
		Thermal	60 (30)	1	
OLI	Landsat 8	Panchromatic	15	1	NASA/USGS
		VNIR	30	6	
		SWIR	30	2	
TIRS	Landsat 8	Thermal	100	2	NASA/USGS
Hyperion	EO-1	Hyperspectral	30	220	NASA/USGS
ALI	EO-1	Panchromatic	10	1	NASA/USGS
		VNIR	30	9	
ASTER	Terra	VNIR	15	3	NASA/Japan METI/Japan Space Systems
		SWIR	20	6	
		Thermal	90	5	
--	RapidEye	VNIR	5	5	RapidEye Blackbridge Ltd.
--	EROS-A	Panchromatic	1.9	1	ImageSat International
--	EROS-B	Panchromatic	0.7	1	ImageSat International
--	Pléiades 1A	Panchromatic	0.7 (0.5)	1	CNES/EADS Astrium/Spot Image
		VNIR	2	4	
--	Pléiades 1B	Panchromatic	0.7 (0.5)	1	CNES/EADS Astrium/Spot Image
		VNIR	2	4	
HRV	SPOT 1-3	Panchromatic	10	1	CNES/EADS Astrium/Spot Image
		VNIR	20	3	
HRVIR	SPOT 4	Panchromatic	10	1	CNES/EADS Astrium/Spot Image
		VNIR	20	3	
		SWIR	20	1	
HRS	SPOT 5	Panchromatic	10	1	CNES/EADS Astrium/Spot Image
HRG	SPOT 5	Panchromatic	5 (2.5)	2	CNES/EADS Astrium/Spot Image
		VNIR	10	3	
		SWIR	20	1	
NAOMI	SPOT 6	Panchromatic	1.5	1	EADS Astrium
		VNIR	6	4	
--	IKONOS	Panchromatic	1	1	DigitalGlobe
		VNIR	4	4	
--	Quickbird	Panchromatic	0.6	1	DigitalGlobe
		VNIR	2.5	4	
--	Geoeye	Panchromatic	0.4	1	DigitalGlobe
		VNIR	1.65	4	
--	Worldview-1	Panchromatic	0.5	1	DigitalGlobe
--	Worldview-2	Panchromatic	0.46	1	DigitalGlobe
		VNIR	1.85	8	
KH1-KH6	CORONA / ARGON / LANYARD	Panchromatic	<1.8	1	USGS
--	Formosat-2	Panchromatic	2	1	China NSPO/EADS Astrium
		VNIR	8	4	
ASAR	Envisat	Microwave	30	2	ESA
SAR	ERS-1	Microwave	30	1	ESA
SAR	ERS-2	Microwave	30	1	ESA
SAR	RADARSAT-1	Microwave	8/30/50/100	1	CSA
SAR	RADARSAT-2	Microwave	2/5/16/30/50/100	1	CSA
--	COSMO-Skymed	Microwave	1/3/15/16/20	1	ASI/eGEOS
--	TerraSAR-X	Microwave	1/3/18	1	DLR/EADS Astrium

Radar imaging applications have, however, been widespread in modern glaciology and studies of contemporary glaciers. Consecutive missions of the RADARSAT-1 Antarctic Mapping Project (RAMP) in 1997 and 2000, for instance, utilized that sensor's unique maneuverable orbit, and steerable antenna array to image the entirety of the Antarctic ice sheet. The 2007 launch of RADARSAT-2 by the Canadian Space Agency (CSA) has opened the door to further ice monitoring using this setup. SAR imagery has also been employed in assessments of surficial ice velocity flux. For instance, optimized feature tracking using SAR imagery during a surge of Sortebræ, east Greenland, revealed an abrupt transition to fast flow rates on the order of 24 m d^{-1}, and an active-phase extending 28-32 months, between November 1992, and June 1995 (Pritchard et al., 2005). Continuation of the European Space Agency's (ESA) series of microwave EOS systems throughout the past two decades (ERS-1, 1991-2000; ERS-2, 1995-2011; Envisat, 2002-2012) has provided the bulk of useable SAR data of interest to glaciologists and glacial geomorphologists. Other systems have been locally employed, including the C-band SAR instruments onboard RADARSAT-1 and 2, and the Phased Array type L-band Synthetic Aperture Radar (PALSAR) payloads of the Japan Aerospace Exploration Agency's (JAXA) Advanced Land Observing Satellite (ALOS) 1 and 2. More recently, in 2007, the German Aerospace Centre (DLR), in partnership with EADS Astrium GmbH, has deployed a commercial X-band radar sensor, TerraSAR-X, capable of returning (in spotlight mode) 1 m spatial resolution SAR imagery. A near-identical system, the TerraSAR-X add-on for Digital Elevation Measurement (TanDEM-X), was launched into tandem orbit configuration in 2010, and together these two platforms offer single-pass interferometry, enabling the generation of gridded elevation data at spatial resolution of 12 m and <2 m vertical accuracy. At present, altimetry support provided by the Synthetic Aperture Interferometric Radar Altimeter (SIRAL) instrument onboard ESA's Cryosat-2 platform is being utilized in ice sheet mass balance and sea-ice flux monitoring (e.g., Laxon et al., 2013), though is also being applied in more novel approaches; for instance, mapping volume changes in subglacial lakes beneath the Antarctic Ice Sheet (McMillan et al., 2013). Outside of these contemporary glaciological studies, SAR applications have been relatively limited (i.e., in glacial geomorphology and palaeoglaciology), potentially owing to a wide variety of errors and geometric distortions associated with off-nadir (side-looking) sensor orientations (Fig. 4.6), as well as the specialist knowledge required to properly process and interpret such imagery (Clark, 1997; Palmann et al., 2008). The unique geometry of SAR sensors is useful for imaging positive relief landforms, though it also implies that layover occurs in front of tall features, and shadow behind. Layover can be processed out, whereas the latter strictly generates areas of no data.

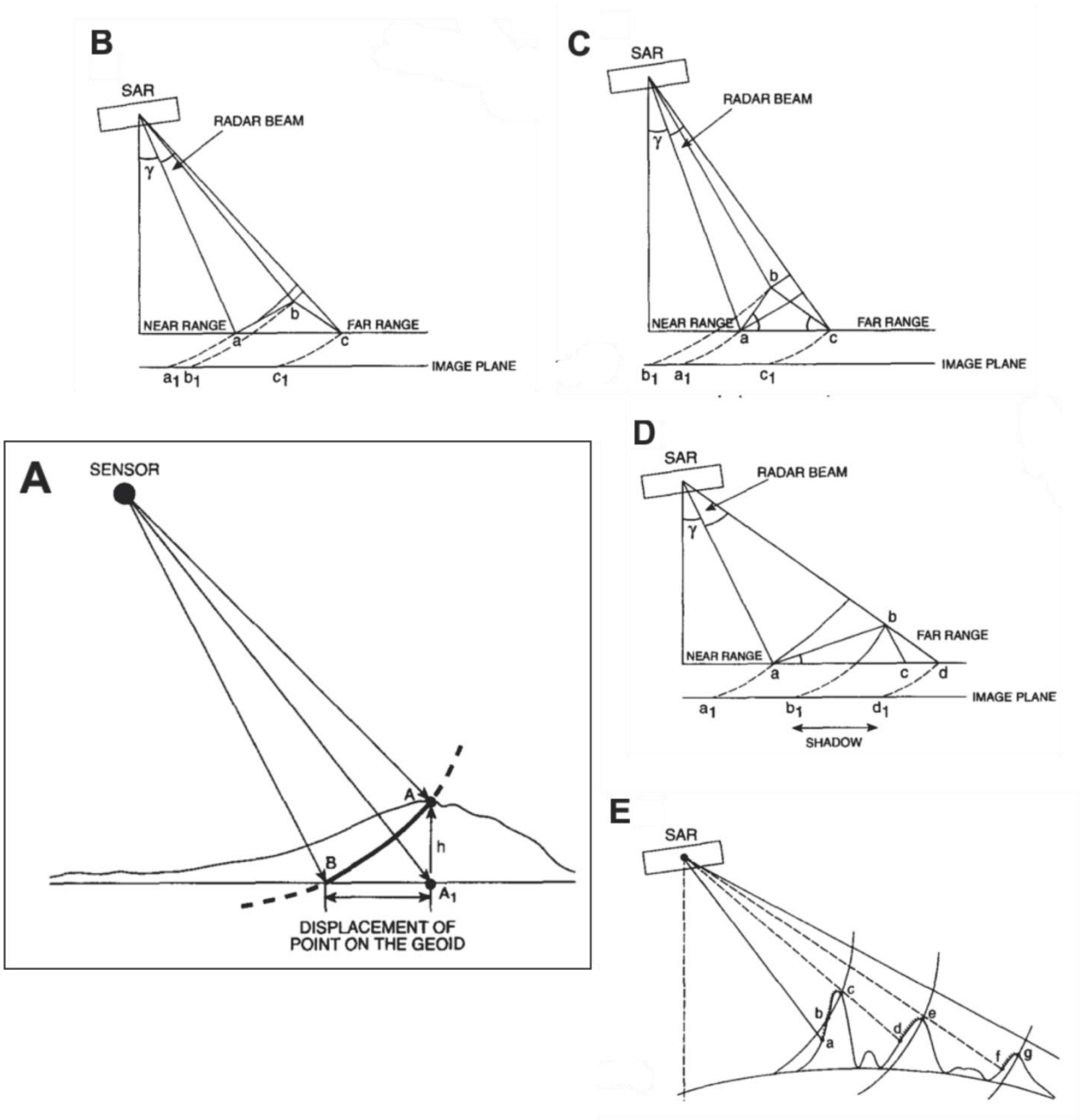

Fig. 4.6 – Geometric distortions associated with SAR data collection owing to side-looking sensor geometry (modified from Clark, 1997). B) Foreshortening occurs when local terrain slope (m) < incidence angle (γ). Sensor-facing slope *a*-*b* is compressed to a_1-b_1.C) Layover occurs when local $m > \gamma$ (i.e., in steep terrain). Since point *b* occurs nearer the sensor than point *a*, the former "lays over", returning an incorrect apparent relative position. D) Radar shadow occurs in rugged terrain. Surface *b*-*c*-*d* lies in the lee of a positive relief feature, resulting in area b_1-d_1 on the image plane being recorded as an area of no data. E) Areas of variable relief suffer from a combination of geometric distortions: *b*-*a* = layover; *c*-*d*, *e*-*f* = radar shadow, *d*-e, f-*g* = foreshortening.

4.3 *Digital Elevation Models*

Undoubtedly the most significant development in geomorphological data collection within recent years has been the introduction of widely available surface elevation datasets, derived variously using several techniques, including traditional photogrammetry, radar altimetry, Light Detection and Ranging (LiDAR), and interferometric synthetic aperture radar (IfSAR, also InSAR). Digital elevation data are commonly processed into a gridded, regularly-sampled dataset, and made available to the end-user as a digital elevation model (DEM). Though often (and erroneously) used interchangeably, the term DEM is a superset of the designations digital terrain model (DTM) and digital surface model (DSM). The latter products differ in that DSMs record only first-return collections, and hence depict the tops of buildings, forest canopies, etc.; conversely, elevation values stored in DTMs represent "bare-earth" models of the ground, and can thus be likened to a DSM with all but final-returns processed out (Fig. 4.7). DTMs tend to be most suitable for the majority of geomorphological mapping applications.

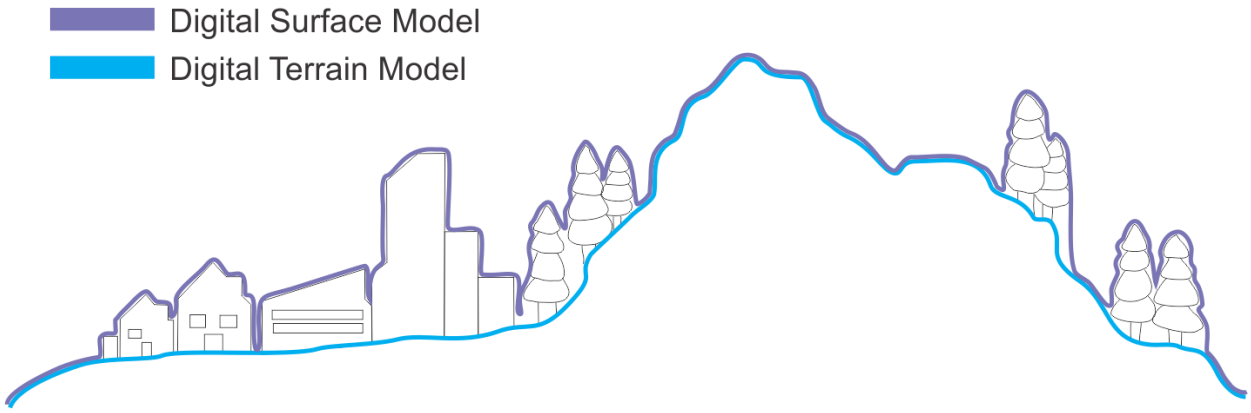

Fig. 4.7 – Schematic diagram illustrating the difference between digital surface models (DSMs) and digital terrain models (DTMs). DSMs include first-return sample elevations and thus reflect the tops of tree canopies, structures, etc. DTMs are created by processing out all but final-return sample elevations and therefore represent "bare earth" models of the terrain.

Photogrammetrically-derived DEMs rely on the collection and processing of repeat-pass (steerable sensor array), or single-pass (multiple fore/aft sensors) stereographic satellite imagery. The Terra ASTER, SPOT 5 and IKONOS systems all support stereo-pair acquisition modes. In particular, Terra ASTER, which features a second, aft-looking sensor, has been used with relative success to produce a near-global (83˚N-83˚S) photogrammetric DEM from along-track, single-pass imagery at 1 arc-second posting interval (~30 m spatial resolution). This data has been used extensively in contemporary glaciological studies, though has had only limited representation within palaeoglaciology. Lytwyn (2010) employed ASTER-derived DEMs to map glacial features throughout Devil's Lake State Park and surrounding areas in Wisconsin, USA. Terrain aspect metrics calculated from the ASTER-derived DEMs were deemed useful in identifying numerous features demonstrating poor detection on aerial photos and multi-spectral Landsat TM and ASTER imagery (Fig. 4.8). Mapping efforts revealed a prominent NE-SW trending fabric towards a termination margin at the Johnstown Moraine, in addition to several outlying N-S trending moraines inferred to have formed during eastward back-stepping of the LIS Green Bay Lobe following the Johnstown Phase. Slope direction highlighted by the ASTER DEM aspect analysis simplified moraine identification (Lytwyn, 2010).

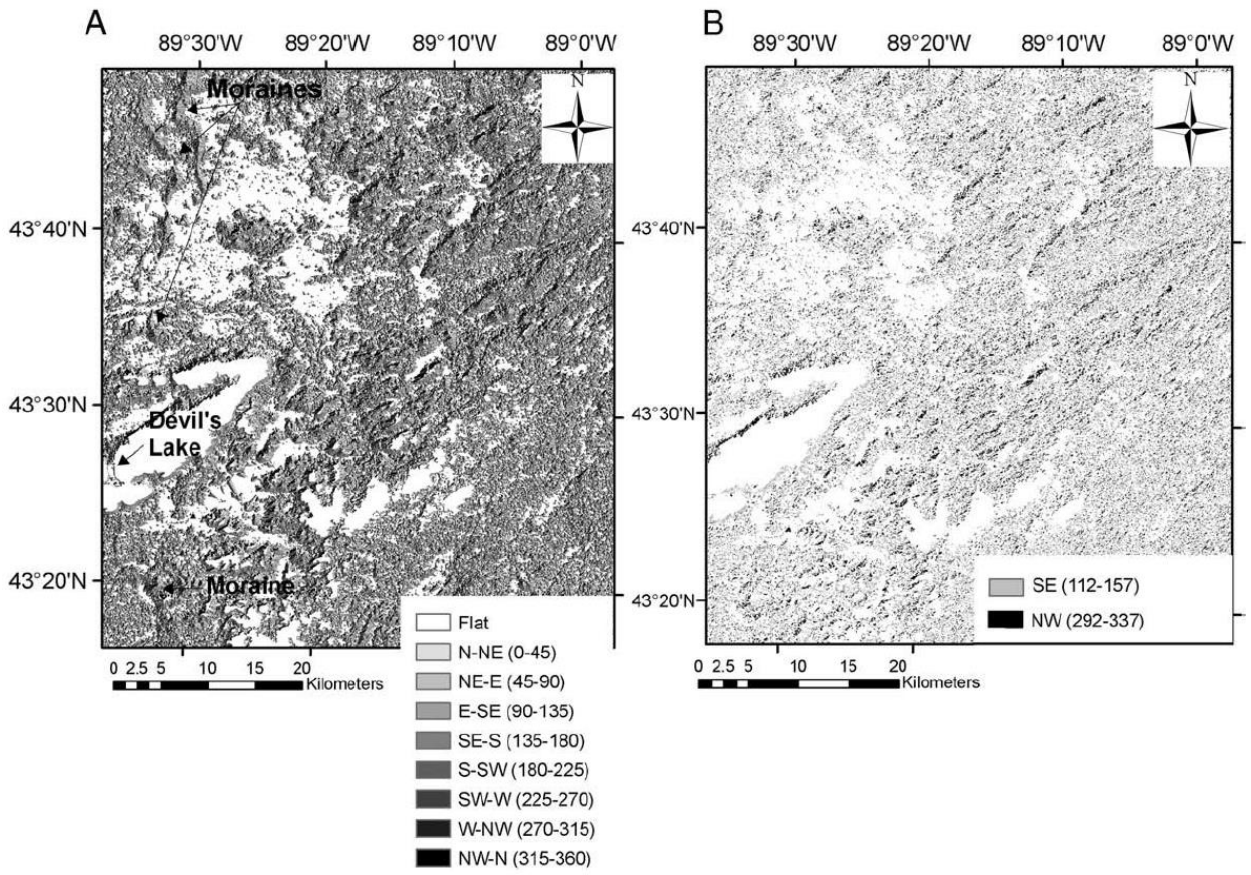

Fig. 4.8 – Aspect analysis of an ASTER-derived DEM, Baraboo Hills, Wisconsin. A) Derived slope directions, highlighting sinuous ridges in the NE and SE portions of the study area, interpreted as moraines. B) Extract of SE and NW facing slopes revealing a prominent NE-SW trending terrain fabric terminating at the sinuous ridges (Lytwyn, 2010).

IfSAR products have likely been the most extensively utilized sources of elevation data in glacial geomorphology. NASA's 11-day Shuttle Radar Topography Mission (SRTM) in February, 2000, exploited space-borne, single-pass IfSAR, flown onboard the Space Shuttle Endeavour, to generate a continuous DEM between latitudes 60˚N and 56˚S at 3 arc-second posting interval (~90 m spatial resolution), with 1 arc-second post spacing (~30 m spatial resolution) for the USA and Australia. These data have been extensively utilized in glacial geomorphological mapping, despite low spatial resolution and lack of coverage at high latitudes. Blundon et al. (2009) provide a brief review of projects within Canada that have incoporated SRTM data. More recently, the commercial acquisition of airborne IfSAR has procured seamless, wide-area digital elevation products (DEMs, DSMs and DTMs) at high resolution (<5 m) for large areas of the globe. In particular, Intermap©'s NextMap® series of products provide coverage across most of the USA and Western Europe, and have been employed widely for glacial geomorphological mapping applications in those areas (e.g., Everest et al., 2005; Smith et al., 2006; Bradwell et al., 2007; Greenwood et al., 2007; Finlayson and Bradwel, 2008; Livingstone et al., 2008, 2010, 2012; Clark et al., 2009, 2012; Evans et al., 2009; Finlayson et al., 2010; Hughes et al., 2010; Knight, 2010; Phillips et al., 2010; Spagnolo et al., 2011; Margold and Jansson, 2012; Hughes et al., 2014). Likewise, airborne LiDAR coverage is increasingly expanding (often yielding datasets with cm-scale resolution) and is becoming a preferred basis for mapping in glacal geomorphology (e.g., Salcher et al., 2010; Jónsson et al., 2014).

5. Ribbed Moraines of South-central Keewatin, Nunavut, Canada – An Examination based on Remotely Sensed Data

5.1 *Introduction*

The widespread occurrence of ribbed moraines across south-central Keewatin, Nunavut, Canada and their apparent preference for expression near former ice divide positions (cf. Kleman and Hättestrand, 1999), presents great opportunity to study the palaeoglaciology of the interior LIS. Recent work by Trommelen and Ross (2009, 2010) and Trommelen et al. (2012, 2013) in northern Manitoba has convincingly demonstrated that ice sheet core regions showcase various degrees of landscape overprinting and inheritance, suggestive of patchy, spatio-temporal transformations in ice-flow direction, basal hydrology, erosional intensity, and basal thermal regime. Such changes condition the development of a fragmented subglacial bed mosaic, within which specific patches, or 'glacial terrain zones' (GTZs), display internally-consistent styles of palaeoglaciodynamic evolution (e.g., palimpsest, high-inheritance, or deglacial terrain). The unique association of ribbed moraines with relict and palimpsest-type GTZs implies that their genesis is likely not a product of deglaciation, and that their preservation throughout later stages of ice flow is enabled by subsequent switches in the state of the ice/bed interface (Trommelen et al., 2014). This study presents further detailed analyses focused on the morphological attributes and spatial distribution of ribbed moraines in south-central Keewatin, with the goal of yielding additional insight into the nature of the bed throughout these transitions.

5.2 *Geology and Glacial History*

The primary area of interest for this thesis is situated within the southern sector of the former District of Keewatin, Northwest Territories, a portion of the present-day region of Kivalliq in south-central Nunavut, Canada (Fig. 5.1). This ~70,600 km^2 area dips eastward across the Kazan upland from an elevation of ~470 m a.s.l. near the Nunavut/Northwest Territories border in the southwest, down to sea level along the fringe of the Hudson Bay depression. Physiographically, the region can be divided into five components, changing primarily along an east-west gradient (Fig. 5.2). Hydrological patterns appear glacially-deranged, and are characterized by short reaches of disordered streams that terminate regularly in small pondings or lakes, many of which are confined between encompassing glacial landforms. Regional drainage is captured by Hudson Bay and, from west to east, crosses three sub-drainage basins: Kazan, Nueltin Lake, and Northwest Central Hudson Bay (Environment Canada, 1986). Topography within the study area is formed generally by a series of plateaus, rolling hills and planation surfaces featuring modest local- (~10 m) and regional- (~50 m) scale relief. A restricted zone of high relief occurs between Mountain Lake and Hurwitz Lake, running towards Padlei northeast of the study area, and passing between North and South Henik lakes. Fossil beaches, flat wave-washed surfaces, spits, bay-mouth bars and organic deposits (e.g., peat bogs) occur prominently within the eastern quarter and are products of incursion of the post-glacial Tyrrell Sea. Most land in this portion of the study area lies below 170 m a.s.l., the altitude of the highest shoreline owing to this transgression (Shilts, 1977). Throughout the greater District of Keewatin, the elevation of the highest shoreline increases from north to south (Wright, 1955). Shoreface and shallow sea deposits east of the marine limit overlie and obscure the subglacial imprint that is prevalent elsewhere in the region (Fig. 5.4).

The subdued surface features of the study area are underlain primarily by Meso- to Neoarchean siliciclastic and, to a lesser degree, chemical sedimentary rocks which were inhomogeneously reworked

throughout tectonic assembly of the Laurentia proto-continent 2.0-1.75 Ga (Rainbird et al., 2010). The region occupies part of the central Canadian Shield, and its bedrock forms a mainland component of the Western Churchill province. Bimodal mafic to felsic volcanic rocks of the Henrik Group overlie syn- to post-tectonically emplaced Archean granites and orthogneisses of the Ennedai-Rankin greenstone belt, with rarer interspersed supracrustal rocks, comprising an inhomogeneous basement. These Archean units are locally crosscut by northeast trending Kaminak dykes, dated to 2,450 Ma (Christie et al. 1975; Sandeman et al., 2003).

Basement rocks in southern Keewatin are unconformably overlain by Palaeoproterozoic siliciclastic sedimentary rocks, predominately associated with the Hurwitz group of the Central-Hearne subdomain at ~2.1 Ga (Paul et al., 2002). The Hurwitz group is an Aphebian erosional remnant of a broad, moderately shallow, intracratonic basin, and is preserved as a thick, 4-tiered sequence of siliciclastics and carbonates, separated mid-succession by a ~200 Ma depositional lag (Aspler et al., 2001). Basal sequences in this group are comprised predominately of white quartzites which form conspicuous hills and ridges throughout southern and central Keewatin, generally paralleling strike. These lower facies, including orthoquartzite-carbonate sequences, are unconformably overlain by conglomerates and greywackes in the western portion of the study area (Eade, 1971; Aspler et al., 1994). The quartzite in these sequences is generally pure white, though rarely features a pink or purple hue, and is fine to medium grained (Lord, 1953). In places, quartzites are schistose and marked by significant mica and orthoclase constituents (Wright, 1955). It has been suggested that extensive, relatively drift-free regions bearing these resistant lithologies in the north and west may have had a modulating role on regional ice dynamics throughout the Pleistocene (and possibly earlier) glaciations by opposing and retarding flow (Goulet et al., 2009).

Though not occurring within the immediate study area, a collection of Late Proterozoic clastic and volcaniclastic formations (the Dubawnt Supergroup, comprising rocks of the Thelon and Baker Lake basins) occurs to the north and northwest, surrounding Dubawnt Lake (Wright, 1955; Donaldson, 1965). These rocks are generally unmetamorphosed and constitute the source of an enormous (>150 km wide, >800 km long) dispersal train of reddish till and distinctive erratics that mantles much of the terrain across southern Keewatin (Shilts et al., 1979; Dyke and Dredge, 1989). Red pigments in these sediments derive from finely comminuted hematite, remnant in surface tills as a pink or grey residue (Shilts, 1978). Tills of the Dubawnt dispersal train are rich in sands and silt, and differ compositionally from parent tills of central and southern Keewatin, which tend to be much less sandy (Shilts, 1977; Dyke and Dredge, 1989).

Quaternary deposits are extensive throughout the study area, with till blanket (thick/continuous) dominating over till veneer (thin/discontinuous), and comprising the dominant surficial deposit overall (Fulton, 1995). In southern Keewatin, the morphology of these deposits is expressed near-ubiquitously as subglacial bedforms, which are arranged in broad, though spatially irregular patches. East of the marine limit, bedforms are extensively terraced, and show evidence of winnowing along the crestline, with fines having been washed into adjacent depressions. Bedform fields emanate outward from a broad, ~15,000 km^2 NE/SW trending zone of low-relief, hummocky moraine surrounding Yathkyed Lake (north of the study area) that is characterized by a pronounced absence of meltwater features, and few subglacial bedforms. Elsewhere in the region, a dendritic network of long (many >100 km), sinuous eskers overprints most bedform assemblages. When not present as single features, esker ridges are commonly joined by up to fourth-order tributaries, and in places occur in association with terraced outwash, or glaciofluvial nodes (beads), fans, and ramps, suggesting subaerial and subaqueous depositional environments, respectively. Though well-formed and continuous in the western portion of the study area, eskers grow exceptionally chaotic and segmented towards Hudson Bay. Lateral

meltwater channels are rare in southern Keewatin, with proglacial and subglacial channels having dominated the deglacial drainage system. Such channels, where commonly persevered, typically show orientations that agree with the surrounding local bedform record, especially in the west, suggesting operation/formation near in time. The headward reaches of most esker assemblages are formed along the perimeter of the 'esker-less' zone surrounding Yathkyed Lake, existing here as a network of N-channels which are largely devoid of glaciofluvial infilling.

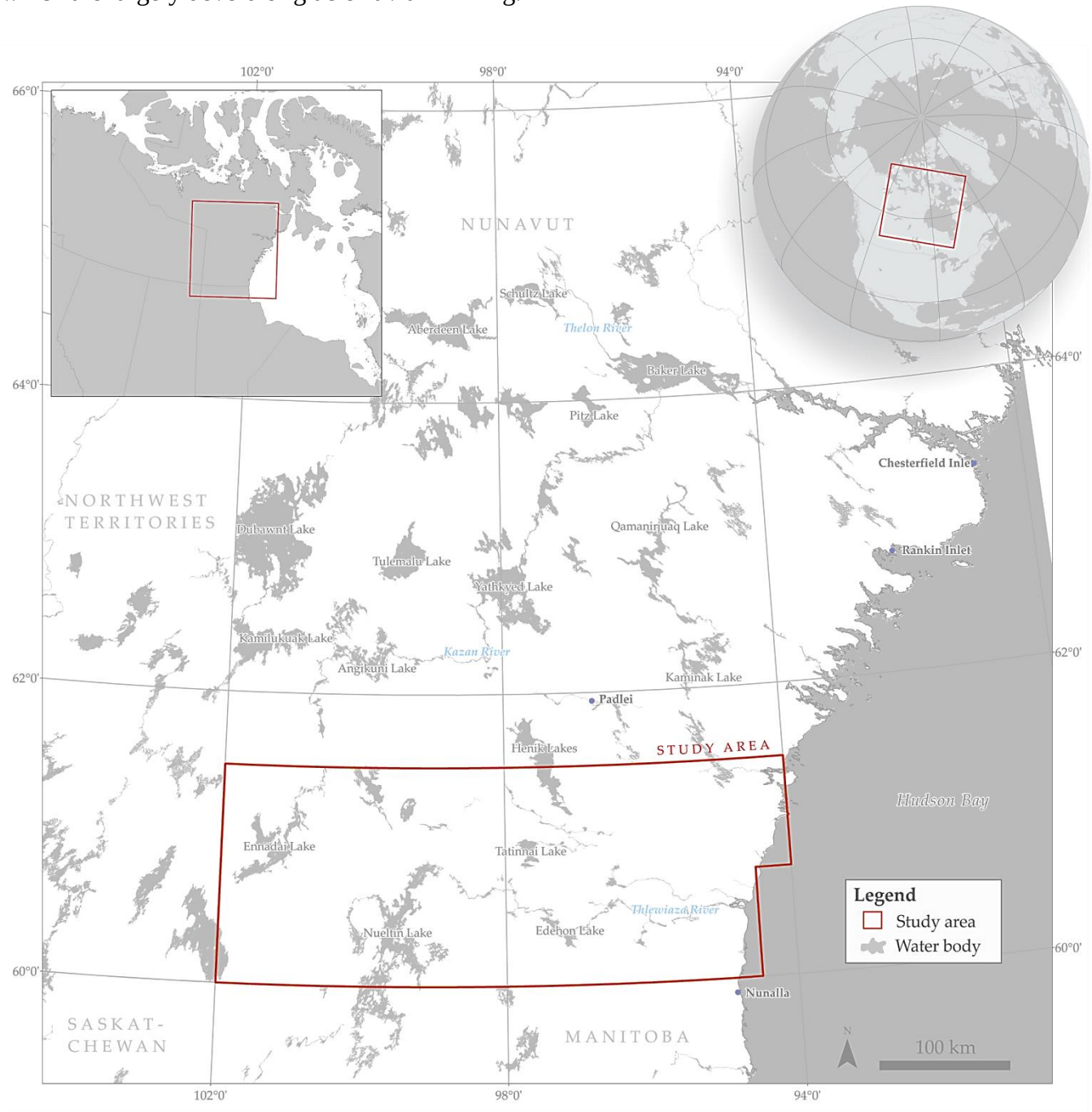

Fig. 5.1 – Map showing location of 70,600 km^2 study area in south-central Keewatin (present-day Kivalliq), Nunavut, Canada. Names of landmarks referred to in this section are indicated on the map.

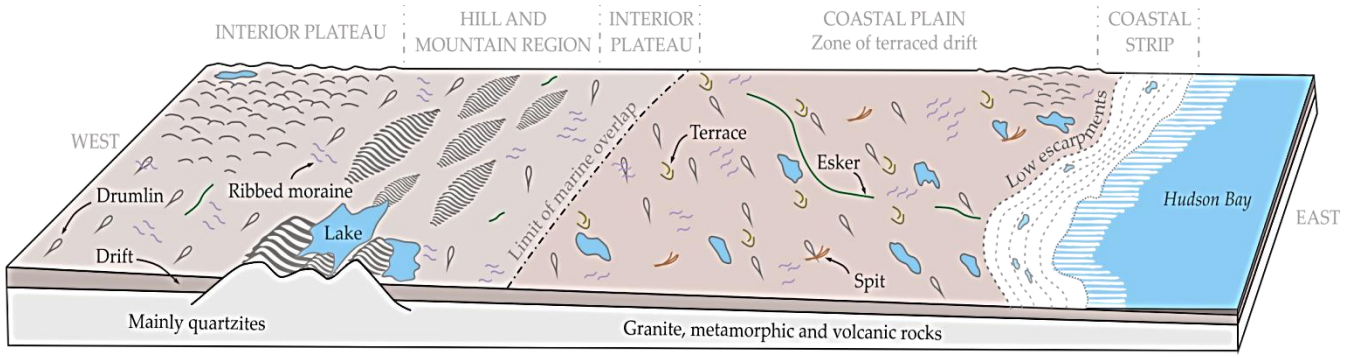

Fig. 5.2 – Physiographic divisions of southern Keewatin, showing characteristic features and topography. Exact locations of features are not shown. Re-interpreted after Lee, 1959.

The "Keewatin sector" (Prest, 1970) occupied one of the core zones of the LIS during the last glaciation (Shilts et al., 1979; Shilts, 1980; Dyke and Prest, 1987; Dyke et al., 2002). Considering the duration and thickness of ice cover in this region, understandings of its glacial history have been informed only by the relative chronology of successive ice flow events (e.g., Boulton and Clark, 1990a,b); very little absolute age constraint exists for glacial deposits in this area. Knowledge of pre-Late Wisconsinan phases, in particular, remains very weak (Dyke et al, 1989). This is in part due to the general low relief of the region and the resistance of its crystalline shield bedrock to erosion, each which precludes the formation of thick drift cover, and allows pre-existing glacial deposits to be removed by subsequent glacial activity. Accordingly, few natural sections from which to study these sediments exist within southern Keewatin, and only a handful of localities retain tills that predate the Late Wisconsinan (Shilts, 1984). Across the larger shield area, however, there is sparse documented evidence of multiple tills within the regional stratigraphy (Shilts, 1984; Dredge and Thorleifson, 1987; Dyke and Dredge, 1989; McMartin and Henderson, 2004). Of the few exposures that have been investigated within the District of Keewatin specifically, all exist north of the study area (i.e., along the banks of the Kazan and Thelon rivers near Baker Lake, in the vicinity of Kaminak Lake). Two tills with contrasting geochemical, textural and petrological characteristics are superposed in these outcrops, and do not feature intervening non-glacial/waterlain units or erosional lags. These tend mostly to be unoxidized below the upper surface, and there is also little evidence to suggest that successive units differ widely in age, implying probable continuous Wisconsinan ice cover and emplacement during shifting ice flow conditions. An alternative interpretation suggests that these sequential, though compositionally distinctive units represent primary englacial layering, once stacked as shear planes in marginal ice, and consecutively draped by downwasting/melt-out (Shilts, 1984).

During the 1970's, a series of geotechnical boreholes were drilled at ~10 km intervals by the Polargas consortium along the route of a proposed natural gas pipeline, connecting the Canadian Arctic Islands to Longlac, Ontario. Three of these boreholes from northern Manitoba and southern Keewatin revealed multiple tills separated by fluvial and/or glaciofluvial sediments. One of these, extracted about 15 km south of the Nunavut/Manitoba border, contained a minimum of two tills exhibiting contrasting geochemistry, and featuring several meters of intervening deformed gravel and till. A nearby core revealed a similar sequence of (probable) glacial diamicts, separated by organic-rich, fluvial sands (Dyke and Dredge, 1989). Boreholes drilled to the north of the study area, just west of Baker Lake, likewise contained at least two distinctive till formations separated by 2 m of waterlain sands with provenance that was distinct from overlying and underlying deposits. At this location in particular, along the perimeter of the Keewatin Ice Divide, non-glacial sediments are of tremendous significance, as their

deposition must necessarily be assigned to a full interglacial (Shilts, 1984). Whether the interglacial sediments uncovered here correlate to those from southern Keewatin and northern Manitoba has yet to be determined.

From this regional stratigraphy and field-based ice flow indicators, two dominant, high-level phases of ice flow have traditionally been recognized in Keewatin. The youngest (Late Wisconsinan) corresponds to a quasi-radial trajectory emanating from a NNE-SSW oriented Keewatin Ice Divide (KID), centered to the south and east of Dubawnt Lake, and potentially connected along a broad saddle across Hudson Bay, to an easterly center of outflow over Labrador/Ungava. An older phase, or phases, of generally southward ice flow *into* southern Keewatin has also been accepted, but is not well-placed within the chronological record.

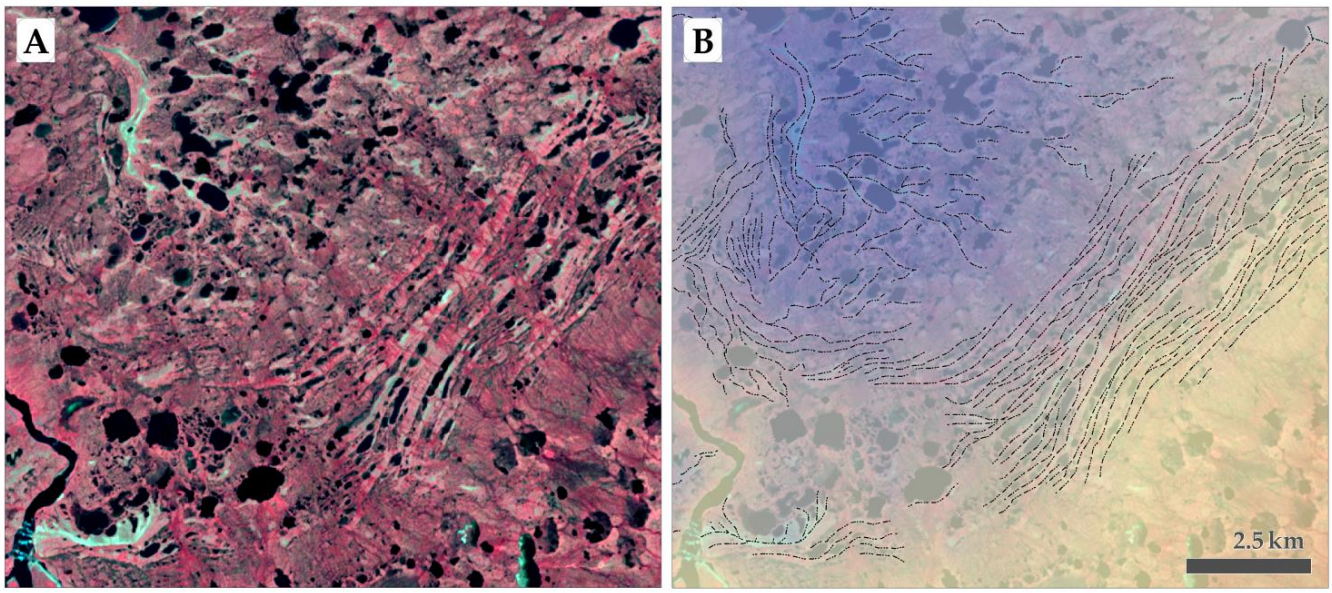

Fig. 5.3 – Strandlines, near-shore and raised marine deposits northwest of Hyde Lake. (A) Landsat 7 ETM+ 4,3,2 (RGB) FCC. (B) Annotated features with elevation transparency overlay (blue = low, yellow = high). Note the esker ramp and spit in the bottom left adjacent the lip of the depicted depression.

The earliest writings on the glacial history of Keewatin were authored by Tyrrell (1898), who described the region as one of many "gathering grounds" for ice masses around Hudson Bay throughout the last glaciation. During his epic 1893-94 survey of the 'barren grounds' (north of 59˚ latitude and west of Hudson Bay), Tyrrell encountered much physical evidence in support of this proposition, arguing that an ice sheet once "flow[ed] south-eastward and south-westward to the west coast of Hudson Bay from its névé ground in the vicinity of Doobaunt and Yath-kyed lakes" (1989, p. 92); thus Tyrrell envisioned the District of Keewatin as a dispersal center for an independent 'Keewatin Ice Sheet', reaching at its southernmost extent to the northern limit of the driftless area in the American Midwest. From his observations, Tyrrell inferred a glacial history for the region that consisted of three stages: 1) An early phase of ice flow stemming from a center of dispersal north or northwest of Dubawnt Lake; 2) A southeastward shift in this accumulation center of up to 400 km, towards the area between the Dubawnt and Kazan Rivers; and 3) A recessional phase, marked by activity from several dispersal centers, one located north of Baker Lake, the other southeast of Yathkyed Lake. As far north as Churchill, Manitoba, Tyrrell also recognized widespread signs of scouring from eastern-sourced ice, but attributed these to a local glacier that expanded westward from the Hudson Bay shoreline along the

Churchill River at the onset of the last glaciation. These are now understood to have originated from interplay between Labrador/Ungava and Keewatin sourced ice (Dyke and Dredge, 1989).

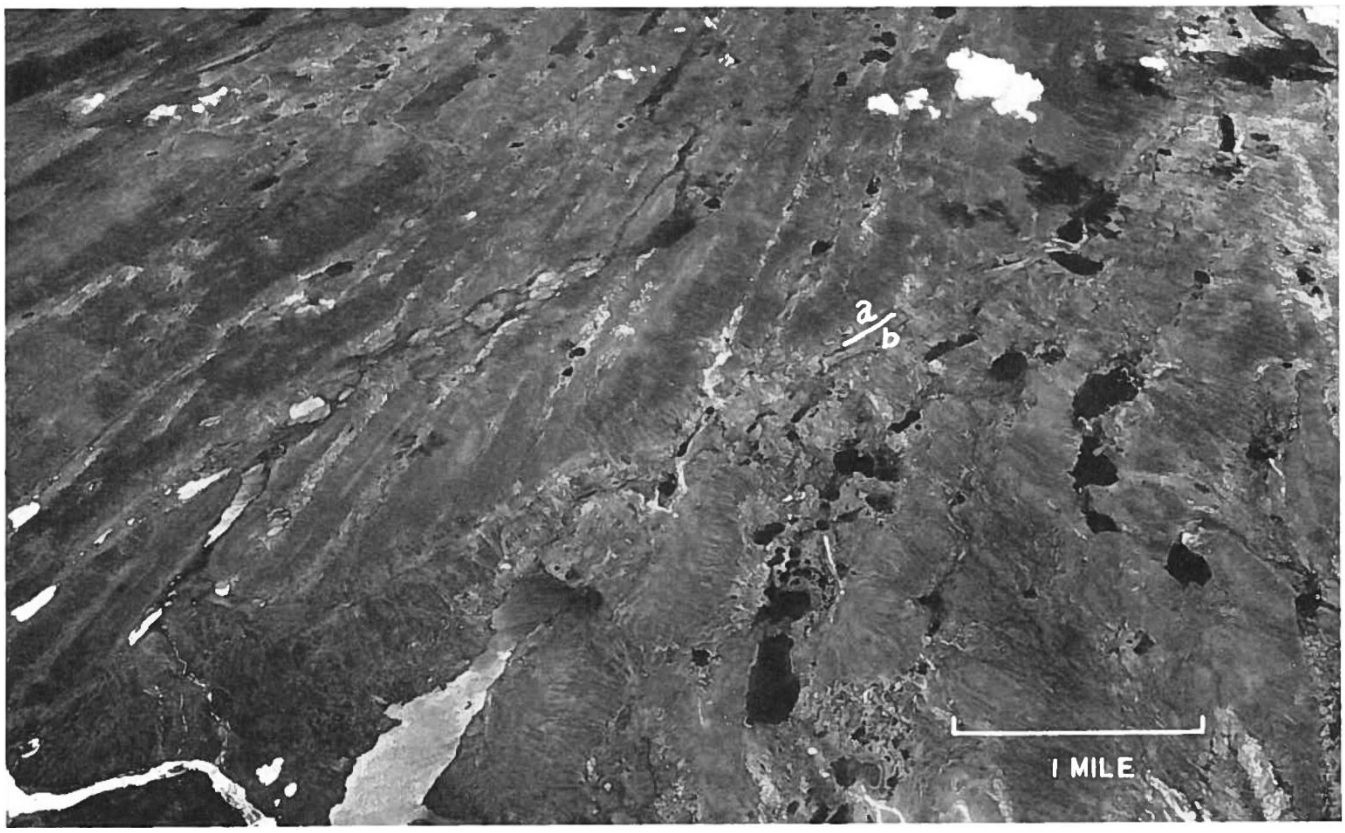

Fig. 5.4 – Oblique low-altitude aerial photograph from southeast Nunavut demonstrating the surface textural and morphological distinction between regions east (b) and west (a) of the marine limit (Plate II in Lee, 1959). Note the well preserved lineations on the west side of the figure and the gullied, wave-washed features on the right overlain by sandy and organic deposits.

Several decades later, Flint (1943) voiced opposition to Tyrrell's model of segregated domes, arguing instead that a single, cohesive ice sheet once covered northern North America; one that was incepted in the northeastern highlands of Québec, Labrador and Baffin Island, and migrated southwest during expansion such that the a "vast, continuous Laurentide ice sheet" emerged that was "thickest over Hudson Bay itself" (Flint, 1943, p. 333, as cited in Shilts et al., 1979). This idea was later upheld by Bird (1953), Dean (1953) and Taylor (1956), who concluded from aerial photographs and limited fieldwork in western and north-central Keewatin, that the most recent ice flow was radially sourced from central Hudson Bay.

This new 'single dome' interpretation was challenged by Lee (in Lord, 1953) and Lee et al. (1957), who convincingly demonstrated that streamlined glacial landforms (in particular, crag-and-tails) east of Hicks Lake, and south of Ferguson Lake, indicate southeastwardly flow *into* Hudson Bay, rather than the opposite. Associatively, indicators south of this zone were proposed to have originated from south-southwest flowing ice, whereas northwestwardly flows are recorded further west. Neil and Putnam (1955) supported Lee et al.'s observations, and contributed additional field evidence from north Ennadai Lake and Ferguson Lake to substantiate the existence of a linear partition across central Keewatin which separated former inland-flowing ice from that which evacuated into Hudson Bay. Fyles (in Wright,

1955) and Wilson (1955) argued also in favour of this partition, and perhaps more importantly, acknowledged it for the first time as a formal ice divide. Wilson (1955) further mapped extensions of this divide northwest and southeast of Yathkyed Lake, though these areas were soon after re-interpreted as 'false-divides', or zones of flow transition during migration of the primary divide (Lee, 1959), given widespread indication of parallel ice flow alongside these linear offshoots.

Set in the context of a multi-domed LIS, Lee et al. (1957) and Lee (1959) judiciously placed the KID as a late (de)glacial feature, suggesting that its apparent footprint discloses the location of the final remnants of continental ice over western mainland North America. On the basis of several ^{14}C ages obtained from marine shells south of Hudson Bay (see also Lee, 1960) these authors proposed initiation of the KID between 7 and 8 Ka BP, in conjunction with the maximum transgression of the Tyrrell Sea, and inferred its collapse by 6 Ka BP, thus implying existence of the divide for only 1-2 Ka, despite its apparently significant influence on the present-day landscape of the central Canadian Shield (cf. Shilts et al., 1987). In contrast, Dyke and Prest (1987), Dyke and Dredge (1989), and Dyke (2004) show much earlier disintegration of the divide in order to reconcile the behaviour of this sector with that of Foxe/Baffin and Hudson Bay, though also recognize its initiation much earlier in the last glacial cycle. Based largely on the reconstructed transport history of geochemical and erratic dispersal trains, later studies by Shilts (1977, 1980) Shilts et al. (1979) and Kaszycki and Shilts (1979) sought to redefine the KID as a relatively stable, long-lived featured of the LIS, rather than the transient deglacial element of Lee (1959). This latter body of work provided critical support to the 'multi-dome' LIS hypothesis, and in particular, challenged earlier models that were constructed on the basis of: 1) isostatic uplift (Andrews and Peltier, 1976); 2) multi-proxy palaeoclimatic reconstruction (Hughes et al., 1977; Andrews and Barry, 1978); 3) large-scale erosional patterns (Ives et al., 1975; Sugden, 1978) and; 4) numerical ice volume calculations (Patterson, 1976); however, little consideration was given to the behaviour of the divide itself, and thus the position of the KID was essentially inferred to be static. Based on similar understandings, Aylsworth and Shilts (1989a, p. 3) argued that "although the [Keewatin] dispersal center had migrated eastward and southward […] it probably migrated no more than 100 km." Prior to the 1990's, this concept informed several reconstructions of the LIS in this sector, which depicted the region's entire landform archive as originating only from the youngest phase of ice flow (e.g., Boulton et al., 1985).

More recently, based on cross-cutting lineation patterns identified from aerial photos and Landsat imagery, Boulton and Clark (1990a,b) provided evidence of a highly dynamic LIS, featuring a migrating (on the order of 1,000-2,000 km), transient divide over Keewatin that contributed to the generation and preservation of a stacked sequence of non-coeval landforms. Since this time, extensive ice flow indicator mapping and stratigraphic studies conducted by McMartin and colleagues of the Geological Survey of Canada (GSC) throughout central and northeastern Keewatin have provided much field evidence to support this view (McMartin and Henderson, 1999, 2004; McMartin, 2000; McMartin et al., 2003a,b; McMartin and Dredge, 2005). Emerging largely from this work, a sequence of up to seven regional ice flow phases is presently recognized in the Keewatin glacial record (Table 5.1). Notably, with respect to the oldest of these reported events, there has been some dissension among different workers, with Boulton and Clark (1990a) and McMartin and Henderson (2004) interpreting an oldest flow from the NE, as widely reported in earlier studies (e.g., Tyrrell, 1898; Bird, 1953; Taylor, 1956; Ridler and Shilts, 1974; Cunningham and Shilts, 1977), though also a subsequent flow from the N/NNW; conversely Lee (1959), Dyke et al. (1989), Dyke (2004) and Kleman et al. (2006) are reluctant to distinguish any formal separation between these stages. Perhaps most critically, the placement of these events with regard to the initiation and subsequent evolution of the KID remains unclear (Fig. 5.5). Moreoever, the chronology of subglacial bed-formation is also ambiguous in Keewatin, where sub-

marginally produced landforms (i.e., drumlins, lineations) occur in close association with ribbed moraines, which (in low-lying topography) have been traditionally interpreted as forming some distance behind the ice sheet terminus (see section 3.4). Given that the parameters controlling ribbed moraine formation have yet to be conclusively established, inferring palaeoglaciodynamic conditions from these assemblages is problematic, and thus the contiguity of these features with streamlined forms remains unexplained. Through detailed spatial and remote geomorphological analysis, this study seeks to improve understandings of controls on ribbed moraine formation in south-central Keewatin, with the goal of utilizing the distribution and morphology of these landforms to strengthen understandings of palaeoglacial dynamics in a centralized sector of the LIS, which bears a complex glacial history.

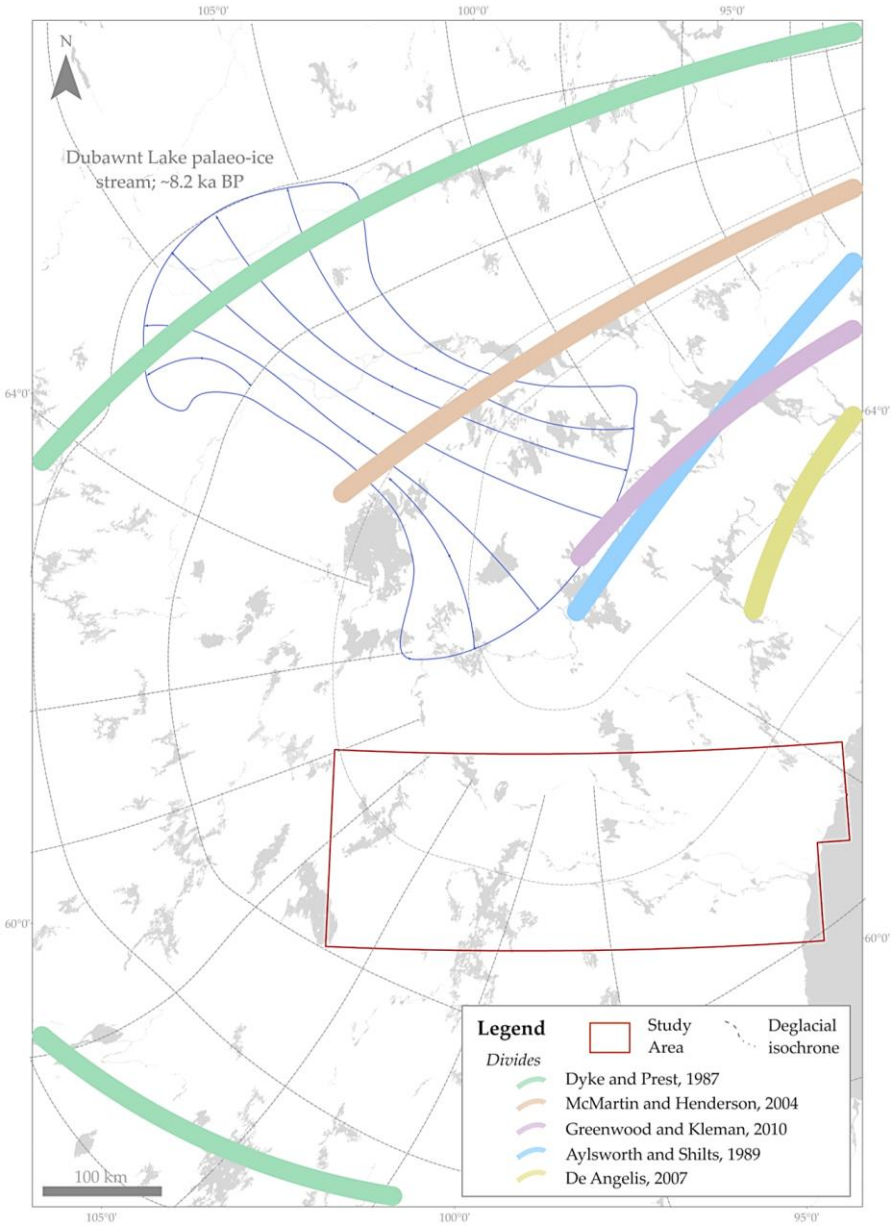

Fig. 5.5 – Previously-proposed locations of the final position of the Keewatin Ice Divide with respect to the study area. Deglacial isochrones from Dyke and Prest (1987) palaeogeographic maps. Outline of the deglacial (~8.2 Ka BP) Dubawnt Lake palaeo-ice stream track (after Stokes et al., 2013b) shown in blue. Adapted from Greenwood and Kleman, 2010.

Table 5.1 – Generalized sequence of ice flows known from Keewatin, primarily derived from McMartin and Henderson (2004).

Flow stage	Cardinal flow direction(s)	Ice Divide		Notes
		Position	Trend	
A	SW	Northeast Keewatin	?	Flow phase predating LGM; development of an early center of outflow in northeast Keewatin or Baffin Island (Boulton and Clark, 1990a), or the Melville and Boothia Peninsulas (Kleman et al., 2002)
B	SSE south of Schultz Lake and east of Tehek Lake; above this, NNW	Crossing Wager Bay, between Committee Bay and Rankin Inlet	WSW -- ENE	Southward expansion of ice across central Keewatin; migration of divide into northern Keewatin
C	ESE	West of Keewatin	NNE--SSW	Early advance of westwardly-sourced ice into Keewatin; likely of pre-LGM, middle-Wisconsinan age
D	SE	?	?	Major erosional phase; responsible for E and SE transport of Dubawnt clasts across central Keewatin
E	S and SE	East-central Keewatin	NE--SW, sinuous	Widespread flow reversal and divide migration by up to 250 km; southeastward rotation of bottom divide region; possible activation of the Dubawnt Lake Ice Stream and triggering of rapid drawdown in response to ice collapse over the Hudson Strait
F	E and SE to W and NW	East-central Keewatin	NE--SW	Retreat of ice to the Chantrey Moraine System and the McAlpine Moraine by ~8.2 Ka BP; associated shut-down of Dubawnt Lake Ice Stream; convergent deglacial flows to the E and SE
G	E-SE-S-SW-W; radial flow around bottom of divide	Central Keewatin, over Pitz, Yathkyed and Western Baker Lake	NE--SW	Expansion of marine calving activity into Hudson Bay; ~100 km shift of divide to NW between ~8 and 7 Ka BP; after 7 Ka BP, bifurcation of divide into two masses N and S of Chesterfield Inlet and incursion of Tyrrell Sea into Thelon River basin before 6.5 Ka BP

5.3 *Methodology*

5.3.1 **Data Products & Sources**

A total of 6 Landsat 7 ETM+ (scan-line corrector on) and 33 SPOT 4/5 HRV-IR/HRG scenes covering south-central Keewatin (Fig. 5.10) were freely obtained from the Canadian Geobase portal (www.geobase.ca) and the NASA/USGS EarthExplorer utility (http://earthexplorer.usgs.gov/), and imported into Exelis ENVI 5.0 for processing. Where multiple scenes were available, those featuring low or localized (<10%) cloud cover, and/or acquired during the winter season at low solar declination were preferentially selected (cf. Smith and Wise, 2007) (Fig. 5.6). SPOT data available through Geobase are provided as georectified orthoimages; sources of planimetric data used in this georectification process are assigned the following priority: (1) The Control Points for Landsat 7 Imagery, Canada, Level 1 (PCILC1); (2) The National Road Network (NRN); and (3) Landsat 7 Orthorectified Imagery over Canada (also available through Geobase). Canadian Digital Elevation Data (CDED) is also used in georectification in certain regions, with the highest quality (most precise) tiles being assigned priority. SPOT 5 (HRG) panchromatic band imagery acquired nominally at 5 m spatial resolution by the detector is resampled to 10 m in order to maintain consistency with SPOT 4 (HRV-IR) datasets, which is hosted also as part of the 'Geobase Orthoimages 2005-2010 over Canada' collection.

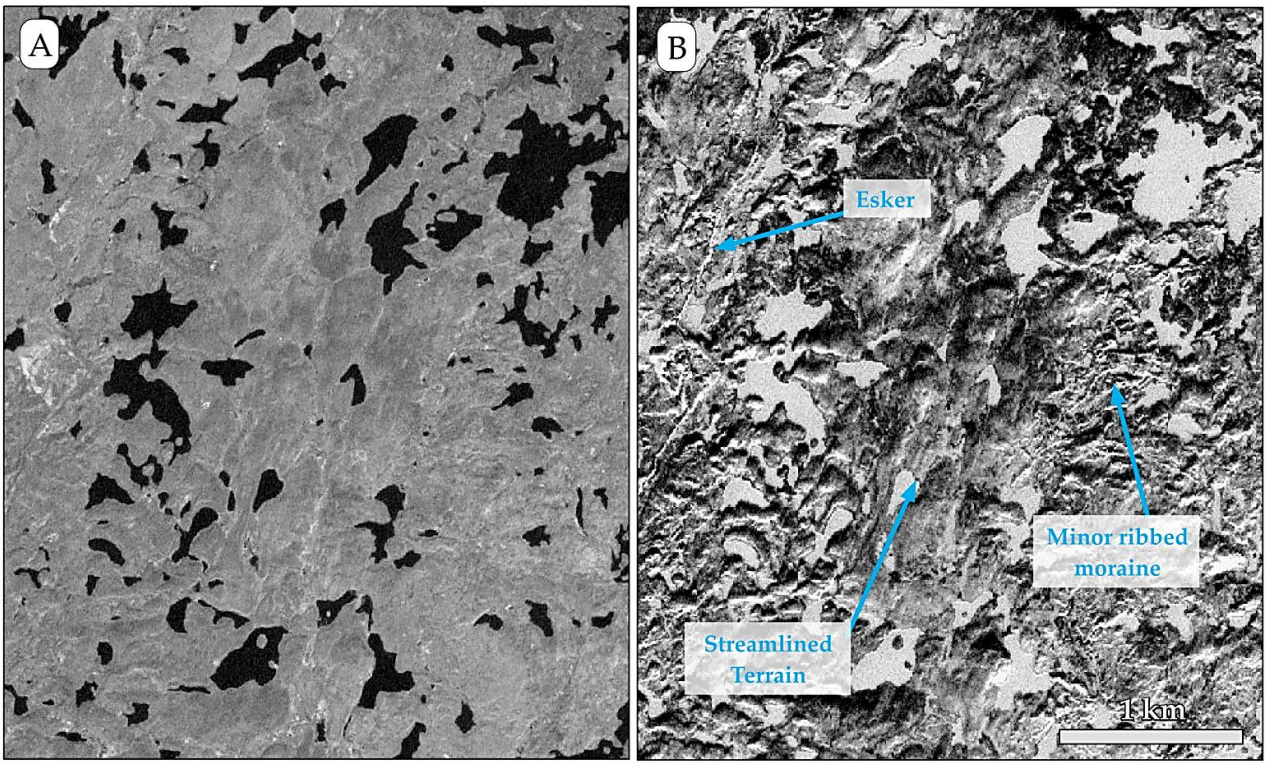

Fig. 5.6 – The effect of solar biasing on glacial landform identification. (A) Landsat 7 ETM+ panchromatic band 8 sub-scene acquired from southern Nunavut during the summer season at high solar declination. (B) Landsat 7 ETM+ panchromatic band 8 sub-scene from the same WRS-2 path/row as (A), but acquired during the winter season under light snow cover and low solar declination. Ice flow is from top right to bottom left. Note the increased detail (shadow, contrast) available in winter imagery over summer imagery, which provides optimal conditions for the detection of glacial landforms. Orthogonal illumination with respect to transverse features permits better detection than for streamlined forms, which in this image are illuminated along a parallel.

Individual Landsat 7 ETM+ scenes cover an area of approximately 170 km north-south, by 183 km east-west, whereas single SPOT footprints cover 60 x 60 km. Spatial resolutions range from 15 m (panchromatic) to 60 m (thermal IR), with 30 m in VNIR bands for Landsat data. Only monospectral (10 m) and panchromatic (10 m, resampled) HRV-IR/HRG data were utilized from the SPOT sensors. Relevant characteristics of the platforms and the sensor bands employed in this study are shown in Table 5.2. A variety of Landsat multi-spectral band combinations were experimented with prior to mapping in order to determine those which enabled the best detection of targets (Fig. 5.7). In agreement with Jansson and Glasser (2005), a 4,3,2 (RGB) VNIR false-colour composite (FCC) utilizing the near-infrared band was found to be most optimal, though alternative configurations (e.g., 7,4,2; 5,3,1) were also employed within limited areas. All subsequent image processing (e.g., statistics and pyramid building) was conducted within ESRI ArcMap 10.1.

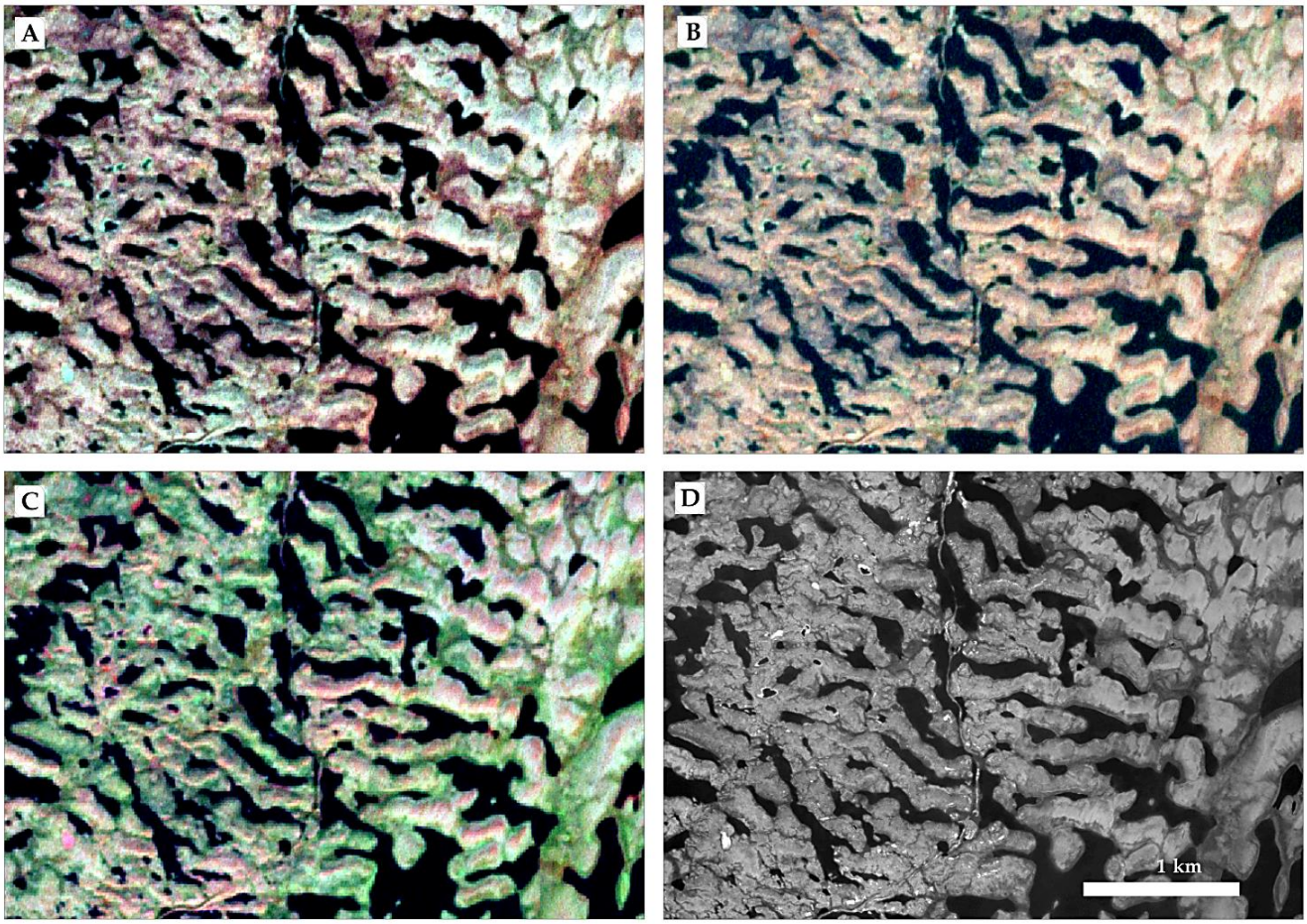

Fig. 5.7 – Examples of ribbed moraines south of Ennadai Lake depicted using various multi-spectral band combinations. All Landsat ternary images have been pan-sharpened using ETM+ panchromatic (15 m resolution) band 8. (A) Landsat 7 ETM+ 4,3,2 (RGB) FCC of visible and near infrared bands. (B) Landsat 7 ETM+ 5,3,2 (RGB) FCC of visible and mid-infrared bands. (C) Landsat 7 ETM+ 7,4,2 (RGB) FCC of infrared, near-infrared and visible bands. (D) SPOT 5 panchromatic image (10 m resolution).

Table 5.2 – Characteristics of the platforms and sensors from which imagery was derived for mapping purposes in this study.

Sensor/Platform	Platform Altitude (km above datum)	Sensor Inclination	Orbit		Revisit Period	Swath	Band	Wavelength (μm)	Resolution (m)
			Period	Type					
Landsat 7 ETM+	705	98.22	98.83	sun-synchronous, polar	16 days	185 x 170 km	Band 1 (Blue)	0.45-0.52	30
							Band 2 (Green)	0.52-0.60	30
							Band 3 (Red)	0.63-0.69	30
							Band 4 (Near-IR)	0.77-0.90	30
							Band 5 (SW-IR)	1.55-1.75	30
							Band 6 (TIR)	10.40-12.50	60 * (30)
							Band 7 (SW-IR)	2.09-2.35	30
							Band 8 (Panchromatic)	0.52-0.90	15
SPOT 4 HRV-IR	822	98.7	101 min.	sun-synchronous, polar	26 days	60 x 60-80 km	Monospectral	0.61-0.68	10
SPOT 5 HRG	822	98.7	101 min.	sun-synchronous, polar	26 days	60 x 60-80 km	Panchromatic	0.51-0.73	10**

*ETM+ Band 6 (thermal infrared) is acquired nominally by the sensor at 60 m resolution, though imagery processed after February 25, 2010 has been resampled to 30 m.
**SPOT 5 HRG data is acquired at nominal 5 m resolution (2.5 m in supermode), though is resampled to 10 m for distribution through Geobase.

Additionally, 186 1:50,000 CDED tiles were freely acquired from the Canadian Geobase portal and imported into the GIS environment to support mapping from the optical datasets. CDED tiles are derived from 1:50,000 and 1:250,000 (depending on desired resolution) digital source data, which is extracted from hypso- and hydrographic attributes of the Canadian National Topographic Database (NTDB), alongside various contributions from provincial governments. Each CDED tile represents either the eastern or western half of a single National Topographic System (NTS) map sheet. For the 1:50,000 products (used here), spatial resolution varies with latitude from 0.75 to 3.00 arc-seconds. Data preprocessing, including mosaicking, pyramid building, and histogram/statistical calculations were completed within ESRI ArcMap 10.1. Relief-shaded surfaces were generated for the study area using low declinations (25-45˚), vertical exaggeration between 3x and 7x, and multiple orthogonal illumination azimuths (cf. Smith and Clark, 2005). All geospatial data, including satellite imagery and DEMs, were projected to Universal Transverse Mercator (UTM) Zone 14 N prior to manipulation.

Following Hillier and Smith (2008), continuous residual relief raster surfaces were derived, in iteration, by processing each mosaicked DEM tile using an *n* x *n* mean filter. DEMs were first passed with a 3 x 3 sliding window in order to correct for the integer quantization of the CDED data (cf. Broscoe et al., 2011) by recomputing a neighbourhood mean to be stored as a floating point value within each grid cell. A second raster was then computed using a coarse filter (e.g., 18 x 18 – 24 x 24, depending on local relief) sliding window, generating a surface which approximated the regional-scale relief. Subtracting the coarse- from the fine- mean filtered dataset using raster mathematics yielded a residual surface exclusively representative of local-scale relief (i.e., with the contributions of 'regional' topography effectively removed) (Fig. 5.11). Subsequent linear stretching of the residual relief histogram prevented issues with value saturation and enabled better visualization of low relief landforms. Particularly with respect to ribbed moraines, mapping from optical remote sensing data alone (e.g., VNIR satellite imagery) is heavily biased towards detection of landforms with submerged inter-crestal troughs (Dunlop and Clark, 2006b). Mapping with support from a residual relief surface proved useful in several regions (Fig. 5.8), and in particular, significantly aided in the detection of landforms which could not be distinguished by spectral contrast with intervening/surrounding water bodies. This method, however, was ineffective in areas of relatively low relief (i.e., much of the eastern portion of the study area) where data artefacts are abundant, and where the digital surface fails to accurately characterize terrain (Fig. 5.9).

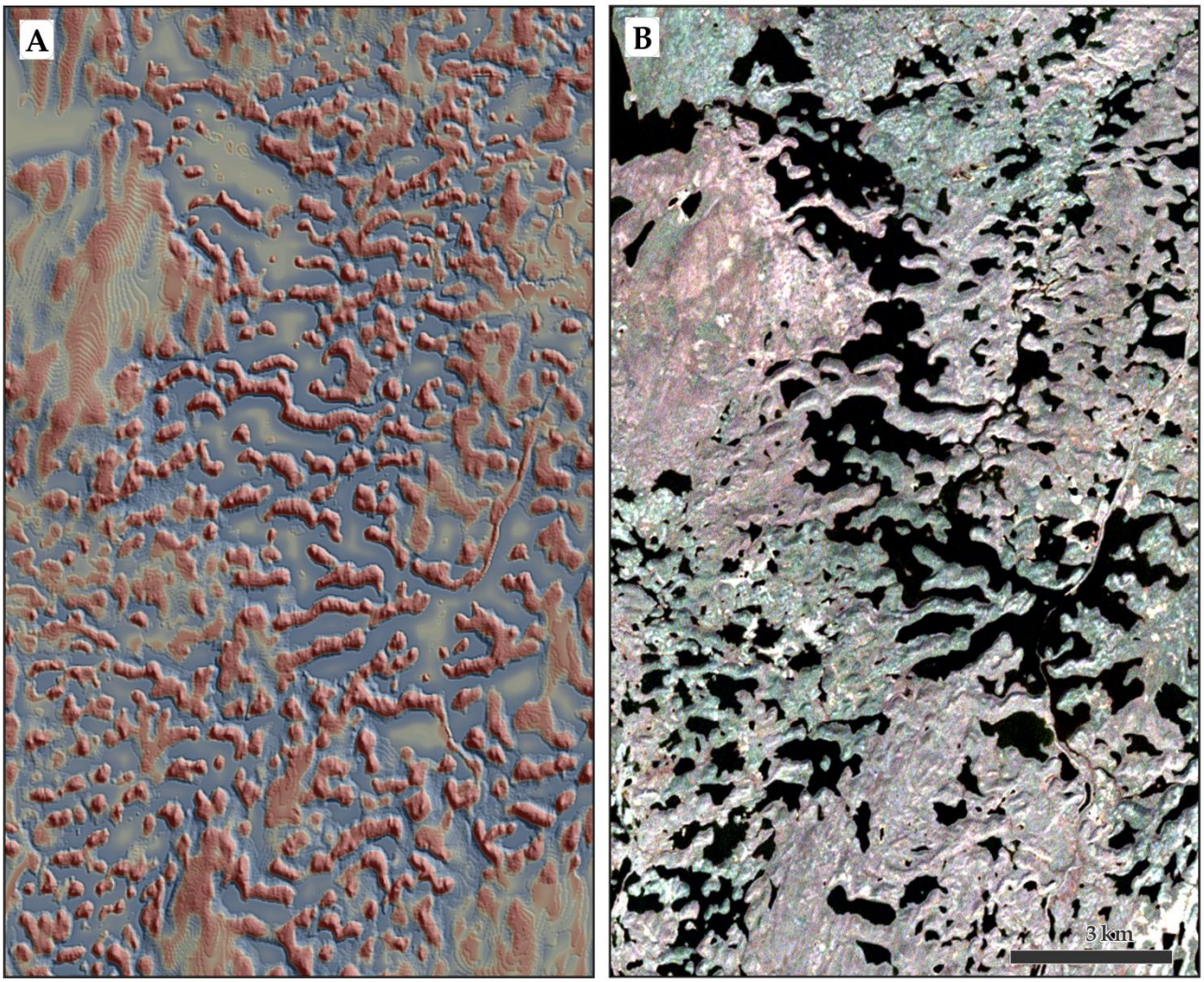

Fig. 5.8 – Examples of data products deemed suitable for remotely mapping glacial landforms in the western portion of the study area. (A) Derived residual relief surface visually-fused with a hillshaded 0.75 arc-second CDED DEM (illumination 45˚, declination 25˚). (B) Landsat 7 ETM+ 4,3,2 (RGB) FCC sub-scene of the same area displayed in (B). Greater local relief and the absence of wave-washing west of the marine limit permit the detection of glacial landforms from moderate-resolution elevation data and its derivatives.

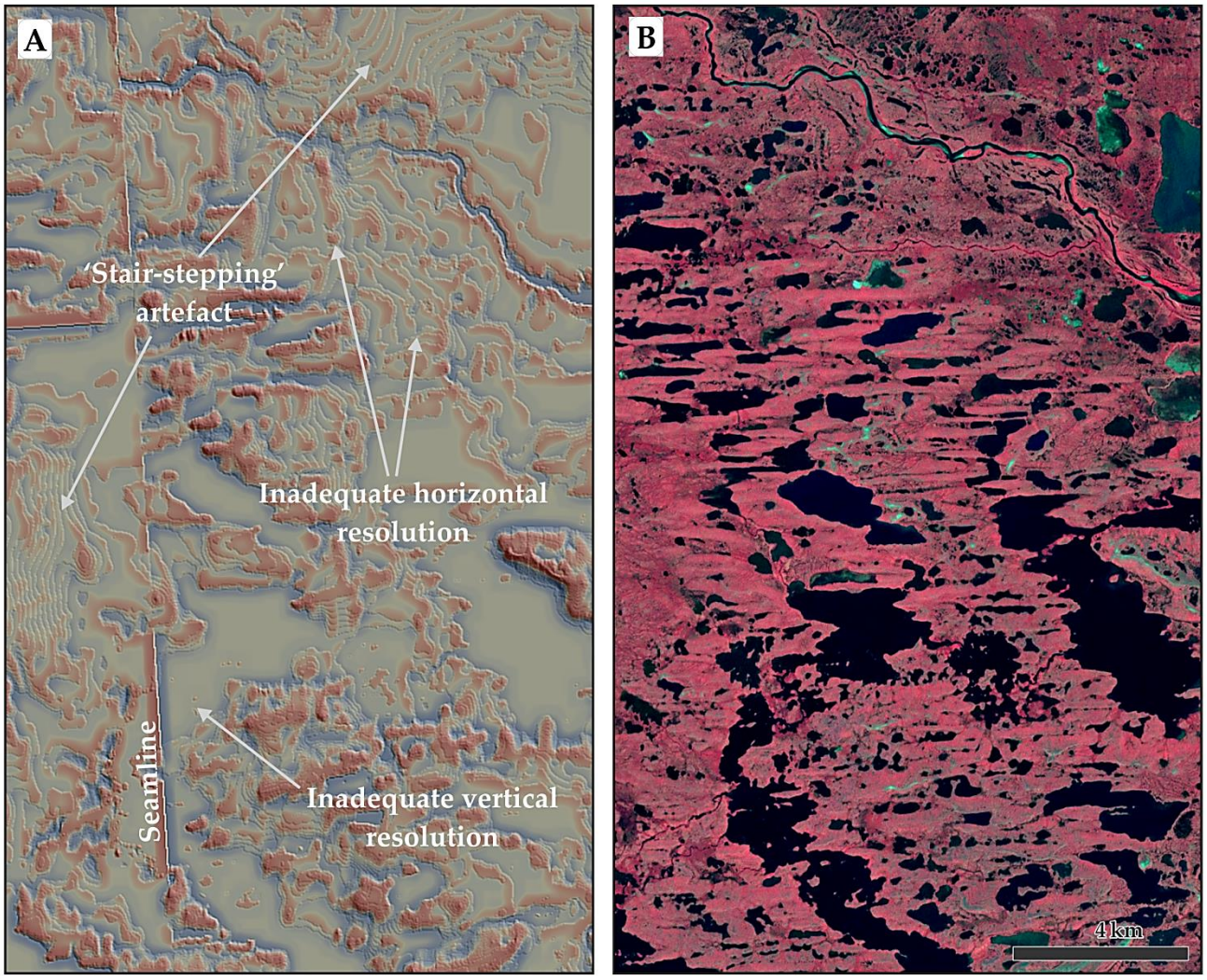

Fig. 5.9 – An example of inadequacies in a CDED DEM for mapping glacial landforms east of the marine limit within the study area. (A) Derived residual relief surface visually-fused with a hillshaded 0.75 arc-second CDED DEM (illumination 45˚, declination 25˚). Note the prominence of 'stair-stepping' artefacts on gentle slopes resulting from errors in CNTD digitization/conversion. Seamlines appear conspicuous along tile boundaries in areas of modest local scale relief. The CDED DEM is incapable of (horizontally) resolving small, clustered lineations and (vertically resolving) irregular, low-elevation surfaces. (B) Landsat 7 ETM+ 4,3,2 (RGB) FCC sub-scene of the same area displayed in (B).

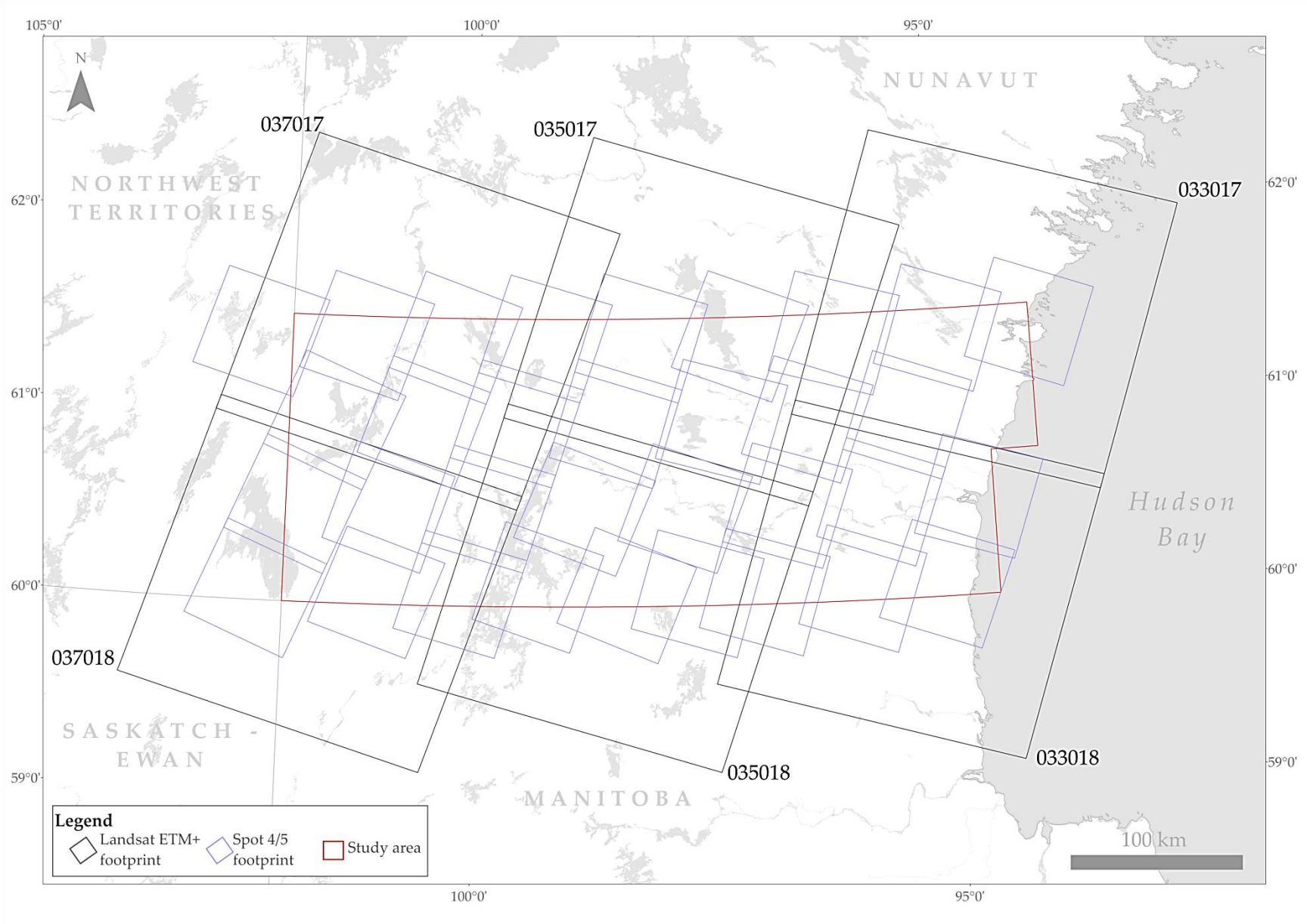

Fig. 5.10 – Landsat 7 ETM+ and SPOT 4/5 satellite images used for glacial geomorphological mapping in the study area. Landsat WRS-2 path/row identifiers are indicated for each ETM+ scene footprint.

5.3.2 **Geomorphological Mapping**

Comprehensive mapping of glacial landforms within south-central Keewatin was conducted in ESRI ArcGIS 10.1 by systematic heads-up digitization using the data sources listed in section 5.3.1. Given their superior spatial resolution, SPOT 4/5 HRV-IR/HRG scenes constituted the primary data source during the mapping process, though pan-sharpened Landsat 7 ETM+ FCCs were also regularly employed, especially when distinctive surficial composition or vegetation cover was available to aid in landform detection (e.g., esker ridges). CDED DEMs and their derivatives (e.g., hill-shaded and residual relief surfaces) proved relatively less suitable for mapping in the region, given the generally low-relief of the study area and the low resolution of these datasets, though remained useful, in particular, west of the marine limit, where primary landform morphologies are best preserved (see Fig. 5.4, Fig. 5.8 and Fig. 5.9). A number of ancillary data sources were also consulted in order to ensure that all mapped features could be confidently assigned to a glacial origin (e.g., to avoid the mapping of bedrock structure). These sources included a series of surficial geological maps, compiled chiefly from aerial photos, by Aylsworth and colleagues of the GSC throughout the 1970's and 1980's (Aylsworth et al., 1978, 1979, 1986, 1990; Arsenault et al., 1980; Aylsworth, 1986a,b, 1989a,b). These maps differentiate till (blanket, veneer), glaciofluvial material, glaciolacustrine deposits, glaciomarine deposits, alluvium, organic sediments, present-day water bodies, and outcropping bedrock. All consulted surficial geological maps were converted to digital image files and stored as raster datasets within a geodatabase; these were then georeferenced and projected to UTM Zone 14 N to facilitate rapid comparison with digitized features in the GIS environment. Checks were also made against bedrock geological maps (Paul et al., 2002), which contained greater detailed information on bedrock structure and lithology. Lastly, continuous reference to published literature throughout all stages of the mapping process provided an additional level of quality assurance and support.

Separate categories of landforms were digitized individually as vector layers after visual interpretation (e.g. Clark, 1997) and stored as shapefiles within a geodatabase. To facilitate internal referencing while mapping, a grid consisting of 226 cells (each 23 x 15.5 km) was superimposed on the RS datasets. Mapping benefited from multiple passes and was completed systematically, landform type by landform type, column by column, mapping east-west across the projected grid. Though the focus of this investigation concerns ribbed moraine morphology and distribution, two additional landforms were mapped in order to permit thorough examination of the relationships between all features; these included undifferentiated glacial lineations (drumlins, flutings, crag-and-tails, mega-scale glacial lineations) and eskers. All features were stored as polylines. A subset of ribbed moraine ridges (n = 200) were also digitized as polygons in order to permit assessment of their width based on convex-hull minimum boundary geometries (see section 5.3.3). Landforms were identified and mapped at a variety of scales, ranging from ~1:10,000-1:100,000, in order to avoid any scale-bias in their detection.

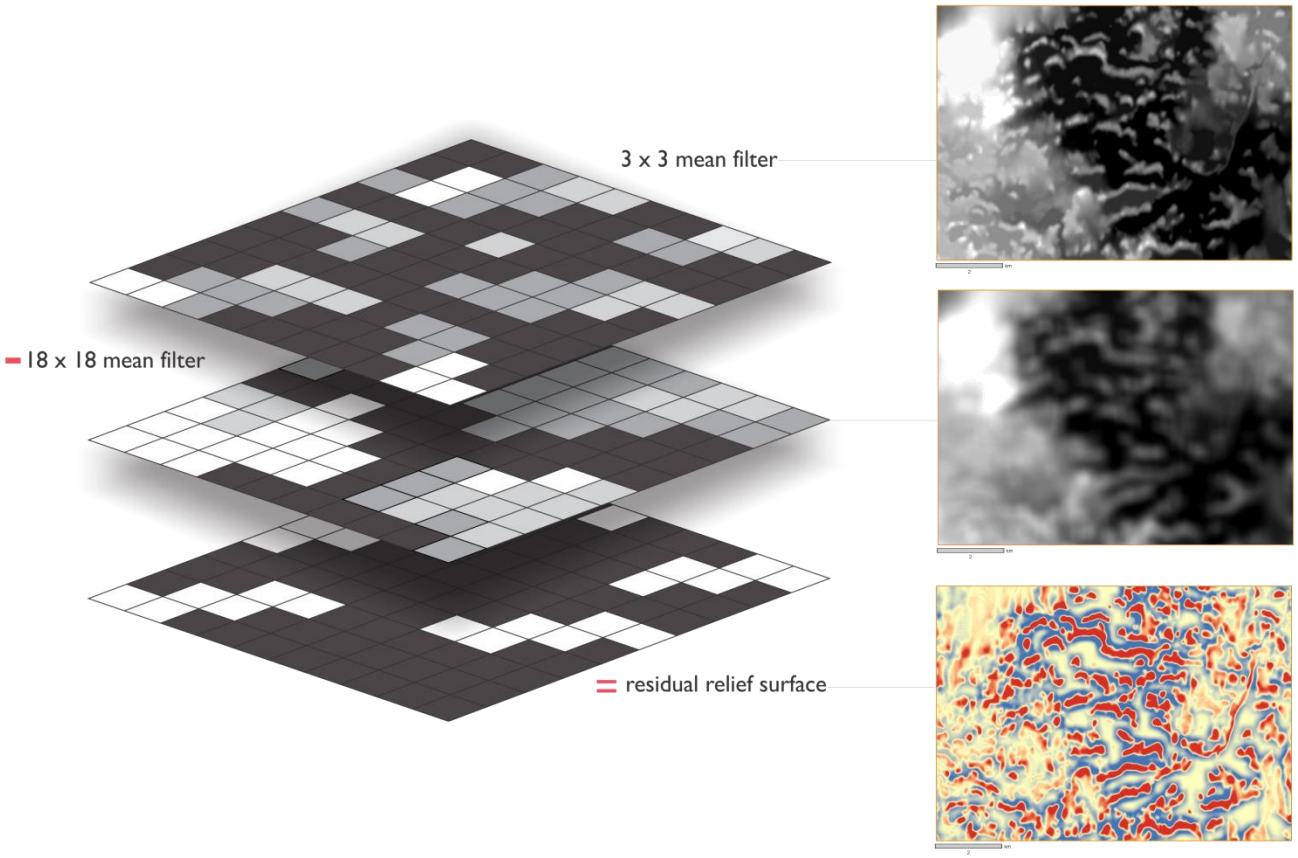

Fig. 5.11 – Schematic diagram illustrating the procedure employed to generate a residual relief surface for south-central Keewatin. A coarse-resolution DEM is subtracted from a fine-resolution DEM after each having been passed by a moving-window mean filter. The residual relief surface is subsequently subjected to a linear histogram stretch in order to eliminate saturation of relief values.

5.3.3 **Morphometric Analyses**

Quantitative analysis of ribbed moraine landforms identified from RS datasets required that each instance was stored as a feature with a unique numeric identifier (e.g., an object ID in ArcGIS 10.1). Attribute values (see Table 5.3 for list and definitions) were then captured and stored using an assortment of GIS workflows. Length values were procured directly from the ribbed moraine attribute table; processes for obtaining the remaining morphometric measurements are detailed below.

Individual widths were retrieved from a sample of 200 ribbed moraine ridges within south-central Keewatin. A grid comprised of 200 cells (20 x 10) was constructed and overlain on the study area, and a single landform sampled from within each cell to prevent geographic bias in selection. In instances where cells did not contain a single ribbed moraine landform, the nearest feature was sampled from a contiguous cell. Sampled ridges were digitized on-screen as polygon features. Upon digitization of 200 ridges, a new polygon feature class of convex hulls was created from the original ribbed moraine polygons, and the width attribute used to approximate the true width of the landform. Given that this measurement is derived from the convex hull, it represents the cross-sectional distance at the widest point along a ridge's longitudinal profile.

Table 5.3 – Definition of attributes calculated for ribbed moraine features.

Attribute	Definition
Length	Calculated as the cumulative distance of the polyline longitudinally overlain on the ridge crestline
Width	Approximated from the width of a convex hull derived from digitized ribbed moraine polygons
Height	Calculated by subtracting the minimum from the maximum elevation value along a transect spanning one break of slope to another, perpendicular to the ridge long axis, across the approximate center point of the ribbed moraine
Wavelength	Calculated as the distance of a single straight line extending from the center point of one ridge crest to the center point of a proximal ridge crest within the same field

Employing the same sampling grid described for ribbed moraine width, 200 ribbed moraine ridges were selected from within the study area in order to determine their height above the surrounding terrain. This process involved carefully constructing transects from proximal to lee side breaks of slope, across the short-axis of each ridge at its approximate longitudinal midpoint. Elevation data were then extracted from DEMs along each transect and exported for processing. The integrity of each transect was checked by plotting cross-profiles as scatterplots and viewing each graphically on-screen. Ribbed moraine height was then approximated by subtracting the minimum from the maximum elevation along the transect.

As a means of examining the wavelength (down-ice, crest-to-crest distance) of ribbed moraines in south-central Keewatin, line features were manually digitized from crestline to crestline, at an angle ~90° to ridge long axes, using edge-to-edge snapping between polylines of the ribbed moraine feature class. Wavelengths were assessed within "tracts", essentially involving the construction of segmented transects down individual flowlines within narrow, linear zones. Along single flowlines, wavelengths were found to exhibit very little variance. Measurement lengths were subsequently obtained directly from their attribute table and exported for further analysis. In total, 1,300 measurements were collected. Measurements were taken from all cells of the 20 x 10 sampling grid (see above) in order to ensure representation throughout the study area.

In addition to the numeric morphological attributes stored for each feature (detailed above), an azimuth field recording individual long axis orientations of lineations and ribbed moraines was calculated using the following custom Python script:

```
azimuth = 180 + math.atan2((!Shape.firstpoint.X! – !Shape.lastpoint.X!), (!Shape.firstpoint.Y! –
!Shape.lastpoint.Y!)) * (180 / math.pi)
```

For the ribbed moraine feature class, an additional `text` field was created to store morphological classification type and was subjectively populated during each instance of digitization. A total of 14 plan-view morphologies are recognized according to a classification scheme modified from Dunlop and Clark (2006b) (Fig. 5.12; see section 5.4.1 for a descriptions). Though developed to describe ribbed moraines in Nouveau Québec/Labrador, Sweden and Ireland, the categories utilized in this scheme were deemed effective (after modification) for differentiating between ribbed moraine plan-view morphologies in south-central Keewatin.

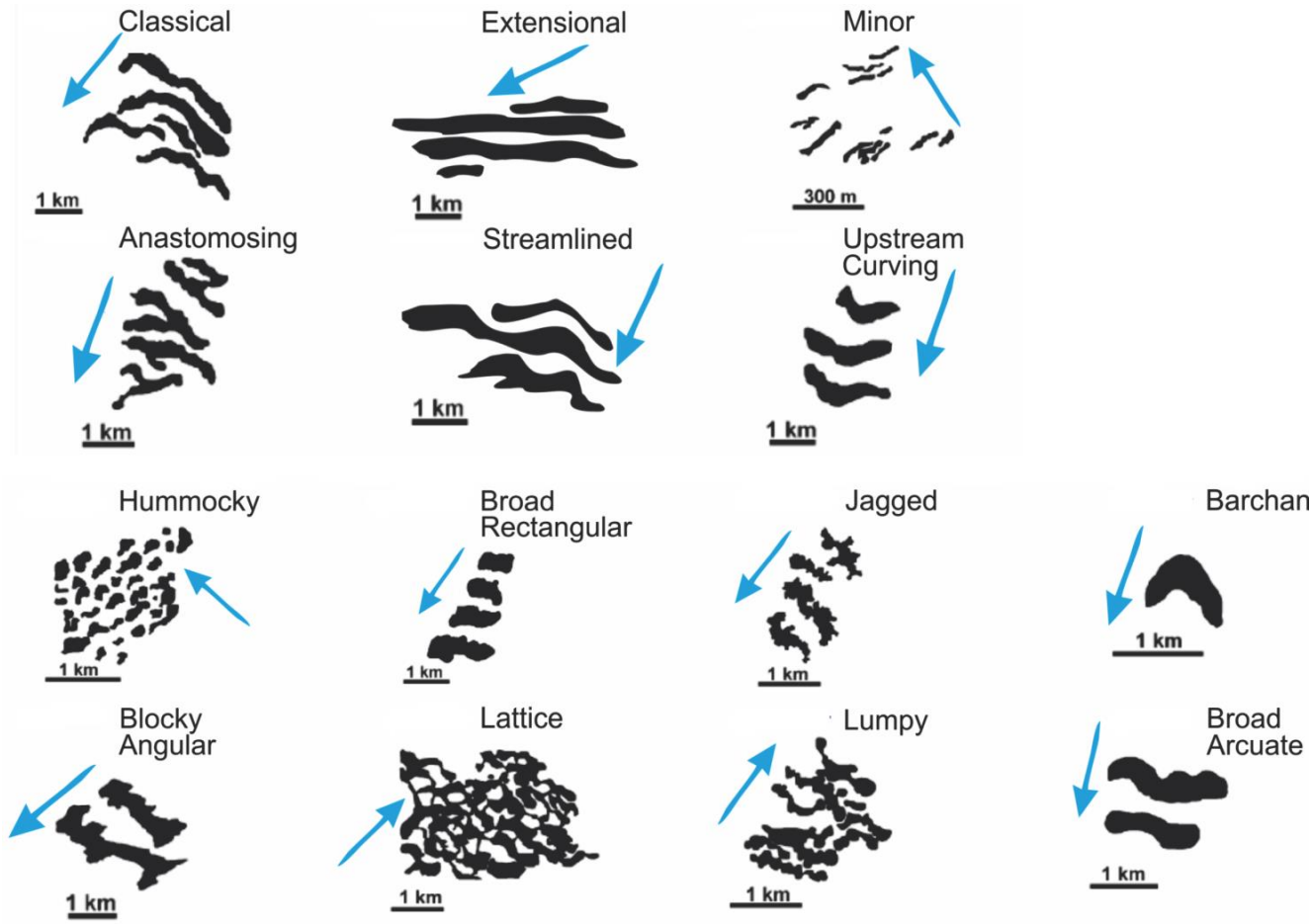

Fig. 5.12 – Classification scheme used to assign mapped ribbed moraines to specific morphological categories. Blue arrows indicate direction of ice flow with respect to ridge form. See discussion in section 5.4.1 for descriptions of each morphology. Adapted and modified from Dunlop and Clark (2006b).

5.3.4 **Multivariate and Cluster Analyses**

5.3.4.1 ***Principal Component Analysis***

Principal component analysis (PCA) is a variable reduction procedure that is most often used as an exploratory tool when dealing with datasets of large dimension. When many related variables exist within a dataset, PCA eliminates redundancy by reducing the overall number of variables through the derivation of new components (principal components, PCs) which are linear combinations of the optimally-weighted existing variables. Principal components can be manipulated to form composite axes which maximize the overall distance between individual data points by encompassing the greatest possible percentage of the total variance in a dataset. Alternatively stated, PCA determines the net effect of each variable on the total variance of the dataset, and then selectively extracts the maximum variance possible from the data, and in the process, deemphasizes redundant variables and reduces multicollinearity (Johnson and Wichern, 1992).

In PCA, the number of components extracted is equivalent to the number of variables input into the analysis, however in most investigations, only the first several components will account for a

meaningful amount of the total variance, and hence only these components are retained for further analysis. By definition, the first component (PC1) extracted in PCA accounts for the greatest proportion of the total variance in the observed variables, and generally implies that this PC will be correlated (either positively or negatively) with at least some (probably many) of the observed variables input into the analysis. The second component (PC2) extracted in PCA accounts for the maximum variance in the data set that was not accounted for by PC1, and this typically implies that variables showing strong correlation with PC2 will not be correlated with PC1. PC1 and PC2 (and all components) are technically orthogonal eigenvectors, implying that correlation between any two PCs is equal to zero. The amount of total variance each eigenvector accounts for is its eigenvalue, and this decreases progressively with the generation of each new mutually orthogonal component. The projection of each variable on a component axis is referred to as its *loading*, whereas the projection of each treatment (e.g., in this case, ribbed moraine morphology) in the new axis space is referred to as its *score* (Johnson and Wichern, 1992). In the present study, PCA is conducted in the SPSS 21 software package and used as the first step in a sequence of procedures for categorizing the 14 ribbed moraine morphologies identified and mapped in south-central Keewatin (see section 5.3.4.1 above) into objective groupings (referred to herein as "morphotypes") based on 10 metrics (variables) which are derived from each morphology's calculated length-frequency distribution (section 5.4.1.6).

5.3.4.2 ***Hierarchical Cluster Analysis***

Cluster analysis is a method for ordering discrete items/entities in a dendrogram, where entities with the highest correlation are grouped together, and those with low correlation are spaced more widely apart. Broadly speaking, *hierarchical* cluster analysis (HCA) is a form of *agglomerative* cluster analysis, in that items begin as individuals (*n* clusters) which are sequentially combined until a single cluster is formed, as opposed to *divisive* procedures which begin at 1 cluster and produce *n* clusters through partitioning. In an HCA algorithm, after a distance matrix has been calculated between all inputs, two entities with the highest correlation in a dataset are merged together to form a single "synthetic" entity. The remaining items in the dataset are then scanned for the highest correlation with the synthetic entity, and the process is iterated until all items are merged to form the single "trunk" of the dendrogram. Correlations among individual items and the synthetic entity at each step in the algorithm are expressed on the dendrogram using one of several distance indices.

In this thesis, HCA is performed on the PCs derived in an earlier procedure (i.e., Hierarchical Clustering of Principal Components, HCPC) in the SPSS 21 software package, and used as a means to classify a large number of ribbed moraine morphologies into a smaller number of more meaningful morphotype clusters which may potentially express underlying genetic similarities. Distances are conceptualized using Ward's minimum variance method which, at each step in the clustering algorithm, pairs items such as to minimize total within-cluster variance. HCA in SPSS 21 follows algorithms defined in Anderberg (1973).

5.3.4.3 ***K-means Clustering***

The *k*-means clustering algorithm is a simple, yet powerful, type of cluster analysis. In *k*-means clustering, items are initially randomly assigned to clusters, and sorting proceeds by iteration of mean vector calculations for all items in each cluster, followed by a cluster reassignment which seeks to minimize distance between item means and cluster centers. In a typical application, the *k*-means clustering method will return a partitioning solution that more optimally minimizes within-cluster sum

of distances than does HCA. The former algorithm, however, receives the number of clusters as an input variable; when this is not known *a priori* (i.e., in exploratory data analysis), an HCA agglomeration schedule can be used to determine the optimal number of initial clusters to seed in the *k*-means approach using the 'elbow rule' (Madhulatha, 2012), as has been completed in this study.

Given that initial cluster assignments are random in the *k*-means approach, successive runs of the procedure can potentially yield diverse clustering solutions. Consequently, the *k*-means algorithm is subjected to iteration according to a pre-determined input variable which specifies the maximum number of trials (in this study, ≤10 runs). When multiple runs achieve convergence due to little or no change in the position of output cluster centers, an optimal clustering solution is assumed to have been found. In this thesis, *K*-means clustering is run using SPSS 21 (following algorithms defined in Hartigan, 1975) and is incorporated as the final step in HCPC for ribbed moraine morphotype classification.

5.3.5 **Exploratory Data Analysis and Spatial Statistics**

5.3.5.1 ***Nearest Neighbour Analysis***

Nearest neighbour analysis (NNA), perhaps one of the most fundamental techniques in point pattern analysis, assesses the distance between a feature centroid and its (first order) nearest neighbour within a dataset, and uses the location and magnitude of these values to determine whether groups of features are clustered, dispersed or randomly distributed. In many examples in nature, the distance between neighbouring instances/events is seen to reflect an underlying process that is responsible for those instances/events, and so might be assumed for the genesis of subglacial bedforms. This procedure was used to evaluate the spatial distribution of ribbed moraines in south-central Keewtin. Once first order (k = 1) nearest neighbour distances are calculated for all features in a dataset, these distances can be averaged and compared with an expected mean under conditions of complete spatial randomness (CSR; i.e., a Poisson distribution) to determine whether clustering or dispersion (if detected) is statistically significant. The average nearest neighbour ratio (NNR) is hence given as:

$$NNR = \frac{D_{obs}}{D_{exp}}$$

where

$$D_{obs} = \frac{\sum_{i=1}^{n} d_i}{n}$$

and

$$D_{exp} = \frac{0.5}{\sqrt{n/A}}$$

and d_i is the distance between feature i and its nearest neigbouring feature, n is the total number of all features in the dataset, and A is the area of the study region. If NNR < 1, features are said to exhibit spatial clustering; associatively, if NNR > 1, features trend towards spatial dispersion. Standard error,

and subsequently, a Z-score can then be calculated using basic statistical procedures to determine the significance of any apparent trend, wherein the null hypothesis is one of absolute spatial randomness. For instance, Z-scores < -1.96 are rejected (at a 95% confidence level) on the basis that clustering is exhibited within the dataset, whereas Z-scores > 1.96 also result in rejection of the null hypothesis (again, at a 95% confidence level) by reason that they indicate dispersion. Nearest neighbour calculations are performed under the assumption that instances/events are free to locate at any position within the boundaries of *A*. Comparisons of NNR are only valid for a fixed *A* with consistent bounding geometry. This technique was performed in the present study using ArcGIS 10.1 to examine the spatial distribution of ribbed moraines in southern Nunavut.

5.3.5.2 ***Kernel Density Mapping***

Density analysis is visualization technique that functions to distribute (discrete) point events across a continuous surface that is representative of the relative concentration of all points (instances/events) that fall within a given portion of the entire study area. Kernel density analysis is a specific variety of density analysis that utilizes a circular *kernel* (a smooth, curved surface with a specified distance, or bandwidth) that is centered on each point within a dataset. The density at each point is calculated by summing the number of instances/events within each kernel, thus generating a continuous surface from discrete location-based point data. In ArcGIS 10.1, the kernel function follows the quadratic kernel function developed in Silverman (1986). Kernel density analysis is used in this thesis to visualize the distribution of glacial bedforms in south-central Keewatin. In this instance, points represent individual ribbed moraine (or drift lineation) centroids, and kernel bandwidths are implemented across several multiples of average nearest neighbor distances (ANND) for each bedform type. There is no objectively ideal bandwidth when performing kernel density analysis, and the choice of using ANND was made here because it is assumed that these values are inherently significant when describing any underlying bedforming process (e.g., nearest neighbour spacing could encompass competition for sediment supply, natural wavelengths in a propagating till instability, etc.). Resulting raster surfaces are transcribed to maps and visually evaluated for the existence of spatial trends. This approach is utilized for visualization of both the entire ribbed moraine population within the study area, as well as for comparison of clustering between ribbed moraines and glacial lineations with high (upper quintile) and low (lower quintile) length values.

5.3.5.3 ***Ripley's K Function***

Whereas many basic quantitative geospatial procedures (e.g., NNA, cumulative distribution functions, etc.) consider only first-order statistics, Ripley's *K* function (Ripley, 1977, 1979) is capable of summarizing spatial dependence over a range of distances or spatial scales. Just as many instances/events in nature exhibit "global" clustering that is indicative of an underlying universal process, many such point patterns also exhibit differences in the intensity of clustering when assessed at multiple spatial scales. Ripley's *K* is a function that is used to evaluate this range of differences by determining how spatial dependence (clustering, dispersion) changes as neighbourhood size changes. In its basic form, Ripley's *K* can be stated as:

$$K(d) = \vartheta^{-1}E$$

where ϑ is the density (number per unit area) of instances/events (e.g., glacial bedforms), and E is the number of additional events within a distance d of any given instance/event selected at random. In this investigation, Ripley's K is utilized as a means to test whether ribbed moraine distributions in south-central Keewatin are consistent with a Poisson process (i.e., CSR) when analyzed across multiple scales. This is a common application of the K function, where it becomes more intuitive to express $K(d)$ in variance-stabilized form:

$$L(d) - \left(\frac{K(d)}{\pi}\right)^{1/2} - d$$

which, conveniently, equates to 0 for all values of d under CSR, since the expectation of $K(d)$ in this scenario is simply πd^2. In the above equation:

$$L(d) = \sqrt{\frac{A \sum_{i=1}^{n} \sum_{j=1, j \neq 1}^{n} k(i,j)}{\pi n(n-1)}}$$

where A is the area of the study region, n is the total number of features, and $k(i,j)$ is a weight determined by the number of points (j) located within a distance (d) of all points in the study area (i). For a standard Poisson distribution, $L(d) = d$ for all values; any exceedance of $L(d)$ indicates clustering at that given distance, whereas $L(d) < d$ signifies a more dispersed pattern than would be expected under conditions of CSR. In this study, values were calculated for $L(d)$ to a maximum of d = 90 km, and Monte Carlo simulations were run for 99 replications to test the significance of deviation from a Poisson distribution at 99% upper and lower confidence limits for CSR using the CrimeStat v3.3 software package.

5.3.5.4 ***Spatial Autocorrelation (Global Moran's I)***

Given a set of features and an associated attribute common to all features, spatial autocorrelation provides a measure of whether near-located features demonstrate similar attribute values; that is – based on the location of a set of valued points, are like values clustered, dispersed or randomly distributed? Moran's I index (Getis and Ord, 1992) is the traditional measure of spatial autocorrelation, and can be defined as:

$$I = \frac{n}{S_0} \frac{\sum_{i=1}^{n} \sum_{j=1}^{n} w_{i,j} z_i z_j}{\sum_{i=1}^{n} z_i^2}$$

where $z_i = (x_i - \bar{X})$ (i.e., the deviation of feature i's attribute value x from its global mean $\bar{X}$), $w_{i,j}$ is a spatial weight applied to the distance evaluation between i and j, and S_0 is a sum of all spatial weights:

$$S_0 = \sum_{i=1}^{n} \sum_{j=1}^{n} w_{i,j}$$

Essentially, z_i values for all neighbouring features within a specified distance are multiplied together, returning a cross-product that is positive when both features' attribute values are larger or smaller than the mean, but negative when $x_i > \bar{X}$, $x_j < \bar{X}$ (or *vice versa*). Larger z_i returns a larger cross-product in all cases. When like values (e.g., high-high, low-low) cluster together spatially, Moran's *I* index will be positive, and conversely, is negative when high values are located amongst low values, or low values amongst high values. A zero Moran's *I* is achieved when there is no spatial trend in the distribution of attribute values. Moran's *I* index is variance-normalized such that all values fall between -1.0 and +1.0. Observed values of Moran's *I* can be statistically evaluated against an expected distribution, assuming a null hypothesis of CSR. Moran's *I* is utilized in this thesis to determine whether ribbed moraines in south-central Keewatin are spatially autocorrelated by length.

5.3.5.5 ***High/Low Clustering (Getis Ord General G)***

In addition to Moran's *I*, which aids in determining whether high and/or low values are spatially clustered, dispersed, or randomly distributed within a dataset, Getis Ord General *G* is a commonly employed statistic in spatial analysis that provides indication of the type of attribute clustering among features (Getis and Ord, 1992). The General *G* statistic is expressed as:

$$G = \frac{\sum_{i=1}^{n}\sum_{j=1}^{n} w_{i,j}x_i x_j}{\sum_{i=1}^{n}\sum_{j=1}^{n} x_i x_j}, \forall j \neq i$$

where x_i and x_j are the attribute values of features *i* and *j* respectively, and $w_{i,j}$ is the distance weight of the spatial relationship between *i* and *j*. As with spatial autocorrelation, the null hypothesis in a statistical test of Getis Ord General *G* assumes CSR (i.e., that there is no spatial clustering of attribute values among features), and an expected value for *G* can be computed to facilitate this testing:

$$E[G] = \frac{\sum_{i=1}^{n}\sum_{j=1}^{n} w_{i,j}}{n(n-1)}, \forall j \neq i$$

Simply stated, when the *p*-value of a statistical test of General *G* on a dataset against CSR is small and permits rejection of the null hypothesis, the sign of the Z-score determines the type of clustering in the study area, wherein positive Z-scores indicate spatial clustering of high attribute values, and low Z-scores indicate spatial clustering of low attribute values. Getis Ord General *G* is employed in this thesis to test whether large or small ribbed moraines are clustered throughout southern Nunavut.

5.3.5.6 ***Local Indicators of Spatial Autocorrelation (LISA)***

Moran's *I*, detailed above, is a *global* measure of spatial autocorrelation, however closer inspection of the index reveals that the computation can be disaggregated into a series of constituent *local* indices. Calculation of Local Indicators of Spatial Autocorrelation (LISA; also referred to as Local Moran's *I*) (Anselin, 1995) is a useful technique for identifying spatial "hotspots" of high or low feature attribute clusters within a specified distance of each point instance/event. The Local Moran's *I* statistic is given as:

$$I_i = \frac{x_j - \bar{X}}{S_i^2} \sum_{j=1, j \neq i}^{n} w_{i,j}(x_j - \bar{X})$$

where

$$S_i^2 = \frac{\sum_{j=1, j \neq i}^{n}(x_j - \bar{X})}{n-1} - \bar{X}^2$$

An expected value for I_i is:

$$E[I_i] = -\frac{\sum_{j=1, j \neq i}^{n} w_{ij}}{n-1}$$

and is used to calculate a Z-score and p-value that determine the significance of each I_i. Positive values of I_i for a feature indicate that surrounding features (within a specified neighbourhood distance) have similar high or low attribute values; hence these features form part of a *cluster*. Conversely, negative values of I_i for a feature indicate that its surrounding features (within a specified neighbourhood distance) exhibit dissimilar values; hence these features are represented as *outliers*. LISA statistics are employed in this thesis to map the distribution of ribbed moraines in south-central Keewatin based on clustering of their ridge lengths throughout the study area.

Fig. 5.13 presents a flowchart detailing the progression of RS/GIS, mapping and spatial and morphometric methodologies employed in this study.

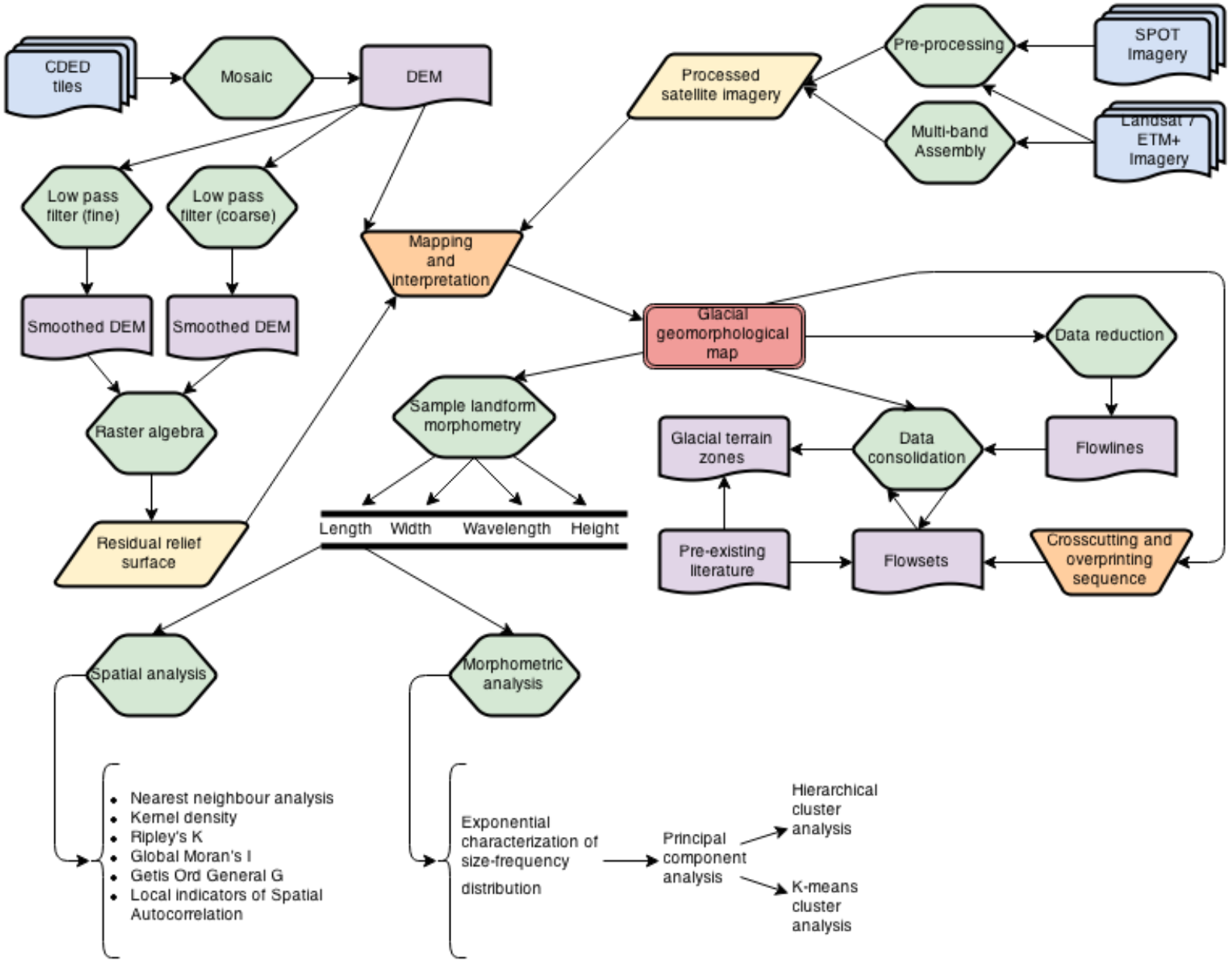

Fig. 5.13 – Flowchart showing methodological overview for glacial landform mapping and analysis completed in this study.

5.4 *Results*

In total, >45,800 individual ribbed moraine ridges, >24,100 undifferentiated glacial lineations, and >3,900 esker segments were mapped within the study area using the data sources listed in section 5.3.1. Final output is shown in Appendix A using minimal cartographic generalization, and in Fig. 5.14 as separate map layers. The following sections describe the results of this mapping and subsequent morphometric and geospatial analyses.

5.4.1 Spatial and Morphological Characteristics of Ribbed Moraines

5.4.1.1 *Patterning, Spacing and Organization*

The spatial organization of ribbed moraines in south-central Keewatin is expressed uniquely at a variety of scales. At the broadest level, ridges appear densely clustered in several locations, most prominently: (a) in a wide corridor southwest of the Kognak River between Kasba and Nueltin Lakes; in patches (b) south of Ennadai Lake and (c) northeast of Edehon Lake in the vicinity of the Thlewiaza River, and; (d) in a broad band extending from South Henik Lake to the southeastern corner of the study site. In order to quantitatively assess this pattern, geometric centers of the ribbed moraine feature class were computed and stored as a separate dataset for subsequent application in point pattern analysis. First order nearest neighbour analysis (NNA) on the point feature class returned an observed average nearest neighbour distance (ANND) of 321.27 m and a nearest neighbour ratio (NNR) of 0.51. When compared against the expected ANND under a scenario of complete spatial randomness (CSR), the results reveal a negative z-score that is statistically significant for underlying non-randomness ($p<0.01$) (Table 5.6), confirming visual observations of ribbed moraine clustering within the study area. A kernel density series (Fig. 5.16) incremented at broadening search radii (ranging from 5x–25x ANND at intervals of 5 ANND) clearly illustrates the preference for ribbed moraines to cluster spatially at multiple scales, and primarily within the locations mentioned above. These results suggest underlying spatial constraints operating on either the formation or preservation processes of ribbed moraine landforms.

The pattern of spatial distribution of individual ribbed moraines within the boundaries of the study area was estimated using the univariate second-order Ripley's *K* function (Ripley, 1977) (section 5.3.5.3) (Ripley, 1979). Fig. 5.15 plots the observed *L(d)* function against distance for south-central Keewatin ribbed moraines. *L(d)* lies above the 99% confidence limit for all intervals, implying multiscalar, statistically significant spatial clustering up to neighbourhood distances of 90 km. Maximum ribbed moraine clustering is observed at ~30 km and ~85 km, which agrees well with the results of kernel density analysis, where clusters are highlighted at scales of ~30-40 km (Fig. 5.16B-C) and ~80-100 km (Fig. 5.16D-E).

Ribbed moraines in south-central Keewatin are organized within ~562 fields covering a total area of 32,975 km^2. This is a substantially greater area of coverage than has previously been mapped in this sector (e.g., 12,207 km^2 in Shaw et al., 2010; Fig. 5.17). Individual fields range in length from 0.56–138.38 km, in width from 0.20–89.1 km, and in area from 0.12-8,307.6 km^2 (Table 5.4). The distributional pattern of ridges within these fields varies such that it is possible to distinguish between ~6 unique configurations (Fig. 5.18; see also Dunlop and Clark, 2006b). Of these 6 varieties, two (elongate ribbons, broad concentrated patches) comprise an overwhelming majority (77%) of the total area covered by ribbed moraines in southern Nunavut (Fig. 5.19).

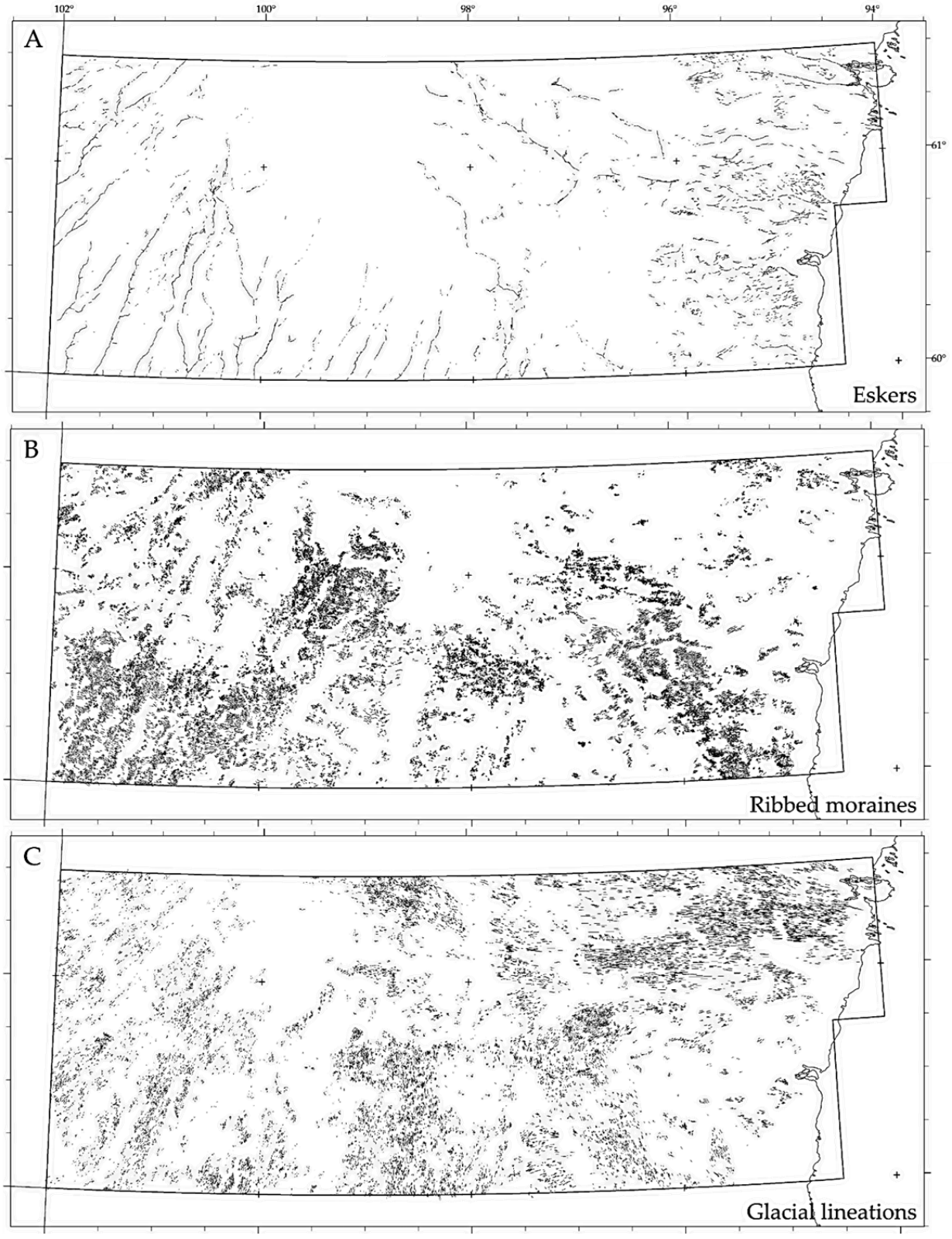

Fig. 5.14 – Glacial landforms mapped from remote sensing datasets in south-central Keewatin depicted as separate map layers. A) Eskers. B) Ribbed moraines. C) Glacial lineations.

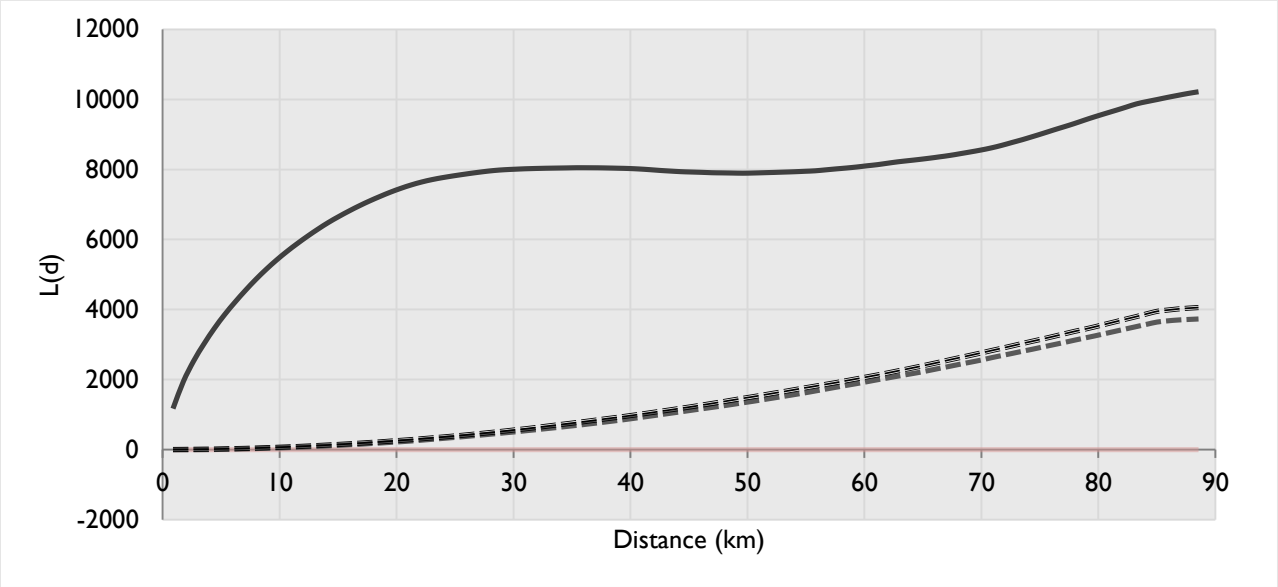

Fig. 5.15 – Ripley's *K* (expressed in variance stabilized form as *L(d)*) for south-central Keewatin ribbed moraines. Solid red line provides reference for *L(d)* under CSR. Dashed lines represent 99% confidence limits for CSR. Distance is expressed in terms of ribbed moraine geometric centroid separation (i.e., ribbed moraines are theoretically overlapping for *d*=0). Observed *L(d)* lies above the upper confidence limit for all distance intervals, indicating multiscalar, statistically significant spatial clustering of ribbed moraines within the study area.

Table 5.4 – Statistics for ribbed moraine field shapes.

	n	Length (km)			Width (km)			Area (km^2)		
		Min.	Max.	Mean	Min.	Max.	Mean	Min.	Max.	Mean
Shaw et al., 2010	653	0.08	77.52	9.42	0.002	45.24	3.76	0.0004	2600.23	44.15
This study	562	0.56	138.38	7.94	0.200	89.85	3.43	0.1200	8307.66	58.66

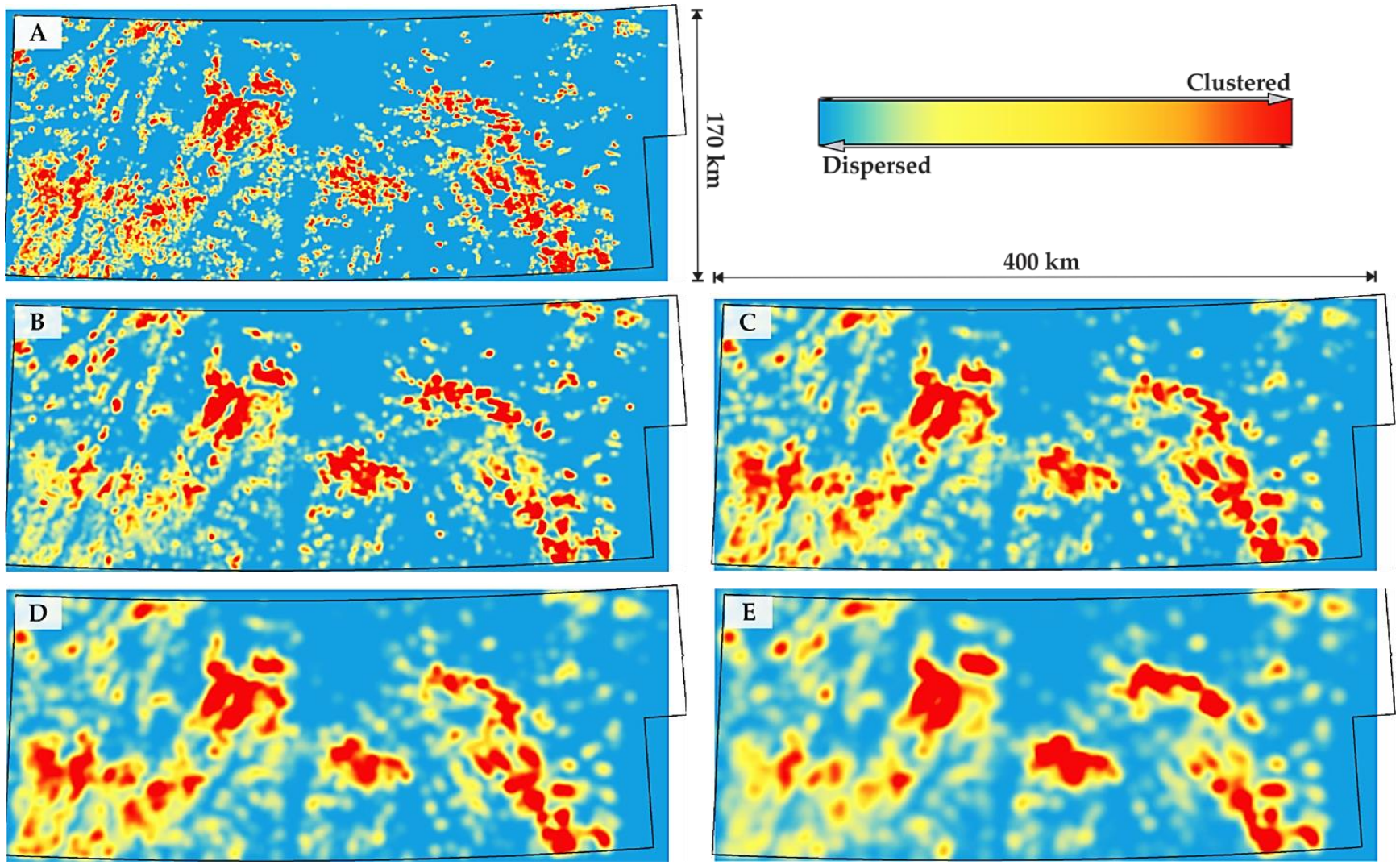

Fig. 5.16 – Kernel density ("heat") maps depicting geographic clustering of ribbed moraines in south-central Keewatin. Maps have been generated using kernel radii at increments of 5x the average nearest neighbor distance (ANND) for ribbed moraines in the study area, beginning with 5x in A) through to 25x in E). Note that spatial clustering can be visually detected at a variety of scales.

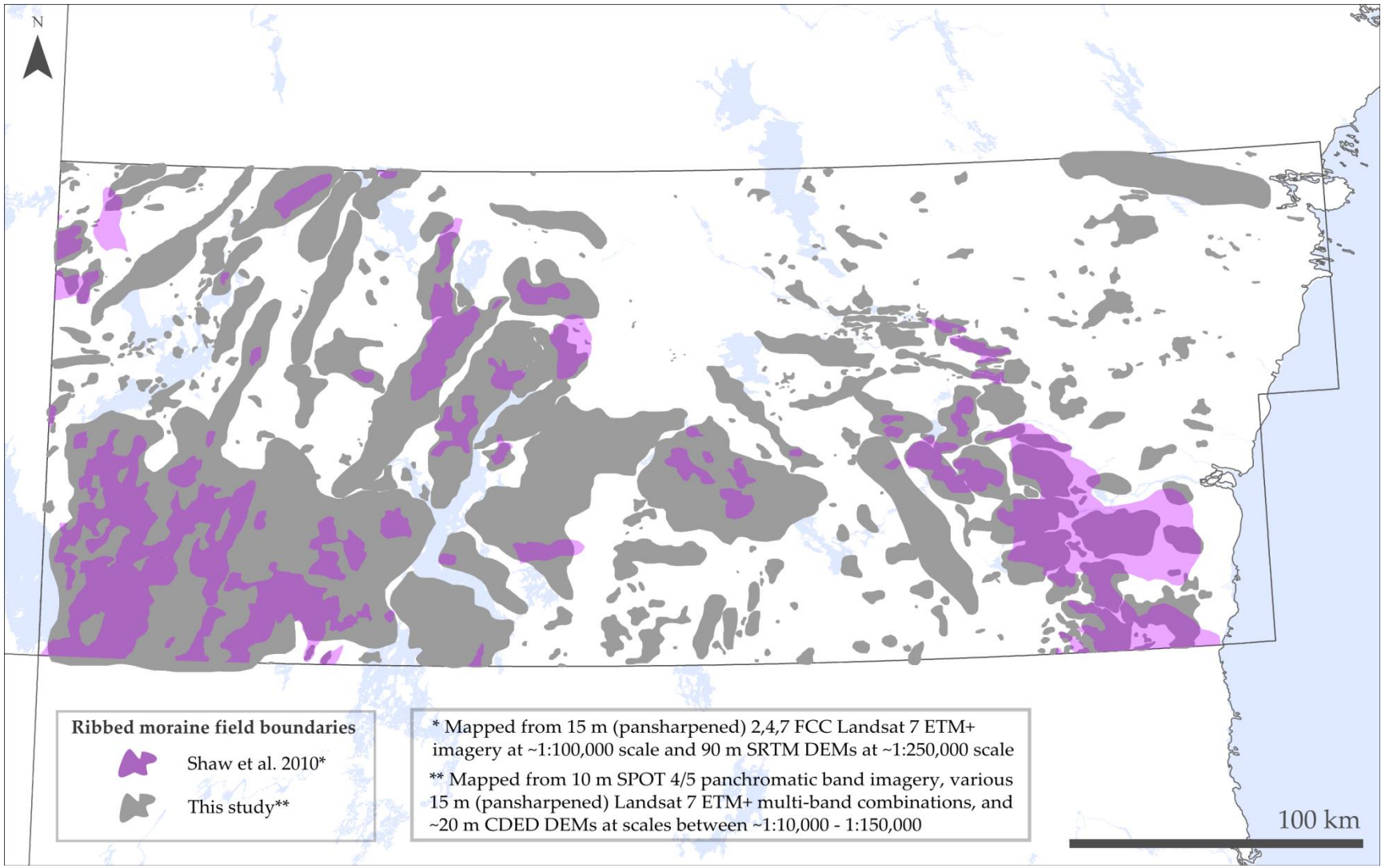

Fig. 5.17 – Ribbed moraine fields in south-central Keewatin. Purple polygons depict the boundaries of individual fields mapped in Shaw et al. (2010), grey polygons show ribbed moraine fields mapped in this study. Ribbed moraine fields are mapped only along their perceived outlines in Shaw et al. (2010) and do not portray individual ridges. In comparison to the present study, there is substantial underrepresentation of ribbed moraines in southern Keewatin depicted by earlier coarse-scale mapping efforts.

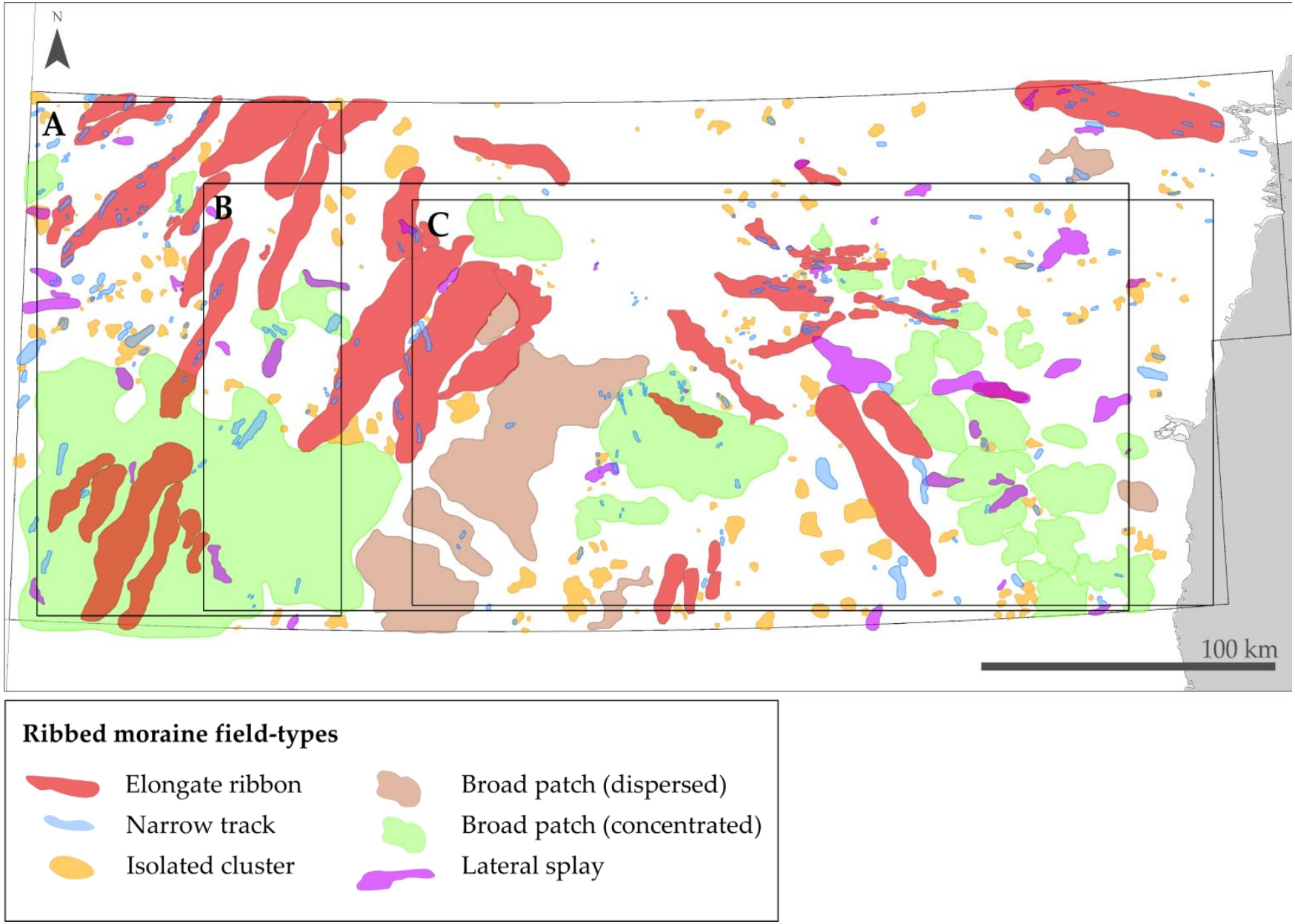

Fig. 5.18 – Classification of ribbed moraine fields in south-central Keewatin. A, B, and C show extent of Fig. 5.20, Fig. 5.21, and Fig. 5.22, respectively.

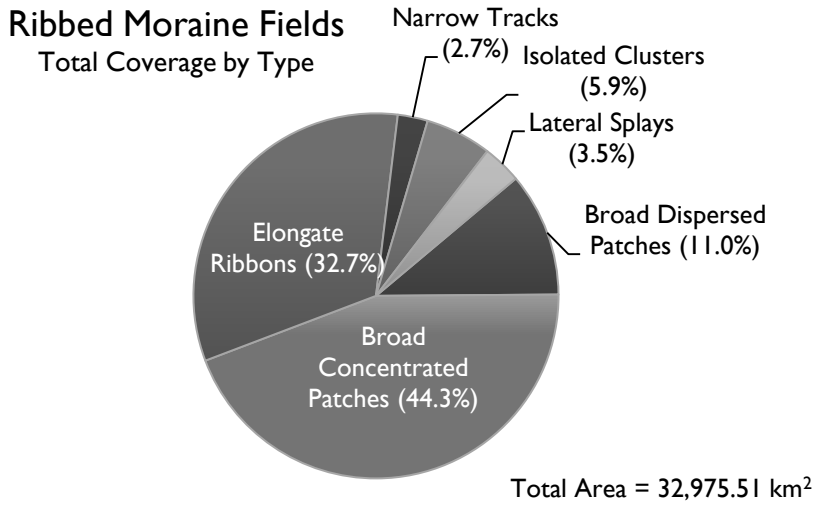

Fig. 5.19 – Percentage of the total ribbed moraine area in south-central Keewatin that is covered by different field-types.

5.4.1.1.1 Elongate Ribbons and Narrow Tracks

Approximately 50 large, ribbon-like tracks of ribbed moraines exist within the study area, covering ~10,780 km^2, most of which extend outwards from a broad zone of thin drift between Watterson, Hicks, South Henik and Tattinai Lakes. Aylsworth and Shilts (1989a) describe similar arrangements of ribbed moraines from eastern Keewatin, formed within trains of boulders that head at outcrops near Kaminuriak Lake. Shilts (1977) also describes extensive "belts" of ribbed moraines in Keewatin which he considers analogous to dispersal trains in both plan shape and composition, and notes a tendency for these belts to pass laterally into drumlinized till plains. This relationship is likewise observed here, most noticeably in the southwestern portion of the study site east of Kasba Lake (Fig. 5.20C), however elongate ribbons of ribbed moraines and tracks of drumlinized terrain are in no way mutually exclusive, and streamlined forms overprint many such fields in the region (see section 5.4.1.2).

Ribbon-like fields of ribbed moraines are found at a variety of scales throughout the study area (Fig. 5.20A), ranging in length from 3.6 to 89.5 km, with widths 1.5–22.9 km, and an average elongation ratio (ER) of 3.71. In places, much smaller, and narrower tracks of ribbed moraines can be identified within elongate ribbons, though also frequently occur independently of other fields (Fig. 5.20C-E). These narrow tracks mirror the larger ribbon-type fields in their general shape, orientation, and elongation (average ER = 2.57), though are distinguished by the tight spacing and generally smaller dimensions of their individual ridges. Typically, narrow tracks are comprised of a single-file arrangement of minor ribbed moraines extending in a down-ice direction, though occasionally, multiple series of ridges formed abreast of one another are best considered as belonging to a single track. Their scale is reflected in a small range (202-5,312 m) and average (1,206 m) of track widths, and also in the comparatively limited dimensions of ribbed moraines within these tracks (mean length = 476.63 m) compared to the population average (652.89 m). The local-scale coexistence of like-oriented narrow tracks and elongate ribbons throughout the study area implies that ribbed moraines of varying spatial and morphometric properties can be generated in close proximity, even if this is not the overall tendency (e.g., Fig. 5.53).

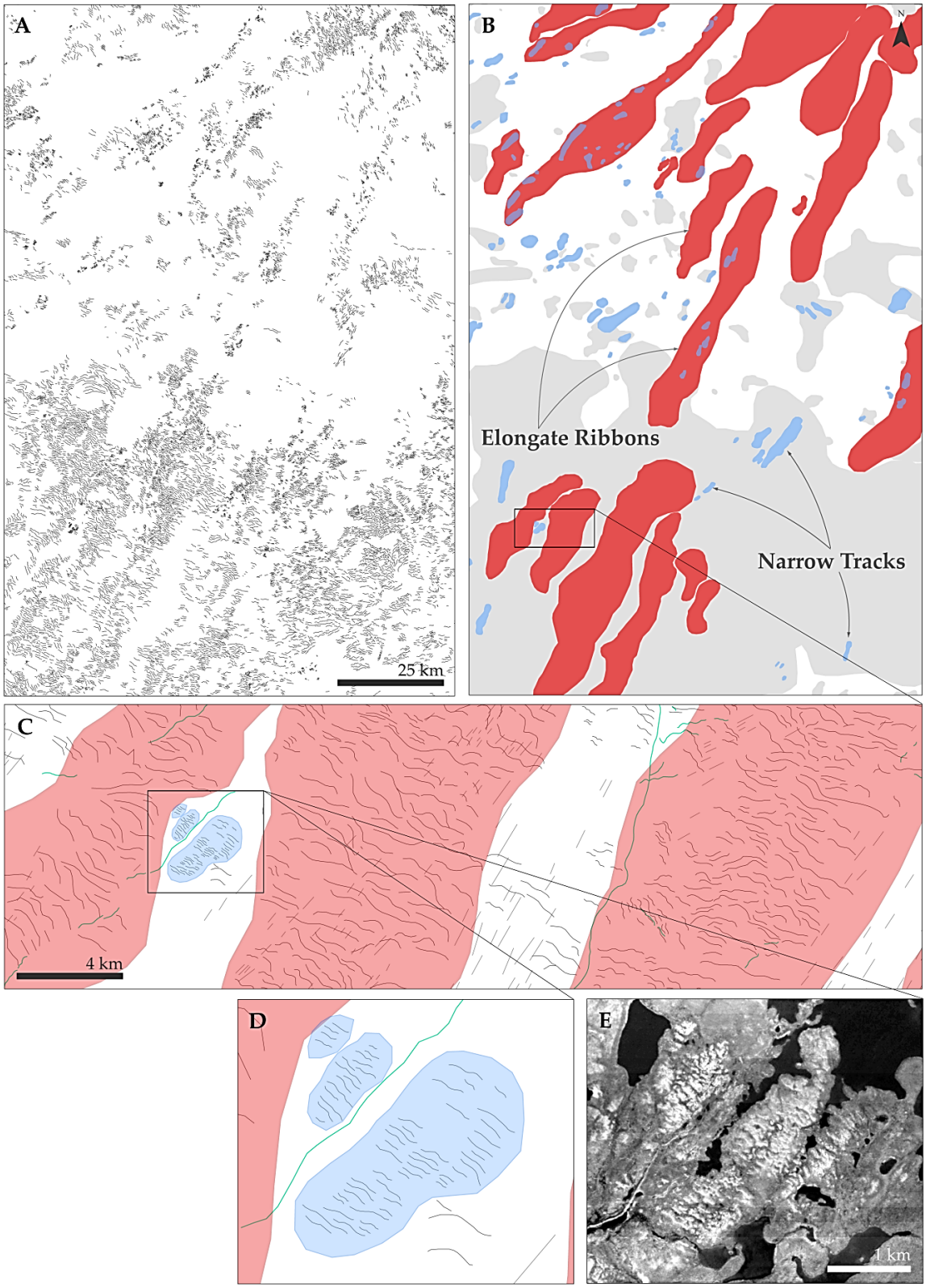

Fig. 5.20 – Examples of elongate fields and narrow tracks of ribbed moraines in the northwestern portion of the study area. B) Narrow tracks exist both within and outside of ribbons. C-E) Narrow tracks feature small-scale ribs which are commonly aligned along one edge. Dark grey lines = ribbed moraines, light grey lines = lineations, green lines = eskers.

5.4.1.1.2 Broad Concentrated and Dispersed Patches

Larger, amorphous patches of ribbed moraines are also found within the study area, featuring, in places, ridges of varying dimensions and orientations. Where nested fields occur, particularly within these patches, cross-cutting ridges are occasionally also identified. Dunlop and Clark (2006b) recognize such instances as forming a distinct type of ribbed moraine field; here, however, separate field types are defined exclusively on the basis of bedform spacing and continuity, and thus no distinctions are assigned to cross-cutting occurrences. Broad concentrated and dispersed patches are primarily differentiated on the basis of landform density, wherein each demonstrates either densely-packed concentrations of ridges, or alternatively, relatively dispersed landforms. Patches of tightly-packed and dispersed ribbed moraines may occur in close proximity (Fig. 5.21C). Together, broad concentrated and dispersed patches comprise the majority (18,248 km^2, 55%) of the total ribbed moraine coverage within south-central Keewatin, and are most prominent in the southern half of the study area (Fig. 5.19 and Fig. 5.21). Coherent patches of dispersed ribbed moraines are primarily restricted to a wide, NE-SW trending zone east of Nueltin Lake, though are found also southwest of Maguse Lake, northeast of Baralzon Lake, and below the Thlewiaza River near Hudson Bay (Fig. 5.21A). Alternatively, a large tightly-packed field comprises most of the area (8,308 km^2) between Kasba and Nueltin Lakes, whereas southeast of the Tha Anna River, smaller concentrated patches are contiguously arranged within a wide band trending NW-SE towards the study area boundary.

Differences in ridge density between broad dispersed and concentrated patches can be verified quantitatively using NNA. Ribbed moraines organized within dispersed patches demonstrate an ANND of 444.72 m (NNR = 0.71). Those found within broad concentrated patches are significantly closer spaced (Fig. 5.21D), and this is reflected by an ANND of 330.14 m (NNR = 0.83). Note that the ANNDs reported here are larger than that for the entire study area (321.27 m, Table 5.6) because the former measures account only for intra-field densities, whereas the latter assesses inter-field distributions averaged over a larger minimum encompassing area (i.e., the bounds of the "study area"). Broad concentrated patches frequently encompass all other varieties of field-types recognized here (excepting, of course, dispersed patches), whereas dispersed patches are commonly exclusive. South of Ennadai Lake, an extensive concentrated patch completely incorporates ~6 elongated ribbon-type fields in addition to several lateral splays and narrow tracks. The latter are found also within a dispersed patch below Maguse Lake, the only example of nested fields involving dispersed ribbed moraines that is here identified.

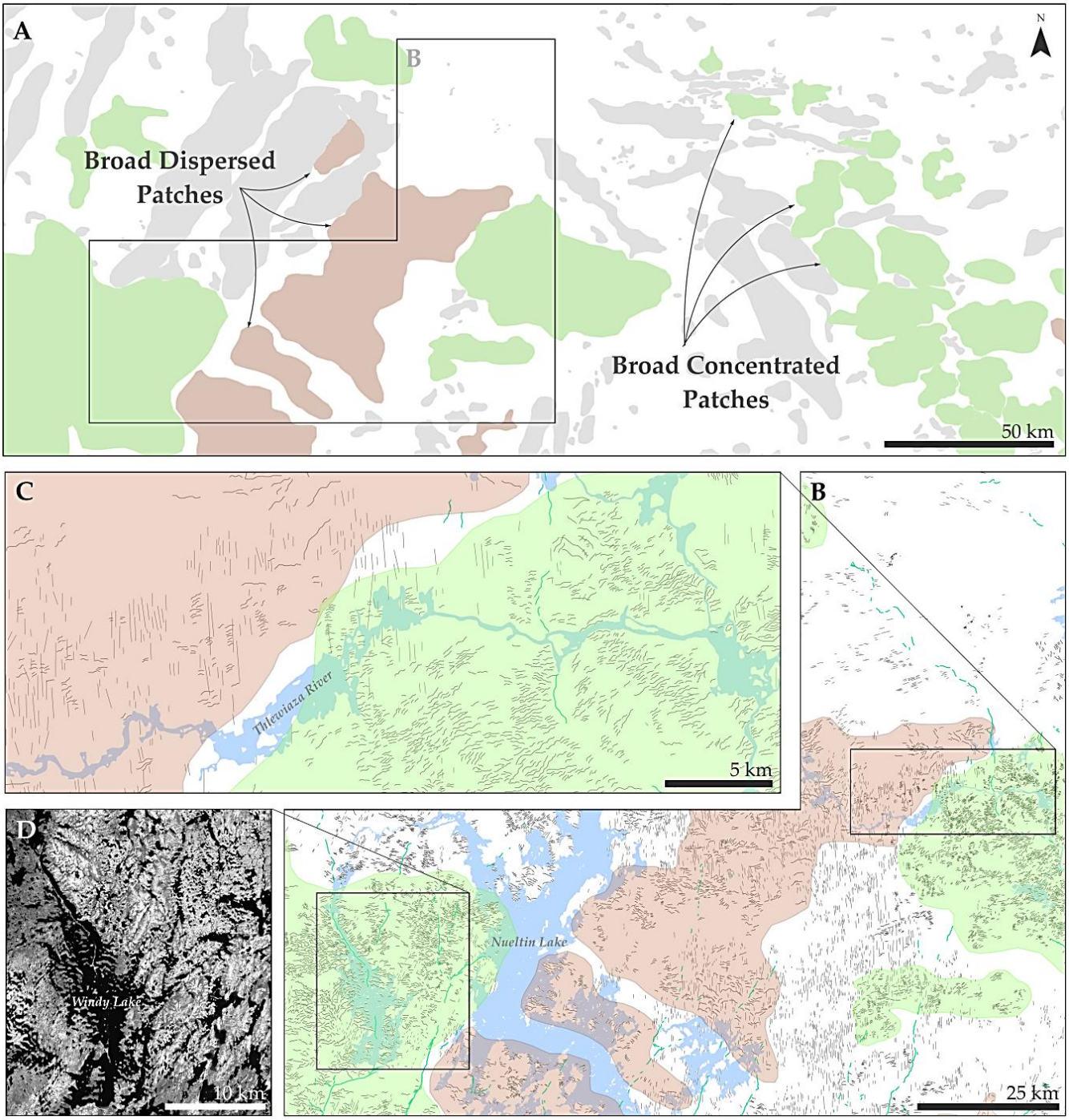

Fig. 5.21 – Examples of broad concentrated and dispersed patches of ribbed moraines in the central portion of the study area. C) Despite differences in ridge spacing, there is often close spatial association between each type of field. B) Dispersed patches are largely confined to a wide band east of Nueltin Lake. D) SPOT 4 sub-scene showing the tight-spacing of ridges in a concentrated patch surrounding Windy Lake. Dark grey lines = ribbed moraines, light grey lines = lineations, green lines = eskers.

5.4.1.1.3 Isolated Clusters

A number of isolated fields of ribbed moraines (defined here as encompassing ≥3 landforms) are found dotted across the study area (Fig. 5.22A). These are typically small (on average, 10.29 km^2) and independent, and are located within gaps between larger ribbons and patches, often interspersed within fields of streamlined landforms (see Fig. 5.22C). Though abundant (188 of 562, or ~33% of total identified fields), isolated clusters constitute only ~6% of the total area occupied by ribbed moraines in south-central Keewatin. Dunlop and Clark (2006b) recognize similarly organized fields of ribbed moraines in Nouveau Québec, citing smaller average landform dimensions in these fields than elsewhere within their limit of mapping. Here, however, ridge lengths are similar both within isolated clusters ($\bar{x}$ = 618.03 m, s = 390.31 m) and outside of these arrangements ($\bar{X}$ = 652.89 m, S = 435.61m). The presence of isolated clusters is significant in that it implies that ridge forming process(es) can, under certain circumstances, be highly localized, and thus may require relatively specific glaciological or geological conditions. Alternatively, spatially dissociated clusters of landforms could be attributable to localized preservation owing to patchy transitions in subglacial thermal regime and/or subglacial hydraulic conditions (e.g., Kleman and Stroevan, 1997; Piotrowski and Kraus, 1997; Piotrowski et al., 2004).

5.4.1.1.4 Lateral Splays

A final field-type, here termed "lateral splays", comprise a relatively small percentage (~3.5%) of the total ribbed moraine occupied area in south-central Keewatin, though are unique in that they exhibit greater lateral, than along-flow continuity. In contrast to ice flow-aligned ribbons and narrow tracks, and amorphous patches and clusters, lateral splays exhibit distinct configurations transverse to ice flow, and thus mirror the orientation of ribbed moraines themselves. These fields tend to be relatively small (on average 27.07 km^2 in area) and isolated. Occasionally, lateral splays are nested within larger ribbons or patches, and in rare instances encompass portions of smaller narrow tracks. Laterally continuous fields are found throughout the study area with little regional preference, though appear, in almost all cases, to occur along scarps or abrupt changes in local topography (Fig. 5.23). Throughout the study area, though particularly in the vicinity of the Thlewiaza and Tha Anna Rivers, lateral splays are found in association with eskers, glaciofluvial outwash trains and contemporary hydrological features. These areas are typically flanked by patches of thin or discontinuous till cover and/or surrounding outcropping bedrock (Fig. 5.24C).

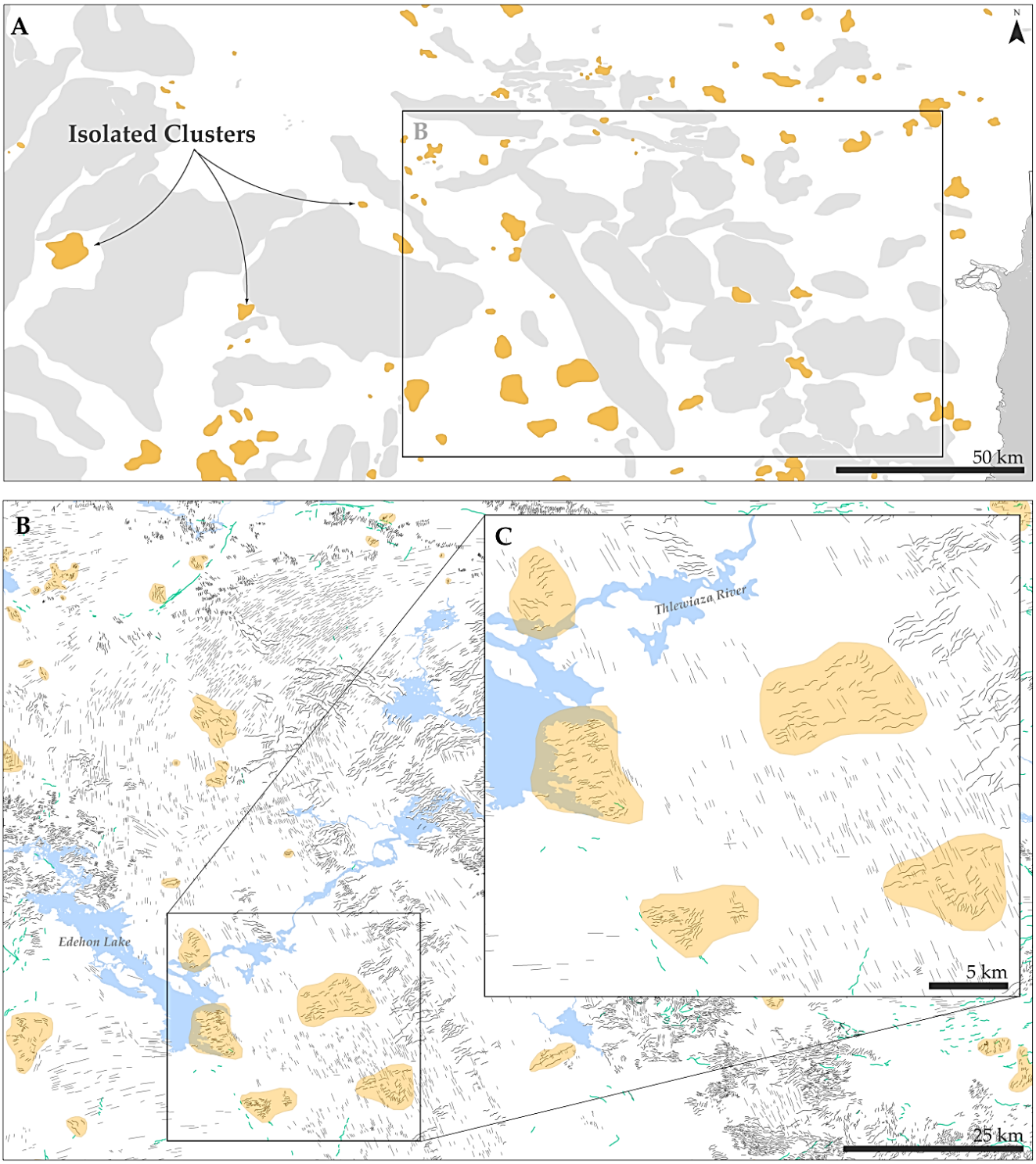

Fig. 5.22 – Examples of isolated clusters of ribbed moraines in the central and southeastern portions of the study area. A,B) Isolated clusters commonly exhibit a patchy, quilt-like pattern over the landscape. C) Small isolated clusters tend to occur amid fields of streamlined terrain. Dark grey lines = ribbed moraines, light grey lines = lineations, green lines = eskers.

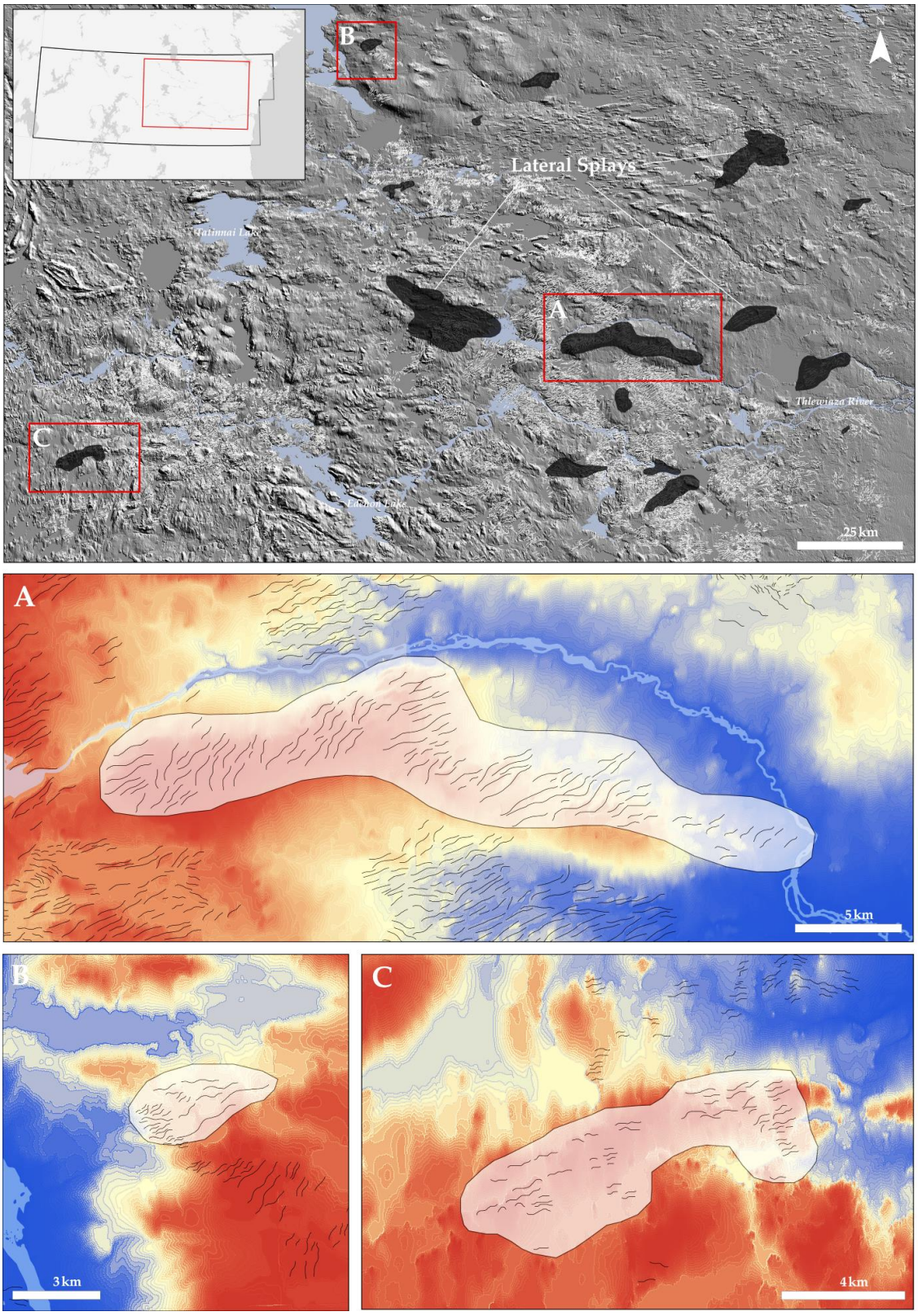

Fig. 5.23 – Examples of lateral splays in south-central Keewatin. A-C) Note the tendency for this type of field to be perched atop abrupt steps in topography. Red denotes high elevation, blue denotes low elevation. Upper panel contains hillshaded CDED DEM, illumination from the NE.

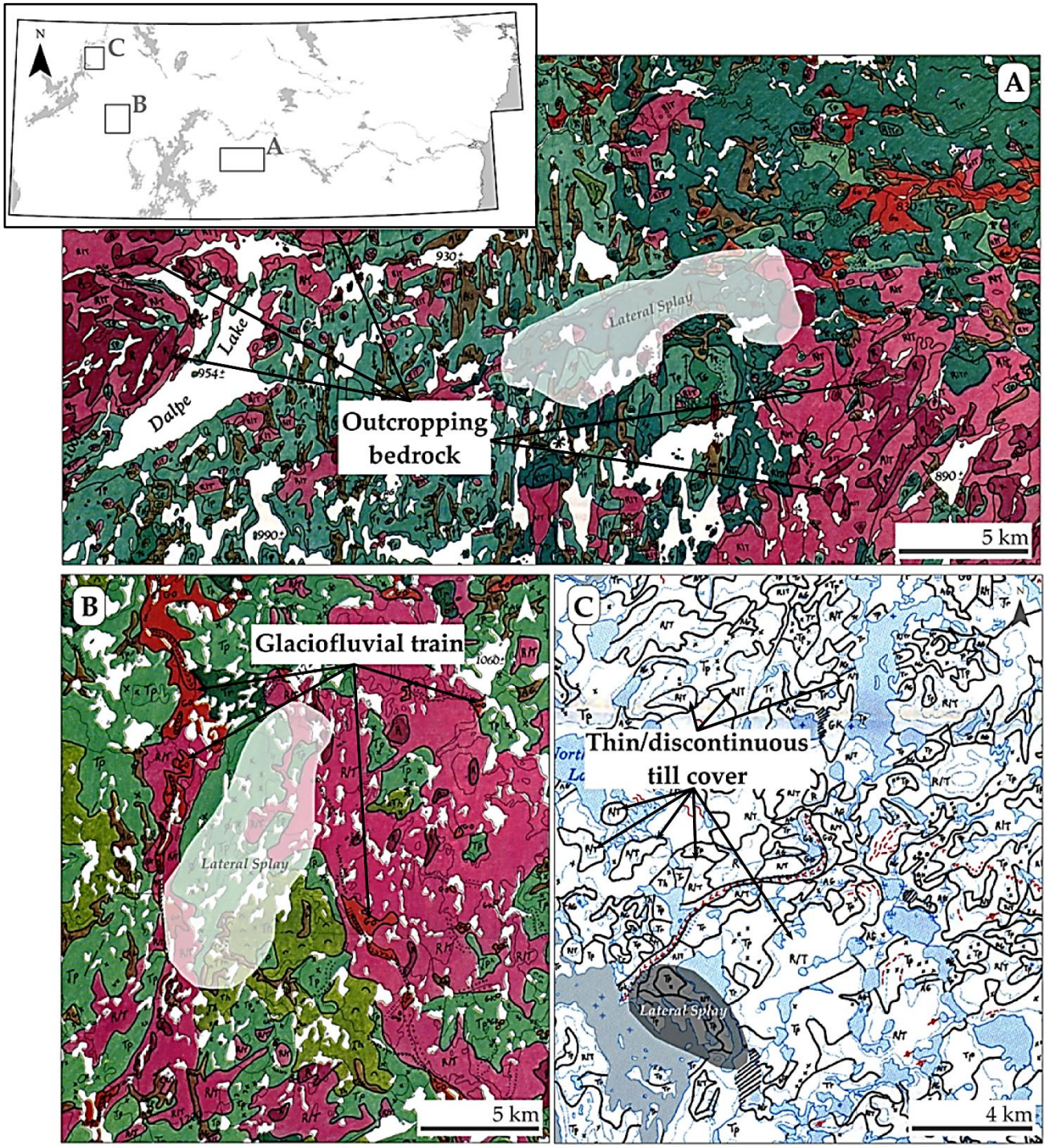

Fig. 5.24 – Features commonly associated with the presence of lateral-splay type ribbed moraine fields. A) Surrounding outcropping bedrock. B) Glaciofluvial trains and associated meltwater deposits. C) Thin and/or discontinuous till cover. Surficial geology from A) Aylsworth, 1986b; B) Aylsworth, 1986a; C) Aylsworth, 1989a.

5.4.1.2 *Ribbed Moraine Topographic Setting and Relationship to Other Landforms*

Ribbed moraines in south-central Keewatin are distributed within a variety of topographic settings. Whereas much of the existing literature reports confinement of these bedforms within topographic lows or basins (e.g., Andrews, 1963, 1969; Lundqvist, 1969, 1989; Marich et al., 2005; Markgren and Lassila, 1980; Shaw, 1979; Sugden and John, 1976; Sollid and Sørbel, 1994; Menzies and Shilts, 1996; Möller, 2006 – see section 3.2.4), there is little evidence for such an exclusive relationship within the study area. Nevertheless, certain areas do show a large topographic influence of bedform pattern; in particular, northeast of Edehon Lake around the Thlewiaza River (Fig. 5.25C); above Ennadai Lake, near the Kazan River (Fig. 5.25A); and around the Tha Anna River, beneath South Henik Lake (Fig. 5.25B). In the west-central portion of the study area, these topographic relationships are apparent only because high local relief is affected by exposed orthoquartzite knobs/hills; hence these areas are not merely lacking ribbed moraines, but glacial deposits in general. Commonly where narrow tracks and lateral splays are found, ridges are fronted by an adjacent step in the local topography. Thus, there is local-scale evidence for topographic influence in ribbed moraine formation and/or preservation, yet the presence of these landforms across all topographic settings at the regional scale implies that this is likely not a fundamental control over large areas.

Many workers have suggested that, where ribbed moraines are found in depressions or within concave terrains, drumlins and other streamlined forms occupy convexities on the surrounding landscape (e.g., hilltops, slopes/rises, etc.) (e.g., Lundqvist, 1969, 1989; Markgren and Lassila, 1980 – see section 3.2.4). In order to test this hypothesis on a regional scale within the study area, the geographic centers of ribbed moraines and lineations were computed and plotted in three dimensions (x = grid east, y = grid north, z = elevation) using the scatterplot3d package in R. Resulting landform scatterplots for the study area are shown in Fig. 5.26 with a view to the southwest, and in Fig. 5.27 with smoothed regression surfaces and a view to the northwest. In terms of the topographic relationship between transverse and flow-parallel glacial bedforms, three patterns are immediately apparent: 1) The topographic position of ribbed moraines and glacial lineations reflect regional relief wherever they are found; 2) ribbed moraines may occupy positions which are topographically higher, lower, or equivalent to glacial lineations when these bedforms occur in close proximity, and; 3) both glacial lineations and ribbed moraines can exhibit broad (<100 m) ranges of topographic positioning at the local scale. It is interesting to note that, in a W-E transect across the study area, the general topographic relationship between bedforms, as evidenced by their regression surfaces (Fig. 5.27), remains relatively constant, with few intersections. The fitted lineation surface tightly drapes the ribbed moraine surface over most of the study area, reflecting widespread observations of fluted and/or drumlinized ribbed moraine landforms (e.g., streamlined morphologies). Near Hudson Bay, however, across the easternmost fringe of the Kazan Upland towards Arviat, the underlying ribbed moraine surface crops up, likely in response to the unique relative age sequence witnessed in this area, where NNE-SSW trending minor ribbed moraine ridges overprint pervasive MSGL assemblages formed during convergent eastwardly flow into Hudson Bay (section 5.4.2.3). Outside of this region, ribbed lineations, or lineations broken up into transverse ridges are comparatively rare. Thus, streamlined landforms do regularly occupy positions of higher local elevation than ribbed moraines, though these differences are typically small (<50 m) and probably owe more to the typical sequence of bedform generation than to any discrete relief-dependent bedform zonation (though see also Fig. 5.31).

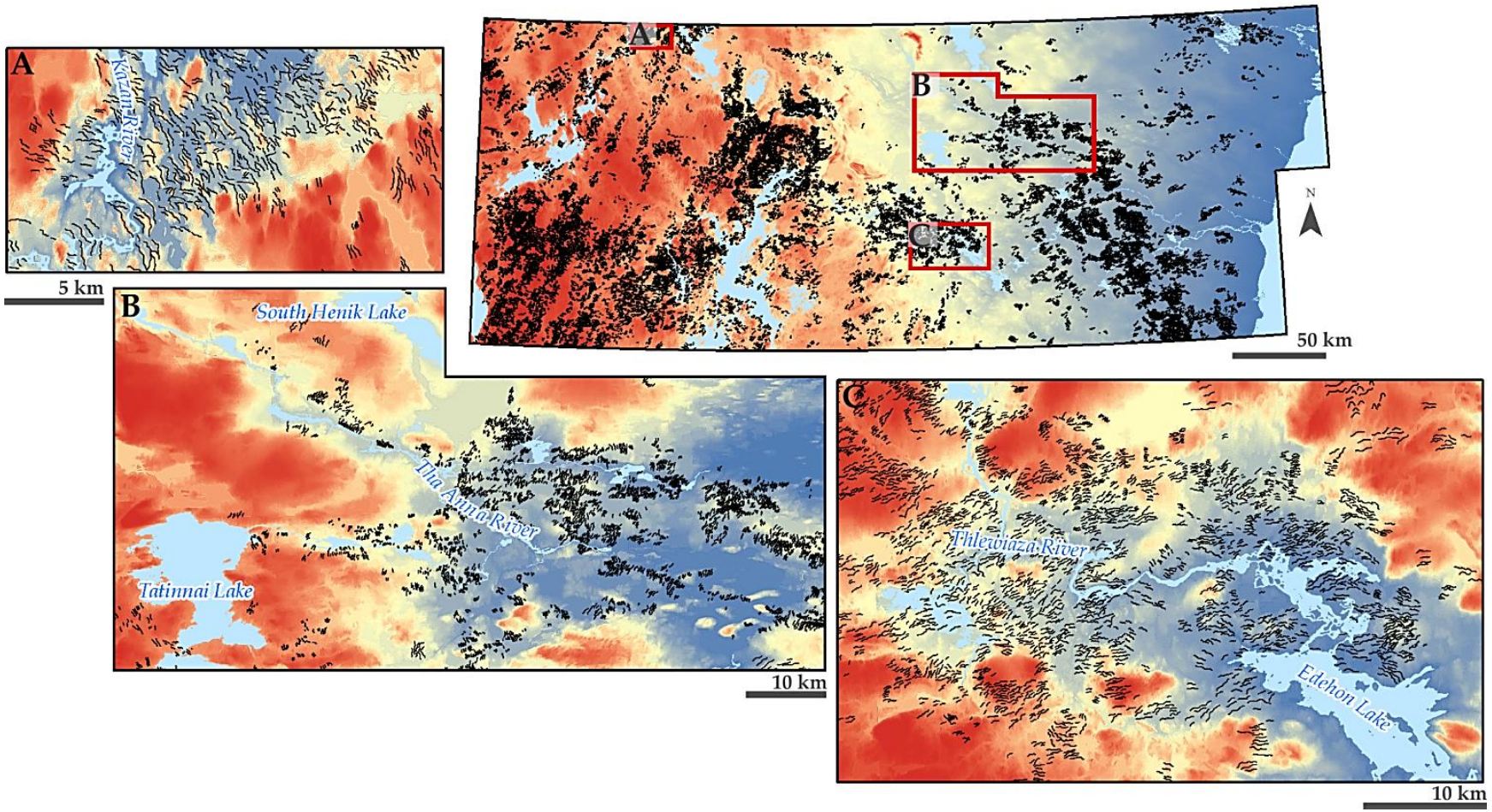

Fig. 5.25 – Examples of ribbed moraine confinement within areas of low topography. Red indicates high elevation, blue indicates low elevation.

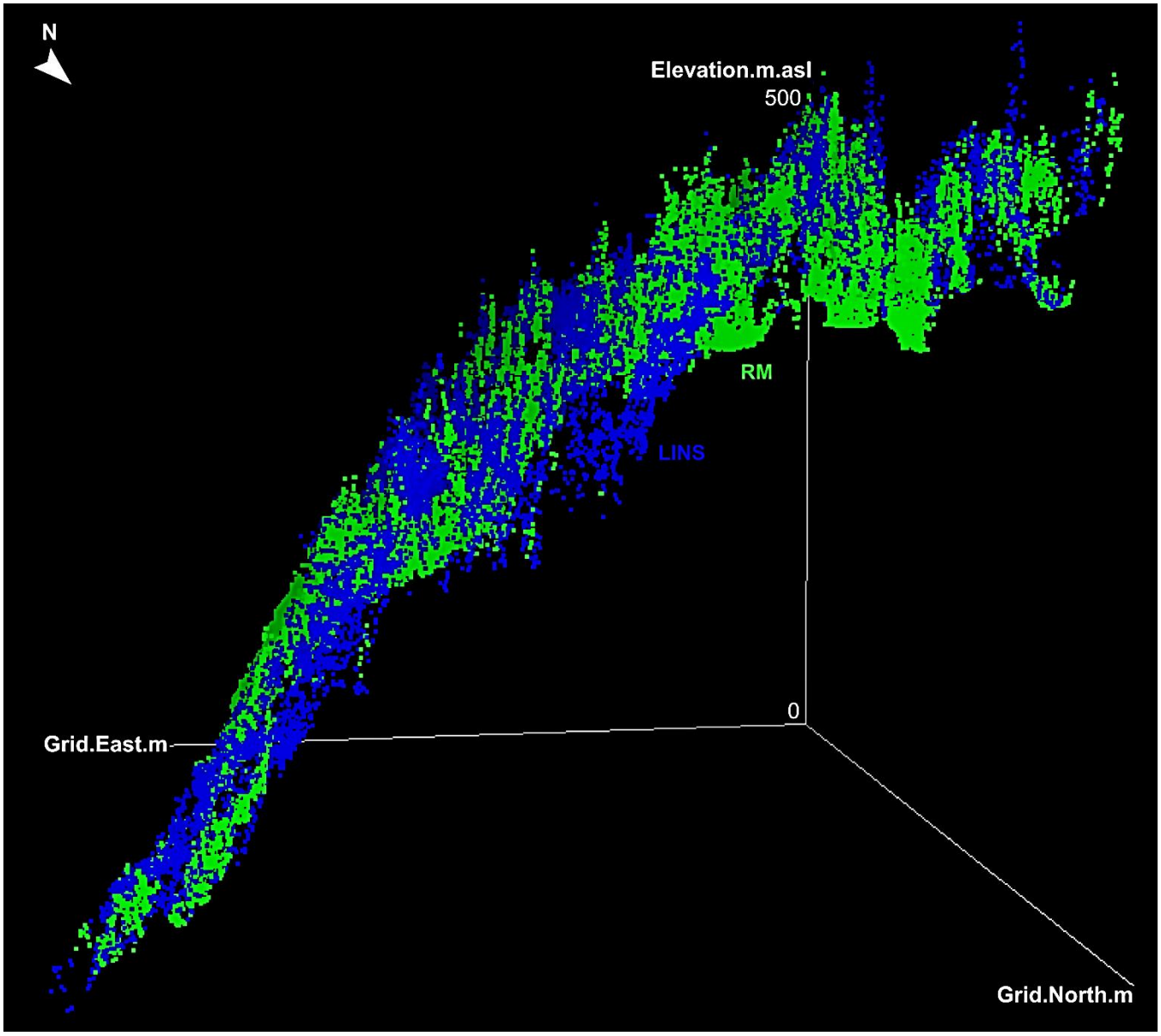

Fig. 5.26 – 3-dimensional scatterplot depicting the altitudinal distribution (m a.s.l.) of glacial bedforms in the study area. RM = ribbed moraines, LINS = glacial lineations. View to the southwest.

Bedform overprinting relationships are not ubiquitous, however, in south-central Keewatin; on the contrary, exclusivity of landforms is observed in many regions. It is common, for instance, that fluted, streamlined, and/or unevenly modified ridges exist in close spatial association with those that retain their pristine morphologies. This is demonstrated in Fig. 5.28 from an area 37 km south of Ennadai Lake, west of Poorfish Lake, where assemblages of heavily fluted ridges to the north and east are found adjacent to a discrete patch of ribbed moraines to the west which exhibit intact, unmodified crestlines. Moreover, surface reflectance varies between fluted and non-fluted ridges (i.e., "pristine" surfaces in Fig. 5.28 appear green to light cyan, overridden surfaces white), suggesting that original

draping deposits (e.g., boulders, supra/englacial detritus) may have been subsequently scavenged from modified ridge crests throughout the process of fluting/drumlinization. Such boundaried variations in morphology and surficial composition imply that thermal and hydraulic conditions at the ice/bed interface evolved independently over localized scales following ribbed moraine formation, and that these dynamic transitions exerted unique geomorphological signatures upon the landscape.

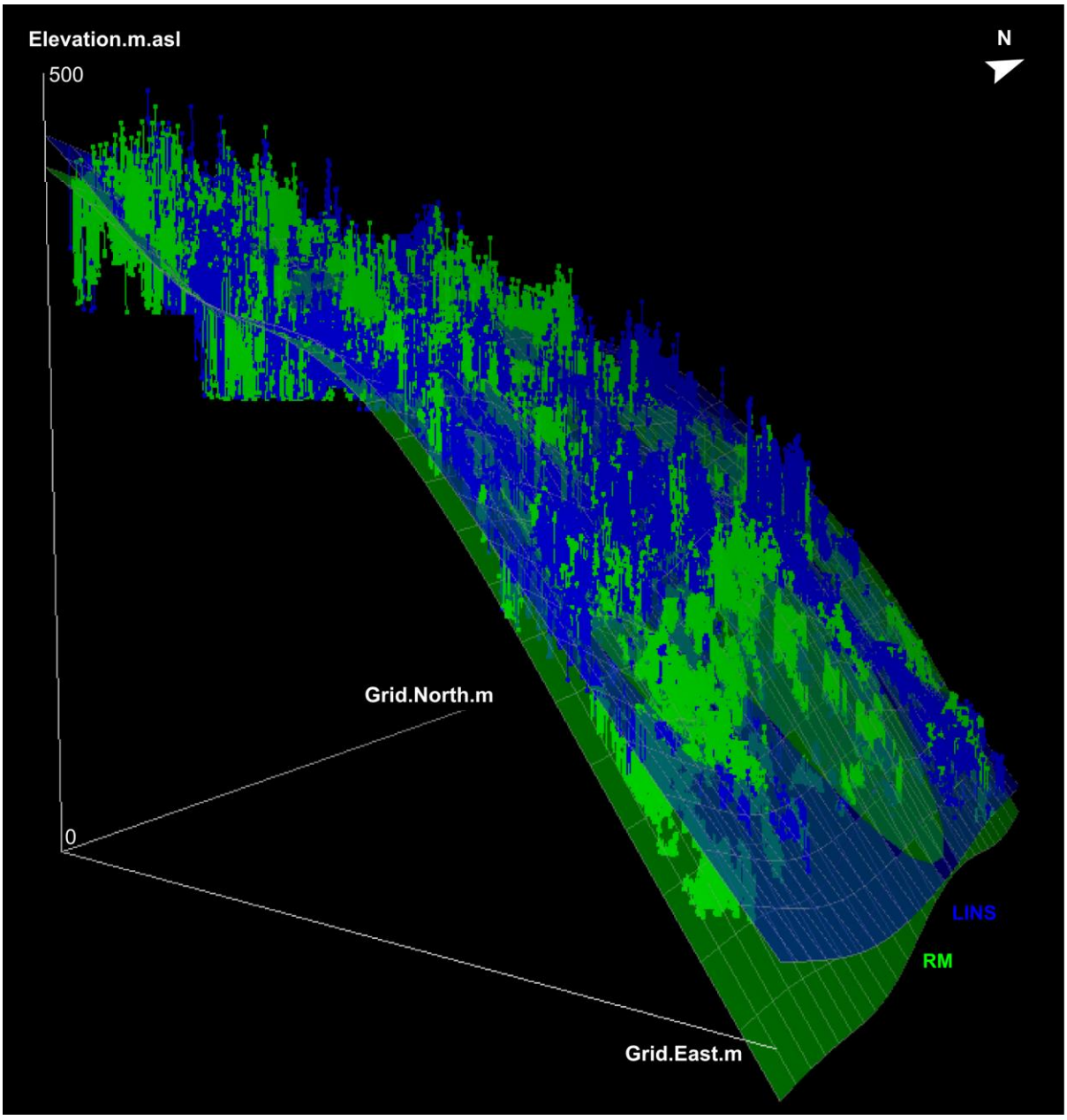

Fig. 5.27 – 3-dimensional scatterplot depicting the altitudinal distribution (m a.s.l.) of glacial bedforms in the study area. Surfaces shown are generated from smoothed regression; data points are shown with difference bars. RM = ribbed moraines, LINS = glacial lineations. View to the northwest.

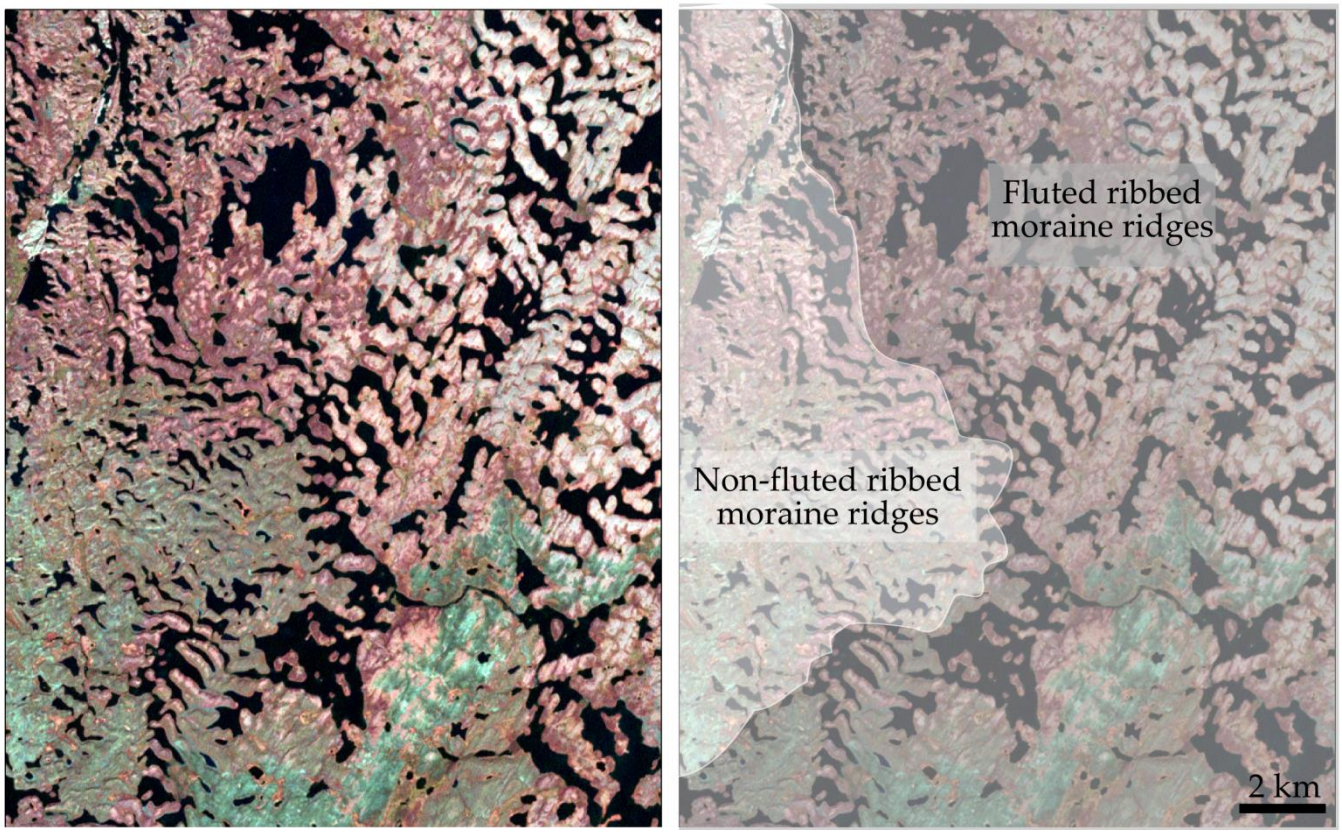

Fig. 5.28 – Landsat ETM + (4,3,2) sub-scene illustrating the close spatial association (and sharp, undulating boundary) between fluted and non-fluted ribbed moraines in an area south of Ennadai Lake. Ice flow is from top right to bottom left.

In south-central Keewatin, the opposite relative age sequence (i.e., ribbed moraines superimposed on glacial lineations) is also observed, though it is acknowledged, in agreement with the pre-existing literature, that this relationship is relatively rare (e.g., Aylsworth and Shilts, 1989a,b; Hättestrand and Kleman, 1999). Descriptions of the specific instances where this sequence is expressed within the study area (and their implications) are offered in section 5.4.2. Here, however, three examples are presented in Fig. 5.29 (see also Fig. 5.41), each showing a unique mode of lineament ribbing and/or overprinting. In Fig. 5.29A, large W-E trending drumlins (transitioning into MSGL to the east, out of frame) are shown in a typical *en echelon* arrangement, east of Thaolintoa Lake, and are flanked to the south by a wide, aligned glaciofluvial corridor infilled with branching eskers and well-sorted glaciofluvial deposits. In the upper left-hand portion of this sub-scene, relatively large, broad crested ribbed moraines obscure faint traces of underlying pre-existing flow-parallel forms, whereas east of this region, small, tightly spaced minor ribbed moraine ridges occupy the swales between adjacent, well-preserved drumlins. Fig. 5.29B presents a separate example, southeast of Debartok Lake, where N-S trending lineations have been completely re-organized into stunted ribbed moraines; evidence of these landforms' earlier pristine morphology is retained by several streamlined landforms in the lower right-hand portion of this sub-scene. Fig. 5.29C depicts elongate NNW-SSE trending streamlined landforms along the Thlewiaza River, southeast of Hurwitz Lake, that are overprinted by diminutive ridges of such minor scale that they approach the threshold for discrete mapping at the spatial resolution of the SPOT imagery datasets.

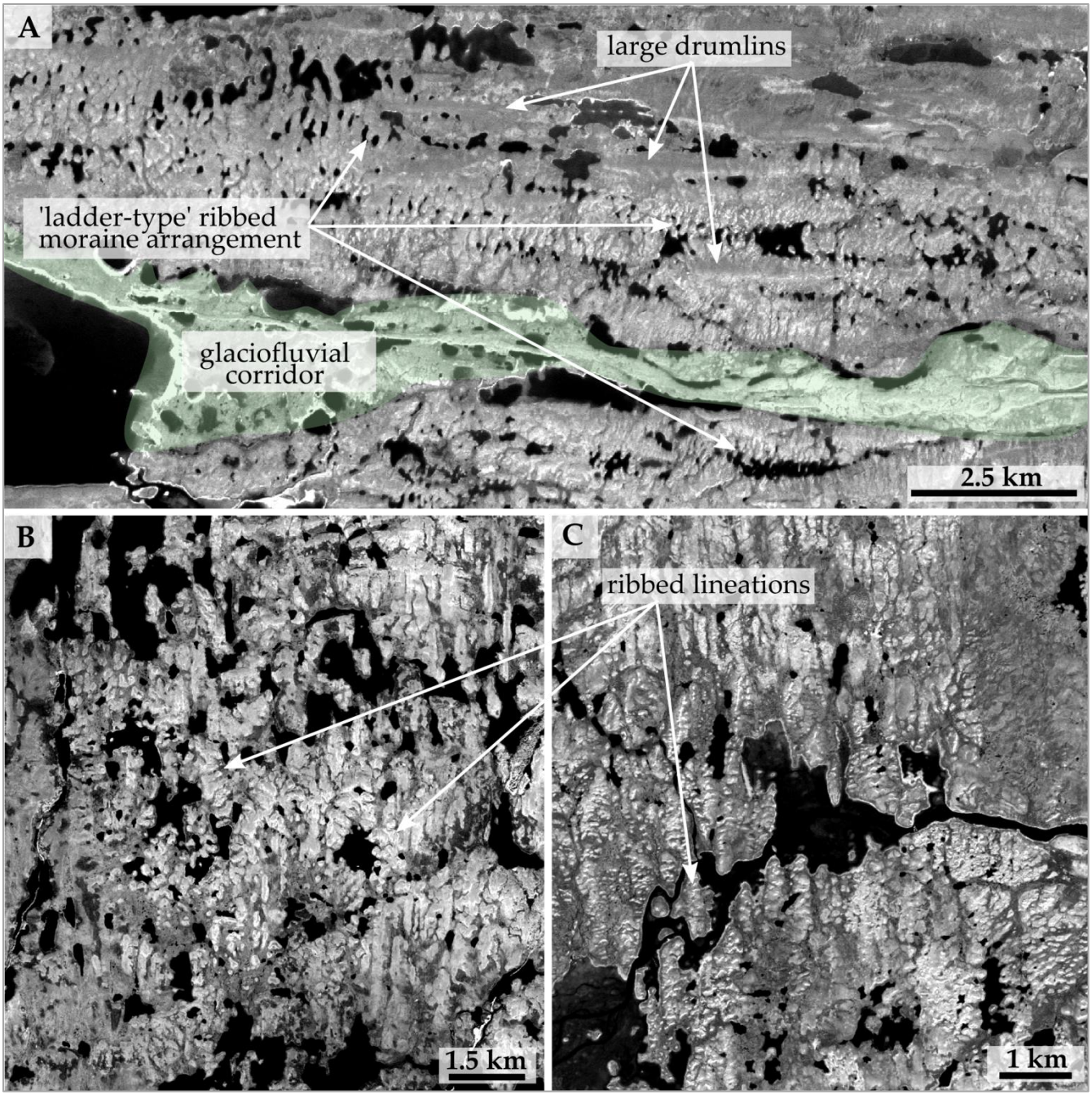

Fig. 5.29 – Examples of rare bedform relationships and relative age sequences in south-central Keewatin. A) Ribbed moraines occupying the swales of surrounding large drumlins, forming a 'ladder-type' arrangement. Ice flow from left to right. B) Glacial lineations broken up into stunted 'ribs'. Ice flow from top to bottom. C) Glacial lineations overprinted by minor ribbed moraines. Ice flow from top to bottom.

Despite the frequency of overprinting mentioned above, exclusive downstream transitions between ribbed moraines and lineations (cf. Lundqvist, 1969, 1989) are also common in south-central Keewatin, as are abrupt lateral transitions (cf. Aylsworth and Shilts, 1989a,b). Fig. 5.30 exemplifies one instance of local landform exclusivity and lateral bedform zonation south of Windy Lake. In this area, hummocky, jagged, and barchan-type ribbed moraines are confined within discrete patches and alternate

in lateral succession with zones dominated by drumlins and flutes. The boundaries between these zones are undulating, though everywhere appear sharp and can be easily delineated. In the right-hand quarter of the sub-scene, a ribbed moraine zone is obliquely overprinted by a prominent esker ridge and partially blanketed by associated glaciofluvial deposits. This relative age sequence (eskers overprinting ribbed moraines) is detected everywhere across the study area without a single observation to the contrary, suggesting that the well-developed esker network that radiates from the position of the late Keewatin Ice Divide was laid down throughout final deglaciation. Above the lowermost portion of this zone, a laterally-continuous, ~3.5 km long, ~30 m tall ridge acts as a partition between hummocky/transverse and streamlined drift deposits; on the basis of its position and morphology, it is hypothesized that this ridge was formed at an abrupt boundary between rapidly-flowing and sluggish basal ice, and is thus tentatively regarded here as a lateral shear margin (cf. Dyke and Morris, 1988). This ridge is one of only a handful of similar features documented within the study area.

Unlike in Fig. 5.30 where bedform zonation is not topographically enforced, Fig. 5.31 provides an example from below Edehon Lake where a prominent NW-SE-oriented bedrock ridge separates low-lying ribbed moraines to the west from SE trending crag-and-tails along the ridge's convex surface. Ribbed moraines in contact with the west-facing slope show faint deflection compared to adjacent ridges towards the lake shoreline, which also record a slightly more easterly ice flow than crag-and-tail ridges along the ridge crest. These ribbed moraines may have experienced topographic shielding and preservation during westerly flowline migration. Alternatively, the distinct zonation and bedform orientation offsets in this area could have arisen from ice deflection, enhanced creep, and local-scale variations at the bed owing to pressure-induced strain differentials between low-lying and convex subglacial terrains.

Gradational and downstream transitions between bedform types are also observed in south-central Keewatin, though these do not everywhere adhere strictly to the classical (proximal-to-distal) ribbed moraine-to-drumlin transition advocated by the "continuum" model (e.g., Aario, 1977a; Boulton, 1987). Fig. 5.32 provides one example of a more complex sequence from below Geillini Lake. Here, a downstream (NW-SE) transition is seen from irregular streamlined terrain into blocky, transverse forms and then finally smaller-scale, intricately arranged hummocky, lumpy and lattice-type ribbed moraine. This zone of transition is circumscribed by a sharp boundary, outside of which exists a dense, disordered network of ribbed moraines and patterned drift draped by well-sorted nearshore deposits and abandoned shorelines and bars. The effect is such that a gradational transition is nested within a strong abrupt lateral transition and surrounded by bedform patterns indicative of varying degrees of overprinting, re-organization and modification (e.g., note the presence of both overridden NW-SE and NNE-SSW trending flutings outside of the main streamlining zone). Fig. 5.33 displays a more simplified transition, wherein NNW-SSE trending drumlins and flutes immediately west of Dutcher Lake transition across a narrow band into blocky angular ribbed moraine ridges, and again further downstream, into elongate streamlined forms.

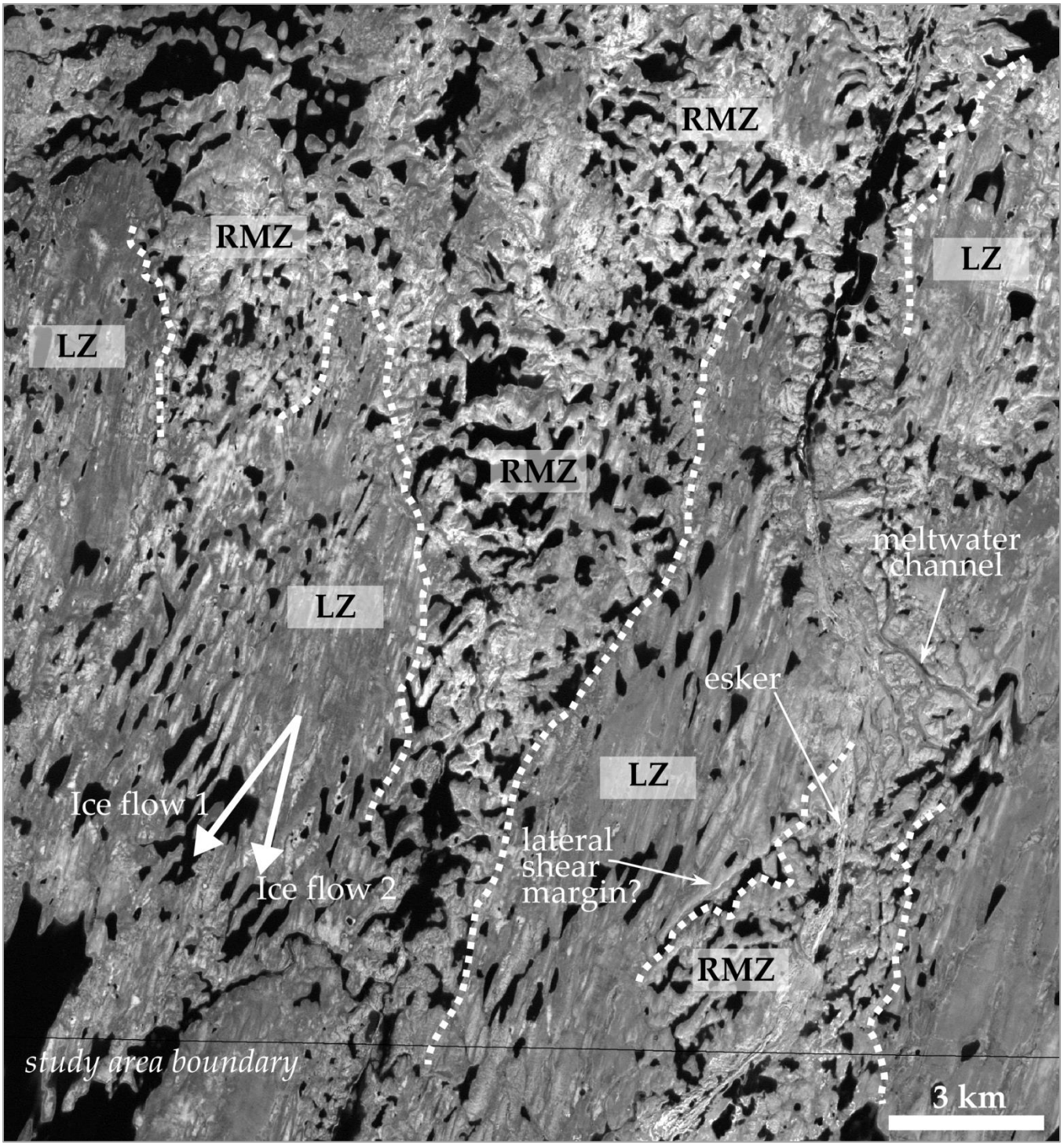

Fig. 5.30 – Abrupt lateral transitions between ribbed moraines and streamlined terrain. LZ = lineation zone, RMZ = ribbed moraine zone. Ice flow is to the SW (1) and SSW (2).

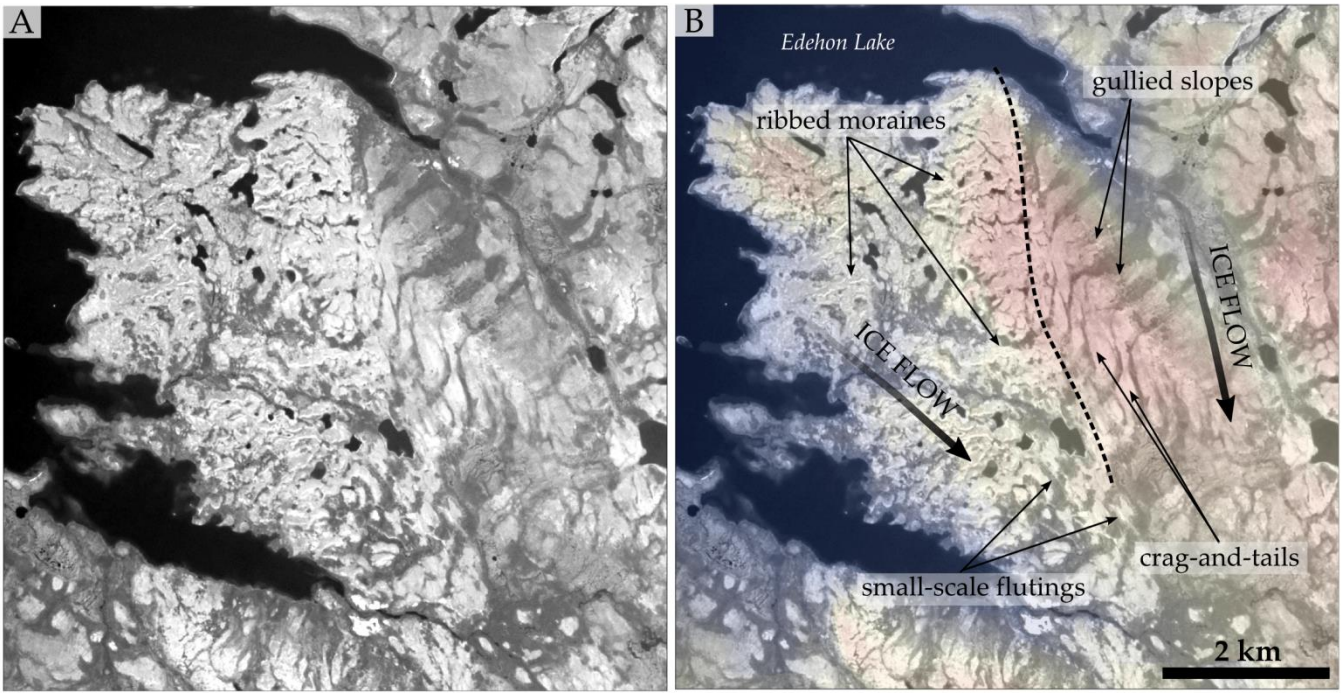

Fig. 5.31 – Abrupt lateral bedform transition south of Edehon Lake. A) Ribbed moraines and small-scale flutings indicating ice flow to the southeast are located adjacent to crag-and-tail landforms oriented ~170° and separated by a bedrock ridge. Ribbed moraines positioned along the flank of the bedrock ridge exhibit slight deflection compared to those situated at lower-lying elevation to the west. B) CDED elevation data draped over SPOT image; warm (cool) colours indicate high (low) elevation. Evidence in this area suggests local-scale topographic influence on landform formation, zonation and preservation.

5.4.1.3 ***Individual Ridge Morphological Characteristics***

Within south-central Keewatin, it is evident that many, and indeed, the majority of identified ribbed moraines fit the "classical" description of transverse-to-ice flow, down-ice concave ridges, featuring relatively regular crest-to-crest spacing, and organized within coherent assemblages or fields (cf. Hättestrand, 1997). Fig. 5.34 provides a good example of these types of landforms. Of the 47 ridges depicted in this sub-scene, most appear curving, and many with horns at their lateral extremities that are bent down-ice. Each ridge displays similar orientation and is tightly aligned within a sequence of parallel bands. Excepting the anastomosing and broad arcuate varieties also shown in this image, most ridges have relatively similar lengths and widths with respect to their neighbouring forms (though as a field, these narrow down ice), and exhibit remarkably consistent, ~250 m crest-to-crest wavelengths. Several of these ridges demonstrate asymmetry in their cross profile (Fig. 5.35), though most appear symmetrical, with both broad- and flat-crested surfaces and feature occasional proximal and/or lee-side terraces. In other places, "classical" asymmetric profiles (steeper sloping distal faces) and lee-side terraces are found more commonly, though these are evidently not universal characteristics among all classically-shaped ribbed moraines in the study area. Despite several of the ridges in Fig. 5.34 (top, center) which bear slight superimposed drumlinoid elements, the relationship with streamlined landforms is mostly exclusive, corresponding to Lundqvist's (1969) classical definition, with the latter transitioning into the former, and then again transitioning into the latter down-ice (out of view) (Fig. 3.4).

Fig. 5.32 – An area of complex bedform transitions. LZ = lineation zone, RMZ = ribbed moraine zone. Lineations are confined to a narrow, down-ice tapering strip where they progressively pull apart blocks of drift into angular, transverse forms. The zone of progressive ribbing is surrounded by fields of smaller scale ribbed moraine which are draped by nearshore deposits and show evidence of development throughout multiple phases of ice flow.

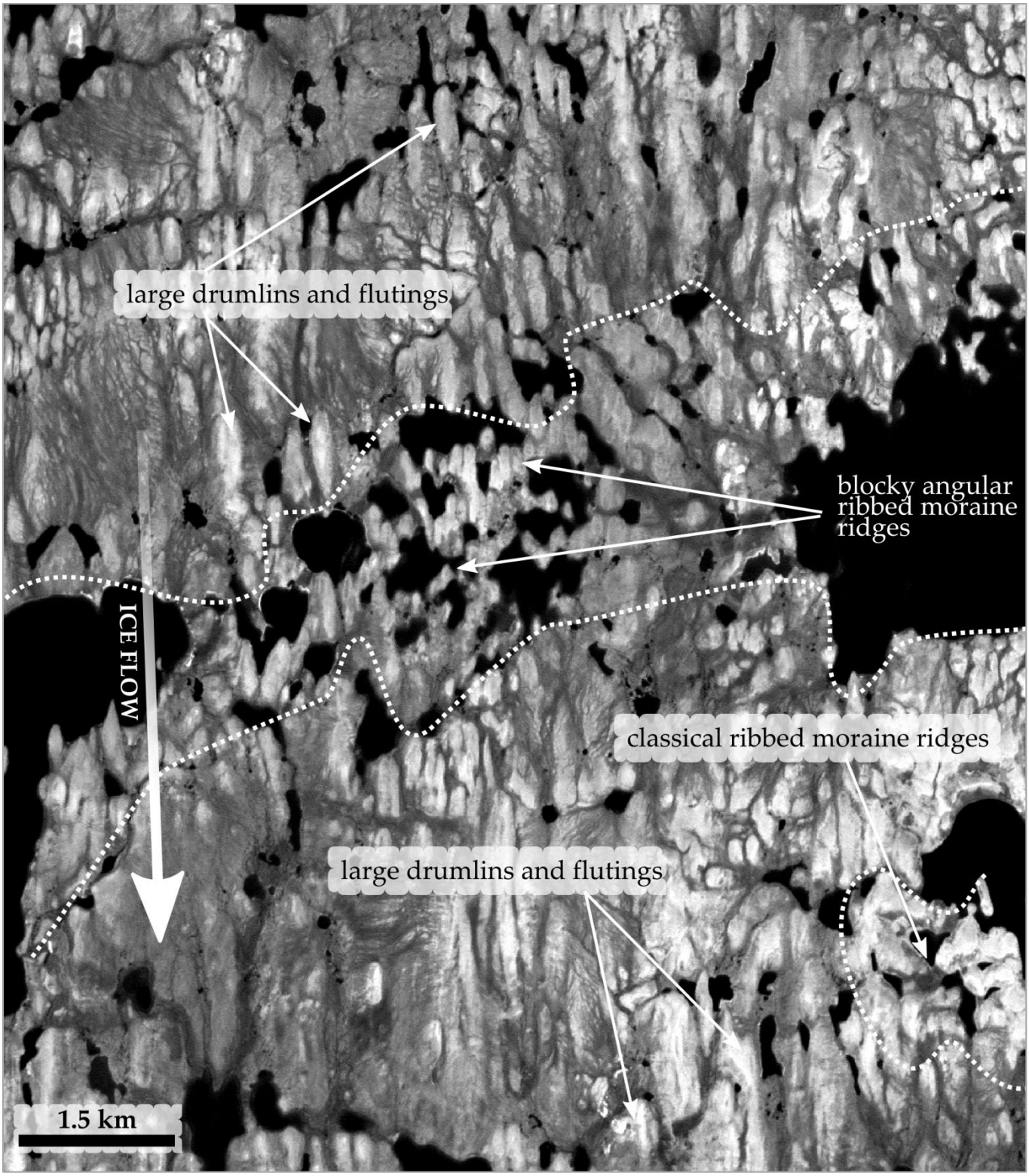

Fig. 5.33 – Example of a “classical” bedform transition, showing clear zonation between drumlins and fluted ribbed moraines and down-ice transitions between forms.

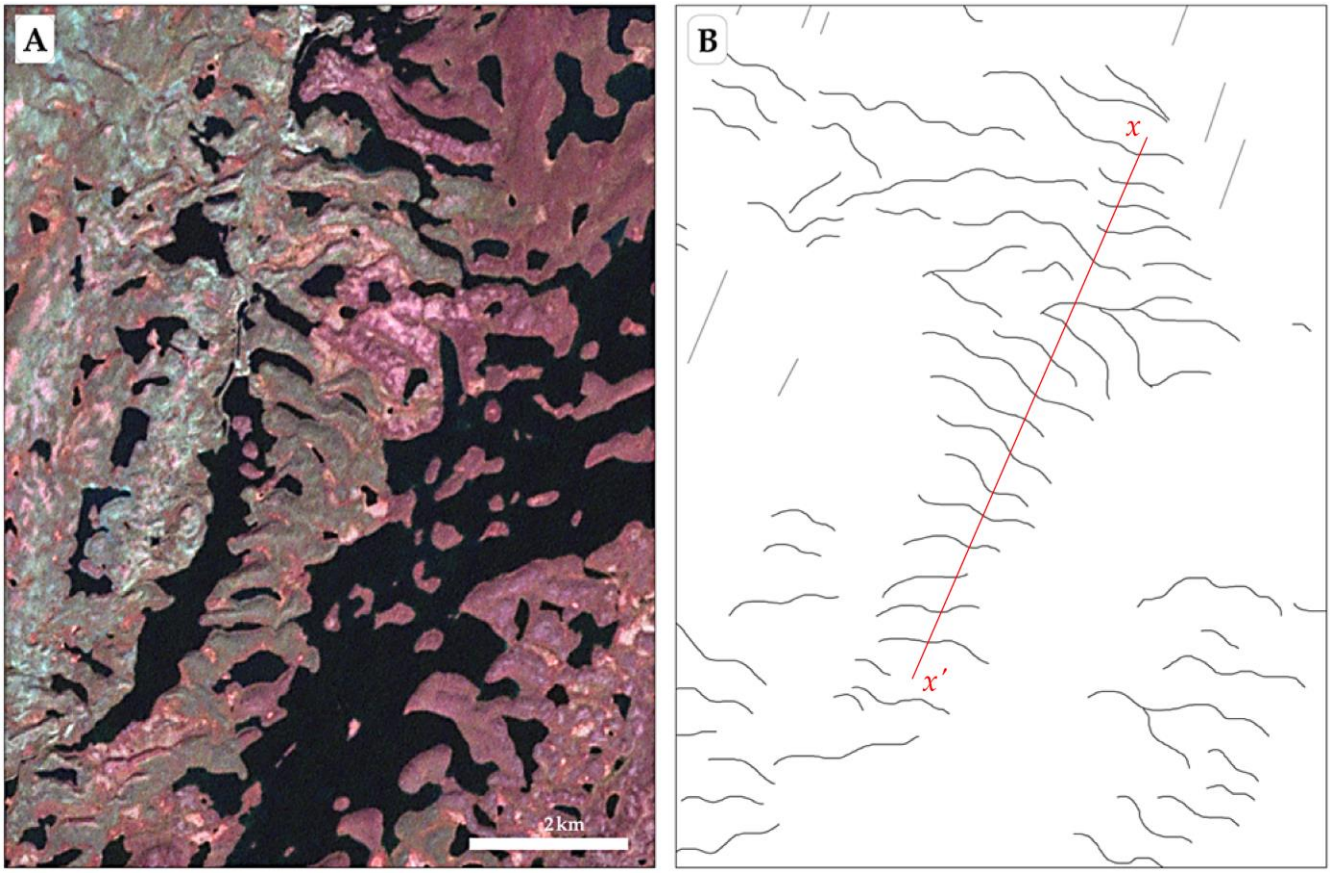

Fig. 5.34 – Classical ribbed moraines, showing arcuate planiforms, consistent spacing and down-ice pointing horns. Transect *x – x'* shown in B) corresponds to Fig. 5.35. Line features in the map view indicate ribbed moraines (black) and streamlined landforms (grey). Ice flow is from the top right to bottom left.

Broader inspection of ribbed moraine ridges in south-central Keewatin attests to the fact that "classical" ribbed moraine attributes are absent in many fields. Thus in addition to ridges displaying the above characteristics, it is possible to recognize a puzzling array of alternative forms, including upstream curving, blocky angular, anastomosing, barchan-shaped, jagged, lumpy, lattice-type, hummocky, minor, and broad arcuate and rectangular ribbed moraine ridges (Fig. 5.12). These classifications were first adopted by Dunlop and Clark (2006b) to describe bedform assemblages throughout north-central Ireland, Québec/Labrador, and the Lake Rogen type locality in Sweden. The usefulness of these terms for relating similar forms in Keewatin is immediately apparent and was utilized in this study to develop individual quantitative datasets for each subpopulation. Two additional templates, "extensional" and "streamlined" are also applied here, though are not explicitly handled in the previous classification scheme.

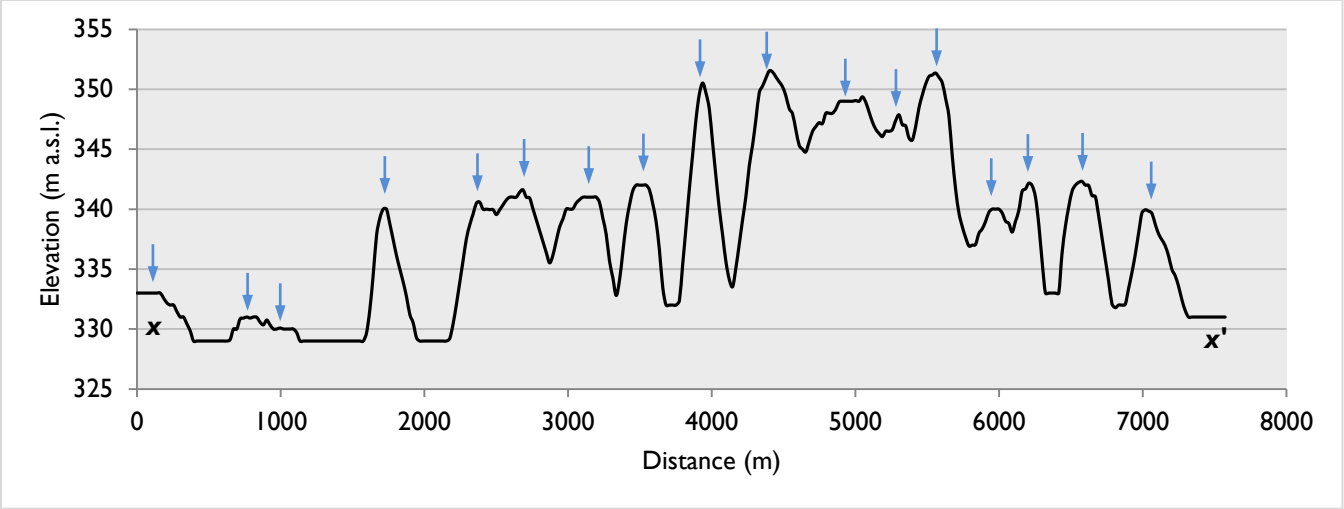

Fig. 5.35 – Transect *x – x'* across the classical ribbed moraine track shown in Fig. 5.34. Blue arrows denote individual ridge crests. Note the general cross-profile symmetry of ridges, their ability to display both broad-crested and sharp surfaces, and their tendency to exhibit multiple crests or terraces.

Fig. 5.37 presents three alternative morphologies recognized in south-central Keewatin. Some of these ridges show very little curvature and lack the smooth outlines of classically-shaped ribbed moraines. A relatively large number of ridges throughout the study area feature rough or *jagged* perimeters with planiforms that have somewhat more ambiguous relation to palaeo-ice flow than the smooth and transverse outline of classical forms (Fig. 5.37A). Where these outlines feature bulbous protrusions, and where ridge width and spacing vary within a small area, clusters of *lumpy* ribbed moraines can be identified. In many places, ribbed moraines lack the "classical" upstream/downstream transition into drumlins, and are instead heavily overprinted by linear elements (Fig. 5.37B and C), the latter of which regularly have orientations perpendicular to that of the ribbed moraine. Very often, the process of drumlinization appears to have re-moulded and/or attenuated portions of the underlying landform down-ice, and in such instances these features can be described as *streamlined*. Where drumlinization has occurred parallel or near-parallel to the ridge long-axis, long, protracted *extensional* ribbed moraines are formed; not surprisingly, these are found almost exclusively in areas of sharp (≥90˚) ice flow direction transitions (Fig. 5.36). Along the fringes of some streamlined landform fields, individual lineaments appear to have been re-moulded perpendicular to their long axes, and these modified forms – demonstrative, perhaps, of Boulton's (1987) two-step ribbed moraine landform – are here also classified as "extensional" ridges.

Certain other ridges are found commonly between fields of streamlined ribbed moraines (though occur also in broad swaths, independent of other forms) which reveal branching or *anastomosing* limbs – a quality argued by Hättestrand (1997) and Hättestrand and Kleman (1999) as belonging to the classical ribbed moraine, but here recognized as the typifying feature of a separate morphology, considering the prevalence of otherwise "classically-shaped" ridges mapped in this study that do not have anastomosing limbs. Those shown in Fig. 5.39B are confined to a ~13 x 10 km area and tend to be somewhat longer (up to 2,700 m) and more closely spaced (~150–200 m) than other morphologies in the vicinity. These also lack the drumlinization of surrounding landforms, suggesting that anastomosing patterns may be primary attributes of this morphology; note however that fluted anastomosing ridges are commonly seen elsewhere throughout the study area.

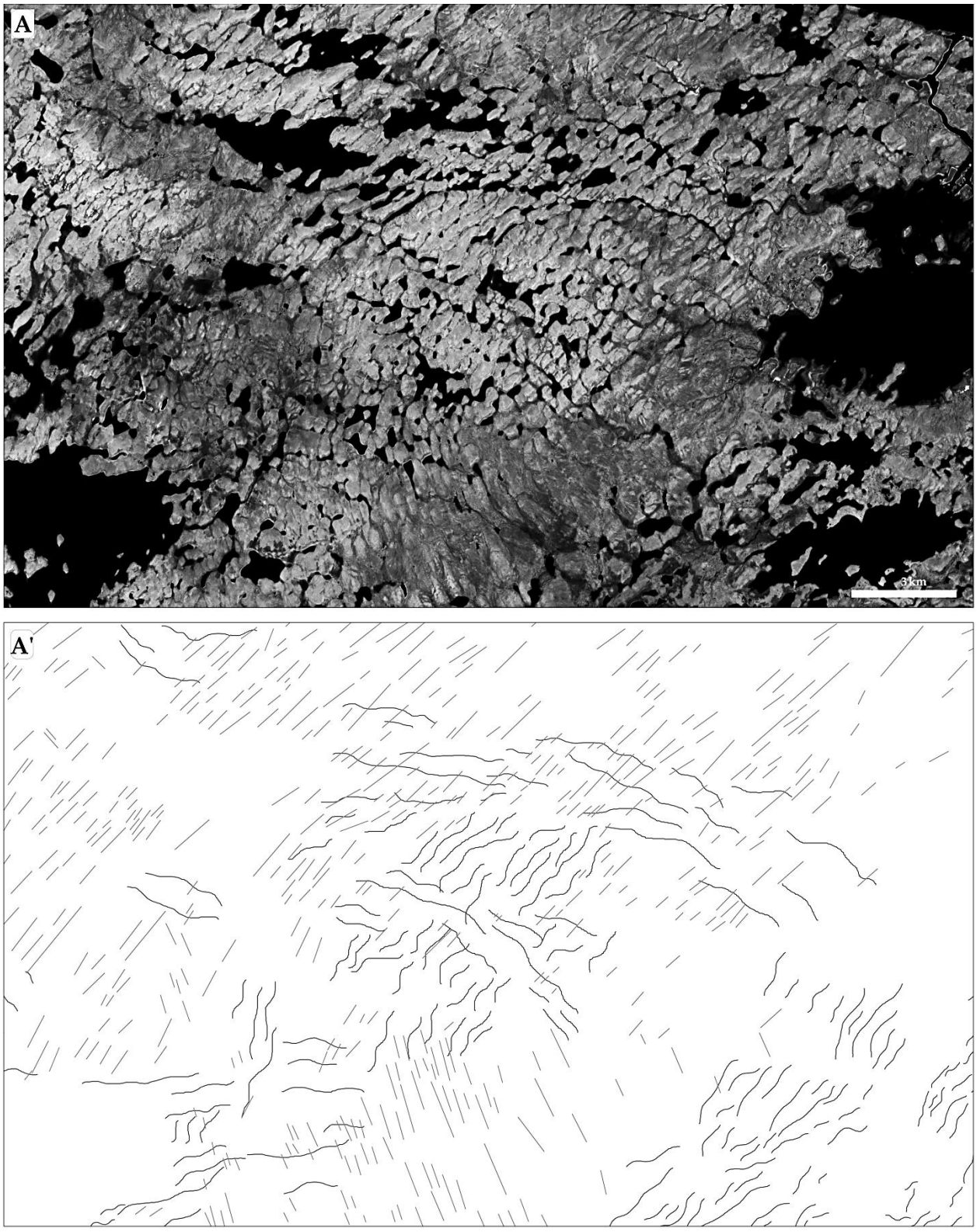

Fig. 5.36 – Extensional ribbed moraines located in an area of clear ice flow transition. Extensional forms are developed by overprinting both parallel and perpendicular to pre-existing ridges. Line features in the map view indicate ribbed moraines (black) and streamlined landforms (grey). Separate ice flows are shown trending towards the top right and bottom right.

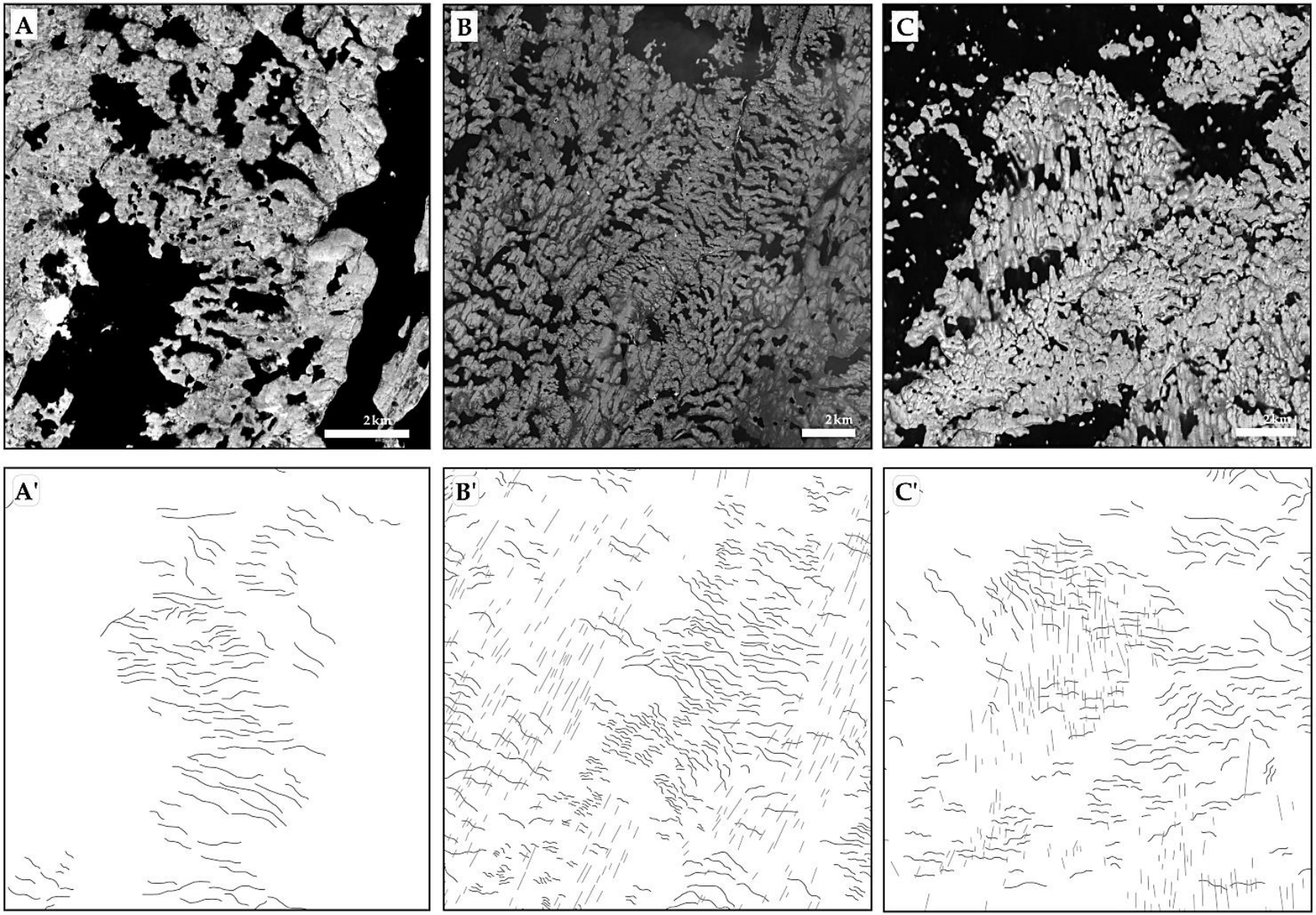

Fig. 5.37 – Examples of non-classical ribbed moraine morphologies. A) Jagged. B) Anastomosing and Streamlined. C) Streamlined. Line features in the map view indicate ribbed moraines (black) and streamlined landforms (grey).

Lattice-type ribbed moraines also demonstrate anastomosing limbs, although these features are generally much smaller in scale, and the visual distinction between the primary ridge element and inter-connecting cross-ribs is much less apparent. Lattice structures tend to occur in isolated pockets and may feature well-defined, geometric edges (e.g., Fig. 5.38), or else have a more irregular, lumpy appearance. In certain areas, these features form dense conjugate ridge networks. Pure overprinting of ribbed moraine landforms is rare, however, where it does occur, it is typically expressed within fields of lattice-type ribbed moraines.

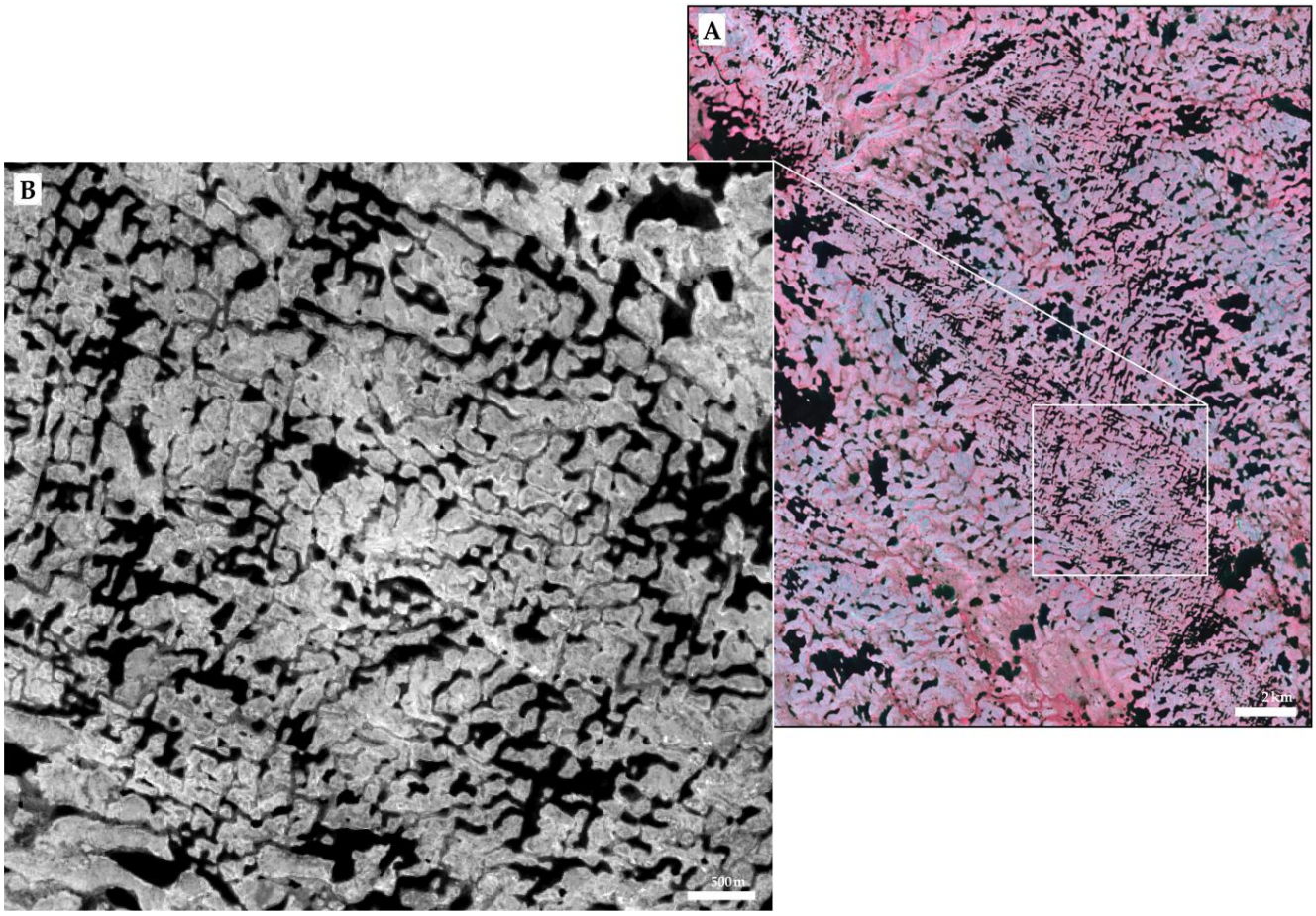

Fig. 5.38 – Lattice-type ribbed moraines south of Geillini Lake. In this example, lattice-structures are comprised of sharp, geometric forms, though elsewhere they are found also with more poorly-defined edges.

Whereas ribbed moraines have in the past been distinguished on the basis of a crescentic long axis profile, capped by prominent spurs and horns that point down-ice (Hättestrand and Kleman, 1999), select morphologies identified in this study instead reveal wide, rectangular, or only slightly curving arrangements, with square long axis edges devoid of any attenuated elements. These *broad arcuate* (Fig. 5.39B) and *broad rectangular* (Fig. 5.39A) ridges are found throughout southern Nunavut, the latter often occupying narrow zones, justified along one of their edges, somewhat akin to the steps of a ladder, though occasionally, as is demonstrated in Fig. 5.39A, existing within wider, laterally- and down-flow continuous patches. Broad arcuate ridges share many characteristics with "classical" ribbed moraines, having both a curving planiform and a typically regular wavelength, however the former demonstrate much lower length/width ratios, are usually less crescentic and normally do not feature pronounced

down-ice pointing spurs. In some areas, as shown in Fig. 5.39B, broad arcuate ridges appear blotchy or poorly formed, with little discernible intra-field organization. In other examples, broad ridges are obliquely overprinted and reshaped by linear elements, giving them a *blocky angular* appearance (Fig. 5.40C). Unlike streamlined ribbed moraines, however, those with blocky angular planiforms are also found in places without evidence of drumlinization or overprinting, tend to be somewhat more localized, and usually have lower length/width ratios.

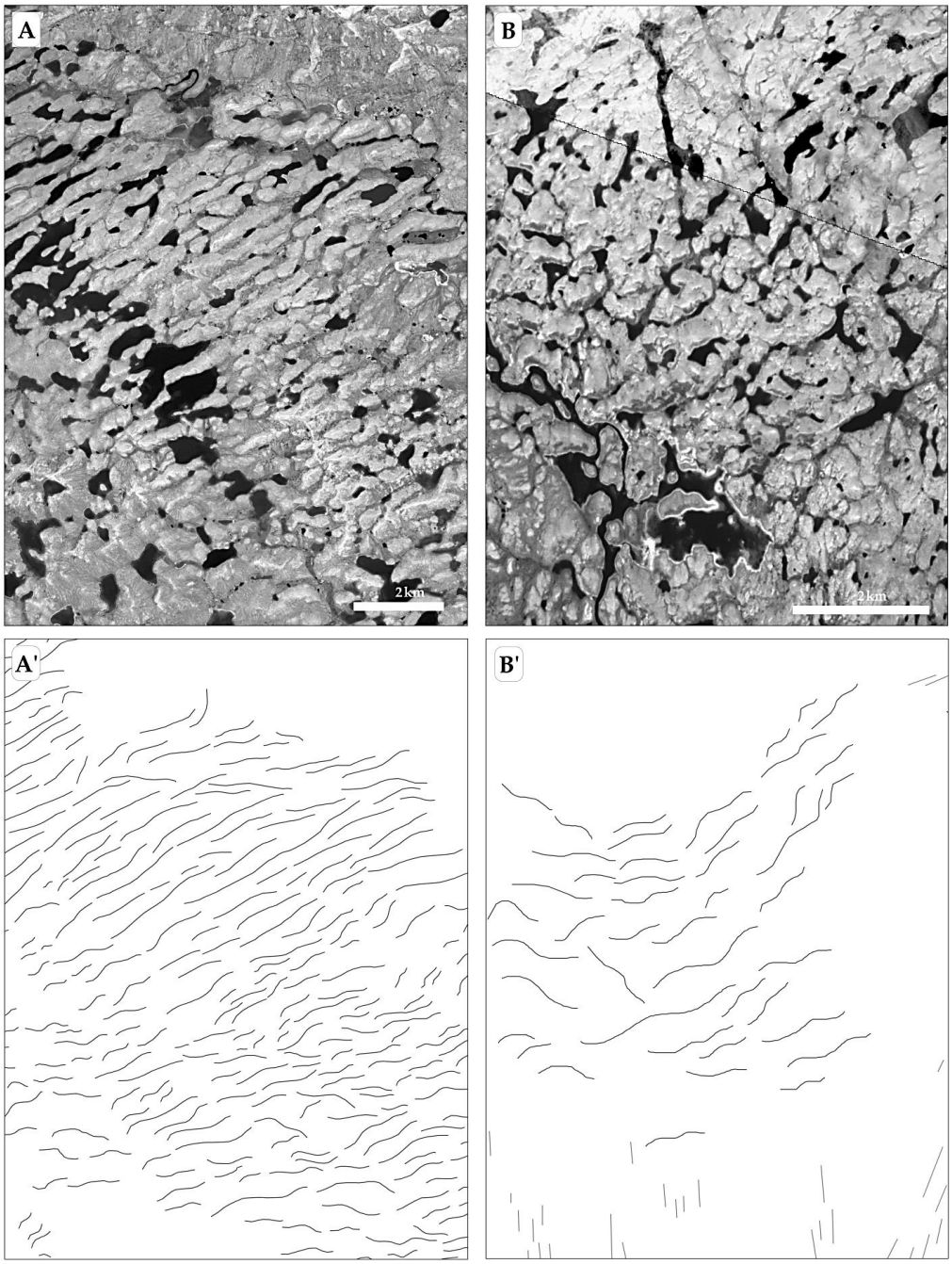

Fig. 5.39 – Examples of non-classical ribbed moraine morphologies in south-central Keewatin. A) Broad rectangular. B) Broad arcuate. Note that ridges in A) show some degree of lateral continuity, though commonly this morphology exhibits narrow, down-ice zonation. Line features in the map view indicate ribbed moraines (black) and streamlined landforms (grey).

Other transverse bedforms in this region depart much more drastically from the classical variety of ribbed moraine. Some of these have characteristics that are, in fact, antithetical to the classical definition, such as *upstream curving* ridges, which are convex in the down-ice direction. Generally these are found as isolated features within fields of hummocky, or conventionally-oriented ribbed moraines (e.g., Fig. 5.40A), though occasionally smaller upstream curving ridges are nested downflow within a series of larger specimens, or they may alternatively occur within regularly-spaced tracks, in similar fashion to their 'classical' counterparts. Certain transverse landforms feature undulating longitudinal profiles, and often take on the shape of irregular mounds or hummocks. Nevertheless, these occur in and amongst better-developed fields of ribbed moraines and are here designated as the *hummocky* ribbed moraine morphology. Hummocky ribbed moraines are found in great numbers throughout the study area though are especially well-represented east of the marine limit, providing good evidence that this morphology may be derived by reworking. Elsewhere in southern Nunavut, hummocky ridges protrude from the centers of shallow lakes or are located along the flanks of large esker ridges or beaded glaciofluvial deposits. These vary greatly in size and shape and are often irregularly spaced within a particular field. They are occasionally overprinted by drumlinoid elements, but the frequency of such overprinting is noticeably less than for most other morphologies.

Where streamlining of a ridge element appears to approach complete reshaping, *barchan shaped* ribbed moraines typically result, noteworthy for their morphological similarity to the aeolian forms of the same designation. The glacigenic variety are very short, stunted landforms that have previously been interpreted as a transitional morphology between ice flow-parallel and ice-flow transverse landforms within a proximal to distal bedforming continuum (section 3.2.5). The examples shown in Fig. 5.40B occur amongst jagged, blocky angular, and classically-shaped ridges and exhibit clear evidence of post-depositional drumlinization and re-moulding at an angle oblique to the primary ridge axis. In this particular instance, barchan shaped ridges have been excised from adjacent features and occur as independent landforms, though quite often, these ridges are connected to neighbouring barchans at their horns, forming a linked array of ridges with slight along-axis offsets in successive hinge positions. In most cases, the limbs of barchan shaped ridges are asymmetric, with one being disproportionately longer than the other, and generally paralleling the strongest ice flow direction imprinted on surrounding terrain.

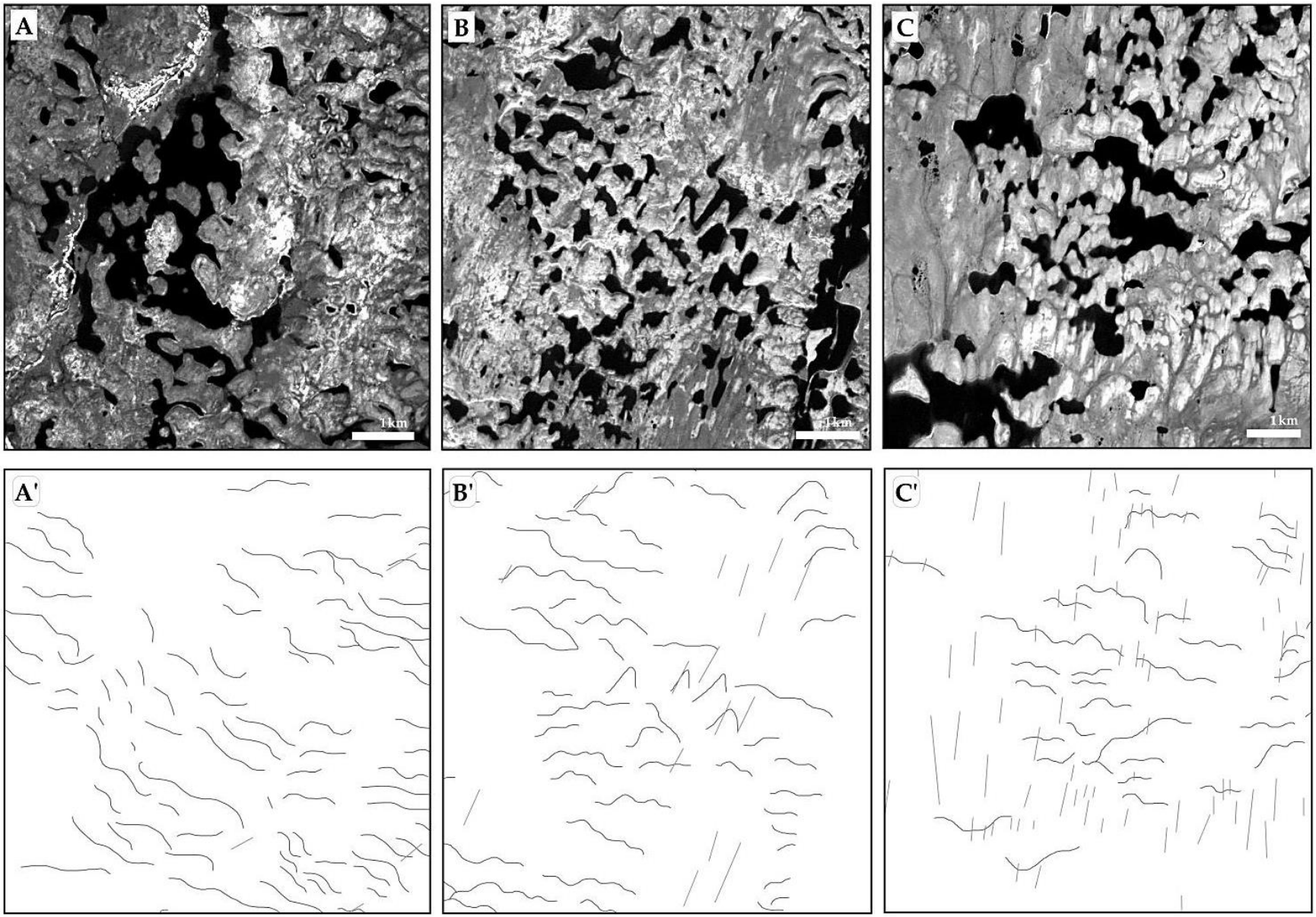

Fig. 5.40 – Examples of non-classical ribbed moraine morphologies in south-central Keewatin. A) Hummocky and upstream curving. B) Lumpy and barchan-type. C) Blocky angular and upstream curving. Line features in the map view indicate ribbed moraines (black) and streamlined landforms (grey).

Assemblages of *minor* ribbed moraines are also documented within the study area, featuring restricted lengths and widths, close spacing and remarkable wavelength consistency. These features possess many of the attributes common to the "classical" ribbed moraine morphology, though occur everywhere at smaller scales. Minor ribbed moraines are only very infrequently drumlinized; instead, they are unique in their tendency to display the opposite relative age relationship with streamlined landforms, where they are commonly found overprinting drumlins and MSGL (Fig. 5.41), or appearing to have fragmented the latter features into a succession of stunted transverse ridges.

Large, so-called "mega-scale" transverse ridges have also been previously identified in southern and central Keewatin (Kleman et al., 2002, 2010; Greenwood and Kleman, 2010). Greenwood and Kleman (2010) mapped over 200 individual "till belts" in this area that they interpreted as forming transverse to ice flow within an active subglacial environment. Their mapping identified numerous fields of these features, exhibiting extremely variable morphologies, and with dimensions much larger than 'typical' ribbed moraines (length $\bar{x}$ = 13.7 km, width $\bar{x}$ = 2.4 km, ER $\bar{x}$ = 5.7). A separate specific grouping of these ridges occurs within a ~350 km long (~50 km wide) band running east from Ennadai Lake towards Hudson Bay. The lateral continuity of this grouping, and its weak concavity towards the northeast, has been interpreted as evidence that this specific subset of "mega-scale" ridges are, in-fact, overridden ice-marginal end moraines, formed during an early S/SE ice flow into the Keewatin region prior to the establishment of a late deglacial Keewatin Ice Divide (Kleman et al., 2002, 2010; Greenwood and Kleman, 2010). Dredge et al. (2007) identify ridges of similar scale from northern Manitoba that they also interpret as overridden ice-marginal end moraines.

Many similar "mega-scale" features were identified in the present study, exhibiting comparably large dimensions, and showing heavy modification and overprinting. An example is provided in Fig. 5.42 from below Downer Lake, illustrating the enormous scale and complex morphology of these features. There exists evidence, however, that the nature of these features has been overconfidently interpreted. For instance, Figure 7a in Kleman et al. (2002) depicts a large, NE-SW trending ridge between Sealhole and Fitzpatrick Lakes that is construed by those authors as a "massive moraine" (forming part of the Ennadai-Nueltin end moraine belt described above). This same feature is shown here in Fig. 5.43B, though is presented within its regional context in Fig. 5.43A, beneath N-S trending quartz arenite outcrops, mapped by Aspler et al. (2000) as the Whiterock and Middle Maguse members of the Paleoproterozoic Hurwitz Group (Central Hearne Domain). The alignment of these bedrock ridges above the "massive moraine" feature of Kleman et al. (2002), in addition to small outcrops/patches of thin drift along the ridge feature itself (shown in cyan on the ETM+ 4,3,2 false-coloured sub-scene in Fig. 5.43B), indicate substantial bedrock control on the organization of surface deposits in this area, and provides good evidence that many large ridges in central and southern Keewatin have perhaps been genetically misinterpreted. Consequently, the existence of outsized transverse ridges within south-central Keewatin is recognized in this study, though lacking ground-truth, and given considerable uncertainty regarding their origin, they have not here been exhaustively mapped, and are not incorporated as a central component of the regional glacial landsystem.

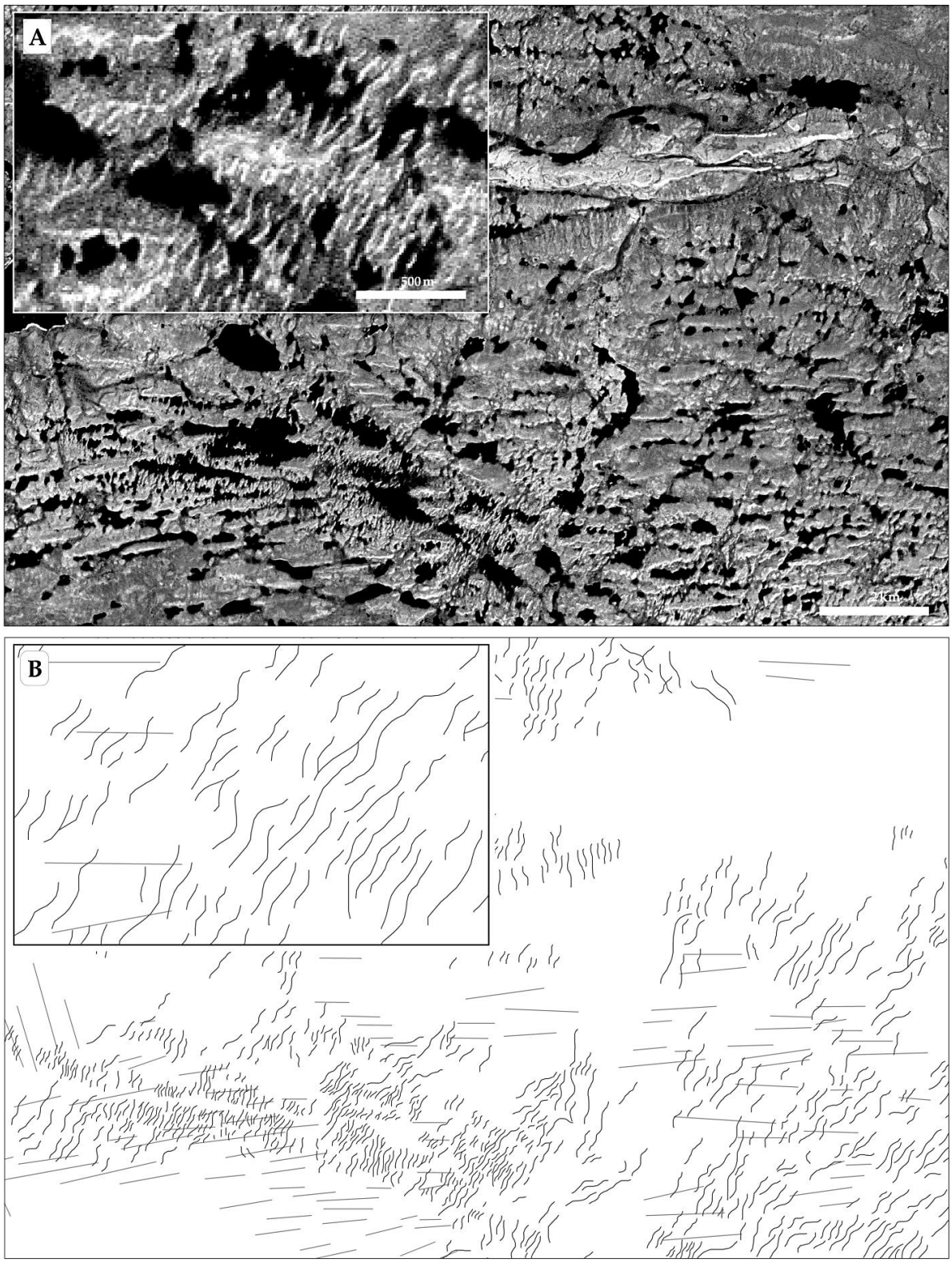

Fig. 5.41 – Minor ribbed moraines, shown here overprinting MSGLs east of Thaolintoa Lake. Inset shows features at enhanced scale. The limited dimensions of these ridges approach the threshold for discrete mapping using SPOT 4/5 (10 m) imagery. Line features in the map view indicate ribbed moraines (black) and streamlined landforms (grey). Ice flow from left to right.

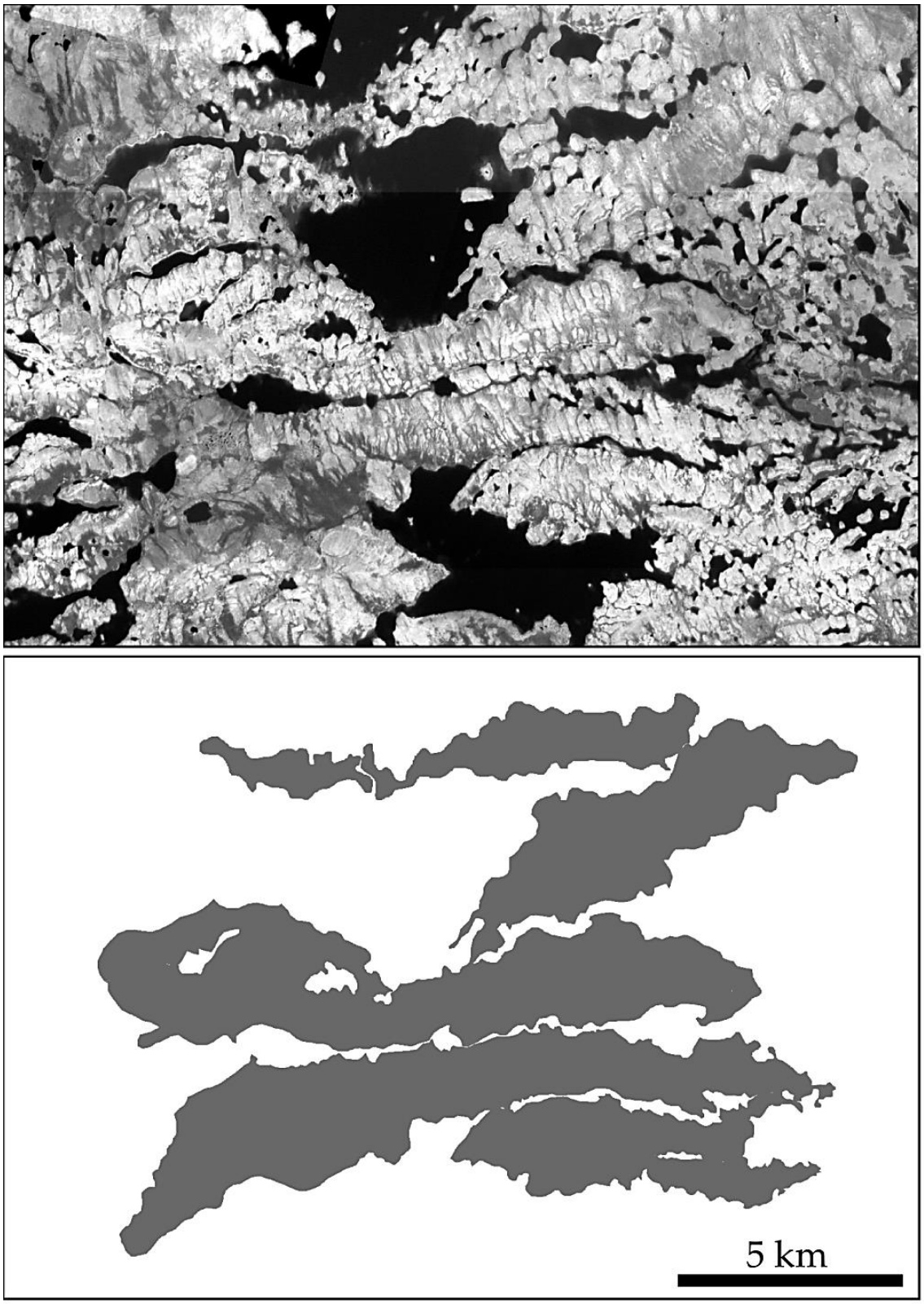

Fig. 5.42 – Heavily drumlinized “mega-scale” transverse ridges, up to 18 km long, surrounding Downer Lake.

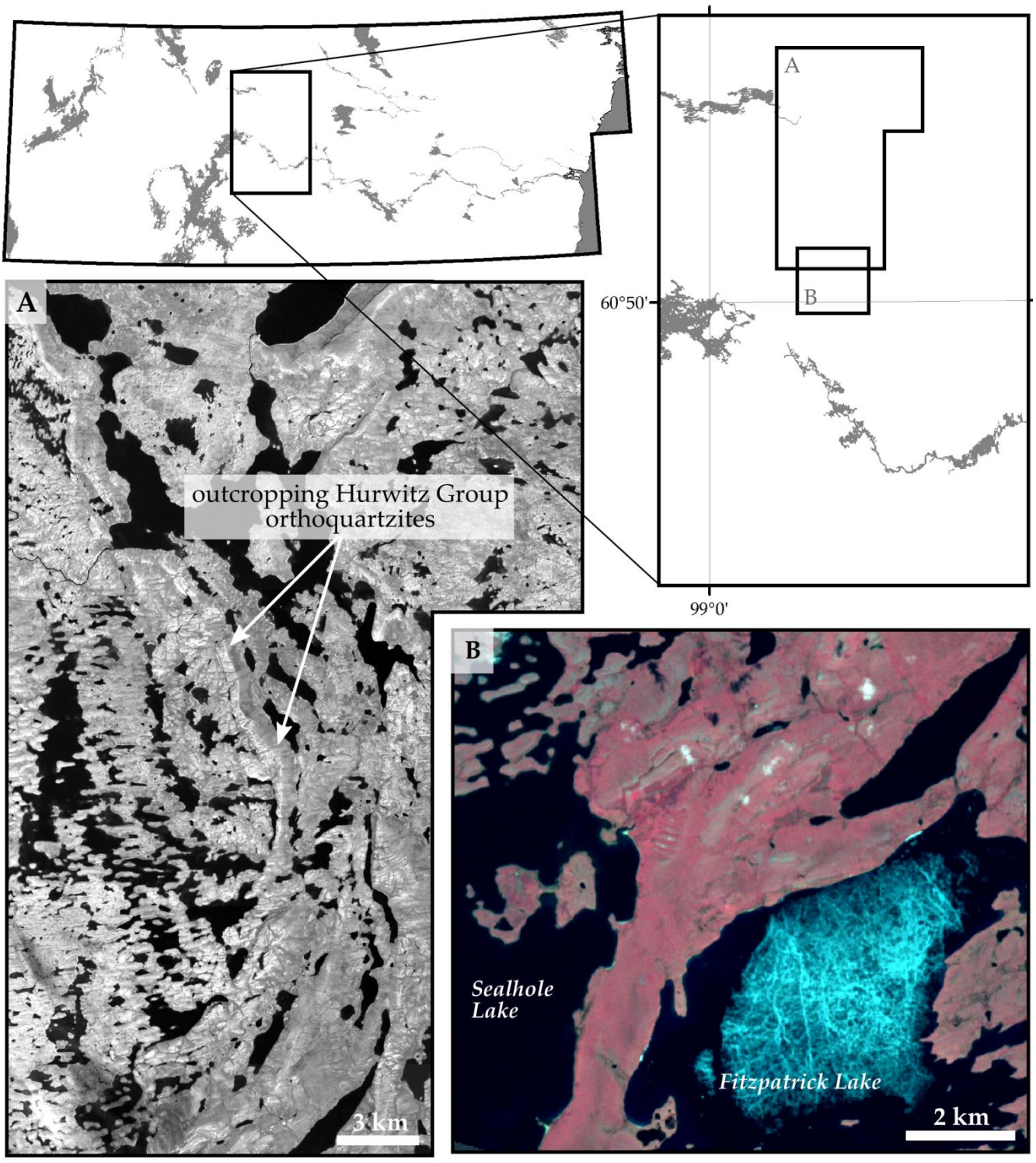

Fig. 5.43 – Large ridge between Sealhole and Fitzpatrick lakes, previously interpreted as a "massive moraine" by Kleman et al. (2002), but shown in (A) clearly paralleling the strike of outcropping Paleoproterozoic Hurwitz Group quartz arenites to the north; illustrated also on the 1:50,000 scale bedrock geology map of Aspler et al., 2000.

5.4.1.4 ***Spatial Distribution of Morphologies***

It is important to recognize that individual ridge morphologies are not confined to type-exclusive fields, but rather are found commonly intermixed within the field-types identified in section 5.4.1.1. Fig. 5.44 provides an example of these overlapping distributions where, at minimum, eight unique ribbed moraine morphologies are identified in a ~20 km^2 area, north of Nueltin Lake. By comparison with the kernel density maps shown in Fig. 5.16, it can be seen that this region of high morphological variety also corresponds to an area of high spatial density of ridges, and in fact this observation applies throughout the entire study area. Fig. 5.45 depicts morphological diversity using 3 km grid spacing, and reveals a striking correlation with kernel density maps of this area (Fig. 5.16), showing high values for morphological variety in areas of high ridge concentration: Southwest of the Kognak River between Kasba and Nueltin Lakes; north of Nueltin Lake; and in a broad zone extending from South Henik Lake southeast across the Thlewiaza and Tha Anna rivers. In certain areas, as many as 6 of the 14 recognized ribbed moraine morphologies are detected within a single 3 km grid cell, shown in Fig. 5.45 as dark-blue coloured pixels.

Separate analysis of the distribution of individual morphologies appears to corroborate this hypothesis, revealing a general lack of locational preference for *most* ribbed moraine morphological categories. Fig. 5.46 displays presence/absence maps for each morphology as a grid with 3 km spacing; blue pixels denote the presence of ≥1 ribbed moraines of a particular morphological category within a given grid cell. Although most maps reveal few trends, several morphological categories do appear to exhibit locational preference. Barchan, streamlined and broad rectangular ribbed moraines are primarily restricted to the southwest and south-central portions of the study area; hummocky ridges have a distribution that covers more area east of the marine limit than most other morphological types; and perhaps most obvious, extensional and minor ribbed moraines are strongly clustered within particular regions – the north- and east-central in the case of the former, and the northeast in the case of the latter. Generally, the frequency at which each morphology is mapped (Fig. 5.47) does not appear to influence its likelihood for exhibiting meaningful spatial organization; alternatively stated, infrequently mapped morphologies (e.g., upstream curving ribbed moraines) appear just as likely to be found within all sub-regions of the study area as frequently mapped morphologies (e.g., classical ribbed moraines). Furthermore, morphologies that exhibit strong locational preference may be either frequently mapped (e.g., minor ribbed moraines), or only moderately prevalent (e.g., extensional ribbed moraines) within the study area. Considered together, these results may imply some element of randomness affecting formation or preservation processes of most ridges. Moreover, given unique spatial organizations and topological relationships with other landforms, certain ridge types (e.g., minor, extensional) may derive from unique formational or preservational histories.

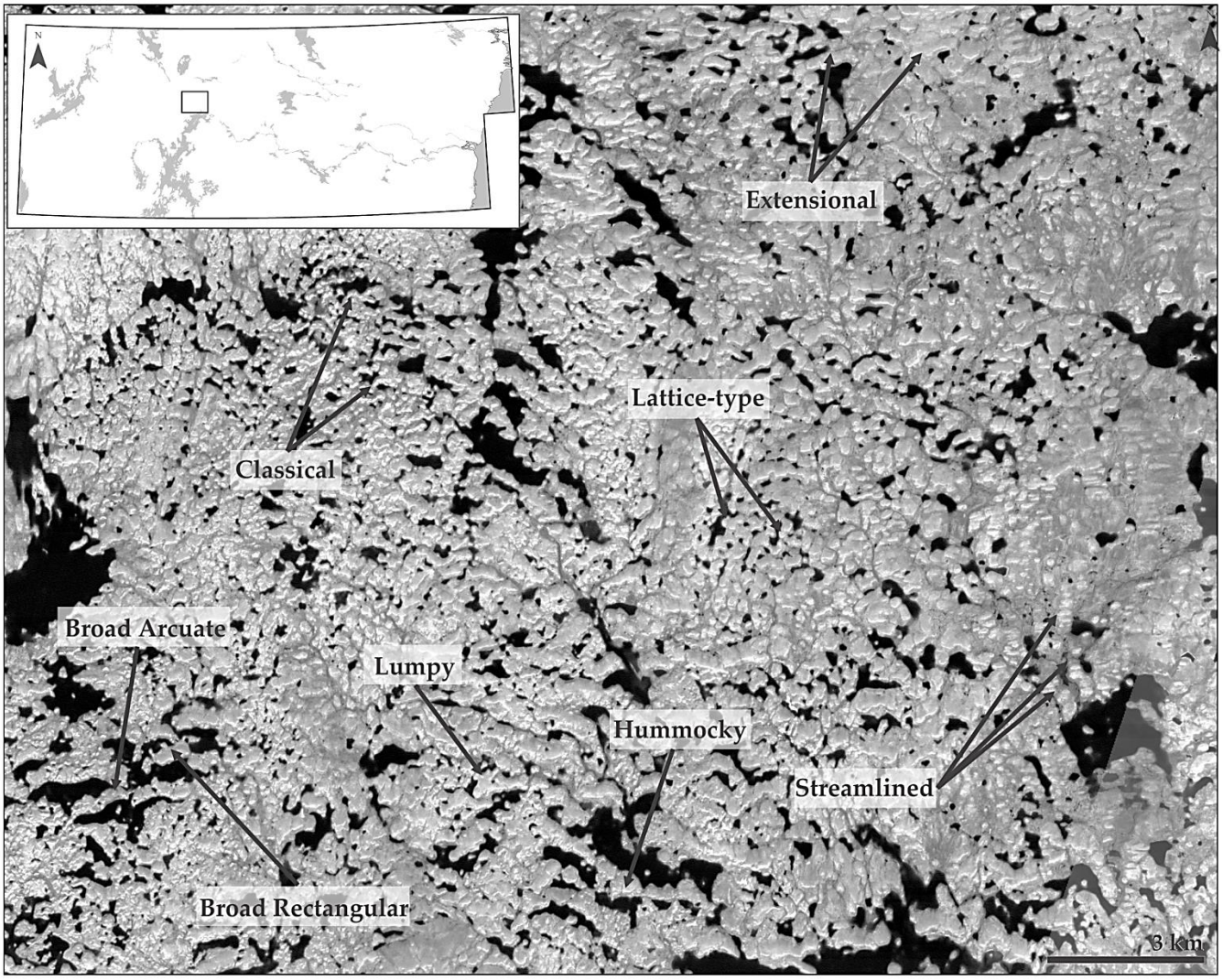

Fig. 5.44 – An area north of Nueltin Lake illustrating the tendency for diverse ribbed moraine morphologies to be co-located. Here, a minimum of 8 different morphologies exist within a ~20 km^2 area.

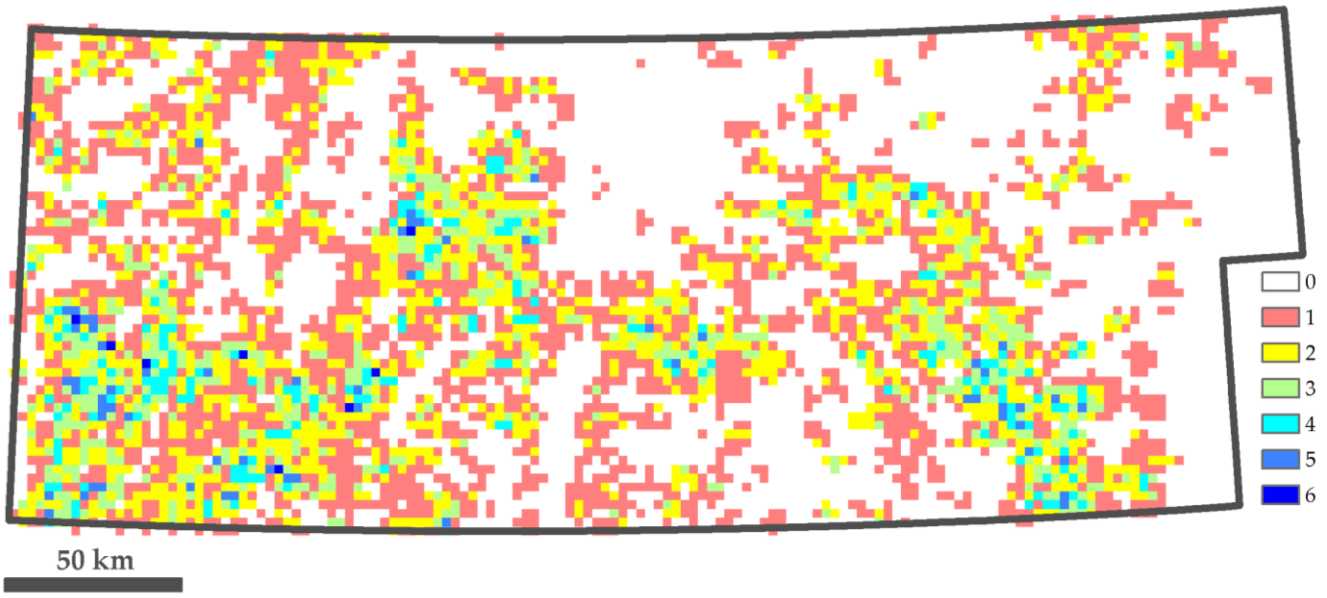

Fig. 5.45 – Map showing ribbed moraine morphological diversity within the study area. Cool colours indicate high morphological diversity (up to 6 different morphologies per pixel), warm colours low diversity (down to 1 morphology per pixel). Areas of high diversity appear to correspond to areas of high ribbed moraine spatial density (Fig. 5.16). Up is north. Pixel size = 3 km.

5.4.1.5 ***Individual Ridge Morphometric Characteristics***

Morphometric measurements were conducted on ribbed moraine ridges in south-central Keewatin in order to develop a quantitative database of landform shape parameters that could be both internally assessed in this study and compared with other measurements previously reported in the literature (e.g., Hättestrand, 1997; Hättestrand and Kleman, 1999; Dunlop and Clark, 2006b). This analysis encompassed four commonly reported characteristics of ribbed moraines: length, width, height, and wavelength (crest-to-crest spacing of consecutive ridges). Standard descriptive statistics of the mapped ribbed moraine population for these variables are presented in Table 5.5. The methods by which parameters were measured are detailed in section 5.3.3.

5.4.1.5.1 Ribbed Moraine Width

The normalized width-frequency distribution for ribbed moraines in the study area is shown as a histogram binned at 30 m in Fig. 5.48. This plot reveals that 90% of all ribbed moraines in south-central Keewatin are between 30 and 600 m in width. Only a very small percentage of ridges (~3.5%) have widths >800 m, and this suggests these features may be outliers or perhaps misidentified landforms. The distribution exhibits positive skew (*skew* = 1.91) and is leptokurtic (*kurtosis* = 5.03), though these variables are sensitive to the bin width and comparatively small sample size used here for surveying widths. Nevertheless, leptokurtic, right-skewed size-frequency distributions appear to be characteristic of most subglacial bedforms and their size parameters (e.g., Clark et al., 2009; Hillier et al., 2013), thus it is tentatively suggested that these observed qualities are truthful descriptions of this distribution also.

Fig. 5.46 – Presence/absence maps for various ribbed moraine morphologies within the study area. Up is north. Pixel size = 3 km. Blue fill indicates the presence of one or more ridges of a given morphology within a particular grid cell.

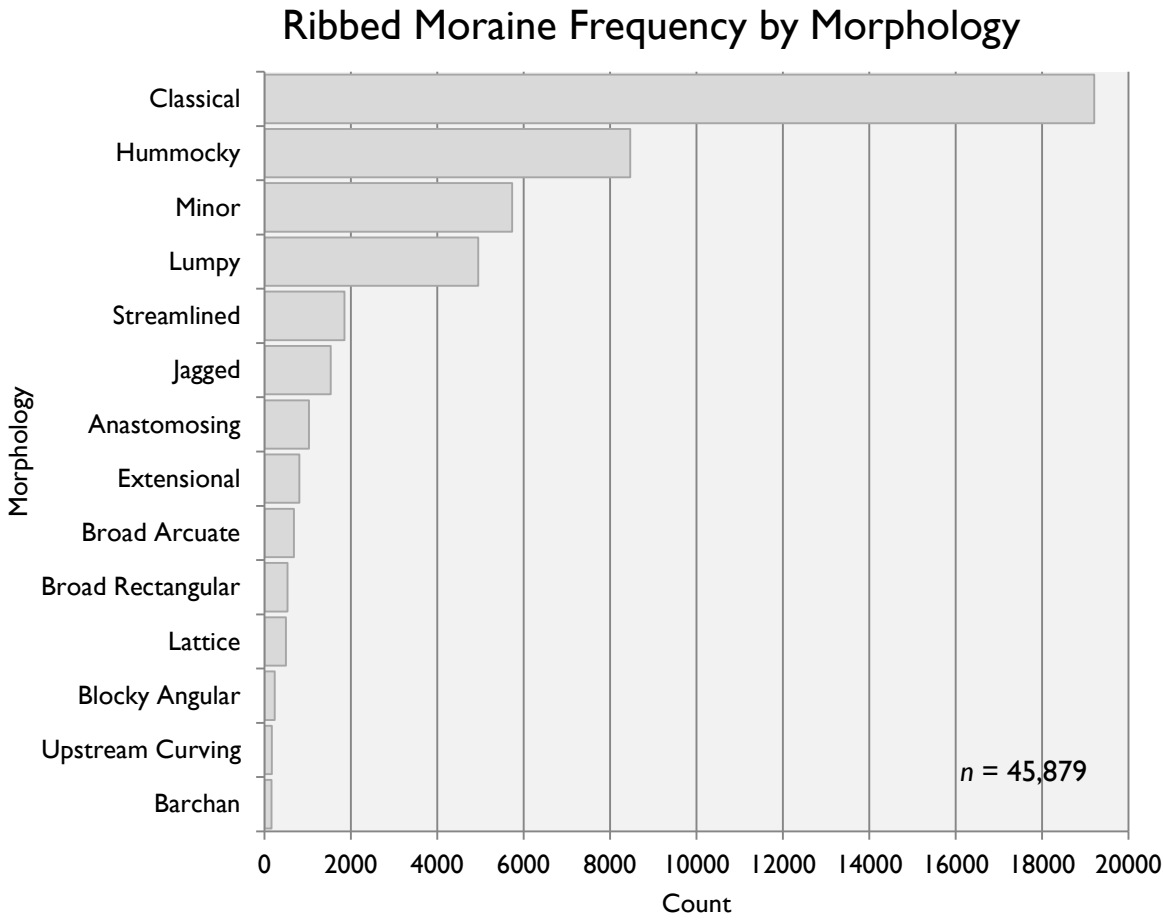

Fig. 5.47 – Count of mapped ribbed moraines by morphology.

5.4.1.5.1 Ribbed Moraine Height

The normalized height-frequency distribution for ribbed moraines in south-central Keewatin is shown as a histogram binned at 5 m in Fig. 5.49. This plot reveals that 90% of all ribbed moraines in the study area are between 5 and 65 m in height. A significant proportion of ridges (38.5%) are <10 m in height, and just over 50% are <30 m. Similar restricted relief values have been reported in other studies (e.g., *range* = 10-30 m, Hättestrand and Kleman, 1999; $\bar{x}$ = 17 m, Dunlop and Clark, 2006b; $\bar{x}$ = 8 m, Finlayson and Bradwell, 2008; $\bar{x}$ = 6 m, Trommelen et al., 2014), however 10% of the ridges in south-central Keewatin have greater relief than the upper limit for any ribbed moraine height recorded in the literature (64 m, Dunlop and Clark, 2006b). Extraction of the ribbed moraine heights reported here relied critically on the vertical accuracy and resolution of the CDED datasets, which in areas may be inconsistent, and thus of all parameters assessed, height is presented here with the lowest level of confidence. The distribution demonstrates slight positive skew (*skew* = 0.47) and is platykurtic (kurtosis = -1.03), though the relatively small sample size may have a large influence on these values, as suggested for widths in section 5.4.1.5.1.

Table 5.5 – Descriptive statistics for ribbed moraine morphometric properties.

	This study	Dunlop & Clark (2006b)
Length (m)		
n	45,879	31,247
Minimum	64	45
Maximum	5,594	16,214
Mean	652	688
Standard deviation	435	-
Modal class	350-400	300-400
Median	539	-
Skewness	2.46	-
(Excess) Kurtosis	10.46	-
Width (m)		
n	200	1000
Minimum	56	17
Maximum	1,300	1,116
Mean	319	278
Standard Deviation	203	-
Modal class	180-210	175-200
Median	275	-
Skewness	1.91	-
(Excess) Kurtosis	5.02	-
Height (m)		
n	200	800
Minimum	1	1
Maximum	88	64
Mean	29	17
Standard Deviation	26	-
Modal class	0-5	6-7
Median	27	-
Skewness	0.47	-
(Excess) Kurtosis	-1.03	-
Wavelength (m)		
n	1300	-
Minimum	43	12
Maximum	2,161	5,800
Mean	311	505
Standard Deviation	196	-
Modal class	150-175	100-150
Median	267	-
Skewness	2.28	-
(Excess) Kurtosis	11.28	-

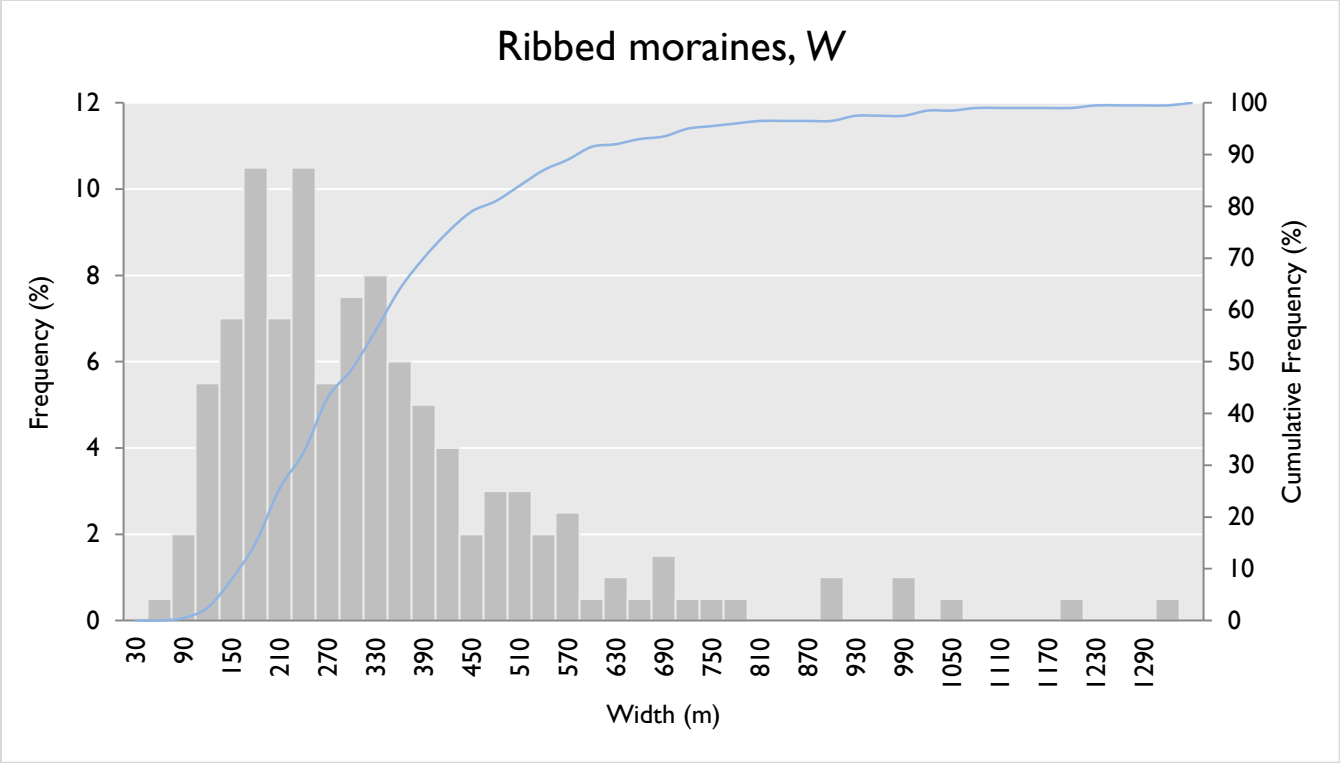

Fig. 5.48 – Width-frequency distribution for south-central Keewatin ribbed moraines.

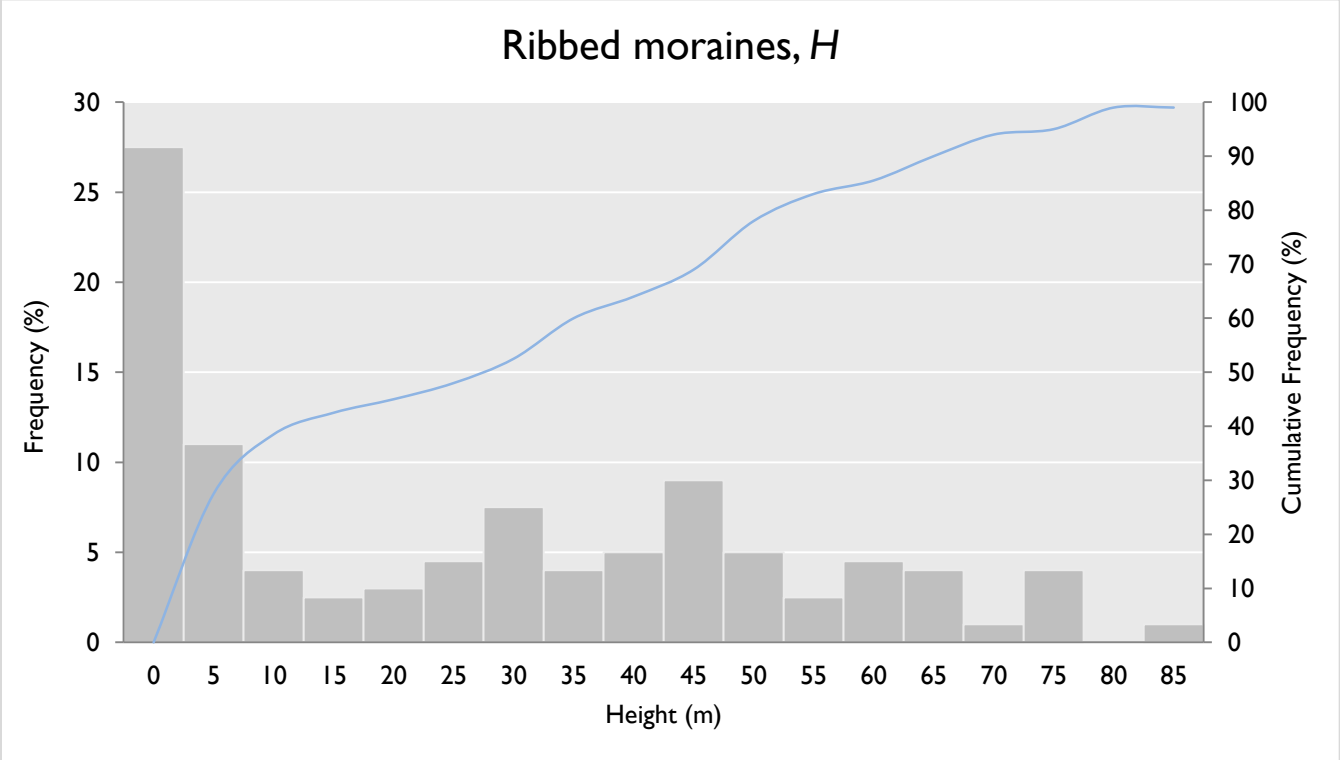

Fig. 5.49 – Height-frequency distribution for south-central Keewatin ribbed moraines.

5.4.1.5.2 Ribbed Moraine Wavelength

The normalized wavelength-frequency distribution for ribbed moraines in south-central Keewatin is provided in Fig. 5.50. Measurements are plotted as a histogram binned at 25 m, revealing a strongly right-skewed (*skew* = 2.28) and leptokurtic (*kurtosis* = 11.28) distribution. Although the histogram produced in this study is shaped very similarly to an equivalent plot in Dunlop and Clark (2006b), the mean ($\bar{x}$ = 311.46) and range (42.74–2,160.99 m) of wavelengths detected in the present study are each much smaller than those described from Labrador/Québec, Ireland and Sweden ($\bar{x}$ = 505, range = 12–5800 m; Dunlop and Clark, 2006b). This could stem from a number of factors; undoubtedly, the high frequency of minor ribbed moraines in the present study area, with their characteristically tight spacing, had a large impact on the sampling mean. Nevertheless, some of the data presented in Dunlop and Clark (2006b) appear suspect, namely their lower limit for wavelength (12 m) which exists at a smaller scale than the nominal spatial resolution of any datasets used for mapping in that study. Differences in collection methodology may also have impacted measurement. Here, wavelengths were obtained directly within the GIS environment; alternatively, Dunlop and Clark (2006b) used mixed methods, including direct measurements in their Swedish study area, approximations from DEM transects in their Irish study area, and spectral (Fourier) analysis of Landsat MSS and ETM+ imagery in Québec.

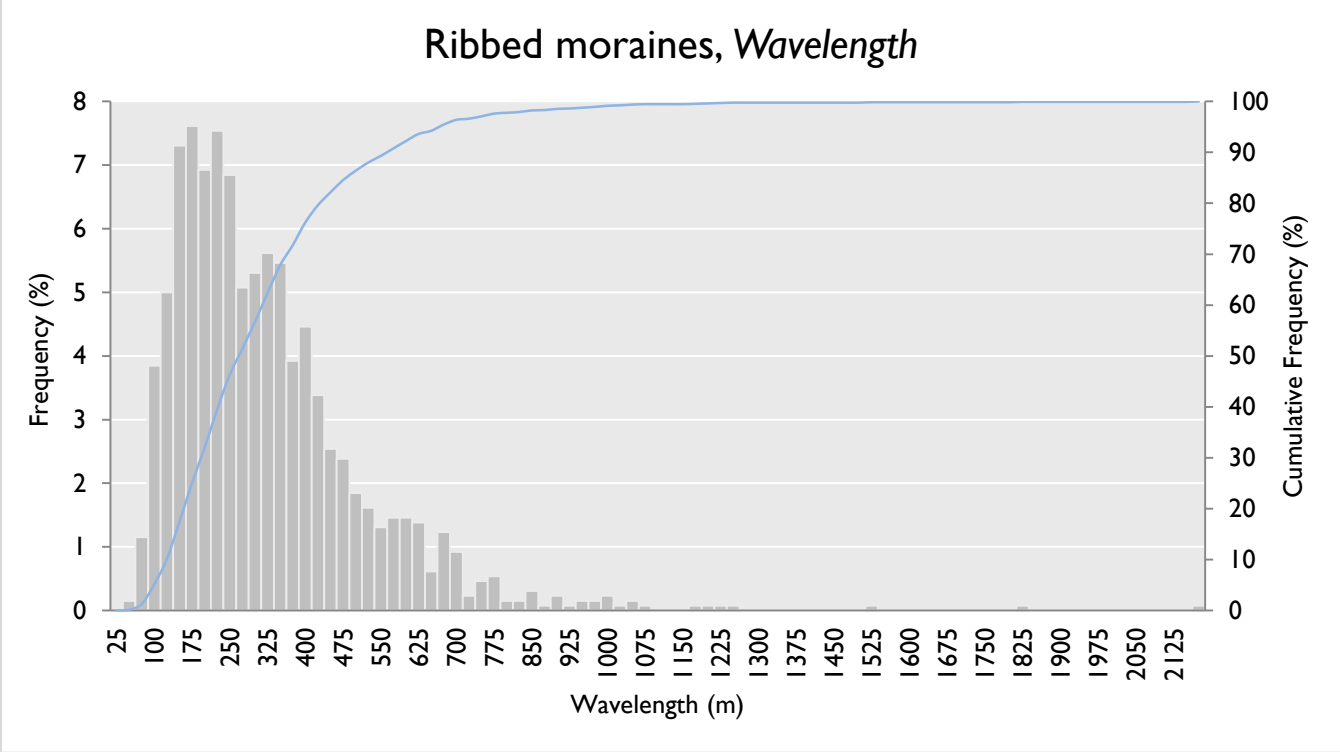

Fig. 5.50 – Wavelength-frequency distribution for south-central Keewatin ribbed moraines.

5.4.1.5.3 Ribbed Moraine Length

Individual lengths for all 45,879 ribbed moraine ridges mapped within the study area were obtained directly from their attribute table. Fig. 5.51 displays the normalized length-frequency

distribution of these values as a histogram binned at 50 m. This plot reveals that 99% of all ribbed moraine ridges in south-central Keewatin are between 50 and 2,500 m in length. Very similarly, Dunlop and Clark (2006a) demonstrated that 90% of ribbed moraine ridges in the Lac Naococane region of Nouveau Québec had lengths between 200 and 2,000 m. Note that lower limits for length detection were likely significantly affected by the use of coarse 80 m Landsat MSS imagery in that study. Additionally, it should be disclosed that personal analysis of supplementary data provided by these authors (Dunlop and Clark, 2006a; http://dx.doi.org/10.4113/jom.2006.44) revealed a large number of inadvertent segments and digitization errors which were accounted for as short ribbed moraines in their analysis. The length-frequency distribution shown here is strongly right-skewed (*skew* = 2.47) and leptokurtic (*kurtosis* = 10.99), and is shaped comparably to the distribution presented in Dunlop and Clark (2006b).

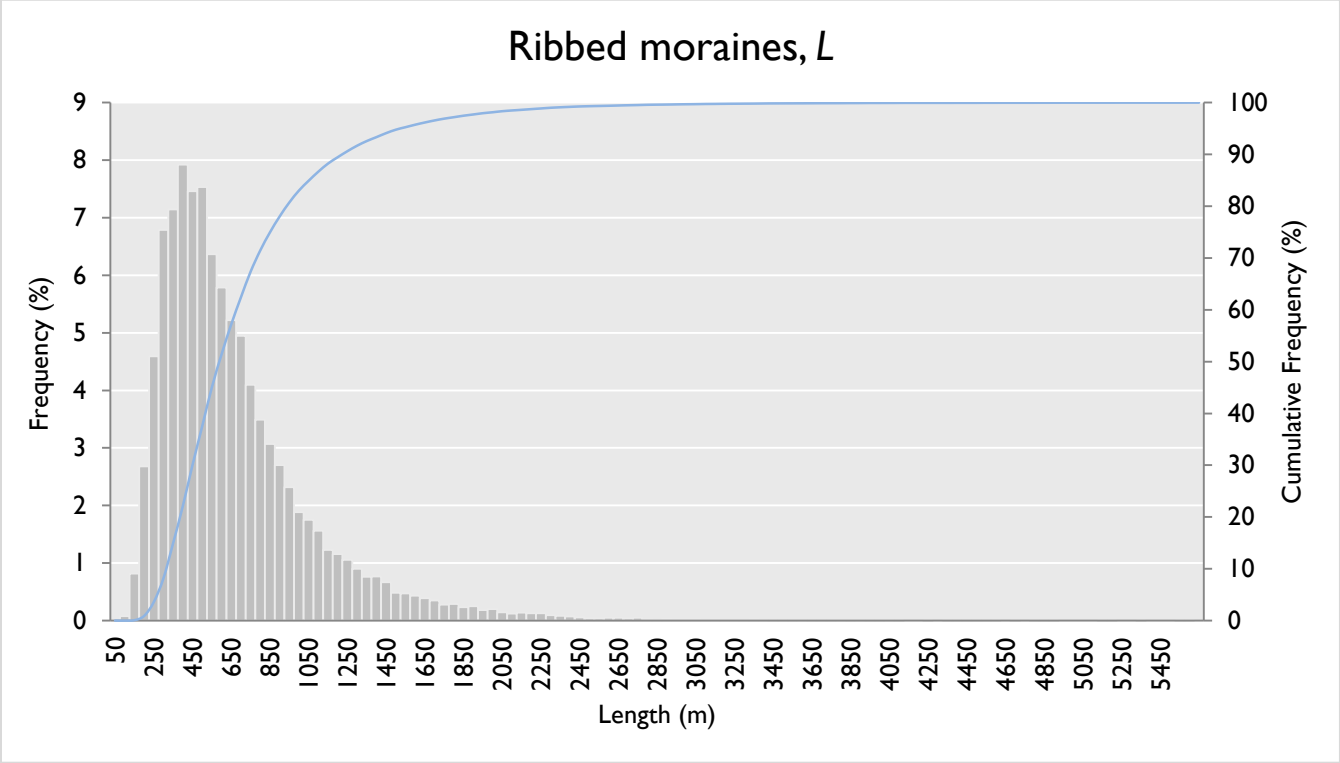

Fig. 5.51 – Length-frequency distribution for south-central Keewatin ribbed moraines.

Ribbed moraine lengths in south-central Keewatin vary considerably by morphology. Fig. 5.52 shows five-number length summaries for each morphological subpopulation. Length distributions for all categories are right-skewed, excepting upstream curving and barchan-type ribbed moraines. Unsurprisingly, 75% of minor ribbed moraines are <750 m in length (excluding outliers), and this distribution plots consistently at lower values for all summary statistics than the other 13 morphologies. This category also exhibits the smallest standard deviation (156.21 m), suggesting that minor ribbed moraines are typically everywhere of similar size. Extensional ribbed moraines feature the greatest spread of lengths, as well as the highest values for all summary statistics save for minimum length, which is surpassed by that for blocky angular ribbed moraines (200 m). Several morphologies generate similar plots (e.g., lumpy, lattice, hummocky, jagged), and all distributions are overlapping. Analysis of Variance (ANOVA) using length as a single factor suggests that observed differences between

morphologies are statistically significant (p<0.01), though admittedly the statistical power of this test is weak in this situation owing to the non-Gaussian distribution of most length-frequency profiles.

Analysis of the spatial distribution of length values yielded stimulating results. Kernel density visualization conducted separately on ribbed moraines of upper (≥886.37 m) and lower (≤334.50 m) quintile lengths revealed unmistakably unique spatial patterns for each subset. Fig. 5.53 demonstrates that large ribbed moraines are found in outsized patches, primarily within three regions: 1) South of Watterson Lake; 2) between Kasba and Nueltin Lakes; and 3) in a NW-SE trending band in the southeast, across the Tha Anna and Thlewiaza Rivers. Alternatively, ribbed moraines of low length occur within more numerous smaller clusters: 1) Above Ennadai Lake; 2) both south and east of Watterson Lake; 3) both south and east of Tatinnai Lake; 4) south of the Thlewiaza River within the marine limit; and 5) in the vicinity of Maguse Lake. The patterns displayed by these quintiles are, of course, comprising of the broader pattern displayed by all ribbed moraines (i.e., Fig. 5.16), however their physical separation is suggestive of underlying determining processes. Interestingly, ribbed moraines of upper quintile length occur primarily in areas of lower quintile length streamlined landforms (and *vice versa*), potentially as a response to thresholds on sediment availability/flux during subglacial bedform production.

This apparent unique spatial distribution of large and small ridges was assessed using common spatial statistical measures (Table 5.6, see section 5.3.4 for methods). First, a test for global spatial autocorrelation (Getis and Ord, 1992) was performed and yielded a positive Moran's *I* index value with statistical significance (p<0.01), confirming the existence of the observed segregation (Fig. 5.53) of high and low ridge length values. Subsequently, a test of Getis Ord General *G* (Getis and Ord, 1992) yielded a statistically significant (p<0.01) negative Z score, implying that this overall global pattern is one of low ridge-length clustering. This result is illustrated also on Fig. 5.53, wherein the pattern displayed by large ridges more strongly reflects the overall pattern of all ridges (Fig. 5.16) than does the spatial distribution of small ribbed moraines.

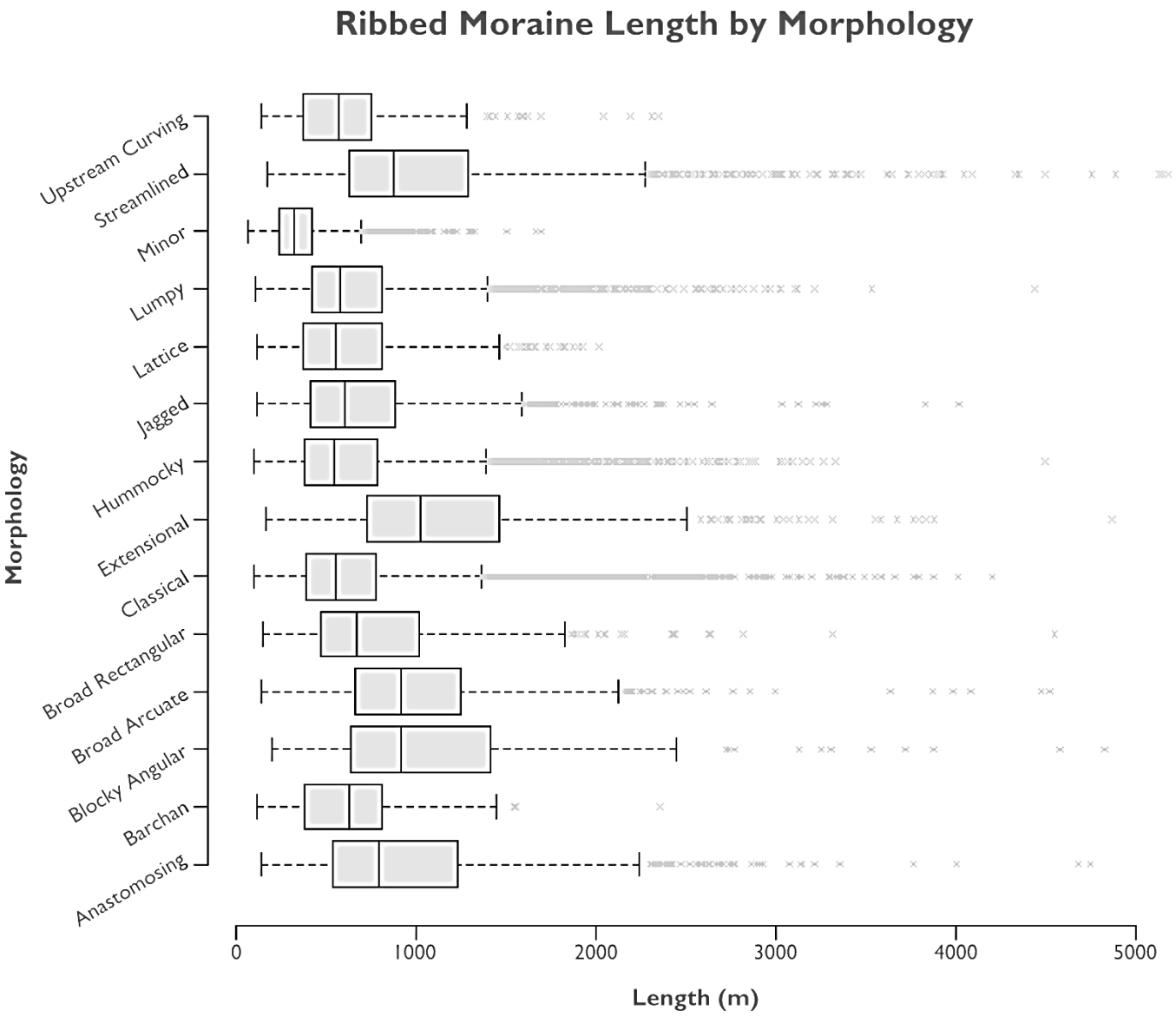

Fig. 5.52 – 5-number summaries (min., lower quartile, median, upper quartile, max.) for south-central Keewatin ribbed moraines by morphology. Grey *x*'s denote potential outliers.

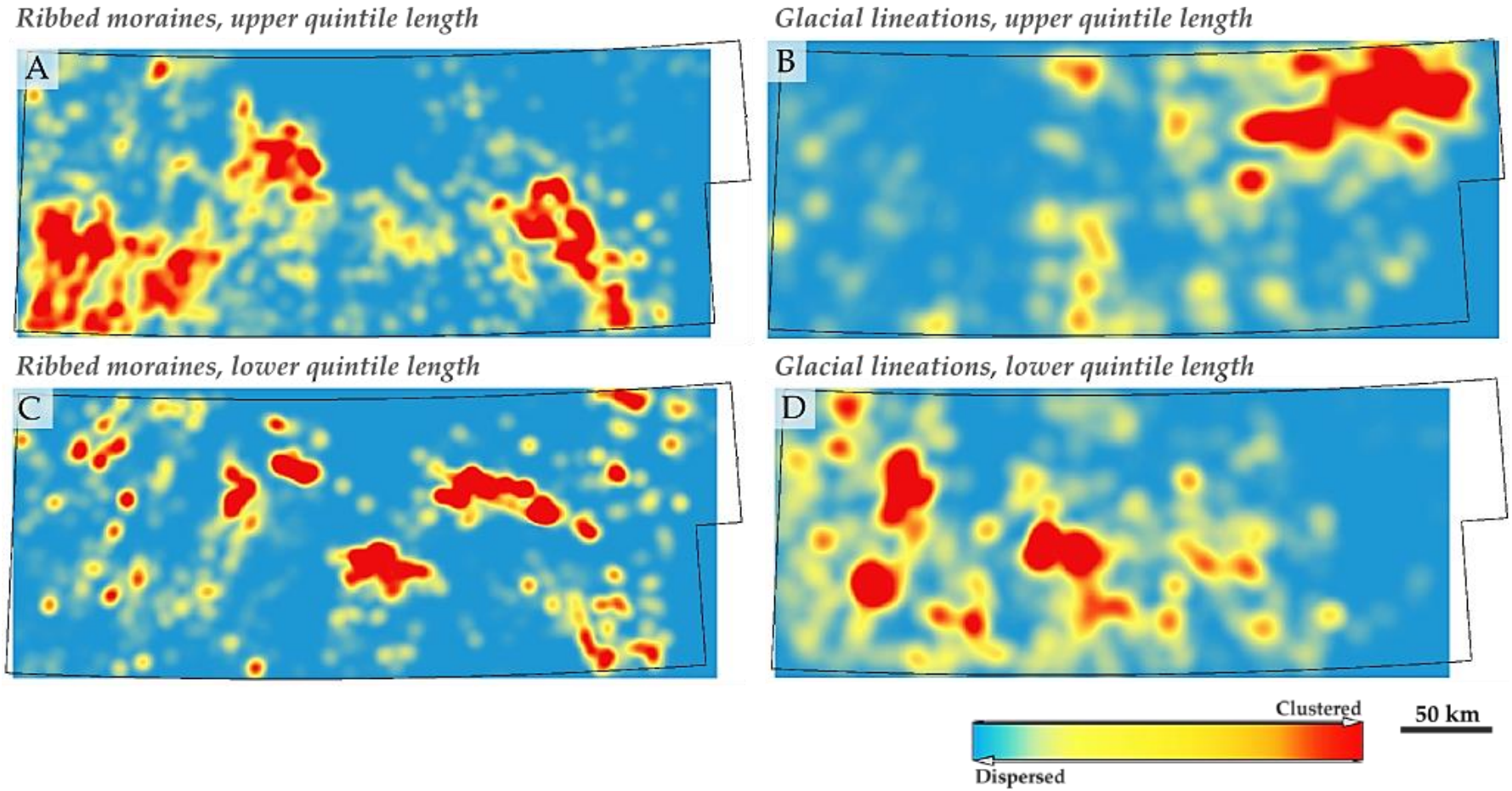

Fig. 5.53 – Kernel density ("heat") maps depicting geographic clustering of glacial bedforms by length in south-central Keewatin. Kernel radii = 25x ANND for each landform. Note that, generally, large (upper quintile) ribbed moraines appear to cluster in areas where small (lower quintile) glacial lineations are found.

Table 5.6 – Spatial statistics for south-central Keewatin ribbed moraines.

	Variable	Observed	Expected	Z score	P Value	Implication
General						
Nearest Neighbour Analysis	Mean nearest neighbour distance	321.27 m	620.21 m	-197.50	<0.01	Statistically significant spatial clustering of ribbed moraine landforms
Parametric						
Moran's I	Moran's Index	0.22897	-0.000022	369.04	<0.01	Statistically significant global spatial autocorrelation of high and/or low ribbed moraine length values
Getis Ord General G	General G	0.000002	0.000002	-33.85	<0.01	Statistically significant global clustering of low ribbed moraine length values

Whereas global Moran's *I* indicated the presence of spatially autocorrelated high *and/or* low length ribbed moraines within the entire study area, Local Indicators of Spatial Association (LISA) were employed using local Moran's *I* (Anselin, 1995) in order to identify the existence of local spatial clusters and outliers. In ArcMap 10.1, this process creates a new feature class containing all original features and their original feature IDs, though also generates a number of new fields, one of which (COType) is populated by cluster and outlier type codes (i.e., HH = high-high, HL = high-low, LH = low-high, LL = low-low, null = not statistically significant) which can be mapped using unique symbologies. Given the size of the ribbed moraine dataset (i.e., 45,879 features), it was necessary to display the output of LISA in a simplified form. Accordingly, an additional field was created (COType_Num) and calculated with nominal numerical COtype equivalents (HH = 4, HL = 3, LH = 2, LL = 1, null = 0) using Python scripting. A majority filter was then applied at 1 km grid spacing using neighbourhood statistics (in this case, neighbourhood = 1x1 cell) to generate a raster of local COType values. From this output, several prominent spatial clusters are observed (Fig. 5.54).

Similar to those displayed on the kernel density distributions (Fig. 5.53), high-high (type 4) clusters are found predominantly in the south, south-central, and southwest; low-low (type 1) clusters alternatively are located in the north, north-central and northeast. Not surprisingly, the spatial distribution of type 1 clusters closely reflects the spatial distribution of minor ribbed moraines (Fig. 5.46); similar linkages between type 4 clusters and morphology are more difficult to ascertain given prominent morphological overlap in those areas, though it is tentatively suggested that streamlined and classical ribbed moraine distributions demonstrate good fit with areas of predominantly type 4 clustering. High-low (type 3) outliers are located near or within all type 1 cluster areas, though are most concentrated in the ribbon-shaped fields E/SE of Hicks Lake and below Watterson Lake, where they probably reflect the nesting of narrow tracks (e.g., Fig. 5.20). Southeast of the Thlewiaza River near Hudson Bay, the presence of type 3 outliers within broad concentrated patches could reflect varying degrees of wave-washing following glaciomarine incursion. In some areas, particularly in the vicinity of Tatinnai Lake, the distribution of type 3 outliers strongly mirrors the distribution of the extensional ribbed moraine morphology, suggesting this latter category of bedform is commonly outsized with respect to surrounding ridges (e.g., Fig. 5.20). Low-high (type 2) outliers are relatively evenly distributed within type 4 cluster areas, where they likely reflect the diversity of ribbed moraine

morphologies in these regions (i.e., Fig. 5.45), a phenomena which itself is possibly indicative of past local diversity in subglacial dynamics (e.g., local-scale preservation, basal hydraulic and/or thermal transitions, varying degrees of overprinting, etc.) or perhaps local-scale variations in substrate properties (though see Greenwood and Clark, 2010). Of all 45,879 ribbed moraines, 53% do not demonstrate statistically significant size clustering. Type 1 clusters (~26%) outnumber type 4 clusters (~15%), hence the strong negative Z score generated by Getis Ord General *G* (Table 5.6). Only ~6% of all ribbed moraines in south-central Keewatin occur as outliers with respect to their size compared to neighbouring ridges.

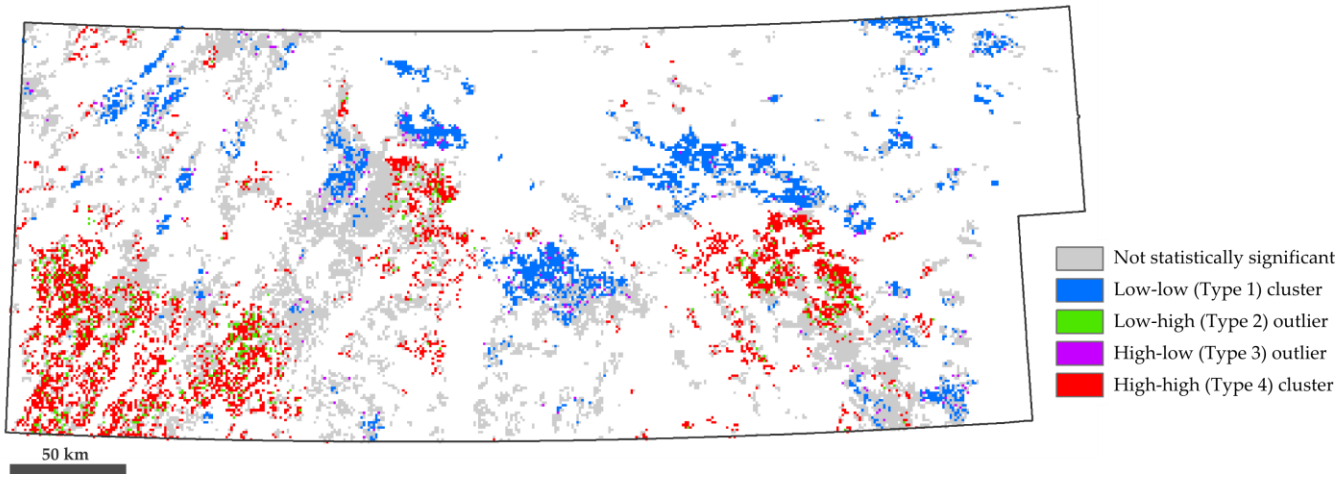

Fig. 5.54 – Modified output of LISA for ribbed moraine length, showing high-high clustering in the south(west)ern, and low-low clustering in the north(east)ern portions of the study area. Result is displayed as a raster (cell values calculated by majority) at 1 km grid spacing.

5.4.1.6 *Exponential Characterization of Ribbed Moraine Length-Frequency Distributions*

Recently, it has been convincingly demonstrated that the size-frequency distribution of key measurement properties (e.g., length, width, height) of subglacial bedforms are exponentially distributed above their mode (Hiller et al., 2013). Through multiple applications, it was established also that the existence of a right-hand exponential tail is not location dependent, related to individual mapper bias, nor the result of aggregation, even when considering data from within large areas (Hillier et al., 2013). The significance of this discovery is that such distributions can be described using only three parameters (gradient, λ; area-normalized y-intercept, $\beta_{0;}$ mode, ϕ). This objective parameterization is less sensitive to measurement artefacts or biases in landform preservation, and more rigorously captures those characteristics of bedforms that are empirically related to ice-sediment interaction. Given the moderate spatial resolution (10–30 m) of the imagery, and the variable quality of the elevation datasets used to map bedforms in this study, this parameterization constitutes an attractive approach for verifying the significance of morphometric insights gained through traditional modes of analysis (e.g., sections 5.4.1.5.1 – 5.4.1.5.3).

Accordingly, the methodology outlined by Hillier et al. (2013) was applied to the dataset of ribbed moraine lengths extracted from south-central Keewatin, and the above three parameters (λ, $\beta_{0,}$ ϕ) calculated from the raw length data. For visualization purposes, data from the binned (50 m) histogram representation of this distribution were plotted on a semi-log graph (Fig. 5.55). It is noted that, to a good

approximation, ribbed moraine lengths from the study area are fit to an exponential right-hand decay above their mode (362.24 m), and a roll-over to low numbers below this. Semi-log plots for each morphology are shown in Fig. 5.56 and, save for a select few morphologies (e.g., barchan, upstream curving), length-frequency distributions are well-described by an above mode exponential decay. Though few comparably parameterized datasets for ribbed moraine length exist in the literature with which to relate what is here derived from southern Nunavut, it is noted that λ of the present distribution (2.43 km^{-1}) matches remarkably well with the sample exponent (λ = 2.33 km^{-1}) calculated and plotted by Hillier et al. (2013) from data (*n* = 31,247) in Dunlop and Clark (2006b). Values for β_0 (here = 9.22; Dunlop and Clark, 2006b ~ 8.5) and ϕ (here, 362.24 m; Dunlop and Clark, 2006b ~ 350 m) are also broadly comparable, which is to be expected given the similarity of these distributions discussed earlier (see section 5.4.1.5.3). Based partly on a relationship proposed by Haschenberger (1999) for relating λ for fluvial scour depths to basal shear stress in that geomorphic setting, Hillier et al. (2013) tentatively suggest that λ in the subglacial domain may directly reflect physical bedforming processes. If this is true, then the similarity between λ derived using data in this study and from Dunlop and Clark (2006b) implies that rib-forming processes are non-distinct over large areas in Nouveau Québec/Labrador, northeastern Ireland, west-central Sweden, and south-central Keewatin.

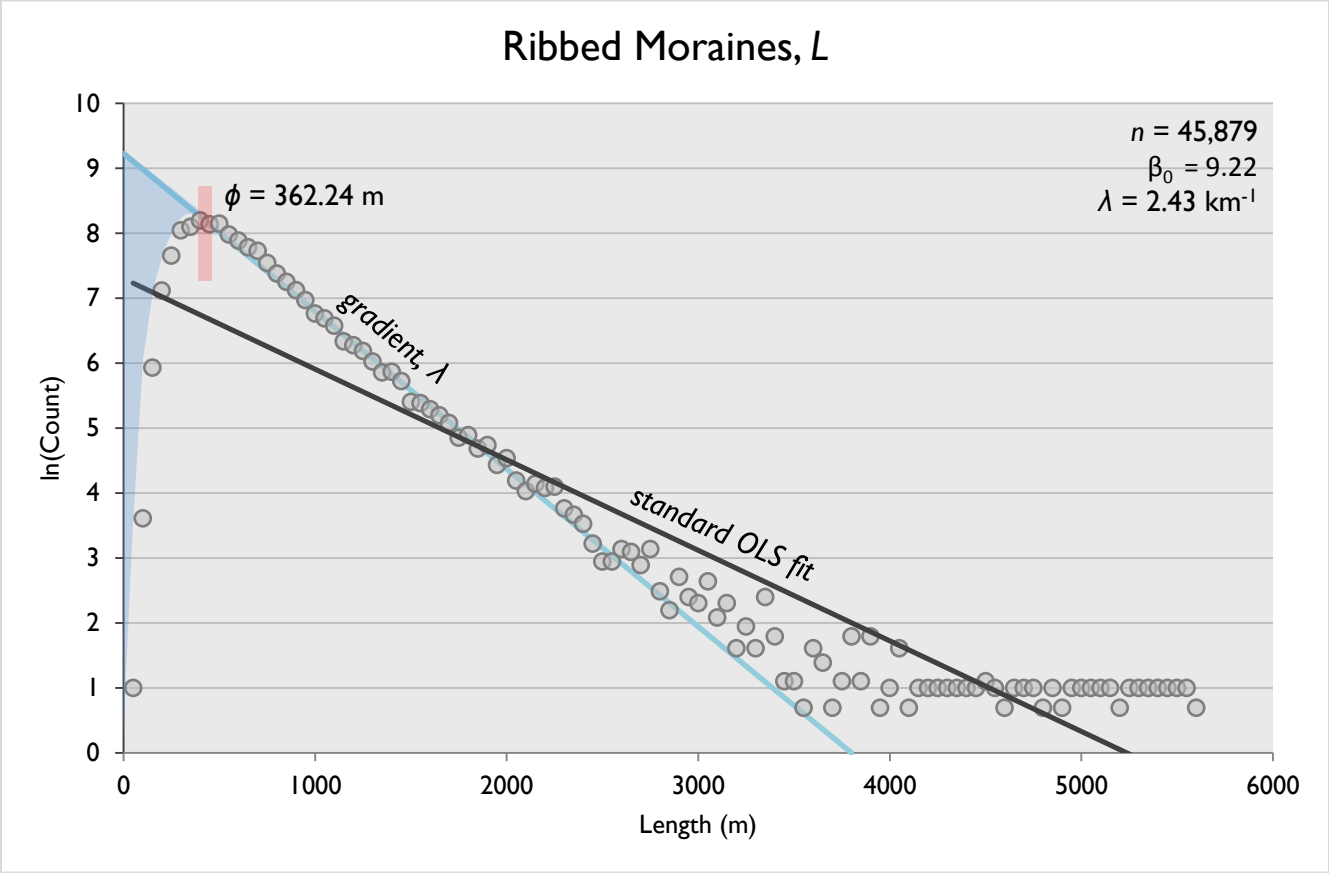

Fig. 5.55 – Semi-log plot for ribbed moraine length. Red box indicates the mode estimated from a gamma distribution. Blue fill to the left of the modal position signifies bedforms which are likely to have been undersampled or misinterpreted due to their small size. Zero counts are placed at a nominal value of 1, regarded as appropriate for *n* >10,000 (Hillier et al., 2013). The standard ordinary least-squares (OLS) regression is also plotted and shows poor fit for bedforms near the modal class, and is influenced considerably by infrequently mapped large bedforms and potential outliers.

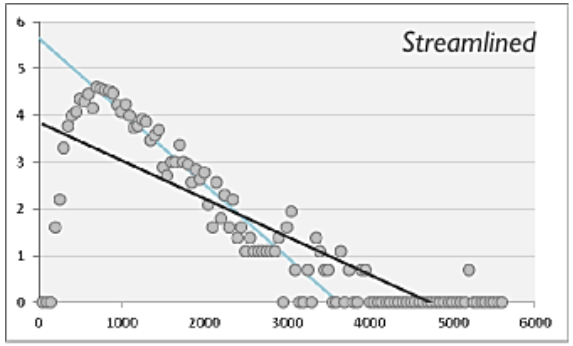
Streamlined

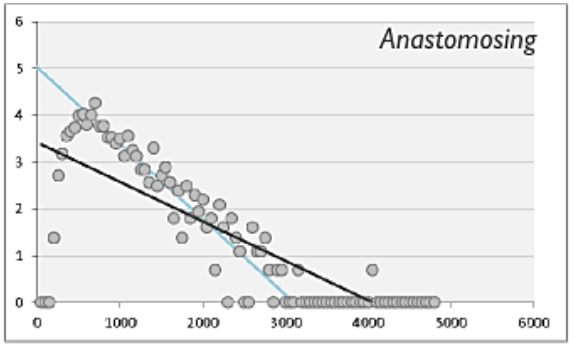
Anastomosing

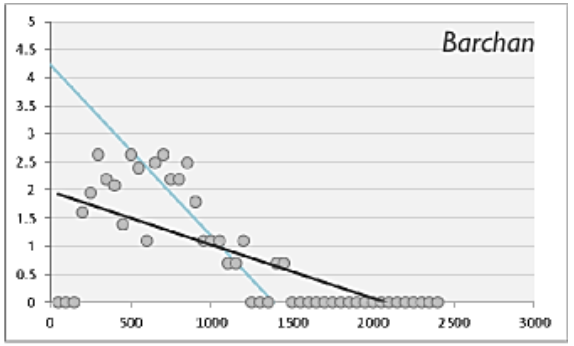
Barchan

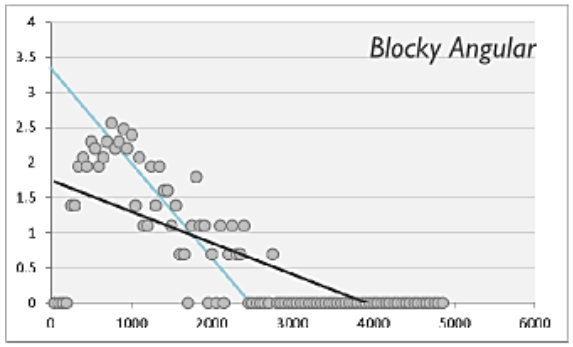
Blocky Angular

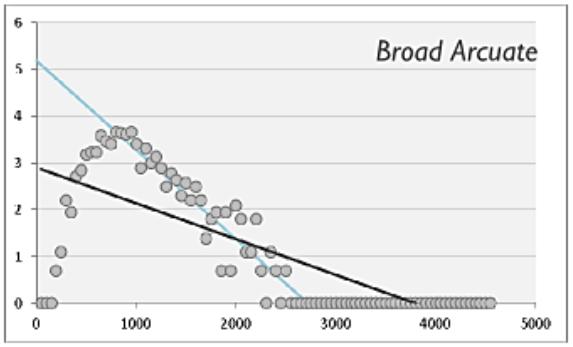
Broad Arcuate

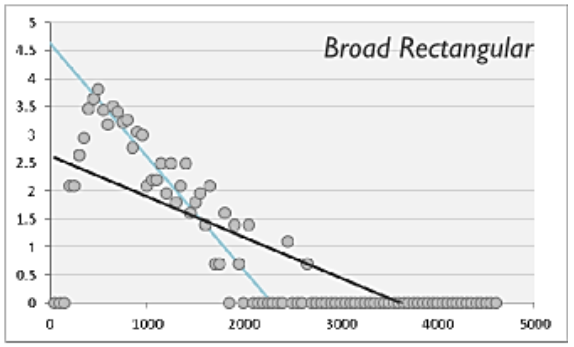
Broad Rectangular

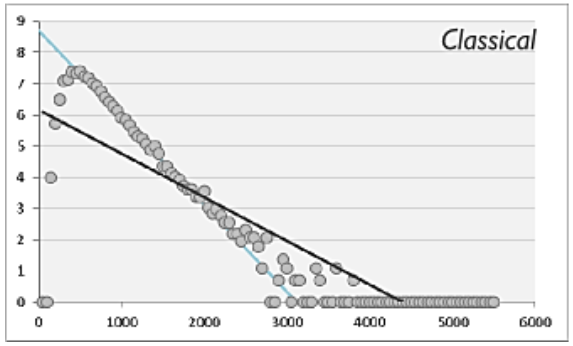
Classical

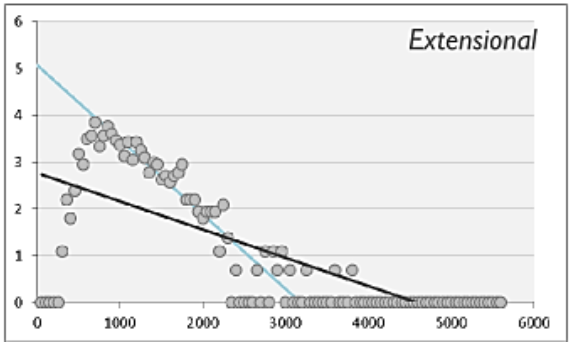
Extensional

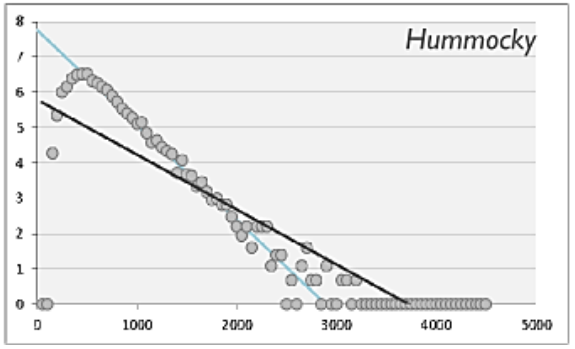
Hummocky

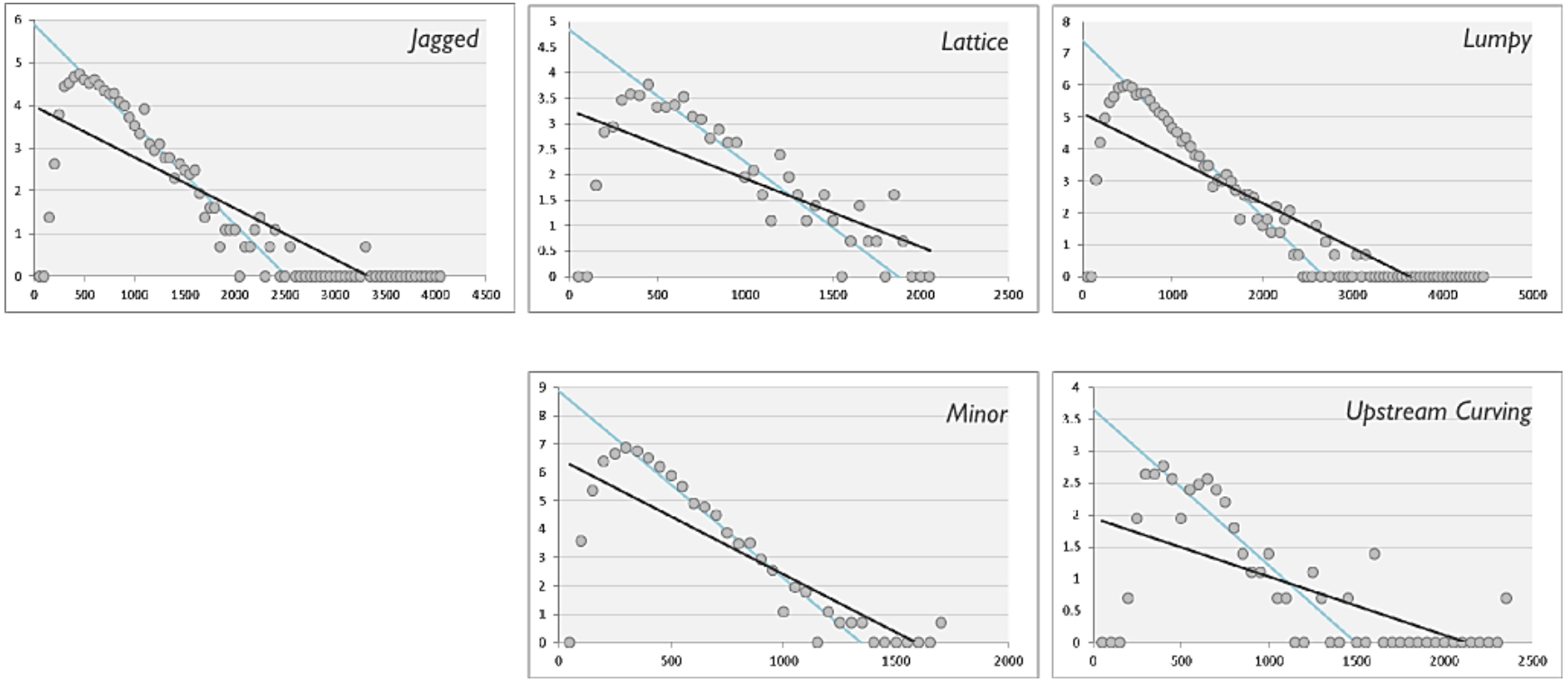

Fig. 5.56 – Semi-log plots for ribbed moraine length by morphology. Blue line indicates calculated slope of the sample exponent. Black line is line of best fit for standard OLS regression, included for reference.

5.4.1.7 *Morphotype Designations*

Of central interest to the present study is the diversity of ribbed moraine morphologies exhibited within south-central Keewatin. Despite the qualitatively distinct visual appearances of the 14 morphologies recognized here (Fig. 5.12), many of their spatial (Fig. 5.46) and size-frequency (Fig. 5.52) distributions overlap, and it is thus instructive to determine whether such a number of discrete morphological classifications is necessary or meaningful, with an ultimate view towards resolving their formational process(es) and, in turn, using their presence to infer specific subglacial conditions at time of formation. As a first step, exponential characterizations were developed (see section 5.4.1.6 above) for ribbed moraine length-frequency distributions, obtaining λ from a maximum likelihood fit for each morphological subpopulation. λ is insensitive to the size of a dataset (Hillier et al., 2013) and hence remains robust even for certain morphologies with low sample size (e.g., barchan-type, n = 162). Fig. 5.57 plots individual exponential decay gradients for each morphology above its mode. Strikingly, λ and β_0 exhibit high variance between morphologies. Sharp gradients (e.g., minor, barchan, lattice, upstream curving) contrast with more gently sloping decays (e.g., streamlined, anastomosing, blocky angular, extensional), and high density morphologies (e.g., minor, classical) contrast with lower density morphologies (e.g., blocky angular, upstream curving).

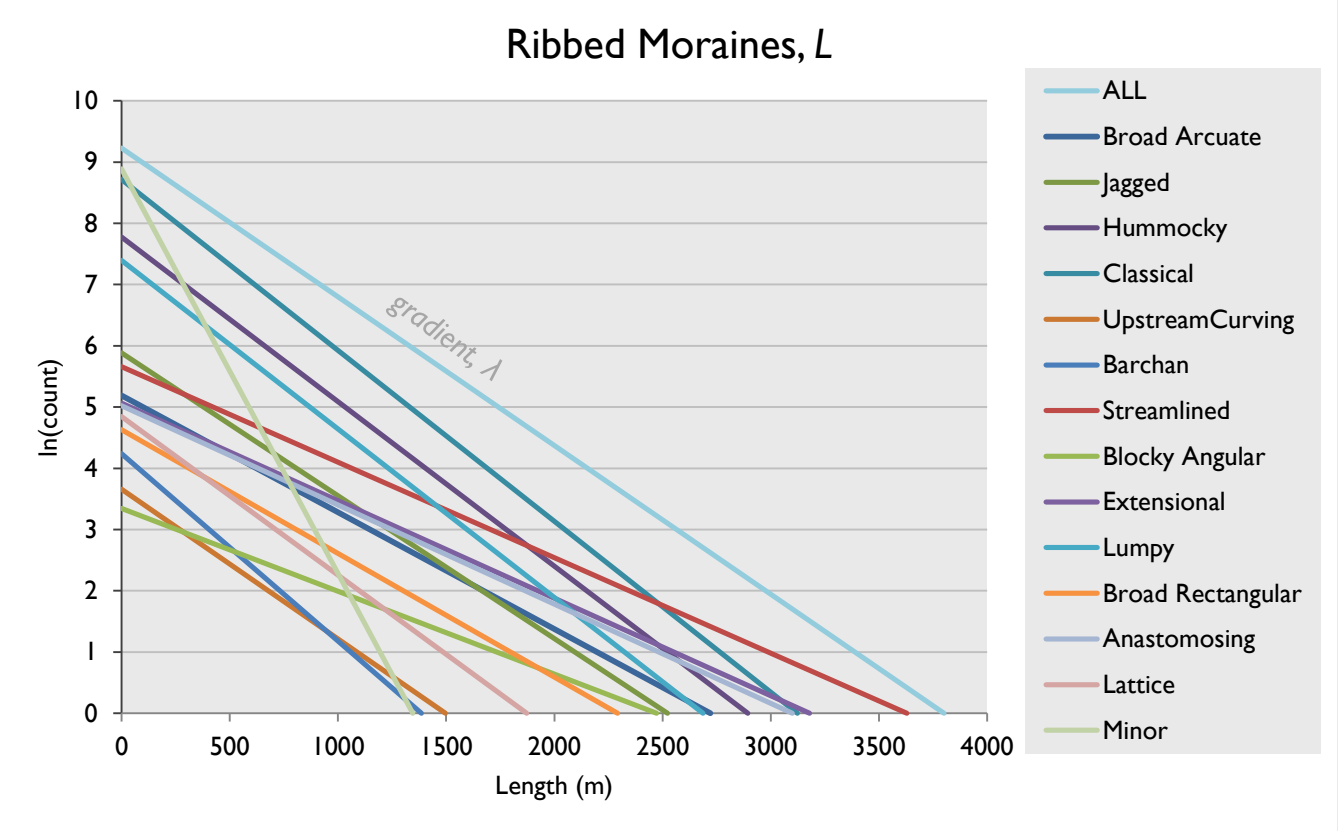

Fig. 5.57 – Semi-log plot of above-mode exponential decay gradients for 14 ribbed moraine morphologies.

Despite these distinctions, it is immediately apparent that certain "groups" of morphologies demonstrate remarkably similar plots. Thus, if λ does in fact reflect physical bedforming processes, then morphological groupings with internally-consistent formation histories (herein referred to as

morphotypes) might be established on the basis of similar λ values and/or the associated length statistics from which λ is derived. In order to test this, λ and β_0, in addition to a suite of 8 length metrics commonly used to describe size-frequency distributions of subglacial bedforms (e.g., Clark et al., 2009) (Table 5.8), were selected and calculated for each morphological subpopulation. Given the probability that separate metrics reflect similar aspects of the ribbed moraine bedforming process, dimensional reduction was necessary in order to mitigate variable redundancy and address potential multicollinearity. Accordingly, principal component analysis (PCA) was first performed (section 5.3.4.1) as a solution to maximizing correlation between the original 10 metrics by creating new artificial variables (principal components (PCs)) which are orthogonal and uncorrelated, and derived from linear combinations of the original variables (see section 5.3.4.1). Two components (PC1, PC2) were extracted in this process based on assessment of the resulting correlation matrix. Eigenvalues reported in Table 5.7 demonstrate that PC1 and PC2 explain 62.86% and 26.10% of the variance in the data, respectively. Interestingly, only λ and β_0 have negative loadings on PC1, implying positive correlation between λ and β_0 along this axis of greatest variance, though negative correlation between each of these variables and the remaining 8 parameters. Also of interest, minimum and maximum length are negatively correlated on PC2, which supports the hypothesis of potential underlying scale-dependent morphological grouping thresholds.

Table 5.7 – 2 component matrix for 10 length metrics showing total and cumulative variance explained by each extracted component.

	Min.	Max.	$\bar{x}$	s	s^2	λ	β_0	ϕ	Skew.	Kurt.	Tot. var.	Cum. Var.
PC1	0.924	0.749	0.981	0.984	0.944	-0.881	-0.574	0.884	0.371	0.154	62.859	62.859
PC2	-0.253	0.605	-0.053	-0.066	-0.096	0.057	0.71	-0.026	0.869	0.949	26.102	88.961

In order to evaluate and compare length-based properties of the 14 ribbed moraine morphological categories, and catalogue those having similar profiles into meaningful morphotype designations, hierarchical clustering of principal components (HCPC) was conducted, involving dimensional reduction (described above) followed by agglomerative hierarchical cluster analysis (HCA) of PCA scores using Ward's linkage, and lastly, distance-based aggregation/partitioning around non-stationary centers (*k*-means clustering). HCPC, and in particular, the latter two-step (agglomerative-partitioning) clustering approach, is widely applied in fields (e.g., genomics, ecotoxicology) that interact with datasets of high dimension (e.g., Genga et al., 2012; Škrbić et al., 2013). The results of HCA using Ward's minimum variance method on the PCs are presented below. Terminal elements indicated on the dendrogram (Fig. 5.58) are individual morphologies; with increasing distance, agglomerative hierarchical clustering continues to group morphologies until all are encompassed within a single cluster. Nesting is exhibited on this dendrogram and implies that clustering of morphologies using the hierarchical approach is sensitive to the chosen cut-off distance. Examination of the agglomeration schedule of Ward's index values reveals that an initial large step (0.039) in coefficients occurs between cluster stages 8 and 9 (Appendix B), yielding a suggested value of 6 clusters which can subsequently be used to seed the *k*-means algorithm (i.e., since, in this example, agglomeration begins with 14 clusters at stage 0; thus 14 – 8 = 6).

Table 5.8 – Length (m) and dimensionless statistics (including PCA scores) for 14 ribbed moraine morphologies.

Morphology	n	Min.	Max.	$\bar{x}$	s	s^2	λ	β_0	ϕ	Skew.	Kurt.	PC1	PC2
Anastomosing	1034	138	4753	971	617	381293	1.62	5.02	578.19	1.74	4.54	0.64	-0.51
Barchan	162	113	2357	633	331	109750	3.06	4.24	459.91	1.34	4.03	-0.74	-1.33
Blocky Angular	241	200	4830	1131	759	575890	1.35	3.35	621.62	1.83	4.61	1.50	-0.90
Broad Arcuate	685	141	4526	1027	560	313506	1.91	5.19	721.22	2.05	7.63	0.74	0.35
Broad Rectangular	533	151	4552	808	494	244354	2.02	4.63	505.26	2.06	8.00	0.33	0.38
Classical	19205	100	5539	642	378	142617	2.79	8.72	419.73	2.21	9.06	-0.45	1.73
Extensional	806	163	5594	1173	638	406803	1.59	5.07	826.68	1.86	6.00	1.26	-0.09
Hummocky	8470	100	4499	635	384	147269	2.69	7.77	403.55	1.96	6.48	-0.57	0.69
Jagged	1537	111	4019	717	437	191337	2.33	5.88	449.99	2.16	8.05	-0.18	0.74
Lattice	494	111	2017	641	374	140017	2.59	4.84	422.66	1.28	1.47	-0.76	-1.81
Lumpy	4951	103	4440	667	386	148728	2.75	7.40	444.44	2.17	8.09	-0.43	1.11
Minor	5731	64	1696	345	156	24403	6.61	8.89	274.25	1.62	5.41	-2.17	0.09
Streamlined	1856	170	5577	1063	687	471642	1.56	5.66	619.70	2.20	7.19	1.18	0.55
Upstream Curving	174	143	2346	651	413	170789	2.45	3.66	388.01	1.83	3.87	-0.35	-1.02

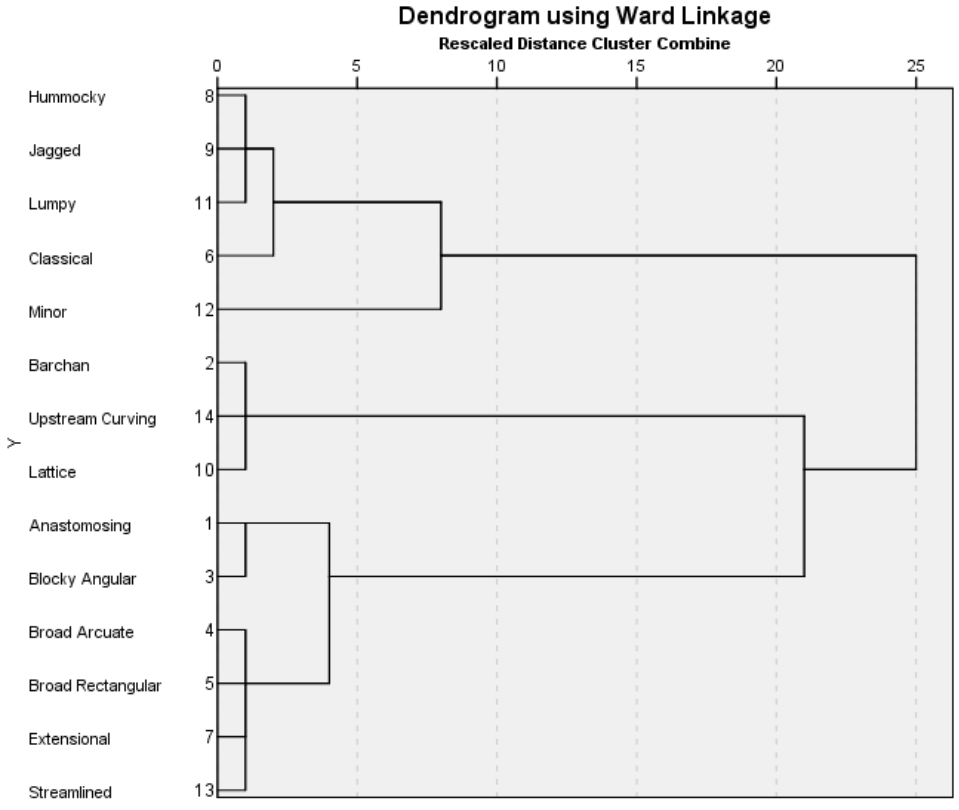

Fig. 5.58 – Dendrogram produced using hierarchical cluster analysis (Ward's minimum variance method) on length PCs for 14 ribbed moraine morphologies.

In this analysis, which utilized 6 initial cluster seeds, convergence was achieved after only two iterations. Table 5.9 presents final cluster centers along PC1 and PC2 output from this analysis for the 6 clusters.

Table 5.9 – PC centers for 6 clusters detected using the *k*-means algorithm.

	Cluster					
	1	2	3	4	5	6
PC1	-.39175	-.61821	1.06751	-2.16900	.87837	-.44964
PC2	.84710	-1.38601	-.70286	.09183	.29903	1.73450

Following successful HCPC, individual elements or treatments can be displayed on a PCA bi-plot according to their cluster membership (Fig. 5.59). Two morphologies, classical and minor, each individually form unique clusters (#6 and #4, respectively). Lumpy, hummocky and jagged morphologies are comprising of a third cluster set (#1) within which all members demonstrate negative scores along PC1 and lower positive scores along PC2 than the classical morphology. Broad rectangular, broad arcuate, streamlined and extensional morphologies together form cluster #5, despite the slight negative score of the latter along PC2. Anastomosing and blocky angular morphologies lie comfortably within the fourth quadrant, constituting cluster #3. Barchan, lattice, and upstream curving morphologies comprise a final cluster (#2) wholly contained within the third quadrant. Note that, assuming the length metrics considered here are at least partly representative of underlying physical processes, the location of one morphology along PC axes with respect to neighbouring morphologies provides some indication of potential similarities in their generative origins, and thus presumably also their location and timing of formation. In this light, certain morphologies that plot near one another on Fig. 5.59 might be expected to exhibit similar geographic distributions across space (Fig. 5.46). Indeed, this appears to be the case, at least for morphologies with very similar PCA scores (e.g., see broad rectangular vs. broad arcuate; upstream curving vs. barchan), though the converse is also true, and it is hence instructive to consider the relative seclusion of the minor ribbed moraine morphological category (i.e., cluster #4) on the bi-plot with reference to the geographically distinct spatial distribution of minor ribbed moraines in south-central Keewatin (Fig. 5.46).

Given that these clusters appear to reflect meaningful separations in the dataset, it becomes perhaps more practical to refer to individual morphologies on the basis of their cluster membership, and as such, these are here assigned to representative morphotypes (M1, M2, M3-A, M3-B, M4, M5) (Fig. 5.60). Subsequently, it is noted that these six morphotypes are also expressed according to λ alone (Fig. 5.61), indicating the usefulness of this parameter for describing subglacial bedforms.

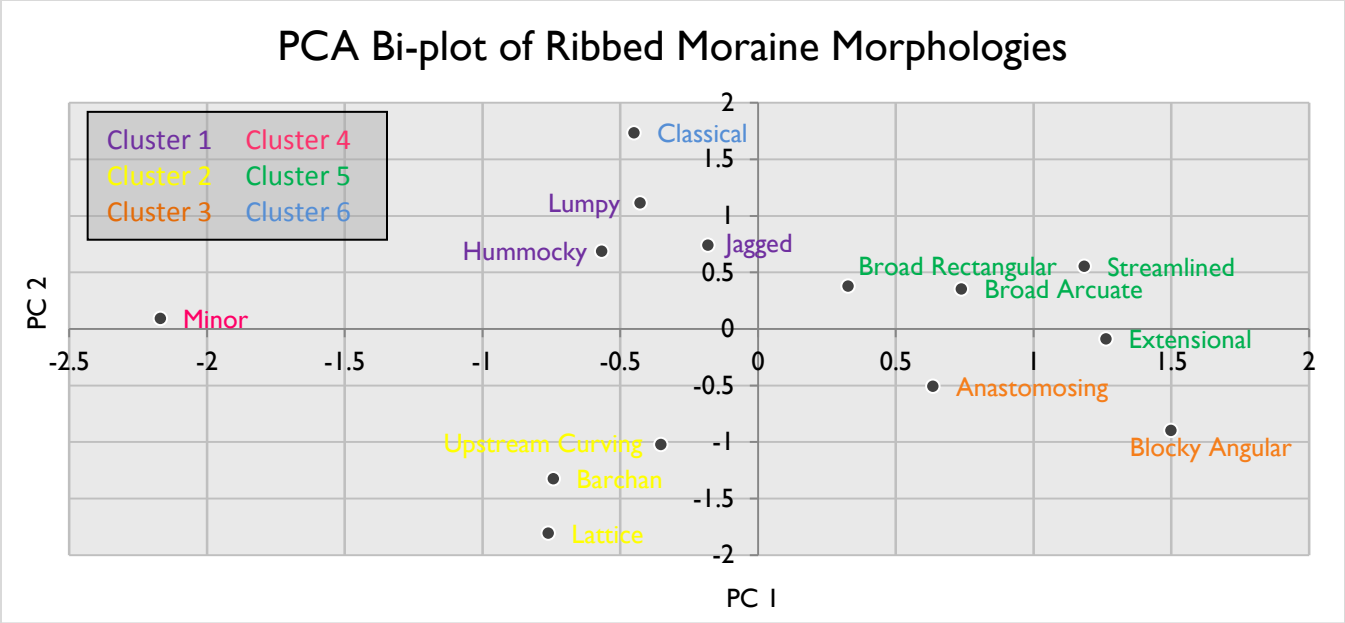

Fig. 5.59 – PCA bi-plot of ribbed moraine morphologies showing cluster membership.

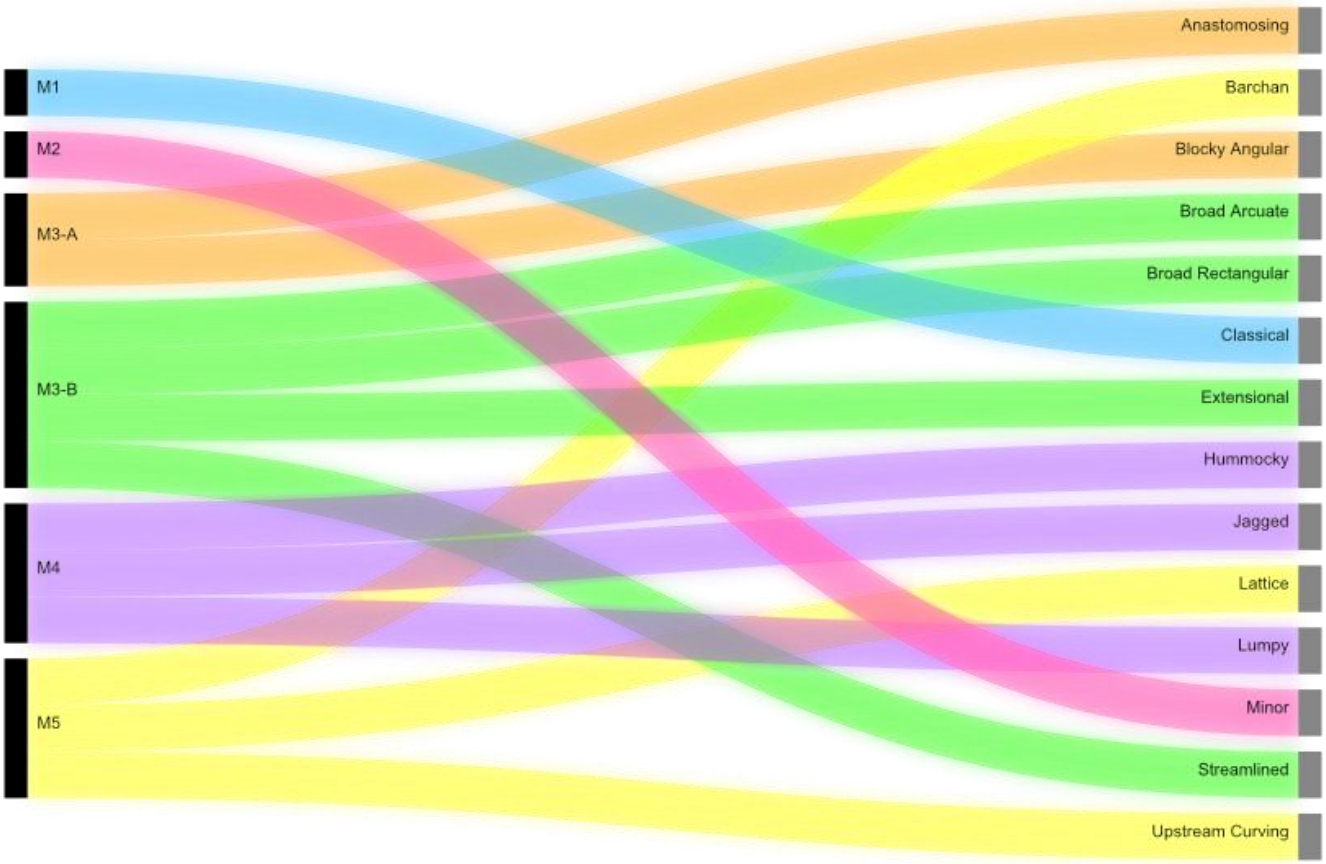

Fig. 5.60 – Morphotype classifications of ribbed moraine morphologies based on cluster memberships output from HCPC.

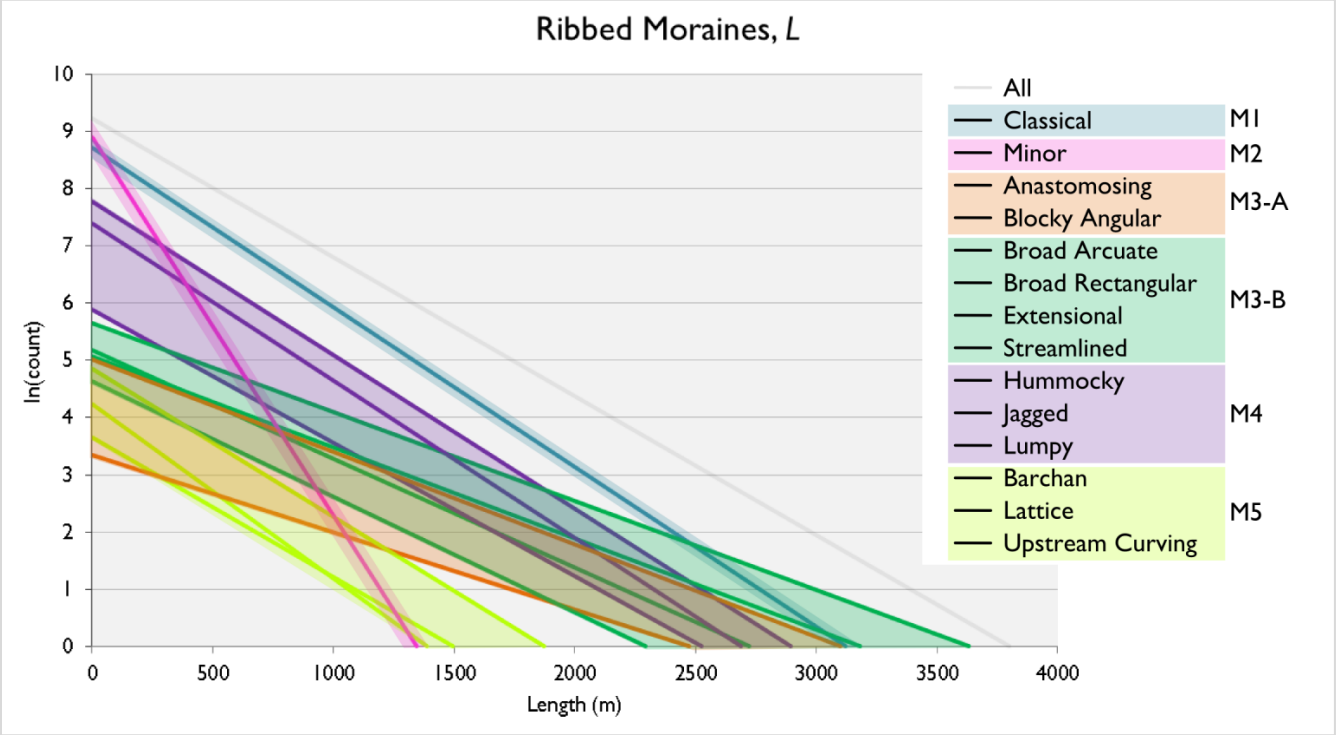

Fig. 5.61 – Morphotype groupings overlain on semi-log plots of λ for each ribbed moraine morphological subpopulation. Note the distinctive range of λ and β_0 that is spanned by each morphotype, and hence the good fit of this classification on the basis of λ alone. See Fig. 5.57 for original plot.

5.4.2 **A Relative Ice Flow Chronology for South-central Keewatin**

In addition to gathering new data on ribbed moraine morphology/morphometry and spatial distribution from south-central Keewatin, it is also the goal of this thesis to utilize the extant glacial landform archive in this sector to improve knowledge of regional glacial history. Given the ambiguity surrounding their mode(s) of formation, ribbed moraines have been scarcely employed in previous palaeoglaciological reconstructions (Kleman et al., 2006). Moreover, in the few places where these landforms have been incorporated into existing models (Greenwood and Clark, 2009a,b; Finlayson et al., 2010; Trommelen et al., 2012; Hughes et al., 2014) variations in their morphology have been poorly or only infrequently (e.g.,. Knight et al., 1999) accounted for. It is hypothesized here that new insights can be gained concerning the regional glacial history of southern Keewatin, in addition to the formational context of ribbed moraines, by considering these topics synergistically.

In order to reconcile these interests, mapping in this study followed a hierarchical approach. After ribbed moraines and streamlined landforms were comprehensively digitized as individual features for morphometric analysis (section 5.4.1), their arrangement within the study area was used to generate flowline maps (Fig. 5.62), derived separately by interpreting each category of landform as an indicator of palaeo-ice flow direction. The upper panel in Fig. 5.62 shows flowlines drawn as parallels to the trend of streamlined landforms. The bottom panel depicts similar linears drawn at orthogonals to the long axes of ribbed moraine ridges, unlike many previous studies which have considered only the orientation of the ribbed moraine field itself (e.g., Jansson et al., 2002; Jansson, 2005; De Angelis, 2007). Theoretically, zones of flowline convergence and divergence disclose former areas of accelerating and

decelerating ice flow, respectively, and can be instrumental in detecting past zones of streaming ice (Dyke and Morris, 1988; Hodge and Doppelhammer, 1996; Kleman et al., 1997; Stokes and Clark, 1999, 2001, 2003; De Angelis and Kleman, 2007, 2008). Conversely, straight, relatively parallel flowlines signify a pervasive sheet-style palaeo-ice flow (Kleman and Borgström, 1996; Clark, 1997, 1999). The maps in Fig. 5.62 reveal broad similarities; each is dominated by S, SW and SE trending flow. A prominent zone of convergence originating in the north-central portion of the study area and extending towards Hudson Bay is easily discerned in lineation flowlines, though is more scarcely traced in the ribbed moraine patterns. Lineation flowlines exhibit a more radial configuration in the western half of the study area and do not express the strong NW-SE trending configuration above Nueltin Lake that is clearly demonstrated by ribbed moraine flowlines. Despite stronger W-E lineation flowline convergence, trends east of 98° W longitude appear broadly correlative using each indicator.

Based on visual assessment of landform proximity (spacing), size (length), morphology, and parallel concordance (orientation) along these flowlines, 17 streamlined landform (*lins*) flowsets (Fig. 5.63) and 21 ribbed moraine (*rm*) flowsets (Fig. 5.64) were identified and mapped across the study area. Flowsets are theoretical tools which represent discrete, coherent groupings of subglacial bedforms. Each flowset cartographically simplifies a subset of the entire bedform record while retaining the spatial and temporal relationships exhibited by its constituent elements (Greenwood and Clark, 2009a) (Fig. 5.65). Whereas flowsets derived from lineations are shown with accompanying directional indicators, ribbed moraine flowsets in Fig. 5.64 are depicted without these components due to the often ambiguous relationship between ribbed moraine form and palaeo-ice flow. In many instances, (e.g., for all M3-A, M3-B, M4 and M5 morphotypes), streamlining of ribbed moraines following formation does not allow for objective interpretation of original form, and indeed some morphologies (e.g., those of M4 morphotype) lack consistent planforms altogether. Palaeo-ice flow directions inferred from *rm* flowsets in Fig. 5.73 are based on the direction of encompassing *lins* assemblages in the relative age model and should therefore be considered good, though objectively uncertain evaluations of the data. The larger number of *rm* compared to *lins* flowsets is arbitrary as a measure of comparison as it simply derives from the more fragmented nature of ribbed moraine fields, relative to fields of streamlined lineations which tend to be spatially continuous and easily aggregated. Field-based ice flow indicators (i.e., striations) were also extracted and mapped from Lee (1959), and used to support interpretations during flowset construction (Fig. 5.66). Flowset assignment is a scale-dependent procedure and varies according to the extent of the study area. Thus, it is possible that select regionally-extensive flowsets (e.g., *lins*6, *rm*8) form composite records of two or more events, despite efforts to discretely separate products of individual ice flows. A conservative approach has been taken in this study, and hence landforms have been assigned to flowsets at relatively large map scale, though the possibility that these may be regionally consistent with nearby flowsets of similar orientation (e.g., *rm*1 and *rm*12; *lins*16 and *lins*17) cannot be discounted. This style of assignment enables more flexibility when attributing various groupings of landforms to individual flow events, though results overall in a larger number of flowsets, and hence more complexity in the reconstruction.

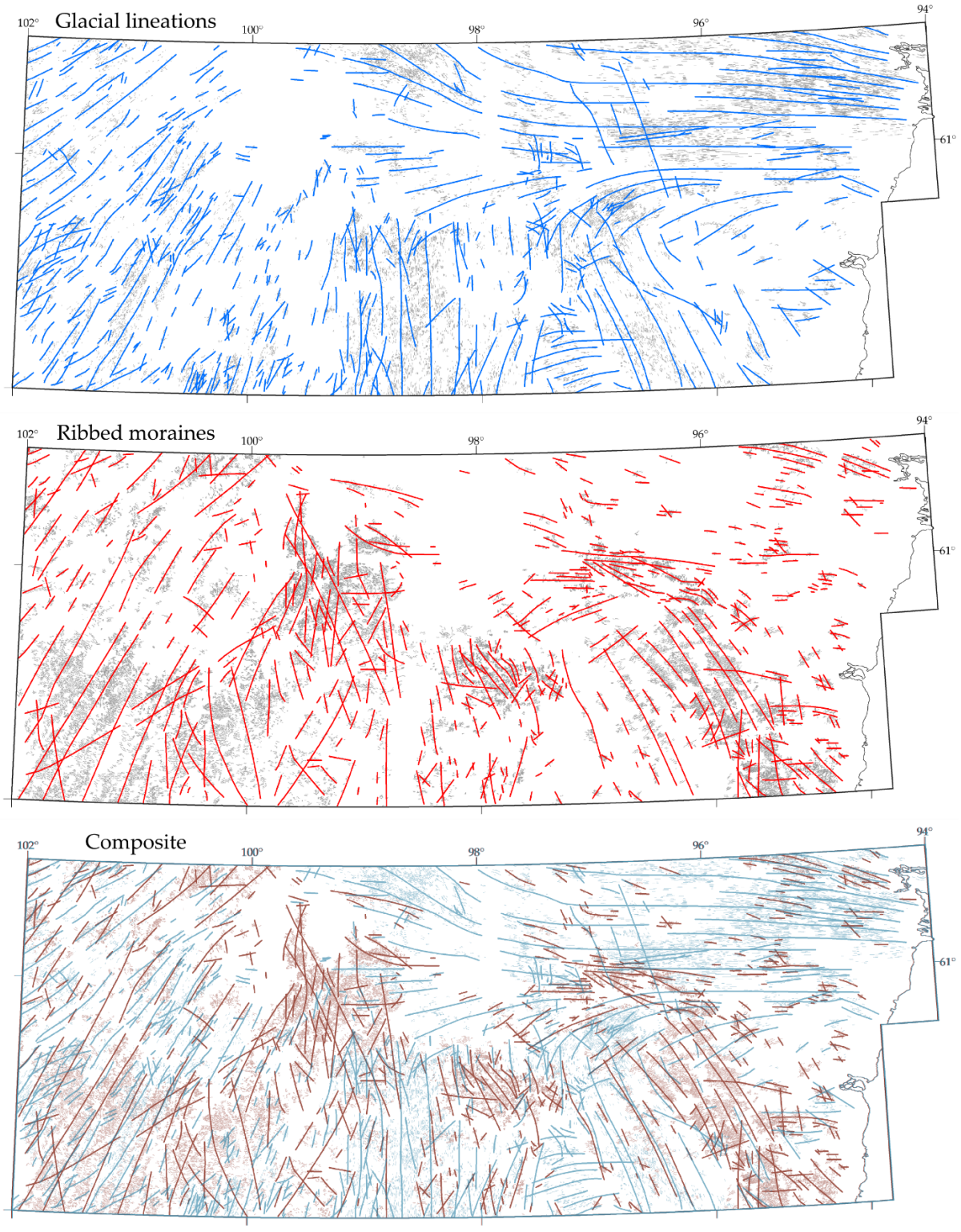

Fig. 5.62 – Flowline maps of south-central Keewatin developed using subglacial bedforms as palaeo-ice flow directional indicators. Upper panel shows flowlines drawn parallel to the trend of glacial lineations; middle panel depicts flowlines drawn perpendicular to the long axes of ribbed moraine ridges, bottom panel displays both sets of flowlines for comparison. Original landform data for each bedform type is included in gray as the background layer. Crossing flowlines do not necessarily imply that individual bedforms cross also at a given location.

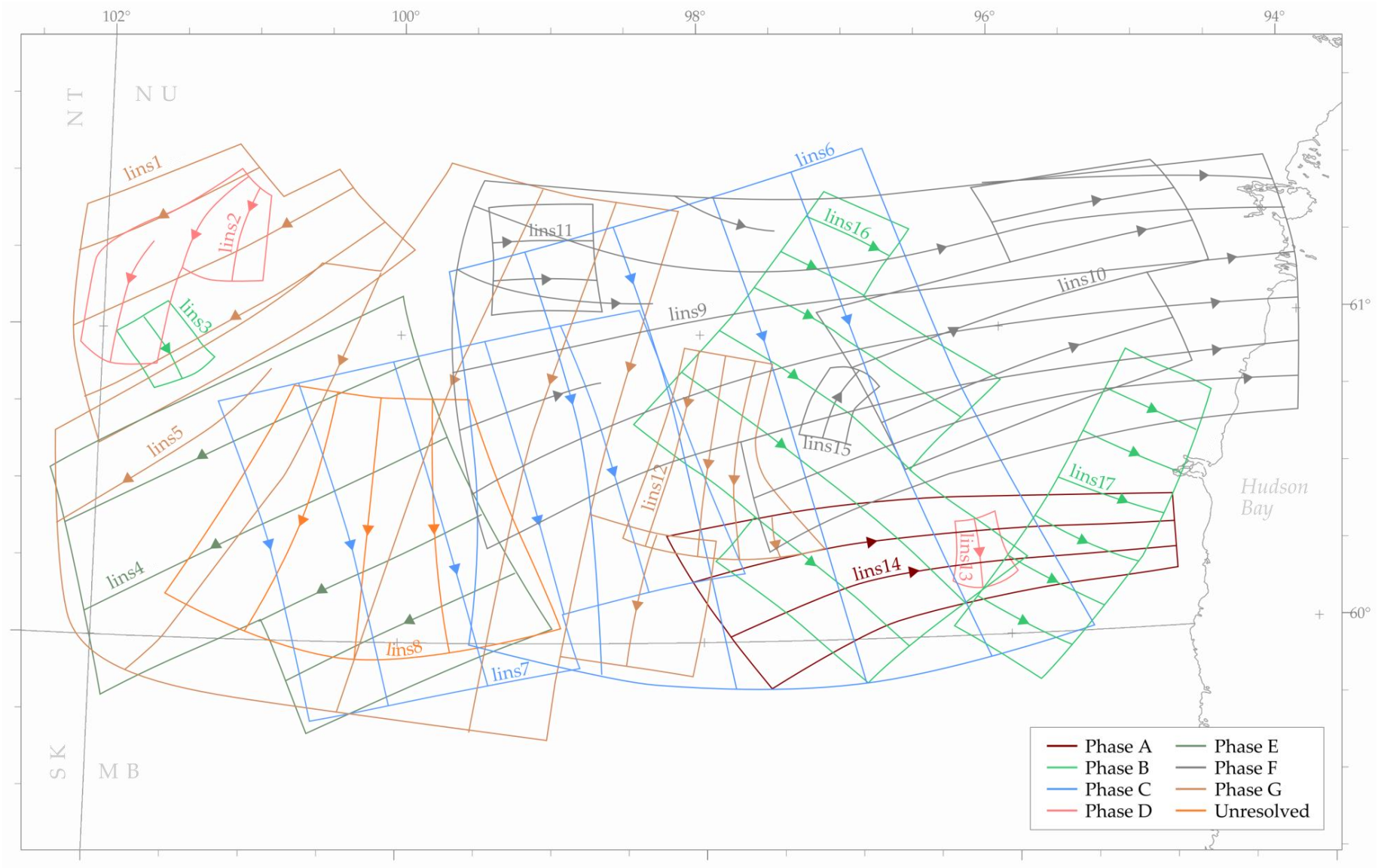

Fig. 5.63 – Results of interpretative flowset assignment for glacial lineations. Arrows along flow lines represent inferred direction of ice flow. Flowsets are coloured by flow phase shown in Fig. 5.73. Flowset numbers are arbitrary but correspond to Fig. 5.73, Table 5.10 and Appendix C.

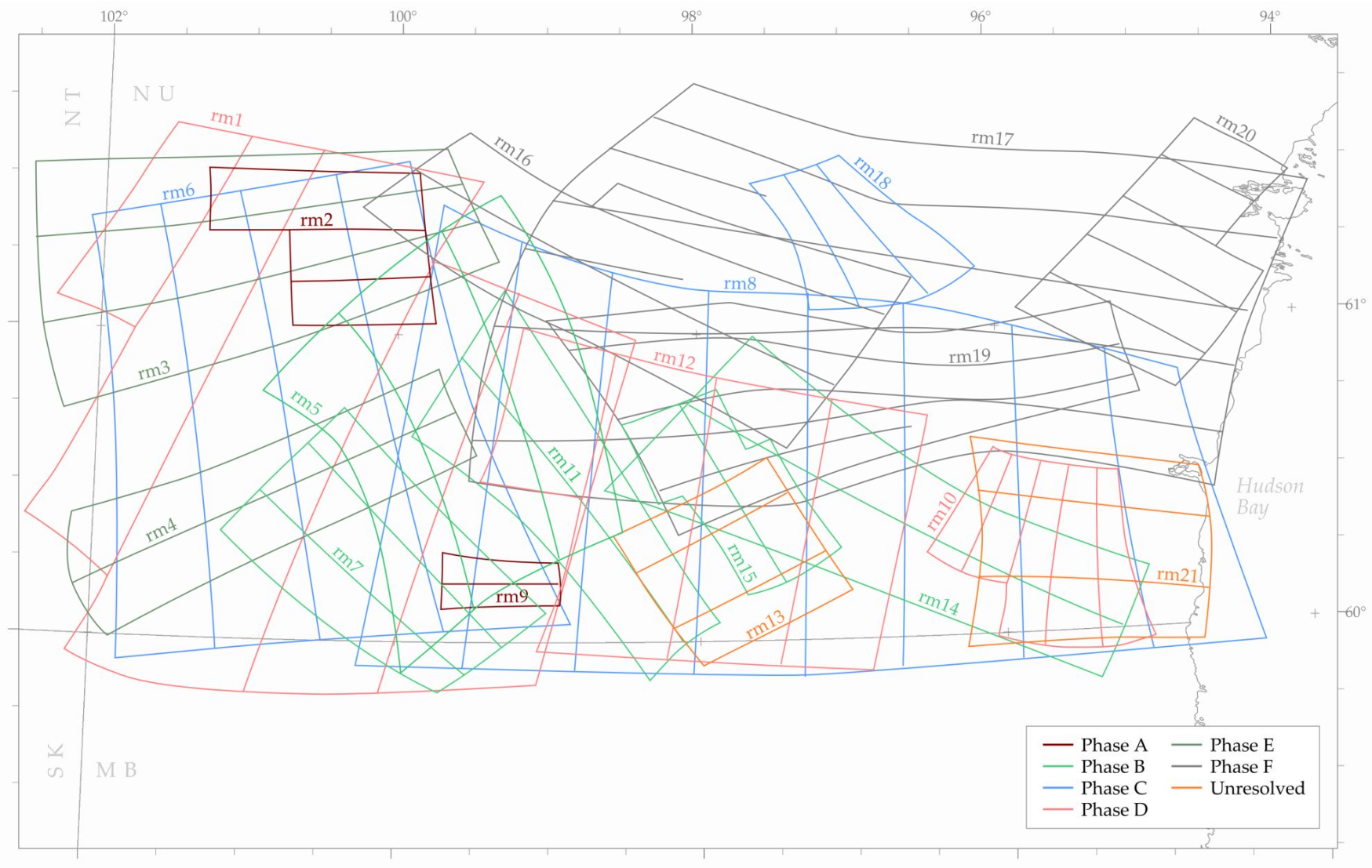

Fig. 5.64 – Results of interpretative flowset assignment for ribbed moraines. Arrows are not shown along flow lines due to uncertainties relating ribbed moraine assemblages to ice flow direction. Flowsets are coloured by flow phase shown in Fig. 5.73. Flowset numbers are arbitrary but correspond to Fig. 5.73, Table 5.10 and Appendix C.

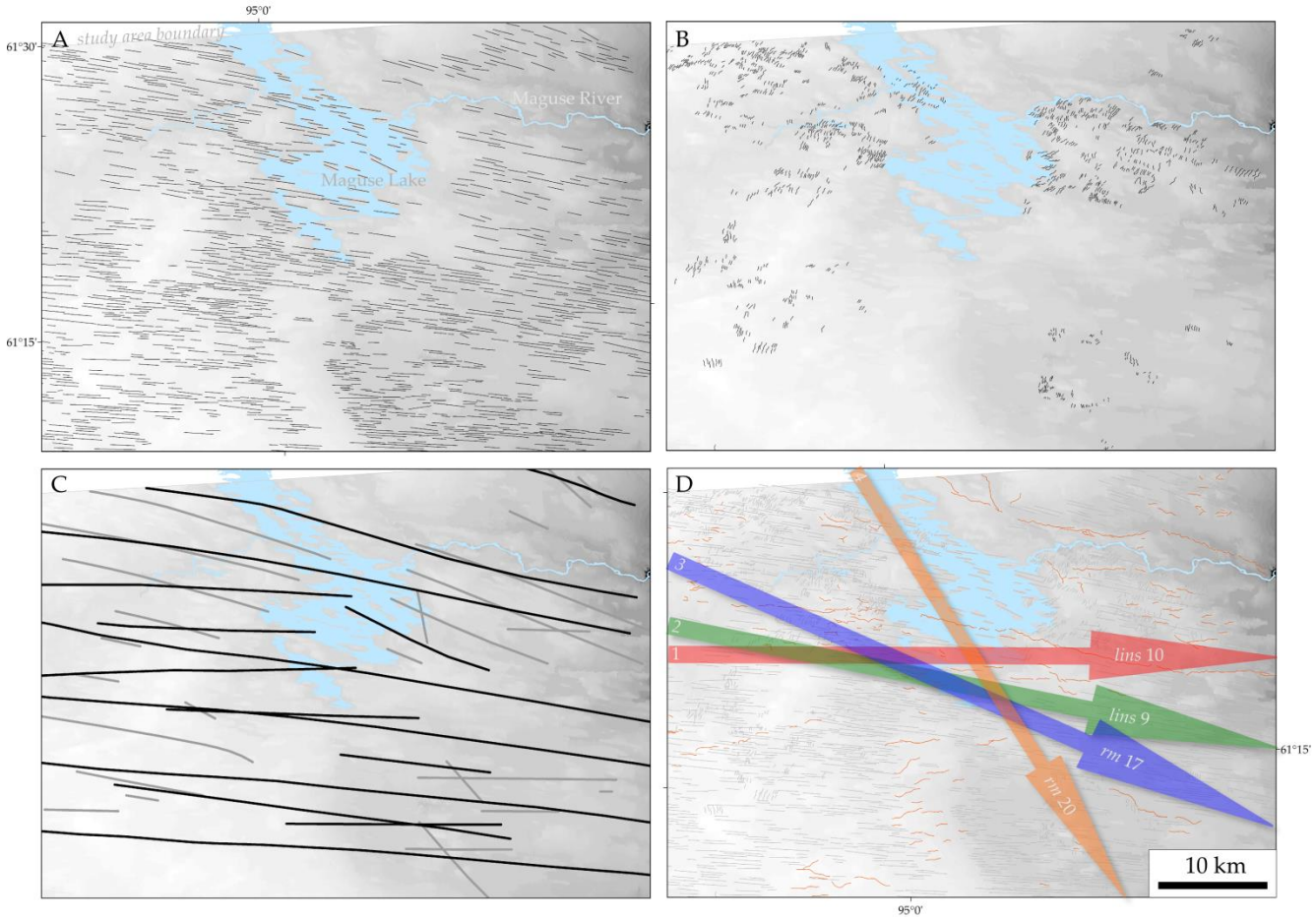

Fig. 5.65 – Illustration of the process of deriving *flowlines* and *flowsets* from the glacial landform record. Glacial lineations (A) and ribbed moraines (B) are mapped and their orientations used to develop separate flowlines (C); black lines drawn parallel to lineation trend, gray lines drawn perpendicular to ribbed moraine crestlines. D) A diachronous series of flowsets is developed by grouping landforms of similar spacing and morphometry along flowlines. Relative age relationships (indicated on arrow tails; 1=oldest) are deduced from instances of cross-cutting and overprinting. Eskers (shown in red) and other meltwater features attest to the organization of ice sheet drainage during deglaciation.

An examination of relative age relationships between individual flowsets (see Appendix C) was conducted based on landform cross-cutting and overprinting relationships, according to the well-rehearsed inversion technique (cf. Clark, 1997, 1999; Kleman and Borgström, 1996; Kleman et al., 2006; Greenwood and Clark, 2009; Hughes, 2014). Despite several previous investigations that seemingly attest to the profusion of cross-cutting sequences in this sector (Boulton and Clark, 1990a,b; Kleman et al., 2010), mapping in the present study determined these relationships to be relatively rare (see also Dyke and Dredge, 1989; De Angelis, 2007; Trommelen and Ross, 2010), at least between flowsets of like category (i.e., *lins* vs. *lins*; *rm* vs. *rm*). Nonetheless, it is common that flowsets (which theoretically encompass the minimum spatial extent of an ice flow event) overlap (Fig. 5.63 and Fig. 5.64), yet the landforms within separate flowsets overprint much less regularly, suggesting they have been (selectively) preserved in place. This lack of relative age control on landform sequences in south-central Keewatin necessitates that abductive reasoning is used to "fill in the gaps" when interpreting this sector's glacial history, in particular when the simplest reconstruction which ensures glaciological

plausibility requires assignment of geographically dissociated flowsets to a single stage. Hence, it is recognized that the process of inversion is inherently subjective, and different workers might form slightly different interpretations when using the same set of evidence. Consequently, all the ingredients of the inversion model utilized here are presented independently such that the interpretation preferred in this thesis can be objectively assessed by future workers, who also may or may not have access to new field-based information.

The results of this inversion process prescribed a reconstruction involving 7 phases of ice flow (Table 5.10, Fig. 5.73). These compartmentalized "time blocks" of bed-formation are introduced below in chronological order, beginning with the oldest recognized flows, through to those which are presumably related to the latest stages of deglaciation in southern Keewatin. Chronologies described within this work are strictly relative, though in some instances, can be tentatively linked to clast macro-fabrics, field-based erosional record indicators, and lithological/geochemical provenance determinations from the regional multiple-till stratigraphy reported in the literature, some of which are geochronologically dated. More thorough discussion and interpretation of the glaciodynamic implications of these flow stages is offered in Chapter 7, involving explicit considerations of possible linkages to the generation and preservation of the 6 ribbed moraine morphotypes introduced in section 5.4.1.7.

Table 5.10 – Flowset groupings by flow phase and the confidence of interpretation used to assign each its place in the relative age model. Three flowsets (*lins*8, *rm*13, *rm*21) cannot be fit to the present reconstruction and are here acknowledged as residuals.

Flow stage	Basis of grouping
Phase A	
*rm*2, *rm*9	Aligned with *lins*14, though no constraint on relative age. Unresolved *rm*21 may belong here but, given its configuration and position near the Bay, could also represent a deglacial imprint. *Rm*2 could fit with Phase F based on orientation, but would necessitate a divide positioned too far to the W; could plausibly fit late-stage Phase E if direction is reversed, or could be pre-LGM (e.g., Churchill Swarm in Kleman et al., 2010.
*lins*14	Patchy but well preserved. Extends into northern Manitoba (Trommelen et al., 2012) and supported by direction of streamlined bedrock. Crag-and-tail sense is to the ENE. Part of flowset 11 in Boulton and Clark (1990a,b).
Phase B	
*rm*7, *rm*11, *rm*14	Narrow banded flowsets with scant bedform preservation. All Phase B flowsets probably associated with SE dispersal of Proterozoic Dubawnt Group erratics from Thelon and Baker Lakes sedimentary basins in central Keewatin (e.g., Shilts, 1977).
*rm*5, *rm*15	*rm*5 offset slightly with respect to *rm*15, but placed here as is verifiably older than Phase C on the basis of superposition. No constraints on relative age for *rm*15, though fits well with alignment of encompassing flowsets.
*lins*3, *lins*16, *lins*17	*Lins*16 and *lins*17 possibly a single flowset. *Lins*3 is very small and geographically dissociated from *lins*16 and *lins*17 though is younger than Phase D flowsets on the basis of superposition.
Phase C	
*rm*6, *rm*8, *rm*18, *lins*7	Large flowsets; *rm*6 and *rm*18 are patchy, *rm8* relatively continuous with high parallel conformity and the dominant *rm* flowset in the eastern half of the study area. *Lins* 7 largely reworked by Phase G deglacial flowsets; no stratigraphic relation to *lins*6 but probably slightly older in order to uphold SE divide shift. Alternatively, may have occurred between *rm*6, *rm*8 and *rm*18 and *lins6. Rm*8 probably near in time or even coeval with *lins*6 in order to explain conjugate ridge belts by brittle subglacial deformation and internal shear.

*lins*6	Large isochronous flowset with high parallel conformity and independence from topography. Possible that early pre-Late Wisconsinan SE-trending flows are mistakenly captured by *lins*6 towards its northern extent, correlative with striae (Lee, 1959; Fig. 5.66), Dubawnt erratics in northern Manitoba (Trommelen et al., 2013) and the Aberdeen swarm in Kleman et al. (2010). In this area, *lins*6 is older than all other flowsets, but below *lins*9, is overprinted by Phase F and G flowsets. Crag-and-tails have southward sense.
Phase D	
*rm*1, *rm*10, *rm*12	Large isochronous flowsets with high parallel conformity; lack radial configuration of overprinting *lins*1 and *lins*5. Trajectory of *rm*1 and *rm*12 disclose SE divide migration on the order of 250-300 km from Phase B position. *Rm*10 reveals development of hook-shaped southern limb of the divide. Alternatively, hook-shape could be interpreted as a "bogus-divide", thereby discrediting this reconstruction, but such a configuration is required for early production of *lins*10 and *lins*15 prior to *lins*9 in Phase F.
*lins*2, *lins*13	Small, topographically influenced flowsets, included here on grounds of alignment but could potentially be late-stage deglacial; if so, this would require an inverse stratigraphic relationship between *lins*2 and *lins*1 (though this relationship as presently assessed is equivocal).
Phase E	
*rm*3, *rm*4	Long and narrow, but continuous flowsets. Parallelism of flowlines implies that ice was still relatively thick in this sector prior to deglacial Phases F and E. *Rm*4 must predate *lins*4 but probably occurred near in time given perfectly perpendicular overprinting of ridges.
*lins*4	Must occur after Phase D on this basis that it overprints *rm*1. Given a hook-shaped southern divide limb, could alternatively be coeval with *lins*10, 11 and 15 in Phase F.
Phase F	
*lins*10, *lins*11, *lins*15	Onset of ice streaming into Hudson Bay. NE-E rotation between these flowsets and *lins*9 records progressive collapse and southward expansion of the calving front in Hudson Bay.
*lins*9	Well-developed, strongly convergent time-transgressive imprint recording rapid ice drainage into Hudson Bay. Increasing basal ice velocity along flowlines exhibited by downstream transition from drumlins to MSGL.
*rm*16, *rm*17, *rm*20	Patchy, time-transgressive flowsets that everywhere overprint *lins*9 ice stream imprint. Slight SE rotation of flowlines compared to *lins*9 record minimal final divide migration to the NE in response to asymmetric ice sheet decay as a partial result of uncoupling of Keewatin and Labrador ice margins in northeast Manitoba. Esker ridges are generally aligned to *rm*17 and *rm*20.
Phase G	
*lins*1, *lins*5	Large radial, time-transgressive flowsets, clearly superimposed over all other bedform assemblages. Lobate pattern and alignment to esker ridges suggests formation near to ice sheet margin throughout final recession. Part of flowset 1 in Boulton and Clark (1990a,b).
*lins*12	Small topographically constrained flowset, possibly recording a confined, late lobate readvance, though could alternatively be assigned to Phase D, as age only constrained by older *lins*6.

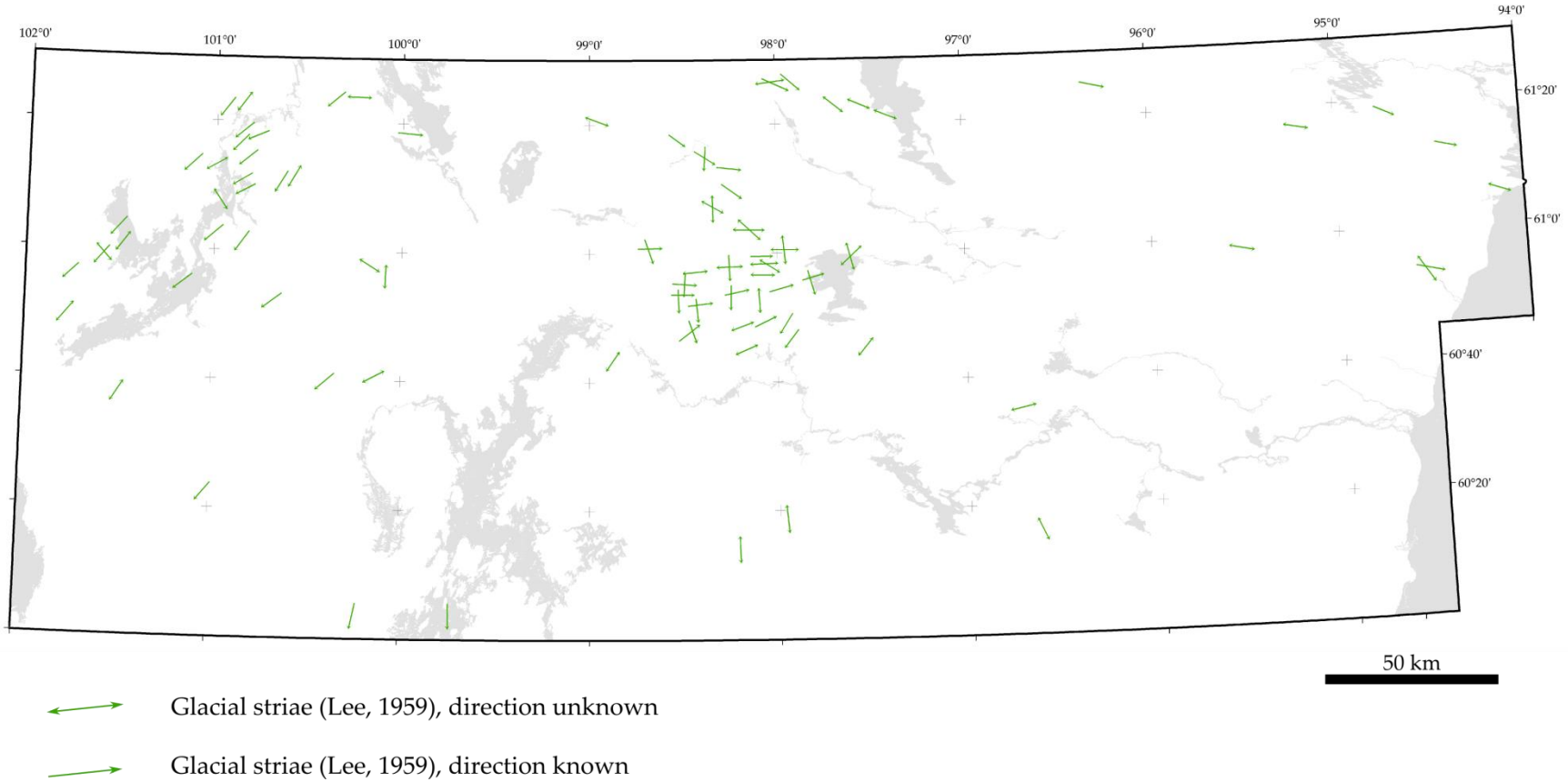

Fig. 5.66 – Glacial striation trends in south-central Keewatin, extracted from Lee (1959).

5.4.2.1 ***Early Flows (Phase A)***

An isolated assemblage of ENE-trending drumlins, megaflutes, crag-and-tails and streamlined bedrock (*lins*14) defines a patch of palimpsest terrain immediately below Edehon Lake, and surrounding Malaher Lake within an area of thin and discontinuous drift. Despite their excellent preservation, these features are notably absent on the Glacial Map of Canada (Prest et al., 1968) though are depicted by the three subsequent mapping projects with coverage in this area (Aylsworth et al., 1990; Boulton and Clark, 1990a,b; De Angelis, 2007). At its headward extent, *lins*14 is draped at right-angles by low-relief, disjointed esker ridges, and is very clearly overprinted by smaller lineations that trend towards the SE (*lins*6) and the SW (*lins*12) (Fig. 5.67).

In line with Boulton and Clark (1990b), these landforms are grouped with similarly oriented lineations near Hudson Bay (their flowset 11), notwithstanding their geographic separation, however it is recognized here that these easternmost features, which lack relative age relationships with any other flowset, may belong to a later deglacial phase, given their alignment to esker ridges in this area. Boulton and Clark (1990a,b), though also acknowledging lack of age control, assign this assemblage to "Stage E" in their chronology (later than the 76 Ka BP marine incursion reported by Andrews et al. (1983)) on the basis that it overprints their convergent flowset 9. This interpretation differs fundamentally from the one presented here, where the northernmost lineations in Boulton and Clark's (1990b) flowset 11 are grouped in this study with the convergent flowset *lins*9 which, in accordance with McMartin and Henderson (2004), is understood as a much younger, time-transgressive imprint, likely having operated in late-stage deglaciation, in contrast to *lins*14, which is clearly an isochronous imprint of an earlier event flow. This age assignment corroborates the findings of Trommelen and Ross (2010) and Trommelen et al. (2012) who recognize NE-trending megaflutes near Big Sand Lake in northern Manitoba (a probable extension of *lins*14) as the oldest streamlined landform flowset within their limit of mapping on the basis of landform cross-cutting and correlations to the regional erosional record. They also position these features within a palimpsest glacial terrain zone (GTZ), implying subsequent phases of overprinting. *Rm*21, which is unresolved in the present chronology, could have formed within Phase A, though this flowset has been significantly degraded by wave-washing, and hence its relationship with *lins*14 cannot be confidently determined.

Old SW and/or S-SE trending flows across Keewatin, for which there is pervasive field-based evidence in the form of striations and southward erratic dispersal (Tyrrell, 1897; Lord, 1953; Taylor, 1956; Lee, 1959; Shilts, 1973, 1977; Cunningham and Shilts, 1977; Shilts et al., 1979; Klassen, 1995; McMartin and Henderson, 2004; McMartin and Dredge, 2005; Trommelen et al., 2012, 2013), are not documented directly within surficial landforms in the present study. Conversely, Boulton and Clark (1990a,b), based on a larger mapping area, show early S-SE oriented drift lineations (their "Stage B") in southern Keewatin. They also correlate this phase with emplacement of the lowermost till (with fabric trends between 155° and 185°) in a sequence of three tills documented from exposures along the Churchill River in northern Manitoba (Dredge and Nielson, 1985; Dredge and McMartin, 2011). Similarly, Ridler and Shilts (1974) attribute a lower grey diamictic unit from a stacked till sequence at Kaminak Lake (Shilts, 1977) to ice flowing across central Keewatin from an area "…100 or more miles north of the region" (pg. 17). Kleman et al. (2010), based partly on mapping in Kleman et al. (2002) and De Angelis (2007), define two SW and S-trending streamlined landform swarms ("Aberdeen" and "Garry", respectively) covering a large area in central and southeastern Northwest Territories and central and southern Nunavut (including a broad portion of the present study area) which they regard as pre-dating the LGM (and tentatively attribute to OIS 3). Similar swarms are also documented here (e.g.,

*lins*8, which is unresolved in this chronology), though within the extent of this mapping and lacking regional correlation, they cannot be confidently assigned to an early, pre-LGM phase of ice flow. Many of the landform assemblages allegedly belonging to these early swarms, shown also in Boulton and Clark's flowset 34, are captured here by the younger flowsets *lins*6 and *lins*7; though the possibility of multiple Mid or Late Wisconsinan S-trending ice flows across this region (cf. Trommelen et al., 2012) is acknowledged, and are probably simply incapable of resolution within the current ~70,000 km^2 mapping limit. Moreover, the large S-trending lineations depicted in De Angelis (2007) just north of Smith Bay are almost certainly primary bedrock structures (Aylsworth et al., 1986a; Paul et al., 2002), which, if so, truncates the eastward extent of Kleman et al.'s (2010) "Aberdeen swarm" in southern Keewatin. SSE-trending lineations further to the east, if relating to an older phase of ice flow, cannot be confidently differentiated from those which form the lowermost extension of *lins*6. Furthermore, in accordance with Trommelen et al. (2012), no evidence of the W-trending "Churchill swarm" reported in Kleman et al. (2010) is found in the study area, though *rm*2, having a relative age imposed only by the regional deglacial assemblage, could be a potential correlative, which would imply that it has here been temporally misplaced and shown with inverted direction.

Recent numerical modeling (Clark et al., 1996; Marshall and Clarke 1997a,b; Marshall et al. 2000; Tarasov and Peltier, 2004; Stokes et al., 2012) has positioned near-LGM (OIS 2) maximum ice sheet surface topographies within the western interior plains. Though it is acknowledged that the Marshall models overpredict LGM ice thickness along the LIS/CIS convergence, these divide structures match broadly with the central dome depicted in the vicinity of Great Slave Lake in Dyke and Prest (1987) at 18,000 Ka BP (despite the numerically-modeled domes being shifted somewhat far to the south in comparison). The flow pattern portrayed in Phase A requires a dispersal center located to the west of the Nunvaut/Northwest Territories border and (especially if including Trommelen et al.'s (2012) flowset A as an extension of *lins*14) also south of 60°N latitude, which is well-matched by the scenarios outlined above. A similar, N-S elongated early Keewatin Ice Divide is positioned across eastern Lake Athabasca in Dredge et al. (1986) (labeled K_0 on their figure 28, pg. 24) in order to explain E-trending striae on the Chekask Hills in northeastern Manitoba. Figure 4 in Dyke et al. (1992) seemingly suggests this center of outflow may also have been a southern extension of the M'Clintock Ice Divide, a position favoured here, and also by Dyke and Dredge (1989) over the interpretation that the latter divide (dome) and the Keewatin Ice Divide were separate, yet coeval features (e.g., Shilts, 1984). LIS inception and build-up modeling of Kleman et al. (2002) and Stokes et al. (2012), however, reveals that this divide structure may have been repeated during earlier maximum stages (e.g., OIS 4), which precludes the secure assignment of Phase A to LGM. The equivalent flow stage in Boulton and Clark (1990a,b; "Stage E") for instance, has been tentatively assigned to pre-Late Wisconsinan time by those authors. It is noted, however, that likely a proportionally greater area of the LIS was warm-based during the later glacial episodes (Kleman et al., 2002; Marshall and Clark, 2002; Stokes et al., 2012), which is a requirement in glacial lineament production (cf. Kleman and Borgström, 1996; Kleman et al., 2006), and also that an LGM assignment of Phase A avoids the need to invoke landform preservation during earlier northward and eastward divide migrations associated with the rapid recession to the OIS 4 minimum (~55 Ka BP), which is a component of recent numerical models (Stokes et al., 2012). Moreover, the 20 Ka BP basal thermal zonations of Marshall et al. (2000) and Tarasov and Peltier (2007) show a warm/cold basal thermal boundary along the approximate headward extent of *rm*9, which could provide a basis for the positioning of this flowset (and *rm*2) within Phase A, if ribbed moraines are taken to be formed at the interface between frozen and thawed bed conditions (cf. Hättestrand, 1997; Hättestrand and Kleman, 1999; Kleman and Hättestrand, 1999; Sarala, 2006 – see section 3.4.1).

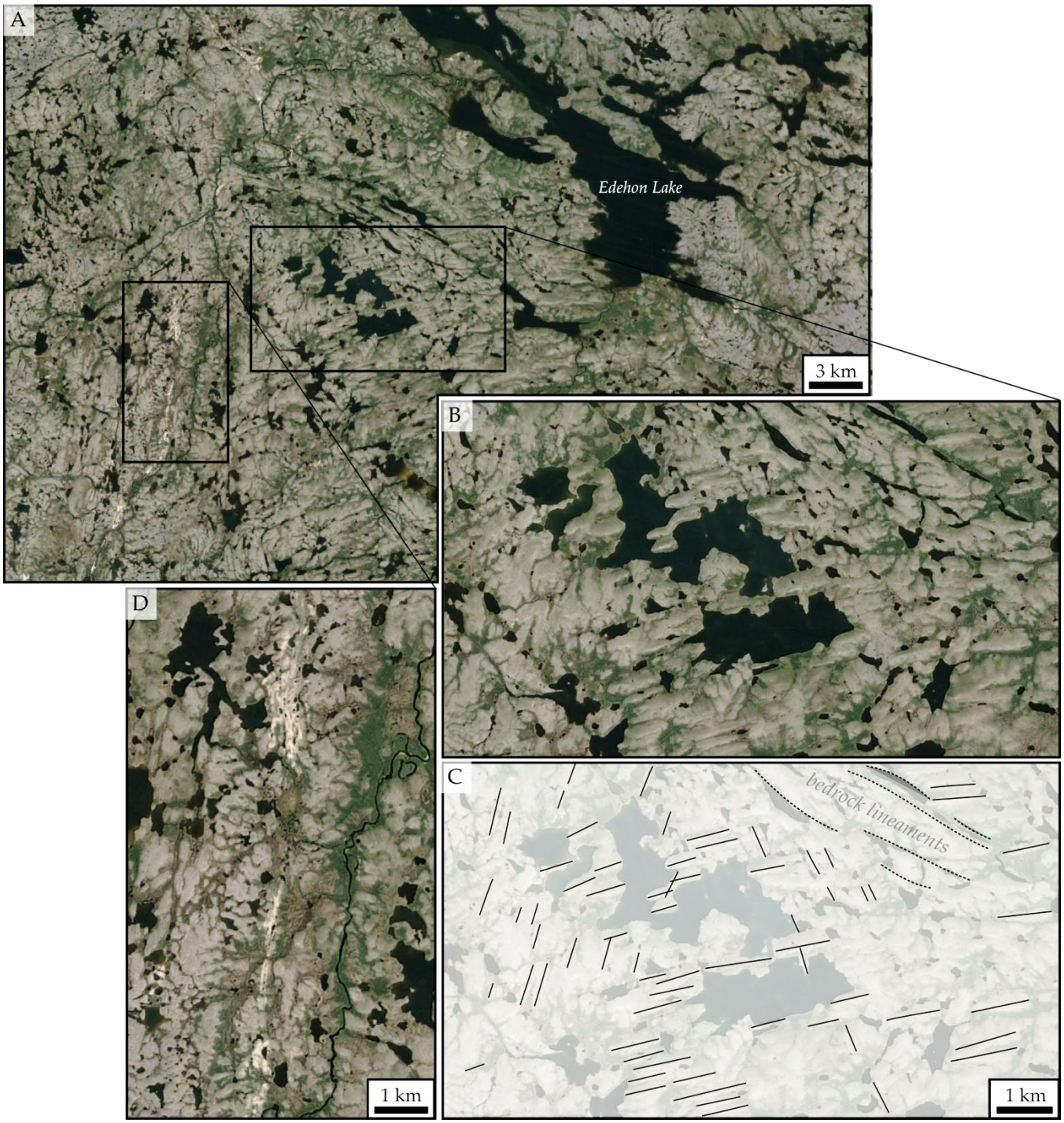

Fig. 5.67 – Three generations of glacial landforms southeast of Edehon Lake. B-C) Well-preserved till lineations and crag-and-tails with ENE sense partially overprinted by SE (younger) and SW (youngest) streamlined landforms. D) Esker ridge and associated glaciofluvial deposits drape lumpy ribbed moraines within a narrow glaciofluvial passageway. Note that ribbed moraines are completely demolished by younger till lineations (upper left, corresponding landforms shown in B) west of a sharp contact, yet ridges adjacent to the esker ridge are reasonably well-preserved.

5.4.2.2 ***Middle Flows (Phases B – E)***

Post-LGM drawdown of the southern LIS margin across the upper Midwest United States and further east in the Great Lakes region, in conjunction with rapid collapse of the CIS (Clague and James, 2002) and associated decreased buttressing along the western margin, facilitated a swing in the lower arm of the Ancestral Keewatin Ice Divide (AKID, cf. Dyke and Prest, 1987) and an enhanced sourcing of ice to central and southern Keewatin from the AKID's northern limb (Tyrrell 1896, Lee, 1959; Dyke et al., 1982; Dredge et al., 1986). Phase B and C, presumably net erosional phases near LGM or early in deglaciation, are consistent with the dispersal of Dubawnt Group erratics from the Thelon and Baker Lake sedimentary basins as far east as the Hudson Bay coast, and further towards Belcher Islands in glaciomarine sediments within the Bay (Shilts, 1973, 1980, 1984; Ridler and Shilts, 1974; Kaszycki and Shilts, 1979; Shilts et al., 1979; Klassen, 1995). McMartin and Dredge (2005) document S-SE trending striae in the Schultz/Pitz/Baker Lakes area, up to 10 km north of Schultz Lake – probably correlative with Phase B – and younger SE trending striae restricted to an area south of Schultz Lake, which they interpret as evidence of a southeastward divide shift across this location, possibly at LGM or shortly thereafter. A subsequent major flow reversal, recorded by NNW trending striae and streamlined landforms as far to the southeast as Kaminuriak Lake (McMartin and Henserson, 2004) indicates a continued southward and eastward migration of the AKID following this stage (shown here in Phases C-E, Fig. 5.73).

In south-central Keewatin, the W-E migration of the AKID is inferred from a series of SE-SW trending landform flowsets supporting relative age relationships that indicate progressive younging with increasing westerly rotation. The concomitant southward migration of the AKID (e.g., Tyrrell, 1897; Lee, 1959; Cunningham and Shilts, 1977; Klassen, 1995; Dyke and Prest, 1987; McMartin and Henderson, 2004) is not resolved within the study area until the latest phases in this sequence, which demonstrate SW (Phase D) and WSW (Phase E) trending ice flow approximately west of Nueltin Lake and attendant S trending flows to the east (Phase D only), the latter of which are only scarcely recorded by *rm*12 and the younger isolated *lins*13. By Phases D and E, south and southwest trending flow traces are absent north and east of Tatinnai Lake, suggesting the existence of a divide in the immediate vicinity (e.g., east of K_3 on figure 28 in Dredge et al., 1986); this is consistent with the clockwise rotation of the AKID's southern limb, and the pinning of its centerpoint below Wager Bay (McMartin and Dredge, 2005), originally proposed by McMartin and Henderson (2004), though implicit also in the reconstruction of Dyke and Dredge (1989). This period of high mobility is presented in the current study as spanning 4 phases (B-E) in order to account for and emphasize what are here interpreted as multiple episodes of ribbed moraine formation (see Chapter 7), though it is otherwise just as correct, and perhaps less complicated, to portray this shift as a single, time-transgressive, SE to SW transitioning imprint. The NW-SE traversal of the AKID across central Keewatin above the study area, and its assignment to the onset of the latest phase of ice decay, is supported also by work in northeastern Manitoba (Dredge and Nixon, 1992; Trommelen et al., 2012) that documents a corresponding transition based on "middle" and "young" aged field-based ice flow indicators (figure 6 in Trommelen et al., 2012) and comparatively younger streamlined landform assemblages (*ibid*., figure 7), the latter of which do not adequately explain inherited SE and ENE clast dispersal patterns from Keewatin-sourced ice (Trommelen et al., 2013) and must necessarily relate to more recent glacial events. Dredge et al. (1986) and Dyke and Dredge (1989) also document a progressive, SE-SW rotation in the orientation of landform assemblages from northwestern Manitoba, and further perceive this to have been punctuated by probable episodes of ice streaming and several major surges (e.g., the Quinn Lake readvance) into Lake Aggassiz prior to its drainage.

*Lins*6, *rm*8 and *rm*18 in the southeastern portion of the study area have been traditionally associated with the regional deglacial envelope (e.g., Dyke and Prest, 1987), though are shown here as belonging to Phase C which clearly pre-dates the youngest landform assemblages in this area, the latter of which are found only in scant traces. Evidence which might link these most expansive swarms to the latest stage of ice decay is lacking or insufficient in earlier works. Near Hudson Bay, eskers trend ENE to ESE and overprint all other landform assemblages. In contrast to their mostly continuous and dendritic arrangement elsewhere over the northwestern Shield, here they are short and highly fragmented, and are grouped into parallel, segmented clusters. Moreover, they occur in intimate association with coalescing glaciofluvial fans, aprons and deltas that are indicative of contracted ice damming along an east-facing margin, oriented approximately parallel to the present-day Hudson Bay coastline (Fig. 5.72A; see also figure 22 in Aylsworth and Shilts, 1989b). Patches of N-S trending De Geer moraines (primarily found above and below the study area) also record successive inland positions of the ice margin. In any case, SE-trending flowlines traced within this area (Fig. 5.62) demonstrate little divergence, suggesting isochronous landform generation under relatively thick ice. Trommelen et al. (2012) map a possible extension of *lins6* in northeastern Manitoba (their flowset B) and likewise interpret this as an inherited imprint from an earlier ice flow phase, which forms a component of their relict-type Caribou River GTZ. Surface tills in that area display anomalously high concentrations of Proterozoic Dubawnt Group erratics (Trommelen et al., 2013), suggesting they may have been sourced from an early stage of flow when the AKID was positioned above the Thelon and Baker Lakes sedimentary basins (Kaszycki and Shilts, 1979; Klassen, 1995). Elsewhere, within surrounding GTZs (e.g., in palimpsest GTZs), these lithologies are comparatively diluted, and together this could reflect subsequent selective scavenging/erosion and deposition promoted by local-scale spatio-temporal transitions in glaciodynamic regimes. Subsequent reconfiguration of surface deposits by convergent eastward flows (e.g., *lins*9) also implies that the SE-trending flowsets are locally not the youngest in age, although this relationship is only observable from an area where SE-trending streamlined landforms (e.g., *lins*6) are of potential pre-LGM age (e.g., Kleman et al.'s (2010) "Aberdeen swarm"; see section 5.4.2.1 above).

5.4.2.3 ***Late Convergent Flows (Phase F)***

By 8.4 Ka BP, the KID had grown relatively stable (Dyke and Dredge, 1989), realizing its terminal configuration and coming to occupy its approximate final resting place (e.g., "Zone 1" in Aylsworth and Shilts, 1989a,b; or the KID *sensu strictro* reported in Lee, 1959). The northern and western extent of ice in Keewatin during this time is delimited by a series of end moraine ridges extending from Committee Bay to Chantrey Inlet (Falconer, 1965), including the prominent McAlpine and Chantrey moraine complexes (Dyke and Prest, 1987) with estimated ages between 8.5 and 8 Ka BP (Blake, 1963; Dyke, 1984; Dyke and Dredge, 1989; Dyke, 2004). Given that they are positioned well inland of marine limit, these systems signify readvances rather than post-calving stabilizations (Dyke, 1984) and are the youngest marginal evidence for deglaciation of the Keewatin sector – subsequent decay geometries are unfortunately chronologically unconstrained (Dyke, 2004). On the western side of the KID, Stokes and Clark (2003) utilized Blake's (1963) 8,160 ± 140 yr BP ^{14}C date recovered from shells on the distal face of the MacAlpine Moraine to assign a minimum age to the operation of the Dubawnt Lake Ice Stream (DLIS), whose geomorphological footprint they have mapped and since exhaustively reported upon (Stokes and Clark, 2001, 2002; Stokes et al., 2006, 2007, 2008, 2013b; Ó Cofaigh et al., 2013). The track of the DLIS terminates distally at the MacAlpine Moraine, which has encouraged these authors' usage of Blake's (1963) date, though they also perceive that this system

represents an isochronous imprint of deglaciation, developed over only a brief, sub-millennial timescale. Conjecturably triggered by the development of proglacial lakes (e.g., glacial Lake Thelon) along the western LIS margin at this time (Craig, 1964), the DLIS, and potentially a secondary ice stream flowing to the northwest in the Back River Basin (McMartin and Henderson, 2004), were critical components of the rapid deglaciation in eastern Northwest Territories and western Nunavut, probably from about 9 Ka BP until their demise.

In the present study area, an expansive assemblage of highly-elongated drumlins, transitioning distally to MSGL, is recorded by a series of E-trending *lins* flowsets converging into Hudson Bay. The earliest flows in this sequence (i.e., *lins*10, *lins*15) indicate slightly more parallel and northerly trajectories, potentially originating from the "hook-shaped" southern limb of the KID across southern Keewatin that is widely portrayed in traditional reconstructions (Dyke and Prest, 1987; Dyke and Dredge, 1989). The geometry of this divide would have partitioned SW flowing ice into northern Manitoba from ENE flows draining into Hudson Bay. By Ka BP, a rapidly retreating calving front in Hudson Bay began siphoning ice from the southeastern and east-central Keewatin mainland (Dyke, 2004), and thus initiated rapid drawdown on the eastern side of the KID. These latter flows (i.e., *lins*9) retain strong indications of streaming ice, including a splaying onset zone and wide catchment area transitioning into a narrow trunk that exhibits progressively more elongate drumlins and eventually MSGL down-ice (Stokes and Clark, 1999, 2002). *Lins*9 contains the longest glacial lineations mapped within any flowset in the study area (Fig. 5.72B and Fig. 5.53). The upper boundary of these converging flows extends north above the mapping limit into east-central Keewatin (Boulton and Clark, 1990a,b; McMartin and Henderson, 2004), whereas the terminus is submerged in Hudson Bay, suggesting operation from at least 8 to 7.7 Ka BP according to the LIS palaeogeographies outlined in Dyke (2004), though streaming on the east side of the KID may have begun as early as 9 Ka BP (in conjunction with the DLIS in the northwest) (McMartin and Henderson, 2004). If the latter argument is true, this would imply that Phase F is coeval with Phase E – a glaciologically plausible scenario, should the southern limb of the KID have been arcuate (as suggested above) and oriented NE-SW, stretched roughly between Hicks and Debartok Lakes, only some 50-100 km west of the 9 Ka BP position depicted in Dyke and Dredge (1989). Conversely, Boulton and Clark (1990a,b) assumed that these flow traces were Middle Wisconsinan in age. In agreement with McMartin and Henderson (2004), evidence from the present study shows that convergent E-trending drift lineations in southeastern Keewatin were generated time-transgressively throughout deglaciation. Most large eskers are aligned with these flowlines, and glaciomarine ice-contact deposits (e.g., sediment fans, ramps and deltas) and De Geer moraines drape lineations at right angles with only minor offsets inside the marine limit (Fig. 5.72A).

Whereas McMartin and Henderson (2004) envision the convergence of *lins*9 (grouped within their Phase F, figure 12, pg. 181) to have simply derived from the arcuate configuration of the KID (i.e., concave towards Hudson Bay) throughout deglaciation, substantial evidence is presented in this study that is indicative rather of first-order glaciodynamic controls on this imprint; namely, convergence due to ice streaming. Even overlying areas of "hard bed" geology such as the Canadian Shield, ice streams can be conditioned exclusively by glaciological parameters, impelled by thermomechanical feedbacks between temperature and ice flow (Payne and Dongelmans, 1997). Likewise, streaming ice east of the KID may have been initiated through positive feedbacks involving enhanced basal strain heating resulting from increasing ice velocities (for which the downstream transition to MSGL within *lins*9 provides plausible evidence; cf. Dyke and Morris, 1988; Mitchell, 1994; Hart, 1999; Canals et al., 2000; Stokes and Clark, 2002, Briner, 2007; Stokes et al., 2013a) due to loss of marginal buttressing and more rapid drainage of terrestrial ice volumes into the Bay. Rapid collapse of ice over Hudson Bay would have stimulated initially high discharge from surrounding outlets, lowering the marginal surface profile

and generating a steep ice sheet topographic gradient outward from the divide, thus engendering further high-velocity flows in order to restore an equilibrium ice sheet topography.

Importantly, patches of ribbed moraines (*rm*16, *rm*17, *rm*19, *rm*20) overprint elongated drumlins and MSGL of *lins*9 everywhere in this region, which is a defining characteristic also of the DLIS on the opposite side of the KID (Stokes and Clark, 2003; Stokes et al. 2006, 2008). Stokes et al. (2007) interpret these unique assemblages of ribbed moraines as indicators of basal freeze-on processes (i.e., "ice stream sticky spots") formed during ice stream shutdown and collapse (see also Christoffersen and Tulaczyk (2003) for a numerically modeled solution for this behaviour). Their field-based evidence also suggests that they were constructed during an abrupt transition from an extensional to compressional flow regime (Stokes et al., 2008) which could have been affected by strong ice/bed recoupling, substrate dewatering and/or a transition to frozen bed conditions (Kleman et al., 1997; Boulton et al., 2009). The presence of ribbed moraines overprinting *lins*9 may imply the operation of similar processes in this area. Here however, *rm*16, *rm*17 and *rm*20 are offset slightly towards the NE/SW, which is consistent with the most recent, minor northwestern migration of the KID following shutdown of the DLIS (McMartin and Henderson, 2004). Evidence from Antarctica suggests that the basal thermal zonation of ice streams is sporadic and spatially non-uniform, specifically within their onset zones (Engelhardt and Kamb, 1998; Bamber et al., 2000; Vaughan et al., 2006), which could have contributed to the patchy distribution of minor ribbed moraines in this area. The final direction of ice retreat in southeastern Keewatin, indicated by Dyke (2004), was to the WNW, and hence it appears that these *rm* flowsets are in fact related to final deglaciation, and succeeded *lins*9 flows.

Fewer instances of ribbed moraines overprinting *lins*9 are observed towards the headward extent of this flowset, and this is likely a function of several factors including: 1) Reduced drift thickness/higher prevalence of outcropping bedrock in this area; 2) exhaustion of sediment supply and/or reduced sediment flux with time during recession; and 3) potential stagnation of ice in the north-central portion of the study area. Stagnation during decay, specifically in this region, is supported by the relative lack of glacial bedforms, the existence of hummocky moraine (cf. Aylsworth and Shilts, 1989b) and the coalescence of esker tributaries at right angles with their trunk streams, all of which are characteristic of thin, active ice transitioning to stagnant, less plastic and/or inactive ice (Fig. 5.68). Perhaps the most prominent of the latter features is the "Ray esker" (shown in Fig. 5.72D, named here after the nearby lake), which trends N-S for ~15 km and cross-cuts elongated drumlins of *lins*9 at ~90°. Several other esker tributaries exhibit similar geometries with their trunk streams in this area. The Ray esker appears to have developed primarily as an erosive channel through the carapaces of *lins*9 drumlins, implying high overburden pressures (e.g., stagnant ice with strong substrate coupling) and low sediment loading of meltwater in this area during deglaciation. The efficient meltwater routing and drainage system of the interior LIS during recession (of which the extensive esker network is a cast) may have promoted spatially variable enhanced coupling of ice and sediment in response to substrate dewatering and effective meltwater evacuation to the margin (Trommelen et al., 2012), hence eliciting localized stiffening of the substrate and cessation or retardation of soft sediment deformation within the mobile deforming bed layer (Menzies, 1989b; Boulton et al., 2009; Menzies and Ellwanger, 2011; Tylmann et al., 2013).

Alleged ice stagnation features have also been observed locally in the southeastern portion of the study area, including hummocky and "reticulate" moraine (Dredge and Nixon, 1992; Dyke and Dredge, 1989; Trommelen and Ross, 2010; Trommelen et al., 2012, 2014) (Fig. 5.69; see also Fig. 5.70). Dredge and Nixon (1992) interpret these latter forms as crevasse-intrusion ridges, generated during *in-situ* downwasting of a brittle, highly fractured and locally stagnant ice mass. Similar features have been described by Boulton et al. (1996) from the marine inundated forefield of the surge-type Sefstrombreen

glacier on Svalbard, and likewise interpreted there as infilled sediment casts of a brittle crevasse network formed by lobe detachment and downwasting following a major surge. In southeast Keewatin however, reticulate moraine ridges are found only within three ~2 km wide belts, stretching southeast for about 40 km into northeastern Manitoba. They alternate laterally with belts of similarly oriented and incompletely overprinted ribbed moraines, and thus are spatially confined and not pervasive as are the features mapped off the coast of Svalbard. In the present study, many of these ridges have been mapped as the "lattice-type" ribbed moraine morphology, and this is not by error, as they are interpreted here to have formed beneath active ice. Trommelen et al. (2014) likewise construe these bands of "conjugate ridges" (pg. 151) as evidence of basal frictional heating between patches of wet-based and sticky (possibly frozen) bed conditions, and thus also prefer a genesis by active subglacial processes. The stacked or "conjugate" quality of these ridges, many of which do not have sharp crests (Fig. 5.70), seemingly precludes a genesis by crevasse injection, but could be indicative of subglacial brittle deformation, as might be accomplished along an interface between rapid and sluggishly flowing basal ice.

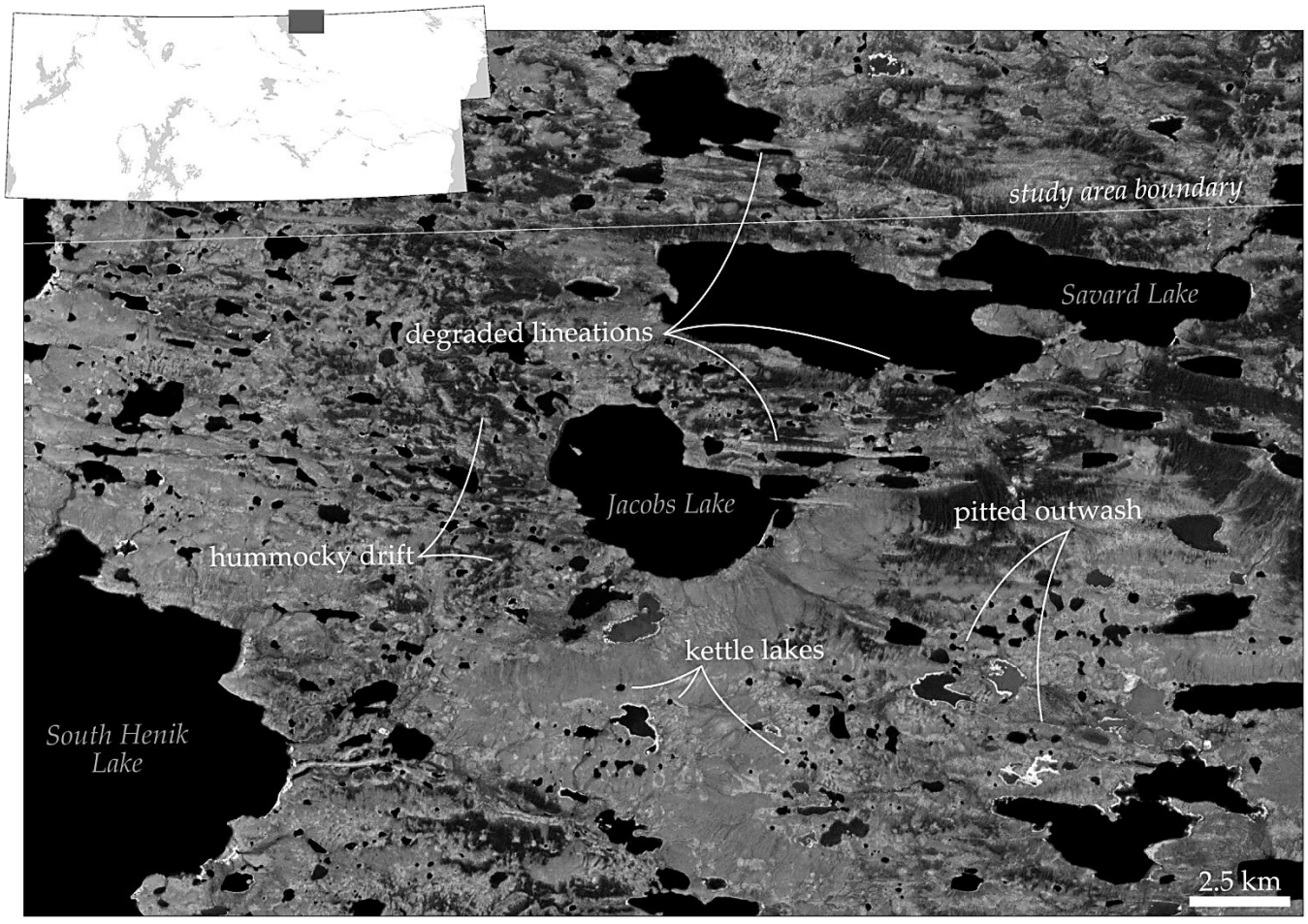

Fig. 5.68 – Hummocky terrain east of South Henik Lake. Surface features are indicative of formation by downwasting and backwasting of stagnant ice.

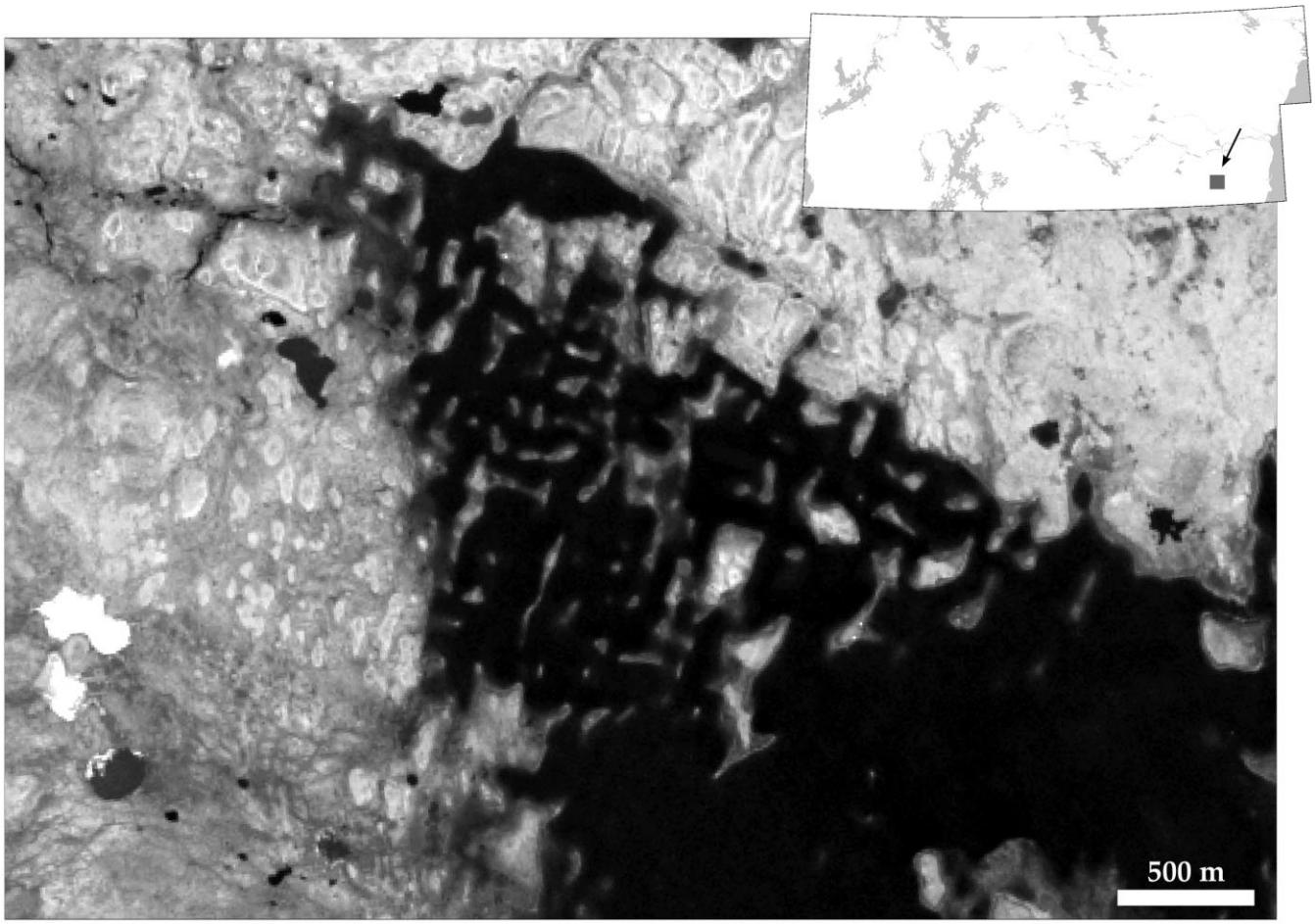

Fig. 5.69 – A partially-submerged patch of reticulate moraines in southeastern Keewatin.

5.4.2.4 ***Deglacial Envelope (Phase G)***

Phase G, consisting exclusively of three *lins* flowsets (*lins*1, *lins*5, *lins*12), in association with the well-developed dendritic esker network in southwestern Keewatin, is comprising of the latest phase of ice flow recorded in surficial landforms within the study area. Temperate glacial landsystems are over-represented in the interior sector of the LIS (Trommelen et al., 2014), as it has already been demonstrated that traces of previous wet-based ice flow phases have been locally preserved intact within the southeastern and north-central regions of the study area under subsequent dewatered, frozen-bed and/or stagnant ice conditions. Contrastingly, *lins*1 and *lins*5 relate verifiably to the final episode of ice flow in southern Keewatin. Their radial trajectory is indicative of time-transgressive formation under thin ice, near an inwardly contracting margin (Kleman and Börgstrom, 1996; Kleman et al., 2006), and their alignment with esker ridges everywhere in this area suggests formation near in time. These two flowsets are shown to overprint all other bedform assemblages in this area, including *rm*1 and *rm*12 which have previously been interpreted as components of the regional deglacial landsystem (Lee, 1959; Kleman and Hättestrand, 1999) but are here included within the earlier Phase D on account of their non-radial flow pattern, independence from topography, high parallel conformity, more southerly orientation, and (though, in some cases, tentatively assigned) older relative age than *lins*1, 2, 4, 5, 8, 9 and/or 11. It might also be argued that the low average length of glacial lineations mapped in this portion of the study

area (Fig. 5.53) is, in this specific case, an indicator of their late deglacial timing of formation, given likely limited subglacial residence duration (cf. Boyce and Eyles, 1981), non-sustained flow direction (cf. Mills, 1967), probable slow, sluggish ice flow (Stokes and Clark, 2002; Briner, 2007) and/or possible sediment starvation (Clark and Stokes, 2001) by late-stage decay.

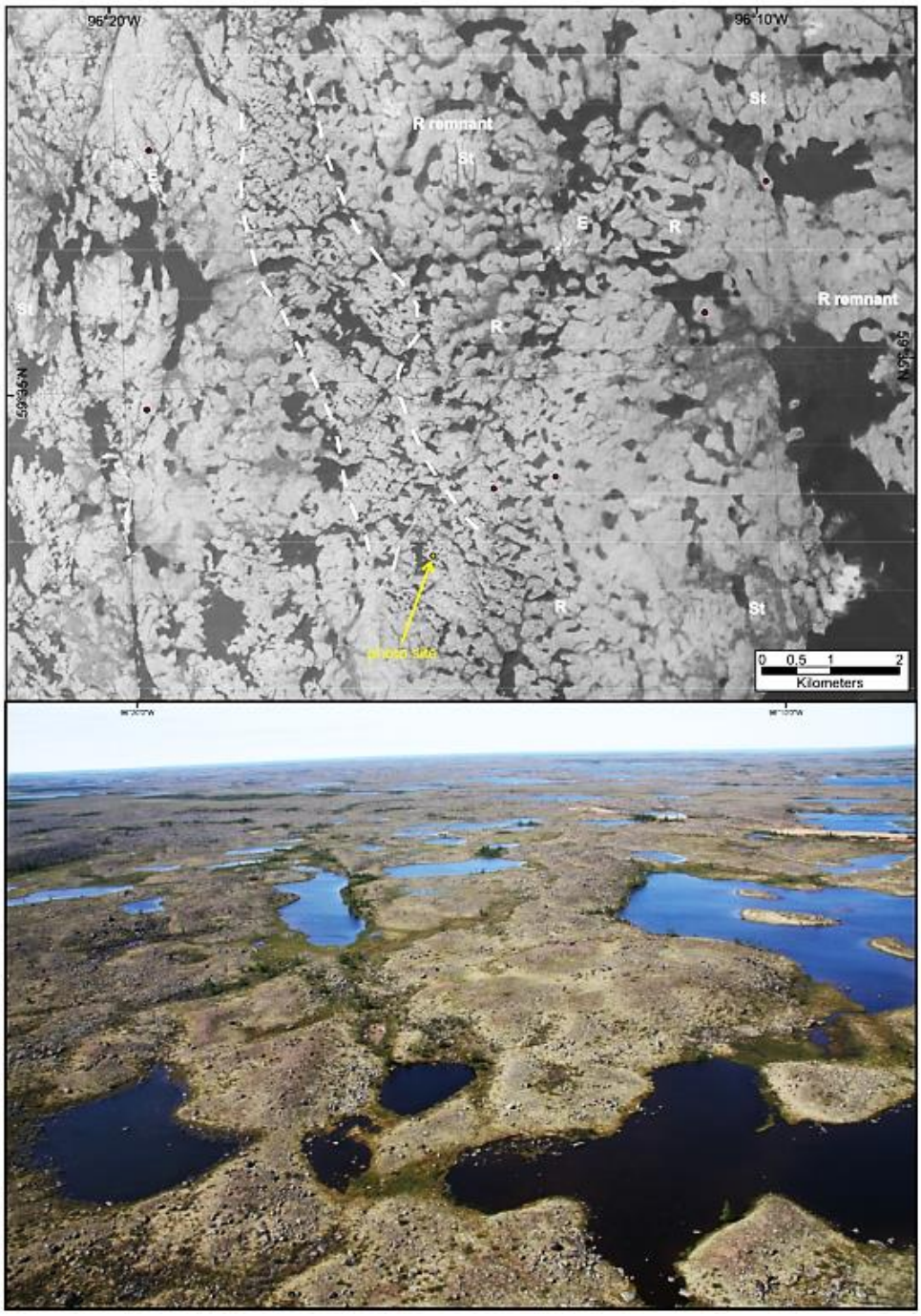

Fig. 5.70 – Conjugate ridge belt in northeastern Manitoba (from Trommelen et al., 2014) (shown between white hatched lines), ribbed moraine fields (R), overprinted ribbed moraine (R remnant), streamlined terrain (St), and esker ridges (E). Low-altitude oblique aerial photograph (bottom panel) shows surface morphology of conjugate ridges.

On the western side of the study area, original retreat directions were towards the northeast (Dyke, 2004). In contrast to areas immediately south and southeast of the KID, ice here remained active until late in deglaciation (Dredge et al., 1986). Boulton and Clark (1990a,b) include these late southwesterly flows as part of their expansive flowset 1 (within their Phase F). The pattern of these radial flows is matched also by reconstructions presented on the Glacial Map of Canada (Prest et al. 1968) and in Dyke and Prest (1987), Boulton et al. (1985) and Dyke and Dredge (1989). At some point early in Phase G (between 8 and 7.7 Ka BP), the marine calving front in Hudson Bay moved rapidly towards the present-day coast, eventually splitting the Keewatin and Hudsonian/Labrador ice masses and permitting Glacial Lake Agassiz to drain into the Bay (Dyke, 2004). This massive reconfiguration of the ice sheet triggered the final migration of the KID ~100 km NW of its Phase D position (McMartin and Henderson, 2004).

Although terrestrial ice-marginal glacial landsystems are mostly lacking in southern Keewatin, glaciomarine ice contact features inside marine limit (as mentioned above) record the final retreat in that area. It is likely that these deposits are coeval with Phase G. Of particular importance are networks of coalescing subaqueous fans, probably formed on the bed of the transgressing Tyrell Sea by density underflows issuing from subglacial meltwater channels (cf. Gustavson and Boothroyed, 1987) (Fig. 5.71). Though many have since been reworked into shorelines, eskers commonly lead up to these fans and are perched along their proximal face at right angles, comprising sediment casts of this former drainage system (appearing bright green in Fig. 5.72A) and suggesting that outwash was subglacially sourced (Fig. 5.71). Proximal zones in front of fans are commonly washed and/or feature only thin veneers of surficial deposits, revealing areas of subglacial erosion by meltwater during fan construction (appearing cyan in Fig. 5.72A). Numerous subglacial channels in relatively close proximity must have facilitated meltwater drainage along the eastern LIS margin, resulting in the development of coalescing fans. The broad-scale configuration of these features reveals that the ice margin became increasingly concave towards the Bay, probably signifying the development of a major calving front into the Tyrrell Sea.

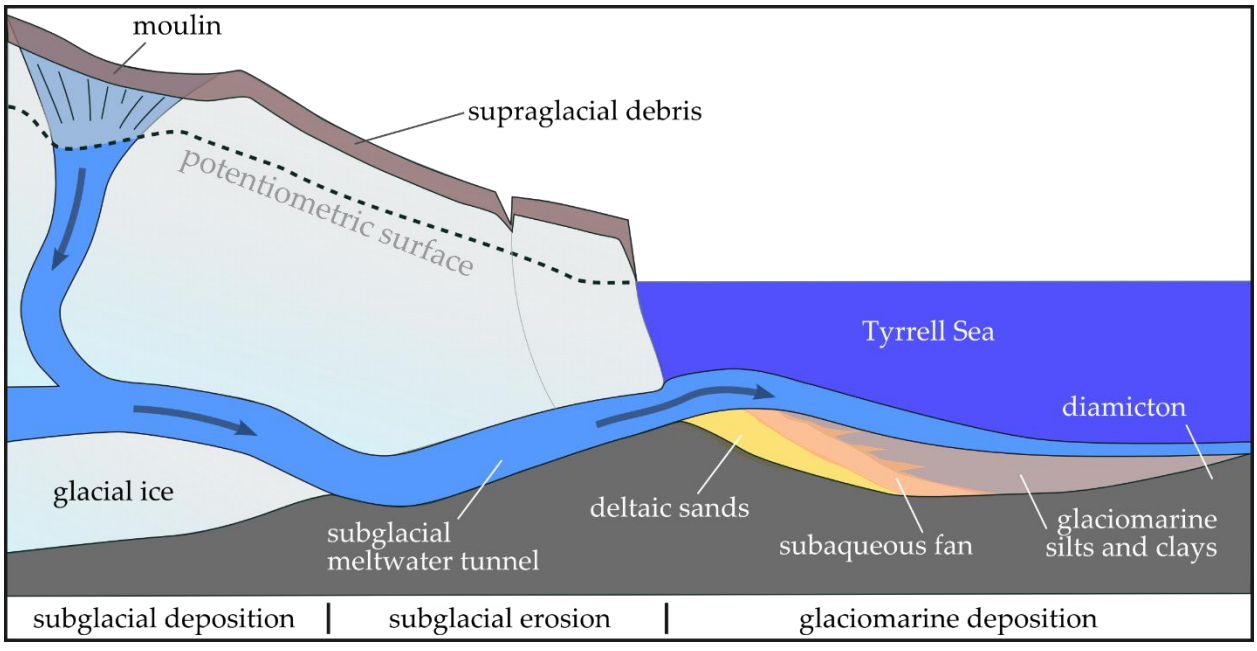

Fig. 5.71 – Conceptual diagram illustrating the formation of ice-contact subaqueous fans inside marine limit in south-central Keewatin. Representation adapted from Gustavson and Boothroyed, 1987.

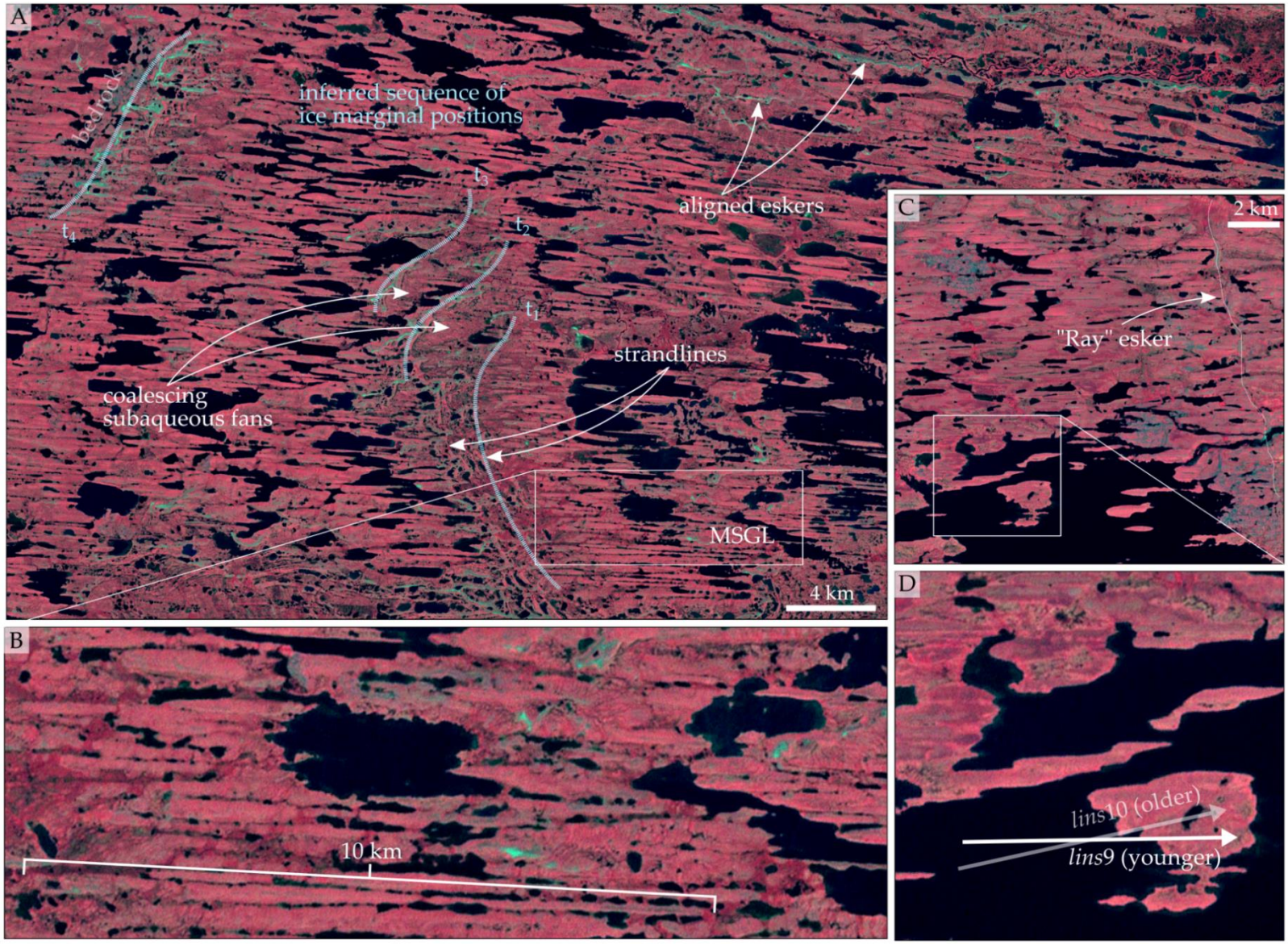

Fig. 5.72 – Geomorphology in the north-eastern portion of the study area. A) Eskers and coalescing ice-contact fans (Fig. 5.71) disclose the style and direction of ice retreat in this area. B) MSGL form part of convergent *lins*9 and indicate streaming ice flow into Hudson Bay. C) Near the headward extent of *lins*9, many esker tributaries converge on their trunks at sharp ~90° angles, the most prominent of which is a ~15 km long specimen near Ray Lake (referred to here as the "Ray esker". D) Two generations are of glacial lineations are preserved in this area, the first (*lins*10) having slightly more northward and parallel trajectory.

Phase A

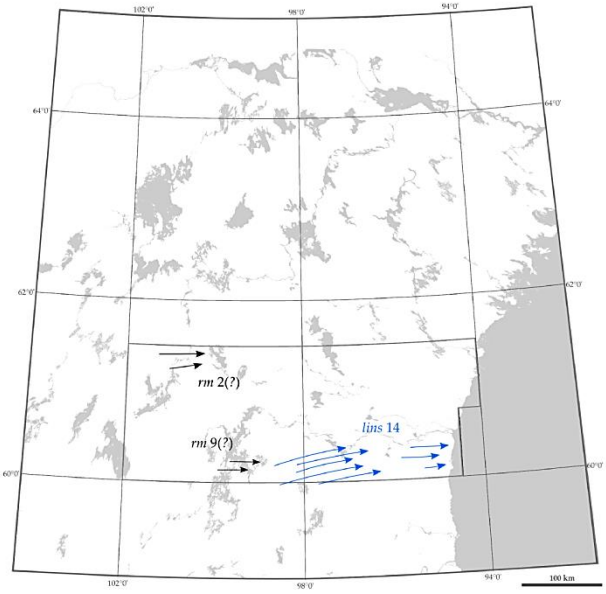

Phase B

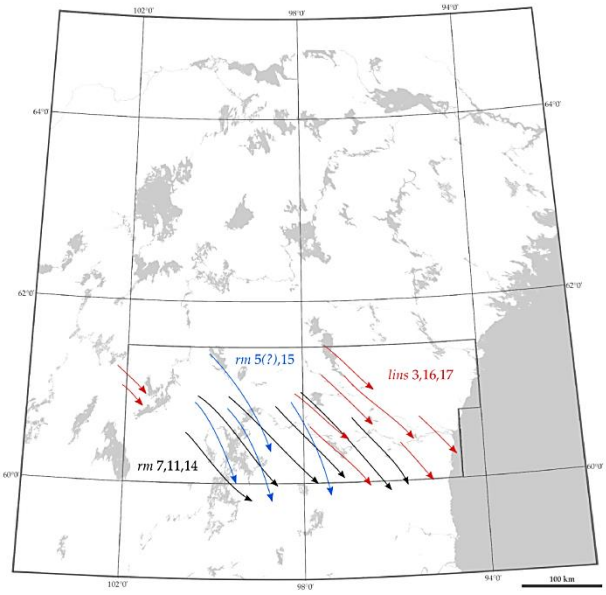

Phase C

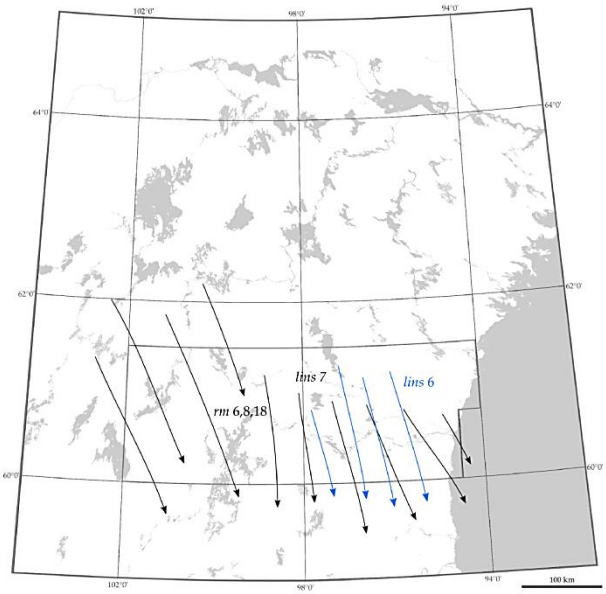

Phase D

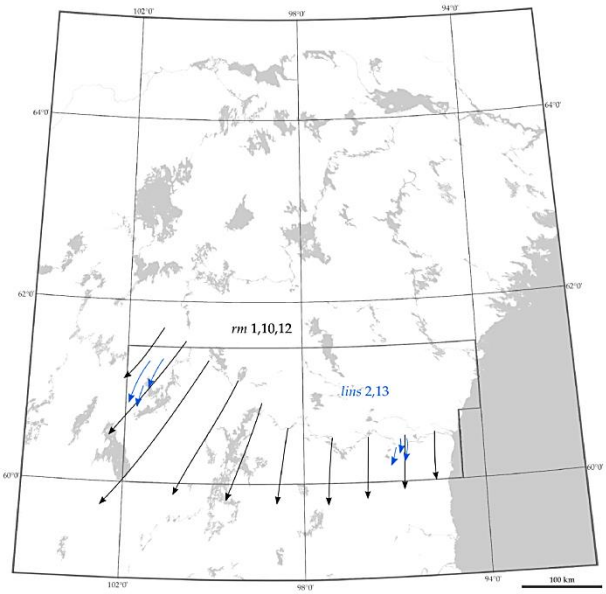

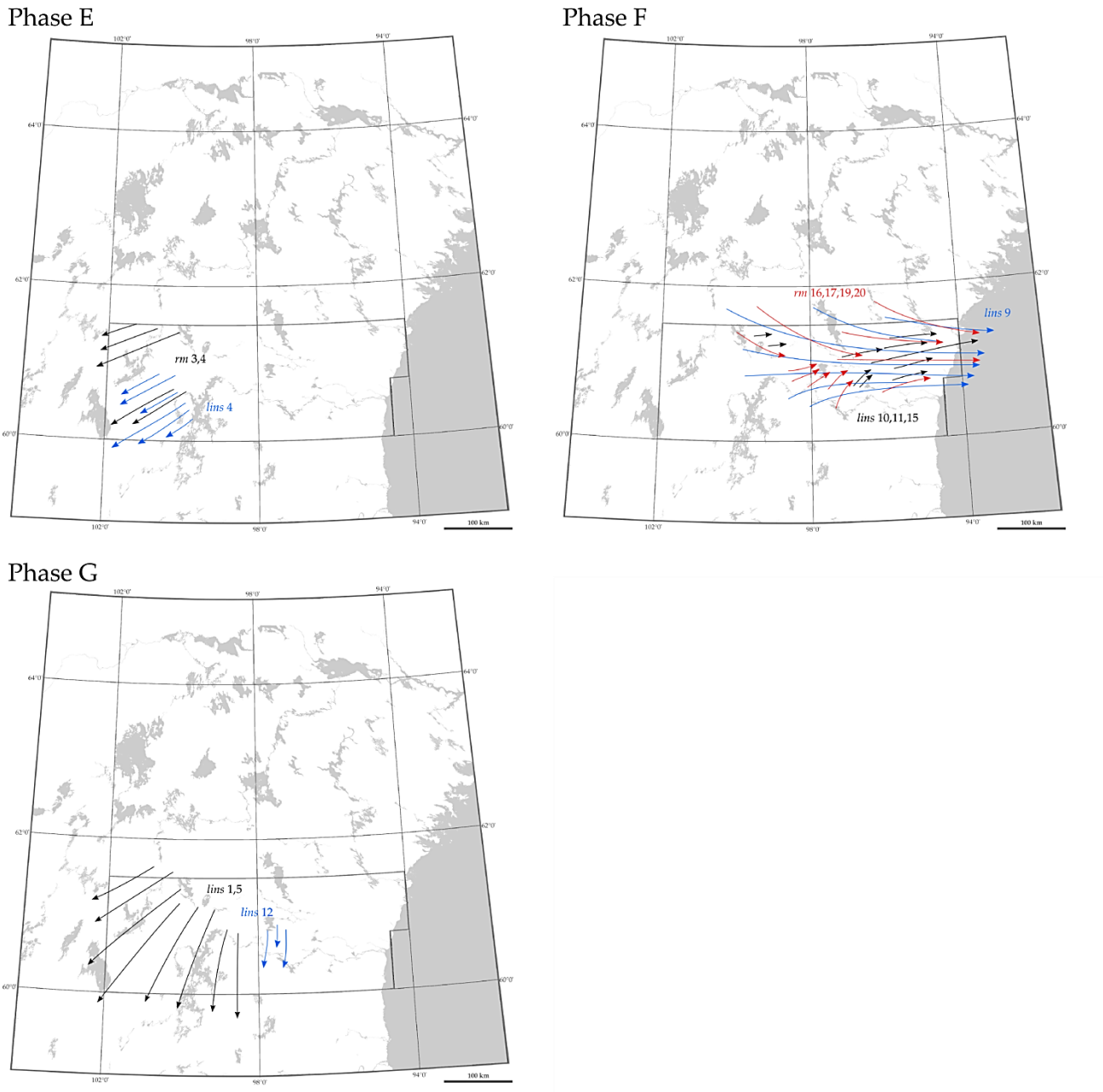

Fig. 5.73 – Glacial history of south-central Keewatin reconstructed from the subglacial bedform record as 7 Phases (A-G) of ice flow. Within each phase, flowline colouration depicts relative age: Red denotes oldest, black youngest, and blue either middle or oldest. In most instances relative age sequences shown in this figure (both between and within Phases) are constrained by cross-cutting/overprinting relationships, though where unavailable, are based on inference or observations from the previous literature alone. Grey outline shows boundary of study area.

6. Field Investigation of Ribbed Moraines in Oppland, Central South Norway

6.1 *Introduction*

It has been demonstrated that λ (i.e., the gradient of above-mode decay in an exponentional characterization of size-frequency distribution) behaves well as an isolated means of discriminating between various ribbed moraine morphologies (Fig. 5.61), and that the mean of λ for ribbed moraine size-frequency distributions, and thus potentially their range of formational and shaping processes, exhibits tremendously low variance between fields and across wide spatial scales (section 5.4.1.6). In light of these considerations, it is possible, and perhaps likely, that physical examinations of ridges from relatively accessible areas can reveal insights about morphologically analogous bedforms located in much more remote and/or inaccessible regions. The northwestern Canadian Shield is an example of the latter – an enormous and fundamentally undeveloped expanse sporting only light aircraft and logging road access. It is, however, also this region which is home to the largest number of ribbed moraines on Earth, and hence this remoteness confounds comprehensive ground-truthing and/or detailed assessment of internal compositional and structural characteristics.

Ribbed moraines are found also in great numbers within another shield environment – namely, on the Scandinavian Peninsula in central South Norway, Finland, and western Sweden. Despite substantial topographic disparity between this area and the northwestern Canadian Shield, both regions once occupied the central, core-interior sectors of the last Wisconsinan/Weichselian ice sheets, and were likely subjected to recurring, at times rapid and spatially discontinuous variations in subglacial hydrological organization and basal thermal regime (Kleman and Glasser, 2007). It is likely the similarity of these processes and each region's placement with respect to ice sheet geometry that have conditioned the similar bedform patterns that are witnessed in these areas today. Moreover, it has been demonstrated by Jørgensen (1977) that the tills of central Norway bear strong textural similarity to those developed on the Canadian Shield (Scott, 1976), in central Finland (Kivekas 1946; Virkkala 1969), and in central and northern Sweden (G. Lundqvist, 1943, 1951; J. Lundqvist, 1958, 1969), suggesting that a sediment-landform association may adequately describe the relationship between ribbed moraines and areas of resistant, crystalline bedrock geology (Haldorsen, 1981), and hence further implying that sedimentological observations from ribbed moraines (of similar morphology) may be somewhat generalizable between these areas. The largest difference between these environments is that the Canadian Shield is a relatively low-relief surface. Bedform patterns in Norway and Sweden have earlier been shown to exhibit strong associations with the sharp topography in those areas (section 3.2.4), hence a comparative analysis of these assemblages may help determine signatures of topographic control.

It is this paradigm that was used to inform physical site selection for ground-truthing in this thesis. Geomorphological and sedimentological investigations were carried out on four ribbed moraine sections at three sites (Fig. 6.1) across central Oppland, west of Gudbrandsdalen and east/southeast of Jotunheimen, central South Norway. Consequently, the primary objective of this chapter is to describe the internal composition and structure of ribbed moraines occurring in this part of the Baltic Shield and consider any potential linkages between these properties and ribbed moraine morphology that could be used to develop better understandings of morphologically analogous forms in south-central Keewatin.

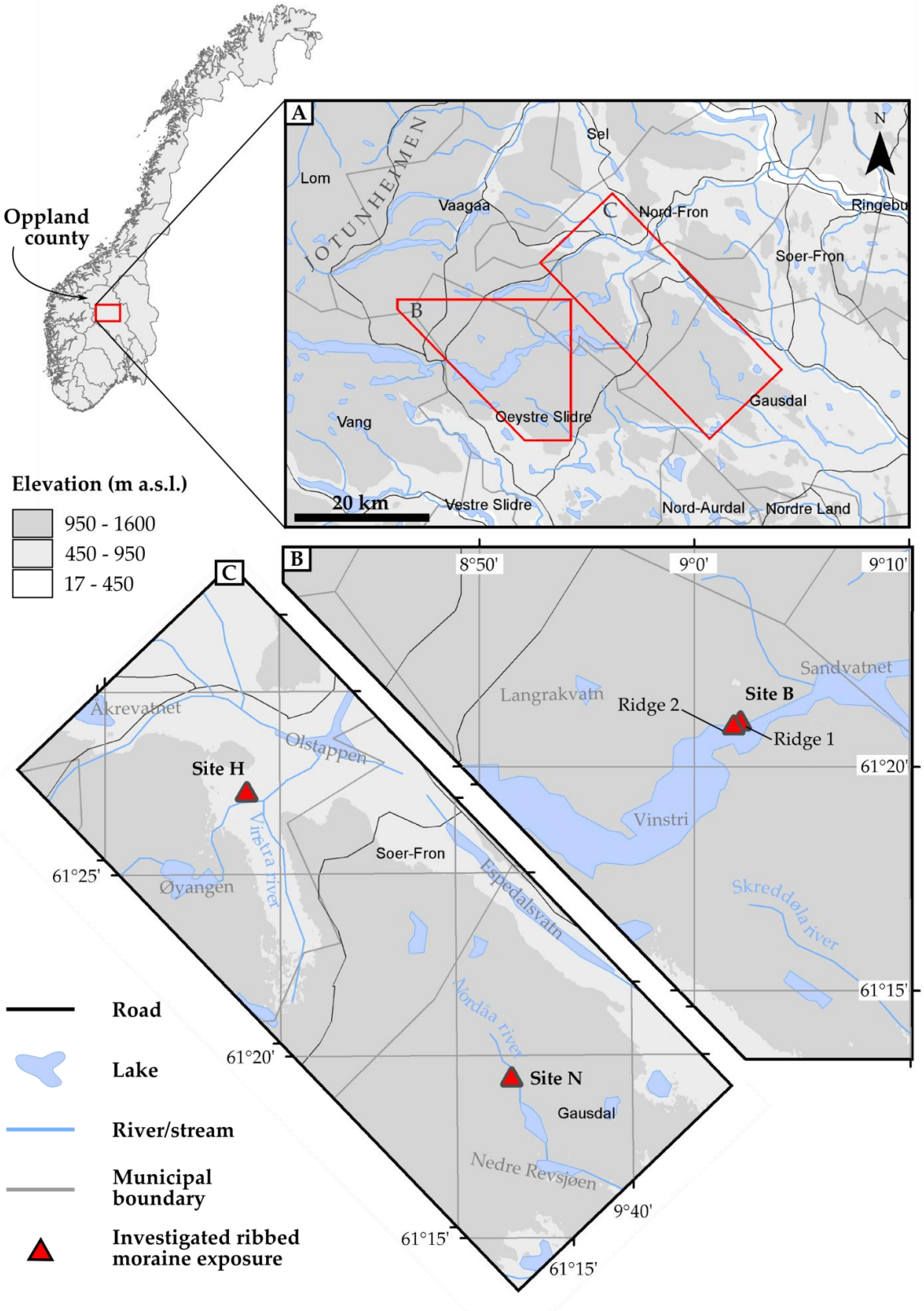

Fig. 6.1 – Overview map of central South Norway. A) Overview of study site locations. B) Locations of ridges 1 and 2 (B-1, B-2) near Bergastølen. C) Locations of ridges H-1 and N-1 near Hølsætra and in the Nordåa river valley, respectively.

6.2 *Physiography and Glacial History of Central Norway*

Oppland is Norway's 5th largest county, spanning ~25,000 km^2 between lakes Randsfjorden and Mjøsa (Norway's largest) in the southeast, to the glacially-sculpted, mountainous Jotunheimen, Rondane and Dovre areas in the north and northwest. The region comprises a diverse topography and range of landcovers. Oppland's northwestern uplands are home to over 300 peaks >2,000 m a.s.l., including Glittertind and Galdhøpiggen, the nation's two highest mountains, although 80% of the entire county lies above 600 m a.s.l. Further east, highland peneplains (termed *vidde* in the Norwegian literature), relicts of pre-Quaternary times, feature flat-topped surfaces scored by shallow channels, and contrast with an impressive network of deeply incised valleys situated ~1,000 m a.s.l., most notably those of Gausdal, Espedalen, Gudbrandsdalen and Sjødalen which, below Jotunheimen, trend generally NW-SE and are partially inundated by deep lakes. Most of the drainage immediately east of Jotunheimen is captured by the Vinstra river valley, which converges on Skåbu and continues northeast towards Gudbransdalen (220 m a.s.l.). Both southeast of Jotunheimen, and from Skåbu, drainage proceeds to the southeast through Espedalen and Vestre Gausdal towards Lake Mjøsa.

The most common surficial deposit within central southeastern Norway is a relatively thick (up to 30 m, though averaging ~5 m) cover of glacial till (primarily in the form of compact ground moraine, though also uniquely here occurring with pockets of loose, coarser grained ablation tills, with or without expressed morphology) and younger organic sediments, including poorly drained peat bogs/fens. Elsewhere in Norway, thick tills are less common, ranging generally between 1-3 m, though the distribution of till thickness appears to be correlated to underlying bedrock type, with thicker tills overlying areas of Cambro-Silurian (meta)sedimentary rock, and thinner, more discontinuous till cover found in regions underlain by resistant Precambrian lithologies (Haldorsen, 1983). These differences in bedrock type have also been shown to elicit divisions in the textural composition of basal tills (Jørgensen, 1977). Excluding peats, younger unconsolidated sediments overlying tills are generally found only along certain valley bottoms or below marine limit (Haldorsen, 1983). Areas of thin superficial deposits and outcropping bedrock are interspersed with these thicker Quaternary units, particularly along the flanks of the Jotun nappe, near Ringebu along lower Gudbrandsdalen, and towards Fagernes in the southwest, though till cover is mostly continuous throughout the central southeast in comparison to most other regions (http://geo.ngu.no/kart/losmasse/).

The Scandinavian mountains, and in particular central Norway, have acted as inception grounds for Scandinavian ice sheets with much iteration during the Quaternary, and probably earlier in geological time (Mangerud, 1983), though only since ~1 Ma has a coherent FIS expanded far south of the Scandinavian Peninsula (Mangerud et al., 2011). Early syntheses of regional- and local-scale investigations into Norwegian glacial history commented on the multiple-phased nature of the most recent (Weichselian) glaciation, recognizing several oscillatory stages of large ice sheet volume and extent. Vorren (1977) argued that this unfolded across four phases (Fig. 6.4), involving variations in ice flow geometry and the positioning of the central ice divide in response to shifting internal ice dynamics and cyclical external forcing. In this reconstruction, early phases I and II share similarities in the direction of their respective ice flow indicators, with each characterized by a westerly situated ice divide, though these are presumed separated in time by an interstadial period (the Fornes thermomer), lasting from 59-45 Ka BP, dated according to palynological evidence and correlation to the Jämtland interstadial in Sweden (Vorren and Roaldset, 1977). Phases I and II are thus argued by Vorren (1977) as corresponding to the Early and Middle Weichselian respectively. Subsequently, phases III and IV are ascribed to build-up/LGM and Preboreal (Younger Dryas) times, with separations between these phases based only on assumption; young ice flow directional indicators probably denote geometries attributable

to a thickening ice sheet, whereas later indicators demonstrate good fit with dated Preboreal end moraines (Vorren, 1977, 1979). During the latest phase (IV), Vorren (1977) argues that the ice divide once again shifted westward and fragmented the FIS into a series of localized domes.

More recent work, supported by the marine geological record, improved geochronologies, and the uncovering of new key stratigraphic sites, expands upon Vorren's (1977) model of Weichselian FIS variability. Based on the micromorphology of marine sediments from the North Sea Basin, and the distribution of Fennoscandian erratics in Danish till, Carr et al. (2006) and Larsen et al. (2009) provide evidence (respectively) of an extensive OIS 4 (Middle Weichselian) FIS covering all of southern Norway and its adjacent shelves. Houmark-Nielsen (2010) documents an early OIS 3 ice advance (Ristinge) from the Baltic Sea basin, corroborating the eastward shift of the central FIS dome surmised in earlier reconstructions (see also Kleman et al., 1997). Presently, it is hypothesized that the FIS extended to the shelf edge along the entire Norwegian coast during OIS 4, and that the extent of the ice sheet during this phase (and/or early OIS 3) was approximately as large in the south and west as it was at LGM (OIS 2) (Mangerud et al., 2011). It is also widely conceded that the interval between OIS 3 (the Ålesund interstadial) and LGM was marked by multiple fluctuations of the ice margin (Mangerud, 2004; Sejrup et al., 2009). Importantly, large areas of Norway, including portions of central Norway, were ice free at least 4 times throughout the Middle and Late Weichselian glaciation (Lundqvist, 1992; Olsen et al., 2013 – though see Mangerud, 1981 for an earlier, dissenting view). New research has even extended the latest (Andøya) interstadial (cf. Vorren et al., 1988) to central Norway, suggesting that the LGM was divided into two stadials by a period of low ice conditions across the entire peninsula (Johnsen et al., 2012).

New bathymetric glacial geomorphological mapping of the Norwegian shelf has largely confirmed that the FIS reached to the shelf edge at LGM, and also importantly, that its dynamics were moderated by a number of fast-flowing ice streams (e.g., Dowdeswell et al., 2007; Andreassen et al., 2008; Ottesen et al., 2008; Sejrup et al., 2009; Winsborrow et al., 2010). The thickness of the ice sheet at this time remains somewhat more widely debated. Certain authors (e.g., Nesje and Dahl, 1992; Nesje et al., 1987; Dahl et al., 2010) have argued that summits protruded from beneath the ice sheet across much of southern Norway during LGM, based primarily on the altitudinal distribution of autochthonous blockfields (see Fig. 6.4B). While this interpretation is plausible for Nordfjord near the western coast, and for much of northern Norway (e.g., the Andøya area), where deep fjords would have promoted surface lowering by accommodating much of the ice flow, as suggested by Mangerud (2004), it is more difficult to reconcile the 800 m maximum ice sheet thickness (1,600 m a.s.l. altitude) required across southern Norway under the parameters of the former model with direct geological evidence of the FIS having transgressed the southern margin of the Scandinavian Peninsula. In direct opposition to the limited ice sheet thickness model, a separate group of writers have provided evidence to suggest that many surfaces in Scandinavia (including a large number of high altitude blockfields) are in fact relicts of past periods of subaerial exposure that have survived unmodified beneath cold-based ice (i.e., frozen bed areas) throughout the LGM (Kleman, 1994; Kleman and Borgström, 1990, 1994; Kleman and Hättestrand, 1999; Lagerbäck, 1988b; Lagerbäck and Robertsson, 1988). Kleman et al. (1997) intimately incorporate this theory into their time-slice, geomorphologically-based reconstruction of the FIS, arguing that the frozen-bed core area was a stable and persistent feature of the FIS during the Middle Weichselian (developing between 70-22 Ka BP), and is responsible for the relative lack of LGM flow traces overlying the shield area. In their reconstruction, the proportion of this frozen bed zone is diminished (though not entirely) throughout the post-LGM stages, where inward-transgressive lineation swarms partially dissect zones of relict terrain.

Within the immediate study area (East Jotunheimen-Gudbrandsdalen), Garnes and Bergerson (1980) have defined four discrete phases of Weichselian ice flow, A-D (Fig. 6.2), the latest of which details the shifting geometry of ice and meltwater drainage throughout deglaciation (Fig. 6.3), largely as a response to vertical downwasting in the interior, which is argued by these authors as being of greater importance to the deglaciation of the FIS in this region than frontal retreat (pg. 267). In the earliest deglacial stage, a NE-sloping ice culmination zone was located in the area between Rondane and Jotunheimen and competed with NW-sloping inland ice to the east, the convergence zone of which became mobile with progressive drawdown of the ice sheet. At this time, the FIS in central South Norway was characterized by a very low surface gradient, as indicated by the slope of lateral meltwater channels carved onto highland rises. During the latest phases of thinning, the ice surface gradient was probably matched by the inclination of the distal land slope, causing large areas to ablate simultaneously. This pattern promoted the development of dead ice over high elevation areas of flat-lying terrain, which were decoupled from dynamically active ice confined within the valleys, the latter of which subsequently retreated as a series of independent lobes, with consequences for the damming of meltwater drainage and fluctuations in marginal stability (Garnes and Bergersen, 1980).

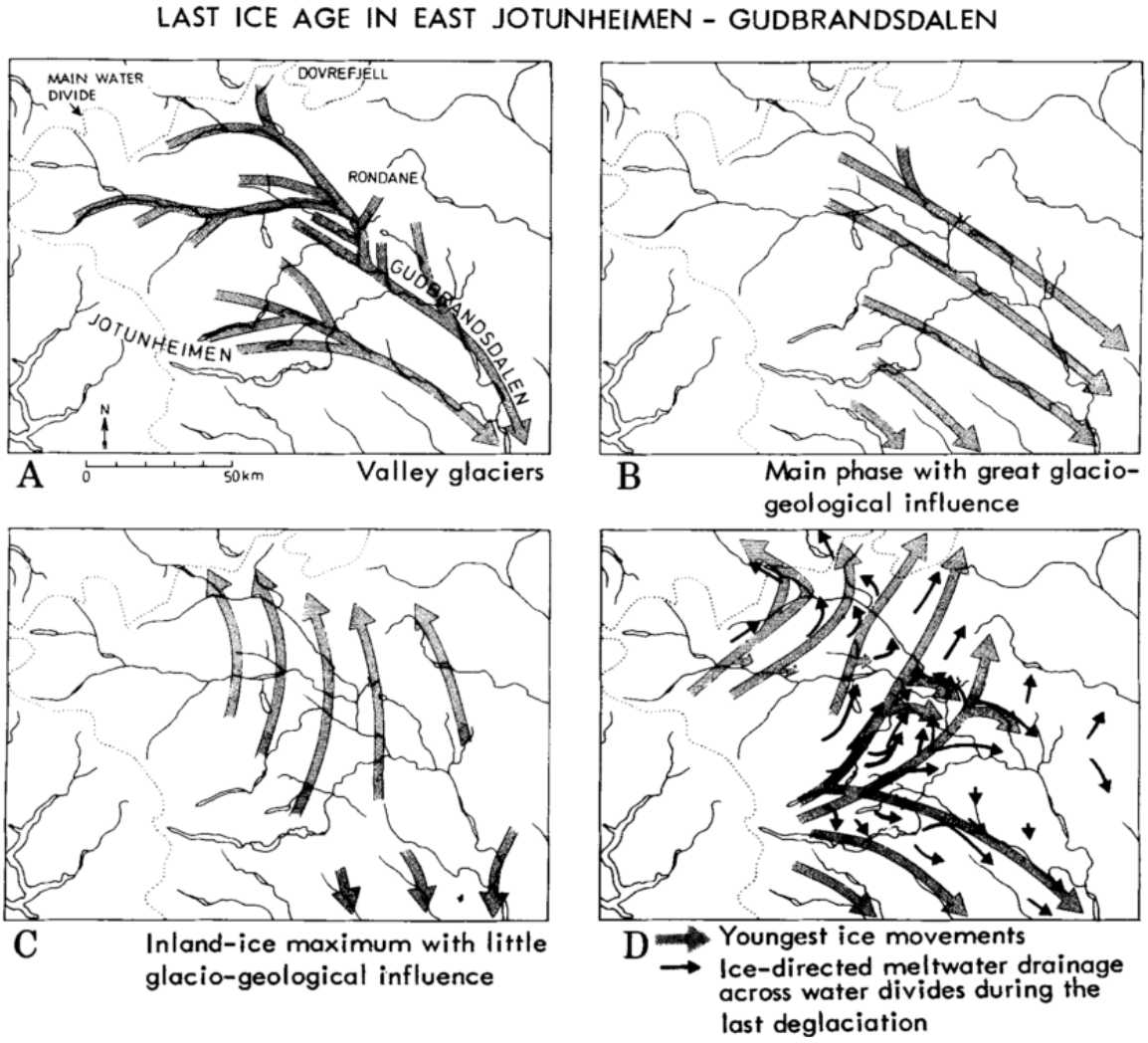

Fig. 6.2 – Reconstructed phases of ice flow in east central South Norway during the Weichselian (Garnes and Bergersen, 1980).

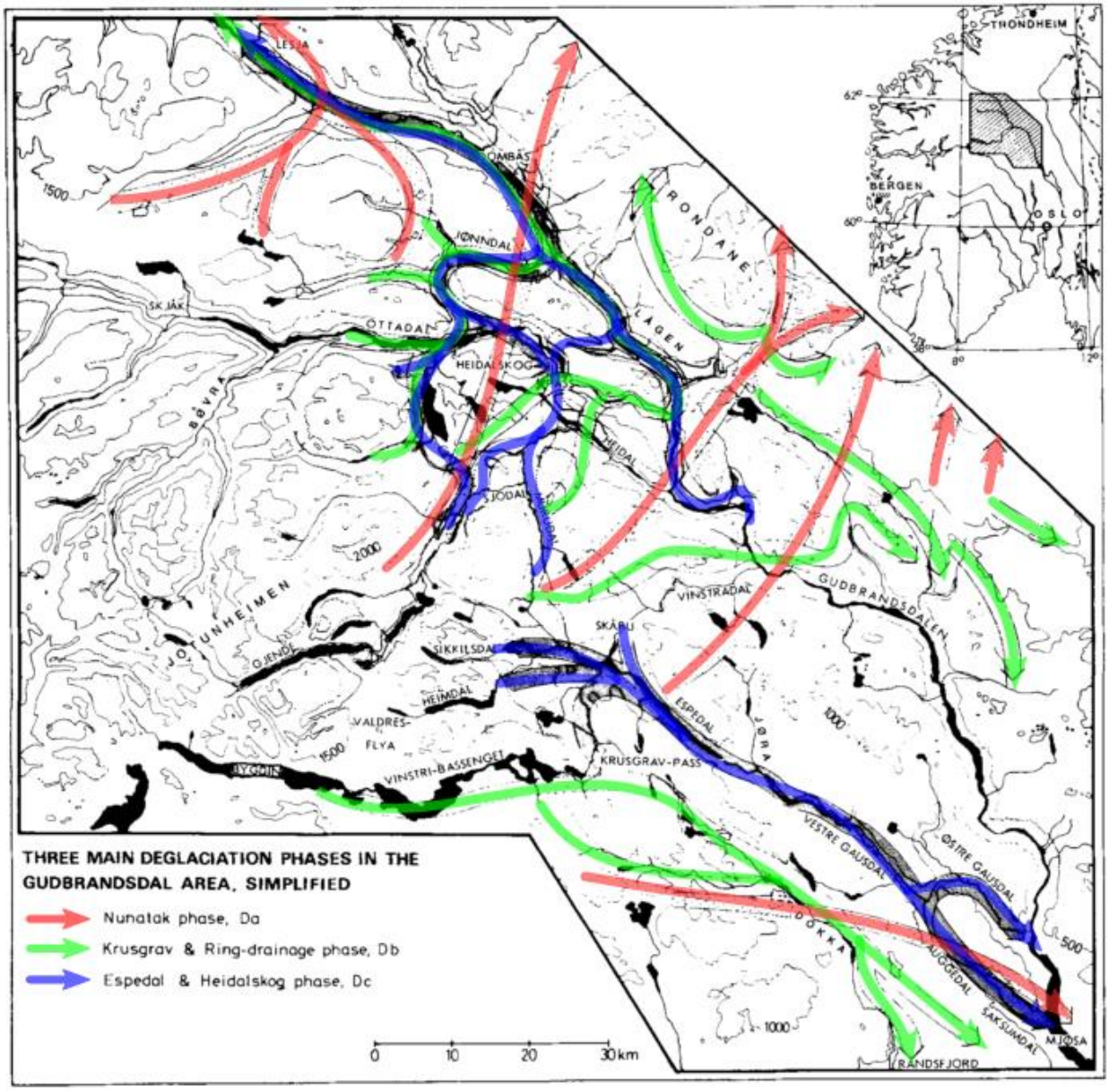

Fig. 6.3 – Evolution of ice flow and meltwater drainage throughout phase D (see Fig. 6.2). Modified from Garnes and Bergersen (1980).

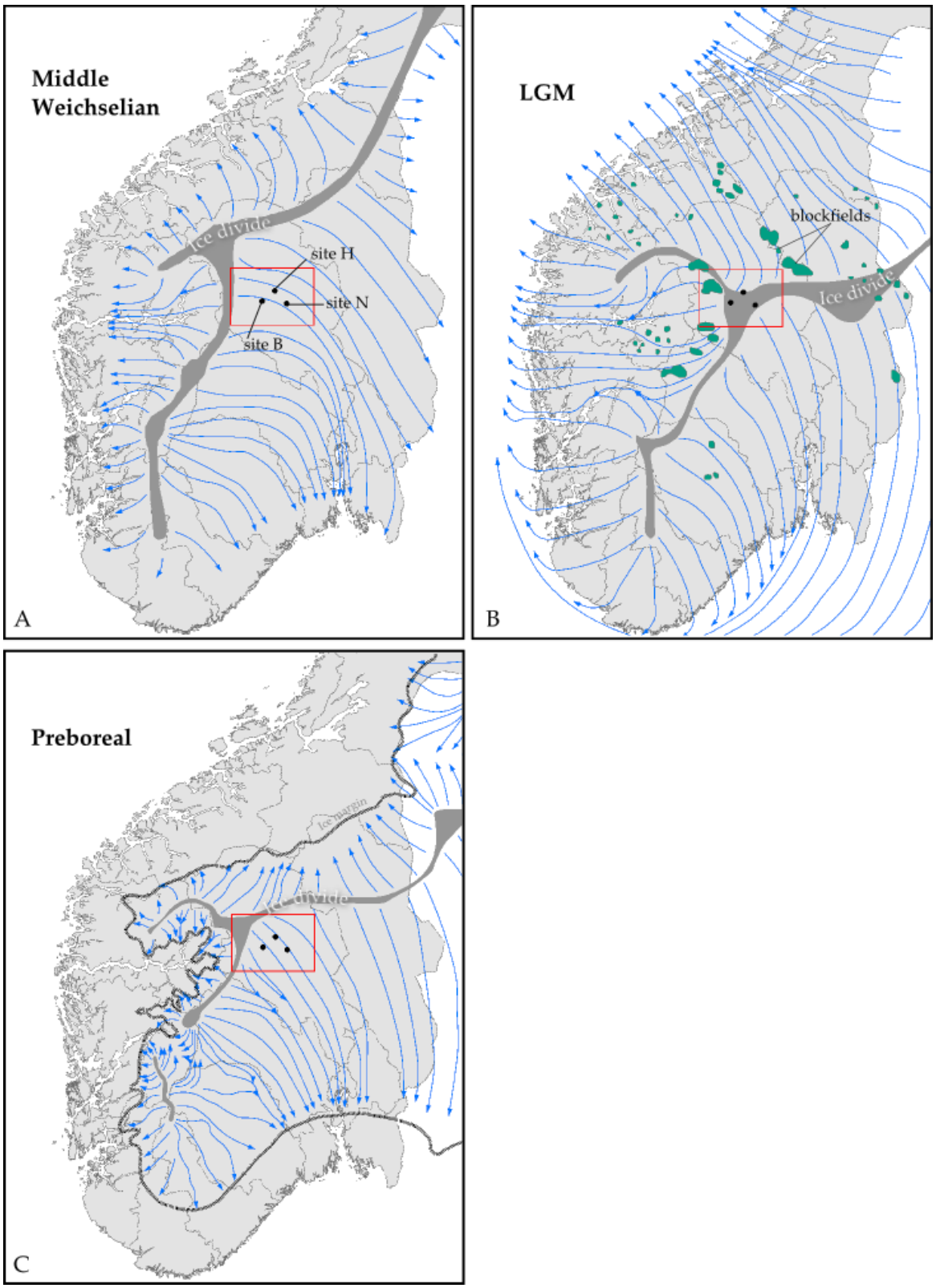

Fig. 6.4 – Reconstruction of FIS ice sheet ice flow geometry throughout A) Middle Weichselian, B) Last Glacial Maximum, and C) Preboreal phases. Adapted from Vorren (1977); location of blockfields from Thoreson (1990). Note that the three study sites occur beneath the presumed location of a triple-junction in the ice divide during LGM.

6.3 *Methodology*

6.3.1 **Field Techniques & Lithostratigraphy**

Geomorphological and sedimentological investigations were carried out in a total of four ribbed moraine sections at three sites (Table 6.1; Fig. 6.1) across central Oppland, west of Gudbrandsdalen and southeast of Jotunheimen, central-south Norway. Due to the paucity of available exposures, all investigations were made from landform horns/extremities. Exposure faces were hand-cleaned using a metal trowel and spade in preparation for sample collection and lithostratigraphic logging. Logging followed widely accepted practices, including the photographic documentation and mapping of lithofacies boundaries, and internal compositional and structural features at scales between 1:10 and 1:20 (Evans and Benn, 2004; Hubbard and Glasser, 2005). Only a limited depth of excavation was obtained at the Nordåa section. Morphological measurements from each ridge were acquired in the field for comparison with measurements collected from Google Earth™ and Landsat 8 Operational Land Imager (OLI) remote sensing datasets.

Table 6.1 – Location and geographic coordinates of studied ribbed moraine exposures from Oppland, central-south Norway

Site	Ridge	Coordinates		Exposure type
		Latitude	Longitude	
Nordåa	N-1	61° 19' 27"	9° 33' 7"	River cut
Bergastølen	B-1	61° 21' 3"	9° 2' 8"	Road cut
	B-2	61° 20' 57"	9° 1' 50"	Road cut
Hølsætra	H-1	61° 27' 18"	9° 18' 6"	Road cut

Two clast macrofabric analyses were conducted on prolate (a:b ≥ 2:1) pebbles of varying lithology extracted from cleaned, 1 m^3 vertical faces in subsurface diamict facies at approximately equal depth within ridges B-1 and B-2. Each fabric set included measurement of the a-axis trend (azimuth) and plunge (dip) of 25 pebbles, where a-axis ≥ 2 cm. Orientation data were statistically assessed in Orient v2.1.2 following the eigenvalue method outlined in Mark (1973), and plotted as rose diagrams and contoured lower hemisphere Kamb nets. Only clasts completely suspended within the diamict matrix were measured; those in contact with other large clasts were disregarded due to the possibility of interference during rotation.

6.3.2 **Grain-size Analysis**

Six bulk sediment samples were collected at various depths from the four studied ridges in order to detect textural deviations between ridge sediments at each site, and to determine the degree of internal compositional variation. Estimates of the proportion of mud (clay, silt), sand, gravel and boulders forming each ridge were made in the field, and sediment colour was determined with reference to the Munsell Book of Colour. Individual bulk samples ranged in mass between ~150 and 200 g and generally included sediments > 4.5 φ. Particle size analysis was conducted in two stages, broadly following ASTM D 422 procedural standards (Standard Test Method for Particle-Size Analysis of Soils): Dry sieving of the < 4.5 φ fraction, and hydrometer analysis of the > 4.0 φ fraction. Dry sieving was carried out using a stack of Endecotts Ltd. mesh sieves with apertures ranging from 0.0 φ to 4.5 φ (US Mesh

#10 – 325), at intervals of 0.5 φ. After 24 hours of air-drying, each sample, in turn, was split using a tin sample splitter and placed onto a sieve stack. Stacks were loaded onto a 60 Hz, RX-29 RoTap® and mechanically shaken for 5 minutes to facilitate particle sorting. After shaking, residual grains from each sieve were collected in plastic weigh boats and their mass measured to three decimal places using a digital weigh scale. Dry sample splits were thereafter reconstituted and prepared for hydrometer analysis.

Prior to fines separation, 40.00 g of each sample containing the > 4.0 φ fraction was weighed and poured into 250 mL beakers. 125 mL of 40 g/L sodium hexametaphosphate dispersant solution was added to each beaker and the slurries were stirred using a metal spatula and left to settle for 24 hours. Samples were processed two at a time over the course of three days. A 1 L control cylinder was prepared for each test with 125 mL of sodium hexametaphosphate and 825 mL of distilled water. Sediment mixtures were washed from 250 mL beakers into metal stirring cups using distilled water and placed on a mechanical mixer for 1 minute. After mixing, each sample was transferred to a 1 L settling cylinder and distilled water was added to make up the slurry to 1 L. ASTM 152H hydrometers were placed in both sample settling cylinders and the blank cylinder, and the meniscus correction factor calculated for each apparatus. Prior to measurement, samples were mixed and re-suspended for 1 minute using a metal plunger. Thermometers were placed in each cylinder, and temperature and hydrometer readings taken from both the blank and sample cylinders at 30 seconds following re-suspension, and thereafter collected at the following time points (in min. from re-suspension): 0.67, 1, 2, 5, 10, 60, 120, 240, 360, 480, 600, 1440.

The rate of particle settling was estimated using Stokes Law (as outlined in Brady and Weill, 2002), which assumes that a solid, perfectly spherical particle of radius r and density ρ_s will settle downward through a fluid of density ρ_l at a calculable rate (detailed below). Considering that individual particles achieve terminal velocity almost instantaneously, the radius of each particle is given by:

$$r = \sqrt{\frac{9\eta s}{2g(\rho s - \rho l)t}}$$

Where s is distance (mm), t is time (s), η is solution viscosity (10^{-3} kg·m^{-1}·s^{-1}) and g is the gravitational constant ($6.67384 \cdot 10^{-11}$ m^3·kg^{-1}·s^{-2}). Given a 1 L volume settling cylinder, the mass of particles finer than the calculated particle size at a given time can then be returned as a percentage (P) according to:

$$P = \left(\frac{C}{C_0}\right) \cdot 100$$

Where P is summation percentage, C_0 is the initial dry weight of the sample (g), and C is concentration of sediment in suspension (g/L). The latter is determined by:

$$C = R - R_l$$

Where R is the uncorrected hydrometer reading at a given time point (g/L) and R_l is the corresponding reading from the blank. The equation for particle radius above can be modified to express particle size in terms of equivalent diameter (d) according to:

$$d = \frac{\theta}{\sqrt{t}}$$

Here, the sedimentation parameter $\boldsymbol{\theta}$ (μm·min$^{1/2}$) is expressed as:

$$\theta = 1000\sqrt{Bh'}$$

where

$$B = 30\frac{\eta}{g(\rho s - \rho l)}$$

and the effective hydrometer depth (h') in cm is:

$$h' = 16.3 - 0.164R$$

For a given temperature (T) and associated water density (ρ°), ρ_s depends on sodium hexametaphosphate concentration (C_s, g/mL) according to:

$$\rho l = \rho^{\circ}(1 + 0.630C_s)$$

Similarly, η is derived for a given T by:

$$\eta = \eta^{\circ}(1 + 4.25C_s)$$

Calculated P for each interval up to 4.0 φ was combined with dry sieving data for the 0 – 4.5 φ range and plotted as cumulative frequency by grain size. Overlapping data points in the 4.5 to 4.0 φ range were removed (with priority given to sieving points) to facilitate smoothing of the curve between test boundaries. All granulometric calculations were carried out in custom spreadsheet software (Meyer and Lawrence, unpublished). All samples were plotted on a ternary textural diagram according to their relative proportion of clay, silt and sand using Tri-plot© v1.4.2 (Graham and Midgely, 2000).

6.3.3 **Pebble Counts & Clast Size/Morphology**

Five samples of 50 clasts each were collected for morphological and lithological analyses at various depths from within ribbed moraine ridges at each investigated site. Clasts were selected without preference for shape or lithology (Bennett et al., 1997), though with b axes 2-6 cm. In the lab, all samples were washed in warm water and the lengths of their three mutually perpendicular axes (a = longest, b = intermediate, c = shortest) were measured to two decimal places using plastic calipers. The lithology of each individual clast, determined with reference to digital bedrock geology maps (www.ngu.no), was recorded in a table, as was the presence/absence of surface features, including facets and striations. Clast roundness/angularity (i.e., the degree of curvature around edges of a clast) was judged by comparison to a Powers roundness chart (Benn and Ballantyne, 1994), and the frequency of classification plotted on a simple histogram for each sample. Axes ratios and disc-rod indices (Sneed and Folk, 1958) were calculated for all clasts, and individual samples plotted on a triangular diagram (Sneed and Folk, 1958; Hockey, 1970) after Benn and Ballantyne (1993) to aid in interpretation of

transport path. Following Ballantyne (1982), the C_{40} index (proportion of clasts with c/a-axes ≤0.4) was calculated and utilized as a measure of platiness. The RA index (percentage of angular and very angular clasts) was also determined for each sample (Benn and Ballantyne, 1994), and plotted against C_{40} on a co-variance diagram. An additional measure, the RWR index (percentage of rounded and well-rounded clasts), was derived and plotted on a RWR-C_{40}-co-variance diagram, in line with more recent practices (e.g., Benn, 2004; Lukas et al., 2012, 2013).

6.3.4 **Micromorphological Sampling & Analysis**

A single, undisturbed and oriented bulk sample was extracted for micromorphological analysis from an overconsolidated sandy diamict exposed within ridge B-1 at Bergastølen. Collection of multiple samples for micromorphological analysis, as originally intended, was inhibited by the coarse matrix and gravelly/bouldery internal composition of ribbed moraine ridges at all sites; thus only a single sample (KW/13/B/1M) was opportunistically obtained. KW/13/B/1M was collected using a sediment knife into a 6 oz. tin packed with plastic film, and carefully wrapped in an additional layer of plastic film to prevent moisture loss and improve sample resilience during shipping. North direction and vertical sense were recorded on both the sample and storage tin. Subsequently, thin section production was carried out at Brock University, following procedures outlined in van der Meer (1993) and Menzies (2000), and described in detail by Rice et al. (2014). Prior to preparation, the sample was air dried and wrapped in a layer of perforated aluminum foil. The sample was then submerged in a resin bath containing a blend of acetone and Ecopoxy© hardener, and left to impregnate in a vacuum chamber for 1 week. Following impregnation and removal of excess resin, the sample was oven cured at 40˚C for 4 days, and thereafter cooled in a fume hood for 24 hours. Once solidified, the impregnated block was bifurcated and mounted using a Servocut®-M250 rock saw, from which a ~1 cm thick slab was cut, and later ground and polished using a PM 2A® polisher. The polished sub-sample was mounted to a 75 x 50 x 1 mm glass plate and hand-ground to a thickness of 30 µm with a Petro-Thin® grinder before finishing with a cover slip.

Thin section analysis was carried out at low magnification (6.3-32x) in plane and cross-polarized light using a Wild-Heerbrugg® M420 macroscope affixed with a Nikon® DS-Fi1 digital imaging instrument. Composite image assembly (‘stitching’) and slide analysis was conducted in Nikon® NIS-Br Elements software. Slide analysis included description and identification of any voids, textures, colours, domains, microstructures, skeleton grains (including size, morphology, and microfabrics) and plasmic fabrics. Microstructural identification followed Menzies (2000, 2012), Menzies and Maltman (1992), Menzies et al. (2006, 2010), van der Meer (1993, 1996) and van der Meer and Menzies (2011), and the terminology developed from Brewer (1976) therein. Microstructures were systematically identified from left to right, top to bottom, and digitally annotated using CorelDraw® X6 vector graphics software.

6.4 ***Results***

Ribbed moraine landforms in central South Norway range in scale and morphology from short, poorly defined hummocks, 2-3 m high, to larger, more distinctive ridges (e.g., near Storjerner and Langvatnet), 10-20 m in height, 100-150 m wide, and up to 1.5 km long. In contrast to those developed on the low-relief Canadian Shield, ribbed moraines in central Norway reveal a high degree of topographic influence, and are commonly confined to valleys or areas of concave terrain. Compared to the Keewatin population (Fig. 5.18), these ridges are also lacking in field-type diversity, and are regularly arranged within laterally restricted, linear bands or tracks. On average, the latter features are

both much smaller in scale, and regionally less abundant compared to those found in southern Nunavut, though each exhibit comparable ranges of ridge spacing (commonly 150-250 m) within fields. The morphology and morphometric parameters of the four individual ribbed moraine landforms investigated in this study are presented in (Table 6.2).

Table 6.2 – Morphology and morphometric properties of ribbed moraine ridges investigated in central South Norway. See section 5.4.1 for references to morphology and morphotypes.

Site	Ridge	Height (m)	Width (m)	Length (m)	Morphology	Morphotype
Nordåa	N-1	11.5	124	395	Classical	M1
Bergastølen	B-1	9	81	142	Minor	M2
	B-2	7	110	305	Minor	M2
Hølsætra	H-1	11	98	432	Hummocky	M4

Many ribbed moraines in central Norway appear to demonstrate the traditional, down-ice concave shape, some with well-developed horns, though it is not uncommon for tracks of ridges to lack clear relation to palaeo-ice flow direction in the curvature of their planform. Southeast of Jotunheimen, ridge axes predominantly trend NE-SW (e.g., ridges N-1 and H-1), although landforms within certain fields display NNW-SSE (e.g., ridges B-1 and B-2), N-S, or NNE-SSW orientations, all of which are transverse to palaeo-ice flow, as indicated by accompanying (occasionally overprinting) drift lineations and streamlined bedrock forms. Properties of macro-scale topography (e.g., valley aspect) appear to form first-order controls on ridge orientation. In certain examples, such as when comparing ridges of the Vinstri-Bygdin river valley near Bergastølen (Site B) to those which protrude from Sandvatnet 2 km down-ice (and also considering the field near Storjerner some ~8 km to the SE), sets of ridge axes can be completely perpendicular to one another within relatively limited distances. At the field site located within the Nordålia valley (Site N), 5 striae measurements were taken from exposed quartzite benches which indicate palaeo-ice flow perpendicular to the Nordålia ribbed moraine long axes and parallel to inflections along the encompassing valley walls (Fig. 6.5 and Fig. 6.6).

For the purposes of this investigation, it was crucial to obtain information on the internal properties of ribbed moraine ridges expressed as a variety of morphologies. It was desired that complete landform cross-sections would be surveyed at approximate ridge midpoints, exposing both proximal and lee-side sediments, however limited natural and/or artificial exposures in this area largely prevented this level of information from being collected. Observations and sampling data from the four surveyed sections are presented below.

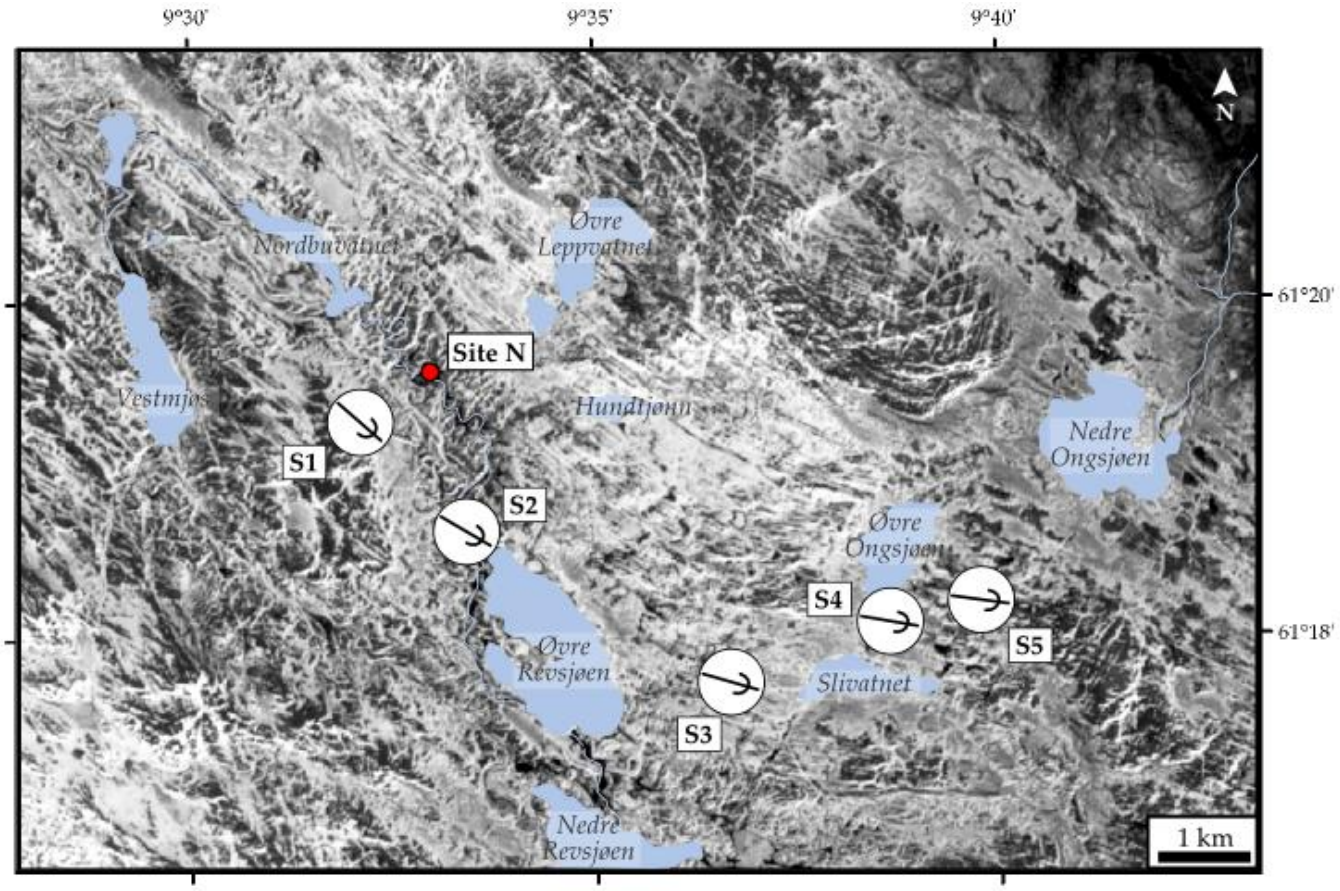

Fig. 6.5 – Landsat 7 ETM+ panchromatic band image, showing location of glacial striae measurements taken from the area surrounding the Nordåa river section (Site N).

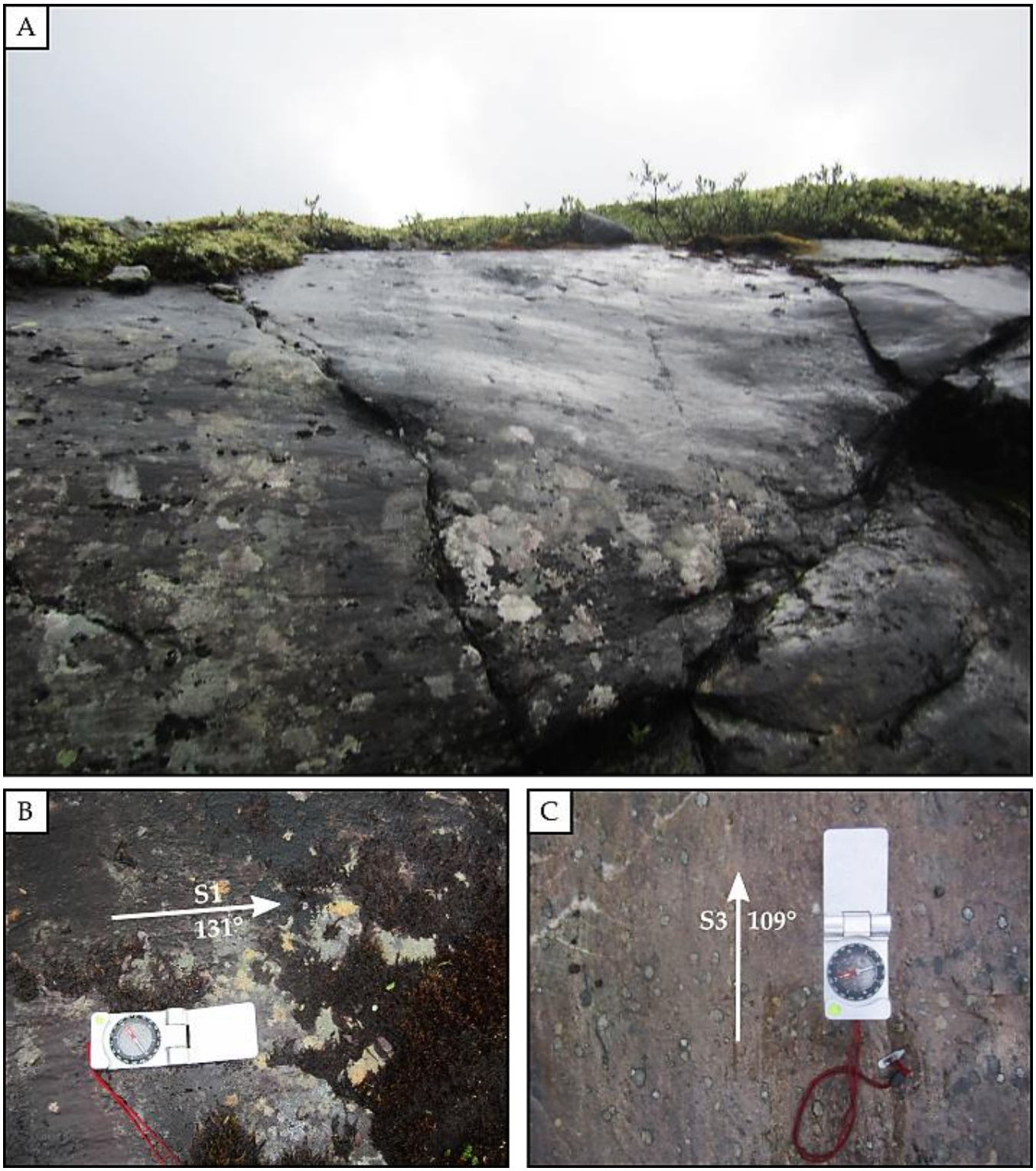

Fig. 6.6 – Examples of palaeo-ice flow indicators in the glacial erosional record surrounding the Nordåa river section. A) Glacially polished and striated grey quartzite outcrop exposed on the east-facing Nordålia valley wall. B) Striae measurement S1 indicating local ice flow to the SE, corresponding to the orientation of the valley. C) Striae measurement S3 indicating local ice flow to the ESE.

6.4.1 **The Bergastølen Sections (Site B)**

The Bergastølen ribbed moraine ridges (B-1, B-2) are located near the eastern tip of Lake Vinstri near Sandvatnet, approximately 45 km east of the head of the Vinstri-Bygdin river valley in Jotunheimen (Fig. 6.7A). Apart from sporadic clusters of glacial landforms, the immediate locality is one of relatively low relief, though is surrounded to the north and southeast by flattened highlands and prominent peaks (Fig. 6.7C and Fig. 6.7D). Some of the Bergastølen ridges are partially submerged beneath Lake Vinstri while other of the larger landforms protrude above lake level into the center of the water body (Fig. 6.7B). The surfaces of the ridges support communities of dwarf shrubs and mosses, and display a dense cover of perched, angular to sub-angular boulders, overwhelmingly of local quartzite lithology (in contrast to lithologies embedded within internal sediments, cf. Fig. 6.23). Boulder cover in this area is not exclusive to ridge tops but occurs everywhere on surrounding flat-lying land. Troughs between ridges support tall grasses and are draped in a thick layer of water saturated, peaty deposits.

Sections were excavated from degraded road-cuts which exposed portions of the south-facing limbs of two ridges. The excavation through the eastern ridge (B-1) was completed in two sections, the uppermost to a depth of 2.5 m below surface, and the lower to an additional 1.1 m depth along a more lee-side exposure (Fig. 6.8A). Ridge B-2 to the west was excavated to a depth of 1 m below surface. Sediments within the ridges predominantly comprise sandy-gravelly to gravelly-sandy, clast- to matrix-supported and massive diamictons. In addition to those perched on their surface, many boulders are found lodged within the ridges, with relatively even distribution throughout. These tend also to be angular to subangular, though are of more varied lithology. They range dramatically in size, yet are characteristically quite large, some with diameter >1 m.

Subtle variations in colour, level of consolidation and texture made it possible to distinguish between three quasi-distinct ridge facies within B-1. Facies 1 occurs primarily as a 130 cm thick unit at the base of the upper section, and constitutes the entire 110 cm of the lower section. It consists of massive, diamictic, grey to grey-brown (7.5 YR 4/2) medium silty sands with subangular pebbles and large subangular boulders, containing an estimated 10%/60%/30% clay-silt/sand/gravel. This facies is matrix-supported and poorly consolidated and exhibits slight normal grading, made most obvious by the prevalence of large boulders near the base of the upper section, though diamicts within the ridge as a whole become clast-supported towards the surface. Contained within this lower unit is a ~35 cm thick (thinning towards the east) layer of facies 2 sediments comprising friable, poorly consolidated dark grey, medium sandy-pebbly diamict (~5%/70%/25% clay-silt/sand/gravel) with comparatively few large cobbles, and exhibiting extremely faint horizontal bedding. The latter is most prominent beneath two boulders lodged at the facies 1/facies 2 contact where facies 2 appears to be at its thickest. Facies 1 is capped by facies 3 – a 60-75 cm thick deposit of overconsolidated, fissile, dark brown-grey (10 YR 4/2) pebble-rich silty-sandy diamict (~15%/45%/40% clay-silt/sand/gravel) with many boulders and a high proportion of angular to subangular clasts. The contact between facies 1 and 3 appears convoluted, though is obscured by the high boulder content in this area. Fe staining was observed beneath boulders (Fig. 6.8E) and thin oxidation halos surrounded a number of clasts within this unit. Some clasts exhibited evidence of frost and/or strain shattering (Fig. 6.8D). The B-1 sequence is capped along a sharp contact by a thick developing soil horizon (Fig. 6.8C) which overlies laterally alternating facies 1 and facies 3 sediments.

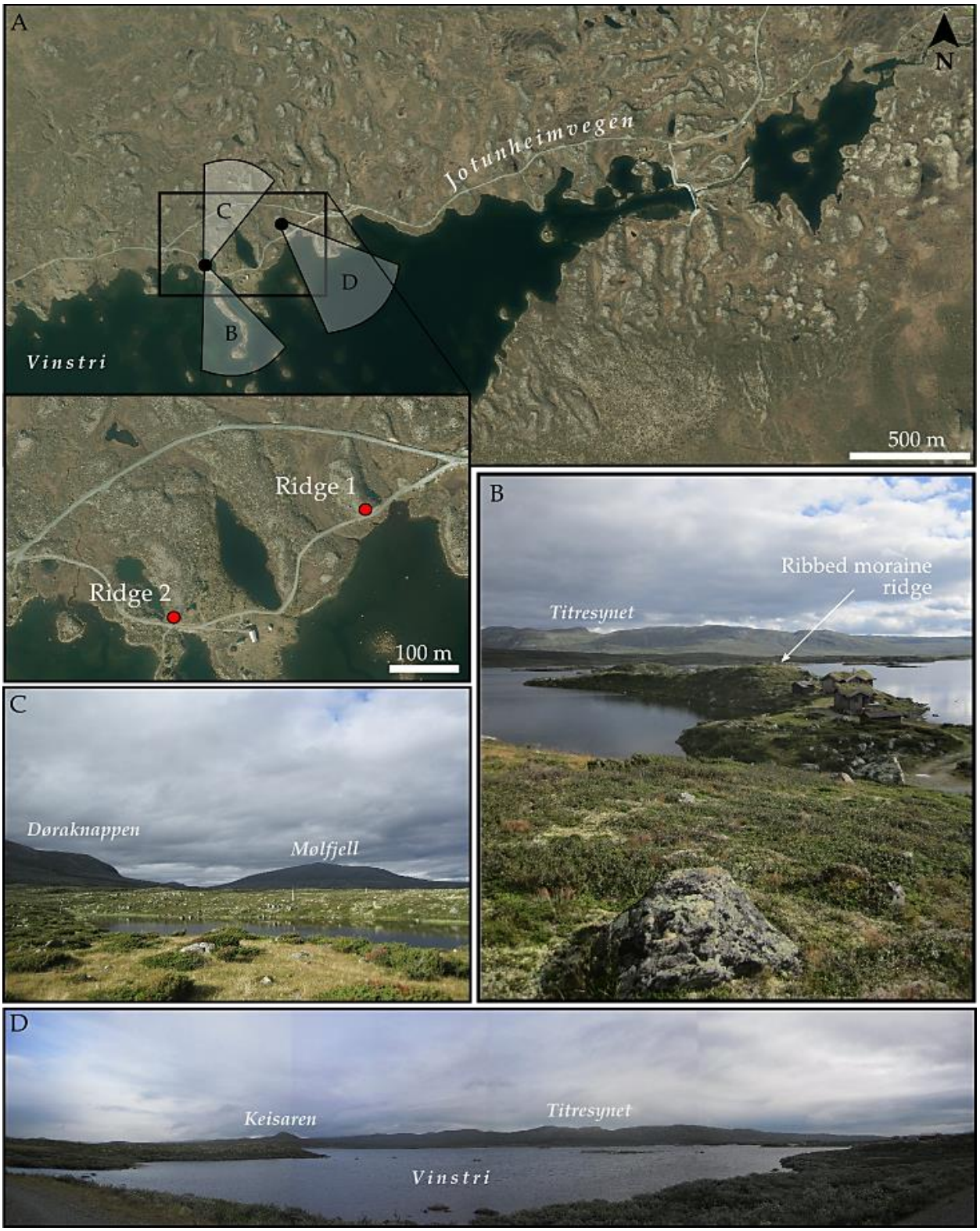

Fig. 6.7 – Overview of the study site near Bergastølen. A) Aerial orthophotographs showing location of eastern and western ridges (B-1, B-2). Cones show location and viewing aspect of photos in C,B,D. B) A ribbed moraine ridge extending into the center of Lake Vinstri. C) View of the area NW of the study site, towards peaks Mølfjell and Døraknappen. D) View to the SE across Lake Vinstri. Aerial orthophotographs obtained from Norge i Bilder (www.norgeibilder.no).

The excavation of the upper portion of ridge B-2 revealed a similar assortment of mainly poorly sorted, structureless sandy-gravelly facies 1 diamicts (Fig. 6.9), and also featured an up to 60 cm thick layer of darker, overconsolidated facies 3 sediments approximately 30 cm below the base of the overlying surficial soil profile. Clast macrofabrics were obtained from facies 3 in both ridge B-1 (n = 30) and ridge B-2 (n = 25) (see section 6.3.1), yielding similar principal eigenvectors (V_1) (B-1 = 234°, B-2 = 245°) with relatively low isotropy/azimuthal dispersal, based on the normalized eigenvalues (S_1) of V_1 (B-1 = 0.661, B-2 = 0.750). These principal eigenvectors suggest a predominant stress transfer direction from the ESE. Fabrics from each ridge demonstrated moderate up-ice plunge (B-1 = 24°, B-2 = 16°). In each instance, V_1 exhibited preferred clustering in a direction perpendicular or slightly oblique to the trend of the sampled ribbed moraine long axis. The B-1 fabric features a greater offset from orthogonal with respect to the landform than does the B-2 fabric (Fig. 6.10).

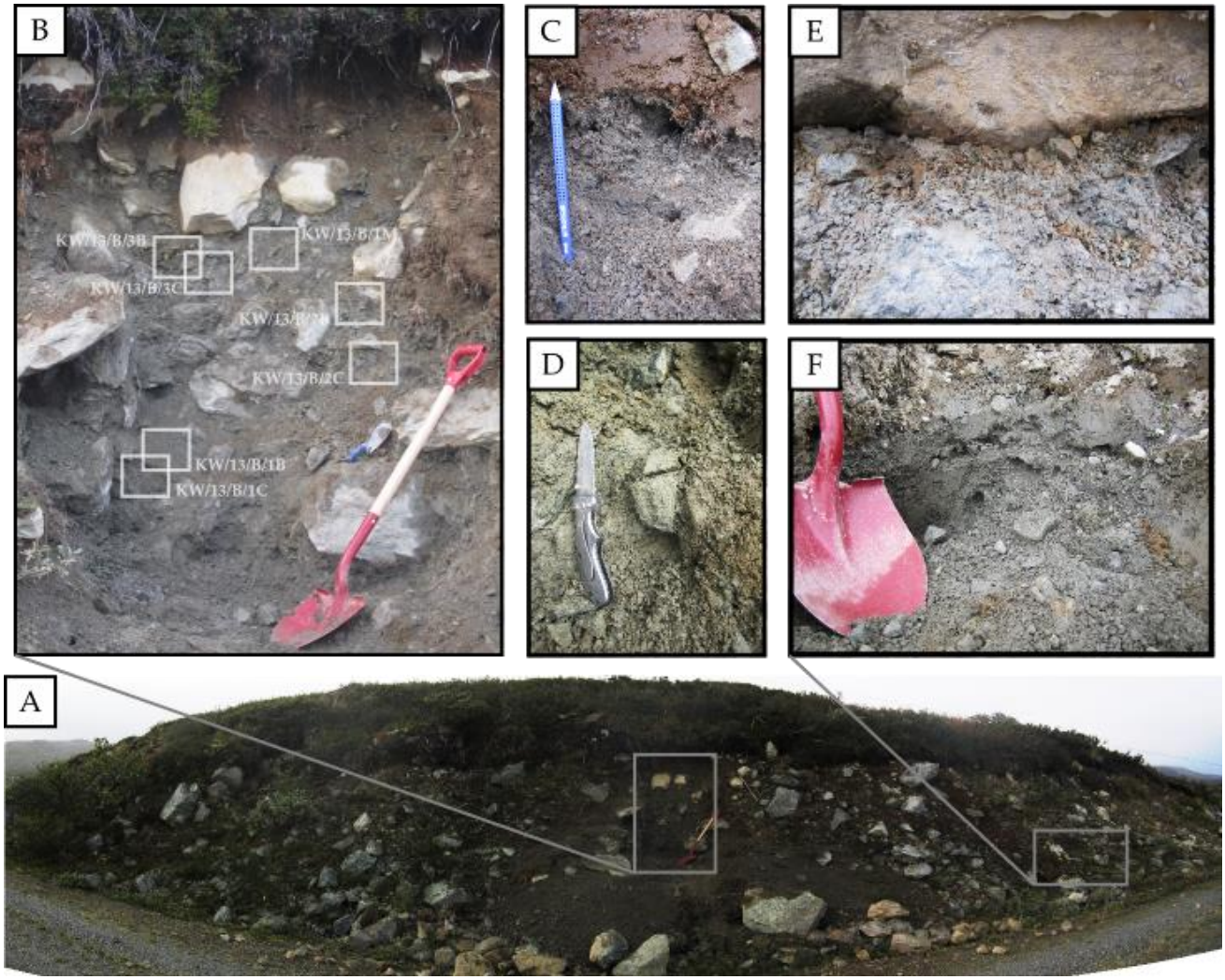

Fig. 6.8 – The excavation at ridge B-1. See text for description. Length of spade = 130 cm. Locations where clast, and bulk sediment samples (oriented and unoriented) were extracted are indicated in B.

A single, undisturbed and oriented bulk sample (KW/13/B/1M) was also obtained for micromorphological analysis from facies 3 within ridge B-1 at 0.5 m depth below the base of the uppermost soil profile (see methods section 6.3.4). It was intended that similar samples would be

collected throughout the entire stratigraphic sequence, though the coarse-grained nature and poor consolidation of facies 1 and 2 precluded their acquisition. Analysis of facies 3 sediments in thin section at low magnification (6.3-32x) enabled the documentation of diagnostic microstructures. Identified microstructures within the sample include single and multiple direction short-distance lineations, grain stacks, rotation structures, grain fractures, edge-to-edge crushing, necking structures, clay banding and translocation structures, and micro-laminae. In accordance with the macro-scale observations of facies 3, this particular thin section displays high clast content (~60%) and a silty-sandy, coarse grained matrix. An imbricate structure is apparent throughout a large portion of the slide, wherein clasts and large grains are packed in a tight, edge-to-edge arrangement and are interspersed with other angular, poorly comminuted materials. Necking structures, indicative of the effusion of a ductile matrix through narrow interstices within the sediment package, occur within gaps between the convergent edges of outsized clasts, and are occasionally associated with instances of grain fracturing and edge-to-edge crushing (Fig. 6.11A) which, alternatively, are indicative of high stress and brittle deformational environments. Similarly, ductile rotation structures are identified around several core stones, though occur in the immediate presence of multiple direction short-distance lineations (Fig. 6.11B) which signify brittle conditions. Disaggregated inclusions of organic material are noted throughout the sample (Fig. 6.11 and Fig. 6.12) and could be indicative of pioneer vegetation assemblages having colonized the proglacial zone throughout one or more interstadials (e.g. Menzies and Ellwanger, 2011) which were later cannibalized by an overriding glacier and incorporated into basal ice. Again in accordance with macro-scale observations, iron/manganese staining is observed on several clasts in the thin section, as are intervening thin bands of oxidized clays (Fig. 6.13B). Stratified silty-clayey infillings occur beneath protected lee-side positions of certain large clasts (Fig. 6.13A) and contrast with the coarse-grained matrix observed throughout the bulk of the sample.

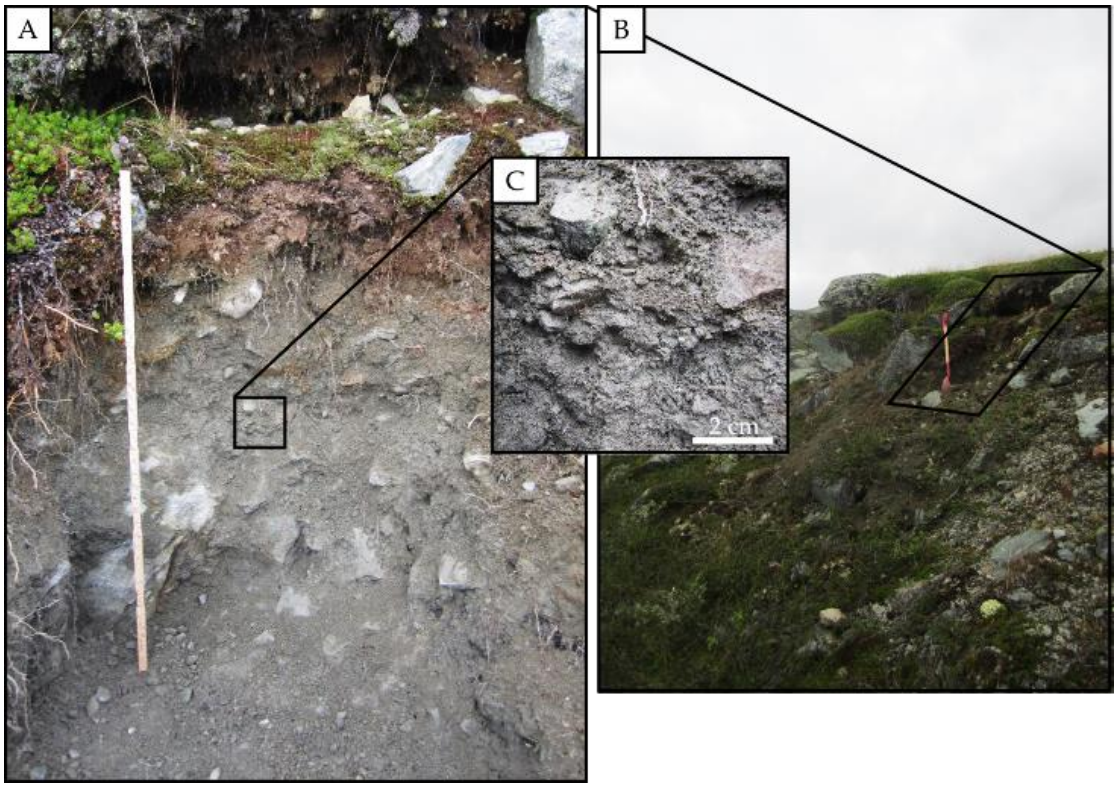

Fig. 6.9 – The section at ridge B-2. See text for description. Length of folding rule = 1 m.

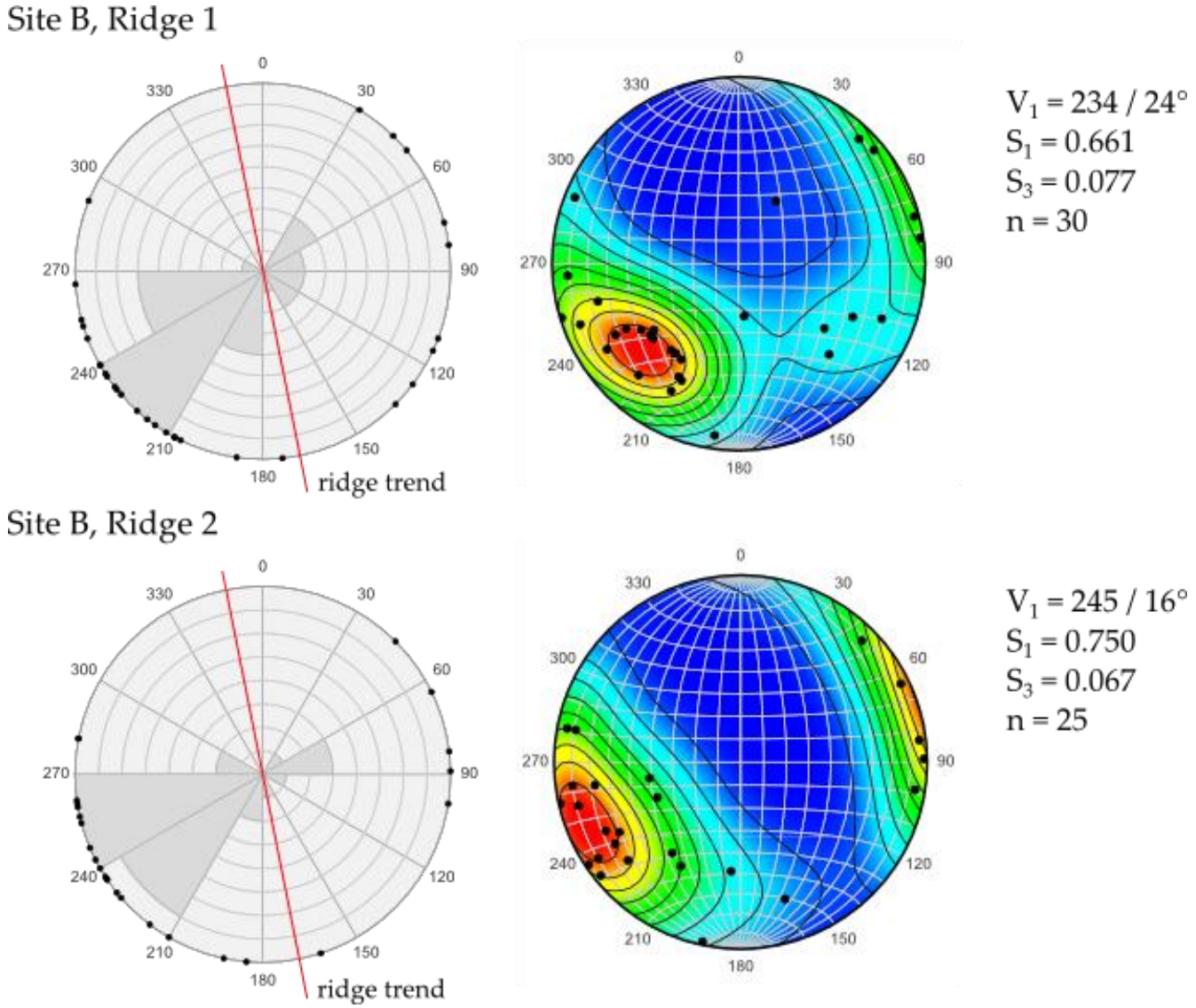

Fig. 6.10 – Clast macrofabrics obtained from facies 3 in ridges B-1 and B-2 at the Bergastølen study site displayed as rose diagrams (left) and contoured lower hemisphere Kamb nets with 3 σ grids (right).

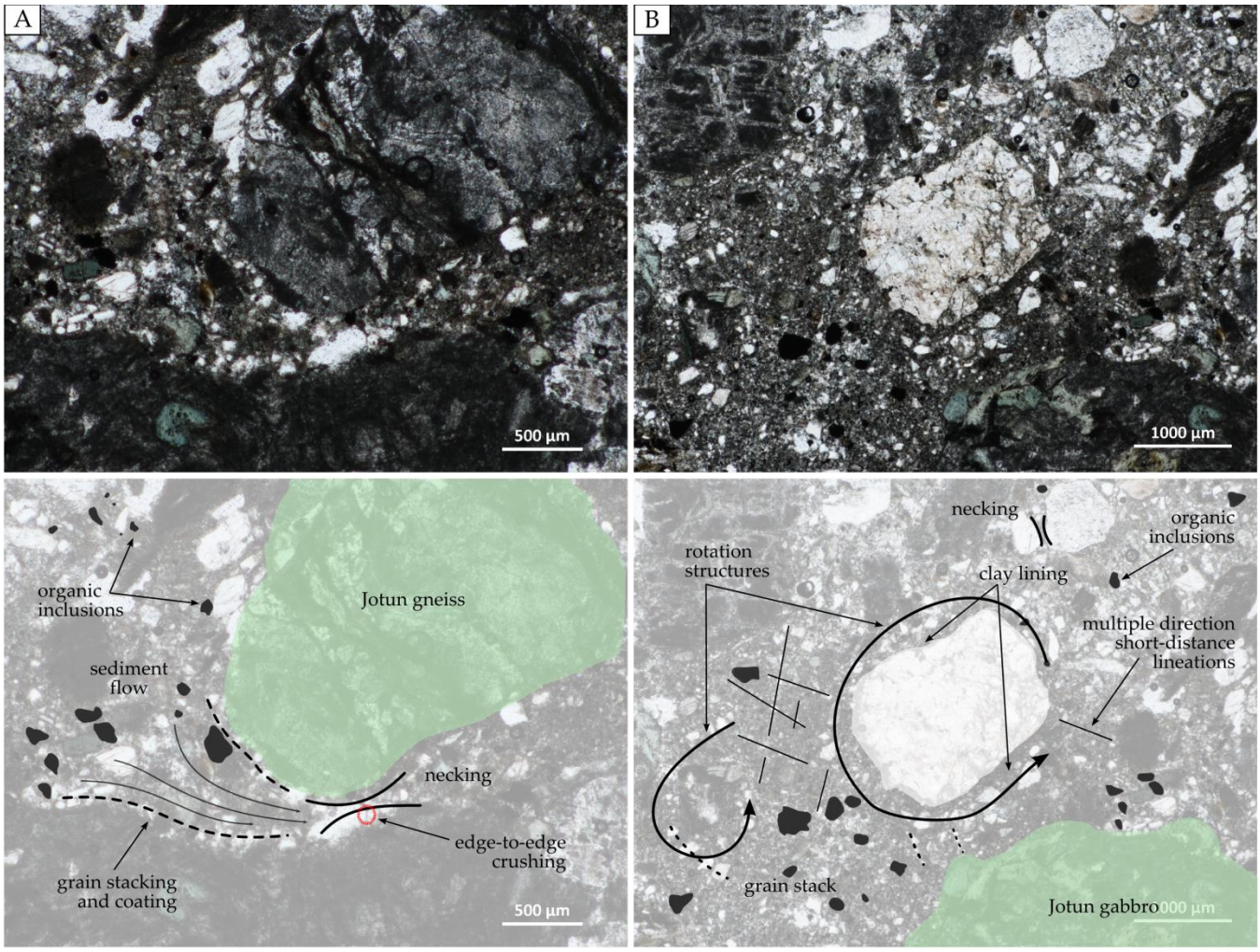

Fig. 6.11 – Photomicrographs (plane light) and corresponding microstructural interpretations from KW/13/B/1M. A) Necking and stacking of skeleton grains indicating the squeezing of materials through gaps between large clasts, which are embedded in the sediment matrix. B) Rotation structures and multiple-direction short-distance lineations indicative of a polyphase strain history.

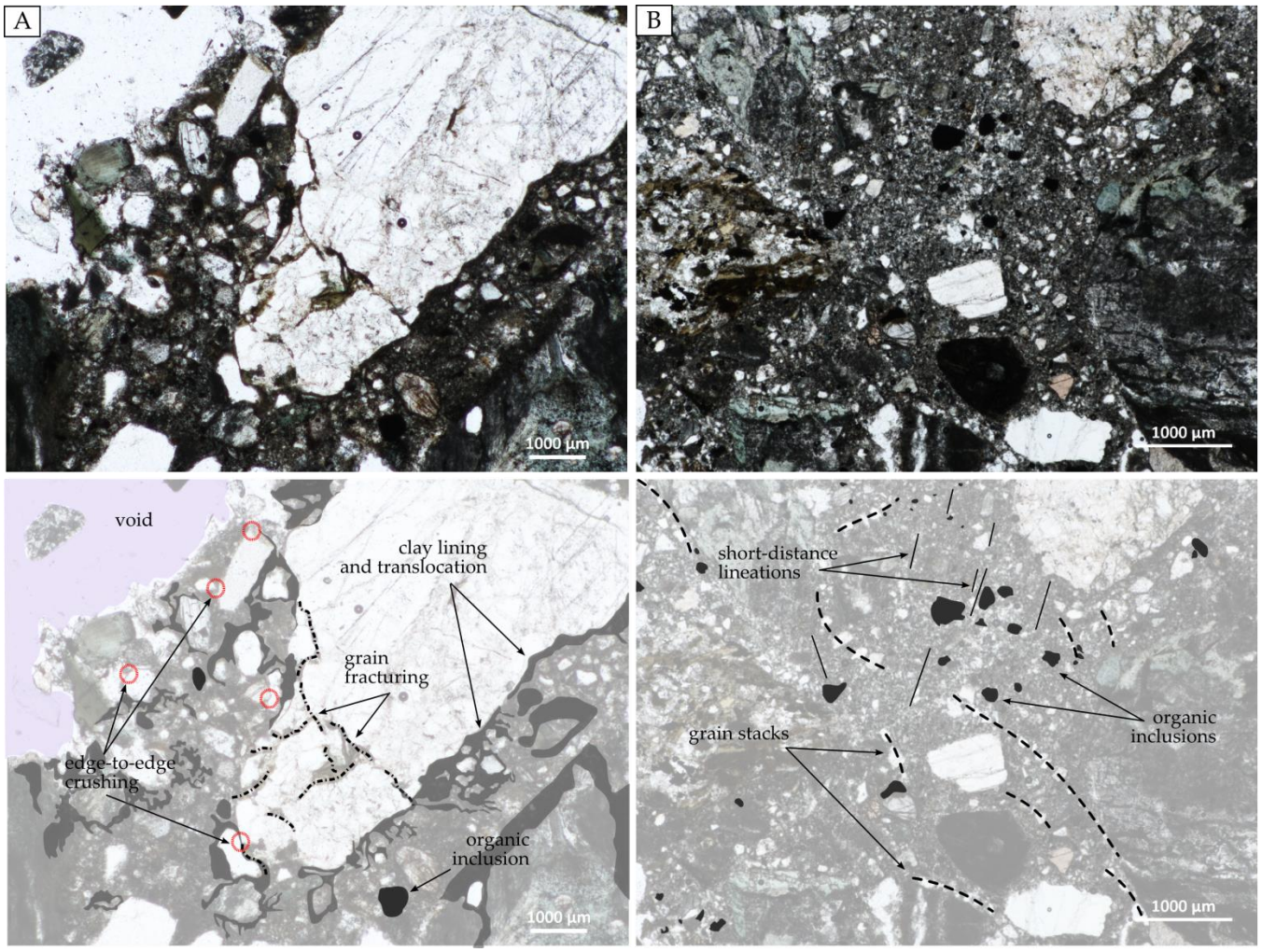

Fig. 6.12 – Photomicrographs (plane light) and corresponding microstructural interpretations from KW/13/B/1M. A) Microstructures indicative of high strain and brittle conditions, including edge-to-edge crushing and grain fracturing events. Clay lining and translocation structures indicate porewater movement following sediment decompression. B) Grain stacks and short distance lineations indicative of a polyphase strain history.

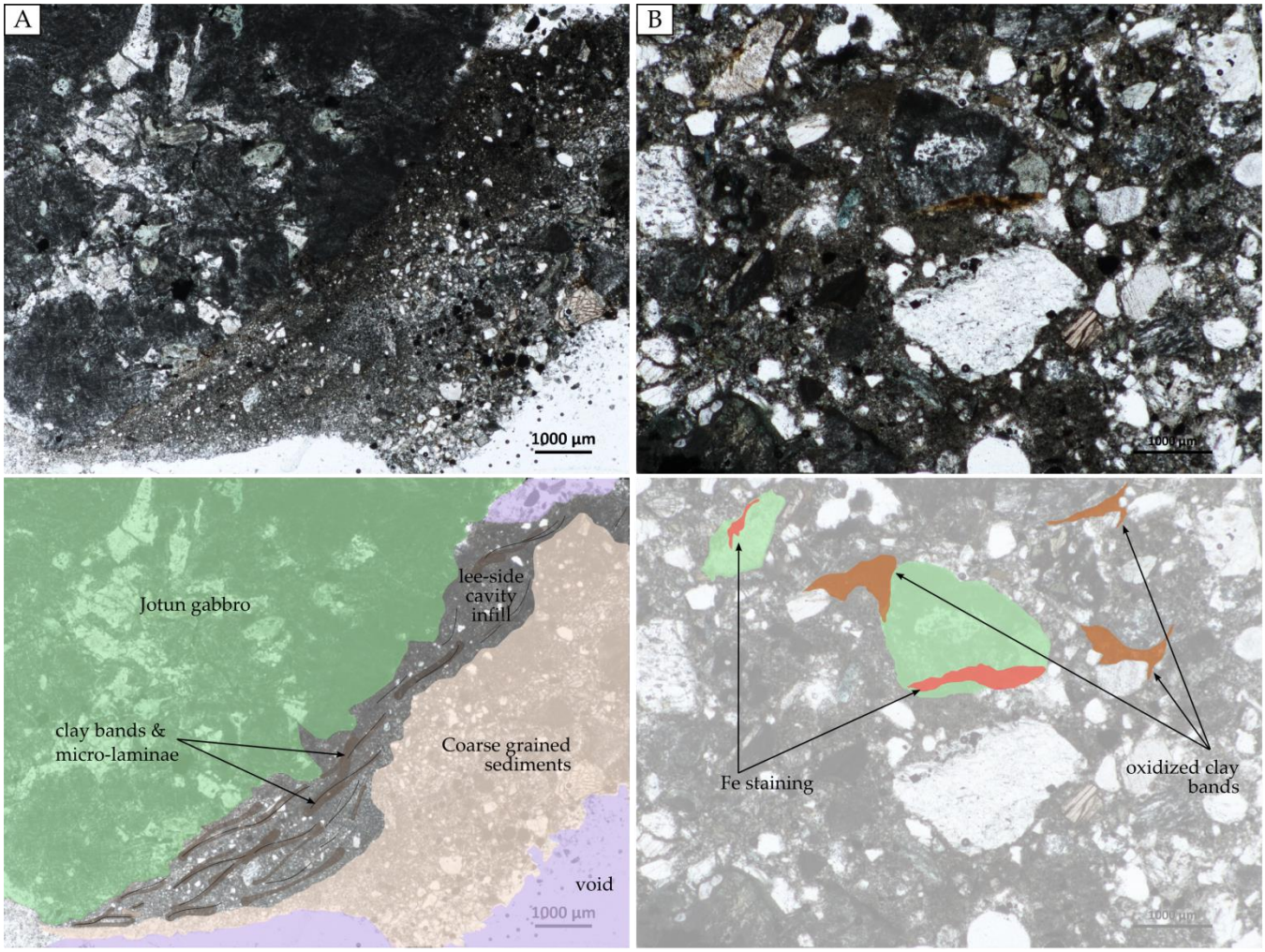

Fig. 6.13 – Photomicrographs (plane light) and corresponding microstructural interpretations from KW/13/B/1M. A) Micro-laminated lee-side infill with clay banding beneath a large clast. B) Iron staining of clasts and oxidized clay matrix.

6.4.2 **The Hølsætra Section (Site H)**

The Site H ribbed moraines are located ~10 km southwest of Skåbu, with access via a crude cottage trail that forks off of Jotunheimvegen towards Hølsætra (Fig. 6.14). Ribbed moraines in this area are large but appear relatively degraded and exhibit a variety of morphologies. This site occurs within a ~2 km wide depression that contributes runoff to the Breddagsklykka river valley immediately to the south. The lateral continuity of the Hølsætra ribbed moraine field is truncated by high land to the west towards Vesfjellkampen (1,312 m a.s.l.), where the ridges have been overridden or otherwise largely demolished by (offset) NW-SE trending drumlins and flutes. Along the western edge of the field, ridges are conspicuously oriented parallel to the valley wall and could be genetically differentiated as lateral moraines. Down-ice, towards the center of the sub-drainage basin, these ribbed moraines transition into pitted hummocky moraine which supports a dense Montane Birch Forest cover. In the Hølsætra field, as elsewhere in central Norway, ribbed moraines are easily distinguishable on aerial photographs by their carapace of terricolous reindeer lichen (*Cladina stellaris*). Clusters of downy birch (*Betula pubescens*)

occur exclusively on ridge tops (Fig. 6.15D), and alternate with peat and marshland vegetation in the intervening swales.

3 sections were made into the NW face of a road-cut exposing the eastern limb interior of a hummocky-type ribbed moraine ridge (H-1) (Fig. 6.15A). The western arm of H-1 extends an additional ~320 m beyond the road cut, the eastern an additional 110 m in the opposite direction. The sections were staggered from bottom to top, moving towards the central axis of the ridge, together covering 2.2 m of the exposed vertical face. 5 units were distinguished and logged in a composite vertical profile (Fig. 6.16). At the base of the lowermost section, 35 cm of matrix supported, medium grey (2.5 YR 4/2) gravelly-sandy diamict was found, containing a high proportion of small sub-angular to sub-rounded pebbles with weak horizontal bedding and occasional imbricate structure (Fig. 6.15E). This unit thins out towards the NNE (i.e., the ridge's eastern limb) and is overlain, along a graded to conformable contact, by 10-15 cm of orange-brown pebbly silt that transitions upwards into an overlying porous soil. Pebbles embedded in the silt are primarily sub-rounded and of mixed lithology. At the base of the middle section, 25 cm of alternating, rhythmically laminated brown fine sand and orange silt pinch out from beneath a lodged sub-angular boulder (Fig. 6.15H). Bedding within this unit exhibits a true dip of 16° towards the N. This unit thins towards the NNE and grades upwards into the thick (110 cm), uppermost unit 5 (Fig. 6.15F). Unit 5 is a massive, clast-rich, matrix supported, medium grey gravelly-sandy diamict with occasional sub-rounded to sub-angular cobbles and boulders (Fig. 6.15B). Some large cobbles demonstrate a high degree of rounding (Fig. 6.15G). This unit begins in the upper portion of the middle section and continues throughout the uppermost section towards the center of the ridge. The diamict matrix in unit 5 demonstrates slight upward coarsening, becoming sandier, and yet more fissile and better consolidated towards the surface. Embedded within unit 5, 30-50 cm below the surface, and beneath a large, rounded granitoid boulder, are two distinct lenses of sorted sediments (Fig. 6.15C); the uppermost consisting of fine gravels, the lower tightly-packed brown-yellow horizontally laminated silt.

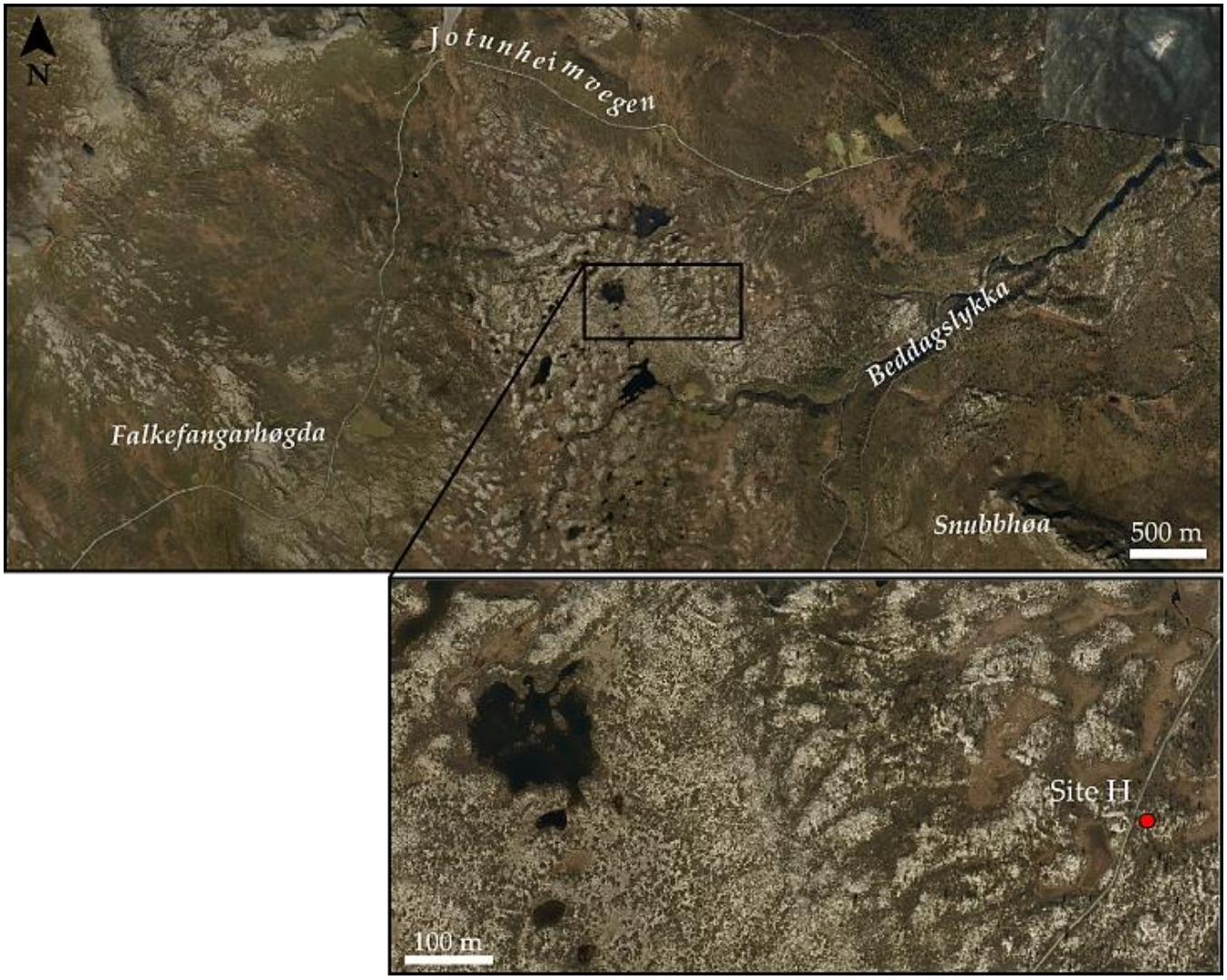

Fig. 6.14 – Overview of the study site near Hølsætra. Aerial orthophotographs obtained from Norge i Bilder (www.norgeibilder.no).

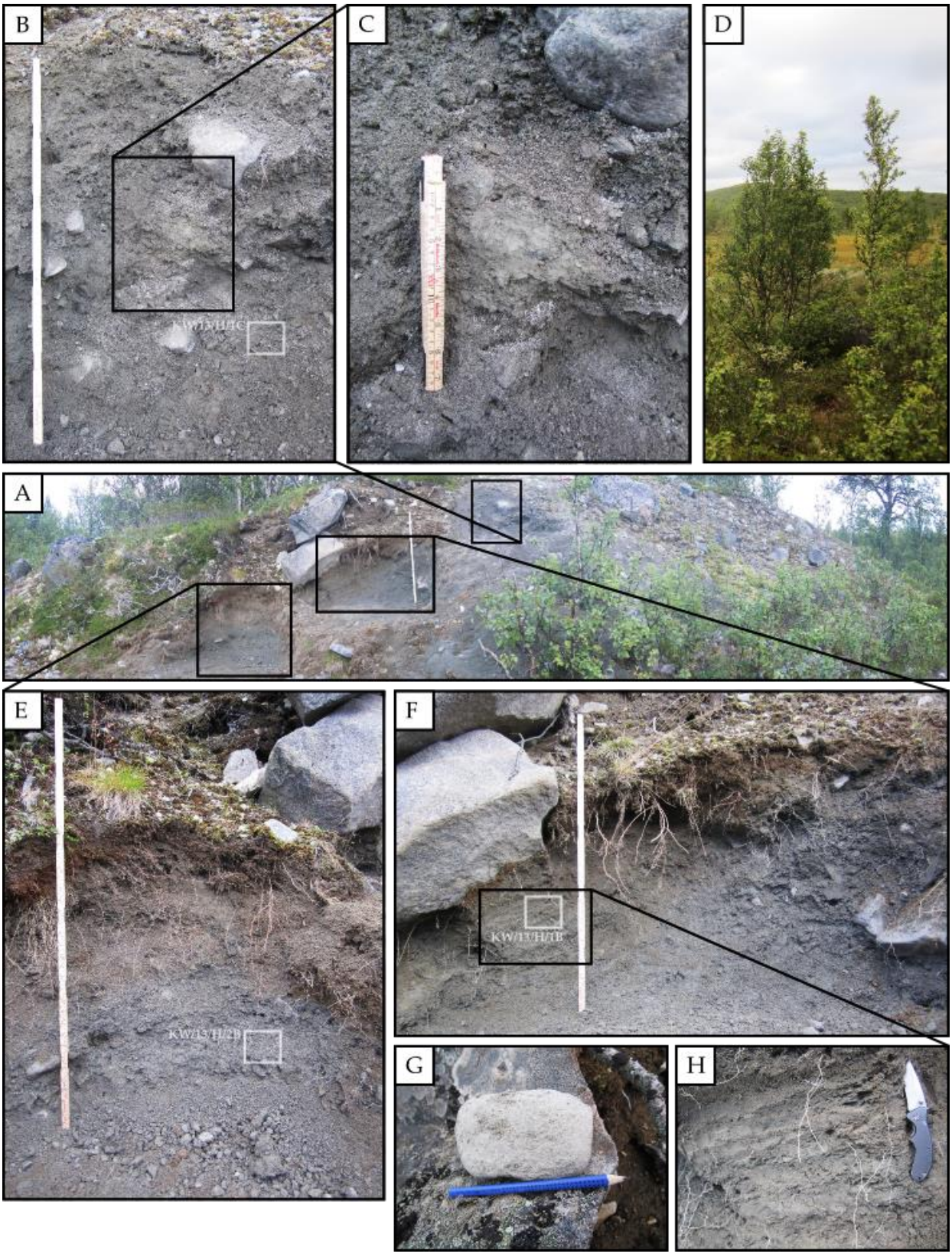

Fig. 6.15 – Sections through ridge H-1 at the Hølsætra site. See text for description. Folding rule = 1 m in E, 80 cm in A, B, and F, and 20 cm in C. Locations where clast and bulk sediment samples were extracted are indicated in B, E and F.

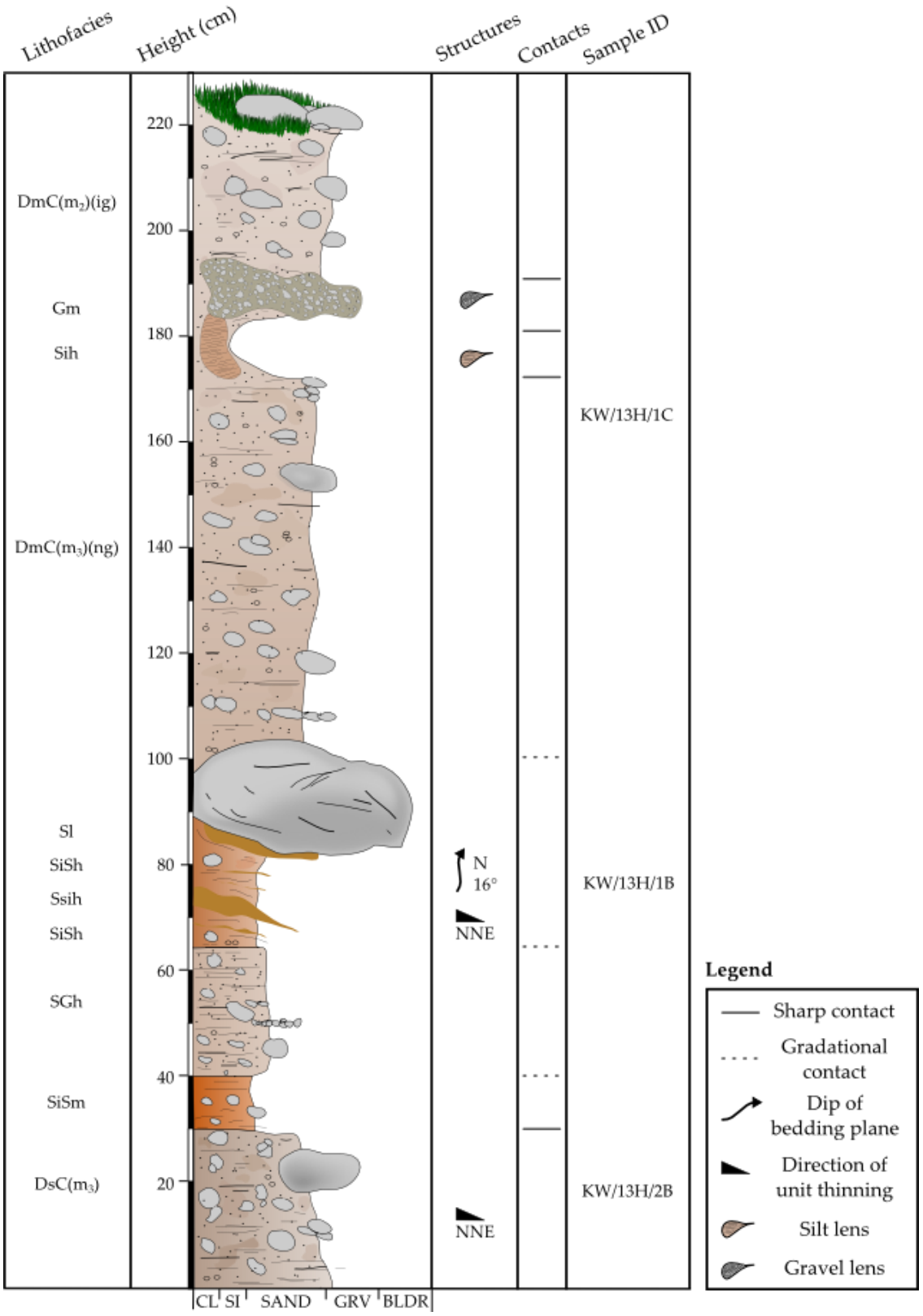

Fig. 6.16 – Composite log of the stratigraphy spanning 3 sections through ridge H-1 at the Hølsætra study site. See Table 6.3 for key to facies codes.

6.4.3 **The Nordåa Section (Site N)**

Ribbed moraines of the Nordålia valley – the most remote of the three investigated sites – are arranged within a narrow, linear strip ~20 km SE (i.e., down-ice) of the Hølsætra section, inside the 537.1 km^2 Langsua National Park, and encompassed within, and near the eastern border of the Storlonen Nature Reserve (Fig. 6.17A). Ribbed moraines at this site are of moderate scale, tightly spaced (average wavelength ca. 150 m), and are dissected by a rapidly meandering segment of the Nordåa river (Fig. 6.17D), which here runs due southeast, eventually draining into Øvre Revsjøen. This small field contains 29 individual ridges grading from proximal bulbous, hummocky forms, through to classically shaped ridges, and eventual small, minor ridges alongside small drumlins (Fig. 6.19) and flutings at its distal extent. A degraded field of ribbed moraines is also located ~1.5 km to the east, perched on the north facing slope of Risåhøgda. The Nordålia valley is surrounded by a series of distant peaks, and the slope breaks along these valley walls support dense stands of conifer forest (Fig. 6.17D). In a similar fashion to those examined at Site H, ridges of the Nordålia valley exhibit a distinctive cover of *C. stellaris*, somewhat more sporadic *B. pubescens*, alongside a patchwork of short grasses, wolf lichen (*Letharia vulpina*), small flowering plants (e.g., *Campanula barbata*, *Pulsatilla vernalis*) and dwarf shrubs (e.g., *Betula nana*) (Fig. 6.18B and H). Troughs between ridges frequently contain standing water and marshland vegetation. The surfaces of these ridges (including the studied ridge, N-1) are also blanketed by typically large (some up to 3 m diameter), sub-angular, local quartzite boulders (Fig. 6.18G), which are perched, rather than lodged into, most ridge crests. A small pit (~1 m deep) was dug into the exposed eastern face of a river cut through a ridge (N-1) of classical morphology near the lower 2/3 of the Nordålia ribbed moraine field. At this location, the river has bisected the ridge (in total, ~400 m long), isolating a ~140 m long segment of its limb on the western bank. Sediments within the ridge comprised massive, matrix-supported, coarse-grained, grey (2.5 Y 4/2), gravelly-sandy diamict (Fig. 6.18E) with many rounded cobbles (typical a-axis ~10-12 cm) and lodged boulders of mixed lithology (Fig. 6.18C and D). One bulk sediment sample and one clast sample (KW/13/N/1B, KW/13/N/1C) were obtained from the excavated pit for subsequent analysis.

Table 6.3 – Facies codes utilized in this study (modified from Eyles et al., 1983, and Krüger and Kjær, 1999).

Diamict		Sorted sediments		Structure	
D		B	Boulders	m	massive
		CoG	Gravelly cobbles	s	stratified
Matrix Texture		G	Gravel	l	laminated
C	coarse-grained (sandy, gravelly)	GS	Sandy gravel	h	horizontally-bedded
M	medium-grained (silty, sandy)	SG	Gravelly sand	(ig)	inversely graded
F	fine-grained (clayey, silty)	S	Sand	(ng)	normally graded
		SiS	Sandy silt		
Organization		Ssi	Silty sand		
(c)	clast-supported	Si	Silt		
(m_1)	matrix-supported, clast-poor	SiC	Clayey silt		
(m_2)	matrix-supported, clast-moderate	Csi	Silty clay		
(m_3)	matrix-supported, clast-rich	C	Clay		

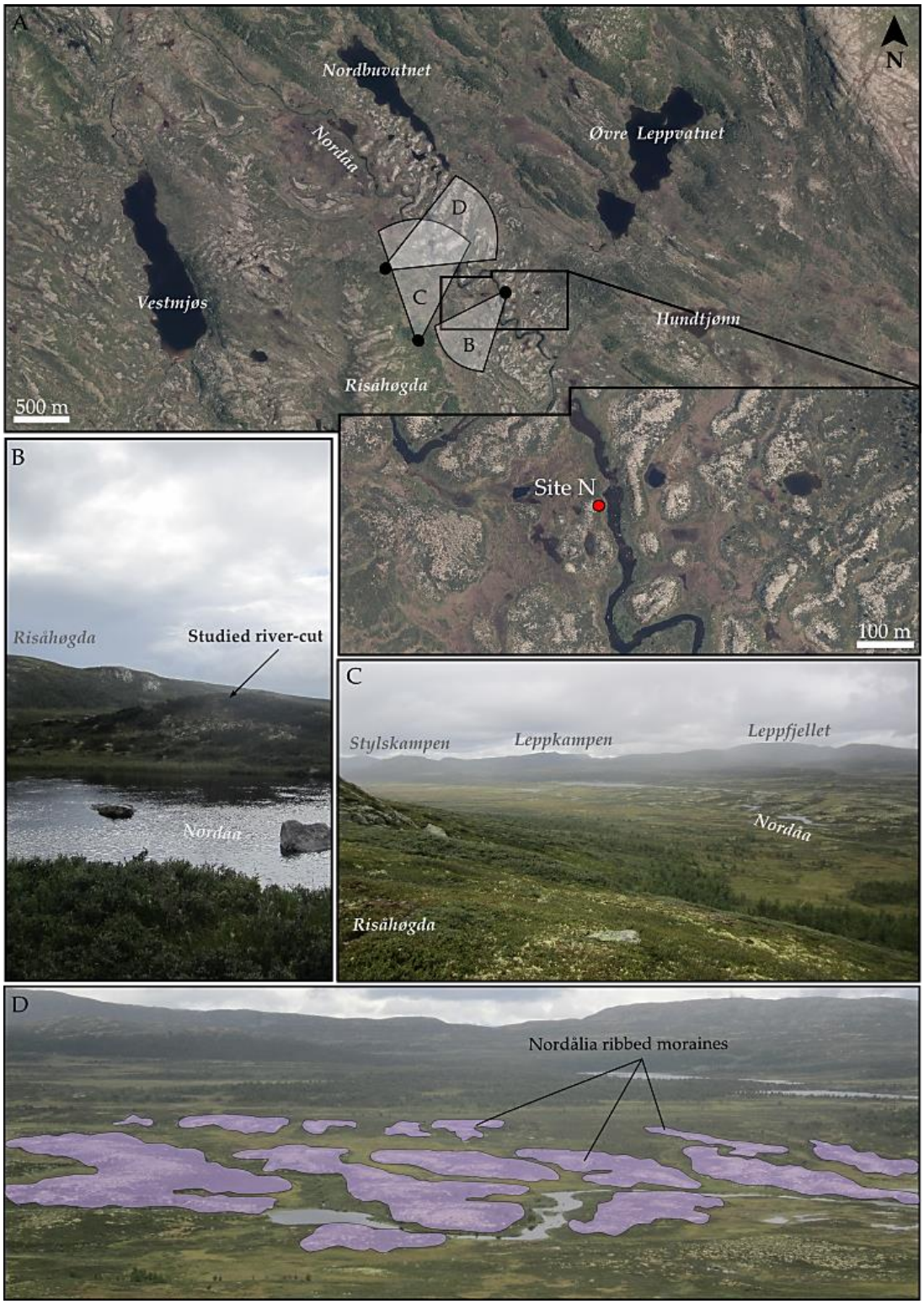

Fig. 6.17 – Overview of the study site in the Nordålia valley. A) Aerial orthophotographs showing location of ridge N-1. Cones show location and viewing aspect of photos in C,B,D. B) View towards the western bank of the Nordåa river, showing exposed sediments along a river cut in ridge N-1. C) View to the NE across the Nordålia valley, showing Stylskampen, Leppkampen and Leppfjellet peaks in the distance. D) The Nordålia ribbed moraines (purple) in the center of the valley, bisected by a meandering segment of the Nordåa river.

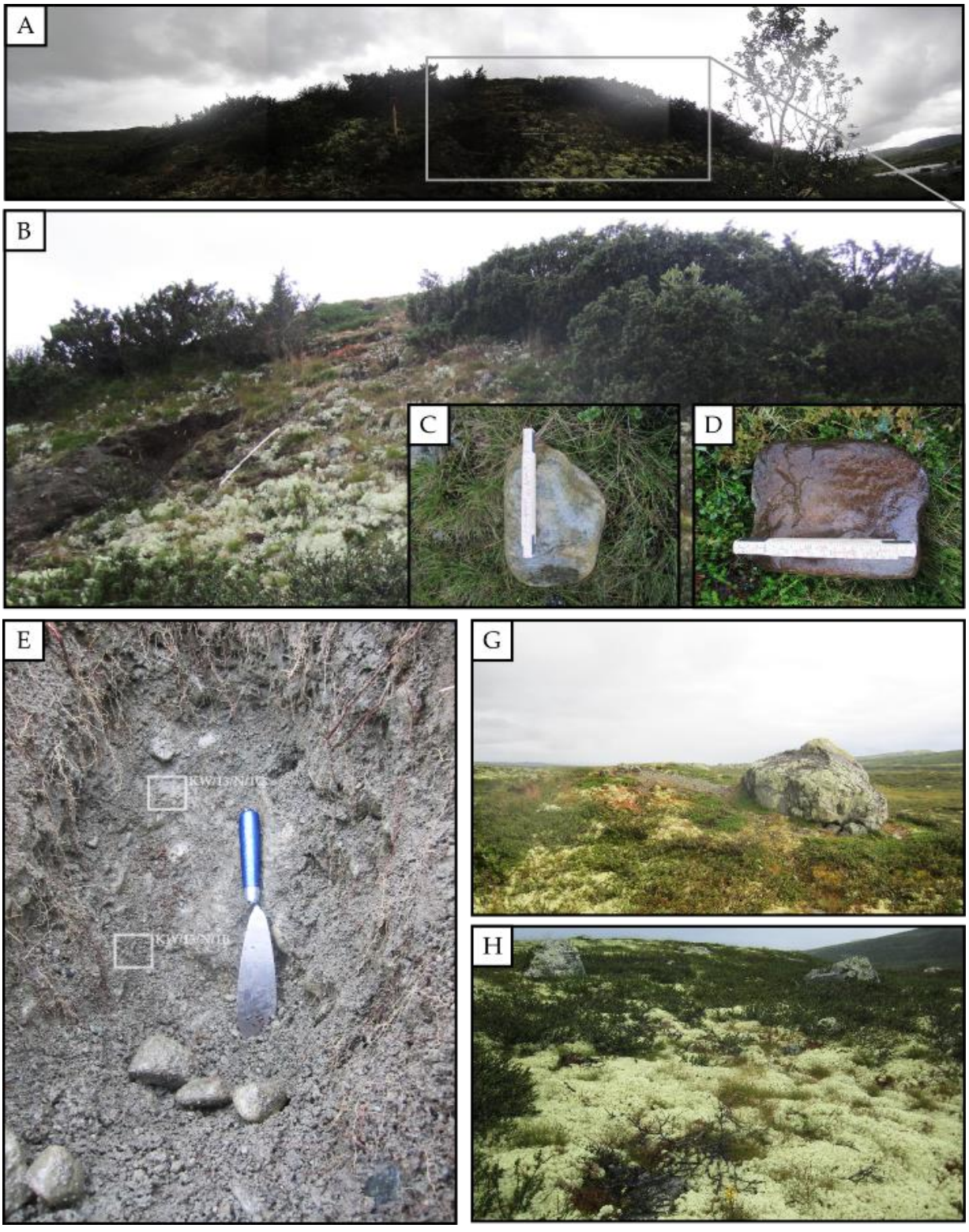

Fig. 6.18 – Ridge N-1 and the contents of a 1 m pit dug into a portion of an exposed river cut along the western bank of the Nordåa river. See text for description. Length of folding rule = 1 m in B and 20 cm in C, and D. Length of trowel in E = 29 cm. Locations where clast and bulk sediment samples were extracted are indicated in E.

Fig. 6.19 – A small drumlin (oriented ~120°), aligned to valley long axis, and located near the mouth of the Nordåa river.

6.4.4 **Till Matrix Granulometry**

Six bulk sediment samples were obtained from various depths within the studied ribbed moraine landforms at each of the 3 field sites (see section 6.3.3 for methods and above figures for locations). Raw data for each sample is given in Appendix D. All samples were collected from diamictons excepting KW/13/H/1B, which was acquired from a sorted and stratified deposit within ridge H-1 (Fig. 6.15H). Cumulative grain size distribution curves for each sample matrix (<2 mm fraction) are presented in Fig. 6.20. The results demonstrate a remarkable similarity in diamicton matrix granulometry between sites despite variation in auxiliary properties (colour, consolidation, etc.); all samples are predominantly coarse-grained (>50% sand), very low in clay content (<10%), and have exceptionally well-behaved cumulative grain size distribution curves within their sand-sized fraction. Samples KW/13/H/1B and KW/13/N/1B exhibit the lowest clay contents (<5%) and have sharp rises at the coarse silt/fine sand boundary, suggesting (re)incorporation of fluvially eroded and/or transported materials. Fig. 6.21B contrasts sample grain size distributions on a ternary diagram plot, revealing a clear separation between the diamictons and sorted sediment sample. Comparison with Fig. 6.21A shows that all samples collected in this analysis fall within a typical textural range for Norwegian basal tills (based on 3,000 samples analyzed in Jørgensen, 1977), providing a basis for similar interpretation of these diamictons.

In addition to correlations with the grain-size envelopes developed in Jørgensen, 1977, diamictons found in section within all studied ridges in the Norwegian field sites are interpreted here as tills on the basis of their generally high boulder content, heterogeneous grain size distribution, predominantly massive (though occasionally vaguely stratified), matrix-supported structure and (in some instances), a high proportion of faceted and subangular clasts. The lack of fissility (a common characteristic of subglacial tills) exhibited by the Norwegian tills (excluding facies 3 tills found within the Bergastølen sections) is attributable to their general deficiency in fine grained (i.e., clay-rich) matrix materials. Nevertheless, a relatively high silt component ensures that the latter deposits remain relatively well-consolidated, though the universal dominance of sands and gravels attributes to them a friable property.

Fig. 6.20 – Cumulative grain size distribution curves and textural composition for 6 bulk sediment samples obtained from 3 ribbed moraines in central South Norway.

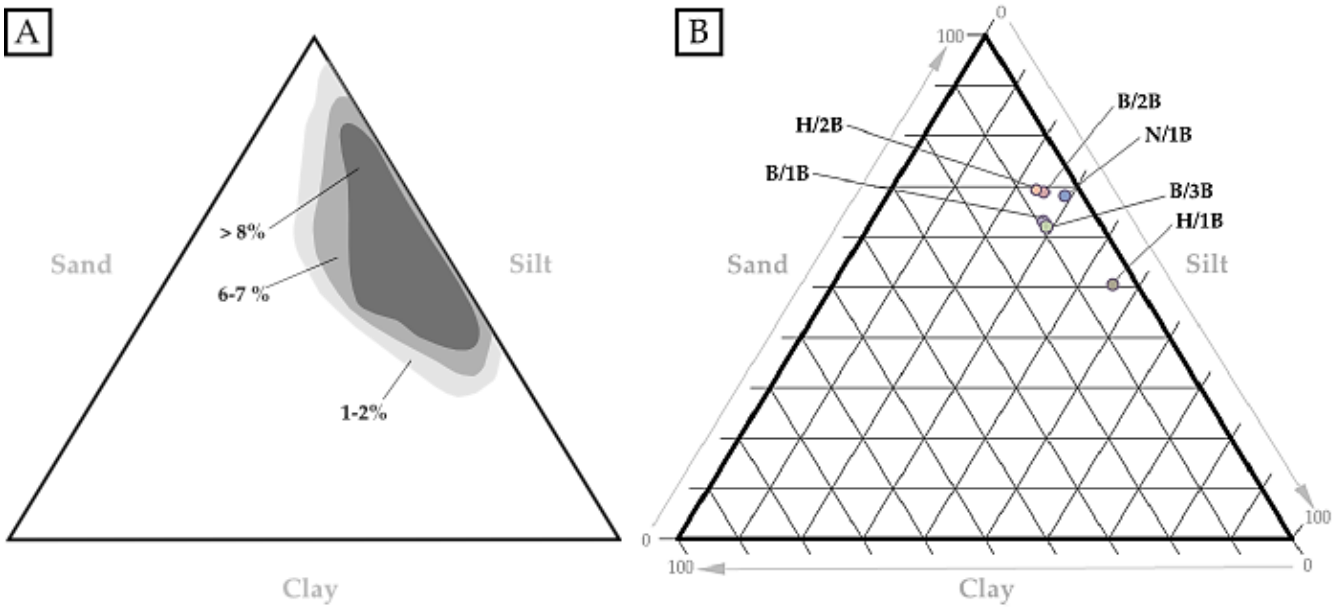

Fig. 6.21 – Ternary diagram plots for sample textural composition. A) Redrawn from Jørgensen (1977); envelopes show percentage of 3,000 Norwegian till samples falling within 1% area of the triangle. B) Bulk sediment samples obtained in this study from 3 ribbed moraines in central South Norway.

6.4.5 **Clast Morphology and Provenance**

Five clast samples (n = 50) were obtained from the studied ribbed moraine ridges at various depths from each of the 3 field sites (see section 6.3.3 for methods and above figures for locations). Raw data for all 5 samples is given in Appendix E. All samples were obtained from diamictons interpreted as glacial tills (see above). All samples lack a dominance of any particular clast shape, but show preference for locating towards the compact range of general shape diagrams (Fig. 6.22) (cf. Sneed and Folk, 1958). The uppermost samples (B/2C, B/3C) from ridge B-1 demonstrate a high proportion of compact blade (CB) and compact elongate (CE) shaped clasts. Sample N/1C contains a larger percentage of platy (P) and compact platy (CP) clasts than samples acquired from the other two sites. All samples occupy comparable ranges of the shape triangle.

Greater distinctions between samples are drawn when assessing clast provenance and roundness. Fig. 6.23 demonstrates that samples from all depths of the easternmost Bergastølen ridge display exceedingly high RA values (B/1C = 0.68, B/2C = 0.92, B/3C = 0.80) and low RWR values (B/1C = 0.20, B/2C = 0.00, B/3C = 0.00) indicating very low transport distances and/or passive modes of transport, whereas sample N/1C from the Nordålia section has a much higher proportion of rounded and well-rounded clasts (RWR = 0.24) and fewer very angular and angular clasts (RA = 0.10), suggestive of long transport or fluvial controls, which is in agreement with bulk sediment analysis (see above). Clasts sampled from the Hølsætra section show a relatively lower RA index value than the Bergastølen samples (0.44) but also exhibit a low RWR (0.04) and are instead mostly sub-angular, signifying intermediate transport distance.

Covariance plots of two shape indices (RA, RWR) against C_{40} (i.e., percentage of clasts with c:a axis ratios ≤0.4) reveal clear separations between clasts sampled from the Nordålia section and those obtained from the other sites (Fig. 6.24). Between the Bergastølen samples, the proportion of slabby/elongate clasts varies, though all plot high on the RA axis. H/1C has a relatively low C_{40} (i.e.,

predominantly blocky clasts) whereas N/1C occupies an intermediate range, though exhibits a high RWR which isolates it from the other samples on the covariance plot. B/3C (and to a lesser degree, B/1C and B/2C) plots far to the upper right of the RA/C_{40} diagram, possibly indicating that it contains a large component of passively transported materials. Ballantyne (1982) found that clasts sampled from Jotunheimen subglacial tills had characteristic aggregate form characteristics, ranging in C_{40} between 0.10 and 0.36. Samples from supraglacial debris, rockwall talus, and *in situ* periglacially weathered detritus occupied much higher C_{40} ranges (0.70 – 0.86, 0.18 – 0.48, and 0.66 – 0.88 respectively), implying that the level of "blockiness" in clast form is affected by transport history. Comparing the form of clasts sampled from ribbed moraine ridges in the Jotunheimen-Gudbrandsdalen area to the results presented by Ballantyne (1982), it is seen that the Hølsætra sample fits a typical pattern for subglacial deposits (i.e., a high proportion of blocky clasts), whereas the aggregate form characteristics of the Bergastølen samples are suggestive of subglacial deposits skewed by the incorporation of "slabby" supraglacial detritus.

The results of clast provenance analysis (Fig. 6.25) largely support interpretations derived from the above characterizations of shape and roundness. Samples B/1C, B/2C, and B/3C all contain ≥90% Jotun rocks (primarily gabbros, gabbro schists, gneissic feldspathic "jotunites", and a lesser component of pyroxenites and granitoid types; cf. Battey, 1965) (Fig. 6.23), indicating a large component of short transported materials within the coarse fraction of these sampled diamictons, which is matched by the high RA values for these samples. The Hølsætra and Nordålia sections are both geographically further from the edge of the Jotunheimen nappe and consequently display lower percentages of Jotun rocks in their composition (Fig. 6.23), however the latter lithologies continue to make up a significant proportion of these samples, constituting 64% and 50% of rock types respectively. High percentages of Jotun rocks within these diamicts points to the capacity for long-distance (e.g., >60 km) transport of materials within Norwegian tills, a characteristic which has previously been regarded as quite rare (Haldorsen, 1983).

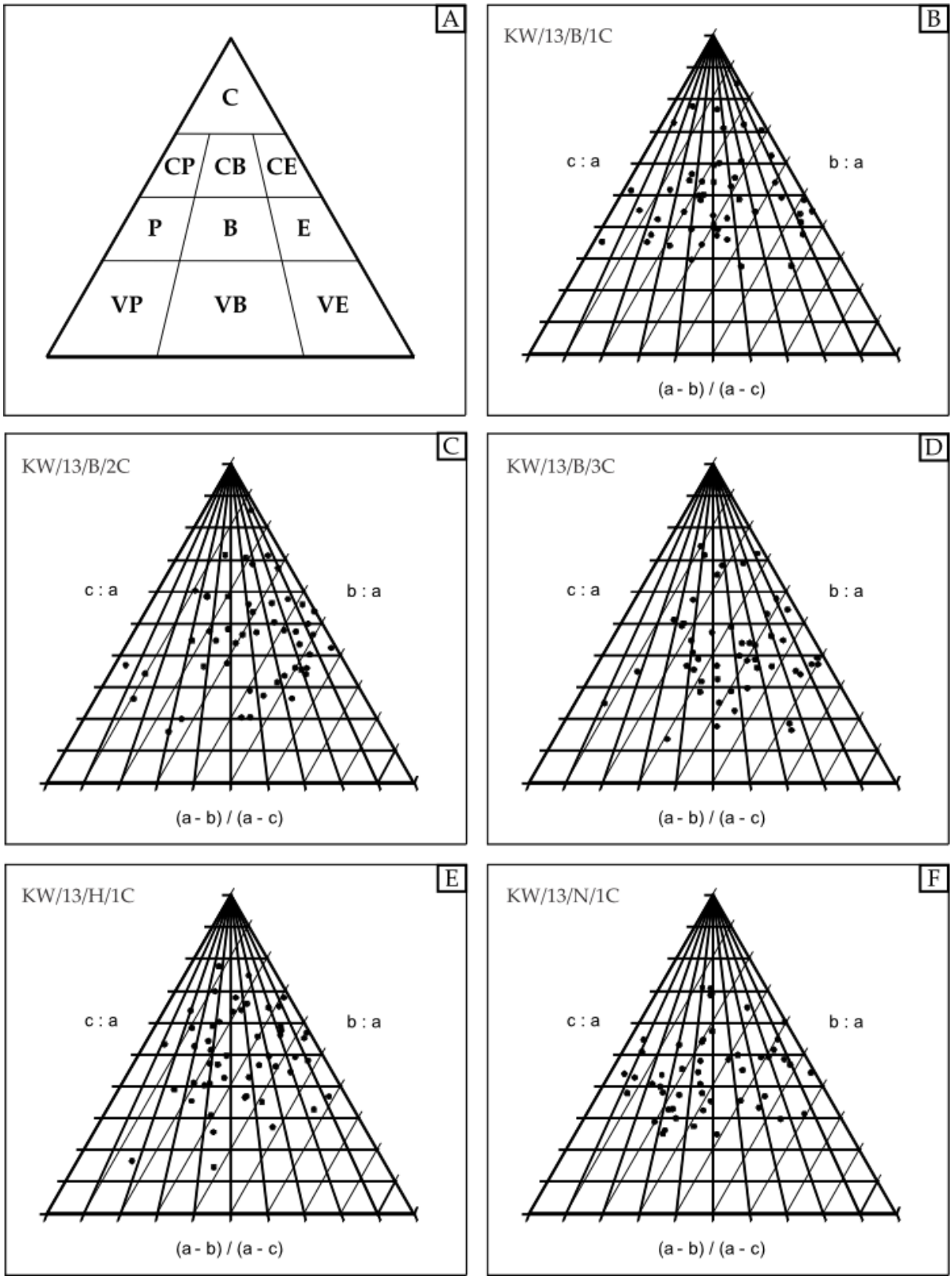

Fig. 6.22 – Ternary diagrams depicting general clast shape for 5 clast samples (*n* = 50) obtained from 3 ribbed moraine ridges in central South Norway. Partitioning of the diagram by shape is indicated in A. P = platy, B = blade, E = elongate, C = compact, V = very.

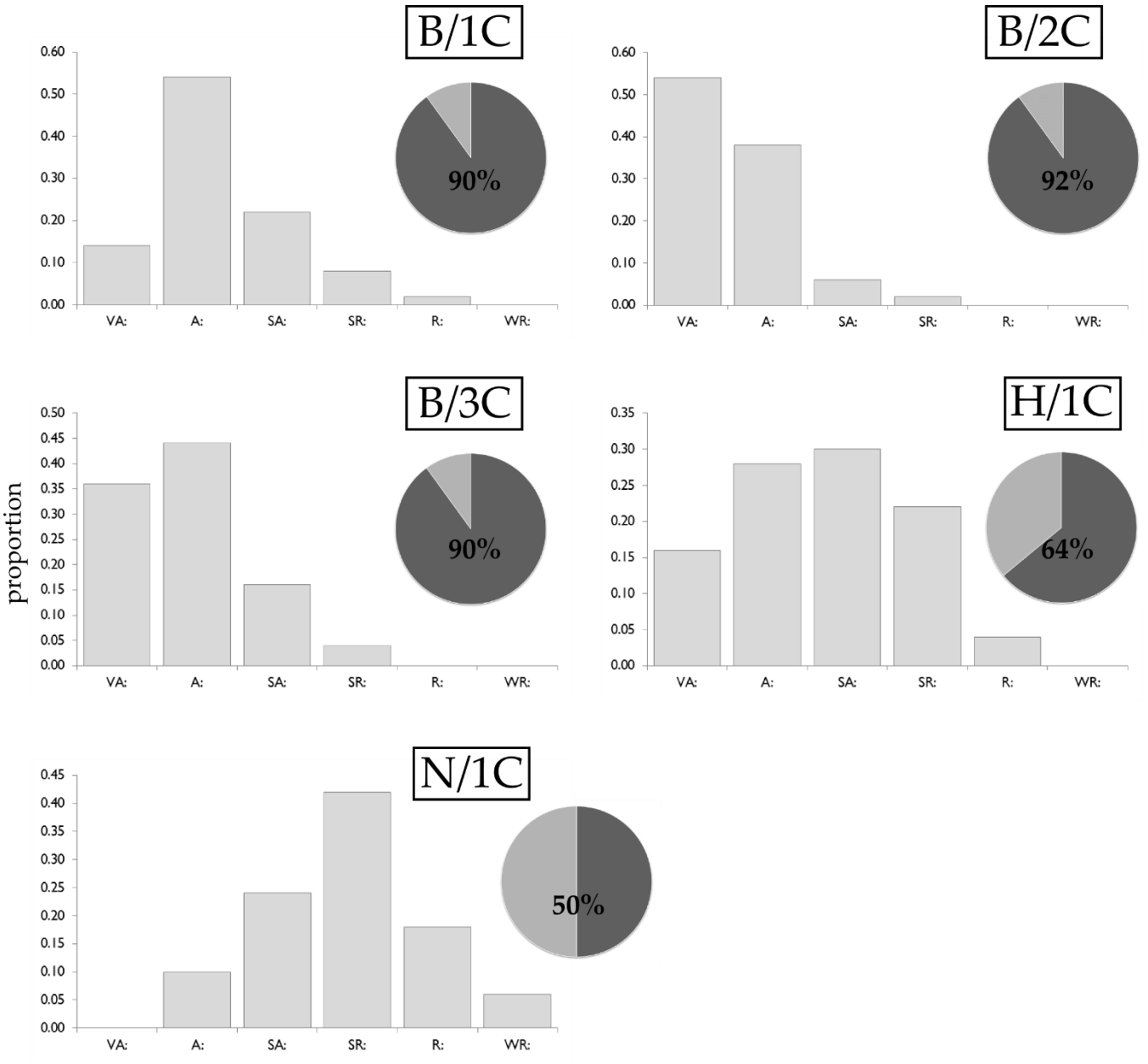

Fig. 6.23 – Histograms showing clast roundness for 5 clast samples (*n* = 50) obtained from 3 ribbed moraine ridges in central South Norway. Accompanying pie charts illustrate the percentage of Jotun lithologies (light grey) in each sample. VA = very angular, A = angular, SA = sub-angular, SR = sub-rounded, R = rounded. WR= well rounded.

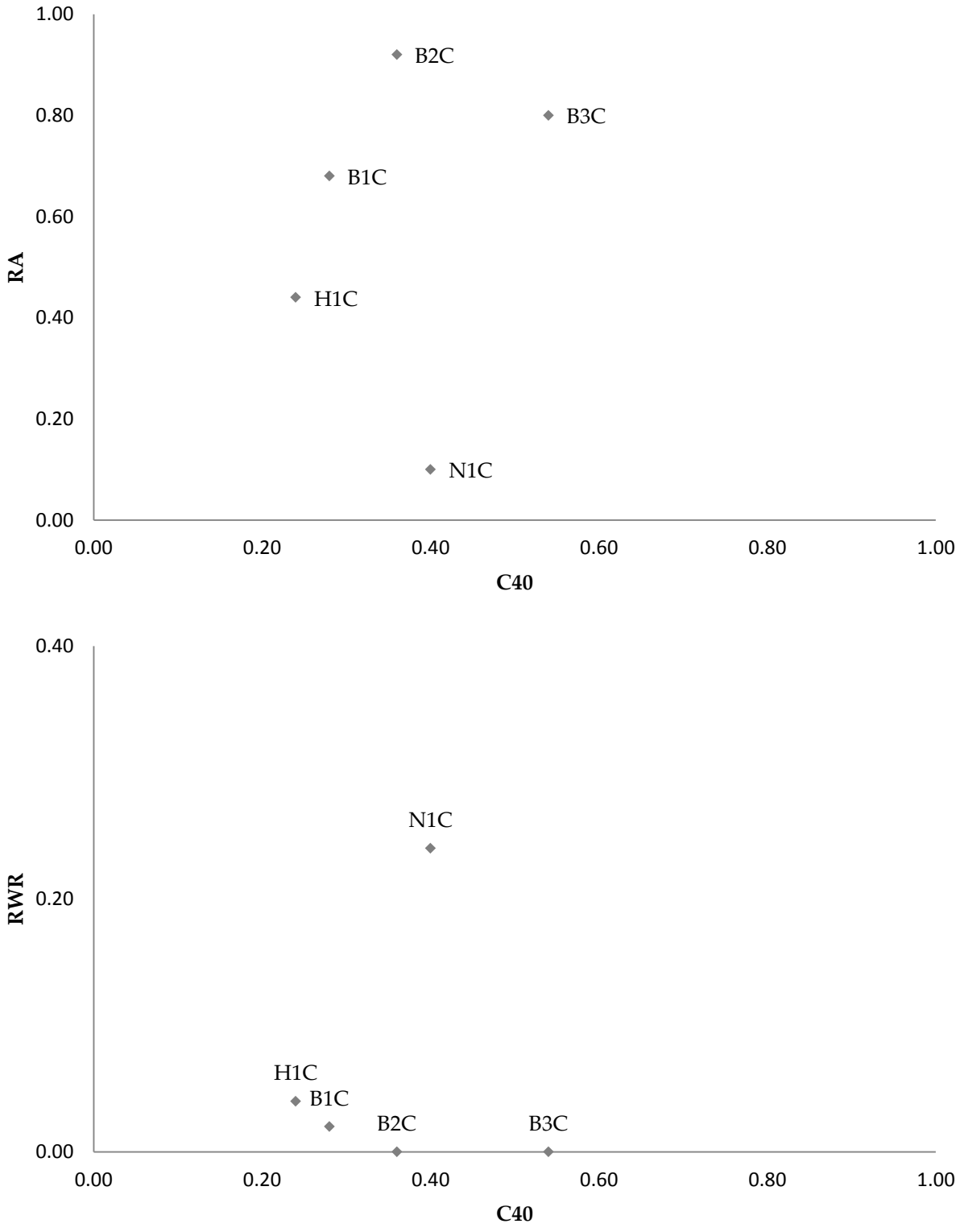

Fig. 6.24 – Shape/roundness covariance diagrams for 5 clast samples (n = 50) obtained from 3 ribbed moraine ridges in central South Norway. RA = % of very angular + angular, RWR = % of well-rounded + rounded. C_{40} = % of c:a ratios ≤0.4.

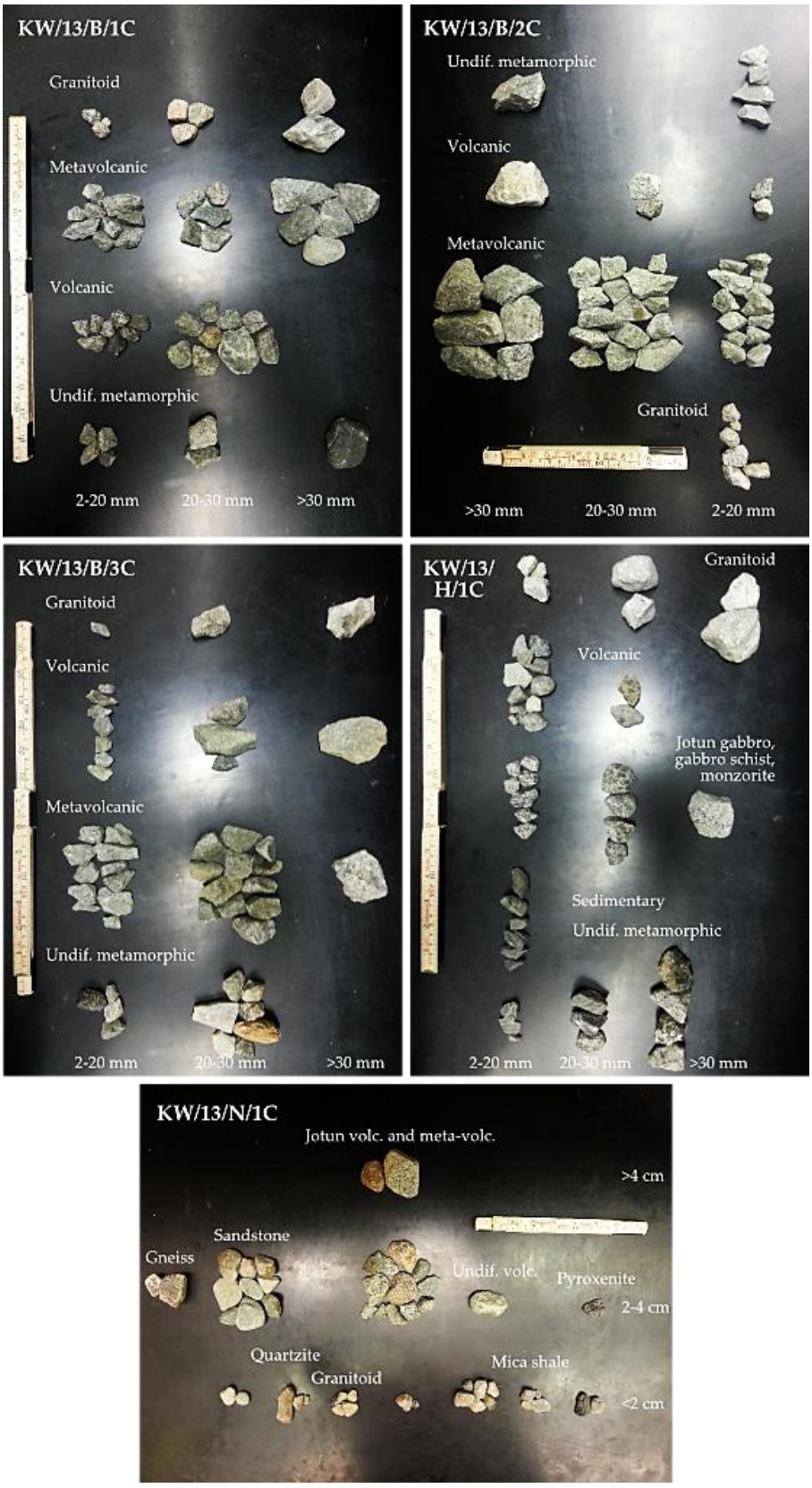

Fig. 6.25 – Photographs of clast samples, grouped by size and lithology/provenance determinations.

7. Discussion

Comprehensive mapping of ribbed moraines in southern Nunavut, Canada, and the collection of basic field data from central South Norway, has enabled a critical evaluation of the mode and timing of ribbed moraine formation with respect to the extent and chronology of the last continental ice sheets. Analysis of the spatial patterns displayed by these (and other) landforms within south-central Keewatin places new constraints on the glaciodynamic behaviour of the LIS throughout the Late Wisconsinan. Together these findings can be used within palaeoglaciology to support an improved empirical model of subglacial landscape evolution for the core regions of ice sheets.

7.1 *Mode and Timing of Ribbed Moraine Formation*

Based on the results of objective geospatial analyses presented in this thesis, it is now clear that any model of subglacial bedform genesis within low-relief core-zones of the Pleistocene ice sheets must account for:

- spatial clustering of ribbed moraines across large areas;
- spatial segregation of large and small ribbed moraines, and in particular, spatial autocorrelation of landforms with low ridge lengths;
- spatial correlation of large ribbed moraines with small glacial drift lineations (and *vice versa*);
- independence of both ribbed moraines and glacial drift lineations from regional topography in areas of low relief; coupling with topography in areas of high relief;
- high morphological diversity in areas of ribbed moraine clustering, and;
- strong spatial clustering of certain morphologies (e.g., minor, extensional), and dispersed distributions of others (e.g., hummocky, classical).

One explanation that can account for the majority of these findings is to consider that what have hitherto been referred to as "ribbed moraines" are, in fact, a polygenetic group of landforms, and that variations in their spatial and morphological properties stem both from differences in their initial mode of genesis, as well as the severity of subsequent reshaping processes. Evidence from southern Nunavut and central South Norway suggests that ribbed moraines are formed time-transgressively, and during multiple intervals throughout a given glacial cycle. Moreover, ribbed moraine morphologies identified in these areas locate along a continuum. This *morphological* continuum parallels – and derives from – a less tangible *process* continuum that determines the degree to which pristine ribbed moraine forms are reshaped. Results also suggest that there are quantifiable breakpoints in specific morphometric parameters that permit the discrete visual classification of ribbed moraine forms (i.e., that partition the morphological continuum), which – in areas of dense ribbed moraine cover – can be utilized as proxy criteria to retrace the evolution of basal ice/substrate interactions.

The existence of morphometric breakpoints is made clear by the ability to perspicuously group ribbed moraine morphologies into *morphotypes* according to explicit ranges of above-mode exponentional decay (λ) on semi-log plots (section 5.4.1.7). By this system of classification, M1 and M2 morphotypes are unique in that they each encompass only single morphologies ("classical" and "minor", respectively); this fact, in addition to the isolation of these morphotype clusters on PCA bi-plots derived from ribbed moraine length metrics (Fig. 5.59), suggests that these morphotypes may be each indicative

of ‘pristine’ ribbed moraine forms that arise through primary formational processes, and presumably each owing to unique formational conditions. Considering the dissimilarity in their wavelengths and physical dimensions (Fig. 5.52 and Fig. 5.57), and the differing relative age relationships they typically exhibit with other glacial landforms (section 5.4.1.2), the simplest assumption is that these are genetically divergent landforms that do not coincide in terms of these attributes. The largest (non-sedimentological) distinction between M1 and M2 morphotype ribbed moraines is undoubtedly their size and spacing, and hence it is possible that their geographic exclusivity in southern Nunavut stems from fundamental differences in their mode and timing of formation. Whereas M1 ribbed moraines are spatially widespread throughout the study area, M2 ribbed moraines are largely confined to a specific region east of South Henik Lake (though are found in more limited numbers elsewhere), and are intimately associated with, and consistently overprint, MSGL converging into Hudson Bay. Clustering of the M2 morphotype in this region is statistically significant and overshadows the clustering signal of other ridge lengths, based on calculated *G* statistics (section 5.4.1.4). In order to explain these separations in geographic distribution and relative-age relations, a spatially pervasive mode of subglacial origin is postulated for the M1 type below, and a genesis by late-stage, localized englacial thrusting – similar to those mechanisms proposed by Dyke et al. (1992) and Stokes et al. (2008) – for the M2 morphotype (see below).

Though the majority of existing models of ribbed moraine formation (section 3.4) could theoretically account for the expansive and apparently non-selective geographic distribution of M1 type ribbed moraines in south-central Keewatin, fewer are compatible with their full suite of attributes. First, considering that the study area features relatively low relief, and that the majority of ridges are distributed independent of topography (Fig. 5.26 and Fig. 5.27), the requirement that M1 ridges are shaped from precursor topographic obstacles (Boulton, 1987; Knight and McCabe, 1997; Moller, 2006; Finlayson et al., 2010; Knight, 2010), or are found only in areas of concave terrain (Lundqvist, 1989, 1997) must be discounted, unless these “obstacles” are inferred to represent stiff patches of pre-existing substrate. Evidence from northern Manitoba (Trommelen et al., 2014) also suggests that ribbed moraines are associated with spatial variability in drift thickness (see also Lundqvist, 1969, 1997; Wastenson, 1983; Knight, 2010), and hence fracture-and-extend models of ribbed moraine formation (Lundqvist, 1969; Hättestrand, 1997; Hättestrand and Kleman, 1999; Kleman and Hättestrand, 1999; Sarala, 2006), which incorporate no explicit mechanism for relief amplification, are not suitable for explaining the genesis and widespread distribution of M1 type ridges in nearby south-central Keewatin. An adequate solution must also be able to explain the mixture of both far travelled (e.g., Dubawnt Group) and local materials making up these ridges (Aylsworth and Shilts, 1989a,b), as well as high levels of inheritance as indicated by clast provenance trends in surficial tills (Trommelen et al., 2013).

With regard to the above considerations, the instability model of ribbed moraine formation (cf. Dunlop et al., 2008; section 3.4.4) appears to offer a plausible explanation of the geographic distribution and morphometric properties of M1 type ribbed moraines in southern Nunavut, and perhaps most importantly, when numerically assessed, produces realistic germinal ridge size and spacing (i.e., wavelength) dependent on localized discrepancies in pre-existing till thickness and bed drainage conditions – the latter of which must have been spatiotemporally variable and constantly evolving in order to generate and preserve intricate patterns of alternating exclusivity and co-location of ribbed moraines and streamlined landforms (section 5.4.1.2). Nevertheless, it is foreseeable that many workers would depart from this interpretation and instead favour one that caters to *pure* equifinality. More explicitly, is possible that the M1 morphotype *itself* is a polygenetic class of transverse subglacial landforms, and there may be a handful of processes capable of generating this single morphotype alone. Although this possibility is not ignored here, the existence of a *dominant* process (even if amongst

multiple processes) is expected in order to account for uniformity in M1 type bedform shape and patterning and uni-modal size-frequency distribution. In an analogous example, Clark (2010) distinguishes between "emergent drumlins", "drumlin clones" and "obstacle drumlins", wherein emergent drumlins arise from a (hypothetically) perfectly flat, pre-existing till sheet through a process of migrating interfacial instability in the coupled flow of ice and subglacial sediment. Obstacle drumlins (growing via agglomeration around bedrock protrusions) and drumlin clones (erosively shaped from stiff sediment patches) are acknowledged as secondary and/or localized modes of drumlin formation, however the emergent drumlin is characteristic of the "true" or "typical" landform, and is an expression of the self-organization of the subglacial bed.

Given extensive overlap in their morphometric characteristics, ribbed moraine morphotypes M3-A, M3-B, M4 and M5 are interpreted as products of varying degrees of drumlinization, overprinting, and modification of the primitive morphotypes (M1, M2) under evolving, polythermal subglacial (and/or later, post-glacial subaerial) conditions. Of these daughter morphotypes, M3-A and M3-B include ribbed moraines which develop directly from the M1 morphotype (or perhaps other landforms, e.g., drift lineations, in the case of the extensional morphology), though in most instances, these retain many characteristics of the parent ridge. Alternatively, M5 type ribbed moraines demonstrate little morphological resemblance to the parent morphotypes and probably either derive from more complete modifications of the bed, or construction in conjunction with patchy variations in substrate rheology. Evidence for the latter is found in certain M5 morphologies (i.e., barchan, upstream curving) which appear to have either resistant hinges or limbs around which the remainder of the ridge has been deformed, whereas lattice-type ribbed moraines are probably indicative of more regional-scale disparities in the competence of the bed (i.e., demarcating zones of transition between fast and slow flowing ice). Based on their irregular appearance, and especially the geographic distribution of the hummocky morphology, the M4 morphotype could derive from post-glacial modification of both parent and daughter morphotypes, probably most significantly by subaerial backwasting and downwasting/ablation, but also by the influence of ponded water given that these ridges are commonly found in poorly drained areas or in the center of shallow lakes.

All of the above daughter (non-parent) morphotypes are therefore interpreted to reflect a spectrum of secondary formational processes resulting from spatiotemporal migrations of hard (H), mobile (M), and quasi-mobile (Q) bed zones (cf. Menzies, 1989b) (Fig. 7.1). In this framework, parent morphotypes (M1, M2) are generated under Q bed conditions, preserved under H bed conditions, and modified under M bed conditions to generate the full spectrum of daughter morphotypes. Quasi-mobile (Q) beds, featuring contiguous patches of stiff and deforming substrate, are likely required to induce and propagate instability in the coupled flow of ice and pre-existing basal tills (i.e., M1 genesis), and also to generate localized zones of compressive ice flow in regions featuring low topographic relief (i.e., M2 genesis). In areas where Q beds transition to H beds (i.e., frozen, or de-watered), parent morphotypes will be preserved, whereas a transition to a fully mobile (M) bed will motivate reorganizations of the substrate, often in the form of drift streamlining and partial or complete destruction of pre-existing morphology. Subsequently, daughter morphotypes are produced and can be similarly modified and/or preserved in response to the translation of rheological properties within the bed. The consideration of migrating substrate "regimes" within a deforming bed model has been outlined previously in van der Meer et al. (2003), though the concept is upscaled here to describe the spatial patterning of bedforms which are generated at this interface.

Multivariate analysis of 10 ribbed moraine length metrics derived from size-frequency distributions in south-central Keewatin suggests there are isolatable and potentially quantifiable processes underlying ribbed moraine formation, implying much potential work for future modeling

studies. Plots of ribbed moraine morphology against principal components derived from these metrics show unambiguous clustering of the 6 identified morphotypes (Fig. 5.59), wherein PC1 – which captures the majority of variance within the dataset – reveals apparent utility as a compression/extension index. Morphotypes with high scores on PC1 (e.g., extensional) are those which are theoretically *modified* under purely extensional ice flow regimes, whereas those with low PC1 scores (e.g., minor) presumably require a source of compressive flow to induce their formation. Morphotypes that locate near the center of the PC1 axis (e.g., classical) show relatively equal influence from compressive and extensional flow regimes, as would be expected from a migrating waveform instability.

With reference to the standard Couloumb-Navier equation:

$$\tau_{crit} = C + (P_n - P_w) \tan \Phi$$

where τ_{crit} is critical shear stress, C is the cohesive resistance of the substrate, P_n is the component of normal stress (equivalent to the sum of ice and sediment overburden pressures), P_w is the internal porewater pressure of the substrate, and $\tan \Phi$ is the angle of internal friction, it can clearly be seen how two processes – de-watering, basal freezing – can have significant impact on the strain response of the bed to a persistent glacial driving stress, and could potentially influence the migration of "bed zones" in a subglacial deforming bed mosaic. Whereas substrate de-watering (e.g., affected via porewater evacuation and switches in the routing of basal meltwater drainage systems) facilitates a lower P_w (and hence augments the effect of P_n), *in situ* freezing of interstitial porewater contributes to increased C, though both phenomena (under hypothetical steady state stress transmission) would result in the development of a stable/non-deforming bed by increasing τ_{crit}. In the latter scenario, vertical and lateral migrations of a subglacial freezing front would facilitate expulsion of porewater into peripheral sediments, hence increasing P_w and lowering τ_{crit} along this fringe, and enabling deformation of the surrounding substrate once τ_{crit} (i.e., the sediment yield strength) falls below driving stress. Conversely, increased basal drag associated with a de-watered or adfrozen ice/bed interface would promote overlying sticky/sluggish ice flow and ice movement primarily by ploughing or internal deformation, respectively. If multiple frozen and/or de-watered sediment patches/nuclei were to arise across the bed due, for instance, to transient water pressure gradients (Engelhardt and Kamb, 1997; Kavanaugh and Clarke, 2001), climatic deterioration, localized ice thinning, or a reduction in frictional heat generation at the glacial sole (Christoffersen and Tulaczyk, 2003), then it is reasonable to envision that a patchwork mosaic of stable/non-deforming and deforming bed regions would manifest, with implications for the spatial expression of subglacial geomorphology.

Thus, it is argued that processes of ribbed moraine genesis, modification and preservation in south-central Keewatin are constrained by evolving basal thermal regimes, substrate porewater contents, and bed rheologies, and as a corollary, that the extant spatial and morphological signature of these bedforms provides useful information regarding palaeoglacial dynamics. Patchwork networks consisting of alternating areas of stable and deforming substrate have been previously described for Pleistocene locations in the literature (Krzyszkowski, 1994; Piotrowski and Kraus, 1997; Knight, 2002, 2010; Jørgensen and Piotrowski, 2003; van der Meer et al., 2003; Larsen et al., 2004; Piotrowski et al., 2004, 2006; Tylmann et al., 2013), and it is proposed here that the local-scale variability in substrate rheology they engender may be a contributor to the development and propagation of coupled ice and subglacial till instabilities. These "subglacial bed mosaics" have also been inferred from seismic investigations of the contemporary West Antarctic Ice Sheet, and there definitively linked to active bedforming processes (Smith and Murray, 2009). Several authors have asserted linkages between subglacial bed mosaics and ribbed moraine genesis (Knight, 2010; Trommelen et al., 2012; 2013) – most recently, Trommelen et al.

(2014), who attribute inherited till signatures and patchy drumlinization of ribbed moraine fields in northeastern Manitoba to selective preservation under transient sticky bed conditions. This model is adopted here as it does well to describe the spatial properties of bedforms in south-central Keewatin also.

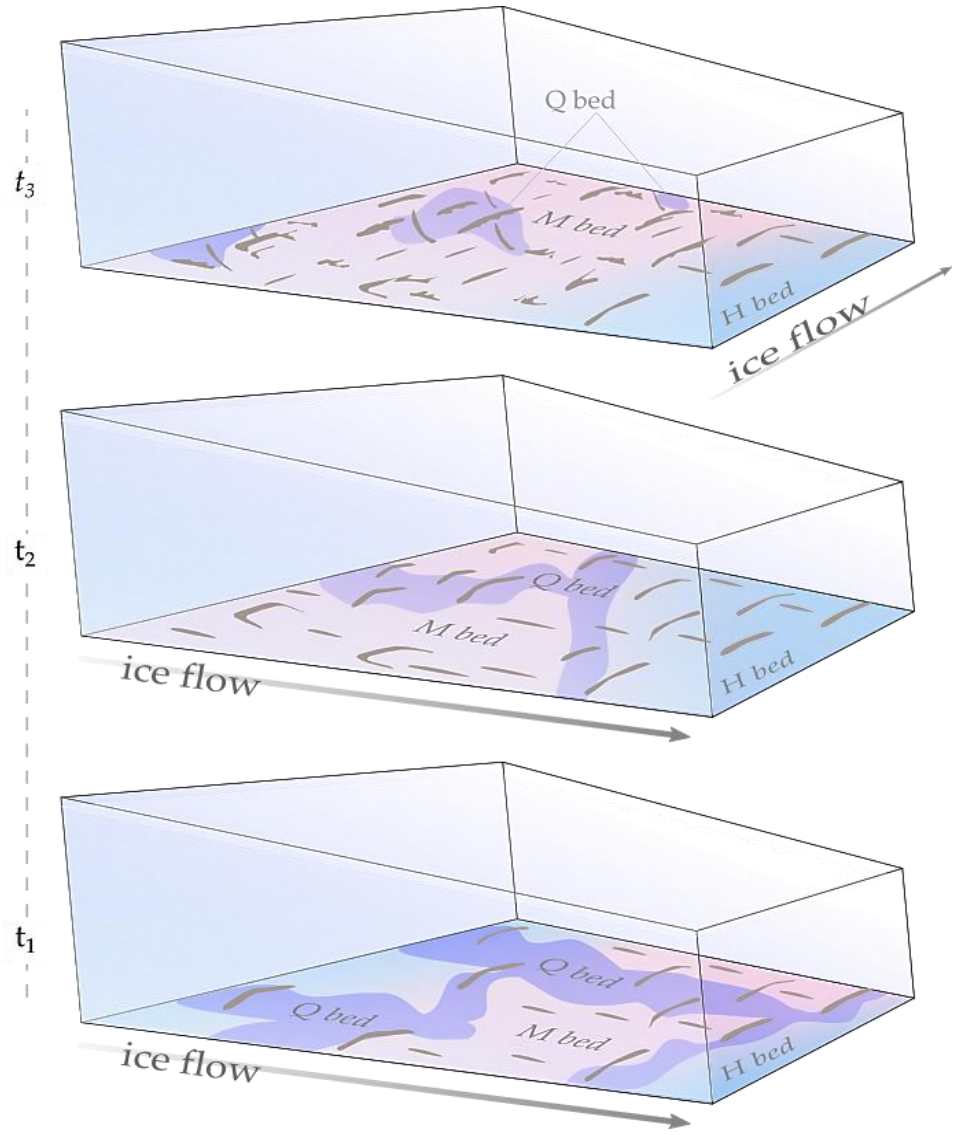

Fig. 7.1 – Conceptual diagram illustrating the generation and modification of M1 type ribbed moraines under a transient subglacial deforming bed mosaic. Partitioning of bedforming processes at t_1 reflects local-scale variations in properties of the bed, with ribbed moraines forming under quasi-mobile (Q) conditions and drift lineations under mobile (M) conditions. Evolution of the subglacial bed mosaic at t_2 facilitates production of new bedforms and streamlining/modification of pre-existing M1 type ribbed moraines within M bed zones. Bedforms generated at t_1 are preserved *in situ* under immobile (H) bed conditions. A shift in ice flow direction in conjuction with the continued translocation of bed zones at t_3 produces a patchwork of selectively preserved and modified flow parallel and transverse bedforms within close proximity. The duration of sustained flow and the magnitude of ice flow directional change determine the path of parent ribbed moraine transition into one of several daughter morphotypes.

7.2 *Were Ribbed Moraine Generating Processes Similar in Central Canada and Scandinavia?*

One difficulty surrounding the instability model of bed-formation is that it does not yield particularly useful constraints on the sedimentology and structure of bedforms. Moreoever, the tremendously variable composition of ribbed moraines in field studies (section 3.3) confounds any attempt to associate unique internal properties with such an overarching/universal process. For instance, if pre-existing sediments from which instability-generated bedforms are developed contain earlier-formed structure or stratigraphy, it is possible that these could be retained within bedforms, despite lacking any actual bedforming process relationships (e.g., Clark, 2010). Unfortunately, results of field investigations from ribbed moraine sections in central South Norway presented in this thesis do little to resolve this particular debate. Specifically, the interpretations offered (below) for ribbed moraine genesis in these locations are the simplest arguments that fit the available evidence, however they depart somewhat from those which best explain the south-central Keewatin population based on spatial/morphological reasoning alone. Given, however, that the instability model does not prescribe any diagnostic structures or facies associations, this is not to say that the present observations will not later be most satisfactorily explained within a subglacial deforming bed mosaic and till instability framework, should models become capable of accounting for variation in bedform structure and stratigraphy. Overall, however, results from this thesis suggest that there were possible inherent differences in bedforming processes beneath the central Laurentide and Fennoscandian ice sheets (despite similarities in till properties and underlying geology, see section 6.1), and that these differences are quite probably relatable to contrasting topographic relief.

The sedimentary sequence revealed in section at H-1, a hummocky (M4 morphotype) ribbed moraine ridge examined at the Hølsætra site in central South Norway, contained a predominantly gravelly-sandy till with high compaction, and faint and sporadic horizontal stratification in lower units, transitioning to a looser, sandier till with minor inverse grading at lesser depths. This till contains parallel dipping units of alternating sand and silt, as well as lenticular inclusions of sorted fine silts and gravels, each of which are sheltered in lee-side positions behind or beneath large, sub-angular boulders embedded within the ridge. In all instances, sorted bedsets and interlaminated sorted deposits do not continue outside of the vertical projection of overlying/adjacent boulders. The uppermost till, occurring beneath a silty boulder-rich soil carapace at the surface, is better consolidated relative to immediately underlying mid-sequence tills, despite experiencing lower sediment overburden pressures. The bulk matrix (<2 mm) grain-size distribution of lower-sequence diamictons, and shape indices of clasts (~2/3 of Jotun provenance) from the uppermost diamicton in H-1 fall well within accepted ranges for typical Norwegian subglacial tills (Jørgensen, 1977; Ballantyne, 1982 – see sections 6.4.4 and 6.4.5). Hence, there are converging lines of evidence to suggest that the primary sediments forming ridge H-1 were initially emplaced along a subglacial interface, and that a significant component of coarse fraction (>2 mm) materials were sourced from the nearby Jotunheimen range and transported/shaped within a subglacial traction layer.

The presence of both lenses and thin stratified units of sorted materials throughout H-1 provides probable indication of switches between pipeflow and thin sheet-style meltwater drainage during the process of ridge formation. Given a decisive lack of macro-scale internal deformational structure, it is likely that the bulk ridge materials were syndepositionally homogenized, and that the sorted sediments were intermittently deposited by transient discharges of subglacial meltwater. The preservation of laminae/current structures within the sorted sediments implies that the latter units were either: a) deposited in channels/sheets as cut-and-fill sequences below a shallowing thin-skin deforming layer, b)

deposited at the subglacial interface during conditions of relaxed ice/bed coupling, c) syngenetically deposited as meltwater scours alongside unsorted materials in a process of subglacial melt-out (see below), or d) deposited and shielded from principal driving stress during till emplacement in the lee of adjacent boulders within an active subglacial deforming layer. One constraint on scenario b) above, however, is that ice/bed recoupling following interfacial meltwater drainage would generate a sharp (i.e., erosive) or deformed contact to overlying tills in the sequence (e.g., Lindén and Möller, 2005), and this is not observed in the Hølsætra sections. If the lenticular sorted units are alternatively interpreted as soft-sediment intraclasts, it could also be argued that they were scavenged and transported within an actively deforming bed while in a frozen state (cf. Menzies, 1990; Larsen et al., 2004), though neither plow marks nor evidence of peripheral dewatering structures are observed and thus this interpretation is not applicable here.

Slight gradations in till matrix texture and level of compaction upwards throughout the profile are likely explained by differential tractive mobile sediment loads and fluctuating rheological responses to evolving subglacial stress regimes. Incremental shear stiffening of the low-sequence tills (i.e., wherein effective normal pressure exceeds the shear strength of the substrate) is implied by their compaction, crude parallel stratification, and the irregular clustering/imbrication of clasts which dip slightly in an ice-proximal direction, however Shaw (1979) has interpreted similar tills as resulting from subglacial sorting due to basal melt-water activity. Compaction and porewater dissipation from this unit likely proceeded alongside cumulative till accretion which would have fostered the development of a rigid, impermeable substrate, and conditioned high compressional stresses leading to enhanced sediment porewater pressures and more pervasive deformation within overlying deposits (i.e., hence the homogenized character of tills above the bottommost unit 1). High subglacial pressure gradients would be expected in such a location, with ice funneling into the valley from the Finnbølshaugen-area uplands. Upon encountering this zone of compressional stress in the presence of high porewater pressure, the accreting substrate probably responded by shear thickening which may have been responsible for initial relief amplification of the ridge.

The absence of distinguishing attributes within H-1 tills thwarts any effort to reconstruct a detailed constructional history for the ridge based on its (lack of) internal diagnostic properties, though it is possible either that these deposits were subjected to repeated, pervasive and/or distributed shearing such as to extinguish most macro-scale sedimentary structures, or that the exceptionally coarse-grained nature of the till matrix, especially if under conditions of low effective normal pressure (e.g., high porewater pressure), simply did not have the competence to retain said structures incipiently. Alternatively, the absence of glaciotectonic and/or deformational markers (e.g., thrust faults, folds, boundinage structures, augens, etc.) could be utilized as basis upon which to obviate consideration of prolonged emplacement by lodgement and/or plastering (at least within the mid-upper sequence units), thereby necessitating deposition under conditions of relaxed ice/bed coupling, or via a "passive" subglacial melt-out process. Indeed, the "blockiness" and frequently faceted surfaces of clasts sampled from within unit 5 are indicative of an active subglacial transport history, however there is abundant evidence from the literature to suggest that elevation of materials from the ice/bed interface into englacial and supraglacial debris pathways is a common phenomenon and is affected in a variety of settings; e.g., by adfreezing (Weertman, 1961; Alley et al., 1998; Lawson et al., 1998; Roberts et al., 2002; Larsen et al., 2006) and folding and thrusting (Boulton, 1970b, 1972), and/or englacial shearing (Hambrey et al. 1997, 1999; Bennett et al. 1998; Glasser and Hambrey, 2003). As the relief of the proto-ridge initially grew via till accretion at the subglacial interface, it is probable that the debris elevation mechanism was intensified as stress on the up-ice face of the protuberance increased, resulting in the thick sequence of unit 5 tills in H-1. Importantly, in the absence of a discontinuity indicating thrust or

slip along a fault, it is assumed that basal debris was pushed atop and laterally around the proto-ridge in a process of continuum flow wherein motion was entirely accommodated by distributed strain, thus leaving little evidence as to the direction or magnitude of shear. Although increased effective pressure inhibits the flux of subglacial till, this is compensated by the heightened basal shear stress required to discharge the ice flow around the protuberance, allowing till flux to increase in the presence of high normal pressure (Schoof, 2007; Fowler, 2009). This mechanism has been linked to the propagation of dynamic instabilities and ribbing patterns at the bed of the Thwaites and Pine Island Glaciers in Antarctica (Sergienko and Hindmarsh, 2013). Given their vague, patchy foliation, the existence of undeformed sandy-silty and sandy-gravelly lenses and interbeds (some of which show disrupted draping over boulders), and absence of deformational structures, it is suggested that the upper sequence tills (unit 5) at the Hølsætra site were deposited from the base of a stagnant ice mass. Similar sequences of diamicton and interlaminated sorted sediments, and in particular, associations of boulders and underlying pockets of undeformed, sorted materials, have also previously been cited as exemplary characteristics of subglacial melt-out deposits (Shaw, 1979; Lawson, 1981; Haldorsen and Shaw, 1982; Shaw, 1982; Piotrowski and Tulaczyk, 1999; Munro-Stasiuk, 2000). Winnowing of fines from these upper tills throughout the ablation process could explain the vague inverse grading in this upper sequence.

Aggregating elements of the above discussion, the interpretation favoured here is that H-1, and immediately adjacent ribbed moraine ridges, were generated by a series of processes involving a progression from lodgement leading to subsequent till emplacement by shear thickening and ductile accretion above the traction layer, and late-stage ablation in a stagnant ice environment. Although the high hydraulic conductivity of these coarse grained tills would have facilitated relatively efficient drainage, localized failure and remobilization likely occurred under fluctuating conditions of increased porewater pressure (perhaps due to intermittent freezing/thawing) because mixing within units is extensive and stratification discontinuous. Implicit in this interpretation is that the ice bed underwent a transition from mobile to immobile conditions that may have been associated with widespread ice thinning and stagnation as has repeatedly been cited as a significant contributor to deglaciation in the Jotunheimen and surrounding highland areas (Garnes and Bergersen, 1980). Möller (2010), Minell (1980) and Shaw (1979) have inferred melt-out origins for ribbed moraines throughout Sweden, though each of their models postulate formation in near-marginal environments and/or implicate glaciotectonic thrusting processes. The interpretation of the Hølsætra ridges that is presented here differs from these models in that compressive flow is thought to be generated within an interior location, and driven both by local topography in addition to changes in the rheology of the bed, with relief amplification owing to accretion of the bed rather than to tectonic thrusting. It is stressed here that melt-out is not perceived as necessarily significant in the constructional process of the ridge, but imparts a signature to the uppermost units and could otherwise be regarded as a "draping facies", which is perhaps more instructive to determining ridge preservation processes.

Ridge B-1 at the Bergastølen site (a "minor" ribbed moraine of M2 morphotype) revealed a composition consisting primarily of coarse-grained, (macroscopically) massive and structureless tills (i.e., facies 1), similar to those found in ridge H-1. As in the lower unit of H-1, however, crude foliation is observed (i.e., facies 2) in places, here beginning ~65 cm from the base of the upper section, though is made difficult to discern due to the ridge's high boulder content. Anticlinal draping of matrix materials and '*en echelon*' clast arrangements are occasionally observed on top of larger boulders in the upper units. Nevertheless, several characteristics of the B-1 exposure do prove distinctive from H-1, including the lack of cohesive sorted inclusions, and the presence of facies 3, a slightly finer grained, well-consolidated till exhibiting a fissile structure, at roughly 0.5–1 m depth below surface. The B-1

sedimentary sequence thus displays many features also observed in the Hølsætra sections, though differs in the presence of facies 3, and the morphology of clasts sampled from throughout the exposure. Clasts sampled from ridge B-1 (samples B/1C, B/2C, B/3C) are highly angular and, while primarily blocky, are skewed by the incorporation of slabby morphologies. All three clast samples from B-1 demonstrate similar high RA values, although the lowermost sample (B/1C, obtained from facies 1 near the base of the upper section) includes a lower ratio of "very angular" to "angular" clasts. High RA/C_{40} co-variance values have been traditionally linked to supraglacial debris and/or otherwise passively transported coarse-fraction deposits (Ballantyne, 1982; Lukas et al., 2013) and, likewise, these samples are interpreted here as reflecting similar transport histories. Frost shattered clasts embedded within subsurface tills at B-1 and B-2 provide additional evidence of prior supraglacial transport. Such materials were likely sourced as rockfall/talus from valley walls by macrogelivation and deposited onto the glacier surface once Jotunheiman peaks became exposed as nunataks throughout the process of ice sheet thinning, however properties of the till matrix, occasional faceting and mixed C_{40} values of clasts suggest these materials were temporarily transported within basal ice. Mechanisms for the lowering of these deposits through the ice include burial above the equilibrium line, sinking and attenuation during extending flow, and deposition into open crevasses. Although clasts throughout the ridge profile are overwhelmingly of Jotunheimen provenance (Fig. 6.23), boulders draping the surfaces of ridges (and surrounding "cover moraine") – at each of the Bergastølen, Hølsætra, and Nordålia study sites – are primarily of local lithologies, demanding that a mechanism exist to excavate and exhume blocks of locally derived materials at the surface. Similar boulder draping of ribbed moraines is widely reported from other locations (Ives, 1956; Lundqvist, 1958; Henderson, 1959; Shaw, 1979; Aylsworth and Shilts, 1989; Sarala, 2007; Möller, 2010; Sutinen et al., 2010; Trommelen et al., 2012, 2014). In low relief terrain, such as the south-central Keewatin study site on the Canadian Shield, blocks were likely plucked up-ice and thrust into englacial positions over stable bed patches, where they were lowered during subsequent surface ablation. In higher relief terrains, like the Jotunheimen-Gudbrandsdalen area, a similar mechanism could have been affected, though initial plucking would be aided by sharper subglacial pressure gradients at valley heads.

Micromorphological analysis of facies 3 sediments revealed a unique suite of microstructures suggestive of a transition from moderate to low internal pore-water content. Single and multiple direction lineations, grain fractures and edge-to-edge grain crushing are mapped throughout the examined thin section, and in places, lineations cross-cut ductile structures, including grain stacks and rotation structures, implying a transition from ductile (i.e., high porewater) to brittle (i.e., de-watered) conditions. The fissile macro-structure of this facies may also be an indicator of such transition, as it has earlier been argued that fissility planes in till not only accommodate shear strain, but also the evacuation of porewater under high pressure gradients (van der Meer et al., 2003). Edge-to-edge grain crushing events are commonly found near the apex of necking structures suggesting compression of the sediment package under ice load following de-watering. Clay translocation structures and skelsepic fabrics are abundant throughout the thin section. Occasional iron/manganese staining around clasts is observed in both micro- and macro-scale observations. Clast macrofabrics sampled from this unit (in both B-1 and B-2) revealed moderately strong clustering in a direction perpendicular to ridge long axes, with a preferred up-ice dip. In light of these observations, facies 3 is interpreted as a remnant deposit of a thin subglacial traction layer (e.g., analogous to "horizon B" in Evans et al., 2006) emplaced following short-lived reactivation of an immobile ice mass which functioned to rework underlying ablation deposits. Overlying sediments were likely subject to pervasive shear and incorporated in this remobilization phase as dilatant horizons (e.g., A, or A/B in Evans et al., 2006) from which pore water was subsequently drained, and clays (and later iron/manganese oxides) eluviated into underlying facies 3 during final

stagnation and subaerial exposure. Clustered clast macrofabrics amid melt-out sequences are often the result of subsequent reworking (Brodzikowski and van Loon, 1990), and the fissility of this unit implies emplacement under high subglacial pressures.

It is not clear from the Bergastølen site whether this inferred remobilization phase belongs to the same stage as the ridge building process. Large offsets in orientation of the Bergastølen ribbed moraines compared to nearby surrounding landforms (e.g., the Storjerner ribbed moraine field, and drift lineations over encompassing plateaus) suggests that geomorphorphic products from multiple ice flow phases are preserved in this location, however non-glacial sediments are not reported from any of the study sites, despite suggestions by Johnsen et al. (2012) of OIS 2 interstadial conditions extending to central Norway. Nevertheless, older sub-till waterlain sediments (of potential Middle Weichselian age) are known from immediately surrounding localities in Mid-Gudbrandsdalen (Bergersen and Garnes, 1981), though none have been uncovered in south Gudbrandsdalen, southeast of Jotunheimen, which might imply continuous Weichselian ice cover in these interior mountain valleys (e.g., Vinstri-Bygdin), as is featured in earlier reconstructions (e.g., Lundqvist, 1992; Mangerud, 2004, 2011). Thus it is probable that sequential flow phases played out in this area under continuous ice cover, and that the preservation of the Bergastølen bedforms was due either to their proximity to the Late Weichselian ice divide and/or protection under cold-based ice (see Fig. 6.4). The orientation of Bergastølen ribbed moraines match broadly with Middle Weichselian flowlines in Vorren (1977) and subsequent protection is afforded by a sub-divide LGM position in that reconstruction. Ribbed moraine orientations at the Hølsætra and Nordålia sites are aligned with Preboreal flowlines in Vorren (1977), though an inland ice maximum phase in Garnes and Bergersen (1980) (see Fig. 6.3 and Fig. 6.4). The latter authors also suggest active ice flow in the Vinstri-Bygdin river valley through mid-stage (last) deglaciation, offering the possibility that the Bergastølen ridges are entirely Late Weichselian features. Indeed the potential exists for abrupt changes in the orientation of ice flow indicators over short distances in areas where ice movement is strongly controlled by topography. In the absence of geochronological dating, the timing of ribbed moraine formation in central South Norway must be left unresolved.

7.3 *Implications for Palaeoglaciology of the Central Laurentide Ice Sheet*

New insights into bedforming processes beneath Pleistocene ice sheet interiors presented in this thesis can be used to form more complete understandings of subglacial landscape evolution in areas where comprehensive bedform mapping has been performed. The ability to link assemblages of bedforms (e.g., eskers, glacial drift lineations, and ribbed moraines exhibiting a continuum of morphologies) to specific conditions at the ice/bed interface during formation and/or reshaping allows the geomorphological record to be utilized in detailed bottom-up reconstructions of ancient glaciodynamic regimes and their transformations. When combined with information on the relative chronology of individual ice flow events gleaned from flowset groupings and cross-cutting/overprinting relationships, a relatively robust picture of regional-scale glacial history emerges.

Analysis of the mapped bedform record in south-central Keewatin reveals a collection of "zones" with internally-consistent glacial histories. Trommelen et al. (2012) recognize a similar zonation in the ice flow indicator record of northeastern Manitoba, and have developed the concept of "Glacial Terrain Zones" (GTZs) to explain fragmented, high-inheritance subglacial landscapes in that area. The GTZ paradigm is adopted here for the purposes of this discussion, as it does well to explain similar complex landscape patterns within southern Nunavut (Fig. 7.2). Trommelen et al. (2012) define three fundamental types of GTZ: Deglacial, Palimpsest and Relict. Three additional templates – Stagnation, Erosive, and Ice Streaming – are utilized here to more fully characterize the present study area. Whereas

the original GTZ categories are classified according to their extent of landscape inheritance vs. overprinting, the latter are instrumental in relaying "dominant" signatures preserved within each zone.

Palimpsest terrains are common along the periphery of former ice divides where they record shifts in ice flow direction and the position of dispersal centers through re-moulded or cross-cutting landform signatures (e.g., Clark, 1999). Palimpsest GTZs are found in south-central Keewatin in the vicinity of the Thlewiaza River between Nueltin and Edehon lakes (GTZ *D*), and in a small patch immediately below Ennadai Lake (GTZ *B*). These GTZs contain concentrated assemblages of M3-A and M3-B (modified) type ribbed moraines and strong imprints from several pre-deglacial *lins* flowsets (e.g., *lins*4 in GTZ *B*, and *lins*6, *lins*7, *lins*12, *lins*14, and *lins*16 in GTZ *D*). Fragmented patches of pre-deglacial flowsets are, in fact, observed throughout the entirety of the study area (section 5.4.2), though elsewhere do not comprise dominant landscape-forming components (whereas they are defining characteristics of GTZs *B* and *D*). In both palimpsest GTZs, eskers drape older streamlined landforms at oblique angles and deglacial flowsets are, in places, superimposed on older landforms. In order to preserve a diachronous landform record within a confined location, younger ice flow phases must have had limited erosional capacity in these areas, and bedforming events must have involved rapid fluctuations between M and Q bed conditions, with selective final preservation under frozen and/or de-watered H bed states throughout deglaciation.

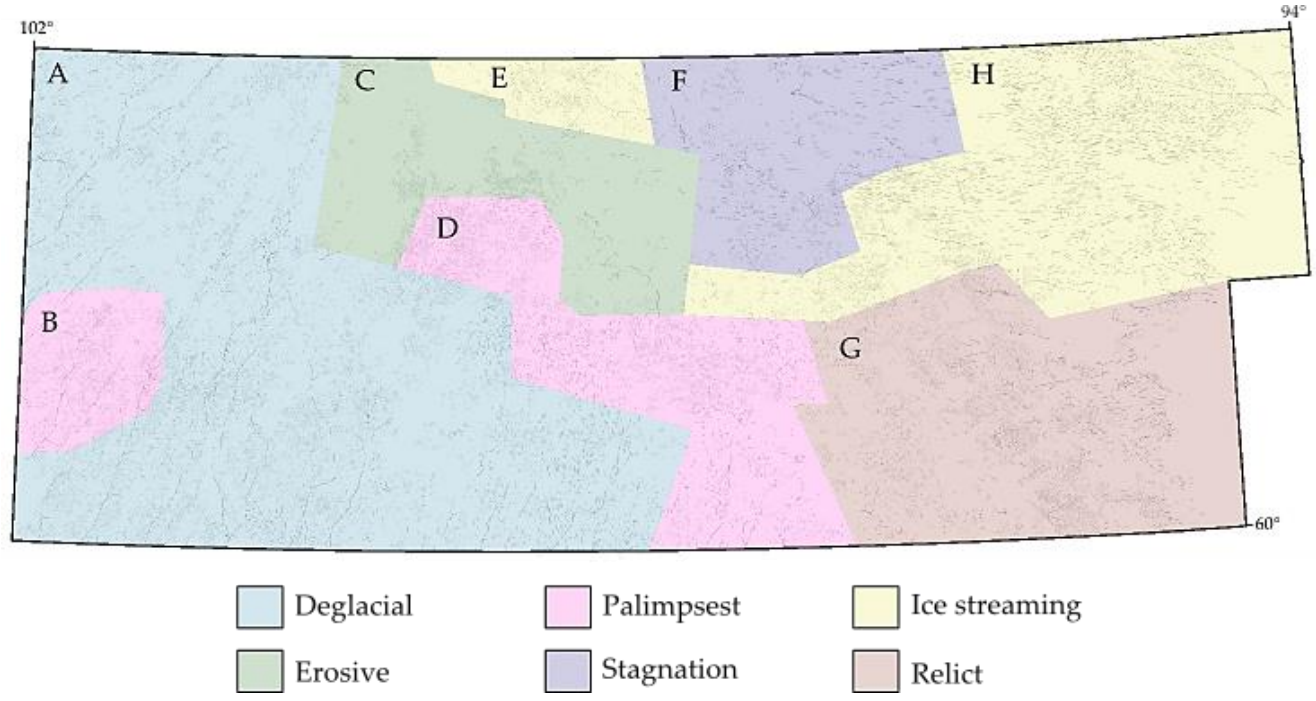

Fig. 7.2 – Glacial terrain zones (GTZs) identified in south-central Keewatin (labeled A through H), each delimiting portions of the study area that demonstrate internally-consistent glacial histories. GTZs are classified by dominant landscape signature.

In contrast to glacial palimpsests, which support a mixture of young and old ice flow indicators, relict terrains comprise areas in which the geomorphological signature of old ice flow phases is over-represented. Relict surfaces are those which contain landscape elements (e.g., tors, blockfields, etc.) formed under different geomorphological or environmental conditions than prevail in present times

(Battiau-Queney, 1996), however the term has been extended to refer to glacial landscapes that survive unmodified throughout one or more glaciations or ice flow phases (Lagerbäck, 1988b; Kleman et al., 1994, 1999; Goodfellow, 2007). Bedform imprints of ice flow phases B through D (section 5.4.2) in the southeastern corner of the study area are preserved within relict GTZ *G*. The SE-trending flowsets encompassed within this GTZ have traditionally been interpreted as deglacial features (e.g., Dyke and Prest, 1987), however detailed mapping conducted in this study has demonstrated that E and ESE-trending ice flow indicators – though extremely fragmented and localized – comprise the youngest in this region and include swarms of truncated eskers, networks of subaqueous ice contact deposits and isolated lineation assemblages. In following with the relative chronology outlined in section 5.4.2, GTZ *G* was probably established during a W-E migration of the ancestral Keewatin Ice Divide (i.e., eliciting a SE-WSW flowline shift across the study area), likely under primarily wet-based M bed conditions, though subsequently transitioned into a coherent H bed (either via substrate dewatering or the development of subglacial permafrost), enabling preservation of flowsets formed throughout phases B-D. GTZ *G* supports a high proportion of M3-B and M4 type ribbed moraines, representative of ridge re-moulding during the phase B-D translocation of the ancestral Keewatin Ice Divide, and subsequent post-glacial reworking by the transgressing Tyrrell Sea. The M1 morphotype is, however, also observed in high numbers within this GTZ, implying that bed regime transitions were patchy and localized in order to preserve the parent ridge morphology only in certain locations.

The largest GTZ in south-central Keewatin (GTZ *A*) forms part of the deglacial envelope in the western portion of the study area. Here, radial swarms of lineations with strong parallel conformity and draped by continuous, aligned sub-parallel esker ridges reflect inward time-transgressive formation behind a retreating ice margin (cf. Kleman et al., 2006; Greenwood and Clark, 2009b). These swaths of lineations overprint pre-existing landform assemblages wherever they are found, including broad patches and elongate ribbons of ribbed moraines, which has consequently spawned a preponderance of M3-B morphotypes (specifically streamlined morphologies) within this GTZ. A distinct presence of the M1 morphotype is also noted in this region (formed earlier in phases C and D), the existence of which likely denotes either a short-lived deglacial phase with limited erosive capacity, or patchy preservation under persistent Q or H bed conditions during younger ice flow phases E-G. Indeed, the tendency for lateral alternation in fluted and non-fluted ridges within this GTZ (e.g., Fig. 5.30; see also Aylsworth and Shilts, 1989b) suggests that only select areas of the bed were progressively thawed during the final ice retreat, possibly forming "islands" of frozen-bed patches surrounded by intervening bands of wet-based substrate, as has been modeled by Hughes (1981) and described in depth by Kleman and Glasser (2007). Patchy thawing and/or increased porewater content of the bed would lead to selective localized deformation and overprinting/re-moulding of M1 type ribbed moraines to form the widespread M3-B daughter morphotypes. Under sustained M bed conditions in these patches, eventual extinction and complete drift streamlining would occur. Translocation of deforming and non-deforming bed zones could have promoted surging by facilitating stiffening and strain hindrance within sub-marginal substrates, allowing lobate ice margins to oversteepen and accumulate stress. Surging glacier landsystems have been reported in northwestern Manitoba, adjacent to the study site and immediately below GTZ *A* (Dredge et al., 1986; Dyke and Dredge, 1989).

Up-ice of GTZ *A*, a broad zone of thin, discontinuous drift and outcropping bedrock comprises GTZ *C*. This was likely an area that experienced net erosion throughout recent ice flow phases. Superficial sediments are generally lacking in GTZ *C*, with the dominant landscape signature being one of widespread areal scouring. Bedrock knobs contribute to a prominent hilly terrain, some of which appear glacially sculpted. Belts of M4 morphotype ribbed moraines (primarily jagged and lumpy

morphologies) occupy depressions between these knobs, suggesting a possible association between the M4 morphotype and thin drift or concave terrain.

GTZs *E, F* and *H* are intimately related in the northeastern section of the study area, primarily including elongate drumlin and MSGL assemblages of flow phase F overlain by dense patches of M2 morphotype ribbed moraines. It is argued in section 5.4.2.3 that these convergent drift lineations and overprinting ridges record the operation and subsequent shut-down of ice streaming activity east of the Keewatin Ice Divide, into Hudson Bay. Enhanced calving, and a reduced buttressing effect of the ice margin within the Bay (following collapse over Hudson Straight by at least 8 Ka BP, cf. Dyke, 2004) would have promoted ice stream speed up, fostering a subdued ice sheet surface topography across eastern Keewatin, and contributing to associated changes in basal hydrology and drainage patterns. Prior to ice stream speed up, basal meltwater would have been effectively flushed towards the margin, given a steeply sloping basal hydrologic potential, in which ice surface slope is of 10:1 greater importance than ice bed slope (cf. Anandakrishnan and Alley, 1997). Following enhanced calving and an increased influx of ice to the Bay, this potential surface would have flattened in response to a leveling of the ice sheet surface, hence reorganizing basal drainage towards a largely distributed system, which is implied also by the chaotic esker network in this area. Re-organization of drainage would have engendered patchy dewatering of the substrate, promoting the development of sticky spots and zones of localized compressive flow, allowing basal debris to be thrust into englacial transport pathways up-ice of these sticky regions, effectively generating the M2 morphotype ribbed moraines which would come to overprint ice stream lineations throughout ongoing ablation and melt-out (cf. Stokes, 2008). Moore et al. (2009) provide numerical support for similar phenomena operating at the margin of contemporary Alaskan glaciers. Recent numerical modeling experiments (Melanson et al., 2013) predict an anomalously high content of englacial debris within GTZ *H*, and a prominent zone of subglacial erosion near GTZ *C* at LGM, which lends further support to suggestions outlined here.

It is worth noting that a combination of processes was likely involved in the collapse of mid-latitude palaeo-ice streams. In this example, it is reasonable to assume that enhanced ice flux towards the Bay would have also increased the rate at which cold ice was advected towards the margin from more interior locations (Patterson, 1994). A steepening of the vertical temperature profile through the ice stream could promote basal freeze-on of the substrate (Fig. 7.3), encourage ice stream shut-down, and create a zone of compressive flow up-ice, again, allowing basal sediments to enter englacial transport pathways by thrusting. East of the highest shoreline, ice stream bedforms were degraded following marine incursion, however they are comparatively better preserved than those which occupy GTZ *F* as ice calved away from the eastern margin, rather than ablated *in situ*. GTZ *F* contains a sprawling zone of ice wastage features (e.g., hummocky moraine, pitted outwash, gravitationally-reworked bedforms, etc.) that records downwasting and backwasting of ice following ice stream collapse. Ribbed moraines of morphotypes other than M2 are rare, if not entirely absent in these GTZs.

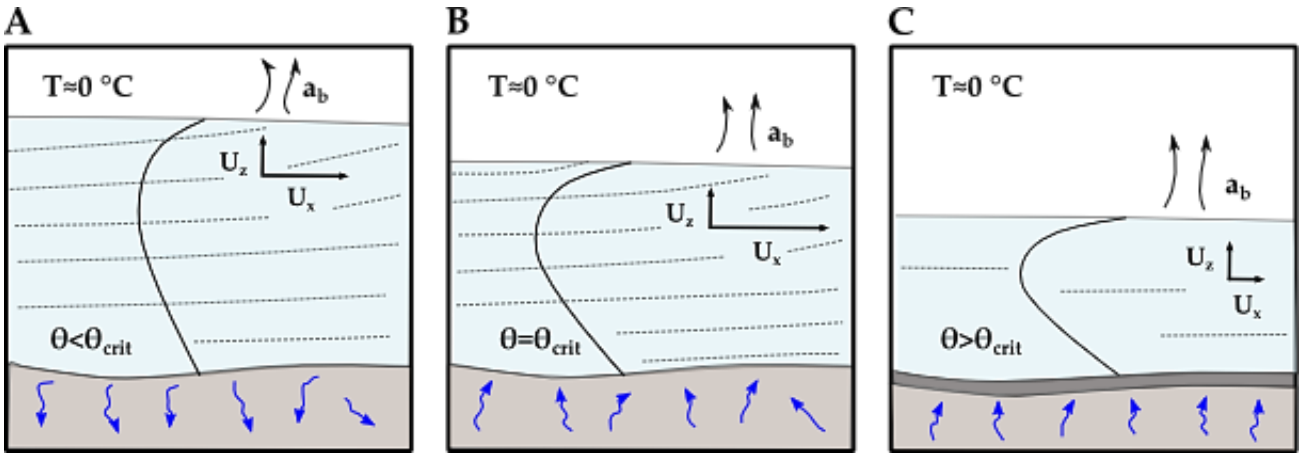

Fig. 7.3 – Vertical temperature profile (solid black line) through a mid-latitude ice stream. A) During steady state conditions, vertical ice velocity is directed towards the surface due to ongoing ablation. B) Horizontal advection of cold ice contributes to a steepening of the basal temperature gradient and may induce basal freeze-on. C) A "collapsed" mid-latitude ice stream wastes rapidly in the absence of ice flux from upstream and ongoing surface ablation. Blue arrows indicate substrate porewater movement, U_x and U_z are vectors which respectively denote horizontal and vertical ice velocity, a_b indicates ablation, and θ_{crit} is the threshold basal temperature gradient for basal freezing. Redrawn from Christoffersen and Tulaczyk, 2003.

The above GTZ assignments for south-central Keewatin are largely supported by recent numerical modeling experiments (Marshall et al., 2000; Kleman et al., 2002; Marshall and Clark, 2002; Tarasov and Peltier, 2004, 2007; Stokes et al., 2012) which indicate primarily cold-based ice and sluggish flow over the western Canadian Shield, and only brief phases of warm-based/wet-bed conditions throughout the last glacial cycle. Most of these models also predict that the ratio of warm:cold based ice increased in association with ice sheet thickening throughout the early-mid phases of the cycle leading up to LGM. Thick ice would have allowed portions of the bed to reach pressure melting point, hence enabling the production of ice flow traces far within interior locations beneath the ice. Tarasov and Peltier (2007) and Stokes et al. (2012) also indicate a decline in the warm:cold based ratio following LGM. As suggested by Trommelen et al. (2014) however, marginal locations likely remained warm-based throughout deglaciation, hence an increasing proportion of cold-based ice implies that large core regions transitioned towards cold-based and/or stucky/sluggish ice flow conditions. Kleman and Hättestrand (1999) have implied that the Keewatin ribbed moraine assemblage reflects an inward-transgressing warm-based temperature gradient during deglaciation, however, such a linear boundary is not supported by this study, which predicts a patchy distribution of warm- and cold-based/de-watered bed zones. Moreover, results of this thesis suggest that ribbed moraines were formed throughout multiple pre-deglacial phases, and hence cannot simply reflect the single stage contraction of a warm-based ice margin.

8. Conclusions

The overall aim of this research was to establish linkages between subglacial bedform geomorphology and palaeoglacial dynamics, and utilize these associations to devise a detailed reconstruction of the glacial history of the Keewatin sector of the LIS that is compatible with modern frameworks for interpreting formerly glaciated terrains. Individual research objectives were outlined in section 1.2, and the following chapter will briefly address the conclusions from this thesis that are pertinent to each of these goals.

8.1 *Research Objectives: Summary of Findings and Conclusions*

1. *Quantitatively assess the spatial and morphological characteristics of ribbed moraines in south-central Keewatin*

Spatial and morphometric analysis has revealed that ribbed moraines in south-central Keewatin are organized within >550 individual fields covering a total area of 32,975 km^2. Within these fields, they have characteristic spacing (mean wavelength = 311 m) and average lengths, widths and heights (652 m, 319 m, 29 m, respectively) that compare favourably with similar bedforms in Ireland, Québec and Sweden (Dunlop and Clark, 2006b). As commonly reported from other areas, ridge wavelengths in south-central Keewatin can be approximated by their widths. Ribbed moraines exhibit statistically significant spatial clustering when considered against the ~70,000 km^2 study area (nearest neighbour ratio = 0.52), and moreover, demonstrate statistically significant spatial clustering by size at the 99% confidence level. This tendency is one of low ridge length clustering (~26% of all ridges). Roughly half (~53%) of all ribbed moraines in the study area are not clustered by size.

2. *Elucidate controls on ribbed moraine formation and development;*

Results presented in this thesis suggest that the generation, modification and preservation of ribbed moraines are controlled by the distribution of hard (H), mobile (M) and quasi-mobile (Q) beds (cf. Menzies, 1989b; van der Meer, 2003). Ridges are incepted under Q bed conditions, either by a propagating subglacial till instability (cf. Dunlop et al., 2008), or by localized englacial thrusting and melt-out, depending on one of two probable formation mechanisms. Subsequently, ridges can be modified and/or streamlined under M bed conditions, and preserved *in situ* under H bed conditions. The velocity and duration of ice flow over M bed zones determines the extent to which ridges are reshaped, and subsequently, where they fall along a continuum of morphologies. Concomitant shifts in ice flow direction and/or translocation of dispersal centers affect the obliquity of ridge overprinting or re-moulding. Spatiotemporal migration of Q, H and M beds stimulates development of a subglacial deforming bed mosaic and, in the geological record, elicits a patchy, fragmented archive of young and old bedforms in close proximity, with varying degrees of reworked morphology.

3. *Contribute additional field-based observations of ribbed moraine internal structure and composition;*

Field observations from central South Norway revealed that ribbed moraines in that area are composed primarily of coarse-grained, sandy-gravelly tills with a high content of boulders and, in some ridges, occasional silty-sandy sorted interbeds and lenses. Matrix grain size and clast morphology

analysis suggests that these are basal tills, some with high input from supraglacial sources. Glaciotectonic and/or deformational structures are mostly absent in these ridges, though upper units may have been subject to gravitational reworking. Clast fabric analysis and striae measurements indicate formation transverse to ice flow direction. The confinement of ribbed moraines to concave surfaces in this area suggests a large influence of topographical effects in their formation.

4. *Determine the extent of convergence between morphologic and genetic ribbed moraine classifications*;

Subjective evaluations supported by statistical clustering procedures based on ridge size allude to the existence of separate ribbed moraine *morphotypes*. Two of these (M1, M2) constitute parent morphotypes, and presumably possess divergent modes of origin. Thus, distinction between M1 and M2 type ribbed moraines can be considered a *genetic* classification. Four other (daughter) morphotypes (M3-A, M3-B, M4, M5) do not exhibit diverse modes of origin, but locate along a continuum that represents varying degrees of modification of the parent morphotypes. Distinctions between the daughter morphotypes are valid, but are strictly *morphological* descriptions, as each of these morphotypes share a common formational history.

5. *Interpret the glacial history of south-central Keewatin within a modern palaeoglaciological framework*

Flowset grouping of bedforms and the establishment of a relative chronology for ice flow events in south-central Keewatin based on cross-cutting and overprinting relationships yielded a reconstruction consisting of seven phases (A-G) of ice flow, most (if not all) of which were probably realized during the Late Wisconsinan. Early flows (Phase A) signify an ice divide position west of the study area, which subsequently migrated eastward across central Nunavut, as is captured in the SE-WSW rotation (Phases B-E) of lineation and ribbed moraine assemblages in south-central Keewatin. A switch to fast ice flow and ice streaming behavior east of the divide, in the northeast portion of the study area, was facilitated by the collapse of ice over Hudson Straight and a calving margin that rapidly encroached upon the Hudson Bay shoreline. Ice stream shutdown later ensued in response to reorganizations in basal hydrology, or the development of sub-ice stream permafrost, causing massive stagnation inside the marine limit. In the western half of the study area, deglaciation proceeded steadily in a radial, lobate fashion, with occasional surging of oversteepened margins. Uneven preservation of these flow phases in the geological record of south-central Keewatin allowed for the partitioning of the study area into 8 distinct glacial terrain zones (GTZs, cf. Trommelen et al., 2012) based on the relative strength of inheritance vs. overprinting signals, and the dominant palaeoglaciological signatures retained within each area. Large zones of relict terrain, and other areas of more local-scale inheritance, suggest that styles of deglaciation were varied across space, and incorporated mechanisms of preserving old ice flow signatures.

8.2 *Limitations*

It is important to draw attention to the methodological limitations in this thesis. Problems of bias when mapping landforms from remotely sensed imagery are well-known and have been comprehensively reviewed in the past (Clark, 1997; Smith and Wise, 2007). These include issues which stem from both a) landform detectability, and b) observer ability. Smith and Clark (2005) demonstrate

that detectability suffers from multiple biases associated with data visualization techniques. Although mapping in this thesis utilized repeat passes, and varied data visualization procedures (e.g., multiple and orthogonal illumination azimuths for elevation data and derivatives, variations in brightness, gamma and contrast for imagery), the possibility that a subset of landforms has escaped detection due to improper visualization cannot be discounted. Smith et al. (2006) have concluded that detectability is also closely associated with the spatial resolution and (for elevation data) vertical accuracy of a data product. Similarly, in an automated landform mapping study, Napieralski and Nalepa (2010) determined that elevation data with sub-10 m resolution produced mapping outputs which were comparable to those from a 1 m DEM; coarser resolution data contributed to landform positional drift and shape-related errors. Spatial resolution and vertical accuracy of elevation data is a tremendous limitation to landform mapping in northern Canada, particularly above 60º N, as sub-20 m products are not available, with the exception of those that could be created by commercial satellite tasking and stereo-DEM creation. Mapping artefacts generated from observer error are surely also captured in the dataset, however this is likely much less significant a limitation than those which stem from the data sources themselves, since image interpretation is highly trainable, and can be improved upon through repeat mapping passes. As indicated in section 5.3.2, checks were also consistently made against published geological maps (both surficial and bedrock) to avoid misinterpretation of structural features. Although difficult to quantify, it is estimated that less than 8% of bedforms mapped in this study have be misidentified. Considering that >73,800 glacial landforms were mapped in the study area, this would imply at most ~6,000 misidentifications due to observer error.

8.3 *Recommendations for Future Work*

During the course of bedform mapping in this study, it was recognized that the identification of glacial landforms from remotely sensed imagery – especially when forming distinctions between several morphologies of a single landform type – is an inherently subjective exercise. As a result, consistent morphological templates (Fig. 5.12) and strict landform definitions were followed for mapping, however the possibility that such identification could be automated in image analysis and remote sensing software must be acknowledged. Several studies have shown the utility of automated mapping procedures for glacial landform identification (Saha, 2009; Napieralski and Nalepa, 2010; Broscoe et al., 2011; Gerçek et al., 2011; Saha et al., 2011; Maclachlan and Eyles, 2013), however none have developed algorithms for mapping ribbed moraines. Moreover, the accuracy and reliability of these techniques are variable in their current form, and manual, single-operator mapping currently remains the preferred method. Further development of automated procedures is likely forthcoming, however there will perpetually be need to ground-truth observations made from remotely-sensed datasets.

Additional field studies are needed from a variety of locations, involving deep sections through ribbed moraine landforms, with multiple, perpendicular aspects in order to gain a full understanding of 3-dimensional internal architecture. Based on the results of this study, ideally these field investigations would target separate morphological types, as there is need to examine the potential for associating diagnostic structures and facies with surficial geomorphology. Ground-truthing and detailed field work are also required in southern Nunavut in order to validate the results of this study. Specifically, examination of the spatial distribution of inherited signatures in till geochemistry and clast provenance, and the mapping of field-based ice flow indicators, must be completed in order to verify the assignment of glacial terrain zones.

Ongoing geophysical studies in Antarctica seeking to characterize active rib-forming processes are required in order to provide better constraints for models of palaeo-subglacial environments, e.g., by

providing actual values for ribbed moraine growth timescales, bed rheology, and ice velocity. Existing models have had moderate success in simulating the formation of instability-generated ribbed moraines (Dunlop et al., 2008; Chapwanya et al., 2011) however they suffer from having poor constraints on the above parameters. Other metrics should also be explored in modeling using datasets mapped from the geological archive. Results of this study nominate an extension/compression index (contained within principal component 1 in section 5.4.1.7) as a good measure of differentiating between ribbed moraine morphologies, however further quantitative work is required to test to this.

9. References

Aario, R. 1977a. Associations of flutings, drumlins, hummocks and transverse ridges. GeoJournal, 1(6): 65-72.

Aario, R. 1977b. Classification and terminology of morainic landforms in Finland. Boreas, 6(2): 87-100.

Aario, R. 1987. Drumlins of Kuusamo and Rogen-ridges of Ranua, northeast Finland. In: J. Menzies and J. Rose (Eds.), *Drumlin Symposium*. Rotterdamn, A.A. Balkema, pp. 87-101.

Aario, R., L. Forsstrom and P. Lahermo. 1974. Glacia1 landforms with special reference to drumlins and fluting in Koillismaa, Finland. Geological Survey of Finland, Bulletin 273: 30 pp.

Alley, R.B. 1991. Deforming-bed origin for southern Laurentide till sheets? Journal of Glaciology, 37: 67-76.

Alley, R.B., D.D Blankenship, S.T. Rooney and C.R. Bentley. 1987b. Till beneath ice stream B 4. A coupled ice-till flow model. Journal of Geophysical Research, 92: 8931-8940.

Alley, R.B., D.D. Blankenship, C.R. Bentley and S.T. Rooney. 1986. Deformation of tills beneath ice stream B, West Antarctica. Nature, 322: 57-59.

Alley, R.B., D.D. Blankenship, C.R. Bentley and S.T. Rooney. 1987a. Till beneath ice stream B 3. Till deformation: evidence and implications. Journal of Geophysical Research, 92: 8921-8929.

Alley, R.B., D.E. Lawson, E.B. Evenson, J.C. Strasser and G.J. Larson. 1998. Glaciohydraulic supercooling: a freeze-on mechanism to create stratified debris-rich basal ice: II. Theory. Journal of Glaciology, 44: 562-568.

Anandakrishnan, S. and R.B. Alley. 1997. Stagnation of ice stream C, West Antarctica by water piracy. Geophysical Research Letters, 24(3): 265-268.

Anandakrishnan, S., D.D. Blankenship, R.B. Alley and P.L. Stoffa. 1998. Influence of subglacial geology on the position of a West Antarctic ice stream from seismic observations. Nature, 394: 62-65.

Anderberg, M.R. 1973. *Cluster Analysis for Applications*. New York: Academic Press, 359 pp.

Andreassen, K., J.S. Laberg and T.O. Vorren. 2008. Seafloor geomorphology of the SW Barents Sea and its glacidynamic implications. Geomorphology, 97(1-2): 157-177.

Andrews, J.T. 1963. The cross-valley moraines of north-central Baffin Island: a quantitative analysis. Geographical Bulletin, 20: 82-129.

Andrews, J.T. 1969. Cross-valley moraines of the Rimrock and Isortoq River valleys, Baffin Island, N.W.T. – a descriptive analysis. In: J.G. Nelson and M.J. Chambers (Eds.), *Process and Method in Canadian Geography: Geomorphology, Selected Readings*. Toronto: Methuen, pp. 111-133. (Reprinted from Geographical Bulletin, 19(1963): 49-77).

Andrews, J.T. and B.B. Smithson. 1966. Till fabric of the cross-valley moraines of north central Baffin Island, Northwest Territories, Canada. Bulletin of the Geological Society of America, 77: 271-290.

Andrews, J.T. and M.A.W. Mahaffy. 1976. Growth rate of the Laurentide ice sheet and sea level lowering (with emphasis on the 115,000 BP sea level low). Quaternary Research, 6: 167-183.

Andrews, J.T. and R.G. Barry. 1978. Glacial inception and disintegration during the last glaciation. Annual Reviews of Earth and Planetary Science, 6, 205-228.

Andrews, J.T. and W.R. Peltier. 1976. Collapse of the Hudson Bay ice center and glacio-isostatic rebound. Geology, 4, 73-75.

Andrews, J.T., W.W. Shilts and G.H. Miller. 1983. Multiple deglaciation of the Hudson Bay Lowlands, Canada, since the deposition of the Missinaibi (Last-Interglacial?) Formation. Quaternary Research, 19: 18-37.

Anselin, L. 1995. Local indicators of spatial association – LISA. Geographical Analysis, 27: 93-115.

Arsenault, L., J.M. Aylsworth, C.M. Cunningham, I.M. Kettles and W.W. Shilts. 1980. Surficial geology, Eskimo Point, District of Keewatin, Northwest Territories. Geological Survey of Canada, Map 8-1980, scale 1:125,000.

Aspler, L.B., C. Höfer and B.J.A. Harvey. 2000. Geology, Sealhole and Fitzpatrick Lakes area, Nunavut. Geological Survey of Canada, Ottawa, Open File 3753, scale 1:50,000.

Aspler, L.B., J.R. Chiarenzelli and T.L. Bursey. 1994. Ripple marks in quartz arenites of the Hurwitz group, Northwest Territories, Canada: Evidence for sedimentation in a vast, early Proterozoic, shallow, fresh-water lake. Journal of Sedimentary Research, Section A: Sedimentary Petrology and Processes. 64A(2), 282-298.

Aspler, L.B., J.R. Chiarenzelli, B.L. Cousens, V.J. McNicoll and W.J. Davis. 2001. Paleoproterozoic intracratonic basin processes, from breakup of Kenorland to assembly of Laurentia: Hurwitz Basin, Nunavut, Canada. Sedimentary Geology, 141-142: 287-318.

Attig, J.W. 1985. Pleistocene geology of Vilas County, Wisconsin. Wisconsin Geology and Natural History Survey, Informational Circular 50: 32.

Aylsworth, J.M. 1986a. Surficial geology, Ennadai Lake, District of Keewatin, Northwest Territories. Geological Survey of Canada, Map 5-1985, scale 1:125,000.

Aylsworth, J.M. 1986b. Surficial geology, Nueltin Lake, District of Keewatin, Northwest Territories. Geological Survey of Canada, Map 6-1985, scale 1:125,000.

Aylsworth, J.M. 1989a. Surficial geology, Ennadai, District of Keewatin, Northwest Territories. Geological Survey of Canada, Map 36-1989, scale 1:125,000.

Aylsworth, J.M. 1989b. Surficial geology, Watterson Lake, District of Keewatin, Northwest Territories. Geological Survey of Canada, Map 1-1988, scale 1:125,000.

Aylsworth, J.M. and W.W. Shilts. 1989a. Bedforms of the Keewatin ice sheet, Canada. Sedimentary Geology, 62: 407-428.

Aylsworth, J.M. and W.W. Shilts. 1989b. Glacial features around the Keewatin ice divide: Districts of Mackenzie and Keewatin. Geological Survey of Canada, Paper 88-24: 21 pp.

Aylsworth, J.M., C.M. Cunningham and W.W. Shilts. 1979. Surficial geology, Hyde Lake, District of Keewatin, Northwest Territories. Geological Survey of Canada, Map 8-1979, scale 1:125:000.

Aylsworth, J.M., C.M. Cunningham and W.W. Shilts. 1990. Surficial geology, Edehon Lake, District of Keewatin, Northwest Territories. Geological Survey of Canada, Map 10-1990, scale 1:125,000.

Aylsworth, J.M., C.M. Cunningham, I.M Kettles and W.W. Shilts. 1986. Surficial geology, Henik Lakes, District of Keewatin, Northwest Territories. Geological Survey of Canada, Map 2-1985, scale 1:125,000.

Aylsworth, J.M., I.M. Kettles and W.W. Shilts. 1978. Surficial geology, Dawson Inlet, District of Keewatin, Northwest Territories. Geological Survey of Canada, Map 9-1979, scale 1:125,000.

Ballantyne, C.K. 1982. Aggregate clast form characteristics of deposits at the margins of four glaciers in the Jotunheimen Massif, Norway. Norsk Geografisk Tidsskrift, 36: 103-113.

Ballantyne, C.K., D. McCarrol and J.O. Stone. 2007. The Donegal ice dome, northwest Ireland: dimensions and chronology. Journal of Quaternary Science, 22: 773-783.

Bamber, J.L., D.G. Vaughan and I. Joughin. 2000. Widespread complex flow in the interior of the Antarctic ice sheet. Science, 287: 1248-1250.

Battey, M.H. 1965. Layered structure in rocks of the Jotunheim Complex. Mineralogical Magazine, 34(268): 35-51.

Battiau-Queney, Y. 1996. A tentative classification of paleoweathering formations based on geomorphological criteria. Geomorphology, 16: 87-102.

Benn, D.I. 1994. Fabric shape and the interpretation of sedimentary fabric data. Journal of Sedimentary Research, A64(4): 910-915.

Benn, D.I. 2004. Clast morphology. In: D.J.A. Evans and D.I. Benn (Eds.), *A Practical Guide to the Study of Glacial Sediments*. Arnold, London, pp. 78-92.

Benn, D.I. and D.J.A. Evans. 2010. *Glaciers & Glaciation*. London: Hodder Education: 816 pp.

Benn, D.I., D.J.A. Evans, J. Shaw and M. Munro-Stasiuk. 2006. Subglacial megafloods: outrageous hypothesis or just outrageous / reply. In: P.G. Knight (Ed.), *Glacier Science and Environmental Change*.Chichester, Wiley-Blackwell, pp. 42-60.

Bennett, M.R., M.J. Hambrey and D. Huddart. 1997. Modification of clast shape in high-arctic glacial environments. Journal of Sedimentary Research, 67(3): 550-559.

Bennett, M.R., M.J. Hambrey, D. Huddart and N.F. Glasser. 1998. Glacial thrusting and moraine-mound formation in Svalbard and Britain: the example of Core a' Cheud-chnoic (Valley of a Hundred Hills). Quaternary Proceedings, 6: 17-34.

Bergersen, O.F. and K. Garnes. 1981. Weichselian in central South Norway: the Gudbrandsdal Interstadial and the following glaciation. Boreas, 10(4), 315-322.

Beskow, G. 1935. Praktiska och kvartärgeologiska resultat av grusinventeringen i Norrbottens län. Geologiska Föreningens i Stockholm Förhandlingar, 57:120-123.

Bird, J.B. 1953. The glaciation of central Keewatin, Northwest Territories, Canada. American Journal of Science, 251: 215-230.

Blake, W. Jr. 1963. Notes on glacial geology, northeastern District of Mackenzie. Geological Survey of Canada, Paper 63-28: 12 pp.

Blankenship, D.D., C.R. Bentley, S.T. Rooney and R.B. Alley. 1986. Seismic measurements reveal a saturated porous layer beneath an active Antarctic ice stream. Nature, 322: 54-57.

Blankenship, D.D., C.R. Bentley, S.T. Rooney and R.B. Alley. 1987. Till beneath ice stream B 1. Properties derived from seismic travel times. Journal of Geophysical Research, 92: 8903-8911.

Blundon, P., T. Bell and M. Batterson. 2009. An evaluation of SRTM digital elevation data for glacial landform mapping in Newfoundland. In: Current Research. Newfoundland Department of Natural Resources, Geological Survey: Report 09-1, pp. 289-303.

Bouchard, M.A. 1980. Late Quaternary geology of the Témiscamie area, central Québec, Canada. Dissertation, Department of Geological Sciences, McGill University: 284 pp.

Bouchard, M.A. 1989. Subglacial landforms and deposits in central and northern Québec, Canada, with emphasis on Rogen moraines. Sedimentary Geology, 62: 293-308.

Bouchard, M.A. and G. Martineau. 1985. Southeastward ice flow in central Quebec and its paleogeographic significance. Canadian Journal of Earth Sciences, 22: 1536-1541.

Bouchard, M.A., H.G. Ignatius and L.-K. Königsson. 1989. Ribbed moraines of North America—A historical account. Geologi, 41: 75-79.

Boulton, G.S. 1970a. On the deposition of subglacial and melt-out tills at the margins of certain Svalbard glaciers. Journal of Glaciology, 9: 231-245.

Boulton, G.S. 1970b. On the origin and transport of englacial debris in Svalbard glaciers. Journal of Glaciology, 5(56): 213-229.

Boulton, G.S. 1971. Till genesis and fabric in Svalbard, Spitzbergen. In: R.P. Goldthwait, R.P. (Ed.), *Till, a Symposium*. Ohio State University Press, pp. 41-72.

Boulton, G.S. 1972. Modern arctic glaciers as depositional models for former ice sheets. Geological Society of London Quarterly Journal, 128: 361-393.

Boulton, G.S. 1979. Processes of glacier erosion on different substrata. Journal of Glaciology, 23, 15-38.

Boulton, G.S. 1986. A paradigm shift in glaciology? Nature, 322: 18.

Boulton, G.S. 1987. A theory of drumlin formation by subglacial sediment deformation. In: J. Menzies and J. Rose (Eds.), *Drumlin Symposium*. Rotterdamn, A.A. Balkema, pp. 25-80.

Boulton, G.S. 1996. Theory of glacial erosion, transport and deposition as a consequence of subglacial sediment deformation. Journal of Glaciology, 42(140): 1996.

Boulton, G.S. and A.S. Jones. 1979. Stability of temperate ice caps and ice sheets resting on beds of deformable sediment. Journal of Glaciology, 24: 29-44.

Boulton, G.S. and C.D. Clark. 1990a. A highly mobile Laurentide Ice Sheet revealed by satellite images of glacial lineations. Nature, 346: 813-817.

Boulton, G.S. and C.D. Clark. 1990b. The Laurentide Ice Sheet through the last glacial cycle: the topology of drift lineations as a key to the dynamic behaviour of former ice sheets. Transactions of the Royal Society of Edinburgh: Earth Sciences, 81: 327-347.

Boulton, G.S. and D.L. Dent. 1974. The nature and rates of post-depositional changes in recently deposited till from south-east Iceland. Geografiska Annaler, 56(A): 121-134.

Boulton, G.S., D.L. Dent and E.M. Morris. 1974. Subglacial shearing and crushing, and the role of water pressures in tills from south-east Iceland. Geografiska Annaler, 56(A): 135-145.

Boulton, G.S., G.D. Smith, A.S. Jones and J. Newsome. 1985. Glacial geology and glaciology of the last mid-latitude ice sheets. Journal of the Geological Society of London, 142: 447-474.

Boulton, G.S., J.J.M. Van der Meer, J. Harts, D. Beets, G.H.J. Rueggs, F.M. Van der Wateren and J. Jarvis. 1996. Till and moraine emplacement in a deforming bed surge – an example from a marine environment. Quaternary Science Reviews, 15: 961-987.

Boulton, G.S., M. Hagdorn, P.B. Maillot and S. Zatsepin. 2009. Drainage beneath ice sheets: groundwater-channel coupling, and the origin of esker systems from former ice sheets. Quaternary Science Reviews, 28: 621-638.

Boulton, G.S., P. Dongelmans, M. Punkari and M. Broadgate. 2001. Paleoglaciology of an ice sheet through a glacial cycle: the European ice sheet through the Weichselian. Quaternary Science Reviews, 20(4): 591-625.

Boyce, J.I. and N. Eyles. 1991. Drumlins carved by deforming till streams below the Laurentide Ice Sheet. Geology, 19: 787-790.

Bradwell, T., M. Stoker and M. Krabbendam. 2008. Megagrooves and streamlined bedrock in NW Scotland: The role of ice streams in landscape evolution. Geomorphology, 97(1-2): 135-156.

Bradwell, T., M. Stoker and R. Larter. 2007. Geomorphological signature and flow dynamics of the Minch palaeo-ice stream, northwest Scotland. Journal of Quaternary Science, 22(6): 609-617.

Brady, N.C. and R.R. Weil. 2002. *The Nature and Properties of Soils*, 13th edition. Prentice Hall, New Jersey, 960 pp.

Brewer, R. 1976. *Fabric and Mineral Analysis of Soils*. Krieger, Huntington, 482 pp.

Briner, J.P. 2007. Supporting evidence from the New York drumlin field that elongate subglacial bedforms indicate fast ice flow. Boreas, 36(2): 143-147.

Broscoe, D., D.I. Cummings, H.A.J. Russel and D.R. Sharpe. 2011. A semi-automated esker detection method (EDM) for improved quantification of glaciated landscapes. Geological Survey of Canada Technical Note 2, 17 pp.

Brown, V.H., C.R. Stokes and C.O. Cofaigh. 2011. The glacial geomorphology of the north-west sector of the Laurentide Ice Sheet. Journal of Maps, 7: 409-428.

Canals, M., Urgeles, R. and Calafat, A.M. 2000. Deep sea-floor evidence of past ice streams off the Antarctic Peninsula. Geology, 28: 31-34.

Carl, J.D. 1978. Ribbed moraine—drumlin transition belt, St. Lawrence Valley, New York. Geology, 6: 562-566.

Carr, S.J., R. Holmes, J.J.M. Van der Meer and J. Rose. 2006. The Last Glacial Maximum in the North Sea Basin: micromorphological evidence of extensive glaciation. Journal of Quaternary Science, 21(2): 131-153.

Chapwanya, M., C.D. Clark and A.C. Fowler. 2011. Numerical computations of a theoretical model of ribbed moraine formation. Earth Surface Processes and Landforms, 36(8): 1105-1112.

Chen, J., X. Zhu, J.E. Vogelmann, F. Gao and S. Jin. 2011. A simple and effective method for filling gaps in Landsat ETM+ SLC-off images. Remote Sensing of Environment, 115(4): 1053-1064.

Christie, K.W., A. Davidson and W.F. Fahrig. 1975. The paleomagnetism of Kaminak dikes—no evidence of significant Hudsonian plate motion. Canadian Journal of Earth Sciences, 12: 2048-2064.

Christoffersen, P. and S. Tulaczyk. 2003. Signature of palaeo-ice-stream stagnation: till consolidation induced by basal freeze-on. Boreas, 32: 114-129.

Clague, J.J. and T.S. James. 2002. History and isostatic effects of the last ice sheet in southern British Columbia. Quaternary Science Reviews, 21: 71-87.

Clark, C. D., A.L.C. Hughes, S.L. Greenwood, M. Spagnolo and F.S.L Ng. 2009. Size and shape characteristics of drumlins derived from a large sample, associated scaling laws. Quaternary Science Reviews, 28: 677-692.

Clark, C.D. 1993. Mega-scale glacial lineations and cross-cutting ice-flow landforms. Earth Surface Processes and Landforms, 18(1): 1-29.

Clark, C.D. 1994. Large scale ice-moulded landforms and their glaciological significance. Sedimentary Geology, 91(1-4): 253-268.

Clark, C.D. 1997. Reconstructing the evolutionary dynamics of former ice sheets using multi-temporal evidence, remote sensing and GIS. Quaternary Science Reviews, 16: 1067-1092.

Clark, C.D. 1999. Glaciodynamic context of subglacial bedform generation and preservation. Annals of Glaciology, 28: 23-32.

Clark, C.D. 2010. Emergent drumlins and their clones: from till dilatancy to flow instability. Journal of Glaciology, 51(200): 1011-1025.

Clark, C.D. and C.R. Stokes. 2001. Extent and basal characteristics of the M'Clintock Channel Ice Stream. Quaternary International, 86: 81-101.

Clark, C.D. and R.T. Meehan. 2001. Subglacial bedform geomorphology of the Irish Ice Sheet reveals major configuration changes during growth and decay. Journal of Quaternary Science, 16(5): 483-496.

Clark, C.D., A.L.C. Hughes, S.L. Greenwood, C. Jordan and H.P. Sejrup. 2012. Pattern and timing of retreat of the last British-Irish Ice Sheet. Quaternary Science Reviews, 44: 112-146

Clark, C.D., D.J.A. Evans, A. Khatwa, T. Bradwell, C. Jordan, S. Marsh, W. Mitchell and M. Bateman. 2004. Map and GIS database of glacial landforms and features related to the last British Ice Sheet. Boreas, 33(4): 359-375.

Clark, C.D., J.K. Knight and T. Gray. 2000. Geomorphological reconstruction of the Labrador Sector of the Laurentide Ice Sheet. Quaternary Science Reviews, 19(13): 1343-1366.

Clark, P.U., J.M. Licciardi, D.R. MacAyeal and J.W. Jenson. 1996. Numerical reconstruction of a soft-bedded Laurentide Ice Sheet during the last glacial maximum. Geology, 24(8): 679-682.

Clarke, G.K.C. 1987. Subglacial till: a physical framework for its properties and processes. Journal of Geophysical Research, 92: 8942-8984.

Clarke, G.K.C. 2005. Subglacial processes. Annual Review of Earth and Planetary Sciences, 33: 247-276.

Clarke, G.K.C., D.W. Leverington, J. Teller, A.S. Dyke and S.J. Marshall. 2005. Fresh arguments against the Shaw megaflood hypothesis. A reply to comments by David Sharpe on 'Paleohydraulics of the last outburst flood from glacial Lake Agassiz and the 8200 BP cold event'. Quaternary Science Reviews, 24: 1533-2541.

Clayton, L. and S.R. Moran. 1974. A glacial process-form model. In: D. Coates (Ed.), Glacial geomorphology, In: *Proceedings, Fifth Annual Geomorphology Symposia Series*. Binghamton, New York, pp. 89-119.

Cowan, W. 1968. Ribbed moraine: Till-fabric analysis and origin. Canadian Journal of Earth Sciences, 5: 1145-1159.

Craig, B.G. 1961. Surficial geology of northern district of Keewatin, Northwest Territories. Canadian Geological Survey. Paper 61(5): 8 pp.

Craig, B.G. 1964. Surficial geology of east-central District of Mackenzie. Geological Survey of Canada Bulletin 99: 41 pp.

Cunningham, C.M. and W.W. Shilts. 1977. Surficial geology of the Baker Lake area, District of Keewatin. Geological Survey of Canada, Paper 77-1B: 311-314.

Dahl, S.O., H. Linge, D. Fabel and A.S. Murray. 2010. Extent and timing of the Scandinavian Ice Sheet during Late Weichselian (MIS3/2) glacier maximum in central southern Norway—link to the Norwegian Channel Ice Stream? [Abstract]. Proceedings of the Geological Society of Norway 1-2010: 37-38.

De Angelis, H. 2007. Glacial geomorphology of the east-central Canadian Arctic. Journal of Maps, v2007: 323-341.

De Angelis, H. and J. Kleman. 2007. Palaeo-ice streams in the Foxe/Baffin sector of the Laurentide Ice Sheet. Quaternary Science Reviews, 26(9-10): 1313-1331.

De Angelis, H. and J. Kleman. 2008. Palaeo-ice stream onsets: examples from the north-eastern Laurentide Ice Sheet. Earth Surface Processes and Landforms, 33: 560-572.

Dean, W.G. 1953. The drumlinoid landforms of the "Barren Grounds", Northwest Territories. The Canadian Geographer, 3: 19-30.

Douglas, M.C.V. and R.N. Drummond. 1955. Map of the physiographic regions of Labrador-Ungava. The Canadian Geographer, 2(5): 9-16.

Dowdeswell, J.A., D. Ottesen, L. Rise and J. Craig. 2007. Identification and preservation of landforms diagnostic of past ice-sheet activity on continental shelves from three-dimensional seismic evidence. Geology, 35(4): 359-362.

Dredge, L.A. and E. Nielson. 1985. Glacial and interglacial deposits in the Hudson Bay Lowlands: a summary of sites in Manitoba. Geological Survey of Canada, Ottawa. Current Research, Part A: Paper 85-1A: 247-257.

Dredge, L.A. and H. Thorleifson. 1987. The Middle Wisconsinan history of the Laurentide Ice Sheet. Géographie physique et Quaternaire, 41: 215-235.

Dredge, L.A. and I. McMartin. 2011. Glacial stratigraphy of northern and central Manitoba. Geological Survey of Canada Bulletin 600: 27 pp.

Dredge, L.A., F.M. Nixon and R.J. Richardson. 1986. Quaternary geology and geomorphology of northwestern Manitoba. Geological Survey of Canada Memoir 418: 38 pp.

Dredge, L.A., I. McMartin and M.Pyne. 2007. Surface materials and landforms, northernmost Manitoba. Geological Survey of Canada, Ottawa, Open File 5435.

Dunlop, P. and C.D. Clark. 2006a. Distribution of ribbed moraine in the Lac Naococane region, central Québec, Canada. Journal of Maps, 2: 59-70.

Dunlop, P. and C.D. Clark. 2006b. The morphological characteristics of ribbed moraine. Quaternary Science Reviews, 25(13-14): 1668-1691.

Dunlop, P., C.D. Clark and R.C.A. Hindmarsh. 2008. Bed Ribbing Instability Explanation: Testing a numerical model of ribbed moraine formation arising from coupled flow of ice and subglacial sediment. Journal of Geophysical Research, 113(F03005): 1-15.

Dyke, A.S. 1984. Quaternary geology of Boothia Peninsula and northern District of Keewatin, Central Canadian Arctic. Geological Survey of Canada Memoir 407: 26 pp.

Dyke, A.S. 2004. An outline of North American deglaciation with emphasis on central and northern Canada. In: J. Ehlers and P.L. Gibbard (Eds.), *Quaternary Glaciations – Extemt and Chronology, Part II*. Amsterdam, Elsevier Science and Technology Books, 2b: 373-424.

Dyke, A.S. and L.A. Dredge. 1989. Quaternary geology of the northwestern Canadian Shield. In: R.J. Fulton (Ed.), *Quaternary Geology of Canada and Greenland*. Geological Survey of Canada, Geology of Canada Series No. 1, pp. 214-235.

Dyke, A.S. and T.F. Morris. 1988. Drumlin fields, dispersal trains, and ice streams in Arctic Canada. Canadian Geographer, 32: 86-90.

Dyke, A.S. and V.K. Prest. 1987. Late Wisconsinan and Holocene history of the Laurentide ice sheet. Géographie Physique et Quaternaire, 41(2): 237-263.

Dyke, A.S., J.-S. Vincent, J.T. Andrews, L.A. Dredge and W.R. Cowan. 1989. The Laurentide Ice Sheet and an introduction to the Quaternary geology of the Canadian Shield. In: R.J. Fulton (Ed.), *Quaternary Geology of Canada and Greenland*. Geological Survey of Canada, Geology of Canada Series No. 1, pp. 178-189.

Dyke, A.S., J.T. Andrews, P.U. Clark, J.H. England, G.H. Miller, J. Shaw and J.J. Veillette. 2002. The Laurentide and Innuitian Ice Sheets during the Last Glacial Maximum. *Quaternary Science Reviews*, 21: 9-31.

Dyke, A.S., L.A. Dredge, and J.-S. Vincent. 1982. Configuration and dynamics of the Laurentide Ice Sheet during the Late Wisconsin maximum. Géographie physique et Quaternaire, 36(1-2): 5-14.

Dyke, A.S., T.F. Morris, D.E.C. Green and J. England. 1992. Quaternary geology of Prince of Wales Island, Arctic Canada. Geological Survey of Canada Memoir 433: 142 pp.

Eade, K.E. 1971. Geology of Ennadai Lake map-area, District of Keewatin. Geological Survey of Canada, Paper 70-45, 19 pp.

Engelhardt, H. 2004. Thermal regime and dynamics of the West Antarctic ice sheet. Annals of Glaciology, 39(1): 85-92.

Engelhardt, H. and B. Kamb. 1997. Basal hydraulic system of a West Antarctic ice stream: constraints from borehole observations. Journal of Glaciology, 43(144): 207-230.

Engelhardt, H. and B. Kamb. 1998. Basal sliding of Ice Stream B, West Antarctica. Journal of Glaciology, 44(147): 223- 230.

Engelhardt, H., N. Humphrey, B. Kamb and M. Fahnestock. 1990. Physical conditions at the base of a fast moving Antarctic ice stream. Science, 248: 57-59.

Environment Canada, 1986. Hydrometric Map Supplement. Inland Waters Directorate, Water Resources Branch, Water Survey of Canada, Ottawa.

Evans, D.J.A. and D.I. Benn. 2004. Facies description and the logging of sedimentary exposures. In: D.J.A. Evans and D.I. Benn (Eds.), *A Practical Guide to the Study of Glacial Sediments*. Arnold, London, pp. 11-51.

Evans, D.J.A., C.D. Clark, and W.A. Mitchell. 2005. The last British Ice Sheet: A review of the evidence utilised in the compilation of the Glacial Map of Britain. Earth-Science Reviews, 70(3-4): 253-312.

Evans, D.J.A., E.R. Phillips, J.F. Hiemstra and C.A. Auton. 2006. Subglacial till: Formation, sedimentary characteristics and classification. Earth-Science Reviews, 78(1-2): 115-176.

Evans, D.J.A., S.J. Livingstone, A. Vieli and C.Ó Cofaigh. 2009. The palaeoglaciology of the central sector of the British and Irish Ice Sheet: reconciling glacial geomorphology and preliminary ice sheet modelling. Quaternary Science Reviews, 28(7-8): 739-757.

Evans, I.S. 2012. Geomorphometry and landform mapping: What is a landform? Geomorphology, 137: 94-106.

Everest, J., T. Bradwell and N. Golledge. 2005. Subglacial landforms of the Tweed Palaeo-Ice Stream. Scottish Geographical Journal, 121(2): 163-173.

Eyles, N. (Ed). 1983. *Glacial Geology: An Introduction for Engineers and Earth Scientists*. Pergamon Press, Oxford, 431 pp.

Eyles, N. 2006. The role of meltwater in glacial processes. Sedimentary Geology, 190: 257-268.

Eyles, N., C.H. Eyles and A.D. Miall. 1983. Lithofacies types and vertical profile models; an alternative approach to the description and environmental interpretation of glacial diamict and diamictite sequences. Sedimentology, 30: 393-410.

Falconer, G., J.D. Ives, O.H. Loken and J.T. Andrews. 1965. Major end moraines in eastern and central Arctic Canada. Geographical Bulletin, 7: 137-153.

Finlayson, A., J. Merritt, M. Browne, A. McMillan and K. Whitbread. 2010. Ice sheet advance, dynamics, and decay configurations: evidence from west central Scotland. Quaternary Science Reviews, 29(7-8): 969-988.

Finlayson, A.G. and T. Bradwell. 2008. Morphological characteristics, formation and glaciological significance of Rogen moraine in northern Scotland. Geomorphology, 101: 607-617.

Finlayson, A.G., D. Fabel, T. Bradwell and D. Sugden. 2014. Growth and decay of a marine terminating sector of the last British–Irish Ice Sheet: a geomorphological reconstruction. Quaternary Science Reviews, 83: 28-45.

Fisher, T. and J. Shaw. 1992. A depositional model for Rogen moraine, with examples from the Avalon Peninsula, Newfoundland. Canadian Journal of Earth-Sciences, 29: 669-686.

Flint, R.F. 1943. Growth of the North American ice sheet during the Wisconsin age. Geological Society of America Bulletin, 54: 325-362.

Ford, J.P. 1981. Mapping of glacial landforms from Seasat radar images. Quaternary Research, 22: 314-327.

Fowler A.C. 2010. The formation of sub-glacial streams and mega-scale glacial lineations. Proceedings of the Royal Society of London A, 466: 3181-3201.

Fowler, A.C. 2000. An instability mechanism for drumlin formation. In: A.J. Maltman, B. Hubbard and M.J. Hambrey (Eds.), *Deformation of Glacial Materials*. Geological Society of London, Special Publication 176, pp. 307-319.

Fowler, A.C. 2009. Instability modelling of drumlin formation incorporating lee-side cavity growth. Proceedings of the Royal Society A: Mathematical, Physical and Engineering Sciences, 465(2109): 2681-2702.

Fowler, R. 2001. Topographic Lidar. In: Maune, D.F. (Ed.), *Digital Elevation Model Technologies and Applications: The DEM Users Manual*. Bethesda: American Society for Photogrammetry and Remote Sensing, pp. 207-236.

Frödin, G. 1913. Bidrag till vastra Jämtlands senglaciala geologi. Sveriges Geologiska Undersökning C, 246 pp.

Frödin, G. 1925. Studien über die Eissheide in Zentralskandinavien. Bulletin of the Geological Institution, University of Uppsala, 19, 214 pp.

Fromm, E. 1965. Beskrivning av jordartskarta över Norrbottens län nedan lappmarksgränsen. Sveriges Geologiska Undersökning C, 39: 232 pp.

Fryer, J.G., H. Mitchell and J. Chandler. 2007. *Applications of 3D measurement from images*. Caithness: Whittles Publishing, 304 pp.

Fulton, R.J. 1995. Surficial Materials of Canada. In: Geological Survey of Canada, "A" Series Map 1880A.

Games, K. and .O.F. Bergersen. 1980. Wastage features of the inland ice sheet in central South Norway. Boreas, 9: 251-269.

Genga, A., F. Baglivi, M. Siciliano, T. Siciliano, M. Tepore, G. Micocci, C. Tortorella and D. Aiello. 2012. SEM-EDS investigation on PM10 data collected in Central Italy: Principal Component Analysis and Hierarchical Cluster Analysis. Chemistry Central Journal 6(Suppl 2): 1-15.

Gerçek, D., V. Toprak and J. Strobl. 2011. Object-based classification of landforms based on their local geometry and geomorphometric context. International Journal of Geographic Information Science, 25(6): 1011-1023.

Getis, A. and J.K. Ord. The analysis of spatial association by use of distance statistics. Geographical Analysis, 24(3) 1992.

Gillberg, G. 1976. Drumlins in southern Sweden. Bulletin of the Geological Institutions of the University of Uppsala. 6: 125-189.

Glasser, N.F and M.J. Hambrey. 2003. Ice-marginal terrestrial landsystems: Svalbard polythermal glaciers. In: D.J.A. Evans (Ed.), *Glacial Landsystems*. Arnold, London, pp. 65-88.

Goodfellow, B.W. 2007. Relict non-glacial surfaces in formerly glaciated landscapes. Earth-Science Reviews, 80: 47-73.

Goulet, C., M. Roy and I. McMartin. 2009. Glacial transport and local ice dynamics under the Keewatin Ice Divide of the Laurentide Ice Sheet, central Nunavut [Abstract]. American Geophysical Union Fall Meeting. December 14-18, 2009. San Francisco, California, USA.

Graham D.J. and N.G. Midgley. Graphical representation of particle shape using triangular diagrams: an Excel spreadsheet method. Earth Surface Processes and Landforms 25(13): 1473-1477.

Granlund, E. 1943. Beskrivning till jordartskarta över Västerbottens län nedanför odlingsgränsen. Sveriges Geologiska Undersökning C, 26: 165 pp.

Greenwood, S.L. and C.D. Clark. 2008. Subglacial bedforms of the Irish Ice Sheet. Journal of Maps, 4: 332-357.

Greenwood, S.L. and C.D. Clark. 2009a. Reconstructing the last Irish Ice Sheet 1: changing flow geometries and ice flow dynamics deciphered from the glacial landform record. Quaternary Science Reviews, 28(27-28): 3085-3100.

Greenwood, S.L. and C.D. Clark. 2009b. Reconstructing the last Irish Ice Sheet 2: a geomorphologically-driven model of ice sheet growth, retreat and dynamics. Quaternary Science Reviews, 28(27-28): 3101-3123.

Greenwood, S.L. and C.D. Clark. 2010. The sensitivity of subglacial bedform size and distribution to substrate lithological control. Sedimentary Geology, 232(3-4): 130-144.

Greenwood, S.L. and J. Kleman. 2010. Glacial landforms of extreme size in the Keewatin sector of the Laurentide Ice Sheet. Quaternary Science Reviews, 29(15-16), 1894-1910.

Greenwood, S.L., C.D. Clark and A.L.C. Hughes. 2007. Formalising an inversion methodology for reconstructing ice-sheet retreat patterns from meltwater channels: application to the British Ice Sheet. Journal of Quaternary Science, 22(6): 637-645.

Gripp, K. 1929. Glaciologische und geologische Ergebnisse der Hamburgischen Spitzbergen-Expedition. 1927. Abhandlungen aus dem Gebiete der Naturwissenschaften, Herausgegeben von dem naturwissenschaftlichen Verein in Hamburg, 22(2-4): 146-249.

Gupta, R.P. 2003. *Remote Sensing Geology*. 2nd Edition. Springer-Verlag, Berlin: 656 pp.

Gustavson, T.C. and J.C. Boothroyd. 1987. A depositional model for outwash, sediment sources, and hydrologic characteristics, Malaspina Glacier, Alaska: A modern analog of the southeastern margin of the Laurentide Ice Sheet. Geological Society of America Bulletin, 99(2): 187-200.

Haldorsen, S. 1981. Grain-size distribution of subglacial till and its relation to glacial crushing and abrasion. Boreas, 10: 91-105.

Haldorsen, S. 1983. The characteristics and genesis of Norwegian tills. In: J. Ehlers (Ed.), *Glacial deposits in North-West Europe*. A.A. Balkema, pp. 11-17.

Haldorsen, S. and J. Shaw. 1982. The problem of recognizing melt out till. Boreas, 11: 261-277

Hambrey, M.J., D. Huddart, M.R. Bennett and N.F. Glasser. 1997. Genesis of 'hummocky moraine' by thrusting in glacier ice: evidence from Svalbard and Britain. Journal of the Geological Society of London, 154: 623-632.

Hambrey, M.J., M.R. Bennett, J.A. Dowdeswell, N.F. Glasser and D. Huddart. 1999. Debris entrainment and transport in polythermal valley glaciers, Svalbard. Journal of Glaciology, 45: 69-86.

Hare, F.K. 1959. A photo-reconnaissance survey of Labrador-Ungava. Canadian Department of Mines Technical Survey, Geographical Branch, Memoir 6: 83 pp.

Hart, J.K. 1999. Identifying fast ice flow from landform assemblages in the geological record: a discussion. Annals of Glaciology, 28(1): 59-66.

Hartigan, J.A. 1975. *Clustering Algorithms*. New York: John Wiley and Sons, 351 pp.

Haschenberger, J. 1999. A probability model of scour and fill depths in gravel-bed channels. Water Resources Research, 35: 2857-2869.

Hättestrand, C. 1997. Ribbed moraines in Sweden – distribution pattern and palaeoglaciological implications. Sedimentary Geology, 111: 41-56.

Hättestrand, C. 1998. The glacial geomorphology of central and northern Sweden. Sveriges Geologiska Undersökning C, 85: 1-47.

Hättestrand, C. and A.P. Stroeven. 2002. A relict landscape in the centre of Fennoscandian glaciation: Geomorphological evidence of minimal Quaternary glacial erosion. Geomorphology, 44: 127-143.

Hättestrand, C. and C.D. Clark. 2006. The glacial geomorphology of Kola Peninsula and adjacent areas in the Murmansk Region, Russia. Journal of Maps, 2: 30-42.

Hättestrand, C. and J. Kleman. 1999. Ribbed moraine formation. Quaternary Science Reviews, 18: 43-61.

Heiser, P.A. and J.J. Roush. 2001. Pleistocene glaciations in Chukotka, Russia: - moraine mapping using satellite synthetic aperture radar (SAR) imagery. Quaternary Science Reviews, 20: 394-404.

Henderson, E.P. 1959. A glacial study of central Quebec-Labrador. Geological Survey of Canada Bulletin 50: 94 pp.

Hensley, S., R. Munjy and P. Rosen. 2001. Interferometric Synthetic Aperture Radar (IFSAR). In: Maune, D.F. (Ed.), *Digital Elevation Model Technologies and Applications: The DEM Users Manual*. Bethesda: American Society for Photogrammetry and Remote Sensing, pp. 142-206.

Hillier, J.K. and M.J. Smith. 2008. Residual relief separation: digital elevation model enhancement for geomorphological mapping. Earth Surface Processes and Landforms, 33: 2266-2276.

Hillier, J.K., M.J. Smith, C.D. Clark, C.R. Stokes and M. Spagnolo. 2013. Subglacial bedforms reveal an exponential size-frequency distribution. Geomorphology, 190: 82-91.

Hindmarsh, R.C.A. 1998a. Drumlinization and drumlin-forming instabilities: Viscous till mechanisms. Journal of Glaciology, 44: 293-314.

Hindmarsh, R.C.A. 1998b. Ice-stream surface texture, sticky-spots, waves and breathers: The coupled flow of ice, till and water. Journal of Glaciology, 44: 589-614.

Hindmarsh, R.C.A. 1998c. The stability of a viscous till sheet coupled with ice flow, considered at wavelengths less than ice thickness. Journal of Glaciology, 44: 288-292.

Hindmarsh, R.C.A., G.S. Boulton and K. Hutter. 1989. Modes of operation of thermo-mechanically coupled ice sheets. Annals of Glaciology, 12: 57-69.

Hockey, B. 1970. An improved coordinate system for particle shape representation. Journal of Sedimentary Petrology, 40: 1054-1056.

Hodge, S.M. and S.K. Doppelhammer. 1996. Satellite imagery of the onset of streaming flow of ice streams C and D, West Antarctica. Journal of Geophysical Research, 101(C3): 6669-6677.

Hodgson, M.E. and P. Bresnahan. 2004. Accuracy of airborne Lidar-derived elevation: empirical assessment and error budget. Photogrammetric Engineering & Remote Sensing, 70(3): 331-339.

Högbom, A.G. 1885. Glaciala och petrografiska iakttagelser i Jemtlands län. Sveriges Geologiska Undersökning C, 70: 39 pp.

Högbom, A.G. 1894. Geologisk beskrifning öfver Jemtlands län. Sveriges Geologiska Undersökning C, 140: 107 pp.

Högbom, A.G. 1920. Geologisk beskrivning öfver Jemtlands län. 2nd ed. Sveriges Geologiska Undersökning C, 140: 139 pp.

Holmsen, G. 1935. Nordre Femund. Beskrivelse til det geologiske rektangelkart. Norsk Geologisk Undersökelse, 144: 55 pp.

Hoppe, G. 1952. Hummocky moraine regions with special reference to the interior of Norrbotten. Geografiska Annaler, 34: 1-72.

Hoppe, G. 1959. Glacial morphology and inland ice recession in northern Sweden. Geografiska Annaler, 41(4): 193-212.

Houmark-Nielsen, M. 2010. Extent, age and dynamics of Marine Isotope Stage 3 glaciations in the southwestern Baltic Basin. Boreas, 39: 343-359.

Hubbard B. and N. Glasser. 2005. *Field techniques in Glaciology and Glacial Geomorphology.* J Wiley & Sons, Chichester, 400 pp.

Hughes, A.L.C., C.D. Clark and C.J. Jordan. 2010. Subglacial bedforms of the last British Ice Sheet. Journal of Maps, 6: 543-563.

Hughes, A.L.C., C.D. Clark and C.J. Jordan. 2014. Flow-pattern evolution of the last British Ice Sheet. Quaternary Science Reviews, 89: 148-168.

Hughes, O.L. 1964. Surficial geology, Nichicun-Kaniapiskau map-area, Quebec. Geological Survey of Canada Bulletin 106: 18 pp.

Hughes, T.J. 1981. Numerical reconstruction of paleo-ice sheets. In: G.H. Denton and T.J. Hughes (Eds.), *The Last Great Ice Sheets*. New York: John Wiley and Sons, pp. 221-261.

Hughes, T.J., G.H. Denton and M.G. Grosswald. 1977. Was there a late-Würm Arctic ice sheet? Nature, 266: 596-602.

Huybechts, P. and S. T'siobbel. 1995. Thermomechanical modeling of Northern Hemisphere ice sheets with a two-level mass-balance parameterization. Annals of Glaciology, 21: 111-116.

Ignatius, H.C. 1958. On the late-Wisconsin deglaciation in Eastern Canada. Acta Geographica, 16(3): 34 pp.

Iverson, N.R., R.W. Baker and T.S. Hooyer. 1997. A ring-shear device for the study of till deformation: Tests on tills with contrasting clay contents. Quaternary Science Reviews, 16(9): 1057-1066.

Iverson, N.R., T.S. Hooyer and R.W. Baker. 1998. Ring-shear studies of till deformation: Coulomb-plastic behavior and distributed strain in glacier beds. Journal of Glaciology, 44(148): 634-642.

Ives, J.D. 1956. Till patterns in central Labrador. The Canadian Geographer, 2(8): 25-33.

Ives, J.D., J.T. Andrews and R.G. Barry. 1975. Growth and decay of the Laurentide Ice Sheet and comparisons with Fenno-Scandinavia. Die Naturwissenschaften, 62: 118-125.

Jansson, K.N. 2005. Map of the glacial geomorphology of north-central Québec-Labrador, Canada. Journal of Maps, v2005: 46-56.

Jansson, K.N. and N.F. Glasser. 2005. Palaeoglaciology of the Welsh sector of the British–Irish Ice Sheet. Journal of the Geological Society of London, 162: 25-37.

Jansson, K.N., J. Kleman and D.R. Marchant. 2002. The succession of ice-flow patterns in north-central Québec-Labrador, Canada. Quaternary Science Reviews, 21: 503-523.

Jensen, J.B.O. 1993. Late Weichselian deglaciation pattern in the southwestern Baltic: Evidence from glacial deposits off the island of Møn, Denmark. Bulletin of the Geological Society of Denmark, 40: 314-331.

Johnsen, T.F., L. Olsen and A. Murray. 2012. OSL ages in central Norway support a MIS 2 interstadial (25-20 ka) and a dynamic Scandinavian ice sheet. Quaternary Science Reviews, 44: 96-111.

Johnson, R.A. and D.W. Wichern. 1992. *Applied Multivariate Statistical Analysis*, Vol. 6. Upper Saddle River, NJ: Prentice Hall, 774 pp.

Jónsson, S.A., A. Schomacker, Í.Ö. Benediktsson, Ó. Ingólfsson and M.D. Johnson. 2014. The drumlin field and the geomorphology of the Múlajökull surge-type glacier, central Iceland. Geomorphology, 207: 213-220.

Jørgensen, F. and J.A. Piotrowski. 2003. Signature of the Baltic Ice Stream on Funen Island, Denmark during the Weichselian Glaciation. Boreas, 32: 242-255.

Jørgensen, P. 1977. Some properties of Norwegian tills. Boreas, 6: 149-157.

Kamb, B. 1987. Glacier surging mechanism based on linked cavity system configuration of the basal water conduit system. Journal of Geophysical Research, 92: 9083-9100.

Kamb, B. 1991. Rheological nonlinearity and flow instability in the deforming bed mechanism of ice stream motion. Journal of Geophysical Research, 96(B10): 16585-16595.

Kamb, B. and E. La Chapelle. 1964. Direct observation of the mechanism of glacier sliding over bedrock. Journal of Glaciology, 5: 159-172.

Kaszycki, C.A. and W.W. Shilts. 1979. Average depth of glacial erosion, Canadian Shield. Geological Survey of Canada, Ottawa, Current Research, Part B: 395-396.

Kavanaugh, J.L. and G.K.C. Clarke. 2001. Abrupt glacier motion and reorganization of basal shear stress following the establishment of a connected drainage system. Journal of Glaciology 47(15): 472-480.

Kavanaugh, J.L. and G.K.C. Clarke. 2006. Discrimination of the flow law for subglacial sediment using in situ measurements and an interpretation model. Journal of Geophysical Research, 111: 20 pp.

King, E.C., J. Woodward and A.M. Smith. 2007. Seismic and radar observation of subglacial bed forms beneath the onset zone of Rutford Ice Stream, Antarctica. Journal of Glaciology, 53(183): 665-672.

King, E.C., R.C.A. Hindmarsh and C.R. Stokes. 2009. Formation of mega-scale glacial lineations observed beneath a West Antarctic ice stream. Nature Geoscience, 2: 585-588.

Kivekäs, E.K. 1946. Zur kenntnis der mechanischen, chemischen und mineralogischen zuzammensetzung der finnischen moränen. Acta agral. Fennica, 60: 122 pp.

Klassen, R.A. 1995. Drift composition and glacial dispersal trains, Baker Lake Area, District of Keewatin, Northwest Territories. Geological Survey of Canada Bulletin 485: 68 pp.

Kleman J. and C. Hättestrand. 1999. Frozen-bed Fennoscandian and Laurentide Ice Sheets during the Last Glacial Maximum. Nature, 402: 63-66.

Kleman, J. and A.P. Stroeven. 1997. Preglacial surface remnants and Quaternary glacial regimes in northwestern Sweden. Geomorphology, 19: 35-54.

Kleman, J. and I. Borgström. 1990. The boulder fields of Mt. Fulufjället, west-central Sweden - Late Weichselian boulder blankets and interstadial periglacial phenomena. Geografiska Annaler, (72)A: 63-78.

Kleman, J. and I. Borgström. 1994. Glacial landforms indicative of a partly frozen glacier bed. Journal of Glaciology, 40(135): 255-264.

Kleman, J. and I. Borgström. 1996. Reconstruction of palaeo-ice sheets: The use of geomorphological data. Earth Surface Processes and Landforms, 21: 893-909.

Kleman, J. and N. Glasser. 2007. The subglacial thermal organization (STO) of ice sheets. Quaternary Science Reviews, 26(5-6): 585-597.

Kleman, J., C. Hättestrand and A. Clarhall. 1999. Zooming in on frozen-bed patches: scale-dependent controls on Fennoscandian ice sheet basal thermal zonation. Annals of Glaciology, 28: 189-194.

Kleman, J., C. Hättestrand, A.P. Stroeven, K.N. Jansson, H. De Angelis and I. Borgström. 2006. Reconstruction of palaeo-ice sheets — inversion of their glacial geomorphological record. In: P.G. Knight (Ed.), *Glacier Science and Environmental Change*. Oxford: Blackwell, pp. 192-198.

Kleman, J., C. Hättestrand, I. Borgström and A. Stroeven. 1997. Fennoscandian paleoglaciology reconstructed using a glacial geological inversion model. Journal of Glaciology, 43(144): 283-299.

Kleman, J., I. Borgström and C. Hättestrand. 1994. Evidence for a relict glacial landscape in Quebec-Labrador. Palaeogeography, Palaeoclimatology, Palaeoecology, III(3-4): 217-228.

Kleman, J., J. Fastook and A.P. Stroeven. 2002. Geologically and geomorphologically constrained numerical model of Laurentide Ice Sheet inception and build-up. Quaternary International, 95-96: 87-98.

Kleman, J., K.N. Jansson, H. De Angelis, A. Stroeven, C. Hattestrand, G. Alm and N.F. Glasser. 2010. North American Ice Sheet build-up during the last glacial cycle, 115-21 kyr. Quaternary Science Reviews, 29: 2036-2051.

Knight, J. 2002. Glacial sedimentary evidence supporting stick-slip basal ice flow. Quaternary Science Reviews, 21: 975-983.

Knight, J. 2006. Geomorphic evidence for active and inactive phases of Late Devensian ice in north-central Ireland. Geomorphology, 75(1-2): 4-19.

Knight, J. 2010. Basin-scale patterns of subglacial sediment mobility: Implications for glaciological inversion modelling. Sedimentary Geology, 232(3-4): 145-160.

Knight, J. and A.M. McCabe. 1997. Identification and significance of ice-flow-transverse subglacial ridges (Rogen moraines) in northern central Ireland. Journal of Quaternary Science, 12(6): 519-524.

Knight, J., S.G. McCarron and A.M. McCabe. 1999. Landform modification by palaeo-ice streams in east central Ireland. Annals of Glaciology, 28: 161-167.

Krüger, J. and K.H. Kjær. 1999. A data chart for field description and genetic interpretation of glacial diamicts and associated sediments…with examples from Greenland, Iceland, and Denmark. Boreas, 28: 386-402.

Krzyszkowski, D. 1994. Forms at the base of till units indicating deposition by lodgement and melt-out, with examples from Wartanian tills near Bełchatow, central Poland. Sedimentary Geology, 91: 229-238.

Kujansuu, R. 1967. On the deglaciation of western Finnish Lapland. Bulletin de la Commission Géologique de Finlande, 232, 98 pp.

Kurimo, H. 1980. Depositional deglaciation forms as indicators of different glacial and glaciomarginal environments. Boreas, 9: 179-191.

Lagerbäck, R. and A.-M. Robertsson. 1988. Kettle holes—stratigraphic archives for Weichselian geology and palaeoenvironment in northernmost Sweden. Boreas, 17: 439-468.

Lagerbäck, R., 1988a. The Veiki moraines in northern Sweden— widespread evidence of an Early Weichselian deglaciation. Boreas, 17: 469-486.

Lagerbäck, R., 1988b. Periglacial phenomena in the wooded areas of north Sweden—relicts from the Tä rendöinterstadial. Boreas 17: 487-499.

Lamsters, K. 2012. Drumlins and related glaciogenic landforms of the Madliena Tilted Plain, Central Latvian Lowland. Bulletin of the Geological Society of Finland, 84: 45-57.

Larsen, N.K., J.A. Piotrowski and C. Kronborg. 2004. A multiproxy study of a basal till: a time-transgressive accretion and deformation hypothesis. Journal of Quaternary Science, 19(1): 9-21.

Larsen, N.K., K.L. Knudsen, C.F. Krohn, C. Kronborg, A.S. Murray, and O.B. Nielsen. 2009. Late Quaternary ice sheet, lake and sea history of southwest Scandinavia—a synthesis. Boreas, 38: 732-761.

Larson, G.J., D.E. Larson, E.B. Evenson, R.B. Alley, O. Knudsen, M.S. Lachniet and S.L. Goetz. 2006. Glaciohydraulic supercooling on former ice sheets? Geomorphology, 75: 20-32.

Lattin, J.M., J.D. Carroll and P.E. Green. 2003. *Analyzing Multivariate Data*. Pacific Grove, CA: Thomson Brooks, 556 pp.

Lawson, D.E. 1981. Distinguishing characteristics of diamictons at the margin of the Matanuska Glacier, Alaska. Annals of Glaciology, 2: 78-84.

Lawson, D.E., J.C. Strasser, E.B. Evenson, R.B. Alley, G.J. Larson and S.A. Arcone. 1998. Glaciohydraulic supercooling: a freeze-on mechanism to create stratified, debris-rich basal ice: I. Field evidence. Journal of Glaciology, 44: 216-226.

Laxon, S., K. Giles, A. Ridout, D. Wingham, R. Willatt, R. Cullen, R. Kwok, A. Schweiger, J.L Zhang, C. Haas, S. Hendricks, R. Krishfield, N. Kurtz, S. Farrell, S. and M. Davidson. 2013. CryoSat-2 estimates of Arctic sea ice thickness and volume. Geophysical Research Letters, 40(4): 732-737.

Lee, H.A. 1959. Surficial geology of southern District of Keewatin and the Keewatin ice divide, Northwest Territories. Geological Survey of Canada Bulletin 51: 42 pp.

Lee, H.A. 1960a. Late-glacial and postglacial Hudson Bay sea episode. Science, 131: 1609-1611.

Lee, H.A. 1960b. Surficial geology, Sakami Lake area, Quebec. Geological Survey of Canada, Map 52-1959.

Lee, H.A., B.G. Craig and J.G. Fyles. 1957. Keewatin Ice Divide. Geological Society of America Bulletin, 68: 1760-1761.

Lee, J.R. and E.R. Phillips. 2008. Progressive soft sediment deformation within a subglacial shear zone—a hybrid mosaic–pervasive deformation model for Middle Pleistocene glaciotectonised sediments from eastern England. Quaternary Science Reviews, 27(13-14): 1350-1362.

Li, X., A.B. Baker. and T. Hutt. 2002. Accuracy of airborne IFSAR mapping. In: Proceedings of FIG XXII International Congress, 19-26 April, Washington, USA, pp. 1-11.

Lindén, M and P. Möller 2005. Marginal formation of De Geer moraines and their implication on the dynamics of grounding-line recession. Journal of Quaternary Science, 20: 113-133.

Lindén, M, P. Möller and L. Adrielsson. 2008. Ribbed moraine formation by subglacial folding, thrust stacking and lee-side cavity infill. Boreas, 37: 102-131.

Lindkvist, Å and S. Svensson. 1957. Glacialmorfologiska studier i Gysenområdet i nordvästra Jämtland. Geographica, 31: 206-222.

Liverman, D., M. Batterson, T. Bell, L. Nolan, A. Marich and M. Putt. 2006. Digital elevation models from Shuttle Radar Topography Mission data - new insights into the Quaternary history of Newfoundland. Current Research, Newfoundland and Labrador Department of Natural Resources Survey, 06(1): 177-189.

Livingstone, S.J., C. Ó Cofaigh and D.J.A. Evans. 2010. A major ice drainage pathway of the last British–Irish Ice Sheet: the Tyne Gap, northern England. Journal of Quaternary Science, 25(3): 354-370.

Livingstone, S.J., C. Ó. Cofaigh and D.J.A. Evans. 2008. Glacial geomorphology of the central sector of the last British-Irish Ice Sheet. Journal of Maps, 4(1): 358-377.

Livingstone, S.J., D.J.A. Evans, C. Ó Cofaigh, B.J. Davies, J.W. Merritt, D. Huddart, W.A. Mitchell, D.H. Roberts and L. Yorke. 2012. Glaciodynamics of the central sector of the last British–Irish Ice Sheet in Northern England. Earth-Science Reviews, 111(1-2): 25-55.

Lord, C.S. 1953. Geological notes on southern District of Keewatin, Northwest Territories. Geological Survey of Canada, Paper 53-22, 11 pp.

Lukas, S., A. Graf, S. Coray and C. Schlüchter. 2012. Genesis, stability and preservation potential of large lateral moraines of Alpine valley glaciers — towards a unifying theory based on Findelengletscher, Switzerland. Quaternary Science Reviews, 38: 27-48.

Lukas, S., D.I. Benn, C.M. Boston, M. Brook, S. Coray, D.J.A. Evans, A. Graf, A. Kellerer-Pirklbauer, M.P. Kirkbride, M. Krabbendam, H. Lovell, M. Machiedo, S.C. Mills, K. Nye, B.T.I. Reinardy, F.H. Ross and M. Signer. 2013. Clast shape analysis and clast transport paths in glacial environments: A critical review of methods and the role of lithology. Earth-Science Reviews, 121: 96-116.

Lundqvist, G. 1935. Isavsmältningen i Bergslagen. Geologiska Föreningens i Stockholm Förhandlingar, 57: 287-381.

Lundqvist, G. 1937. Sjösediment från Rogenområdet i Härjedalen. Sveriges Geologiska Undersökning C, 408: 90 pp.

Lundqvist, G. 1943. Norlands Jordater. Sveriges Geologiska Undersökning C, 457: 166 pp.

Lundqvist, G. 1951. Beskrivning till jordartskartaöver Kopparbergs län. Sveriges Geologiska Undersökning, 21: 213 pp.

Lundqvist, J. 1958. Studies of the Quaternary history and deposits of Värmland, Sweden: Experiences made while preparing a survey map. Sveriges Geologiska Undersökning C, 52(2), 57 pp.

Lundqvist, J. 1969. Problems of the so-called Rogen moraine. Sveriges Geologiska Undersökning C, 648: 32 pp.

Lundqvist, J. 1981. Moraine morphology – Terminological remarks and regional aspects. Geografiska Annaler, 63(A): 127-138.

Lundqvist, J. 1989. Rogen (ribbed) moraine – identification and possible origin. Sedimentary Geology, 62: 281-292.

Lundqvist, J. 1992. Glacial stratigraphy in Sweden. Geological Survey of Finland, Special Paper 15, pp. 43-59.

Lundqvist, J. 1997. Rogen moraine – an example of two step formation of glacial landscapes. Sedimentary Geology, 111: 27-40.

Lytwyn, J. 2010. Remote sensing and GIS investigation of glacial features in the region of Devil's Lake State Park, South-Central Wisconsin, USA. Geomorphology, 123(1-2): 46-60.

Maclachlan, J.C. and C.H. Eyles. 2013. Quantitative geomorphological analysis of drumlins in the Peterborough drumlin field, Ontario, Canada. Geografiska Annaler: Series A, Physical Geography, 95(2): 125-144.

Madhulatha, T.S. 2012. An overview of clustering methods. IOSR Journal of Engineering, 2(4): 719-725.

Maltman, A.J. and A. Bolton. 2003. How sediments become mobilized. In: P. Van Rensbergen, R.R. Hillis, A.J. Maltman and C.K. Morley (Eds.), *Subsurface Sediment Mobilization*. London, Geological Society of London, pp. 9-20.

Mangerud, J. 1981. The Early and Middle Weichselian in Norway: a review. Boreas, 10: 381-383.

Mangerud, J. 1983. The glacial history of Norway. In: J. Ehlers (Ed.), *Glacial deposits in North-West Europe*, A.A. Balkema, Rotterdam, pp. 3-9.

Mangerud, J. 2004. Ice sheet limits on Norway and the Norwegian continental shelf. In: J. Ehlers and P.L. Gibbard (Eds.), *Quaternary Glaciations—Extent and Chronology*, vol. 1. Elsevier, Amsterdam, pp. 271-294.

Mangerud, J., R. Gyllencreutz, Ø. Lohne and J.I. Svendsen. 2011. Glacial History of Norway. In: J. Ehlers, P.L. Gibbard and P.D. Hughes (Eds), *Developments in Quaternary Science*, 15, Elsevier, Amsterdam, pp. 279-298.

Mannerfelt, C. 1945. Nas gra glacialgeologiska formelement och deras vittnesbörd om inlandsisens avsmältningsmekanik i svensk ochnorsk fjällterräng. Geografiska Annaler, 27(A): 1-239.

Margold, M. and K.N. Jansson. 2012. Evaluation of data sources for mapping glacial meltwater features. International Journal of Remote Sensing, 33(8): 2355-2377.

Marich, A., M. Batterson and T. Bell. 2005. The morphology and sedimentological analyses of Rogen moraines, central Avalon Peninsula, Newfoundland. Newfoundland and Labrador Department of Natural Resources Geological Survey, Report 05-1: 14 pp.

Mark, D.M. 1973. Analysis of axial orientation data, including till fabrics. Geological Society of America Bulletin, 84: 1369-1374.

Markgren, M. and M. Lassila. 1980. Problems of moraine morphology: Rogen moraine and Blattnick moraine. Boreas, 9: 271-274.

Marshall, S.J. and G.K.C Clarke. 1997a. A continuum mixture model of ice stream thermomechanics in the Laurentide Ice Sheet 1. Theory. Journal of Geophysical Research, 102(B9): 20599–20614.

Marshall, S.J. and G.K.C Clarke. 1997b. A continuum mixture model of ice stream thermomechanics in the Laurentide Ice Sheet 2. Application to the Hudson Strait Ice Stream. Journal of Geophysical Research, 102(B9): 20615–20638.

Marshall, S.J. and P.U. Clark. 2002. Basal temperature evolution of North American ice sheets and implications for the 100-kyr cycle. Geophysical Research Letters, 29(4): 2214.

Marshall, S.J., L. Tarasov, G.K.C. Clarke and W.R. Peltier. 2000. Glaciological reconstruction of the Laurentide Ice Sheet: physical processes and modelling challenges. Canadian Journal of Earth Sciences, 37: 769-793.

McCabe, A.M., J. Knight and McCarron, S.G. 1999. Ice-flow stages and glacial bedforms in north central Ireland: a record of rapid environmental change during the last glacial termination. Journal of the Geological Society of London, 156: 63-72.

McClenaghan, M.B., P.T. Bobrowski, G.E.M. Hall and S.J. Cook (Eds.). 2001. *Drift Exploration in Glaciated Terrain*. Geological Society of London, Special Publications, 185: 350 pp.

McMartin, I. 2000. Till composition across the Meliadine Trend, Rankin Inlet area, Keewatin Region, Nunavut. Geological Survey of Canada, Ottawa, Open File 3747, 329 pp.

McMartin, I. and L.A. Dredge. 2005. History of ice flow in the Schultz Lake (NTS 66A) and Wager Bay (NTS 56G) areas, Kivalliq Region, Nunavut. Geological Survey of Canada, Ottawa, Current Research 2005-B-2, 10 pp.

McMartin, I. and P.J. Henderson. 1999. A relative ice-flow chronology for the Keewatin Sector of the Laurentide Ice Sheet, Northwest Territories (Kivalliq Region, Nunavut). Geological Survey of Canada, Ottawa, Current Research 1999-C: 129-138.

McMartin, I. and P.J. Henderson. 2004. Evidence from Keewatin (central Nunavut) for paleo-ice divide migration. Géographie Physique et Quaternaire, 58(2-3): 163-186.

McMartin, I., E.C. Little, T. Ferbey, C.A. Ozyer and D. Utting. 2003b. Ice flow history and drift prospecting in the Committee Bay belt, central Nunavut: results from the Targeted Geoscience Initiative. Geological Survey Canada, Ottawa, Current Research 2003-C4, 11 pp.

McMartin, I., P.J. Henderson, B.A. Kjarsgaard, and K. Venance. 2003a. Regional distribution and chemistry of kimberlite indicator minerals, Rankin Inlet and MacQuoid Lake areas, Kivalliq Region, Nunavut. Geological Survey of Canada, Ottawa, Open File 1575, 110 p.

McMillan, M., H. Corr, A. Shepherd, A. Ridout, S. Laxon and R. Cullen. 2013. Three-dimensional mapping by CryoSat-2 of subglacial lake volume changes. Geophysical Research Letters, 40(16): 4321.

Melanson, A., T. Bell and L. Tarasov. 2013. Numerical modelling of subglacial erosion and sediment transport and its application to the North American ice sheets over the Last Glacial cycle. Quaternary Science Reviews, 68: 154-174.

Menzies, J. 1979. A review of the literature on the formation and location of drumlins. Earth-Science Reviews, 14(4): 315-359.

Menzies, J. 1987. Towards a general hypothesis on the formation of drumlins. In: J. Menzies and J. Rose (Eds.), *Drumlin Symposium*. Rotterdam, A.A. Balkema, pp. 9-24.

Menzies, J. 1989a. Drumlins – products of controlled or uncontrolled glaciodynamic response? Quaternary Science Reviews, 8: 151-158.

Menzies, J. 1989b. Subglacial hydraulic conditions and their possible impact upon subglacial bed formation. Sedimentary Geology, 62: 125-150.

Menzies, J. 1990. Sand intraclasts within a diamicton mélange, southern Niagara Peninsula, Ontario, Canada. Journal of Quaternary Science, 5: 189-206.

Menzies, J. 2000. Micromorphological analysis of microfabrics and microstructures indicative of deformational processes in glacial sediments, In: A.J. Maltman, B. Hubbard and M.J. Hambrey (Eds.), *Deformation of Glacial Materials*. Geological Society Special Publication 176, London, pp. 245-258.

Menzies, J. 2002. Problems and perspectives. In: J. Menzies (Ed.), *Modern and Past Glacial Environments: A Revised Student Edition*. Oxford: Butterworth-Heineman, pp. 475-481.

Menzies, J. and A.J. Maltman. 1992. Microstructures in diamictons – evidence of subglacial bed conditions. Geomorphology, 6: 27-40.

Menzies, J. and D. Ellwanger. 2011. Insights into subglacial processes inferred from the micromorphological analyses of complex diamicton stratigraphy near Illmensee-Lichtenegg, Höchsten, Germany. Boreas, 40(2): 271-288.

Menzies, J. and J. Rose. 1989. Subglacial bedforms – an introduction. Sedimentary Geology, 62(2-4): 117-122.

Menzies, J. and W.W. Shilts. 1996. Subglacial environments. In: J. Menzies (Ed.), *Past Glacial Environments: Sediments, Forms and Techniques*. Oxford: Butterworth-Heineman, pp. 15-136.

Menzies, J. and W.W. Shilts. 2002. Subglacial environments. In: J. Menzies (Ed.), *Modern and Past Glacial Environments: A Revised Student Edition.* Oxford: Butterworth-Heineman, pp. 183-278.

Menzies, J., J.J.M. van der Meer and J. Rose. 2006. Till as a glacial “tectomict”, its internal architecture, and the development of a "typing" method for till differentiation. Geomorphology, 75: 172-200.

Menzies, J., J.J.M. van der Meer, E. Domack and J.S. Wellner. 2010. Micromorphology: as a tool in the detection, analyses and interpretation of (glacial) sediments and man-made materials. Proceedings of the Geologists Association, 121: 281-292.

Mercer, B., 2001. Comparing LIDAR and IFSAR: What Can You Expect? In: Proceedings of Photogrammetric Week 2001, Stuttgart, Germany, pp. 2-10.

Mills, H.H. 1987. Morphometry of drumlins in the northeastern and north-central USA. In: J. Menzies and J. Rose (Eds.), *Drumlin Symposium*. Rotterdamn, A.A. Balkema, pp. 131-147.

Minell, H. 1977. Transverse moraine ridges of basal origin in Härjedalen. Geologiska Föreningens i Stockholm Förhandlingar, 99: 271-277.

Minell, H. 1980. The distribution of local bedrock material in some moraine forms from the inner part of northern Sweden. Boreas, 9(4): 275-281.

Mitchell, W.A. 1994. Drumlins in ice sheet reconstructions, with reference to the western Pennines, northern England. Sedimentary Geology, 91: 313-331.

Möller, P. 2006. Rogen moraine: an example of glacial reshaping of pre-existing landforms. Quaternary Science Reviews, 25: 362-389.

Möller, P. 2010. Melt-out till and ribbed moraine formation, a case study from south Sweden. Sedimentary Geology, 232(3-4): 161-180.

Moore, P.L., N.R. Iverson and D. Cohen. 2009. Ice flow across a warm-based/cold-based transition at a glacier margin. Annals of Glaciology, 50(52): 1-8.

Moore, P.L., N.R. Iverson, K.T. Uno, M.P. Dettinger, K.A. Brugger and P. Jansson. 2013. Entrainment and emplacement of englacial debris bands near the margin of Storglaciären, Sweden. Boreas, 42(1): 71-83.

Munro-Stasiuk, M.J. 2000. Rhythmic till sedimentation: evidence for repeated hydraulic lifting of a stagnant ice mass. Journal of Sedimentary Research, 70: 94-106.

Murray, T. 1997. Assessing the paradigm shift: deformable glacier beds. Quaternary Science Reviews, 16: 995-1016.

Napieralski, J. 2007. GIS and field-based spatiotemporal analysis for evaluation of paleo–ice sheet simulations. The Professional Geographer, 59(2): 173-183.

Napieralski, J. and N. Nalepa. 2010. The application of control charts to determine the effect of grid cell size on landform morphometry. Computers & Geosciences, 36(2): 222-230.

Napieralski, J., J. Harbor and Y. Li. 2007. Glacial geomorphology and geographic information systems. Earth-Science Reviews, 85(1-2): 1-22.

Nesje, A. and S.O. Dahl. 1992. Geometry, thickness and isostatic loading of the Late Weichselian Scandinavian ice sheet. Norsk Geografisk Tidsskrift, 72: 271-273.

Nesje, A., E. Anda, N. Rye, R. Lien, P.A. Hole and L.H. Blikra. 1987. The vertical extent of the Late Weichselian ice sheet in the Nordfjord-Møre area, western Norway. Norsk Geologisk Tidsskrift, 67: 125-141.

Ó Cofaigh, C., C.R. Stokes, O.B. Lian, C.D. Clark and S. Tulacyzk. 2013. Formation of mega-scale glacial lineations on the Dubawnt Lake Ice Stream bed: 2. Sedimentology and stratigraphy. Quaternary Science Reviews, 77: 210-227.

Olsen, L., H. Sveian, B. Bergstrøm, D. Ottesen and L. Rise. 2013. Quaternary glaciations and their variations in Norway and on the Norwegian continental shelf. In: L. Olsen, O. Fredin and O. Olesen (Eds.), *Quaternary Geology of Norway*. Geological Survey of Norway Special Publication 13, pp. 27-78.

Ottesen, D., C.R. Stokes, L. Rise and L. Olsen. 2008. Ice-sheet dynamics and ice streaming along the coastal parts of northern Norway. Quaternary Science Reviews. 27(9-10): 922-940.

Palmann, C., M. Mavromatis, J. Sequeira and B. Brisco. 2008. Earth observation using radar data: an overview of applications and challenges. International Journal of Digital Earth, 1: 171-195.

Paterson, W.S.B. 1972. Laurentide Ice Sheet: Estimated volumes during late Wisconsin. Reviews of Geophysics and Space Physics, 10: 885-917.

Paterson, W.S.B. 1994. *The Physics of Glaciers*. Oxford: Butterworth-Heinemann, 480 pp.

Patterson, C.J., and R.L. Hooke. 1995. Physical environment of drumlin formation. Journal of Glaciology, 41(137): 30-38.

Paul, D., S. Hanmer, S. Tella, T.D. Peterson and A.N. LeCheminant. 2002. Compilation, bedrock geology of part of the Western Churchill Province, Nunavut – Northwest Territories. Geological Survey of Canada, Open File 4236.

Paul, M.A. 1983. The supraglacial landsystem. In: N. Eyles (Ed.), *Glacial Geology. An Introduction for Engineers and Earth Scientists*. Oxford: Pergamon Press, pp. 71-90.

Paulen, R.C. and M.B. McClenaghan (Eds.). 2013. *New frontiers for exploration in glaciated terrain.* Geological Survey of Canada, Open File 7374: 85 pp.

Payne, A.J. and P.W. Dongelmans. 1997. Self-organization in the thermomechanical flow of ice sheets: Journal of Geophysical Research, 102: 12219-12234.

Peters, L.E., S. Anandakrishnan, R.B. Alley, J.P. Winberry, D.E. Voight, A.M. Smith and D.L. Morse. 2006. Subglacial sediments as a control on the onset and localization of two Siple Coast ice streams, West Antarctica. Journal of Geophysical Research, 111(B01302): 14 pp.

Phillips, E., J. Everest and D. Diaz-Doce. 2010. Bedrock controls on subglacial landform distribution and geomorphological processes: Evidence from the Late Devensian Irish Sea Ice Stream. Sedimentary Geology, 232(3-4): 98-118.

Piotrowski, J. and S. Tulaczyk. 1999. Subglacial conditions under the last ice sheet on northwest Germany: ice-bed separation and enhanced basal sliding? Quaternary Science Reviews, 18: 737-751.

Piotrowski, J.A. and A. Kraus. 1997. Response of sediment to ice sheet loading in northwestern Germany: effective stresses and glacier bed stability. Journal of Glaciology, 43: 495-502.

Piotrowski, J.A., N.K. Larsen and F.W. Junge 2004. Reflections on soft subglacial beds as a mosaic of deforming and stable spots. Quaternary Science Reviews: 23, 993-1000.

Piotrowski, J.A., N.K. Larsen, J. Menzies and W. Wysoata. 2006. Formation of subglacial till under transient bed conditions: deposition, deformation, and basal decoupling under a Weichselian ice sheet lobe, central Poland. Sedimentology, 53: 83-106.

Prest, V.K. 1968. Nomenclature of moraines and ice-flow features as applied to the glacial map of Canada. Geological Survey of Canada Paper, 67-57: 32 pp.

Prest, V.K. 1970. Quaternary geology of Canada. In: R.J.W. Douglas (Ed.), *Geology and Economic Minerals of Canada*. Ottawa. Geological Survey of Canada, Economic Geology Report No. 1, pp. 676-764.

Prest, V.K., D.R. Grant and V.N. Rampton. 1968. Glacial map of Canada. Geological Survey of Canada, Map 1253A.

Pritchard, H., T. Murray, A. Luckman, T. Strozzi and S. Barr. 2005. Glacier surge dynamics of Sortebræ, east Greenland, from synthetic aperture radar feature tracking. Journal of Geophysical Research, 110: F03005.

Punkari, M. 1984. The relations between glacial dynamics and the tills in the eastern part of the Baltic shield. Striae, 20: 49-54.

Rainbird, R.H., W.J. Davis, S.J. Pehrsson, N. Wodicka, N. Rayner and T. Skulski. 2010. Early Paleoproterozoic supracrustal assemblages of the Rae domain, Nunavut, Canada: Intracratonic basin development during supercontinent break-up and assembly. Precambrian Research, 181(1-4): 167-186.

Rasmusson, G. and N. Tarras-Wahlberg. 1951. Terrängformerna vid Saxvattnet. Svensk Geografisk Årsbok, 27: 173-176.

Rathbun, A.P., C. Marone, R.B. Alley and S. Anandakrishnan. 2008. Laboratory study of the frictional rheology of sheared till. Journal of Geophysical Research, 113(F2): 1-14.

Raunholm, S., H.P. Sejrup and E. Larsen. 2003. Lateglacial landform associations at Jæren (SW Norway) and their glaci-dynamic implications. Boreas, 32(3): 462-475.

Reed, B., C.J. Jr. Galvin and J.P. Miller. 1962. Some aspects of drumlin geometry. American Journal of Science, 260: 200-210.

Rice, J.M., R.C. Paulen, J. Menzies and M.B. McClenaghan. 2014. Micromorphological descriptions of till from pit K-62, Pine Point mining district, Northwest Territories. Geological Survey of Canada, Open File 7526, 30 pp.

Ridler, K.H. and W.W. Shilts. 1974. Exploration for Archean polymetallic sulphide deposits in permafrost terrain; an integrated geological/geochemical tehchnique; District of Keewatin, Kaminak Lake area. Geological Survey of Canada, Paper 73-34, 33 pp.

Ripley, B.D. 1977. Modelling spatial patterns. Journal of the Royal Statistical Society, 2: 172-212.

Ripley, B.D. 1979. Tests of 'randomness' for spatial point patterns. Journal of the Royal Statistical Society, Series B, 41: 368-374.

Roberts, M.J., F.S. Tweed, A.J. Russell, O. Knudsen, D.E. Lawson, G.J. Larson, E.B. Evenson and H. Bjornsson. 2002. Glaciohydraulic supercooling in Iceland. Geology, 30: 439-442.

Rogerson, R.J. and C.M. Tucker. 1972. Observations on the glacial history of the Avalon Peninsula. Maritime Sediments, 8: 25-31.

Rose, J. 1987. Drumlins as part of a glacier bedform continuum. In: J. Menzies and J. Rose (Eds.), *Drumlin Symposium*. Rotterdamn, A.A. Balkema, pp. 103-116.

Rose, J. 1989. Glacier stress patterns and sediment transfer associated with the formation of superimposed flutes. Sedimentary Geology, 62(214): 151-176.

Rose, J. and J. Letzer. 1975. Drumlin measurements: a test of the reliability of data derived from 1:25,000 scale topographic maps. Geological Magazine, 112: 361-371.

Saha, K. 2009. Semi-automated to automated-refined method for mid-scale glacial landform mapping. Papers of the Applied Geography Conferences, 32: 362-371.

Saha, K., N.A. Wells and M. Munro-Stasiuk. 2011. An object-oriented approach to automated landform mapping: A case study of drumlins. Computers & Geosciences, 37(9): 1324-1336.

Salcher, B.C., R. Hinsch and M. Wagreich. 2010. High-resolution mapping of glacial landforms in the North Alpine Foreland, Austria. Geomorphology, 122(3-4): 283-293.

Sandeman, H.A., B.L. Cousens and C.J. Hemmingway. 2003. Continental tholeiitic mafic rocks of the Paleoproterozoic Hurwitz Group, Central Hearne sub-domain, Nunavut: insight into the evolution of the Hearne sub-continental lithosphere. Canadian Journal of Earth Science, 40: 1219-1237.

Sarala, P. 2006. Ribbed moraine stratigraphy and formation in southern Finnish Lapland. Journal of Quaternary Science, 21(4): 387-398.

Sarala, P. 2007. Glacial morphology and ice lobation in southern Finnish Lapland. Geological Survey of Finland, Special Paper 46; 9-18.

Sarala, P. and V. Peuraniemi. 2007. Exploration using till geochemistry and heavy minerals in the ribbed moraine area of southern Finnish Lapland. Geochemistry: Exploration, Environment, Analysis, 7: 195-205.

Schoof, C. 2007. Pressure-dependent viscosity and interfacial instability in coupled ice-sediment flow. Journal of Fluid Mechanics, 570: 227-252.

Sejrup, H.P., A. Nygård, A.M. Hall and H. Haflidason. 2009. Middle and Late Weichselian (Devensian) glaciation history of south-western Norway, North Sea and eastern UK. Quaternary Science Reviews, 28(3-4): 370-380.

Sergienko, O. and R. Hindmarsh. 2013. Regular patterns in frictional resistance of ice-stream beds seen by surface data inversion. Science, 342: 1086-1089.

Shaw, J. 1979. Genesis of the Sveg tills and Rogen moraines of central Sweden, a model of basal melt out. Boreas, 8: 409-426.

Shaw, J. 1982. Melt out till in the Edmonton area, Alberta, Canada. Canadian Journal of Earth Sciences, 19: 1548-1569.

Shaw, J. 1983. Drumlin formation related to inverted meltwater erosional marks. Journal of Glaciology, 29: 461-479.

Shaw, J. 2002. The meltwater hypothesis for subglacial landforms. Quaternary International, 90: 5-22.

Shaw, J., D. Sharp and J. Harris. 2010. A flowline map of glaciated Canada based on remote sensing data. Canadian Journal of Earth Science, 47: 89-101.

Shilts, W.W. 1973. Drift prospecting; geochemistry of eskers and till in permanently frozen terrain: District of Keewatin; Northwest Territories. Geological Survey of Canada, Ottawa, Paper 72-45: 34 pp.

Shilts, W.W. 1977. Geochemistry of till in perennially frozen terrain of the Canadian Shield - application to prospecting. Boreas, 5: 203-212.

Shilts, W.W. 1978. Nature and genesis of mud boils, central Keewatin, Canada. Canadian Journal of Earth Sciences, 15, 1053-1068.

Shilts, W.W. 1980. Flow patterns in the central North American ice sheet. Nature, 286: 213-286.

Shilts, W.W. 1984. Quaternary events - Hudson Bay Lowland and southern District of Keewatin. In: R.J. Fulton (Ed.), *Quaternary Stratigraphy of Canada - A Canadian Contribution to IGCP Project 24*. Geological Survey of Canada, Paper 84-10, pp. 117-126.

Shilts, W.W., C. Cunningham and C. Kaszycki. 1979. Keewatin Ice Sheet — Re-evaluation of the traditional concept of the Laurentide Ice Sheet. Geology, 7: 537-541.

Shilts, W.W., J.M. Aylsworth, C.A. Kaszycki and R.A. Klassen. 1987. Canadian Shield. In: W.L. Graf (Ed.), *Geomorphic systems of North America*. Geological Society of America. Centennial Special Volume, 2: 119-161.

Silverman, B.W. 1986. *Density Estimation for Statistics and Data Analysis*. New York: Chapman and Hall, 176 pp.

Škrbić, B., K. Héberger and N. Đurišić-Mladenović. 2013. Comparison of multianalyte proficiency test results by sum of ranking differences, principal component analysis, and hierarchical cluster analysis. Analytical and Bioanalytical Chemistry, 405(25): 8363-8375.

Smalley, I.J. 1966. Drumlin formation: A rheological model. Science, 151(3716): 1379-1380

Smalley, I.J. and D.J. Unwin. 1968. The formation and shapes of drumlins and their distribution and orientation in drumlin fields. Journal of Glaciology, 7: 377-390.

Smalley, I.J. and J. Warburton. 1994. The shape of drumlins, their distribution in drumlin fields, and the nature of sub-ice shaping processes. Sedimentary Geology, 91: 241-252.

Smith, A.M. and T. Murray. 2009. Bedform topography and basal conditions beneath a fast-flowing West Antarctic ice stream. Quaternary Science Reviews, 28(7-8): 584-596.

Smith, M.J. and C.D. Clark. 2005. Methods for the visualization of digital elevation models for landform mapping. Earth Surface Processes and Landforms, 30(7): 885-900.

Smith, M.J. and C.F. Pain. 2009. Applications of remote sensing in geomorphology. Progress in Physical Geography, 33(4): 568-582.

Smith, M.J. and S.M. Wise. 2007. Problems of bias in mapping linear landforms from satellite imagery. International Journal of Applied Earth Observation and Geoinformation, 9(1): 65-78.

Smith, M.J., J. Rose and S. Booth. 2006. Geomorphological mapping of glacial landforms from remotely sensed data: An evaluation of the principal data sources and an assessment of their quality. Geomorphology, 76(1-2): 148-165.

Smith, M.J., P. Dunlop and C.D. Clark. 2005. An overview of sub-glacial bedforms in Ireland, mapped from digital elevation data. In: P. Knight (Ed.), *Glacier Science and Environmental Change*. Blackwell Publishing, pp. 384-387.

Sneed, E.D. and R.L. Folk. 1958. Pebbles in the lower Colorado River, Texas, a study in particle morphogenesis. Journal of Geology, 66: 114-150.

Sollid, J. and L, Sørbel. 1994. Distribution of glacial landforms in Southern Norway in relation to the thermal regime of the last continental ice sheet. Geografiska Annaler, 76(1/2): 25-35.

Sollid, J. and L. Sørbel. 1984. Distribution and genesis of moraines in Central Norway. In: L.-K. Koningsson (Ed.), Ten years of Nordic till research. Striae, 20: 63-67.

Soyez, D. 1974. Studien zur Geomorphologie und zum letztglacialen Eisrückzug in den Gebirgen Süd-Lapplands/Schweden. Geografiska Annaler, 56(A): 1-71.

Spagnolo, M., C.D. Clark, A.L.C. Hughes and P. Dunlop. 2011. The topography of drumlins; assessing their long profile shape. Earth Surface Processes and Landforms, 36(6): 790-804.

Spagnolo, M., C.D. Clark, J.C Ely, C.R. Stokes, J.B. Anderson, K. Andreassen, A.G.C Graham and E.C. King. 2014. Size, shape and spatial arrangement of mega-scale glacial lineations from a large and diverse dataset. Earth Surface Processes and Landforms, 39(11): 1432-1448.

Stanford, S.D. and D.M. Mickelson. 1985. Till fabric and deformational structures in drumlins near Waukesha, Wisconsin, U.S.A. Journal of Glaciology, 31(109): 1985.

Stokes, C.R. and C.D. Clark. 2001. Palaeo-ice streams.Quaternary Science Reviews 20: 1437-1457.

Stokes, C.R. and C.D. Clark. 2002. Are long subglacial bedforms indicative of fast ice flow? Boreas, 31: 239-249.

Stokes, C.R. and C.D. Clark. 2003. The Dubawnt Lake palaeo-ice stream: evidence for dynamic ice sheet behaviour on the Canadian Shield and insights regarding the controls on ice-stream location and vigour. Boreas, 32: 263-279.

Stokes, C.R., A.C. Fowler, C.D. Clark, R.C.A. Hindmarsh and M. Spagnolo. 2013a. The instability theory of drumlin formation and its explanation of their varied composition and internal structure. Quaternary Science Reviews, 62: 77-96.

Stokes, C.R., C.D. Clark, O.B. Lian and S. Tulaczyk. 2006. Geomorphological map of ribbed moraines on the Dubawnt Lake palaeo-ice stream bed: a signature of ice stream shut-down? Journal of Maps, v2006: 1-9.

Stokes, C.R., C.D. Clark, O.B. Lian and S. Tulaczyk. 2007. Ice stream sticky spots: A review of their identification and influence beneath contemporary and palaeo-ice streams. Earth-Science Reviews, 81(3-4): 217-249.

Stokes, C.R., L. Tarasov and A.S Dyke. 2012. Dynamics of the North American Ice Sheet Complex during its inception and build-up to the Last Glacial Maximum. Quaternary Science Reviews, 50: 86–104.

Stokes, C.R., M. Spagnolo and C.D. Clark. 2011. The composition and internal structure of drumlins. Earth-Science Reviews, 107(3-4): 394-422.

Stokes, C.R., M. Spagnolo, C.D. Clark, C. Ó Cofaigh, O.B. Lian and R.B. Dunstone. 2013b. Formation of mega-scale glacial lineations on the Dubawnt Lake Ice Stream bed: 1. size, shape and spacing from a large remote sensing dataset. Quaternary Science Reviews, 77(1): 190-209.

Stokes, C.R., O.B. Lian, S. Tulaczyk and C.D. Clark. 2008. Superimposition of ribbed moraines on a palaeo-ice-stream bed: implications for ice stream dynamics and shutdown. Earth Surface Processes and Landforms, 33: 593-609.

Sugden, D.E. 1978. Glacial erosion by the Laurentide Ice Sheet. Journal of Glaciology, 21: 367-391.

Sugden, D.E. and B.S. John. 1976. *Glaciers and Landscape*. London, Edward Arnold Publishers, 376 pp.

Sutinen, R., M. Jakonen, M. Piekkari, P. Haavikko, P. Närhi and M. Middleton. 2010. Electrical-sedimentary anisotropy of Rogen moraine, Lake Rogen area, Sweden. Sedimentary Geology, 232(3-4): 181-189.

Sutinen, R., M. Middleton, P. Liwata, M. Piekkari and E. Hyvönen. 2009. Sediment anisotropy coincides with moraine ridge trend in south-central Finnish Lapland. Boreas, 38(3): 638–646.

Tanner, V. 1914. Studier öfver kvartärsystemet i Fennoskandias nordliga delar III. Bulletin de la Comission Géologique de Finland, 38: 815 pp.

Tarasov, L. and W.R. Peltier. 2004. A geophysically constrained large ensemble analysis of the deglacial history of the North American ice-sheet complex. Quaternary Science Reviews, 23(3-4): 359-388.

Tarasov, L. and W.R. Peltier. 2007. Coevolution of continental ice cover and permafrost extent over the last glacial-interglacial cycle in North America. Journal of Geophysical Research-Earth Surface: 112.

Taylor, R.S. 1956. Glacial geology of north-central Keewatin, Northwest Territories, Canada. Geological Society of America Bulletin, 67: 943-956.

Thompson, W.B. and H.W. Borns (Eds.). 1985. Surficial geology map of Maine. Maine Geological Survey, Department of Conservation, scale 1:50,000.

Thoresen, M. 1990. Quaternary map of Norway. Geological Survey of Norway, scale 1:1,000,000.

Tikkanen, M. 2002. The changing landforms of Finland. Fennia, 180(1-2): 21-30.

Trenhaile, A.S. 1971. Drumlins, their distribution and morphology. Canadian Geographer, 15: 113-126.

Trenhaile, A.S. 1975. The morphology of a drumlin field. Annals of the Association of American Geographers, 65: 297-312.

Trommelen, M. and M. Ross. 2009. Manitoba Far North Geomapping Initiative: field reconnaissance of surficial sediments, glacial landforms and ice-flow indicators, Great Island and Kellas Lake areas, Manitoba (NTS 54L, 64I, P). In: Report of Activities 2009, Manitoba Innovation, Energy and Mines. Manitoba Geological Survey, pp. 148-153.

Trommelen, M. and M. Ross. 2010. Subglacial landforms in northern Manitoba, Canada, based on remote sensing data. Journal of Maps, 6: 618–638.

Trommelen, M.S., M. Ross and A. Ismail. 2014. Ribbed moraines in northern Manitoba, Canada: characteristics and preservation as part of a subglacial bed mosaic near the core regions of ice sheets. Quaternary Science Reviews, 87: 135-155.

Trommelen, M.S., M. Ross and J.E. Campbell. 2012. Glacial terrain zone analysis of a fragmented paleoglaciologic record, southeast Keewatin sector of the Laurentide Ice Sheet. Quaternary Science Reviews, 40: 1-20.

Trommelen, M.S., M. Ross and J.E. Campbell. 2013. Inherited clast dispersal patterns: Implications for palaeoglaciology of the SE Keewatin Sector of the Laurentide Ice Sheet. Boreas, 42(3): 693-713.

Tulaczyk, S. 1998. Sedimentary processes at the base of a West Antarctic ice stream: Constraints from textural and compositional properties of subglacial debris. Journal of Sedimentary Research, 68: 487-496.

Tulaczyk, S., W.B. Kamb and H.F. Engelhardt. 2000. Basal mechanics of Ice Stream B, West Antarctica: 1. Till mechanics. Journal of Geophysical Research, 105(B1): 463-481.

Tylmann, K., J.A. Piotrowski and W. Wysota. 2013. The ice/bed interface mosaic: deforming spots intervening with stable areas under the fringe of the Scandinavian Ice Sheet at Sampława, Poland. Boreas, 42(2): 428-441.

Tyrrell, J.B. 1898. Report on the Doobaunt, Kazan, and Ferguson Rivers, and the north-west coast of Hudson Bay; and on two over-land routes from Hudson Bay to Lake Winnipeg. Geological Survey of Canada, Annual Report, Part F, 9: 218 pp.

van der Meer, J.J.M, J. Menzies and J. Rose. 2003. Subglacial till: the deforming glacier bed. Quaternary Science Reviews, 22(15-17): 1659-1685.

van der Meer, J.J.M. 1996. Micromorphology. In: J. Menzies (Ed.), *Past Glacial Environments – Sediments, Forms and Techniques*. Butterworth-Heinemann, Oxford, pp. 335-356.

van der Meer, J.J.M. and J. Menzies. 2011. The micromorphology of unconsolidated sediments. Sedimentary Geology, 238: 213-232.

van der Meer, J.J.M.. 1993. Microscopic evidence of subglacial deformation. Quaternary Science Reviews, 12: 553-587.

Van Landeghem, K.J.J., A.J. Wheeler and N.C. Mitchell. 2009. Seafloor evidence for palaeo-ice streaming and calving of the grounded Irish Sea Ice Stream: Implications for the interpretation of its final deglaciation phase. Boreas, 38(1): 119-131.

Vaughan, D.G., H. Corr, F. Ferraccioli, N. Frearson, N. O'Hare, D. Mach, J. Holt, D. Blankenship, D. Morse and D. Young. 2006. New boundary conditions for the West Antarctic ice sheet: subglacial topography beneath Pine Island Glacier. Geophysical Research Letters, 33: L09501.

Vernon, P. 1966. Drumlins and Pleistocene ice flow over the Ards Peninsula/Strangford Lough area, County Down, Ireland. Journal of Glaciology, 7(51): 377-390.

Virkkala, K. 1969. Suomen moreenien rakeisuusluokitus. Terra, 81: 273-278.

Vorren, T.O. 1977. Weichselian ice movement in South Norway and adjacent areas. Boreas, 6: 247-257.

Vorren, T.O. 1979. Weichselian ice movements, sediments and stratigraphy on Hardangervidda, South Norway. Norges geologiske undersøkelse, 350: 1-117.

Vorren, T.O. and E. Roaldset. 1977. Stratigraphy and lithology of Quaternary sediments at Møsvatn, Hardangervidda, South Norway. Boreas, 6: 53-69.

Walsh, S.J., D.R. Butler and G.P. Malanson. 1998. An overview of scale, pattern, process relationships in geomorphology: a remote sensing and GIS perspective. Geomorphology, 21(3-4): 183-205.

Wastenson, L. 1983. Rogen-Myskelsjöområdet. In: I. Borgström (Ed.), *Geomorphological Map 17C Funäsdalen—Description and Assessment of Areas of Geomorphological Importance*. Stockholm, Statens Naturvårdsverk, PM 1709, pp. 25-31.

Weertman, J. 1961. Mechanism for the formation of inner moraines found near the edge of cold ice caps and ice sheets. Journal of Glaciology, 3: 965-978.

Wellner J.S., D.C. Heroy and J.B. Anderson. 2006. The death mask of the Antarctic Ice Sheet: comparison of glacial geomorphic features across the continental shelf. Geomorphology, 75: 157-171.

Winsborrow, M.C.M., K. Andreassen, G.D. Corner and J.S. Laberg. 2010. Deglaciation of a marine-based ice sheet: Late Weichselian palaeo-ice dynamics and retreat in the southern Barents Sea reconstructed from onshore and offshore glacial geomorphology. Quaternary Science Reviews. 29(3-4): 424-442.

Wright, G.M. 1955. Geological notes on the central District of Keewatin Northwest Territories. Geological Survey of Canada, Paper 55-17: 15 pp.

Zhongchang, S., H. Guo, X. Li, X. Yue and Q. Huang. 2011. DEM generation and error analysis using the first Chinese airborne dual-antenna interferometric SAR data. International Journal of Remote Sensing, 32(23): 8485-8504.

Appendix A

The Distribution of Subglacial Landforms in South-Central Keewatin, Nunavut, Canada

Kaleb G. Wagner[1*], John Menzies[1], Jacob Napieralski[2] and John Delgaty[3]

[1]Department of Earth Sciences, Brock University *(kw11wm@brocku.ca), [2]Department of Natural Sciences, University of Michigan-Dearborn, [3]De Beers Canada

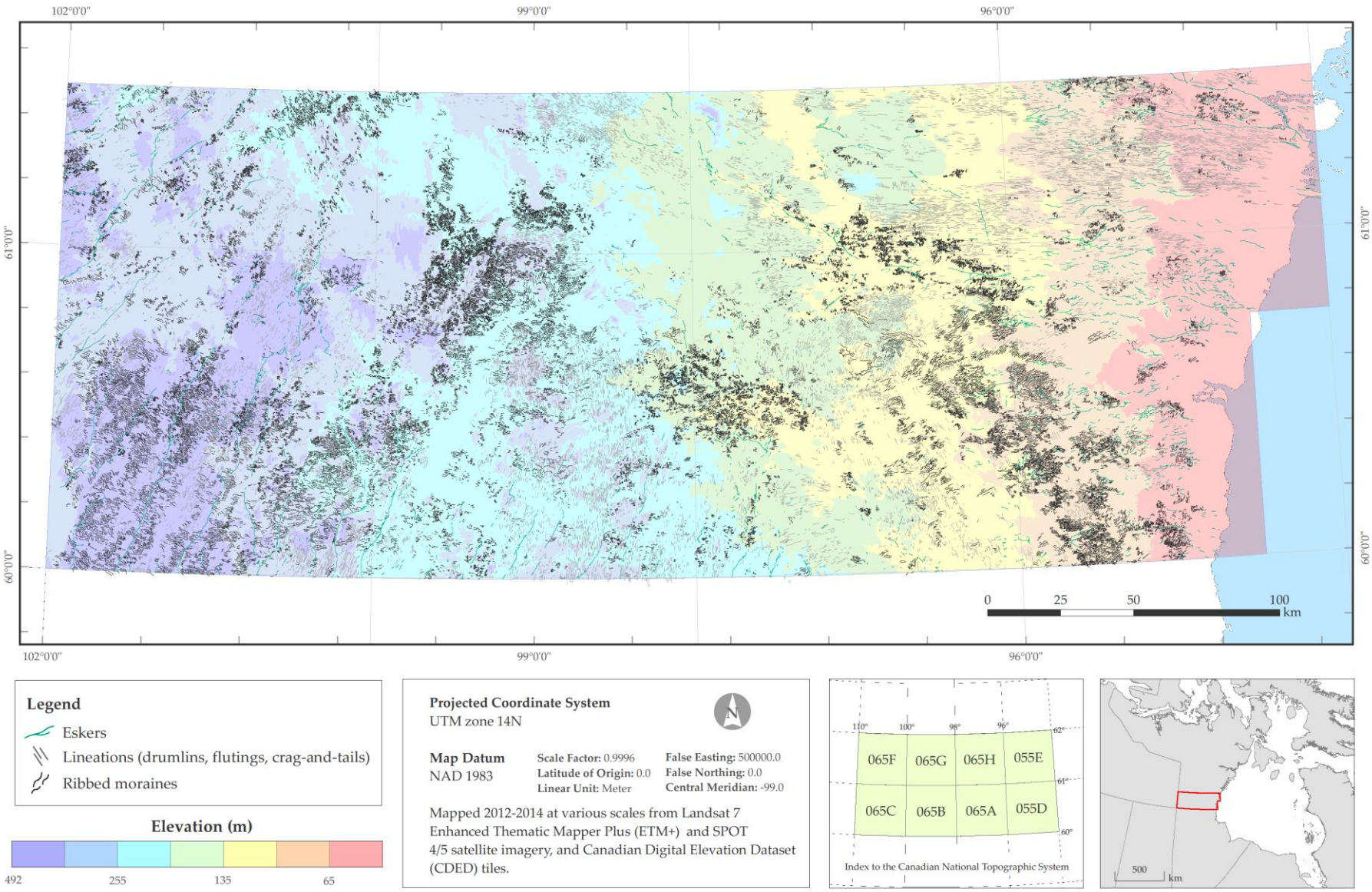

Appendix B – HCA Agglomeration Schedule and Scree Plot

Agglomeration schedule for hierarchical cluster analysis using Ward's minimum variance method.

	Cluster Combined			Stage Cluster First Appears		
Stage	Cluster 1	Cluster 2	Coefficients	Cluster 1	Cluster 2	Next Stage
1	8	9	.000	0	0	3
2	4	5	.001	0	0	8
3	8	11	.003	1	0	9
4	2	14	.007	0	0	6
5	7	13	.017	0	0	8
6	2	10	.034	4	0	12
7	1	3	.060	0	0	10
8	4	7	.090	2	5	10
9	6	8	.129	0	3	11
10	1	4	.227	7	8	12
11	6	12	.451	9	0	13
12	1	2	1.058	10	6	13
13	1	6	1.808	12	11	0

Scree plot of Ward's index values produced in HCA, showing a suggested level of 6 clusters to seed in the *k*-means algorithm based on the 'elbow rule'.

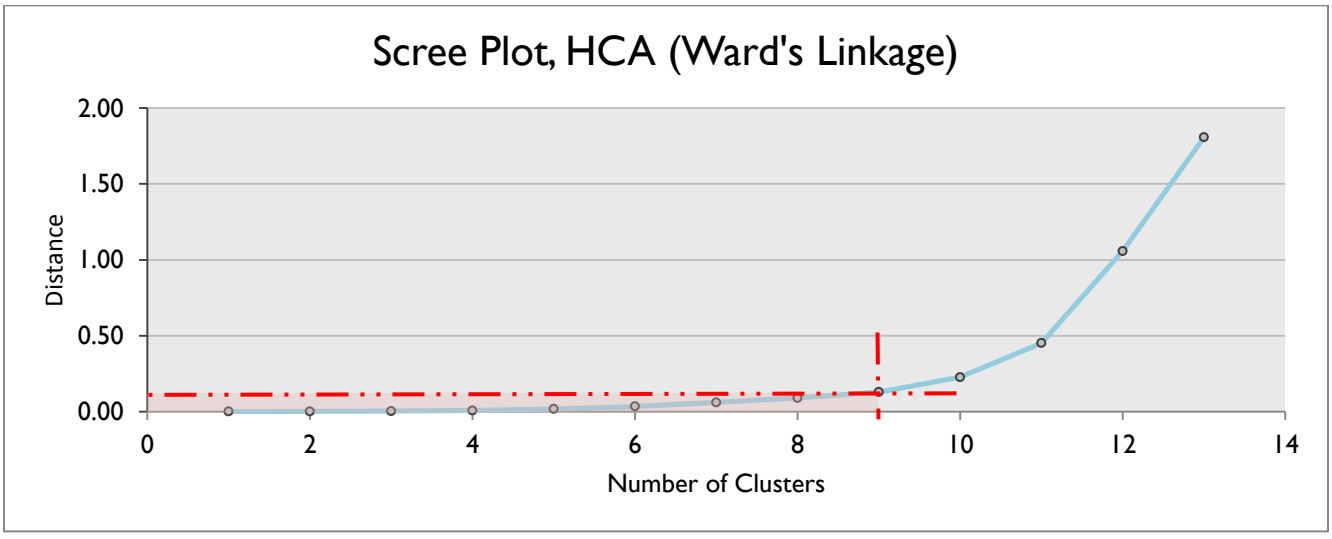

Appendix C – Table of Flowset Relative Age Relationships

Tabulation of flowset relative age relationships for south-central Keewatin based on instances of glacial landform cross-cutting and overprinting. Red (green) fill indicates a flowset listed along a given row is older (younger) than the flowset listed along the intersecting column. Purple fill indicates unknown relative age relationships. Question marks imply tentative relative age assignments. Blue fill indicates flowsets at intersecting rows/columns are presumed (without categorical evidence) to be of the same approximate age. Lins = streamlined landform flowset, rm = ribbed moraine flowset.

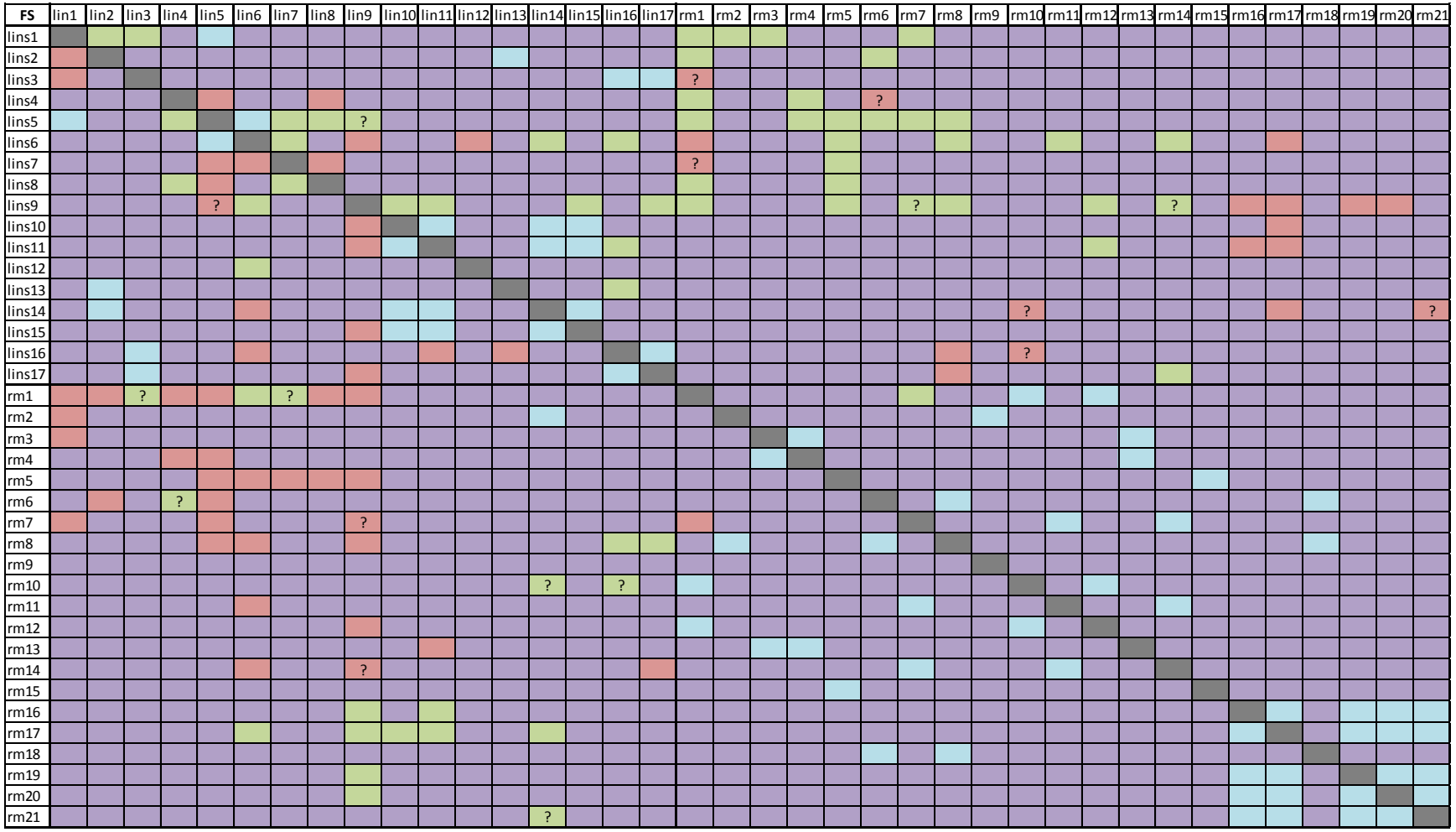

Appendix D – Raw Grain Size Data (Sieved Fraction)

Sample:	**KW/13/B/1B**
Initial wt. (g):	82.45

mm	phi	wt. retained (g)	cumulative (g)	pct. wt. (%)	pct. coarser. (%)	pt. finer (%)
>2.000	<-1.0	0.08	0.08	0.0970	0.0970	99.9030
1.400	-0.5	4.65	4.73	5.6398	5.7368	94.2632
1.000	0.0	5.39	10.12	6.5373	12.2741	87.7259
0.710	0.5	5.05	15.17	6.1249	18.3990	81.6010
0.500	1.0	5.14	20.31	6.2341	24.6331	75.3669
0.355	1.5	4.89	25.20	5.9309	30.5640	69.4360
0.250	2.0	5.33	30.53	6.4645	37.0285	62.9715
0.180	2.5	4.66	35.19	5.6519	42.6804	57.3196
0.125	3.0	5.62	40.81	6.8163	49.4967	50.5033
0.090	3.5	5.23	46.04	6.3432	55.8399	44.1601
0.063	4.0	5.92	51.96	7.1801	63.0200	36.9800
0.044	4.5	4.48	56.44	5.4336	68.4536	31.5464
pan		25.38	81.82	30.7823	99.2359	

Recovery (%)	99.24

Sample:	**KW/13/B/2B**
Initial wt. (g):	63.25

mm	phi	wt. retained (g)	cumulative (g)	pct. wt. (%)	cum pct. wt. (%)	pt. finer (%)
>2.000	<-1.0	0.09	0.09	0.1423	0.1423	99.8577
1.400	-0.5	5.11	5.20	8.0791	8.2213	91.7787
1.000	0.0	5.69	10.89	8.9960	17.2174	82.7826
0.710	0.5	4.72	15.61	7.4625	24.6798	75.3202
0.500	1.0	4.49	20.10	7.0988	31.7787	68.2213
0.355	1.5	4.02	24.12	6.3557	38.1344	61.8656
0.250	2.0	4.14	28.26	6.5455	44.6798	55.3202
0.180	2.5	3.48	31.74	5.5020	50.1818	49.8182
0.125	3.0	4.10	35.84	6.4822	56.6640	43.3360
0.090	3.5	3.68	39.52	5.8182	62.4822	37.5178
0.063	4.0	4.06	43.58	6.4190	68.9012	31.0988
0.044	4.5	2.94	46.52	4.6482	73.5494	26.4506
pan		16.08	62.60	25.4229	98.9723	

Recovery (%)	98.97

Sample:	KW/13/B/3B
Initial wt. (g):	63.45

mm	phi	wt. retained (g)	cumulative (g)	pct. wt. (%)	cum pct. wt. (%)	pt. finer (%)
>2.000	<-1.0	0.07	0.07	0.1103	0.1103	99.8897
1.400	-0.5	3.38	3.45	5.3270	5.4374	94.5626
1.000	0.0	3.81	7.26	6.0047	11.4421	88.5579
0.710	0.5	3.44	10.70	5.4216	16.8637	83.1363
0.500	1.0	3.45	14.15	5.4374	22.3010	77.6990
0.355	1.5	3.25	17.40	5.1221	27.4232	72.5768
0.250	2.0	3.71	21.11	5.8471	33.2703	66.7297
0.180	2.5	3.38	24.49	5.3270	38.5973	61.4027
0.125	3.0	4.52	29.01	7.1237	45.7210	54.2790
0.090	3.5	4.71	33.72	7.4232	53.1442	46.8558
0.063	4.0	5.63	39.35	8.8731	62.0173	37.9827
0.044	4.5	4.21	43.56	6.6351	68.6525	31.3475
pan		19.35	62.91	30.4965	99.1489	

Recovery (%)	99.15

Sample:	KW/13/H/1B
Initial wt. (g):	86.8

mm	phi	wt. retained (g)	cumulative (g)	pct. wt. (%)	cum pct. wt. (%)	pt. finer (%)
>2.000	<-1.0	0.02	0.02	0.0230	0.0230	99.9770
1.400	-0.5	0.81	0.83	0.9332	0.9562	99.0438
1.000	0.0	1.46	2.29	1.6820	2.6382	97.3618
0.710	0.5	1.71	4.00	1.9700	4.6083	95.3917
0.500	1.0	2.40	6.40	2.7650	7.3733	92.6267
0.355	1.5	3.03	9.43	3.4908	10.8641	89.1359
0.250	2.0	3.80	13.23	4.3779	15.2419	84.7581
0.180	2.5	3.97	17.20	4.5737	19.8157	80.1843
0.125	3.0	6.16	23.36	7.0968	26.9124	73.0876
0.090	3.5	7.92	31.28	9.1244	36.0369	63.9631
0.063	4.0	12.58	43.86	14.4931	50.5300	49.4700
0.044	4.5	10.73	54.59	12.3618	62.8917	37.1083
pan		31.81	86.40	36.6475	99.5392	

Recovery (%)	99.54

Sample:	KW/13/H/2B
Initial wt. (g):	73.42

mm	phi	wt. retained (g)	cumulative (g)	pct. wt. (%)	cum pct. wt. (%)	pt. finer (%)
>2.000	<-1.0	0.17	0.17	0.2315	0.2315	99.7685
1.400	-0.5	5.59	5.76	7.6137	7.8453	92.1547
1.000	0.0	6.07	11.83	8.2675	16.1128	83.8872
0.710	0.5	5.53	17.36	7.5320	23.6448	76.3552
0.500	1.0	5.31	22.67	7.2324	30.8771	69.1229
0.355	1.5	4.72	27.39	6.4288	37.3059	62.6941
0.250	2.0	4.94	32.33	6.7284	44.0343	55.9657
0.180	2.5	4.15	36.48	5.6524	49.6867	50.3133
0.125	3.0	4.90	41.38	6.6739	56.3607	43.6393
0.090	3.5	4.46	45.84	6.0746	62.4353	37.5647
0.063	4.0	5.11	50.95	6.9600	69.3953	30.6047
0.044	4.5	3.85	54.80	5.2438	74.6391	25.3609
pan		18.02	72.82	24.5437	99.1828	

Recovery (%)	99.18

Sample:	KW/13/N/1B
Initial wt. (g):	68.77

mm	phi	wt. retained (g)	cumulative (g)	pct. wt. (%)	cum pct. wt. (%)	pt. finer (%)
>2.000	<-1.0	0.28	0.28	0.4072	0.4072	99.5928
1.400	-0.5	5.27	5.55	7.6632	8.0704	91.9296
1.000	0.0	5.83	11.38	8.4775	16.5479	83.4521
0.710	0.5	5.22	16.60	7.5905	24.1384	75.8616
0.500	1.0	5.00	21.60	7.2706	31.4090	68.5910
0.355	1.5	4.63	26.23	6.7326	38.1416	61.8584
0.250	2.0	4.26	30.49	6.1946	44.3362	55.6638
0.180	2.5	3.37	33.86	4.9004	49.2366	50.7634
0.125	3.0	3.98	37.84	5.7874	55.0240	44.9760
0.090	3.5	4.00	41.84	5.8165	60.8405	39.1595
0.063	4.0	4.86	46.70	7.0670	67.9075	32.0925
0.044	4.5	3.70	50.40	5.3803	73.2878	26.7122
pan		17.97	68.37	26.1306	99.4184	

Recovery (%)	99.42

Appendix E – Raw Clast Sample Data

KW/13/B/1C

Clast #	Size (mm)			b/a	c/b	c/a	a-b	a-c	Sphericity	Angularity	Lithology	Faceted	Striated
	a axis	b axis	c axis										
1	4.89	4.10	2.67	0.8384	0.6512	0.5460	0.7900	2.22	M	VA	Gabbro Schist	y	n
2	3.7	3.06	2.63	0.8270	0.8595	0.7108	0.6400	1.07	H	SA	Diorite	n	n
3	4.02	1.99	1.95	0.4950	0.9799	0.4851	2.0300	2.07	L	A	Gabbro Schist	y	n
4	4.32	3.04	1.49	0.7037	0.4901	0.3449	1.2800	2.83	L	R	Gabbro Schist	y	n
5	2.75	2.67	2.00	0.9709	0.7491	0.7273	0.0800	0.75	H	SA	Gabbro	y	n
6	6.94	2.96	1.93	0.4265	0.6520	0.2781	3.9800	5.01	L	VA	Gabbro Schist	y	n
7	5.44	4.29	2.71	0.7886	0.6317	0.4982	1.1500	2.73	M	SR	Peridotite	y	y
8	4.17	3.60	1.77	0.8633	0.4917	0.4245	0.5700	2.40	L	A	Gabbro Schist	n	n
9	2.84	2.03	1.50	0.7148	0.7389	0.5282	0.8100	1.34	M	A	Granitoid	n	n
10	6.56	3.67	3.23	0.5595	0.8801	0.4924	2.8900	3.33	L	A	Gabbro Schist	y	n
11	2.7	2.65	1.39	0.9815	0.5245	0.5148	0.0500	1.31	M	A	Granitoid	n	n
12	3.2	2.19	1.26	0.6844	0.5753	0.3938	1.0100	1.94	L	A	Gabbro Schist	y	n
13	3.71	2.98	1.66	0.8032	0.5570	0.4474	0.7300	2.05	M	SA	Gabbro	n	n
14	3.86	2.35	1.73	0.6088	0.7362	0.4482	1.5100	2.13	L	A	Gabbro	y	n
15	3.02	2.54	1.71	0.8411	0.6732	0.5662	0.4800	1.31	M	SA	Gabbro	y	n
16	3.05	2.37	2.20	0.7770	0.9283	0.7213	0.6800	0.85	H	SA	Gabbro	y	n
17	2.04	1.93	1.59	0.9461	0.8238	0.7794	0.1100	0.45	H	A	Gabbro	y	n
18	2.54	2.49	0.90	0.9803	0.3614	0.3543	0.0500	1.64	M	A	Peridotite	y	n
19	2.42	1.83	0.95	0.7562	0.5191	0.3926	0.5900	1.47	M	SA	Peridotite	n	n
20	2.18	1.71	1.31	0.7844	0.7661	0.6009	0.4700	0.87	M	A	Diorite	n	n
21	2.86	1.27	1.08	0.4441	0.8504	0.3776	1.5900	1.78	L	A	Gabbro Schist	y	n
22	3.7	2.50	1.58	0.6757	0.6320	0.4270	1.2000	2.12	L	A	Gneiss	y	n
23	2.52	2.16	0.89	0.8571	0.4120	0.3532	0.3600	1.63	M	A	Gabbro Schist	y	n
24	3.47	1.95	0.96	0.5620	0.4923	0.2767	1.5200	2.51	L	VA	Gabbro Schist	y	n
25	2.13	1.28	1.15	0.6009	0.8984	0.5399	0.8500	0.98	M	SR	Gabbro	y	n
26	2.42	1.58	1.51	0.6529	0.9557	0.6240	0.8400	0.91	H	A	Gabbro Schist	y	n

27	2.63	2.44	1.19	0.9278	0.4877	0.4525	0.1900	1.44	M	A	Gabbro	n	n
28	4.21	3.27	2.11	0.7767	0.6453	0.5012	0.9400	2.10	M	SA	Gabbro Schist	y	n
29	2.24	1.92	0.84	0.8571	0.4375	0.3750	0.3200	1.40	M	A	Slate	n	n
30	2.27	1.63	1.26	0.7181	0.7730	0.5551	0.6400	1.01	M	VA	Gabbro	y	n
31	2.38	1.65	0.94	0.6933	0.5697	0.3950	0.7300	1.44	L	A	Gabbro Schist	n	n
32	2.49	1.98	1.48	0.7952	0.7475	0.5944	0.5100	1.01	H	SR	Peridotite	y	n
33	2.19	1.55	0.65	0.7078	0.4194	0.2968	0.6400	1.54	M	A	Slate	y	n
34	2.57	1.74	0.96	0.6770	0.5517	0.3735	0.8300	1.61	L	A	Gabbro Schist	n	n
35	4.16	2.67	1.50	0.6418	0.5618	0.3606	1.4900	2.66	L	VA	Gabbro Schist	n	n
36	3.55	2.73	1.92	0.7690	0.7033	0.5408	0.8200	1.63	M	SR	Mica Schist	n	n
37	1.82	1.31	1.28	0.7198	0.9771	0.7033	0.5100	0.54	M	SA	Gabbro	n	n
38	2.13	1.53	0.93	0.7183	0.6078	0.4366	0.6000	1.20	M	A	Slate	n	n
39	2.99	1.40	1.24	0.4682	0.8857	0.4147	1.5900	1.75	L	SA	Gabbro	y	n
40	2.83	1.37	1.25	0.4841	0.9124	0.4417	1.4600	1.58	L	SA	Quartzite	y	n
41	2.12	1.70	1.15	0.8019	0.6765	0.5425	0.4200	0.97	M	A	Gabbro	y	n
42	1.82	1.59	1.40	0.8736	0.8805	0.7692	0.2300	0.42	H	A	Granitoid	n	n
43	3.89	1.77	1.75	0.4550	0.9887	0.4499	2.1200	2.14	L	VA	Gabbro Schist	n	n
44	3.66	2.57	1.49	0.7022	0.5798	0.4071	1.0900	2.17	L	A	Gabbro Schist	y	n
45	3.53	2.74	1.71	0.7762	0.6241	0.4844	0.7900	1.82	L	VA	Gabbro Schist	y	n
46	2.84	2.49	1.47	0.8768	0.5904	0.5176	0.3500	1.37	M	SA	Granitoid	n	n
47	2.05	1.62	0.70	0.7902	0.4321	0.3415	0.4300	1.35	L	A	Gabbro Schist	n	n
48	1.13	0.76	0.55	0.6726	0.7237	0.4867	0.3700	0.58	M	A	Granitoid	n	n
49	2.6	1.89	1.58	0.7269	0.8360	0.6077	0.7100	1.02	M	A	Gabbro Schist	y	n
50	2.74	2.36	2.33	0.8613	0.9873	0.8504	0.3800	0.41	H	A	Amphibolite	y	n

KW/13/B/2C

Clast #	Size (mm)			b/a	c/b	c/a	a-b	a-c	Sphericity	Angularity	Lithology	Faceted	Striated
	a axis	b axis	c axis										
1	6.45	3.26	2.33	0.5054	0.7147	0.3612	3.1900	4.12	L	VA	Gabbro Schist	n	n
2	3.19	2.23	1.20	0.6991	0.5381	0.3762	0.9600	1.99	L	VA	Gabbro Schist	y	n

3	4	2.24	1.90	0.5600	0.8482	0.4750	1.7600	2.10	L	A	Gabbro Schist	y	n
4	4.27	2.17	1.99	0.5082	0.9171	0.4660	2.1000	2.28	L	A	Gabbro Schist	y	n
5	2.69	1.97	1.51	0.7323	0.7665	0.5613	0.7200	1.18	M	A	Gabbro Schist	y	n
6	5.28	3.70	2.46	0.7008	0.6649	0.4659	1.5800	2.82	L	VA	Slate	y	n
7	5.97	3.55	2.86	0.5946	0.8056	0.4791	2.4200	3.11	L	VA	Gabbro Schist	n	n
8	6.41	5.50	3.76	0.8580	0.6836	0.5866	0.9100	2.65	M	A	Gabbro Schist	y	n
9	5.29	2.51	1.91	0.4745	0.7610	0.3611	2.7800	3.38	L	VA	Gabbro Schist	n	n
10	3.06	1.66	1.65	0.5425	0.9940	0.5392	1.4000	1.41	L	VA	Diorite	n	n
11	2.01	1.34	0.95	0.6667	0.7090	0.4726	0.6700	1.06	M	A	Gabbro Schist	n	n
12	2.87	1.82	1.45	0.6341	0.7967	0.5052	1.0500	1.42	L	VA	Gabbro Schist	y	n
13	3.13	2.34	1.51	0.7476	0.6453	0.4824	0.7900	1.62	L	VA	Gabbro Schist	y	n
14	3.02	1.47	1.22	0.4868	0.8299	0.4040	1.5500	1.80	L	VA	Slate	y	n
15	3.99	1.86	1.06	0.4662	0.5699	0.2657	2.1300	2.93	L	A	Slate	y	n
16	3.35	2.78	1.50	0.8299	0.5396	0.4478	0.5700	1.85	M	A	Gabbro Schist	y	n
17	2.05	1.20	1.15	0.5854	0.9583	0.5610	0.8500	0.90	H	SA	Gabbro	n	n
18	3.4	2.60	1.52	0.7647	0.5846	0.4471	0.8000	1.88	M	A	Gabbro Schist	y	n
19	3.99	1.94	1.42	0.4862	0.7320	0.3559	2.0500	2.57	M	VA	Gabbro Schist	n	n
20	2.14	1.68	1.47	0.7850	0.8750	0.6869	0.4600	0.67	H	SR	Diorite	y	n
21	4.27	2.23	1.44	0.5222	0.6457	0.3372	2.0400	2.83	L	VA	Gabbro Schist	n	n
22	6.69	3.97	1.94	0.5934	0.4887	0.2900	2.7200	4.75	L	VA	Gabbro	y	n
23	1.9	1.66	1.36	0.8737	0.8193	0.7158	0.2400	0.54	H	SA	Diorite	n	n
24	4.09	2.17	1.78	0.5306	0.8203	0.4352	1.9200	2.31	L	VA	Gabbro Schist	n	n
25	5.86	4.16	3.15	0.7099	0.7572	0.5375	1.7000	2.71	M	A	Gabbro	n	n
26	2.38	2.04	1.39	0.8571	0.6814	0.5840	0.3400	0.99	M	VA	Peridotite	n	n
27	4.16	1.94	1.42	0.4663	0.7320	0.3413	2.2200	2.74	L	SA	Gabbro Schist	y	n
28	1.18	1.03	1.01	0.8729	0.9806	0.8559	0.1500	0.17	H	A	Granitoid	y	n
29	1.78	1.26	1.20	0.7079	0.9524	0.6742	0.5200	0.58	H	A	Granitoid	y	n
30	2.52	1.36	1.26	0.5397	0.9265	0.5000	1.1600	1.26	L	A	Granitoid	n	n
31	4.89	3.90	2.33	0.7975	0.5974	0.4765	0.9900	2.56	M	A	Gabbro Schist	n	n
32	5.1	4.58	1.35	0.8980	0.2948	0.2647	0.5200	3.75	L	VA	Gabbro Schist	n	n
33	2.83	1.24	1.20	0.4382	0.9677	0.4240	1.5900	1.63	L	VA	Gabbro Schist	n	n

34	2.39	1.69	1.05	0.7071	0.6213	0.4393	0.7000	1.34	L	A	Peridotite	n	n
35	2.84	1.80	1.64	0.6338	0.9111	0.5775	1.0400	1.20	L	VA	Gabbro Schist	n	n
36	3.16	2.53	1.85	0.8006	0.7312	0.5854	0.6300	1.31	L	VA	Gabbro Schist	y	n
37	2.26	1.84	1.60	0.8142	0.8696	0.7080	0.4200	0.66	H	VA	Gabbro Schist	n	n
38	3.29	2.47	0.53	0.7508	0.2146	0.1611	0.8200	2.76	L	VA	Gabbro	n	n
39	3.09	2.80	1.06	0.9061	0.3786	0.3430	0.2900	2.03	L	VA	Gabbro Schist	n	n
40	2.55	1.40	0.70	0.5490	0.5000	0.2745	1.1500	1.85	L	VA	Gabbro Schist	y	n
41	2.16	2.10	0.80	0.9722	0.3810	0.3704	0.0600	1.36	M	A	Gabbro Schist	n	n
42	2.96	2.22	1.43	0.7500	0.6441	0.4831	0.7400	1.53	L	VA	Gabbro Schist	n	n
43	2.77	1.59	0.57	0.5740	0.3585	0.2058	1.1800	2.20	L	VA	Gabbro Schist	n	n
44	5.19	2.76	1.64	0.5318	0.5942	0.3160	2.4300	3.55	L	A	Gabbro Schist	y	n
45	2.04	1.50	0.41	0.7353	0.2733	0.2010	0.5400	1.63	L	VA	Gabbro Schist	n	n
46	3	2.70	1.81	0.9000	0.6704	0.6033	0.3000	1.19	M	A	Gabbro Schist	n	n
47	2.17	1.64	1.55	0.7558	0.9451	0.7143	0.5300	0.62	M	A	Slate	n	n
48	2.81	2.13	1.03	0.7580	0.4836	0.3665	0.6800	1.78	L	VA	Gabbro Schist	n	n
49	2.55	1.71	1.44	0.6706	0.8421	0.5647	0.8400	1.11	M	VA	Gabbro Schist	n	n
50	2.85	1.57	0.59	0.5509	0.3758	0.2070	1.2800	2.26	L	A	Gabbro Schist	n	n

KW/13/B/3C

Clast #	Size (mm)			b/a	c/b	c/a	a-b	a-c	Sphericity	Angularity	Lithology	Faceted	Striated
	a axis	b axis	c axis										
1	2.66	2.24	1.53	0.8421	0.6830	0.5752	0.4200	1.13	M	A	Gneiss	n	n
2	2.77	2.05	1.31	0.7401	0.6390	0.4729	0.7200	1.46	L	SA	Gneiss	n	n
3	1.9	1.14	0.73	0.6000	0.6404	0.3842	0.7600	1.17	L	SR	Gneiss	n	n
4	3.26	1.94	0.94	0.5951	0.4845	0.2883	1.3200	2.32	L	VA	Gabbro Schist	n	n
5	4.72	2.65	1.71	0.5614	0.6453	0.3623	2.0700	3.01	L	SR	Phyllite	n	n
6	3.09	2.26	1.10	0.7314	0.4867	0.3560	0.8300	1.99	L	A	Amphibolite	n	n
7	2.55	2.12	1.28	0.8314	0.6038	0.5020	0.4300	1.27	M	VA	Gabbro Schist	n	n
8	2.65	1.96	1.91	0.7396	0.9745	0.7208	0.6900	0.74	M	SA	Gneiss	n	n
9	1.98	1.10	0.45	0.5556	0.4091	0.2273	0.8800	1.53	L	VA	Gabbro Schist	n	n

10	2.02	1.92	1.87	0.9505	0.9740	0.9257	0.1000	0.15	M	A	Gneiss	n	n
11	3.4	1.47	1.16	0.4324	0.7891	0.3412	1.9300	2.24	L	VA	Gabbro Schist	y	n
12	4.46	1.65	0.74	0.3700	0.4485	0.1659	2.8100	3.72	L	VA	Gabbro Schist	n	n
13	3.68	2.11	1.70	0.5734	0.8057	0.4620	1.5700	1.98	L	A	Gabbro Schist	n	n
14	2.82	1.13	1.05	0.4007	0.9292	0.3723	1.6900	1.77	L	SA	Gabbro Schist	y	n
15	3.51	2.25	1.54	0.6410	0.6844	0.4387	1.2600	1.97	L	A	Gabbro Schist	y	n
16	4.6	2.45	2.06	0.5326	0.8408	0.4478	2.1500	2.54	L	A	Gabbro Schist	y	n
17	3.07	2.07	1.13	0.6743	0.5459	0.3681	1.0000	1.94	M	A	Gabbro Schist	n	n
18	3.3	1.91	1.28	0.5788	0.6702	0.3879	1.3900	2.02	L	A	Gabbro Schist	y	n
19	4.49	2.60	0.80	0.5791	0.3077	0.1782	1.8900	3.69	L	VA	Gabbro Schist	n	n
20	3.9	2.71	0.54	0.6949	0.1993	0.1385	1.1900	3.36	L	VA	Gabbro Schist	y	n
21	5.68	4.32	2.33	0.7606	0.5394	0.4102	1.3600	3.35	M	A	Gabbro Schist	y	n
22	3.59	3.31	0.90	0.9220	0.2719	0.2507	0.2800	2.69	L	VA	Gabbro Schist	n	n
23	1.48	1.34	1.10	0.9054	0.8209	0.7432	0.1400	0.38	H	A	Gabbro Schist	n	n
24	2.27	1.89	1.12	0.8326	0.5926	0.4934	0.3800	1.15	L	VA	Gabbro Schist	y	n
25	3.15	2.14	0.90	0.6794	0.4206	0.2857	1.0100	2.25	L	VA	Gabbro Schist	y	n
26	4.4	2.30	1.61	0.5227	0.7000	0.3659	2.1000	2.79	L	A	Gabbro Schist	y	n
27	2.6	2.29	1.86	0.8808	0.8122	0.7154	0.3100	0.74	M	VA	Gabbro Schist	y	n
28	3.03	1.25	1.19	0.4125	0.9520	0.3927	1.7800	1.84	L	VA	Gabbro Schist	n	n
29	3	2.35	1.34	0.7833	0.5702	0.4467	0.6500	1.66	M	VA	Gabbro Schist	y	n
30	2.83	1.09	0.53	0.3852	0.4862	0.1873	1.7400	2.30	L	VA	Gabbro Schist	y	n
31	3.13	2.39	2.16	0.7636	0.9038	0.6901	0.7400	0.97	H	VA	Gabbro Schist	n	n
32	6.46	4.47	2.06	0.6920	0.4609	0.3189	1.9900	4.40	L	VA	Gabbro	n	n
33	3.13	1.93	1.81	0.6166	0.9378	0.5783	1.2000	1.32	M	A	Exotic	y	n
34	1.75	1.10	0.70	0.6286	0.6364	0.4000	0.6500	1.05	L	A	Gabbro	y	n
35	4.3	2.45	2.34	0.5698	0.9551	0.5442	1.8500	1.96	L	A	Gabbro	n	n
36	6.7	2.80	2.50	0.4179	0.8929	0.3731	3.9000	4.20	L	SA	Gabbro	y	n
37	3.13	1.41	1.10	0.4505	0.7801	0.3514	1.7200	2.03	L	A	Peridotite	y	n
38	2.42	2.09	1.24	0.8636	0.5933	0.5124	0.3300	1.18	M	A	Peridotite	n	n
39	1.73	1.41	1.13	0.8150	0.8014	0.6532	0.3200	0.60	L	VA	Peridotite	y	n
40	2.2	1.94	0.77	0.8818	0.3969	0.3500	0.2600	1.43	M	A	Peridotite	n	n

41	2.01	1.52	0.74	0.7562	0.4868	0.3682	0.4900	1.27	M	A	Gabbro	n	n
42	1.86	1.52	1.27	0.8172	0.8355	0.6828	0.3400	0.59	M	SA	Gabbro	y	n
43	3.38	2.20	1.10	0.6509	0.5000	0.3254	1.1800	2.28	L	SA	Gabbro Schist	y	n
44	2.52	1.40	0.75	0.5556	0.5357	0.2976	1.1200	1.77	L	VA	Gabbro	y	n
45	4.9	3.03	2.60	0.6184	0.8581	0.5306	1.8700	2.30	L	A	Diorite	n	n
46	4.09	2.46	1.77	0.6015	0.7195	0.4328	1.6300	2.32	L	A	Diorite	y	n
47	2.16	1.34	0.95	0.6204	0.7090	0.4398	0.8200	1.21	L	A	Diorite	n	n
48	3.12	2.17	1.53	0.6955	0.7051	0.4904	0.9500	1.59	M	SA	Phyllite	y	n
49	2.72	2.00	1.06	0.7353	0.5300	0.3897	0.7200	1.66	M	SA	Metasandstone	y	n
50	4.36	2.66	1.10	0.6101	0.4135	0.2523	1.7000	3.26	L	A	Phyllite	y	n

KW/13/N/1C

Clast #	Size (mm)			b/a	c/b	c/a	a-b	a-c	Sphericity	Angularity	Lithology	Faceted	Striated
	a axis	b axis	c axis										
1	2.41	2.32	1.06	0.9627	0.4569	0.4398	0.0900	1.35	L	SR	Sandstone	y	n
2	4.36	3.01	1.20	0.6904	0.3987	0.2752	1.3500	3.16	L	R	Sandstone	y	n
3	4.17	3.58	1.82	0.8585	0.5084	0.4365	0.5900	2.35	M	R	Sandstone	y	n
4	3.4	2.05	1.21	0.6029	0.5902	0.3559	1.3500	2.19	L	WR	Sandstone	n	n
5	3.29	2.27	1.07	0.6900	0.4714	0.3252	1.0200	2.22	M	R	Sandstone	n	n
6	3	2.29	0.79	0.7633	0.3450	0.2633	0.7100	2.21	L	SR	Sandstone	n	n
7	2.5	1.80	0.95	0.7200	0.5278	0.3800	0.7000	1.55	M	R	Sandstone	y	n
8	1.77	1.68	0.90	0.9492	0.5357	0.5085	0.0900	0.87	M	WR	Sandstone	n	n
9	1.32	1.22	0.50	0.9242	0.4098	0.3788	0.1000	0.82	L	A	Mica Shale	n	n
10	2.5	1.88	0.75	0.7520	0.3989	0.3000	0.6200	1.75	L	A	Mica Shale	y	n
11	6.24	4.38	3.03	0.7019	0.6918	0.4856	1.8600	3.21	M	SR	Amphibolite	y	n
12	4.31	3.36	1.61	0.7796	0.4792	0.3735	0.9500	2.70	L	SR	Amphibolite	n	n
13	2.94	2.28	0.97	0.7755	0.4254	0.3299	0.6600	1.97	M	SR	Amphibolite	n	n
14	2.91	2.41	1.11	0.8282	0.4606	0.3814	0.5000	1.80	L	SA	Amphibolite	n	n
15	2.35	2.08	1.67	0.8851	0.8029	0.7106	0.2700	0.68	H	R	Amphibolite	n	n
16	4.37	3.50	2.36	0.8009	0.6743	0.5400	0.8700	2.01	M	R	Amphibolite	n	n

17	4.24	3.10	2.75	0.7311	0.8871	0.6486	1.1400	1.49	M	WR	Amphibolite	n	n
18	1.08	1.04	0.59	0.9630	0.5673	0.5463	0.0400	0.49	M	SR	Amphibolite	n	n
19	2.62	2.06	0.86	0.7863	0.4175	0.3282	0.5600	1.76	L	SA	Pyroxenite	n	n
20	3.87	2.64	1.93	0.6822	0.7311	0.4987	1.2300	1.94	M	SR	Metasandstone	y	n
21	3.41	1.85	1.14	0.5425	0.6162	0.3343	1.5600	2.27	L	SA	Gabbro	y	n
22	2.52	1.55	0.63	0.6151	0.4065	0.2500	0.9700	1.89	L	SA	Gabbro Schist	n	n
23	2.92	1.59	1.08	0.5445	0.6792	0.3699	1.3300	1.84	L	SA	Pyroxenite	n	n
24	2.25	1.34	1.11	0.5956	0.8284	0.4933	0.9100	1.14	L	SA	Gabbro Schist	y	n
25	2.25	1.90	0.90	0.8444	0.4737	0.4000	0.3500	1.35	L	SA	Monzorite	n	n
26	1.75	0.96	0.85	0.5486	0.8854	0.4857	0.7900	0.90	M	SA	Granitoid	n	n
27	2.44	1.11	1.08	0.4549	0.9730	0.4426	1.3300	1.36	L	SR	Diorite	n	n
28	3.91	3.13	2.14	0.8005	0.6837	0.5473	0.7800	1.77	M	Sr	Amphibolite	y	n
29	2.25	1.96	0.92	0.8711	0.4694	0.4089	0.2900	1.33	L	SR	Pyroxenite	n	n
30	4.8	1.96	1.51	0.4083	0.7704	0.3146	2.8400	3.29	L	SR	Quartzite	y	n
31	2.24	1.82	1.02	0.8125	0.5604	0.4554	0.4200	1.22	L	SR	Gabbro	n	n
32	3.47	2.37	1.23	0.6830	0.5190	0.3545	1.1000	2.24	L	SR	Gabbro	y	n
33	3.54	1.86	1.66	0.5254	0.8925	0.4689	1.6800	1.88	L	SR	Gabbro	y	n
34	1.81	1.34	0.74	0.7403	0.5522	0.4088	0.4700	1.07	M	SA	Quartzite	n	n
35	1.51	1.30	1.07	0.8609	0.8231	0.7086	0.2100	0.44	H	R	Diorite	n	n
36	1.82	1.39	0.46	0.7637	0.3309	0.2527	0.4300	1.36	L	SR	Slate	n	n
37	2.58	2.00	1.24	0.7752	0.6200	0.4806	0.5800	1.34	M	SR	Metasandstone	y	n
38	1.53	1.30	1.05	0.8497	0.8077	0.6863	0.2300	0.48	H	R	Volcanic	n	n
39	1.28	1.03	0.37	0.8047	0.3592	0.2891	0.2500	0.91	L	A	Slate	n	n
40	1.14	0.53	0.34	0.4649	0.6415	0.2982	0.6100	0.80	L	A	Quartzite	n	n
41	2.6	1.54	1.34	0.5923	0.8701	0.5154	1.0600	1.26	M	SR	Volcanic	n	n
42	2.92	2.23	1.30	0.7637	0.5830	0.4452	0.6900	1.62	L	SR	Gneiss	n	n
43	2.07	1.76	1.43	0.8502	0.8125	0.6908	0.3100	0.64	H	SR	Volcanic	n	n
44	3.19	2.52	1.83	0.7900	0.7262	0.5737	0.6700	1.36	M	R	Metasandstone	n	n
45	4.61	2.76	2.53	0.5987	0.9167	0.5488	1.8500	2.08	L	SR	Volcanic	n	n
46	2.26	1.94	1.20	0.8584	0.6186	0.5310	0.3200	1.06	M	SA	Volcanic	n	n
47	2.64	1.60	1.59	0.6061	0.9938	0.6023	1.0400	1.05	L	SR	Basalt	y	n

48	4.76	2.93	2.34	0.6155	0.7986	0.4916	1.8300	2.42	L	A	Gneiss	n	n
49	2.78	2.58	1.19	0.9281	0.4612	0.4281	0.2000	1.59	M	SA	Volcanic	n	n
50	3.1	2.00	1.40	0.6452	0.7000	0.4516	1.1000	1.70	L	SA	Gabbro Schist	n	n

KW/13/H/1C

Clast #	Size (mm)			b/a	c/b	c/a	a-b	a-c	Sphericity	Angularity	Lithology	Faceted	Striated
	a axis	b axis	c axis										
1	4.94	3.99	2.03	0.8077	0.5088	0.4109	0.9500	2.91	M	SA	Mangerite	n	n
2	3.58	2.96	2.43	0.8268	0.8209	0.6788	0.6200	1.15	H	SR	Monzorite	n	n
3	3.24	2.55	2.14	0.7870	0.8392	0.6605	0.6900	1.10	H	SR	Monzorite	n	n
4	2.96	1.66	1.32	0.5608	0.7952	0.4459	1.3000	1.64	L	SR	Monzorite	n	n
5	1.92	1.48	0.90	0.7708	0.6081	0.4688	0.4400	1.02	M	SR	Mangerite	n	n
6	1.99	1.66	1.20	0.8342	0.7229	0.6030	0.3300	0.79	H	SR	Gabbro	n	n
7	3.22	2.45	1.60	0.7609	0.6531	0.4969	0.7700	1.62	M	SR	Gabbro	y	n
8	2.92	1.67	1.44	0.5719	0.8623	0.4932	1.2500	1.48	L	SA	Gabbro	n	n
9	2.42	1.59	1.13	0.6570	0.7107	0.4669	0.8300	1.29	L	A	Gabbro Schist	n	n
10	2.225	1.57	1.24	0.7056	0.7898	0.5573	0.6550	0.99	M	SR	Monzorite	n	n
11	1.75	1.42	0.90	0.8114	0.6338	0.5143	0.3300	0.85	H	SR	Monzorite	n	n
12	3.47	3.29	1.85	0.9481	0.5623	0.5331	0.1800	1.62	M	SA	Granitoid	n	n
13	2.06	1.84	1.44	0.8932	0.7826	0.6990	0.2200	0.62	H	A	Granitoid	n	n
14	1.8	1.66	1.40	0.9222	0.8434	0.7778	0.1400	0.40	H	SR	Anorthosite	n	n
15	2.81	1.62	1.55	0.5765	0.9568	0.5516	1.1900	1.26	L	R	Sandstone	y	y
16	3.12	1.63	0.85	0.5224	0.5215	0.2724	1.4900	2.27	L	R	Sandstone	y	y
17	3.84	2.04	1.85	0.5313	0.9069	0.4818	1.8000	1.99	L	SA	Gneiss	y	n
18	4.09	3.25	1.93	0.7946	0.5938	0.4719	0.8400	2.16	L	VA	Gneiss	n	n
19	2.33	1.68	1.51	0.7210	0.8988	0.6481	0.6500	0.82	H	SR	Amphibolite	y	n
20	2.1	1.95	1.34	0.9286	0.6872	0.6381	0.1500	0.76	M	A	Gneiss	n	n
21	1.55	1.28	1.16	0.8258	0.9063	0.7484	0.2700	0.39	H	SA	Gabbro	n	n
22	1.87	1.30	1.22	0.6952	0.9385	0.6524	0.5700	0.65	M	SA	Shale	n	n
23	2.26	1.49	1.33	0.6593	0.8926	0.5885	0.7700	0.93	M	VA	Volcanic	n	n

24	0.95	0.82	0.50	0.8632	0.6098	0.5263	0.1300	0.45	M	A	Volcanic	n	n
25	4	3.25	2.54	0.8125	0.7815	0.6350	0.7500	1.46	M	SA	Gneiss	n	n
26	3.83	3.19	2.08	0.8329	0.6520	0.5431	0.6400	1.75	M	A	Gneiss	n	n
27	1.64	1.20	0.70	0.7317	0.5833	0.4268	0.4400	0.94	L	A	Granitoid	n	n
28	3.19	2.05	1.18	0.6426	0.5756	0.3699	1.1400	2.01	L	VA	Amphibolite	n	n
29	2.2	1.87	0.86	0.8500	0.4599	0.3909	0.3300	1.34	L	A	Volcanic	n	n
30	2.33	1.55	1.00	0.6652	0.6452	0.4292	0.7800	1.33	L	A	Volcanic	n	n
31	2.26	2.03	1.32	0.8982	0.6502	0.5841	0.2300	0.94	H	SR	Volcanic	n	n
32	3.62	2.33	1.79	0.6436	0.7682	0.4945	1.2900	1.83	L	SA	Gneiss	n	n
33	2	1.69	1.18	0.8450	0.6982	0.5900	0.3100	0.82	M	SA	Volcanic	y	n
34	4.1	3.13	1.68	0.7634	0.5367	0.4098	0.9700	2.42	L	SA	Gneiss	n	n
35	3.1	2.20	0.96	0.7097	0.4364	0.3097	0.9000	2.14	L	A	Gneiss	y	n
36	2.74	1.67	1.27	0.6095	0.7605	0.4635	1.0700	1.47	L	A	Mica Shale	y	n
37	2.71	1.13	1.00	0.4170	0.8850	0.3690	1.5800	1.71	L	A	Mica Shale	y	n
38	2.11	1.22	1.20	0.5782	0.9836	0.5687	0.8900	0.91	L	A	Mica Shale	n	n
39	2.94	2.51	0.49	0.8537	0.1952	0.1667	0.4300	2.45	L	VA	Amphibolite	n	n
40	3.38	2.00	1.19	0.5917	0.5950	0.3521	1.3800	2.19	L	SA	Amphibolite	n	n
41	1.87	1.30	1.27	0.6952	0.9769	0.6791	0.5700	0.60	L	VA	Volcanic	y	n
42	2.45	1.52	0.36	0.6204	0.2368	0.1469	0.9300	2.09	L	VA	Phyllite	y	n
43	1.37	0.60	0.45	0.4380	0.7500	0.3285	0.7700	0.92	L	A	Phyllite	n	n
44	4.49	2.90	2.52	0.6459	0.8690	0.5612	1.5900	1.97	M	SA	Granitoid	y	n
45	5.55	4.30	2.24	0.7748	0.5209	0.4036	1.2500	3.31	M	SA	Granitoid	n	n
46	2.86	1.86	1.65	0.6503	0.8871	0.5769	1.0000	1.21	L	A	Granitoid	n	n
47	2.98	2.36	1.91	0.7919	0.8093	0.6409	0.6200	1.07	H	SA	Granitoid	n	n
48	0.93	0.73	0.33	0.7849	0.4521	0.3548	0.2000	0.60	L	SA	Volcanic	n	n
49	0.93	0.60	0.34	0.6452	0.5667	0.3656	0.3300	0.59	L	VA	Volcanic	n	n
50	1.05	0.71	0.27	0.6762	0.3803	0.2571	0.3400	0.78	L	VA	Volcanic	n	n